UNIVERSIDADE FEDERAL DE SANTA CATARINA
PROGRAMA DE PÓS-GRADUAÇÃO
EM ENGENHARIA MECÂNICA

MODELO BIFÁSICO PARA A LUBRIFICAÇÃO DO PISTÃO EM COMPRESSORES HERMÉTICOS ALTERNATIVOS

TESE SUBMETIDA À

UNIVERSIDADE FEDERAL DE SANTA CATARINA

PARA OBTENÇÃO DO GRAU DE

DOUTOR EM ENGENHARIA MECÂNICA

FERNANDO PAULO GRANDO

FLORIANÓPOLIS
SETEMBRO DE 2007

MODELO BIFÁSICO PARA A LUBRIFICAÇÃO DO PISTÃO EM COMPRESSORES HERMÉTICOS ALTERNATIVOS

FERNANDO PAULO GRANDO

TESE SUBMETIDA À UNIVERSIDADE FEDERAL DE SANTA CATARINA
PARA A OBTENÇÃO DO TÍTULO DE

DOUTOR EM ENGENHARIA MECÂNICA

NA ÁREA DE CONCENTRAÇÃO DE ENGENHARIA E CIÊNCIAS TÉRMICAS

Prof. Alvaro Toubes Prata, Ph.D. (Orientador)

Prof. Fernando Cabral, Ph.D. (Coordenador do Programa)

BANCA EXAMINADORA:

Prof. Alvaro T. Prata, PhD (Presidente)

Prof. Valder Steffen Junior, Dr. (Relator)

Prof. Marco Tulio C. de Faria, Ph.D.

Prof. Antonio Fábio Carvalho da Silva, Dr.

Prof. Jader Riso Barbosa Junior, Ph.D.

Ao Tio Henrique,
pelo exemplo e constante apoio.
Sem sua ajuda não chegaria até aqui.

À minha July,
por aceitar este desafio comigo.

AGRADECIMENTOS

Ao CNPq, pelo financiamento deste trabalho durante sua execução no Brasil.

Ao Programa Alβan, Programa da União Européia de Bolsas de Alto Nível para a América Latina, por financiar este trabalho durante minha estadia na Universidade de Leeds, identificação E03D22219BR.

À EMBRACO, pelo apoio técnico e também colaboração no financiamento deste trabalho.

Ao professor Alvaro Toubes Prata, por sua sempre presentes instruções e grande motivação nos aspectos técnicos bem como em todos os desafios que enfrentamos em busca de tornar este um inédito trabalho de dupla titulação. Nos últimos tempos, em virtude da mudança de minhas circunstâncias profissionais, sou extremamente grato por sua paciência e determinação que colaboraram para a conclusão desta tese.

Ao professor Martin Priest, da Universidade de Leeds, por seu apoio e orientação nesta tese. Sua colaboração criou novos horizontes no desenvolvimento deste trabalho e também permitiu grande interação com outros institutos de pesquisa, bem como minha participação em diversos congressos internacionais, em particular nos Congressos de Leeds-Lyon onde tive oportunidade de encontrar muitos dos pesquisadores que foram grande fonte de motivação e admiração em meus anos acadêmicos.

Ao professor José Antônio Bellini, por, enquanto coordenador do POSMEC, compreender a importância que colocávamos em elaborar e concluir este trabalho de pesquisa no âmbito de um trabalho cooperativo entre a Universidade Federal de Santa Catarina e a Universidade de Leeds. E, apesar do longo e difícil processo, sua fundamental cooperação levou-nos ao sucesso nesta causa.

Mais recentemente, ao professor Fernando Cabral, por sua compreensão das difíceis circunstâncias em que encontrei-me para concluir este trabalho, mas permitir-me chegar nesta derradeira etapa.

A todos os demais professores, funcionários e colegas do NRVA, agora POLO, pela agradável companhia. Também aos novos colegas com quem pude compartilhar meu período em Leeds.

A todos aqueles que ajudaram na manutenção de minha motivação, alegria e entusiasmo durante esta importante etapa de minha vida, e em particular a minha família que sempre deu-me total apoio e colaborou enormemente nos momentos mais difíceis.

SUMÁRIO

LISTA DE FIGURAS

LISTA DE TABELAS

LISTA DE SÍMBOLOS

Símbolo	Descrição	Unidade SI
A_*	Coeficientes das equações algébricas no método dos volumes finitos	-
c	Folga radial do mancal, folga pistão-cilindro	*[m]*
D	Diâmetro do mancal ou pistão	*[m]*
e	Excentricidade	*[m]*
e_t	Excentricidade do topo do pistão	*[m]*
e_b	Excentricidade da base do pistão	*[m]*
F_f	Força de atrito viscoso	*[N]*
F_f^*	Força de atrito viscoso, considerando separação do filme (eq.12)	*[N]*
F_g	Força exercida pelo gás na câmara de compressão sobre o pistão	*[N]*
F_h	Força hidrodinâmica	*[N]*
F_ε	Força hidrodinâmica no mancal, componente na direção ε	*[N]*
F_ξ	Força hidrodinâmica no mancal, componente na direção ξ	*[N]*
F_{rx}	Força de reação da biela sobre o pistão, direção *x*	*[N]*
h	Espessura do filme de óleo	*[m]*
I_P	Momento de inércia do pistão em relação ao pino	*[N.m2]*
L	Comprimento do mancal ou do pistão	*[m]*
m	Massa do mancal ou do pistão	*[kg]*
M_f	Momento devido à força de atrito (plano *xz*, em relação ao pino)	*[N.m]*
M_h	Momento devido à força hidrodinâmica (plano *xz*, rel. ao pino)	*[N.m]*
p	Pressão	*[Pa]*

p_{cyl}	Pressão na câmara de compressão	$[Pa]$
p_{suc}	Pressão ambiente no compressor	$[Pa]$
Pot	Potência consumida por atrito viscoso	$[W]$
q	Taxa de escoamento	$[m^2/s]$
R	Raio do eixo ou do pistão	$[m]$
S	Termo fonte no método dos volumes finitos	-
t	Tempo	$[s]$
u	Componente da velocidade na direção x	$[m/s]$
u_a	Velocidade para o mancal na direção x	$[m/s]$
u_b	Velocidade para o eixo na direção x	$[m/s]$
U	Velocidade do eixo	$[m/s]$
v	Componente da velocidade na direção y	$[m/s]$
v_a	Velocidade para o mancal na direção y	$[m/s]$
v_b	Velocidade para o eixo na direção y	$[m/s]$
V_P	Velocidade axial do pistão	$[m/s]$
w_r	Concentração de refrigerante na mistura (fração mássica)	$[kg_{ref}/kg_{mist}]$
w_e, w_i	Concentração de refrigerante na entrada do escoamento	$[kg_{ref}/kg_{mist}]$
w_o	Concentração total de refrigerante na mistura (*overall*)	$[kg_{ref}/kg_{mist}]$
w_{sat}	Solubilidade do refrigerante no óleo	$[kg_{ref}/kg_{mist}]$
W	Carga aplicada ao mancal	$[N]$
x	Coordenada do sistema cartesiano	$[m]$
y	Coordenada do sistema cartesiano	$[m]$
z	Coordenada do sistema cartesiano	$[m]$
z_{CM}	Posição axial do centro de massa do pistão	$[m]$

Símbolos Gregos

δ , Δ	Incrementos	-
$\delta\theta_w$, $\delta\theta_e$	Distância entre pontos nodais vizinhos na direção θ	[^{o} ,*rad*]
$\delta\xi_s$, $\delta\xi_n$	Distância entre pontos nodais vizinhos na direção ξ	[*adimensional*]
$\Delta\theta$	Dimensão do volume de controle na direção θ	[^{o} ,*rad*]
$\Delta\xi$	Dimensão do volume de controle na direção ξ	[*adimensional*]
ε	Excentricidade adimensional, ou simplesmente excentricidade	[*adimensional*]
θ	Coordenada angular do sistema polar	[^{o} ,*rad*]
κ	Coeficiente de absorção, equação (3)	[s^{-1}]
μ	Viscosidade dinâmica	[$N.s / m^2$]
$\overline{\mu}$	Viscosidade dinâmica aparente do fluido homogêneo	[$N.s / m^2$]
ξ	Coordenada adimensional para a direção *z*	[*adimensional*]
ρ	Massa específica (densidade volumétrica)	[kg / m^3]
$\overline{\rho}$	Densidade aparente do fluido homogêneo	[kg / m^3]
τ	Ângulo de manivela (ωt)	[^{o} ,*rad*]
ϕ	Fração de vazio, equação (5)	[*adimensional*]
ϕ_a	Fração de vazio estimada para a solução de Reynolds, eq. (13)	[*adimensional*]
χ	Título, equação (4)	[$kg_{gás}/kg_{tot}$]
ψ	Ângulo de atuação do mancal	[^{o},*rad*]
ψ_W	Ângulo da carga aplicada sobre o mancal em relação à vertical	[^{o},*rad*]
ω	Velocidade angular do mancal ou da manivela	[*rad/s*]

Subíndices

bottom	Saia do pistão
cav	Posição de cavitação
e,i	Entrada do escoamento

g	Fase gás
l	Fase líquida
rl	Refrigerante líquido
o	Saída
x	Direção x
y	Direção y
z	Direção z

Índices Sobrescritos

t	Tempo para o instante atual
$t+1, t+\Delta t$	Tempo avançado de um incremento
τ	Ângulo de manivela atual, para o instante t
$\tau+\Delta\tau$	Ângulo de manivela avançado de um incremento
$\dot{}$	Derivada temporal de primeira ordem
$\ddot{}$	Derivada temporal de segunda ordem

RESUMO

O estudo da lubrificação por filme fluido em componentes mecânicos é de fundamental importância na análise do comportamento dinâmico e na determinação das perdas devido ao atrito entre as partes móveis. Em muitos casos, gases presentes no sistema podem interagir com o óleo e alterar significativamente as características da lubrificação – pela sua dissolução e desprendimento no óleo, com a formação de bolhas e até mesmo de espuma. Adicionalmente, em regiões de baixa pressão o lubrificante perde a capacidade de escoar como um filme contínuo, ocorrendo o fenômeno da cavitação.

De um modo geral, o fenômeno da cavitação é tratado em modelos numéricos através das condições de contorno para a equação da pressão, que então é usada somente para o cálculo na região de filme pleno, e não todo o domínio de solução. Diversos critérios estão disponíveis para tanto, e os resultados freqüentemente são sensíveis à condição escolhida.

O presente trabalho propõe o estudo da cavitação considerando as mudanças que o lubrificante sofre ao longo do escoamento no componente sendo lubrificado, considerando a liberação de gás pelo líquido e a existência de um escoamento bifásico. O modelo numérico trata a mistura líquido/gás como um fluido homogêneo, com propriedades calculadas por médias das propriedades das fases constituintes. O modelo então resolve numericamente a equação da lubrificação pelo método dos volumes finitos, considerando as propriedades do fluido variáveis e sem utilizar qualquer condição de contorno intermediária. O lubrificante é considerado uma mistura de óleo e refrigerante, amplamente estudada por sua importância em problemas de lubrificação e transferência de calor em sistemas de refrigeração.

Para avançar no entendimento do modelo bifásico, inicialmente estuda-se a lubrificação em geometrias simplificadas, como a de um mancal radial parcial, e gradativamente as simplificações são relaxadas, aplicando-se o modelo aos mancais radiais plenos, onde comparações com resultados experimentais são possíveis, finalmente avançando para a solução do movimento alternativo do pistão em um compressor de refrigeração.

Os resultados obtidos são comparados com aqueles obtidos utilizando métodos usuais de lubrificação, como as condições de contorno de Reynolds. Variando os principais parâmetros operacionais e o comportamento da mistura em simulações, os resultados são discutidos, especialmente em relação às propriedades do fluido. O modelo explora a diferença de comportamento para misturas distintas de óleo e refrigerante, e também sua distinção para soluções considerando óleo puro.

ABSTRACT

The study of fluid film lubrication in mechanical components is fundamental to the analysis of their dynamic behaviour as well as determining friction losses between moving parts. In several cases, gases present in the system can interact with the oil changing lubrication characteristics – by their dissolution and release from the oil, forming bubbles or even producing foam. Additionally, at low pressure regions the lubricant loses the capacity to flow as a continuous film, and cavitation occurs.

Generally cavitation is treated in numerical model via boundary conditions for the pressure equation, which is then used to solve the problem only in the full film region instead of the whole solution domain. Several criteria are available, and the results are often sensitive to the chosen conditions.

The present work proposes the study of cavitation considering the changes suffered by the lubricant as it flows through the lubricated component, considering the release of gas from the liquid and the existence of a two-phase flow. The numerical model treats the liquid-gas mixture as a homogeneous fluid, whose properties are calculated as weighted averages of the properties from the constituent phases. The model then solves the lubrication equation numerically using the finite volume methodology, considering variable fluid properties and without using any intermediate boundary conditions. The lubricant is considered a mixture of oil and refrigerant, widely studied due to its importance in lubrication and heat transfer problems in refrigeration systems.

To advance in the understanding of the two-phase flow model, it is initially applied to simplified geometries, such as that of a partial journal bearing, and gradually the geometrical assumptions are relaxed, applying the model to a full journal bearing, where comparison against experimental results are possible. Finally, the problem is considered in the study of the reciprocating motion of the piston in a refrigeration compressor.

The results are compared to those obtained using usual lubrication methodologies, such as the Reynolds boundary conditions. By varying in simulations the main operational parameters and the mixture behaviour, the results are discussed with particular attention to the fluid properties. The model also explores the difference in behaviour for distinct oil and refrigerant mixtures, and further how those are distinguished from solutions considering pure oil as the lubricant.

1. Introdução

A interação entre o gás dissolvido em uma fase líquida pode proporcionar uma difícil tarefa no projeto e operação de sistemas mecânicos. Não é incomum a falta de conhecimento sobre o que afeta tal interação e também sobre suas conseqüências, o que por sua vez traz incerteza e até mesmo imprevisibilidade ao projeto e monitoramento dos componentes. Uma área de grande importância neste contexto é a tribologia, e em particular a ocorrência da cavitação na lubrificação hidrodinâmica.

1.1. Considerações Iniciais

A cavitação é convencionalmente definida em lubrificação como a perda de continuidade em um fino filme líquido que separa duas superfícies em movimento relativo. Este fenômeno pode ocorrer tanto pela presença de gás como de vapor, e influencia grandemente o comportamento de componentes mecânicos lubrificados, em aspectos como a capacidade de carga, força de atrito e estabilidade de operação.

Embora a cavitação seja estudada de longa data, sua diversificada ocorrência para diferentes geometrias e condições de operação resultou na proposição de uma variedade de critérios numéricos para sua análise. Embora estes critérios normalmente operem de forma semelhante, provendo condições de contorno em posições intermediárias do domínio de solução do problema, nota-se que há grande sensibilidade dos resultados com relação ao critério escolhido.

Como não é sempre evidente ou identificável o critério ideal a ser utilizado, pode-se obter resultados bastante diversificados para um mesmo problema. Um exemplo onde há dificuldade para se definir o critério de cavitação é aquele de um pistão em compressores alternativos de refrigeração, mostrado na figura 1.

O filme lubrificante separando pistão e cilindro é comunicado com a pressão ambiente na base do pistão e com a pressão da câmara de compressão no topo. É pouco provável que uma condição singular de cavitação possa ser definida para este caso, e condições para posições intermediárias podem ser ainda mais difíceis de avaliar. Assim, hipóteses adotadas em uma fraca base física podem ser extremamente arriscadas, e conduzir a resultados inapropriados. Por outro lado, dada a importância desse problema no estudo de muitos

processos críticos relacionados ao escoamento no interior do compressor, uma solução mais adequada deve ser investigada.

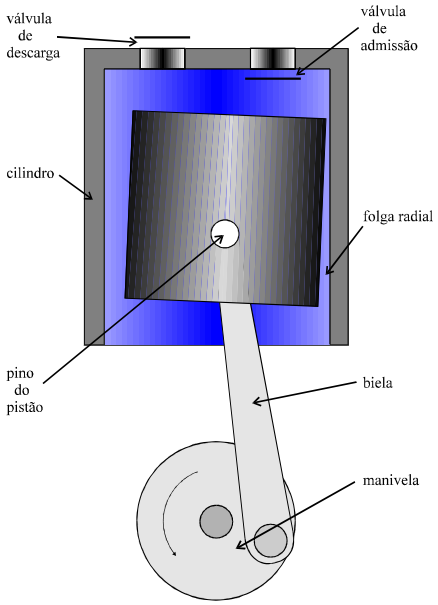

Figura 1. Pistão em movimento alternativo no interior do cilindro de um compressor.

Uma idéia para avançar na solução deste e outros problemas é a de estudar a interação entre as duas fases presentes, líquido e gás, o que inevitavelmente remete a uma modelação bifásica. Visto que também é comum a todas as teorias estudando a cavitação descrever sua existência em função da interação entre estas fases, potencialmente um modelo baseado em tal conhecimento pode resultar em maior generalidade de aplicação do que os modelos disponíveis atualmente.

Neste contexto, a proposta deste trabalho é a de estudar a lubrificação de acordo com a idéia de escoamento bifásico, assim considerando o comportamento da mistura lubrificante ao longo de todo o escoamento e podendo ampliar o entendimento de como este comportamento pode afetar a operação do componente lubrificado.

1.2. Motivação e Objetivos do Trabalho

A crescente pressão por eficiência energética na indústria mecânica em geral, e em particular do setor de refrigeração, requer o uso de ferramentas mais avançadas de modelagem e monitoramento para permitir um projeto otimizado. Pesquisas têm sido extensivamente realizadas em todos os principais componentes do compressor, buscando reduzir as perdas termodinâmicas, elétricas e por atrito (Possamai e Todescat, 2004). Com relação às perdas por

atrito, atualmente uma linha de investigação sugere que a interação do lubrificante com o ambiente de operação é importante para uma estimativa mais apurada das condições de lubrificação e o desgaste em componentes mecânicos (Dowson e Neville, 2005). Entre muitas outras vantagens, esta abordagem tem o potencial the contribuir para o entendimento de situações de lubrificação onde um escoamento bifásico é observado, presentemente uma área onde há muita controvérsia entre as modelagens propostas, e também grande discrepância nos resultados obtidos (Choi e Kim, 2002).

Assim, é interessante que se avance no entendimento de como a cavitação ocorre em sistemas de refrigeração, e qual sua relação com as características da mistura lubrificante. Para tanto, é necessário o conhecimento das propriedades desta mistura, especialmente em aspectos como a solubilidade entre as fases constituintes, massa específica, viscosidade e a variação das mesmas com pressão e temperatura. Também deve-se compreender e modelar o escoamento bifásico existente, nenhum destes plenamente dominado no contexto da lubrificação.

Assim, o desenvolvimento do modelo bifásico tem como metas principais:

- Propor uma equação que governe o fenômeno da lubrificação, que possa ser aplicada aos escoamentos bifásicos compressíveis e que considere o desprendimento e absorção de gás;
- Investigar o comportamento transiente da mistura lubrificante;
- Comparar os resultados da metodologia proposta com as soluções usuais, em particular para as geometrias mais comumente utilizadas;
- Aplicar o conhecimento desenvolvido à solução do problema do pistão no compressor.

As principais contribuições almejadas, nas duas principais áreas estudadas são enumeradas a seguir,

Lubrificação:

- Avançar no conhecimento que contribua para o desenvolvimento e estabelecimento da teoria de lubrificação bifásica;
- Desenvolver um modelo de lubrificação bifásica, onde incopora-se o desprendimento de gás pela mistura lubrificante, permitindo a solução de problemas de lubrificação sem utilizar critérios de cavitação;

- Comparar resultados obtidos com o modelo bifásico com aqueles de modelos de cavitação, visando avançar no entendimento da cavitação e viabilizar uma alternativa mais apurada para a solução de problemas de lubrificação;
- Contribuir para o entendimento dos mancais e pistões, tanto em carregamentos estáticos como dinâmicos.

Refrigeração:

- Disponibilizar através de um amplo trabalho, maior conhecimento sobre os efeitos da interação entre óleo e refrigerante, bem como do seu escoamento, com particular atenção para geometrias complexas como aquelas encontradas no interior do compressor;
- Tornar disponíveis maiores informações que assegurem a correta simulação de mancais e pistões em refrigeração;
- Avaliar parâmetros que influenciam a dinâmica do pistão, bem como investigar e melhorar as ferramentas utilizadas para caracterizar a lubrificação em componentes de refrigeração.

1.3. Estrutura do Documento

Este trabalho foi realizado no contexto de cooperação e dupla titulação entre a Universidade Federal de Santa Catarina e a Universidade de Leeds, resultando no documento de tese entitulado *Two-Phase Lubrication Model for Refrigeration Reciprocating Compressors* (Grando, 2007), submetido à Universidade de Leeds para obtenção do equivalente grau de doutoramento. No presente documento, uma síntese do trabalho é apresentada, discutindo os aspectos envolvidos na formulação do modelo bifásico, a partir da revisão da literatura, incluindo o desenvolvimento do modelo matemático e os testes realizados para as diferentes geometrias estudadas, e as finalmente as principais conclusões são descritas. Entretanto, referência se faz ao documento anterior para maiores detalhes e discussões sobre todo o trabalho de tese desenvolvido.

2. Revisão Bibliográfica

Se o lubrificante é considerado como óleo puro, o estudo da lubrificação aplicada à refrigeração é bastante semelhante à lubrificação de outros componentes, como motores de combustão interna, eixos, rotores, etc. A maior parte dos trabalhos disponíveis nesta área não tratam especificamente de modelos de lubrificação aplicados a componentes de refrigeração; mesmo assim, serão de grande utilidade para desenvolver um modelo geral de lubrificação.

Para a modelagem teórica do problema, é necessário revisar alguns importantes fundamentos da lubrificação por filme fluido, como a cavitação, que consiste na ruptura do filme líquido por este não suportar condições de pressão negativa. A cavitação não é um fenômeno plenamente dominado e modelado, e, através dos trabalhos previamente realizados, pode-se verificar os fatores que devem ser considerados para comparação quando da validação do modelo bifásico. Também devem ser revisados os modelos de lubrificação que consideram a presença de bolhas inertes de ar dissolvidas no óleo, bem como os modelos de lubrificação para pistões disponíveis até o momento, com e sem anéis.

Os trabalhos dedicados à lubrificação de componentes de refrigeração são em sua maior parte experimentais, e estudam dois pontos principais: a influência que o ambiente abundante de refrigerante no interior do compressor tem sobre a lubrificação dos componentes, e a modelagem do escoamento de misturas óleo-refrigerante, colaborando no entendimento do comportamento da mistura em operação.

Representando de forma esquemática na figura 2, essas contribuições serão muito importantes no gradual desenvolvimento do modelo numérico para a solução de problemas de lubrificação onde um escoamento bifásico pode ocorrer, em particular com desprendimento de gás. Em particular, o problema do movimento do pistão considerará todas as influências estudadas.

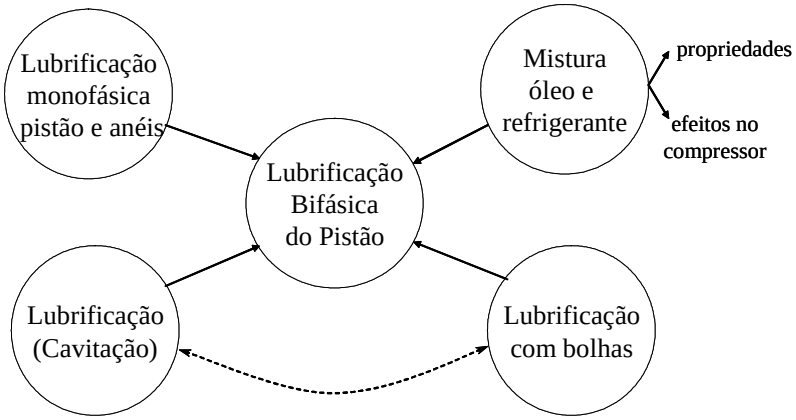

Figura 2. Principais áreas de pesquisa avaliadas para o desenvolvimento do modelo bifásico.

3. Metodologia

3.1. Modelo Físico

O caso em estudo representa um componente mecânico onde há movimento relativo entre superfícies e uma carga externa é aplicada. A geometria do componente é tal que uma geometria convergente-divergente pode ser observada em pelo menos uma região, como apresentado na figura 3. Um lubrificante separa as superfícies, e devido à sua interação com o ambiente de operação, este pode ser caracterizado como um óleo com uma certa quantidade de refrigerante dissolvido, normalmente conhecida a priori.

Na região convergente, a pressão tende a aumentar, e as propriedades permanecerão as mesmas enquanto apenas uma mistura líquida existir. Em caso de existência de bolhas de gás nesta região, é necessário considerar a compressibilidade e a absorção do gás pelo líquido.

Entretanto, na região divergente, um gradiente de pressão negativo ocorre e os níveis de pressão podem atingir os níveis de saturação para a mistura lubrificante. Devido à baixa pressão de vapor do óleo, assume-se que apenas refrigerante está presente na fase gasosa. Com o aumento na folga de escoamento, desprendimentos adicionais ocorrem e gradualmente um volume maior de gás se observa, tanto pelo desprendimento adicional de gás como pela sua expansão (figura 3).

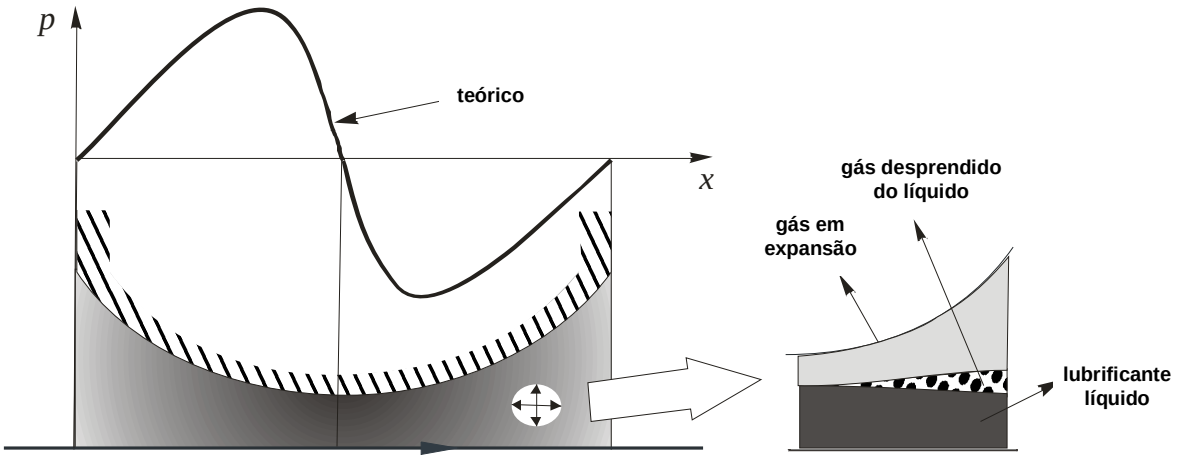

Figura 3. Geometria convergente-divergente e o comportamento do lubrificante ao longo do folga.

Caso haja recirculação de fluido ou uma região de recuperação de pressão seja observada, a mistura líquido-gás experimentará um aumento de pressão, e uma parcela do gás potencialmente poderá ser reabsorvida no óleo, embora a uma taxa de dissolução muito mais lenta que aquela para o desprendimento de gás. Apesar do limitado conhecimento sobre este processo, esta situação precisa ser considerada. Utilizando diferentes hipóteses com respeito à

reabsorção, uma análise qualitativa é possível. Entretanto, a necessidade de investigação adicional sobre o comportamento transiente em absorção é de fundamental importância para uma determinação precisa das condições de operação.

3.2. Modelo Matemático

O desenvolvimento de um modelo numérico para resolver quaisquer dos problemas em avaliação neste trabalho segue um procedimento similar, baseado em três etapas: *(i)* entender as propriedades da mistura e representar o escoamento bifásico; *(ii)* obter a equação que apropriadamente governa o problema; *(iii)* aplicar um método de integração numérica à equação governante, que após a solução do problema, fornecerá valores para as variáveis de interesse em posições discretas ao longo do domínio. Estes procedimentos seguem uma linha comum e representam a solução completa para o problema. Entretanto, para geometrias simplificadas ou baseando-se em hipóteses sobre a física do problema, uma situação mais simples poderá ser resolvida e o procedimento genérico é reajustado de modo que o esforço computacional se reduz.

Na seqüência os três passos principais necessários na metodologia de solução são abordados, e posteriormente as simplificações para cada problema estudado são discutidas.

3.2.1. Caracterização da mistura líquida e do escoamento bifásico

Para caracterizar as variações em propriedades sofridas pelo fuido ao longo do escoamento, uma série de parâmetros se faz necessária, tais como a composição fracional do refrigerante e do óleo na mistura líquida, e as proporções de líquido e gás no escoamento bifásico, definidos a seguir.

Fração mássica de refrigerante: a quantidade de refrigerante dissolvida na mistura líquida, em fração de massa, é definida pela equação (1),

$$w_r = \frac{m_{lr}}{m_l} \tag{1}$$

onde m_{lr} é a massa de refrigerante líquido e m_l a massa total de líquido (óleo e refrigerante).

A quantidade máxima de refrigerante que pode ser dissolvida no líquido para determinadas condições de pressão e temperatura é definida como *solubilidade*,

$$w_{sat} = w_{sat}(p, T) \tag{2}$$

onde p é a pressão absoluta e T a temperatura da mistura.

Para determinar a fração mássica de refrigerante ao longo do escoamento, informações sobre o desprendimento e absorção do gás são necessárias. No presente trabalho, baseado numa analogia com circuitos elétricos, uma equação de potencial pode ser utilizada, como indica a equação (3),

$$w_r^t = w_r^{t-1} + \kappa \cdot \Delta t \cdot \left(w_{sat} - w_r^{t-1} \right) \tag{3}$$

onde κ é o coeficiente de absorção/desprendimento, e *t*, *t-1* representam dois instantes de tempo consecutivos onde a fração mássica é considerada, separados por um intervalo de tempo Δt.

Duas condições termodinâmicas limite são conhecidas para o processo. Em *equilíbrio*, absorção ou desprendimento são instantâneos e $\kappa \cdot \Delta t = 1$. Em *não-equilíbrio pleno*, não há interação e $\kappa \cdot \Delta t = 0$. O desprendimento de gás ocorre próximo das condições de equilíbrio, sendo a metaestabilidade desprezível. Entretanto, a absorção é um processo muito mais lento e tal condição é menos provável. No presente trabalho, as duas condições limites são testadas para a absorção, bem como valores intermediários para o coeficiente de absorção.

Título: é a razão entre a massa de gás e a massa total da mistura em uma seção do escoamento. Em termos da fração mássica de refrigerante, é possível relacionar o título à composição total de referência (w_o), então resultando,

$$\chi = \frac{w_o - w_r}{1 - w_r} \tag{4}$$

Fração de Vazio: é a razão entre o volume de gás e o volume total da mistura numa seção do escoamento. Para um modelo bifásico homogêneo, onde as velocidades são idênticas para ambas as fases, esta razão pode ser calculada como indicado na equação (5),

$$\phi = \frac{1}{\left(1 + \left(\frac{1}{\chi} - 1 \right) \frac{\rho_g}{\rho_l} \right)} \tag{5}$$

onde ρ_g e ρ_l são as massas específicas do gás e do líquido, respectivamente.

Definidos estes parâmetros, a mistura líquido-gás pode ser substituída no modelo bifásico homogêneo por um pseudo-fluido monofásico, cujas densidade aparente ($\overline{\rho}$) e viscosidade ($\overline{\mu}$) são dadas por (Carey, 1992),

$$\bar{\rho} = \phi\rho_g + (1-\phi)\rho_l \tag{6}$$

$$\bar{\mu} = \chi\mu_g + (1-\chi)\mu_l \tag{7}$$

onde ρ_g e ρ_l, μ_g e μ_l são massas específicas e viscosidades para líquido e gás, respectivamente.

3.2.2. Equação governante para o fenômeno da lubrificação: A Equação de Reynolds

As hipóteses relacionadas ao comportamento do fluido são adicionadas às simplificações usuais adotadas para o problema de lubrificação (Cameron, 1966), de modo que a equação convencional para a lubrificação permanece válida no presente modelo matemático. Assim, com as forças de pressão e atrito viscoso dominantes, o escoamento é governado pela equação de Reynolds, apresentada em sua forma mais geral na equação (8), onde as propriedades aparentes do escoamento bifásico são consideradas,

$$\frac{\partial}{\partial x}\left(\frac{\bar{\rho}h^3}{12\bar{\mu}}\frac{\partial p}{\partial x}\right)+\frac{\partial}{\partial y}\left(\frac{\bar{\rho}h^3}{12\bar{\mu}}\frac{\partial p}{\partial y}\right)=\frac{\partial}{\partial x}\left[\bar{\rho}h\left(\frac{u_a+u_b}{2}\right)\right]+\frac{\partial}{\partial y}\left[\bar{\rho}h\left(\frac{v_a+v_b}{2}\right)\right]+\frac{\partial}{\partial t}\left(\bar{\rho}h\right) \tag{8}$$

onde x e y são as coordenadas cartesianas num plano perpendicular à espessura do filme lubrificante, $\bar{\rho}$ e $\bar{\mu}$ as propriedades aparentes da mistura bifásica, h a espessura do filme lubrificante, p a pressão, u e v velocidades das superfícies em movimento. Em casos onde uma das dimensões características do componente estudado é circular e de raio R, é comum normalizar as variáveis x e y por esta dimensão característica, sendo então a equação apresentada em função de coordenadas normalizadas θ e ξ.

A equação governante é válida para toda a extensão do componente e respeita a conservação da massa. São necessárias duas condições de contorno para cada direção considerada (x e y), e uma condição inicial para a variável temporal. As condições de contorno variam entre os distintos problemas, e são detalhadas para cada caso específico.

Uma vez determinado o campo de pressão, as forças resultantes dos efeitos de lubrificação podem ser calculadas. A força hidrodinâmica é dada por,

$$F_h = \sqrt{F_\varepsilon^2 + F_\xi^2} \tag{9}$$

onde,

$$F_\varepsilon = -\int_{\xi_i}^{\xi_o}\int_{\theta_i}^{\theta_o} p(\theta)R^2\cos\theta d\theta d\xi \tag{10.i}$$

$$F_{\xi} = \int_{\xi_i}^{\xi_o} \int_{\theta_i}^{\theta_o} p(\theta) R^2 \sin\theta d\theta d\xi \tag{10.ii}$$

Enquanto que a força de atrito é calculada como,

$$F_f = \int_{\xi_i}^{\xi_o} \int_{\theta_i}^{\theta_o} \left(\frac{h}{2R} \frac{dp}{d\theta} + \bar{\mu} \frac{U}{h} \right) R^2 d\theta d\xi \tag{11}$$

Deve ser observado que a força de atrito é calculada usando a mesma expressão ao longo de todo o componente. No caso de mancais radiais, isto resulta numa forma distinta daquela em uma metodologia convencional (Pinkus e Sternlicht, 1961), que considera a ruptura do filme e sugere que o atrito pode ser calculado considerando estrias separadas de líquido e gás. Por exemplo, para um mancal radial onde forças tranversais são desprezíveis, e cuja largura é dada por *L*, o atrito é calculado pela equação (12),

$$F_f^* = \int_{\theta_i}^{\theta_{cav}} \left(\frac{h}{2R} \frac{dp}{d\theta} + \mu_i \frac{U}{h} \right) RL d\theta + \int_{\theta_{cav}}^{\theta_o} (1 - \phi_a) \mu_i \frac{U}{h} RL d\theta \tag{12}$$

onde θ_{cav} é a posição angular onde ocorre cavitação e ϕ_a é a fração do filme preenchida por regiões de gás ao redor das quais o óleo escoa em estrias. O atrito viscoso no gás é assumido desprezível, e a viscosidade é considerada constante e igual à da entrada do escoamento. Adicionalmente, ϕ_a pode ser considerada como a fração de vazio do filme rompido e calculada por,

$$\phi_a = \frac{h - h_{cav}}{h}, \text{ for } \theta \geq \theta_{cav} \tag{13}$$

Num modelo de escoamento homogêneo, a equação (12) não se aplica, visto que uma velocidade comum e boa misturação entre as fases foram consideradas. O efeito da presença de gás é introduzido pela viscosidade aparente, equação (7). A diferença entre os resultados obtidos com estas diferentes metodologias é discutida em maiores detalhes ao longo dos resultados.

3.2.3. Solução Numérica: A Metodologia dos Volumes Finitos

Soluções analíticas não são obtidas comumente para a equação de Reynolds, apenas em casos bastante simplificados. Desta forma, via de regra a equação governante é resolvida numericamente para um domínio discretizado a partir da geometria do filme lubrificante. Para

discretizar e resolver o problema de lubrificação neste trabalho, a metodologia dos volumes finitos é adotada (Patankar, 1980).

Esta metodologia transforma o domínio contínuo do problema em volumes discretizados, como apresentado na figura 4, onde o detalhe de um volume em particular também é representado. Para cada volume, a equação governante do problema deverá ser satisfeita.

Portanto, a equação de Reynolds deve ser respeitada em cada volume. A título de exemplo, uma versão simplificada da equação de Reynolds, para um escoamento incompressível, é integrada ao longo de um volume de controle genérico, então resultando,

$$\int_s^n \int_w^e \frac{\partial}{\partial \theta}\left(h^3 \frac{\partial p}{\partial \theta} \right) d\theta d\xi + \int_s^n \int_w^e \frac{\partial}{\partial \xi}\left(h^3 \frac{\partial p}{\partial \xi} \right) d\theta d\xi = -\int_s^n \int_w^e 12\mu R^2 \left[\frac{v_a}{2R} \frac{\partial h}{\partial \xi} - \frac{\partial h}{\partial t} \right] d\theta d\xi \qquad (14)$$

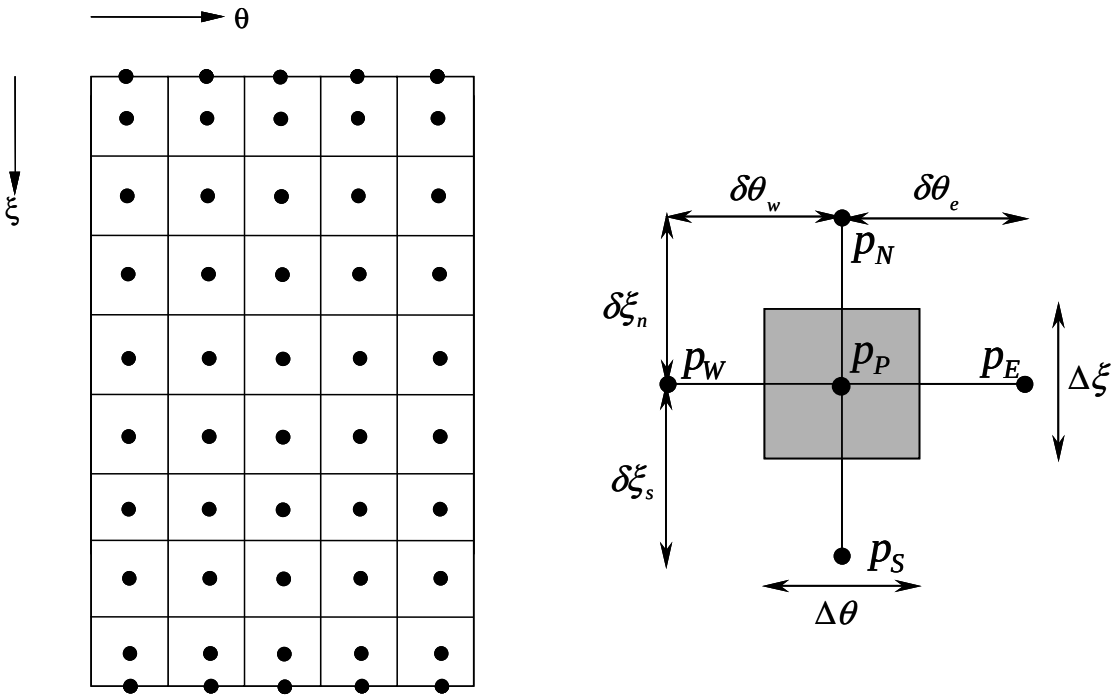

Figura 4. Discretização do domínio de solução pelo método dos volumes finitos.

Se a expressão para a espessura do filme lubrificante *h* é conhecida, e aproximando as derivadas pelo esquema das diferenças centrais, resulta uma equação algébrica,

$$A_p p_P = A_n p_N + A_s p_S + A_e p_E + A_w p_W + S \tag{15}$$

onde,

$$A_n = h_n^3 \frac{\Delta\theta}{\delta\xi_n} \qquad A_s = h_s^3 \frac{\Delta\theta}{\delta\xi_s}$$

$$A_e = h_e^3 \frac{\Delta\xi}{\delta\theta_n} \qquad A_w = h_w^3 \frac{\Delta\xi}{\delta\theta_w}$$

$$A_p = A_n + A_s + A_e + A_w$$

$$S = -12\mu R^2 \left[\frac{v_a}{2} h_P \Delta\xi + \frac{\partial h}{\partial t} \Delta\theta \Delta\xi \right]$$

Ao determinar uma equação para cada ponto interior, um sistema linear composto do conjunto de equações algébricas é obtido, que pode ser organizado em forma matricial e resolvido por uma variedade de métodos, direta ou iterativamente; neste trabalho, o modelo é resolvido pelo algoritmo TDMA (Patankar, 1980). Alternativamente, uma solução direta tal como a Eliminação Gaussiana pode ser utilizada (Roache, 1998). Ao resolver o sistema linear, valores de pressão para o conjunto discreto de pontos é determinado.

À luz desta formulação, diferentes problemas podem ser resolvidos, incluindo situações particulares. Os três problemas resolvidos no presente trabalho são brevemente descritos na seqüência.

3.3. Aplicação do Modelo

3.3.1. Problema 1: Mancal Parcial Radial Longo

Para um mancal radial parcial, onde um eixo rotativo é sustentado por um suporte aberto, as condições de entrada e saída podem ser identificadas. A geometria do problema é apresentada na figura 5.

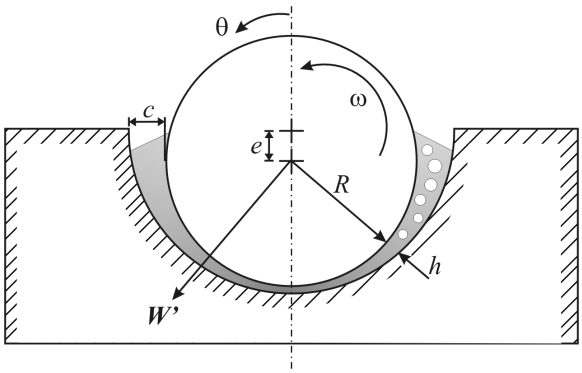

Figura 5. Geometria do mancal parcial e indicação da carga aplicada.

A partir da equação (8), considerando regime permanente, escoamento unidimensional e isotérmico, a equação de Reynolds é simplificada à equação (16), definida por,

$$\frac{\partial}{\partial\theta}\left(\frac{\overline{\rho}h^3}{\overline{\mu}}\frac{\partial p}{\partial\theta}\right) = 6UR\frac{\partial}{\partial\theta}(\overline{\rho}h) \tag{16}$$

A equação governante é valida para todo o domínio angular do mancal, o que também indica que a solução respeita a conservação da massa. Adicionalmente, como as pressões à entrada e saída do escoamento são conhecidas, as seguintes condições de contorno se aplicam,

$$\begin{aligned} \theta &= \theta_i,\ p = p_i \\ \theta &= \theta_o, p = p_o \end{aligned} \tag{17}$$

Com a equação (16) e em posse das condições de contorno, a metodologia dos volumes finitos pode ser aplicada e o problema resolvido. Como as propriedades do lubrificante dependem da pressão do filme, um processo iterativo é necessário para atingir um par coerente de pressões e propriedades do lubrificante. O algoritmo de solução adotado é esboçado na figura 6.

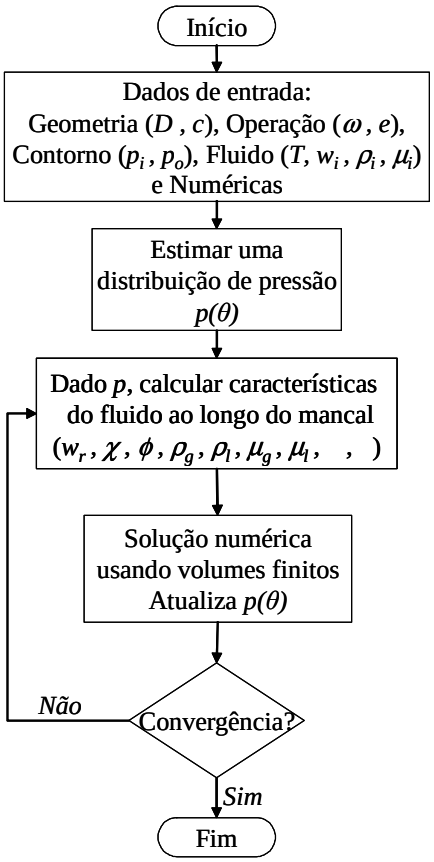

Figura 6. Algoritmo do processo numérico para a solução do problema do mancal radial parcial.

3.3.2. Problema 2: Mancal Radial Pleno Longo

No caso de um mancal radial fechado, as condições de entrada e saída não são facilmente identificadas. De fato, recirculação de fluido ocorre e consequentemente um escoamento bifásico pode também existir na região convergente. O comportamento da mistura pode ser ilustrado na figura 7.

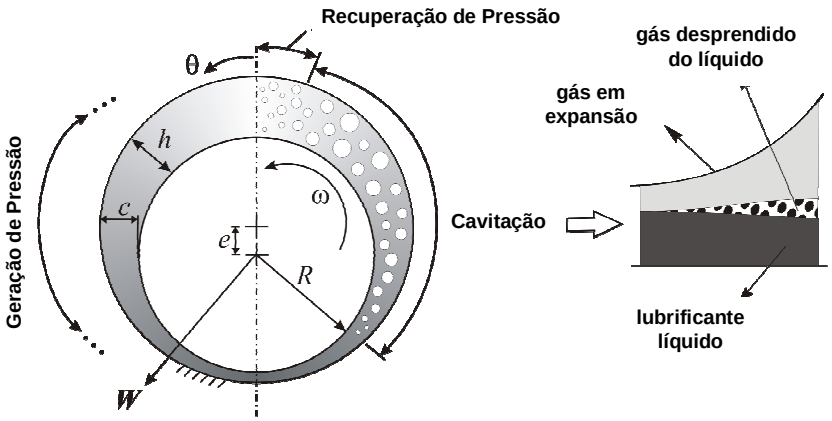

Figura 7. Geometria do mancal radial pleno e esboço das diferentes regiões do escoamento.

Devido à recirculação do fluido, condições de regime transiente serão sempre observadas no mancal, exceção ao caso onde equilíbrio termodinâmico é considerado. Em adição às condições transientes de escoamento, a carga aplicada no mancal também pode variar e um carregamento dinâmico deverá ser considerado. Assim, com base nas hipóteses observadas no problema anterior, mas também tendo em conta a dependência temporal, a forma simplificada da equação de Reynolds para o problema é dada por,

$$\frac{1}{R^2}\frac{\partial}{\partial\theta}\left(\frac{\overline{\rho}h^3}{12\overline{\mu}}\frac{\partial p}{\partial\theta}\right)=\frac{1}{R}\frac{\partial}{\partial\theta}\left(\frac{\overline{\rho}Uh}{2}\right)+\frac{\partial}{\partial t}(\overline{\rho}h) \tag{18}$$

A equação governante é resolvida para um específico passo de tempo onde a espessura do filme lubrificante é conhecida. Neste instante, as seguintes condições de contorno são válidas,

$$\begin{aligned} &p = p_{ref} \quad \text{for } \theta = \theta_{ref} \\ &p(\theta = 0) = p(\theta = 2\pi) \end{aligned} \tag{19}$$

e uma condição inicial também deve ser considerada. Entretanto, para mancais carregados estaticamente, a solução convergida não depende da condição inicial adotada.

Para determinar as condições de operação do mancal, não é suficiente apenas resolver a equação de Reynolds. É necessário também conhecer o comportamento do termo de filme

espremido, $\partial(\bar{\rho}h)/\partial t$, para os intervalos de tempo considerados. Adicionalmente, para determinar o comportamento transiente do mancal, a solução para a dinâmica do eixo é requerida. Para este fim, o balanço de forças no eixo é estabelecido com relação a um novo sistema de coordenadas fixo, adicional ao sistema de coordenadas usual que passa pela linha de centros do mancal e do eixo. Estas referências são apresentadas na figura 8.

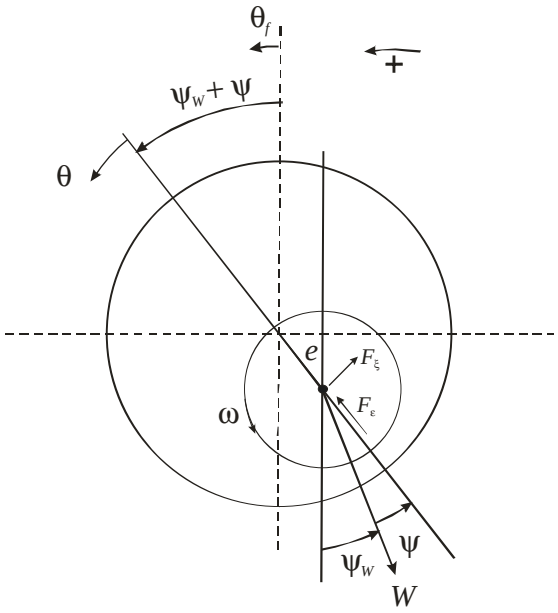

Figura 8. Balanço de forças atuando no eixo e os distintos sistemas de coordenadas adotados.

Considerando as forças que atuam no eixo, o balanço de forças pode ser escrito como,

$$mc[\ddot{\varepsilon} - \varepsilon(\dot{\psi}_W + \dot{\psi})^2] = W\cos\psi - F_\varepsilon \tag{20}$$

e,

$$mc[2\dot{\varepsilon}(\dot{\psi}_W + \dot{\psi}) + \varepsilon(\ddot{\psi}_W + \ddot{\psi})] = F_\xi - W\sin\psi \tag{21}$$

Das equações (20) e (21), para definidas condições de carga W, ψ_l, $\dot{\psi}_l$ e $\ddot{\psi}_l$, e adicionalmente em posse da posição e velocidade do eixo para um instante de tempo t, as acelerações podem ser determinadas como segue,

$$\ddot{\varepsilon}^t = \varepsilon^t(\dot{\psi}_W^t + \dot{\psi}^t)^2 + \frac{1}{mc}(W\cos\psi^t - F_\varepsilon) \tag{22}$$

$$\ddot{\psi}^t = -\ddot{\psi}_W^t - \frac{1}{\varepsilon^t}\left[2\dot{\varepsilon}^t(\dot{\psi}_w^t + \dot{\psi}^t) + \frac{1}{mc}(W\sin\psi^t - F_\xi)\right] \tag{23}$$

A partir das acelerações calculadas, velocidade e posição do eixo podem ser extrapolados com o uso de um esquema de marcha, por exemplo o método de Euler,

$$\dot{\varepsilon}^{t+\Delta t} = \dot{\varepsilon}^{t} + \ddot{\varepsilon}^{t} \cdot \Delta t \tag{24}$$

$$\dot{\psi}^{t+\Delta t} = \dot{\psi}^{t} + \ddot{\psi}^{t} \cdot \Delta t \tag{25}$$

e,

$$\varepsilon^{t+\Delta t} = \varepsilon^{t} + \dot{\varepsilon}^{t+\Delta t} \cdot \Delta t \tag{26}$$

$$\psi^{t+\Delta t} = \psi^{t} + \dot{\psi}^{t+\Delta t} \cdot \Delta t \tag{27}$$

Assim, a solução do problema consiste de passos integrados de cálculo da excentricidade e ângulos para o próximo intervalo de tempo, e a determinação dos valores de pressão utilizando a equação de Reynolds discretizada, onde um processo iterativo já é necessário dada a interdependência entre propriedades e pressão. A solução convergida, por exemplo em um mancal radial estaticamente carregado, ocorre quando posição e pressão cessam de variar, como esquematicamente apresentado na figura 9.

3.3.3. Problema 3: A Folga Pistão-Cilindro

Na operação do pistão, ao invés de rotação, uma translação axial é o movimento principal, responsável pela compressão do gás refrigerante que circula ao longo do sistema de refrigeração. A complexidade do movimento alternativo inevitavelmente resulta em condições dinâmicas, desta forma exigindo equações adicionais para o fechamento do problema. Adicionalmente, o pistão pode transladar e girar na folga radial ao longo do tempo (movimento secundário), sendo necessárias variáveis adicionais para determinar seu pleno posicionamento. Uma opção possível é a de caracterizar o componente utilizando posições e velocidades no topo e base do pistão, como indicado na figura 10 junto da geometria da folga pistão-cilindro e dos principais esforços atuando no pistão.

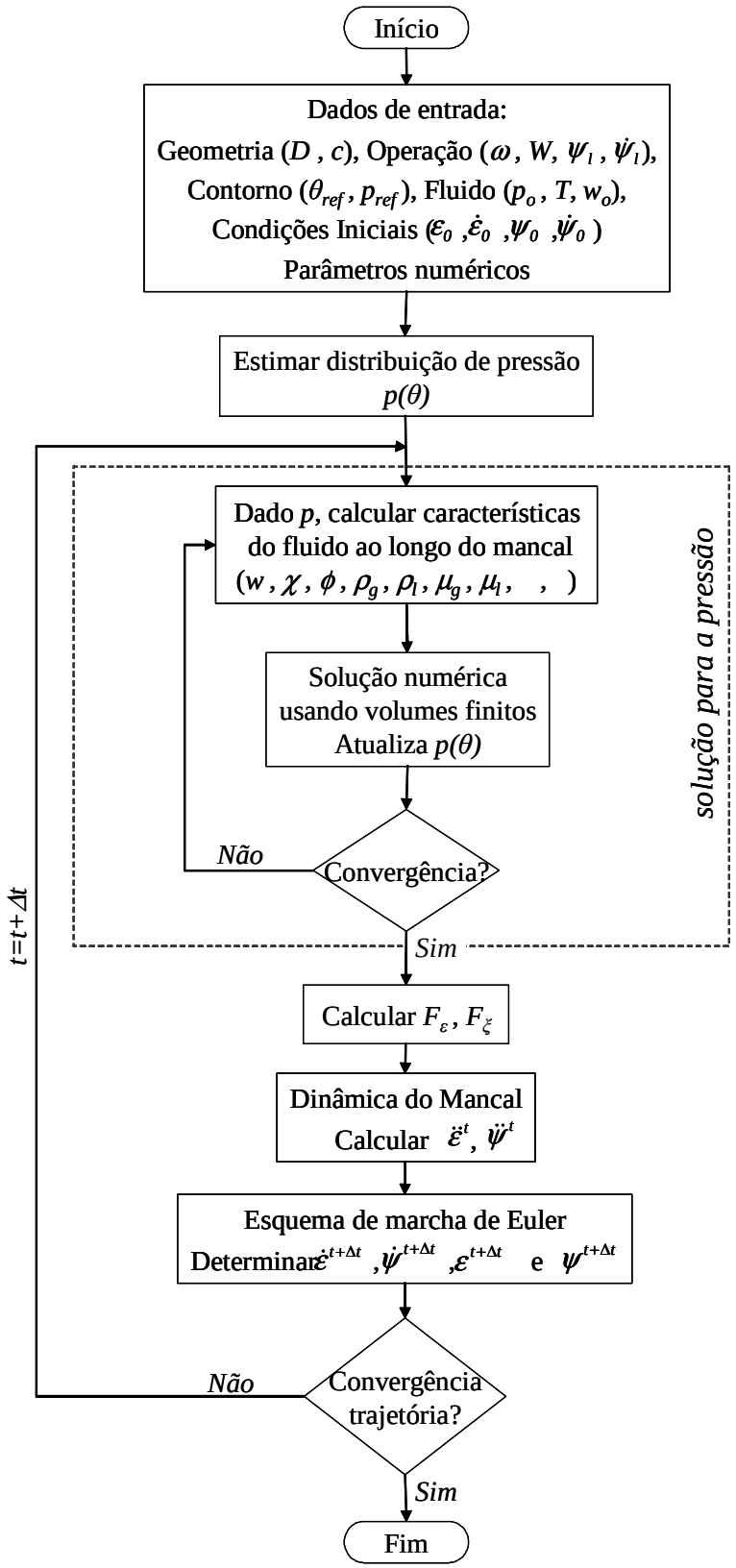

Figura 9. Procedimento numérico de solução para o mancal radial carregado dinamicamente.

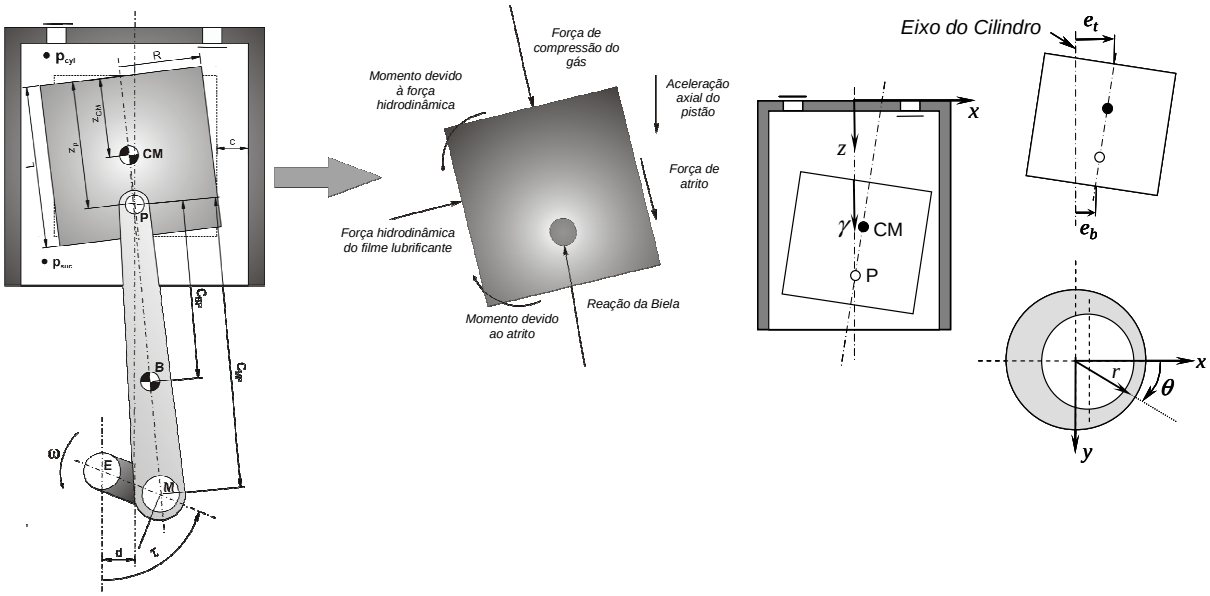

Figura 10. Geometria da folga pistão-cilindro, forças atuantes e sistemas de coordenadas utilizados.

Para a geometria considerada, e considerando que a velocidade axial do pistão V_P é muito maior que as componentes radiais, a equação de Reynolds pode ser simplificada a,

$$\frac{\partial}{\partial\theta}\left(\frac{\overline{\rho}h^3}{12\overline{\mu}R^2}\frac{\partial p}{\partial\theta}\right)+\frac{\partial}{\partial\xi}\left(\frac{\overline{\rho}h^3}{12\overline{\mu}R^2}\frac{\partial p}{\partial\xi}\right)=\frac{V_P}{2R}\frac{\partial(\overline{\rho}h)}{\partial\xi}-\frac{\partial(\overline{\rho}h)}{\partial t} \tag{28}$$

onde as seguintes condições de contorno se aplicam,

$$\begin{aligned}&\xi=0\rightarrow p=p_{cyl}\\&\xi=\frac{R}{L}\rightarrow p=p_{suc}\\&p(\theta=0)=p(\theta=2\pi)\end{aligned} \tag{29}$$

Como nos problemas anteriores, não são necessárias condições intermediárias para cavitação, sendo esta automaticamente determinada pelo desprendimento de gás quando a pressão de saturação é atingida.

Ao determinar o campo de pressões ao longo do filme lubrificante, simultaneamente o balanço de forças e momentos no pistão deve ser satisfeito. As forças principais que atuam no pistão são a força de compressão do gás, o esforço da biela, efeitos de inércia, força de atrito e a força hidrodinâmica devido ao filme lubrificante. As forças de atrito e hidrodinâmica podem também produzir momento com relação ao pino biela-pistão.

Com base no esquema previamente apresentado na figura 10, as seguintes equações podem ser escritas para o pistão,

$$\sum F_x = F_h + F_{rx} = mc\omega^2\left(\ddot{\varepsilon}_t - z_{CM}\frac{\ddot{\varepsilon}_t - \ddot{\varepsilon}_b}{L}\right) \tag{30}$$

$$\sum M_{pin} = M_h + M_f = I_P c\omega^2 \frac{\ddot{\varepsilon}_t - \ddot{\varepsilon}_b}{L} \tag{31}$$

onde *F* e *M* indicam respectivamente forças e momentos.

Para o esforço hidrodinâmico, força e a componente em relação ao pino são necessárias,

$$F_h = -\int_0^L \int_0^{2\pi} p(\theta,\xi) R^2 \cos\theta d\theta d\xi \tag{32}$$

$$M_h = -\int_0^L \int_0^{2\pi} p(\theta,\xi)(z_P - R\xi) R^2 \cos\theta d\theta d\xi \tag{33}$$

E para a força de atrito e o seu momento em relação ao pino, tem-se,

$$F_f = -\int_0^L \int_0^{2\pi} \left(\frac{h}{2R}\frac{\partial p}{\partial \xi} + \mu\frac{V_P}{h}\right) R^2 d\theta d\xi \tag{34}$$

$$M_f = -\int_0^L \int_0^{2\pi} \left(\frac{h}{2R}\frac{\partial p}{\partial \xi} + \mu\frac{V_P}{h}\right) R^3 \cos\theta d\theta d\xi \tag{35}$$

Para a solução das equações (30) e (31), utilizando por exemplo o método de Newton-Raphson, as velocidades do movimento secundário podem ser determinadas. De maneira análoga ao problema do mancal radial, acelerações e posições podem então ser obtidas, tanto para o topo como para a base do pistão, de acordo com as equações (36) e (37),

$$\varepsilon_t^{\tau+\Delta\tau} = \varepsilon_t^{\tau} + \dot{\varepsilon}_t^{\tau+\Delta\tau}\cdot\Delta\tau \text{ e } \varepsilon_b^{\tau+\Delta\tau} = \varepsilon_b^{\tau} + \dot{\varepsilon}_b^{\tau+\Delta\tau}\cdot\Delta\tau \tag{36}$$

onde o tempo é adimensioonalizado para referenciar ao ângulo de manivela τ.

Para as acelerações, tem-se,

$$\ddot{\varepsilon}_t^{\tau+\Delta\tau} = \frac{\dot{\varepsilon}_t^{\tau+\Delta\tau} - \dot{\varepsilon}_t^{\tau}}{\Delta\tau} \text{ e } \ddot{\varepsilon}_b^{\tau+\Delta\tau} = \frac{\dot{\varepsilon}_b^{\tau+\Delta\tau} - \dot{\varepsilon}_b^{\tau}}{\Delta\tau} \tag{37}$$

De posse destes valores, o tempo é avançado em um passo para $\tau+\Delta\tau$ e um processo iterativo é utilizado para obter o correspondente valor das velocidades radiais que satisfaz o balanço de forças.

A metodologia de solução pode ser ilustrada como na figura 11,

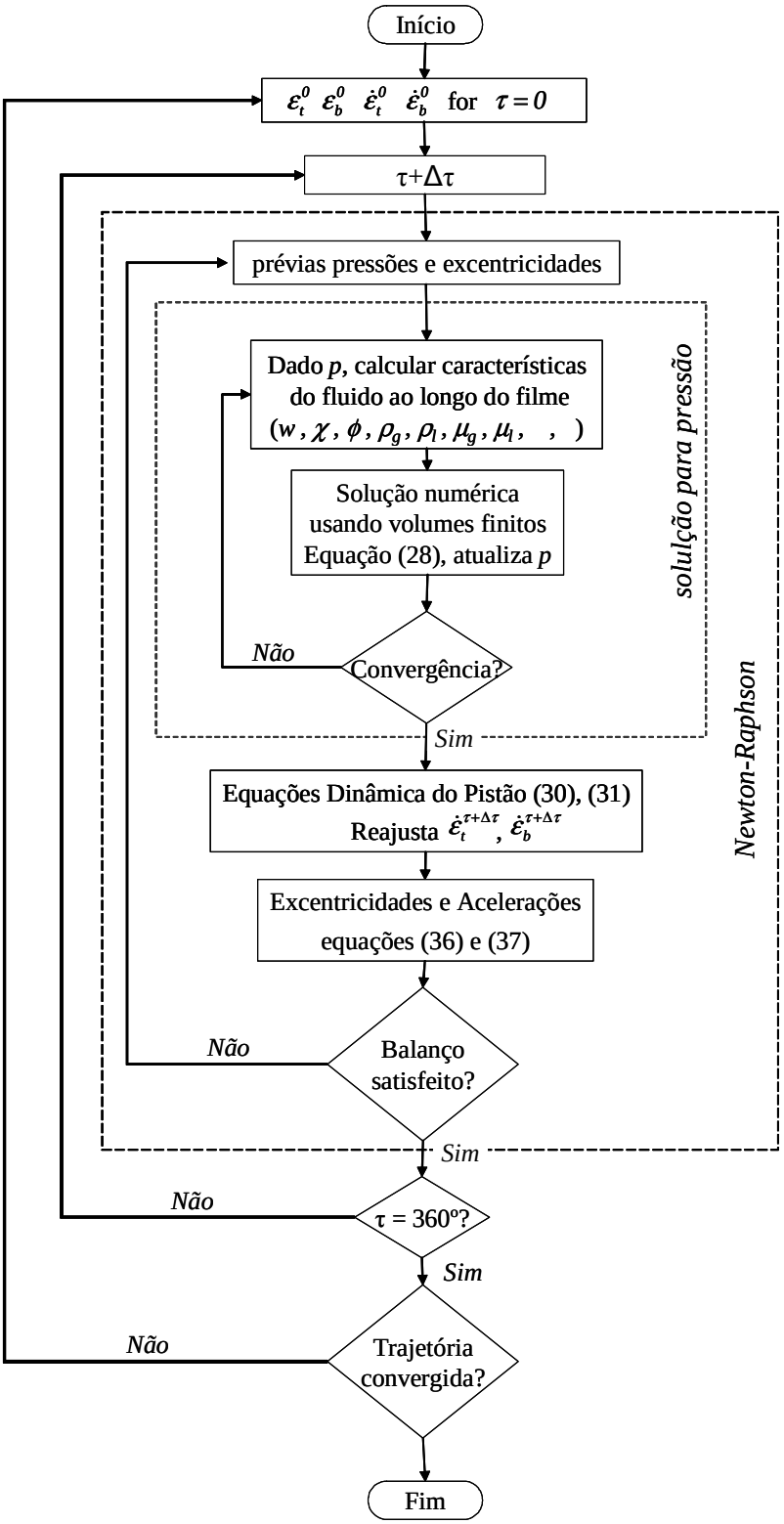

Figura 11. Algoritmo de solução para a dinâmica do pistão utilizando a metodologia proposta.

4. Resultados e Discussão

O modelo bifásico foi aplicado a uma mistura do refrigerante HFC-R134a e óleo poliol-éster ICI EMKARATE RL10H, cujas propriedades foram obtidas pelo fabricante do óleo e ajustadas empiricamente. Adicionalmente, as propriedades gasosas para o R134a foram calculadas utilizando o software REFPROP (McLinden et al., 1998). As correlações adotadas podem ser encontradas em Grando (2004), e maiores detalhes das propriedades são discutidos em Silva (2004).

4.1. **Mancal Radial Parcial Longo** (Grando et al., 2005)

Tendo a mistura definida, valores característicos de geometria e operação foram escolhidos para um mancal radial parcial de 180º, próximas de condições de operação de um compressor de refrigeração, a saber,

$$D=20mm,\ c=20\mu m,\ \omega=60Hz=3600rpm,\ \varepsilon=0.8,\ p_i=p_o=200kPa,\ T=40ºC,\ w_o=w_{sat}=7.13\%$$

Resultados para o campo de pressão são apresentados na figura 12. O resultado do modelo bifásico é comparado com a solução analítica obtida considerando condições de contorno de Reynolds (Pinkus e Sternlicht, 1961), onde a viscosidade é considerada constante e igual àquela na entrada do mancal, tanto para óleo puro como para uma mistura saturada. Devido a maior viscosidade, o mancal lubrificado com óleo puro atinge pressões consideravelmente mais altas, confirmando a redução de capacidade de carga com a dissolução de refrigerante no óleo.

A concordância entre o modelo bifásico e a solução analítica é muito boa quando as mesmas propriedades do fluido à entrada são consideradas. Entretanto, diferenças são observadas ao detalhar a região cavitada, onde pode-se notar para o modelo bifásico que a pressão diminui com o aumento da espessura do filme. Próximo da saída do mancal, a pressão ambiente é comunicada ao fluido por difusão de momento, resultando em recuperação de pressão. É possível verificar que os níveis de pressão na região cavitada são bastante pequenos em comparação à pressão máxima no filme. Assim, neste caso particular, com um mancal fortemente carregado, confirma-se que a condição de contorno de Reynolds provê uma boa aproximação (Dowson e Taylor, 1979). Porém, testes adicionais usando o modelo em condições moderadas de carga (por exemplo, baixas excentricidades e grandes folgas) mostram os resultados tendendo gradualmente da condição de Reynolds para a condição de Sommerfeld (Grando, 2004).

A redução de pressão na região de cavitação é controlada pelo desprendimento de gás da mistura líquida, como ilustrado pela diminuição da massa específica (figura 13a). Na região convergente, apesar do aumento de pressão, esta permanece constante visto que não são observados efeitos de compressibilidade. Na região divergente, a pressão decai até $\theta \approx 200^o$; como a solubilidade diminui com a pressão, desprendimento de gás passa a ocorrer a partir desta posição para que a mistura se mantenha saturada, de modo que a mistura bifásica preenche completamente a folga eixo-mancal. A grande amplitude de variação deve-se à reduzida massa específica do gás, menor que $10 kg/m^3$ nas condições deste estudo, enquanto que a massa específica da mistura líquida é aproximadamente $950 kg/m^3$. Nos últimos 10^o, com a recuperação de pressão, a solubilidade volta a aumentar, mas considerando que gás não é absorvido, a mistura líquida se mantém subsaturada e interagindo com gás livre. Devido aos efeitos de compressibilidade, porém, a densidade aumenta levemente.

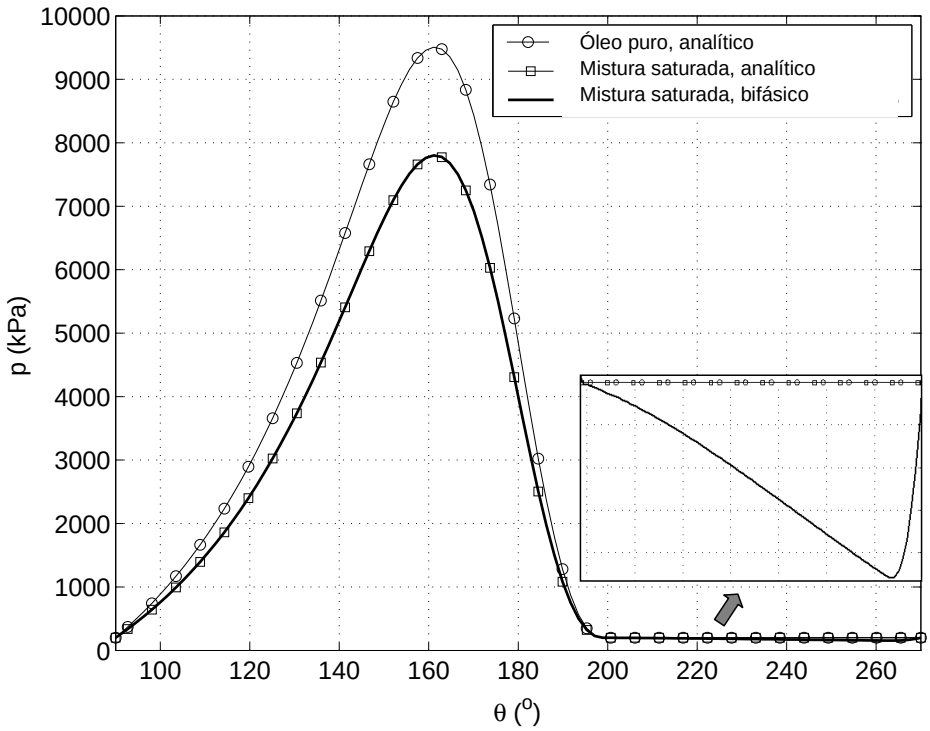

Figura 12. Resultados de pressão para o mancal radial parcial.

Utilizando a equação (4), uma estimativa do título a partir da fração mássica mostra que menos de 2% de gás está presente na saída, indicando que uma quantidade muito pequena de gás é necessária para preencher a folga na região divergente. Contudo, a baixa massa específica desta pequena quantidade de gás desprendido resulta em frações de vazio atingindo valores bastante grandes, acima de 70%.

Apesar da desprezível massa de gás, em fração mássica, as mudanças experimentadas pelo fluido ao longo do escoamento promovem mudanças de viscosidade, como mostra a figura 13b para a viscosidade da mistura líquida e aparente. Para a última, mesmo com a crescente presença de uma fase de baixíssima viscosidade ($\mu_g \approx 12.5 \mu Pa.s$), a viscosidade na verdade aumenta, o que reflete a variação da viscosidade do líquido com a redução na quantidade de refrigerante dissolvido. Entretanto, esta variação não é extremamente significativa ($\approx 3.5\%$), de modo que considerar uma viscosidade constante não seria a priori uma má aproximação para aplicações práticas.

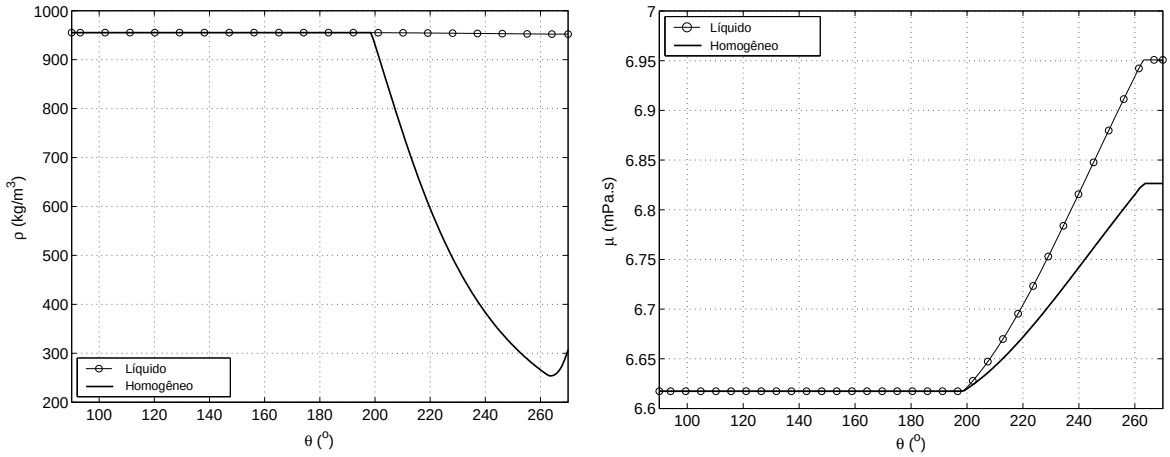

a) Massa específica **b)** Viscosidade

Figura 13. Massa específica e viscosidade ao longo do escoamento no mancal parcial.

Para três diferentes casos estudados, carga suportada e atrito foram calculados e os resultados são apresentados na tabela 1. Para a mistura saturada na entrada, boa concordância entre o modelo bifásico e a solução analítica é confirmada pelos resultados de carga e atrito F_f', calculado desconsiderando a ruptura do filme. Porém, ambas as forças são 22% maiores se óleo puro é considerado como lubrificante. Isto se deve exclusivamente à maior viscosidade do óleo quando comparada à da mistura.

Uma redução de *10%* é observada ao calcular o atrito em caso de ruptura do filme (F_f^*). Em tese, a ruptura do filme deveria ocorrer em óleo puro, onde não há gás disponível para desprendimento. Entretanto, para uma mistura óleo-refrigerante, com o desprendimento de gás em bolhas que permanecem aprisionadas no filme lubrificante (Lacerda et al., 2000), a ruptura não deve ser esperada e F_f' deve ser usada. A equação (11) também é pragmaticamente adotada em situações onde a fronteira de cavitação

não é facilmente identificável, como para um pistão sem anéis. Uma abordagem similar também foi utilizada por Qi et al. (1997) no estudo da lubrificação por óleo com bolhas.

Tabela 1. Resultados para carga suportada e atrito

	Óleo Puro μ_i=8.10mPa.s		*Mistura Saturada* μ_i=6.62mPa.s
	Analítico	*Analítico*	*Bifásico*
W' *(kN/m)*	*76.64*	*62.56*	*62.62*
F_f' *(N/m)*	*155.48*	*126.93*	*127.52*
F_f^* *(N/m)*	*139.63*	*113.99*	-

4.2. **Mancal Radial Pleno Longo** (Grando et al., 2006a)

A metodologia apresentada anteriormente foi utilizada para avaliar a diferença entre a solução clássica com as condições de Reynolds e a abordagem bifásica, tanto considerando equilíbrio como não-equilíbrio termodinâmico para a absorção de gás. Uma primeira simulação considera uma mistura saturada de óleo-refrigerante inicialmente em equilíbrio e sem carga aplicada. Uma carga vertical é então aplicada no centro do eixo do mancal, e os valores de geometria e operação são dados por,

D=20mm, c=20μm, ω=30Hz, W=48kN/m, p_{ref}=200kPa a θ_f=45º, T=40ºC, w_o=w_{sat}=7.13%

A solução numérica do problema foi executada utilizando 100 volumes uniformemente distribuídos, e com um passo de tempo de 1ms. Resultados para a situação convergida de carregamento estático permitem comparar a solução bifásica com o algoritmo de cavitação (Parkins, 1985), que emprega as condições de contorno de Reynolds, onde viscosidade e densidade constantes são assumidas. Os resultados para pressão são apresentados na figura 14.

Como no caso do mancal parcial radial, uma grande similaridade existe entre as pressões calculadas usando o modelo bifásico considerando equilíbrio termodinâmico e aquelas utilizando as condições de contorno de Reynolds, como esperado para cargas moderadas e elevadas. No modelo bifásico, porém, a pressão diminui à medida em que a folga local entre eixo e mancal aumenta, de modo que pressões sub-ambiente existem, embora em magnitudes muito pequenas em comparação com a pressão máxima observada no mancal.

Por outro lado, se a mistura está em condições de não-equilíbrio, com gás presente em toda a extensão do mancal, um menor valor é observado para o máximo da pressão, ao mesmo tempo em que a região de pressão positiva alonga-se em comparação com os resultados obtidos para a solução em condição de equilíbrio e também com o algoritmo de cavitação. Isto indica que o mancal suporta a mesma carga com uma menor excentricidade, assim potencialmente reduzindo a força de atrito.

O comportamento distinto para o perfil de pressão no caso de não-equilíbrio pode ser explicado pelos efeitos de compressibilidade, como pode ser visto na figura 15a para a densidade aparente. Deve ser lembrado que a densidade estimada para a solução clássica utilizando as condições de contorno de Reynolds é definida como $\overline{\rho}_R = \phi_a \cdot \rho_l$.

Assumindo equilíbrio termodinâmico, apenas líquido está presente na região convergente, e quando o escoamento avança na região de cavitação, a densidade reduz continuamente, indicando o efeito da expansão de gás em adição ao desprendimento do líquido. Os resultados para a densidade também permitem estimar a fração volumétrica de gás, alcançando um máximo de 85% próximo dos 360º.

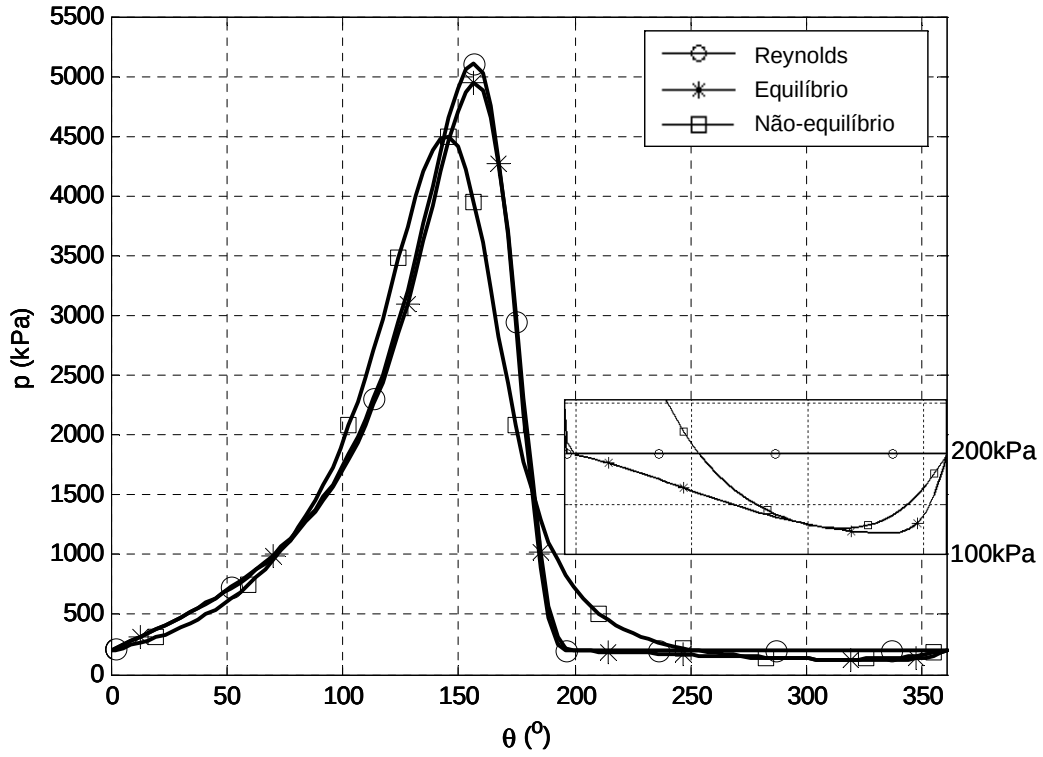

Figura 14. Pressão no mancal radial considerando condições estáticas e diferentes metodologias.

Considerando não-equilíbrio, o gás está presente em todo o mancal, e sua compressibilidade permite ao fluido adaptar-se mais suavemente às mudanças geométricas do mancal, num efeito definido como cunha de massa (Hamrock, 1994), que assiste o efeito de cunha física na geração de pressão. Assim, a menor excentricidade pode ser explicada. Considerando a região cavitada, pela presença de mais gás no início da região divergente, uma menor taxa de variação de densidade é observada, similar àquela da condição de equilíbrio somente em níveis de aeração muito elevados.

O comportamento da viscosidade homogênea absoluta para as diferentes simulações executadas é apresentado na figura 15b. Pode ser notado que, apesar da menor viscosidade do gás, a viscosidade da mistura bifásica na verdade aumenta na medida em que o gás desprende-se do líquido. Contudo, deve-se observar que a variação na viscosidade é pequena comparada àquela da densidade, visto que a última depende na fração de volume ($\phi_{max} \approx 85\%$), enquanto a primeira relaciona-se com a massa de gás ($\chi_{max} \approx 3\%$). No caso de não-equilíbrio, a maior viscosidade aponta para um maior desprendimento de gás. Ainda, o comportamento constante ao longo do mancal indica que o efeito da variação da viscosidade do gás com a pressão pode ser assumida desprezível no tratamento da viscosidade homogênea.

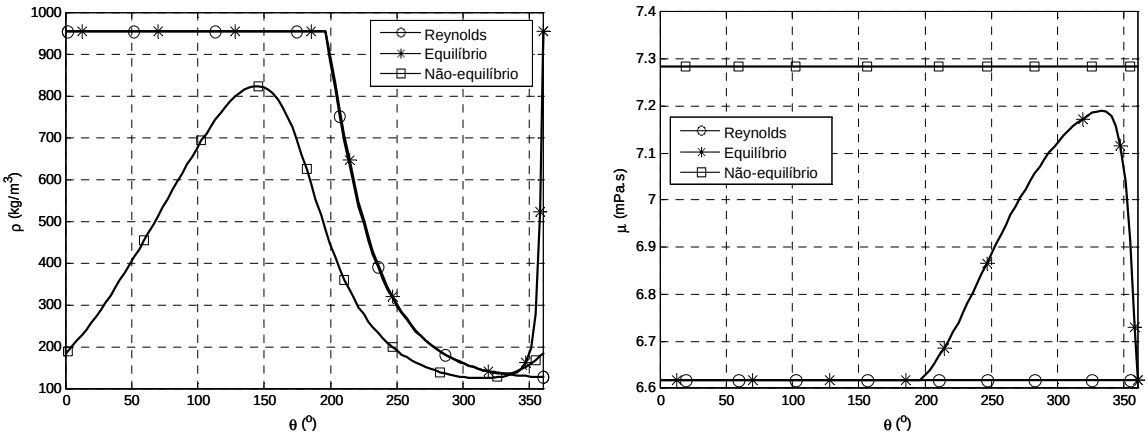

a) Massa Específica **b)** Viscosidade

Figura 15. Propriedades homogêneas ao longo do mancal.

Dadas as variações que as propriedades da mistura pode experiementar, é relevante avaliar como diferentes condições iniciais da mistura afetam o desempenho do mancal radial. Para este fim, uma análise paramétrica é executada considerando diferentes frações mássicas como condição inicial. Este efeito poderia alternativamente ser obtido através de diferentes condições de temperatura e pressão, que por sua vez afetam diretamente a solubilidade.

Avaliando separadamente as condições de equilíbrio e não-equilíbrio, os testes consideram a fração mássica variando entre 0.8 e 1.2 vezes o valor da solubilidade na condição inicial de pressão e temperatura, usando adicionalmente os seguintes dados,

$D=20mm$, $c=20\mu m$, $\omega=60Hz=3600rpm$, $\varepsilon=0.8$, $p_{ref}=200kPa$ *a* $\theta=0^o$, $T=40^oC$, $w_o=w_{sat}=7.13\%$

A influência das propriedades do fluido nas variáveis que caracterizam a operação do mancal é apresentada na figura 16. Para absorção em equilíbrio termodinâmico, figura 16a, pode-se notar para variáveis como a capacidade de carga, força de atrito e pressão máxima variam proporcionalmente à viscosidade. Isso pode parecer inverossímil para misturas acima da saturação w_{sat} – entretanto, nesta condição deve-se lembrar que algum gás está disponível na posição de referência, e é rapidamente absorvido no líquido tão logo a pressão aumenta, reduzindo assim a viscosidade. Por outro lado, variáveis como o coeficiente de atrito e fluxo de massa não dependem da viscosidade e permanecem praticamente constantes, independentemente das condições da mistura. Estes resultados também são esperados para a solução clássica do mancal parcial (Pinkus e Sternlicht, 1961). O ângulo de atuação, porém, varia mais do que o esperado, indicando alguma influência do fluido na região de cavitação, o que não é previsto na solução clássica.

Conclusões similares podem ser obtidas para as simulações considerando a hipótese de não-equilíbrio, como apresentado na figura 16b. Mas as variáveis do mancal são afetadas mais significativamente do que observado no caso de equilíbrio termodinâmico. A máxima pressão e capacidade de carga variam linearmente com a viscosidade da mistura, como esperado. As a força de atrito varia em maior proporção que a viscosidade, o que pode ser relacionado com a maior extensão do perfil de pressão positiva, de modo que a viscosidade influencia o atrito por meio dos escoamentos de Couette e Poiseuille em todo o mancal, diferentemente da condição de equilíbrio que apresenta uma região de pressão constante na região divergente. O coeficiente de atrito reflete o comportamento distinto entre capacidade de carga e atrito, diminuindo na medida em que a fração mássica cresce. O fluxo de massa também reduz com o aumento da fração mássica, o que pode ser explicado pela densidade do fluido – como uma menor massa de gás é desprendida, mais refrigerante dissolve-se no óleo, assim aumentando a viscosidade aparente.

Para a condição de não-equilíbrio, o ângulo de atuação é a variável apresentando a maior alteração com a concentração inicial da mistura. A grande variação no ângulo de atuação é um dos fatores que devem ser investigados para o entendimento da instabilidade numérica observada durante as simulações em condições de não-equilíbrio.

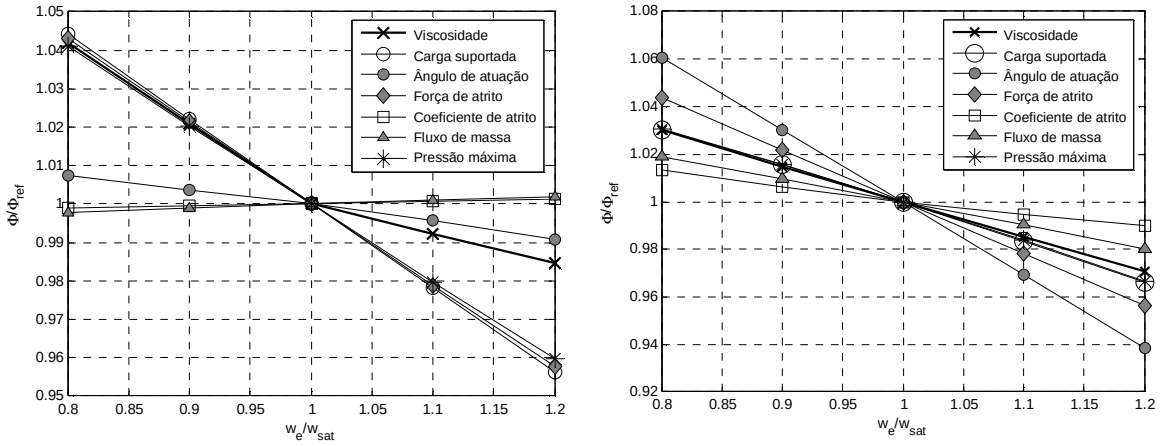

a) Equilíbrio termodinâmico
(μ_{sat}=6.62mPa.s, W_{sat}=95kN/m, $F_{f,sat}$=183N/m, ψ_{sat}=42º, f_{sat}=0.0019, $q_{\theta,sat}$=89g/(s.m), $p_{max,sat}$=9.64MPa)

b) Não-equilíbrio
(μ_{sat}=7.00mPa.s, W_{sat}=111kN/m, $F_{f,sat}$=183N/m, ψ_{sat}=31º, f_{sat}=0.0017, $q_{\theta,sat}$=80g/(s.m), $p_{max,sat}$=10.80MPa)

Figura 16. Variação das variáveis de operação do mancal em relação a fração mássica da mistura.

Como os resultados anteriores indicam, uma significativa diferença existe entre as hipóteses de equilíbrio e não-equilíbrio, sendo necessária uma análise mais profunda para determinar a exata taxa de absorção e conseqüentemente prever de maneira mais precisa o real comportamento do mancal. Embora os resultados para a condição de equilíbrio apresentam boa concordância com a solução clássica, que utiliza as condições de contorno de Reynolds, o tempo requerido para a absorção deve ser investigado. Por exemplo, considerando o caso apresentado na figura 14, a reabsorção ocorre nos últimos 25º do mancal, correspondendo a um tempo de escoamento de 2ms, o que aparenta não ser realístico dado o esforço normalmente requerido para dissolver o refrigerante no óleo (Lacerda, 2000).

4.3. **Folga Pistão-Cilndro: A Dinâmica do Pistão** (Grando et al., 2006b)

A metodologia proposta foi utilizada para simular a dinâmica de um sistema pistão-cilindro pré-definido. Adicionalmente, a pressão no cilindro como função do ângulo de manivela é dada. Por simplicidade, o fluido é assumido em temperatura constante. Os dados do compressor necessários para a simulação são apresentados na tabela 2, bem como os parâmetros definidos para a simulação numérica.

Em referência a equação (3), duas condições diferentes de absorção foram testadas: a primeira simulando uma condição de baixa absorção ($\kappa \cdot \Delta t = 0.05$), enquanto que a segunda ($\kappa \cdot \Delta t = 0.50$) indica fácil dissolução do refrigerante no óleo mesmo em transientes rápidos. Esta última condição apresenta uma dissolução de refrigerante duas vezes superior à

primeira condição, o que indica que uma menor viscosidade da mistura lubrificante serão observadas, bem como um maior potencial de desprendimento de gás em gradientes de pressão negativas, o que se relaciona à maior pressão de saturação. Entretanto, para menores coeficientes de absorção de refrigerante, a dissolução ocorre por um maior intervalo de tempo.

Tabela 2. Geometria e dados numéricos utilizados nas simulações da folga pistão-cilindro.

	Parâmetro	Valor
Geometria	$R\ (mm)$	10.5
	$L\ (mm)$	21.0
	$c\ (\mu m)$	5.0
	$z_P\ (mm)$	12.08
	$z_{CM}\ (mm)$	9.53
	$C_{BP}\ (mm)$	25.54
	$C_{MP}\ (mm)$	36.47
	$d\ (mm)$	2.0
	$\omega\ (rad/s)$	370
	$m\ (g)$	34.6
	$m_b\ (g)$	24.2
	$I_P\ (kg{\cdot}m^2)$	$0.287{\cdot}10^{-5}$
	$p_{suc}\ (kPa)$	238.50
	$T\ (^oC)$	60
Numéricos	*Malha* (θ, ξ)	18x30
	$\Delta\tau\ (^o)$	5
	Tolerância (p)	$1{\cdot}10^{-6}$
	Tolerância (ε_i)	$1{\cdot}10^{-4}$

Os resultados para o modelo bifásico são comparados com aqueles obtidos por metodologias usuais, para um fluido monofásico, tanto óleo puro como uma mistura óleo-refrigerante. Três diferentes critérios de cavitação foram utilizados, identificados por NCav (não-cavitação), Cav (variação linear da pressão de cavitação) e Cav_{min} (mínimo entre a pressão no topo ou base do pistão).

A figura 17 apresenta a excentricidade para o topo e base do pistão como uma função do ângulo de cavitação. As diferenças observadas se devem exclusivamente à viscosidade do lubrificante, ou seja, *Oil NCav v OR NCav* e equivalentes, mostraram não ser de significância.

Porém, o critério de cavitação adotado mostra ser determinante para descrever a trajetória. Maiores excentricidades são observadas quando a cavitação não é considerada, enquanto que o topo do pistão move-se mais próximo do eixo do cilindro quando um critério de cavitação é adotado. Os resultados para o modelo bifásico são similares aqueles desprezando a cavitação. Um aumento na excentricidade de topo é observado para a mistura absorvendo uma menor quantidade de refrigerante (OR $2p_{05}$). Também é notória a maior amplitude do movimento para os resultados onde critérios de cavitação são adotados, indicando esforços adicionais do pistão para o balanço de forças ao longo do ciclo. Em adição à condição mais inclinada com que o pistão se move, um efeito de cunha hidrodinâmica é esperado para satisfazer o balanço de forças. Por outro lado, o modelo bifásico prevê um movimento mais estável, o que também é observado para a solução onde a cavitação é desconsiderada.

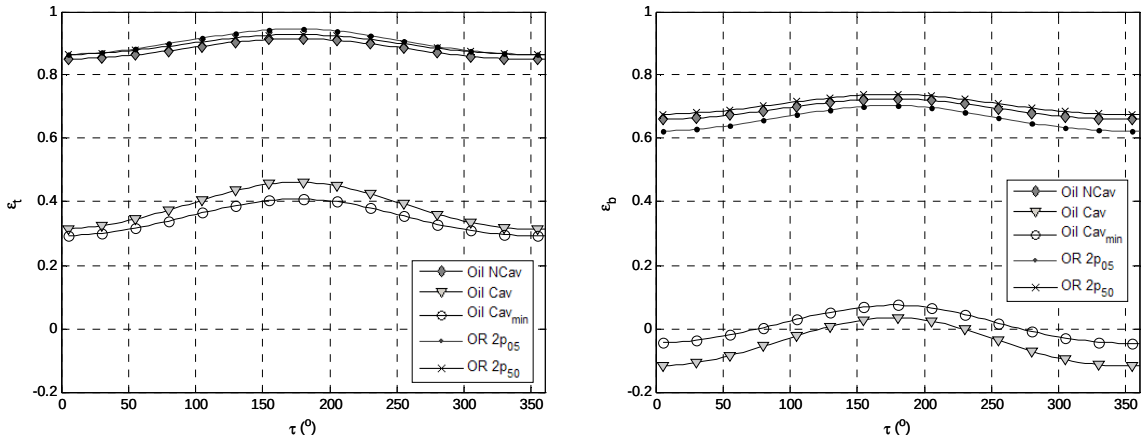

a) Topo do pistão **b)** Base do pistão

Figura 17. Excentricidade para o pistão como função do ângulo de manivela

Uma explicação detalhada do comportamento do pistão requer uma análise dos perfis de pressão ao longo do movimento. Maiores detalhes podem ser obtidos em Grando et al. (2006b).

Como um importante parâmetro para o projeto do pistão, o consumo de energia também foi determinado. Após calcular a força de atrito usando a equação (34), as perdas devido ao atrito viscoso podem ser calculadas por,

$$Pot = F_f \cdot V_P \tag{38}$$

Os valores são apresentados na figura 18 onde também pode ser observado que menores valores são obtidos quando a cavitação é artificialmente considerada, visto que os pontos na região de cavitação são removidos do cálculo (taxa de deformação desprezível).

Aqui, a viscosidade apresenta grande importância e quando a mistura óleo-refrigerante é considerada como lubrificante, menores valores de potência consumida são obtidos. Os resultados para o modelo bifásico estão mais próximos daqueles para óleo-refrigerante desconsiderando a cavitação, embora marginalmente maiores. Uma das razões para tanto é que, quando gás desprende-se do lubrificante, a viscosidade aparente aumenta como resultado da menor fração de refrigerante na mistura lubrificante, apesar da presença da fase gasosa de baixa viscosidade. Mínimas diferenças ocorrem para as diferentes condições de mistura, com maior atrito para a mistura com mais refrigerante dissolvido.

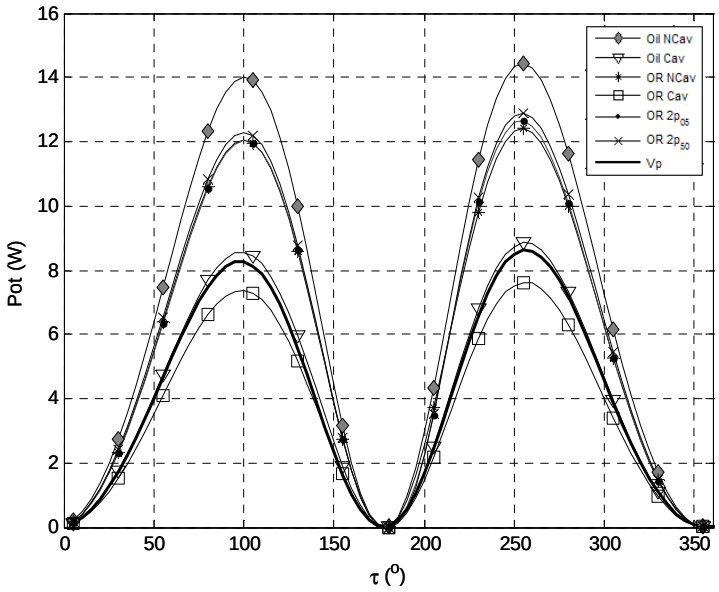

Figura 18. Potência consumida por atrito viscoso como função do ângulo de manivela.

Finalmente, o vazamento de óleo pode ser estimado a partir do campo de pressão determinado. Na base do pistão, a vazão é dada por,

$$q_{bottom} = \int_0^{2\pi} \left(-\frac{h^3}{12\bar{\mu}R}\frac{\partial p}{\partial \xi} + V_P \frac{h}{2} \right)\Bigg|_{z=L} Rd\theta \tag{39}$$

A figura 19 apresenta os resultados para a vazão volumétrica. O principal efeito é o do movimento axial do pistão (*qVp*), com mínimas diferenças entre os distintos casos, o que indica que a capacidade de vedação é promovida pela pequena folga. Esse valor é significativo para quaisquer das simulações monofásicas, mas uma oportunidade para estimar o vazamento de refrigerante como gás pode ser realizado utilizando o modelo bifásico, avaliando tal vazamento com a equação (5) com a fração de vazio do lubrificante líquido-gás abandonando a saia do pistão. O escoamento de refrigerante inicia pouco antes de 180º,

quando o pistão muda de direção, e a presença de gás naturalmente aumenta a vazão volumétrica. Ajustes adicionais são necessários visto que o escoamento devido ao gradiente de pressão é em tese importante nesta região. Entretanto, pode-se notar que o máximo vazamento ocorre nas menores velocidades do pistão, onde não se impõe resistência contra o gradiente de pressão e a mistura apresenta uma elevada fração mássica. Deste instante em diante, o vazamento de gás gradualmente se reduz à medida em que as pressões no cilindro começam a diminuir, reduzindo a quantidade de refrigerante dissolvido. Surpreendentemente, a mistura com a menor fração mássica apresenta um maior vazamento que aquela capaz de absorver mais refrigerante, como pode ser visto no detalhe da figura 19. Enquanto que a mistura com maior coeficiente de absorção apresenta refrigerante em excesso dissolvido, desde o início, ocorre desprendimento na câmara tão logo a pressão no cilindro diminui. Por outro lado, a mistura com menor coeficiente de absorção pode ainda dissolver refrigerante; mesmo com a pressão diminuindo, os níveis ainda são razoavelmente elevados e o refrigerante permanece dissolvendo no óleo, sendo então carregado da câmara ao longo da folga e liberado na saia do pistão. Deve-se ressaltar que neste modelo preliminar os resultados visam comprovar a capacidade preditiva do modelo, embora significativos desenvolvimentos ainda sejam necessários para a precisa determinação da condição de mistura óleo-refrigerante dentro do cilindro, assim também melhorando o entendimento do desprendimento de refrigerante ao longo do estágio de sucção.

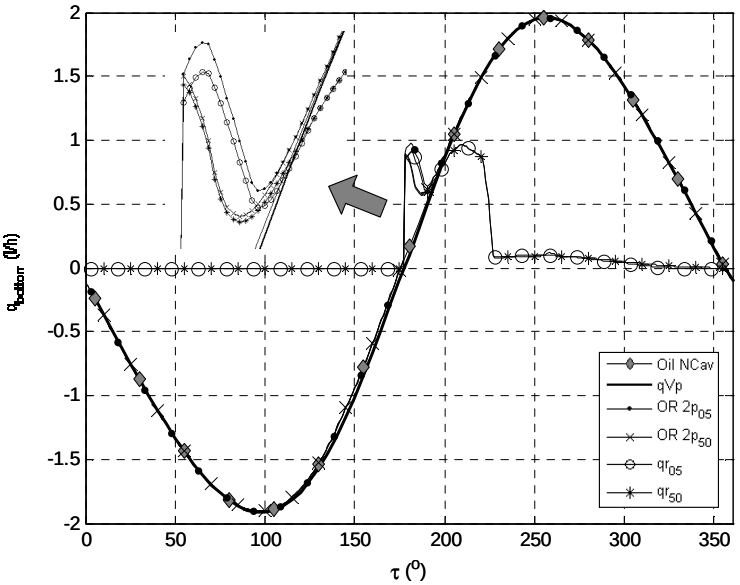

Figura 19. Vazão volumétrica e a participação do gás refrigerante para cada caso bifásico.

5. Conclusões

Um modelo de lubrificação bifásica considerando a interação entre óleo e refrigerante durante a operação do compressor foi proposta. O modelo sugere uma alternativa para a modelação numérica da lubrificação hidrodinâmica, onde ao invés do uso de condições de contorno intermediárias, a cavitação é considerada a partir das propriedades do lubrificante, analizadas para o caso particular de uma mistura óleo e refrigerante; neste caso, a cavitação é definida pelo desprendimento de refrigerante da mistura líquida em condições de saturação. O efeito da dissolução de refrigerante no desempenho de mancais radiais e pistões foi avaliado, comparando os resultados àqueles de metodologias clássicas disponíveis na literatura. Um mancal radial parcial foi escolhido para os testes iniciais devido a sua geometria simplificada e pelas condições bem definidas de pressão na entrada e saída do escoamento, enquanto que um mancal radial pleno foi considerado na seqüência para iniciar o estudo de problemas transientes. Muitos destes desenvolvimentos foram então aplicados ao problema objetivo deste trabalho, a lubrificação da folga radial pistão-cilindro.

O modelo bifásico pode prever automaticamente a região de cavitação, enquanto que não se observam mudanças de comportamento na região de pressão positiva caso líquido seja a única fase presente. Neste caso, a posição da cavitação e a fração de vazio resultantes são similares aquelas obtidas na solução clássica e estão fortemente relacionadas aos fatores geométricos. Entretanto, pressões sub-atmosféricas são observadas na região cavitada. O nível destas pressões se relaciona com a densidade do gás desprendido. Uma região de recuperação de pressão próximo ao fim da região divergente também é identificada, e pode ser relacionada com a difusão da quantidade de movimento.

As principais conclusões podem ser listadas como segue,

- Comparando os resultados para uma mistura óleo-refrigerante com aqueles para óleo puro, uma significativa redução na capacidade de carga é observada com a mistura, resultante da redução de viscosidade observada com a dissolução de refrigerante;
- Uma análise paramétrica mosta que a viscosidade é a propriedade mais importante da mistura na região não cavitada. Como a mistura apresenta maiores viscosidades em menor pressão, temperatura e fração mássica, nestas condições maiores pressões serão observadas no mancal. Adicionalmente, a redução da folga e o aumento na velocidade ou excentricidade também geram maiores pressões. Na região de cavitação, a excentricidade é o único fator geométrico a influenciar o comportamento, como também previsto na teoria de lubrificação clássica;

- Em condições de não-equilíbrio termodinâmico, o comportamento do mancal é significativamente alterado. Gás está presente em todo o mancal e sua compressibilidade melhora a capacidade de acomodar mudanças geométricas. Conseqüentemente, o perfil de pressão se espalha por uma região mais longa do mancal e uma carga específica pode ser suportada com menores excentricidades, quando comparado com as condições de equilíbrio, o que potencialmente pode reduzir o atrito. Com os níveis de aeração observados nas simulações, adotar uma condição de gradiente nulo de pressão próximo à região divergente pode levar a resultados consideravelmente imprecisos;
- Os resultados para o pistão apresentam uma tendência diferente aos dos mancais; considerando soluções prévias utilizando óleo puro com propriedades constantes, pequenas diferenças são observadas em relação às condições de não-cavitação, e não foi observada concordância com as soluções utilizando critérios de cavitação, o que seria esperado para mancais apenas em condições de carga bastante leves. Isto reforça a controvérsia com relação às condições de contorno de cavitação, visto que considerável diferença é observada. Portanto, as condições de cavitação para o pistão necessitam de revisão;
- Considerando a potência consumida por atrito pelo pistão, os resultados apresentados pelos modelos monofásico e bifásicos são bastante semelhantes. Utilizando critérios de cavitação, valores muito menores são previstos;
- A influência do coeficiente de absorção no comportamento da mistura não provou muito significativa, embora um maior vazamento de gás foi previsto para menores taxas de absorção. Entretanto, são necessários mais precisos estudos para o entendimento do comportamento transiente da mistura, e cruciais para seu futuro aperfeiçoamento. Simultaneamente, trabalhos futuros também devem considerar uma melhor estimativa para o escoamento de óleo próximo ao ponto morto superior do ciclo, potencialmente a região onde a maior parte do vazamento de refrigerante ocorre;

Devido à diferença de comportameto obtida com as diferentes situações termodinâmicas consideradas, futuras investigações devem focar na determinação da taxa real de absorção, permitindo assim prever com maior precisão o comportamento de mancais e pistões, entre outros componentes mecânicos lubrificados em condições similares. Neste caso, um modelo de absorção de refrigerante pelo óleo é necessário, particularmente para transientes rápidos, o que ainda não foi estabelecido. Ainda, o desenvolvimento futuro do

modelo deve considerar sua aplicação a geometrias cada vez mais realísticas, tanto do mancal como do pistão; aumentando o entendimento do modelo ante estas condições permitirá proporcionar informações de como otimizar o projeto dos mesmos, definindo mais precisamente as áreas de aplicação desta ferramenta.

Referências Bibliográficas

Como previamente indicado, este documento toma por referência a tese, de mesmo autor e mesmo conteúdo, submetida à Universidade de Leeds para grau equivalente ao que é submetido à Universidade Federal de Santa Catarina por este documento.

GRANDO F.P. **Two-Phase Lubrication Model for Refrigeration Reciprocating Compressors**. Tese de Doutorado, Universidade de Leeds, Leeds, 2007. 247p.

Referências Adicionais,

CAMERON, A. **The principles of lubrication.** London: Longmans, 1966.

CAREY V.P. **Liquid-vapor phase-change phenomena**. New York: Hemisphere, 1992.

CHOI, S., KIM, K.W. **Analysis of bubbly lubrication in journal bearings.** JSME International Journal, Series C, Vol.45, No.3, p.802-808, 2002.

DOWSON, D., NEVILLE, A. **Bio-tribology and the operating environment**. Synopses of the 32nd Leeds-Lyon Symposium on Tribology, 6-9 September, Villeurbanne, France, 2005.

DOWSON D., TAYLOR C.M. **Cavitation in bearings**. Annual Review of Fluid Mechanics, Vol.11, p.35-66, 1979.

GRANDO F.P. **A two-phase flow approach to cavitation modelling in partial journal bearings. Case study: The oil and refrigerant mixture**. Technical report, University of Leeds, 2004. 160p.

GRANDO F.P., PRIEST M., PRATA A.T. **Lubrication in refrigeration systems: Performance of journal bearings lubricated with oil and refrigerant mixtures**. Life Cycle Tribology, Proc. 31st Leeds-Lyon Symposium on Tribology, Leeds 2004, Tribology and Interface Engineering Series, Elsevier, Amsterdam, p.481-491, 2005.

GRANDO F.P., PRIEST M., PRATA A.T. **A two-phase flow approach to cavitation modelling in journal bearings.** Tribology Letters, Vol.21, No.3, p.233-244, 2006a.

GRANDO F.P., PRIEST M., PRATA A.T. **Lubrication in refrigeration systems: A numerical model for piston dynamics considering oil-refrigerant interaction.** Proc. IMechE, Journal of Engineering Tribology, Vol.220, No.3, p.245-258, 2006b.

HAMROCK, B.J. **Fundamentals of fluid film lubrication.** New York: McGraw-Hill, 1994. 690p.

LACERDA, V.T. **Caracterização Experimental do Escoamento Bifásico de uma Mistura Óleo e Refrigerante em Dutos de Pequeno Diâmetro.** Dissertação de Mestrado, Departamento de Engenharia Mecânica, Universidade Federal de Santa Catarina, Florianópolis, 2000. 165p.

LACERDA V.T., PRATA A.T., FAGOTTI F. **Experimental characterisation of oil-refrigerant two-phase flow**. Proceedings of the ASME – Advanced Energy Systems Division, Vol.40, p.101-109, 2000.

MCLINDEN M.O., KLEIN S.A., LEMMON E.W., PESKIN A.W. **REFPROP: Thermodynamic and transport properties of refrigerants and refrigerant mixtures**, version 6.0. Washington(DC): NIST, 1998.

PARKINS, D.W. **Conference report: Cavitation in fluid films: 17 October 1984, Cranfield Institute of Technology, UK.** Tribology International, Vol.18, No.1, p.50-51, 1985.

PATANKAR S.V. **Numerical heat transfer and fluid flow**. New York: McGraw-Hill, 1980.

PINKUS O., STERNLICHT B. **Theory of hydrodynamic lubrication**. New York: McGraw-Hill, 1961.

POSSAMAI F.C., TODESCAT M.L. **A review of compressors energy performance**. Proceedings of the 17th International Compressor Engineering Conference at Purdue, Purdue, USA, Paper C046, 2004.

QI A., YINSHENG Z., YONGXIN Q. **Study on the viscosity properties of bubbly oil and the static characteristics of journal bearing lubricated with bubbly oil**. Wear, Vol.213, p.159-164, 1997.

ROACHE, P.J. **Fundamentals of Computational Fluid Dynamics.** Albuquerque: Hermosa, 1998. 648p.

SILVA A. **Cinética e Dinâmica da Absorção de Gás pelo Óleo Lubrificante.** Tese de Doutorado, Universidade Federal de Santa Catarina, Florianópolis, Brasil, 2004.

ANEXO

Two-Phase Lubrication Model for Refrigeration Reciprocating Compressors

Fernando Paulo Grando

Two-Phase Lubrication Model for Refrigeration Reciprocating Compressors

Fernando Paulo Grando

Submitted in accordance with the requirements for the degree of Doctor of Philosophy

The University of Leeds
School of Mechanical Engineering
Federal University of Santa Catarina
Mechanical Engineering Postgraduate Programme

September, 2007

ACKNOWLEDGEMENTS

I would like to express my extreme gratitude to Professor Martin Priest, for his invaluable support, advice and encouragement and patience throughout this study. It has been an honour to spend this time is Leeds under his outstanding supervision.

I would like to thank Professor Alvaro Toubes Prata, for giving me the opportunity undertake this research from Leeds and his continued support throughout this period. His contributions exceed the dimensions of this academic work.

My gratitude to the Programme Alβan, the European Union Programme of High Level Scholarships for Latin America, sponsors of this work under identification number E03D22219BR.

Assistance from the Brazilian Compressor Company EMBRACO SA is duly acknowledged.

I would also like to thank Professor R.C. Coy for his expert opinions on the experimental and predicted results throughout the project, in addition to his extreme enthusiasm.

I would like to express my gratitude to Mrs. Jackie Findlay, who, under such special circumstances, helped me to appropriately register as a student in Leeds.

Throughout this study colleagues of the School made the work extremely enjoyable, particularly Oliver Smith, Rob Hewson, Bertam Mallia and Dinan Wang, and also Dr. David Barrell for his always enjoyable company. My colleagues from Brazil are also surely missed.

Finally I wish to thank my wife, for her support and help throughout my life and in particular in the final stages of this work. Also my parents, for their care, that distance does not make barrier. Finally, my uncle, “Tio Henrique”, for all the support that he gave me during our period at University – without your help this would not come true.

ABSTRACT

The study of fluid film lubrication in mechanical components is fundamental to the analysis of their dynamic behaviour as well as determining friction losses between moving parts. In several cases, gases present in the system can interact with the oil changing lubrication characteristics – by their dissolution and release from the oil, forming bubbles or even producing foam. Additionally, in low pressure regions the lubricant loses the capacity to flow as a continuous film, and cavitation occurs.

Generally cavitation is treated in numerical models via boundary conditions for the pressure equation, which is then used to solve the problem only in the full film region instead of the whole solution domain. Several criteria are available, and the results are often sensitive to the chosen conditions.

The present work proposes the study of cavitation considering the changes suffered by the lubricant as it flows through the lubricated component, considering the release of gas from the liquid and the existence of a two-phase flow. The numerical model treats the liquid-gas mixture as a homogeneous fluid, whose properties are calculated as weighted averages of the properties from the constituent phases. The model then solves the lubrication equation numerically using the finite volume methodology, considering variable fluid properties and without using any intermediate boundary conditions. The lubricant is considered a mixture of oil and refrigerant, widely studied due to its importance in lubrication and heat transfer problems in refrigeration systems.

To advance in the understanding of the two-phase flow model, it was initially applied to simplified geometries, such as that of a partial journal bearing, and gradually the geometrical assumptions were relaxed, applying the model to a full journal bearing, where a discussion against experimental results was possible. Finally, the problem of the reciprocating motion of the piston in a refrigeration compressor was considered.

From the results, it is shown that the model can automatically predict three regions for the lubricated component, the positive pressure region, cavitation and pressure recovery. When the model is compared to solutions considering Reynolds boundary conditions, good agreement is observed for moderate and heavy loads. Studying the main operational parameters and the mixture behaviour, the discussion focuses on the fluid properties, which affect particularly density and as a result the cavitation region – or even the full bearing if bubbles are considered in all the bearing extent. Finally, in the light of the two-phase solution for piston lubrication, existing cavitation criteria for the problem seem inappropriate.

CONTENTS

LIST OF TABLES

LIST OF FIGURES

LIST OF SYMBOLS

Symbol	Description	SI Units
A_*	Coefficients of the algebraic equations in the finite volume methodology	-
A	Cross-section area	$[m^2]$
A_g	Cross-section area filled with gas	$[m^2]$
c	Radial clearance of the bearing	$[m]$
C_{BP}	Distance between connecting rod centre of mass and the piston gudgeon pin	$[m]$
C_{MB}	Connecting rod length	$[m]$
D	Shaft diameter	$[m]$
d	Offset between crankshaft centre and cylinder axis	$[m]$
e	Eccentricity	$[m]$
f	Friction coefficient, equation (4.25)	[*dimensionless*]
F_f	Viscous friction force	$[N]$
F_g	Force due to compression of gas	$[N]$
F_h	Hydrodynamic force	$[N]$
F_r	Connecting rod reaction force	$[N]$
h	Lubricant film thickness	$[m]$
H	Dimensionless film thickness, divided by radial clearance	[*dimensionless*]
I_P	Moment of inertia of piston about the gudgeon pin	$[N.m^2]$
L	Bearing width	$[m]$
m	Mass	$[kg]$
m_b	Connecting rod mass	$[kg]$
M	Moment	$[N.m]$

n_θ	Number of elements in direction θ (x) to the finite volume methodology	-
p	Pressure	[Pa]
p_e	Entrance pressure	[Pa]
p_o	Pressure at the outlet of the bearing, back pressure	[Pa]
p^*	Dimensionless pressure, equation (4.23)	[*dimensionless*]
Pot	Power consumption due to viscous friction	[W]
q_θ	Mass flow rate per unit length	[$kg/(s.m)$]
r	Radial coordinate of the polar system	[m]
R	Shaft (journal) radius	[m]
S	Source term in finite volume methodology	-
t	Time	[s]
T	Temperature	[^oC]
T_f	Friction torque for journal bearings	[$N.m$]
u	Velocity component in direction x (θ)	[m/s]
u_a	Journal velocity component in direction x (θ)	[m/s]
u_b	Bearing velocity component in direction x (θ)	[m/s]
u_{mean}	Mean velocity in a cross-section	[m/s]
U	Shaft tangential velocity ($2\pi\omega R$)	[m/s]
$\forall_g$	Volume of gas in a cross-section area	[m^3]
$\forall_{tot}$	Total volume in a cross-section area	[m^3]
$\breve{w}$	Velocity component in direction z	[m/s]
$\breve{w}_a$	Shaft velocity component in direction z	[m/s]
$\breve{w}_b$	Bearing velocity component in direction z	[m/s]
w_r	Refrigerant mass fraction in the oil/refrigerant mixture	[kg_{ref}/kg_{mixt}]
w_e	Refrigerant mass fraction at flow entrance	[kg_{ref}/kg_{mixt}]
w_{sat}	Refrigerant solubility (saturation mass fraction) in the oil	[kg_{ref}/kg_{mixt}]

W	Hydrodynamic force, applied load or load carrying capacity	[N]
W_1	Hydrodynamic force, component in the line of centres direction	[N]
W_2	Hydrodynamic force, component perpendicular to W_1	[N]
x	Coordinate of the cartesian system	[m]
y	Coordinate of the cartesian system	[m]
z	Coordinate of the cartesian system	[m]

Greek Symbols

α	Cavitation angle	[^{o},rad]
β	Cavitation angle, Sommerfeld variable	[^{o},rad]
β_p	Under-relaxation for pressure	-
β_ρ	Under-relaxation for density	-
γ	Sommerfeld variable, equation (5.3)	[^{o},rad]
$\delta\theta_w$, $\delta\theta_e$	Distance between neighbour nodal point in direction θ	[^{o},rad]
Δ	Sommerfeld number, equation (4.24)	[*dimensionless*]
$\Delta\theta$	Dimension of the control volume in direction θ	[^{o},rad]
$\Delta\theta_{pjb}$	Length of the partial journal bearing	[^{o},rad]
ε	Dimensionless eccentricity ratio, or simply eccentricity	[*dimensionless*]
θ	Angular coordinate in the polar system	[^{o},rad]
θ_0	Initial angle of the partial journal bearing (entrance)	[^{o},rad]
θ_f	Final angle of the partial journal bearing (exit)	[^{o},rad]
λ	Dimensionless density used in Elrod's algorithm, equation (2.12)	[*dimensionless*]
μ	Dynamic viscosity	[$N.s/m^2$]
$\overline{\mu}$	Apparent dynamic viscosity of the homogeneous fluid	[$N.s/m^2$]
μ^*	Dimensionless viscosity, relative to the entrance viscosity	[*dimensionless*]

ρ	Density	[kg / m^3]
$\bar{\rho}$	Apparent density of the homogeneous fluid	[kg / m^3]
ρ^*	Dimensionless density, relative to the entrance density	[*dimensionless*]
σ	Surface tension	[*N/m*]
$\tau_{r\theta}$	Shear stress	[N/m^2]
υ	Specific volume	[m^3 / kg]
ϕ	Void fraction, equation (3.4)	[*dimensionless*]
χ	Quality, equation (3.3)	[kg_{gas}/kg_{tot}]
ψ	Attitude angle	[^{o} ,*rad*]
ω	Angular velocity	[*rad/s*]

Subscripts

cav	Cavitation position
CM	Centre of mass
e	Flow entrance, inlet position
f	Friction
g	Gaseous phase
h	Hydrodynamic
l	Liquid phase
o	Oil
P	Position of the piston gudgeon pin
r	Refrigerant
lr	Liquid refrigerant

Superscripts

k	Current iteration
k – 1	Previous iteration

Chapter 1

INTRODUCTION

1.1 OVERVIEW

The interaction of gas dissolved in a liquid phase can pose a difficult challenge for the design and operation of mechanical systems. Not uncommonly there is a dearth of knowledge on what affects such interaction and its consequences, which in turn brings uncertainties and even unpredictability to the design and life management of the components. One area of great importance in this context is tribology, and in particular the occurrence of cavitation during hydrodynamic lubrication.

Cavitation is conventionally defined in lubrication as the loss of continuity in a thin liquid film separating two surfaces in relative motion. This loss of continuity can either occur due to the presence of gas or vapour, and this phenomenon influences significantly the behaviour of lubricated mechanical components in aspects such as the load carrying capacity, friction and stability. Cavitation has been studied for more than a century, but it still remains as a concern in the design of mechanical components.

Gaseous cavitation is the most common case. It is usually observed in divergent geometries, and it happens due to one or more of the following factors: *release of gas dissolved in the oil*, as oils can contain considerable quantities of dissolved gas; *expansion of gas bubbles* that have been carried by the oil when flowing through other components, such as pumps; and *ventilation* (entrainment) of gas from the neighbourhood. The occurrence of these effects avoids the lubricant film reaching very low pressures, remaining close to atmospheric levels. Ventilation is not observed in sealed bearings, and the population of bubbles being carried from other sources can be sometimes avoided using mechanical separation. However, the dissolution of air in oils is practically unavoidable.

Different patterns of cavitation are observed for different geometries and different operation conditions. This results in a variety of criteria to physically explain

the occurrence of cavitation, such as film rupture, flow separation and others (Dowson and Taylor, 1979). However, these different criteria are usually dealt in the same way in numerical models: cavitation is set as a boundary condition in an intermediate position of the solution domain, and the governing equation is then solved only for the full-film region (before cavitation takes place). Several approaches are also available and very often they are very efficient. Nevertheless, results are very sensitive to the criterion adopted (Priest et al., 2000), which can lead to considerably different results.

As a result of the sensitivity to the different criteria, defining the correct criterion is essential in cavitation analysis. However, it is not always easy to identify the conditions in which cavitation is observed. Squeeze film dampers and dynamically loaded journals bearings are common examples where this occurs (Feng and Hahn, 1986).

Another example of the difficulty to define the cavitation condition is the ringless piston, commonly used in hermetic refrigeration compressors and shown in figure 1.1. The lubricant film separating piston and cylinder is communicated to the ambient pressure at the bottom of the piston, but a different pressure is observed at the top of the piston, in the compression chamber. In this case, it is highly unlikely to have a single cavitation pressure, and conditions for the intermediate positions can be even more difficult to ascertain. Therefore, assumptions made in a weak physical basis may lead to uncertain and inappropriate results.

As the piston dynamics plays a fundamental role in several critical processes related to fluid flow in reciprocating compressors, such a situation is extremely undesirable. A more precise solution for this problem is of particular importance in the refrigeration industry, where increasing pressure for energy efficiency exists, given that the sector is estimated to be responsible for about 10% of world's energy demand (McMullan, 2002).

One idea to overcome such difficulties is to study the interactions between the two phases present, liquid and gas. This would include, among other aspects, modelling the solubility of the gas in the oil, when the lubricant would be considered a mixture instead of pure oil. Examples of mixtures occurring in lubrication are the oil and air in open bearings, oil and vaporised gasoline in internal combustion engines and oil and refrigerant in refrigeration systems. The two-phase analysis is certainly more complex than the usual models, but it may provide useful information regarding the difficulties

previously presented. Furthermore, it can advance the physical understanding of cavitation, since the full domain is now studied in contrast to the study limited to the full-film region in previous models.

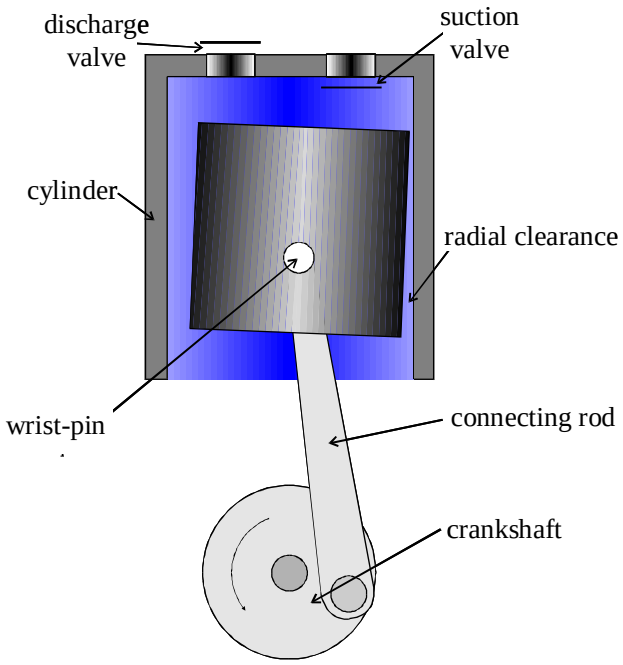

Figure 1.1. Ringless piston in alternative movement inside a cylinder.

This work proposes the study of lubrication according to this idea of two-phase flow, thus considering the behaviour of the lubricant mixture throughout the flow and how this can affect the behaviour of the lubricated component.

Two-phase flows are encountered very often in engineering problems, and the correct approach can be decisive to the appropriate design and operation of a system.

Liquid and gas flows can present different patterns, depending on the mixture components and their concentration, in addition to the flow conditions. For example, in a horizontal circular pipe, figure 1.2, among others one can have (Carey, 1992),

(a) *Bubbly flow:* generally for reduced vapour contents, and is characterised by the presence of a dispersion of small size bubbles in a continuous liquid phase;

(b) *Plug flow:* increasing the vapour content in comparison with the previous case enables some of the bubbles to coalesce, resulting in bigger bubbles in the flow;

(c) *Stratified flow:* for flows with reduced flow rate and high vapour content, separation of phases is observed, with vapour at the top and the liquid below a relatively uniform interface;

(d) Annular flow: in this case, a liquid film flows near the walls and a gas phase moves in the centre part of the pipe. Such flow is usually observed for high speed gas and moderate liquid flow rate.

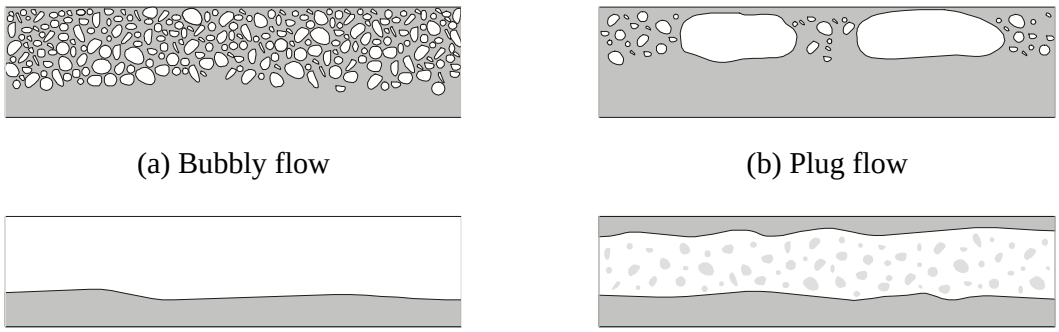

(a) Bubbly flow (b) Plug flow

(c) Stratified flow (d) Annular flow

Figure 1.2. Graphic scheme of different patterns for two-phase flows in a horizontal pipe.

Determining the pattern of the two-phase flow is not simple, as flow visualisation is not always possible and, even if so, the phases may not be easily distinguishable.

Not easy either is the choice of a methodology to analyse the flow considered. Two-phase flows are generally more complex than single-phase. Interaction between phases and their interaction with the boundaries need to be taken into account.

Nevertheless, analyses are often an extrapolation of the ones used for single-phase flows, writing the governing equations for the fluid mechanics problem and solving them via an analytical or numerical procedure. Amongst the methodologies, the most common are,

- *Homogenous methodology:* this model assumes that the phases move with the same velocity, so that slip between them is not observed. Therefore, the two-phase flow can be treated as an equivalent single-phase. Good results are usually conditioned to a good mixing between phases;
- *Separated phases methodology:* this model considers complete segregation of the two phases in two streams, which can have different properties and velocities. Equations have to be solved for each phase, and more information is required in comparison to the homogeneous model.
- *Two-fluids model:* formulated in terms of two sets of conservation equations governing balances of mass, momentum and energy for each phase; further to the separated phases methodology, this model also considers transport terms through the interface, averaged in time or space using appropriate techniques.

Some examples in lubrication have pointed to a separation of phases, observing the formation of distinct regions of liquid and gas film (Dowson and Taylor, 1979). Many of those cases generally presented an interacting neighbourhood more abundant in gas than in the lubricant mixture. Visualisation is also here a challenge to determine patterns, but it has been shown that the shape of the cavitated region can depend on factors such as the gas content and sliding velocity in thrust bearings (Young, 1989).

Figure 1.3 exemplifies a two-phase situation with the flow of a lubricant mixture of a mineral oil and a chlorofluorocarbon refrigerant R12 in a horizontal pipe, where release of gas is observed as pressure decreases. Additionally, the numerical solution for the problem using a homogeneous model can be seen. Despite the difference of properties between phases, and the increasing content of gas, the bubbles are actually reducing in size and becoming more evenly distributed in the liquid, supporting therefore the assumptions adopted for the homogeneous model and in part justifying its good agreement.

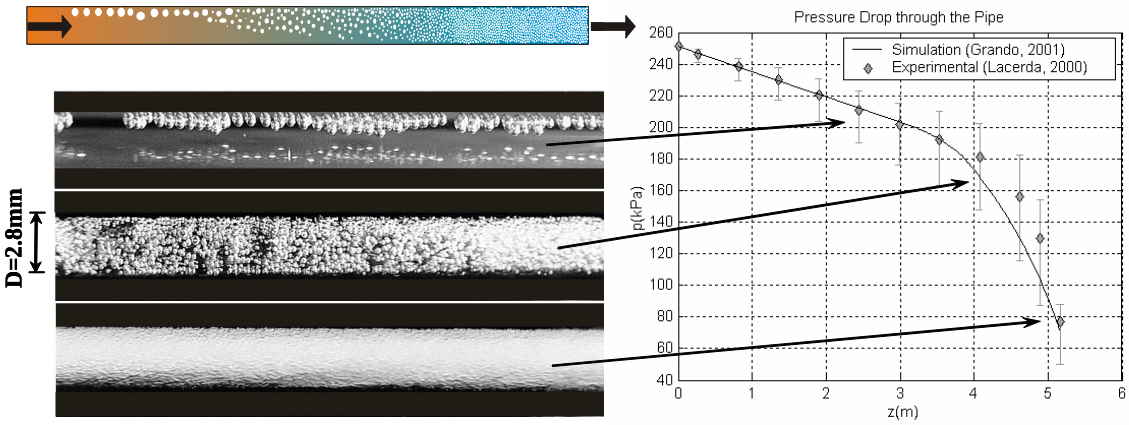

Figure 1.3. Pressure drop in a horizontal pipe for a two-phase flow of a mixture of oil and refrigerant – comparison of experimental and numerical results (Grando, 2001).

Some attempts have been made to study two-phase lubrication, especially in bubbly oils and squeeze film dampers (Nikolajsen, 1999, Someya, 2003), all of them adopting the homogeneous methodology. However, there is no work until now considering the release of gas from the lubricant mixture; current works only consider oil/gas interaction in terms of deformation and expansion of a constant mass of gas in the form of bubbles. In addition, the study of the lubricant mixture properties is still very limited, either for oil and non-condensable gases as well as for oil and volatile liquids. Among the common mixtures, probably the most studied is the oil and refrigerant mixture, which will be the choice for this work.

Oil and refrigerant mixtures are very common in refrigeration systems, influencing both lubrication of the compressor and the heat exchanges through the circuit. The majority of the studies consider rich refrigerant mixtures, but some consider mixtures with a rich oil content and those will provide the basis to calculate properties of the lubricant mixture considered (Grando, 2001). Furthermore, as presented previously in figure 1.3, studies have been characterising the two-phase flow of oil and refrigerant mixtures, both experimentally (Lacerda et al., 2000) and numerically (Grando, 2001, and Barbosa Jr. et al., 2004). Increasing attention has also being paid to absorption and release of refrigerant by the lubricant oil (Silva, 2004, Gessner and Barbosa Jr., 2006), providing useful information to the present work.

1.2 OBJECTIVES OF THE WORK

The main objective of this work is to derive a general model for lubrication phenomena, in which the transient behaviour of the lubricant mixture can be tracked, particularly regarding compressible flows or two-phase mixtures, and apply such equations to solve problems such as journal bearings and piston dynamics.

In choosing the oil and refrigerant mixture as the main lubricant to be studied in this work, contributions are not only to be made for the field of tribology, but also to studies on the refrigeration industry, which are expected to be as follows,

Tribology:

- To provide relevant information that contributes to the development of a two-phase lubrication theory;
- To develop a generalised two-phase lubrication model, where the gas is released from the mixture, thus allowing solution of problems without using a cavitation criterion;
- To compare the results obtained with the two-phase models with those from cavitation models. It is expected to contribute in the understanding of cavitation and to provide a more physical alternative to the solution of lubrication problems;
- To offer a generalised equation governing lubrication problems which facilitates consideration of additional mechanisms to just pressure and viscous effects;

- To contribute in the understanding of the behaviour of bearings and pistons, both statically and dynamically loaded.

Refrigeration:

- To perform a wide industry-ranging study, rich in details, which can advance the knowledge of the interaction effects of the oil/refrigerant mixture as well as the mixture flow and its controlling parameters, mainly in complex geometries such as those found inside the compressor;
- To provide more realistic models to the simulation of bearings and pistons in refrigeration;
- To make available information about the main parameters that influence piston dynamics, as well as to develop a useful tool that provides more precise information about the behaviour of such components in refrigeration systems.

1.3 STRUCTURE OF THE THESIS

The purpose of the work is to develop a general model for two-phase lubrication, based on assumptions about the interaction of the liquid and gas phase of the lubricant, and in the sequence apply the model to a series of components, with increasing level of geometry and operation complexity, exploring in each stage the physical phenomena involved, with special attention to the influence of the oil-gas interaction.

CHAPTER 1

This chapter gives an overview of the challenges involved with dealing with oil-gas mixtures in lubrication, in order to justify the work carried out and clarify the objectives involved.

CHAPTER 2

A detailed literature review is performed on the several areas relevant to the development of the two-phase lubrication model, focusing also on their overlaps. These areas include the theory of lubrication with particular emphasis on cavitation modelling; the previous efforts on two-phase lubrication research; the study of the oil-refrigerant mixture, the interaction between phases, determination of physical properties and their

variation with pressure and temperature; numerical models for bearing and piston lubrication; and lubrication in the context of reciprocating compressors used in refrigeration.

CHAPTER 3

The general two-phase lubrication model is developed in this chapter. The general assumptions will be stated and the uncertainties involved presented. The overview of the methodology to solve two-phase lubrication problems is discussed.

CHAPTER 4

The model developed in chapter 3 is applied for the simplified case of a partial journal bearing subjected to a static load. For this component, focus can be given to the behaviour of the model at the onset of cavitation (i.e., release of gas from the liquid mixture). A comparison with the results provided by other methodologies, whose suitability was previously discussed in Chapter 2, is included.

CHAPTER 5

Still considering the simplified geometry of the partial journal bearing, a detailed parametric assessment is performed, analysing the various factors affecting lubrication, both from the operational point-of-view as well as from fluid properties, including different mixtures.

CHAPTER 6

The solution for a full journal bearing is presented. The solution is now transient, and how the simplified solution of Chapter 4 evolves to the problems in Chapter 6 is presented. Attention is initially given to the thermodynamic considerations related to the recirculation of fluid around the bearing (equilibrium of the oil-gas mixture). In the sequence, operation of the bearing is discussed, particularly for load capacity and friction. Some of the assumptions of the model are further explored and a qualitative comparison against experimental results from Couto (2006) is performed.

CHAPTER 7

The model is now used to solve the target problem of this thesis, the lubrication of ringless reciprocating pistons used in refrigeration. Based on results from the previous

chapters, the model is finally extended to the full piston lubrication, discussing the particular methodology for this case. Results for the secondary motion of the piston are presented, tracking at each step the characteristics of the oil-refrigerant mixture. The performance of the piston is also assessed in terms of friction and gas leakage.

CHAPTER 8

The conclusions from the work undertaken are listed, summarising its main contributions. Suggestions for further development and other opportunities are also discussed.

1.4 ASSOCIATED PRODUCTION

The development of this research has resulted in 3 published papers and 4 presentations in Congresses, as listed below,

Published papers:

- Grando, F.P., Priest, M. and Prata, A.T. **Lubrication in Refrigeration Systems: Performance of Journal Bearings Lubricated with Oil and Refrigerant Mixtures**. Life Cycle Tribology, Proc. 31st Leeds-Lyon Symposium on Tribology, Leeds 2004, Tribology and Interface Engineering Series, Elsevier, Amsterdam, 2005, pp.481-491.

- Grando, F.P., Priest, M. and Prata, A.T. **A Two-Phase Flow Approach to Cavitation Modelling in Journal Bearings**. Tribology Letters, v.21, n.3, 2006, pp.233-244.

- Grando, F.P., Priest, M. and Prata, A.T. **Lubrication in Refrigeration Systems: Numerical Model for Piston Dynamics considering Oil-Refrigerant Interaction**. Proc. IMechE, Part J, Journal of Engineering Tribology, v.220, n.3, 2006, pp.245-258.

Participation in Congresses:

- Grando, F.P., Priest, M. and Prata, A.T. **Lubrication in Refrigeration Systems: Performance of Journal Bearings Lubricated with Oil and Refrigerant Mixtures**. 31st Leeds-Lyon Symposium on Tribology: Life Cycle Tribology, Trinity and All Saints College, Leeds, September 2004, paper XIV (iii).

- Grando, F.P., Priest, M. and Prata, A.T. **A Two-Phase Flow Approach to Cavitation Modelling in Journal Bearings**. International Tribology Conference, International Conference Center, Kobe, Japan, June 2005, paper B-25.

- Grando, F.P., Priest, M. and Prata, A.T. **Lubrication in Refrigeration Systems: Numerical Model for Piston Dynamics considering Oil-Refrigerant Interaction**. 32nd Leeds-Lyon Symposium on Tribology: Interactions of Tribology and the Operating Environment, INSA-Lyon, Villeurbanne, France, September 2005, paper XVI (vi).

- Grando, F.P. **Piston two-phase lubrication considering oil-refrigerant**. Mission of Tribology Research 14, Institution of Mechanical Engineers, London, December 2005.

Copies of the papers are given in the Appendix at the end of the thesis.

Chapter 2

LITERATURE REVIEW

In this chapter a survey of the literature related to two-phase lubrication is performed. As there is no work specifically investigating the solubility of gases in oils and its effect on lubrication, related themes are reviewed. Firstly, a brief review of the usual methodologies adopted in lubrication to deal with cavitation is performed, and also the alternatives proposing two-phase flow approaches (bubbly oils). Later, the oil and refrigerant mixture is characterised in its thermodynamic and thermophysic aspects, as well as in its behaviour in refrigeration systems. Furthermore, to gain knowledge on the practical applications and understand the main challenges that happen in these cases, details of piston lubrication models are discussed.

2.1 OVERVIEW

The great majority of studies involving hydrodynamic lubrication consider pure oil as the lubricant, very often assuming constant properties or temperature dependent only. However, it is acknowledged that gases can be dissolved in the oil in fractions up to 10% in volume under atmospheric conditions (Kicinski, 1983, Nosov and Gomez-Mancilla, 2004), and it can be released from the oil in the divergent region for pressures close to the atmospheric. In this case, viscosity and density are important properties of mixture that affect characteristics of the bearings (Choi and Kim, 2002). Few works have been dedicated to the study of solubility of air in oils. Although the importance of the bubbly oil has been mentioned, precise correlations are not available (Cameron, 1966, Nikolajsen, 1999a). Nevertheless, it is important to review the fundamental aspects of fluid film lubrication, in order to develop a model based on coherent physical assumptions and respecting laws of conservation and to compare the different results in a later stage.

Regarding the oil and refrigerant mixture, the number of works studying the solubility of refrigerant in the oil can be considered significant if compared to the air/oil mixtures, despite most of the research being concerned with rich refrigerant mixtures (with oil as a contaminant) and its effects in heat transfer processes. Nonetheless, research has also focused on understanding the influence that an environment rich in refrigerant can have on the lubrication inside the compressor. Studies of the flow of oil and refrigerant mixtures and experimental studies of lubrication of components in a pressurised refrigerant environment also collaborate to the modelling of mixture lubrication during system operation.

If the presence of refrigerant dissolved in the oil is not considered, i.e., if the lubricant is a pure oil, the study of lubrication in refrigeration components is quite similar to those from other mechanical areas, such as internal combustion engines, shafts, rotors, etc. The majority of the works here reviewed are not specifically related to the lubrication of components in a refrigeration system; nevertheless they still are very useful to assist in developing a numerical code for piston simulation in particular.

2.2 CAVITATION IN LUBRICATION

In Fluid Mechanics, cavitation is the phenomenon that occurs when a liquid vaporizes due to a local pressure reduction, forming bubbles that might implode in sequence if experiencing a positive pressure gradient, causing erosion on the material over which the liquid flows. The levels of pressure in this case are below the vapour pressure of the liquid, therefore generally much lower than the atmospheric pressure.

In lubrication, cavitation is conventionally defined as the loss of continuity in a liquid film due to the presence of gas, vapour or both. Despite this difference, the term cavitation has remained in use and is widely adopted with this meaning. This phenomenon has been examined for more than a century in tribology and in several other areas, as in the study of impellers, valves and turbines. In lubrication, since the first works it has been observed a clear influence of cavitation on bearing behaviour, resulting in a substantial change in variables such as the supported load. Several cavitation models have been developed to predict the behaviour of fluid film lubricated components, but the physical understanding of cavitation in bearings is not yet

satisfactory. A wide and complete review about cavitation in bearings was done by Dowson and Taylor (1979), and it is basis for the present study.

In order to explain the occurrence of cavitation, the governing equation for lubrication can be recalled. This equation, more often denominated Reynolds equation, is discussed in details in Chapter 3. For the purposes of this discussion, a simplified form, derived for an incompressible film can be used, and is given by (Hamrock, 1994),

$$\frac{\partial}{\partial x}\left(\frac{h^3}{\mu}\frac{\partial p}{\partial x}\right)+\frac{\partial}{\partial y}\left(\frac{h^3}{\mu}\frac{\partial p}{\partial y}\right)=6\left(u_a+u_b\right)\frac{\partial h}{\partial x}+12\frac{\partial h}{\partial t} \tag{2.1}$$

where,

h = oil film thickness [m];

μ = lubricant viscosity [$Pa.s$];

p = pressure along the oil film [Pa];

u_a, u_b = surface velocities for the x direction [m/s];

x = coordinate along the variation of the clearance between the surfaces [m];

y = coordinate perpendicular to x [m];

Using Reynolds equation, it can be shown that a positive pressure field is obtained in convergent region of the clearance and a negative pressure field is obtained in the divergent region. Cavitation takes place in the divergent region of the film, as shown in figure 2.1. Due to incompressibility of the oil, in the convergent region it is forced to flow in a direction perpendicular to that in which surfaces are moving, in order to respect conservation of mass. But when the gap becomes divergent, not enough oil is available to fill the whole clearance and then cavitation occurs. Could the film could be kept intact, negative pressures calculated by Reynolds equation would be observed. However, as the bearing is communicated to the ambient pressure on the surroundings, and since this pressure is higher than the negative pressures of the film, air enters in the bearing and avoids a greater pressure drop. Therefore, while the film can accommodate itself in the convergent region and generates pressure, in the divergent region the film is unable to conform to the change in flow section and ruptures, such that a striated flow is commonly observed after this position. This is the principle of ventilation for a finite bearing, but other effects, such as the release of gas from the oil, can also collaborate with the behaviour in the divergent region.

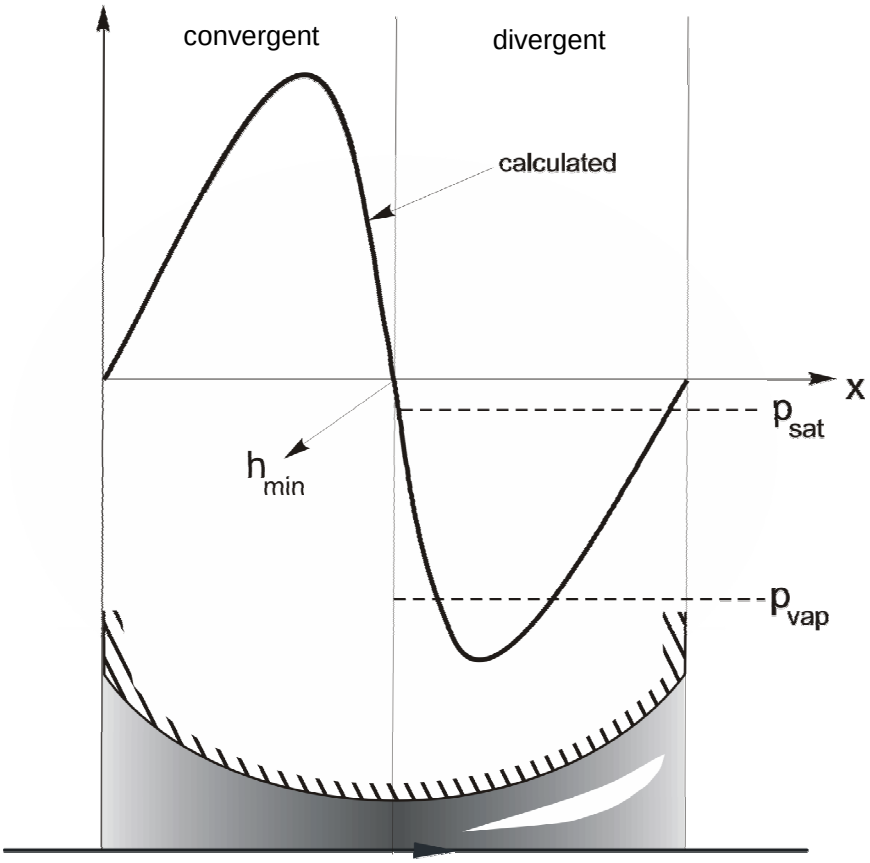

Figure 2.1. Pressure profile on a convergent-divergent surface filled with oil.

The occurrence of cavitation in lubrication does not present only deleterious effects. In fact, a component of force normal to the surfaces is present under cavitation, which is not observed otherwise. When no film rupture is observed, a symmetric pressure profile occurs and the film responds in a normal direction to the applied load, and presents a zero capacity in the load direction. This situation is verified only in very lightly loaded bearings, which would turn their application very restricted.

At this point, two basic forms of cavitation shall be distinguished:

- **Gaseous cavitation:** most commonly observed form, in which the ambient gas can move into the film if subambient pressures occur, as well as the release of gas dissolved in the oil, which results in a film flowing in streamers whose pressure is almost constant and equal to the atmospheric pressure in the surroundings of the divergent region.
- **Vapour cavitation:** in sealed bearings or in fast dynamic loadings, the pressure in the film can fall to the oil vapour pressure, when it boils at ambient temperature. The bubbles formed can later collapse, causing cavitation erosion. In this situation, the pressure levels are much lower than those observed in gaseous cavitation.

Although many experiments have been performed to visualise cavitation, there is still a great challenge in determining in which conditions it occurs, which mathematically correspond to the boundary conditions in the solution of the pressure field on bearings via equation (2.1). This occurs due to the film rupture, in the divergent region of the bearing, as well as to the film reformation, when the pressure increases again and the film restores its liquid continuity. In several cases the bearing is fed with oil near the maximum clearance position, and the film reformation is not a problem of major concern, since the supported load is little influenced by this information (Prata, 1992). The same is not observed if starvation is observed in oil supply, when film reformation needs to be taken into account (Santos, 1995).

Considering statically loaded bearings, the usual conditions used in lubrication problems are described below.

- **Sommerfeld Condition** (Hamrock, 1994)**:** The first solution to a pressure field in a journal bearing was obtained in 1904 by Sommerfeld, assuming that the lubricant film completely fills the clearance, that is, if cavitation is neglected. In this case, boundary conditions are given by,

$$p(x=0) = p(x=x_f) = 0 \tag{2.2}$$

where x is the coordinate along bearing circumference, and x_f is the final position of the oil film.

The pressure field resulting from the solution using this boundary condition is presented in figure 2.2. This pressure field is valid only on very light loaded bearings. For heavier loads, this solution is inconsistent due to the presence of positive and negative pressures of the same magnitude, as well as resulting in a force normal to the applied load.

- **Half-Sommerfeld or Gümbel Condition** (Hamrock, 1994)**:** A suggestion to solve the problem of negative pressures in the bearing is simply to neglect them in the Sommerfeld solution.

  Therefore, in a symmetric bearing, boundary conditions turn into,

$$p(x=0) = p(x=0{,}5x_f) = 0; \quad p(0{,}5x_f \le x \le x_f) = 0 \tag{2.3}$$

The Half-Sommerfeld solution in presented in figure 2.3. It can be shown that this condition violates flow continuity. Nevertheless, due to its simplicity and as results

many times do not lead to considerable errors, this condition is still commonly used and in many cases provides a good estimate for bearing behaviour.

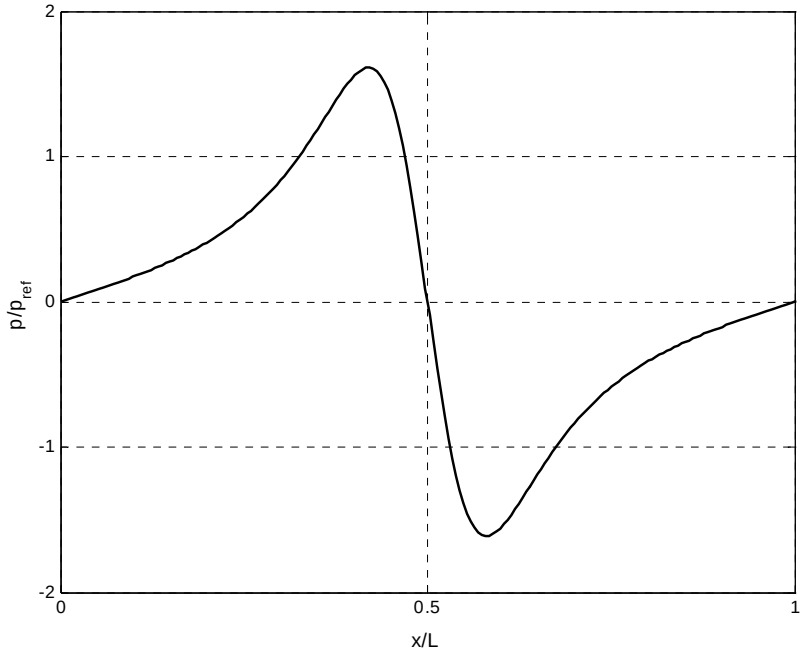

Figure 2.2. Pressure field in a journal bearing using Sommerfeld conditions.

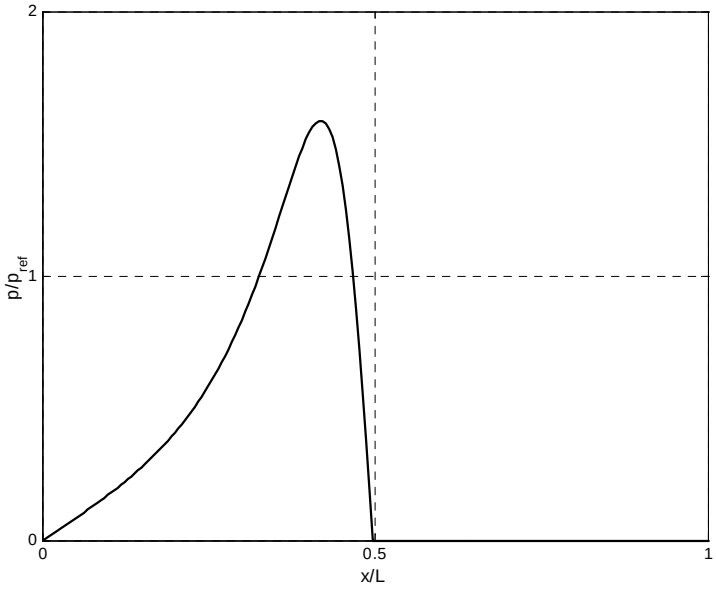

Figure 2.3. Pressure field in a journal bearing using Half-Sommerfeld condition.

- **Reynolds or Swift-Stieber Condition** (Prata, 1992)**:** This condition has been formulated to solve the inconsistency on mass balance in half-Sommerfeld condition, and it considers flow continuity.

  The flow rate of lubricant in a two-dimensional case is given by,

$$q_x = -\frac{h^3}{12\mu}\frac{dp}{dx} + \frac{Uh}{2} \qquad \left[\frac{m^3/s}{m}\right] \tag{2.4}$$

In the cavitated region, it is assumed that the pressure is constant and equal to the ambient pressure. Therefore, there is no influence of the pressure terms and the flow rate is given by,

$$q_x = \frac{Uh}{2} \qquad \left[\frac{m^3/s}{m}\right] \tag{2.5}$$

Comparing the flow immediately before and after film rupture, it can be seen that the conservation of mass will be satisfied if a zero pressure gradient occurs at the onset of cavitation. Thus, half-Sommerfeld inconsistency can be verified (due to its negative gradient in cavitation), and also the boundary conditions for cavitation can be defined as,

$$x = x_{cav}, \; p = \frac{\partial p}{\partial x} = 0 \tag{2.6}$$

which is commonly known as Reynolds boundary condition.

In the previous equation, it was assumed that ambient pressure was zero. For such case, the pressure profile is shown in figure 2.4.

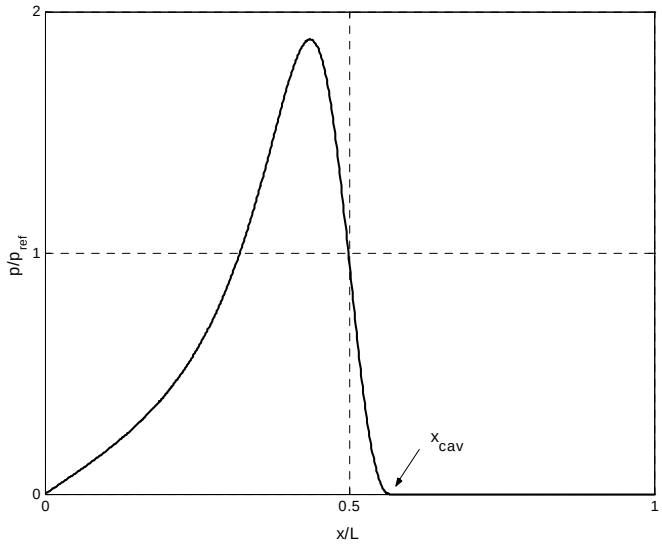

Figure 2.4. Pressure field in a journal bearing using Reynolds condition.

Pinkus and Sternlicht (1961) proved that both conditions for the cavitation boundary are mutually dependent, that is, the zero pressure gradient results in a zero pressure and vice-versa, such that the problem has always a solution. The difficulty lies on the fact that the position for the cavitation boundary, x_{cav}, is initially unknown, and must be obtained during the solution of the problem, which results in a free boundary problem.

- **Separation Boundary Condition** (Coyne and Elrod, 1970)**:** By observing that in some experimental results a subcavity pressure occurred led to the idea that flow separation could be important to film rupture. In this case, a considerable amount of fluid would be carried by surface movements, as opposed to the Reynolds condition which assumes oil flow between gas cavities.

It is considered that flow separation occurs from the stationary surface of the bearing in the divergent region when the cross-film velocity gradient (*du/dz*) is zero. From Navier-Stokes equations for a two-dimensional flow, this conditions results in,

$$\frac{dp}{dx} = \frac{2\mu U}{h^2} \tag{2.7}$$

If cavitation pressure is also known, the rupture interface can be determined. Additionally, if the reverse flow region is associated with a preferential region to the entrance of bubbles in the flow, the film will lose its continuity, as shown in figure 2.5.

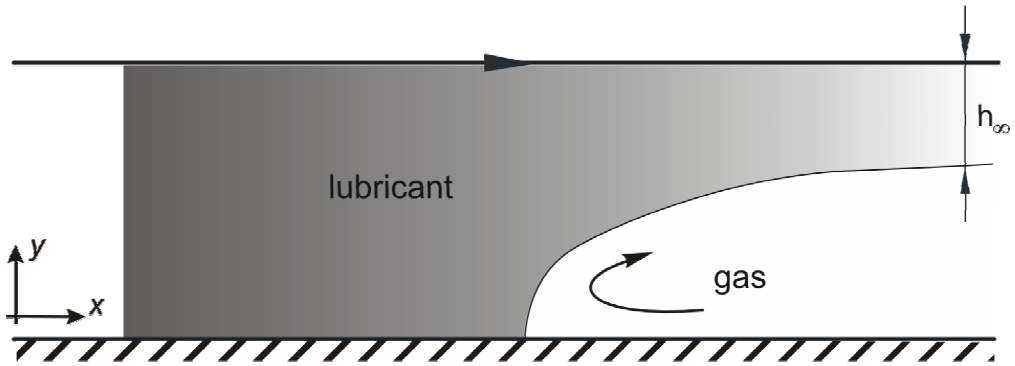

Figure 2.5. Behaviour of the flow considering separation boundary condition.

It is necessary to use the continuity equation and the equation for surface tension to determine boundary conditions for this situation. Considering an asymptotic film thickness downstream the bearing, it is obtained,

$$\frac{\partial p}{\partial x} = \frac{6\mu U}{h^2}\left(1 - 2\frac{h_\infty}{h}\right) \tag{2.8}$$

where h_∞ is determined through considerations on surface tension (Coyne and Elrod, 1970).

Finally, having the interface pressure condition, the problem is defined. According to Coyne and Elrod (1970),

$$p = -\frac{\sigma}{R_0} + \Delta p \tag{2.9}$$

where,

R_0 = radius of curvature of the free film at separation point (m);

Δp = pressure change across the transition region (Pa);

- **Jacobsson-Floberg Boundary Condition:** Floberg (1965) assumed that all the lubricant after film rupture is carried away in between the air cavities. However, considering that no net flow exists in a cavity, he proposed a boundary condition defining the shape of a single cavity in the cavitation boundary, which is,

$$\frac{\partial p}{\partial x} - \frac{\partial p}{\partial z}\frac{\partial x}{\partial z}\bigg|_{cav} = \frac{6\mu U}{h^2} \tag{2.10}$$

In addition to that, the zero pressure condition in cavitation can be used as the second boundary condition. Alternatively to the zero pressure, it can be considered a pressure diference at the interface due to surface tension effects. In this case, a region with subambient pressures will be observed, as it was the case for the separation boundary condition.

Separation and Jacobsson-Floberg boundary conditions therefore can result in similar pressure fields, qualitatively presented in figure 2.6.

It is not always simple to decide which of the boundary conditions is more suitable for a specific problem. Dowson and Taylor (1979), however, verified that Reynolds condition represents better moderate and heavy loads, since, despite subambient pressures are observed, their magnitude is negligible compared to the positive pressures at the convergent region. On the other hand, separation mechanisms are dominant in film rupture in light loads, and the Jacobsson-Floberg condition provides better results.

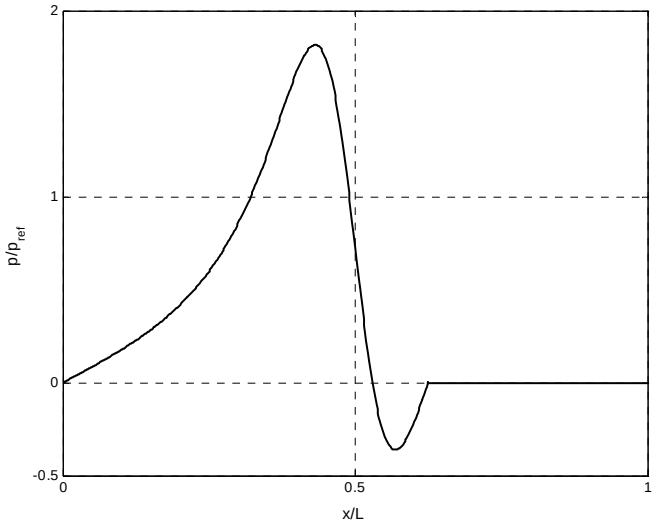

Figure 2.6. Pressure field for separation and Jacobsson-Floberg boundary conditions.

In addition to the diversity of theoretical propositions concerning cavitation conditions, another challenge is how to implement them numerically, mainly the more realistic ones (Reynolds and Jacobsson-Floberg). Sommerfeld and half-Sommerfeld conditions do not require special algorithms as the others. For these, the most commonly used methodologies are briefly described in the sequence:

- **Boundary Adaptative Mesh:** Developed by Prata and Ferreira (1990), it uses Reynolds conditions and proposes a change of variables in order to transform the free unknown boundary in another variable of the problem. Therefore the problem is solved in a transformed domain, fixed, simultaneously with an additional equation that enables the cavitation position to be determined. This additional equation is the continuity equation along the oil film. Once a converged solution is obtained, the original domain can be restored and the pressure field and cavitation boundaries are obtained. Figure 2.7 illustrates this change in domain. The solution methodology using adaptative meshes is presented in details by Prata and Ferreira (1990), Manke (1991) and Prata (1992).

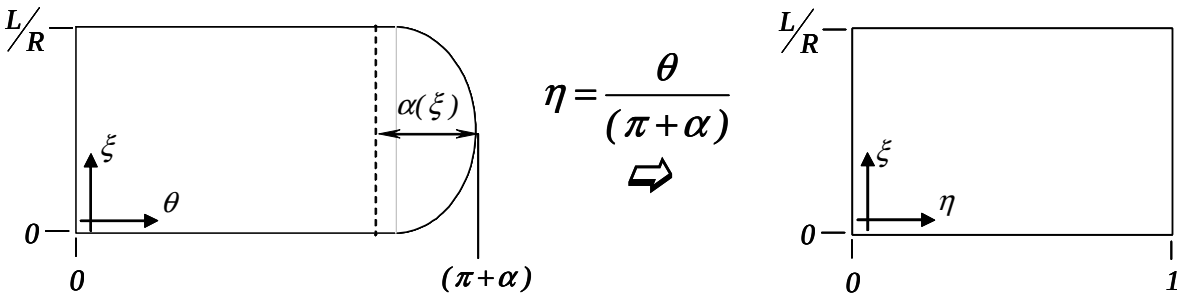

Figure 2.7. Domain transformation to the solution of cavitation problem with adaptative mesh.

- **Cavitation Algorithm:** Developed by Christopherson (1942), and also resulting in Reynolds condition, this iterative algorithm simply turns into zero the negative pressure values obtained during numerical calculations. Parkins (1985) states that this procedure fortuitously leads to a zero gradient pressure at the cavitation boundary. Santos (1995) compares this methodology with the others here described for a dynamically loaded journal bearing. It should be noted that this methodology will only work if an iterative algorithm is adopted to the solution of the resultant linear system.
- **Universal Cavitation Algorithm (The Elrod Algorithm):** Elrod (1981) proposed a universal equation which can represent the lubrication phenomenon either before or after cavitation. To this aim, he considered the compressibility of the liquid, then stating the relationship between density and pressure as,

$$\kappa_l = \rho \frac{\partial p}{\partial \rho} \tag{2.11}$$

where κ_l is the liquid bulk modulus, ρ the liquid density and p the film pressure.

Another key definition of his method is the ratio between densities along the flow and that at the cavitation onset (ρ_c), denoted by λ and calculated as,

$$\lambda = \frac{\rho}{\rho_c} \tag{2.12}$$

Elrod rewrites equation (2.11) in an alternative manner, at the same time as he introduces a logical function that is probably the kernel of his algorithm,

$$g\kappa_l = \frac{\rho}{\rho_c} \frac{\partial p}{\partial \left(\rho / \rho_c \right)} = \lambda \frac{\partial p}{\partial \lambda} \tag{2.13}$$

where g is known as the *switch function*, defined as,

$$g = \begin{cases} 1, & \textit{for the full film region} \\ 0, & \textit{cavitation zone} \end{cases} \tag{2.14}$$

Integrating equation (2.13) returns,

$$p = p_{cav} + g\kappa_l \ln(\lambda) \tag{2.15}$$

A final simplification states that,

$$p_1 - p_2 = \kappa_l \left[\ln(\lambda_1) - \ln(\lambda_2) \right] \approx \kappa_l \left(\lambda_1 - \lambda_2 \right) \tag{2.16}$$

Using this information, the equation for the Elrod algorithm can be obtained by algebraic manipulation from the Reynolds equation. Comparing to equation (2.1), the equivalent equation for the Elrod algorithm, now compressible, will be given by,

$$\frac{\partial}{\partial x}\left(\frac{\kappa_l h^3}{12\mu} g \frac{\partial \lambda}{\partial x}\right)+\frac{\partial}{\partial y}\left(\frac{\kappa_l h^3}{12\mu} g \frac{\partial \lambda}{\partial y}\right)=\frac{\partial}{\partial x}\left[\frac{\lambda(u_a+u_b)h}{2}\right]+\frac{\partial(\lambda h)}{\partial t} \tag{2.17}$$

From equation (2.17), it can be seen that, depending on the region of the flow, whether full film ($g=1$) or cavitation ($g=0$), the equation differs. For the full film region, the numerical process renders an elliptical formula, while for the cavitation zone a parabolic, upwind formula results. This distinction required Elrod to suggest special considerations when discretising the equation, particularly for film that can be in the film transition.

The cavitation boundary conditions usually follows the Jacobson-Floberg proposal, however this results in the Reynolds boundary condition for the onset of cavitation if no subambient pressure is assumed in the bearing. The boundary condition is directly obtained via the logical function.

The Elrod Algorithm has been extensively used, but one of the challenges remains the value assigned to the bulk modulus. As it is typically a rather large number, small differences in the density ratio lead to large differences in pressure, which may bring difficulties for the numerical solution. Additionally, the appropriate definition of the bulk modulus is required to obtain a precise solution for the problem. In the light of this problem, recent works have further developed this algorithm to incorporate a variable bulk modulus for the lubricant considered (Sahlin et al., 2007).

Despite its wider application in lubrication problems, it does come with some irony the observation that the algorithm develops a compressibility-based model for a region which can easily be deemed as incompressible, but avoids the appropriate compressible handling of the actual existing two-phase flow being observed in the cavitated region.

Several works have pursued validation of the proposed boundary conditions as well as numerical methodologies, particularly for bearing problems. It is also important to note that film behaviour under dynamic loads might differ from that observed under static loads. The algorithms used, however, do not show significant changes. The literature related to solving the lubrication problem for bearings is extremely vast and

diverse. In the sequence some selected works are described, which have applied the previous proposals to several lubrication problems, presenting different geometries and loads, and even suggesting many improvements to existing methodologies.

Crosby (1982) solved numerically finite journal bearings considering film separation at the divergent region of the component, using a boundary condition similar to Jacobsson-Floberg. In the axial direction, a curve is adjusted to reduce computational effort. The resulting equation is then solved in a marching scheme (initial value problem) until convergence of cavitation (separation) pressure and its gradient. Comparing the results with other simulations using Reynolds condition, a significant deviation is observed in heavily loaded berings, which justifies to the author to apply his method. The computational effort is low, what can be considered a positive aspect, since Jacobsson-Floberg condition is of difficult establishment.

Rowe and Chong (1984) proposed an algorithm that satisfies principle of mass conservation for film rupture as well as for film reformation, and which is easily accommodated to existing bearing programs. The algorithm uses Reynolds condition to film rupture and Jacobsson-Floberg to film reformation. Cavitation boundaries are estimated and corrected at every iteration, which is finished with a check for the conservation of mass. Results demonstrated the discrepancy between the mass flow rate entering the bearing and the side flow rate when only Reynolds condition is considered. It was achieved a good agreement with experimental results, mainly for small ratios of supply pressure and maximum pressure.

Vijayaraghavan and Keith (1990) have used an implicit numerical scheme with the Elrod algorithm to directly predict the boundaries for rupture and reformation of a film in a dynamically loaded journal bearing. The numerical scheme is based on approximate factorisations to reduce a two-dimensional problem to another in one-dimension, whose solution is obtained via a Newton-Raphson method at each time step. They tested several orthogonal and non-orthogonal grids in aligned and misaligned finite journal bearings, and obtained more precise solutions for steady state conditions. Their methodology also has a great potential of reducing computational effort in transient problems.

Manke (1991) studied finite journal bearings submitted to dynamic loading, integrating the Reynolds equation using finite volume methodology. His formulation includes cavitation, which is treated with Reynolds boundary condition, and also

considers laminar or turbulent flow regimes. He suggested several procedures to calculate the cavitation boundary using adaptative meshes, as well as to solve of shaft trajectory, which characterises the dynamic behaviour of the bearing. His model is used to verify operational conditions of the bearing such as different oil flow rates and power losses due to friction.

Ingham et al. (1992) used the boundary element method (BEM) to solve the problem of flow separation at a corner. This method is an analytical model for free boundary problems. Being governed by a bi-harmonic equation, the free surface problem is solved by approximation of a series of analytical functions. Boundary conditions are assumed to be the inexistence of flow across the interface, the zero shear stress on the free surface and the balance of normal stresses by pressure and surface tension. The use of function series guarantees the smooth continuity of the free surface profile, which is not observed in other methods to the same problem. Despite the good agreement with experimental results, it is still necessary to develop numerical methods capable of solving the problem with lower computational effort.

Yu and Keith (1995) have also applied the boundary element method to predict cavitation in journal bearings. For the Reynolds equation, boundary conditions used were those from Jacobsson-Floberg. The boundaries are simulated by two interpolation polynomials, and the governing equation is transformed into an undetermined boundary problem. This procedure reduced numerical instabilities experienced by the conventional Elrod algorithm, which occurred due to inadaptable grid shape in finite difference algorithms. The good results obtained for various bearings led the authors to believe the method is feasible for dynamic loading, surface deformation and variable lubricant properties.

Santos (1995) reviewed and compared different cavitation algorithms to solve problems involving dynamically loaded journal bearings subjected to cavitation. He tested several conditions, such as half-Sommerfeld, Reynolds (via adaptative mesh and via cavitation algorithm) applied to Reynolds equation solved with a finite volume methodology. The Elrod algorithm was also tested in a numerical solution using finite differences. It is verified that the adaptative mesh gives better results for static loads without considerable computational effort, while Elrod and the cavitation algorithm require refined grids. The Half-Sommerfeld condition is reasonable if only qualitative results are necessary. However, under dynamic loading, the Elrod algorithm has shown

to be more efficient due to its lower computational effort, since the cavitation boundary can be obtained directly.

Lemaître and Berker (1995) extended the Elrod algorithm to use with non-Newtonian fluids, and then implemented it to an axially symmetric finite journal bearing. They obtained initially a generalised Reynolds equation to the non-Newtonian fluid case, which considers the non-linear dependence of shear stress tensor with shear rate of fluid. They also generalised Elrod algorithm, including the logical function *g* (0/1) to the mass flux expression. The method is applied to various situations: journal bearing filled with a Newtonian fluid, a journal bearing with a shear-thinning fluid under static load, and a dynamically loaded journal bearing with a Newtonian lubricant. Results showed a good agreement with existing literature, and the authors concluded that the deviation of behaviour from Newtonian to shear-thinning is more significant in heavier loads, where the eccentricity ratio is higher and higher load capacity is seen for the Newtonian fluid.

Vincent et al. (1996) numerically investigated cavitation in dynamically loaded journal bearings. The numerical procedure applies the Elrod algorithm both for film rupture and reformation. To solve equations for journal dynamics, the authors used the mobility method, which consists on writing radial and angular velocities for the centre of the shaft as components of a *mobility vector*, whose magnitude is *M* and whose angle with the centre line is α; this vector is present in the governing equation of the problem, Reynolds and also in the equation for journal dynamics, and the iterative process leads to values for *M,* α and the density ratio field, which consequently determines the pressure field. Additionally the mean temperature in the bearing along the cycle is calculated by a simplified model which assumes that heat dissipation is partially carried out by the lubricant. After simulations for a connecting rod bearing of a diesel engine, they concluded that the Elrod algorithm (with Jacobson-Floberg) and Reynolds boundary conditions provide very similar results, but systematically with more length for the full film region on the Elrod algorithm solution than the Reynolds condition, as well as greater friction torque and smaller side leakage. Concerning thermal analysis, they verified that values for minimum film thickness and friction torque are reduced due to temperature rise and consequent reduction of oil viscosity. It is also observed that the side leakage is greater for cases where thermal effects are neglected.

In the sequence, Vincent et al. (1997) have used the same procedure to study noncircular journal bearings. Comparing the performance of circular and elliptical bearings they verified that smaller values for minimum film thickness are obtained to the elliptical bearing using Reynolds condition. This is not repeated if the Elrod algorithm is applied, which can be atributed to the additional condition of mass flow conservation on film reformation.

Alvarez and Oujja (2001) considered the nonlinear unidimensional problem of the infinite journal bearing under static load, and obtained an approximate solution through a process of successive approximations, where the non-homogeneous term of the differential equation searches the cavitated region. The results obtained coincide with the usual solution using Reynolds rupture and reformation conditions.

Nosov and Gomes-Mancilla (2004) evaluates the cavitation boundary, based on energy and mass balances in conjunction with the classical Reynolds equation. Considering the kinetic energy changes near the cavitation region, and comparing it to the surface energy generated in the interface of liquid and gas, this methodology enables to estimate the number of streamers that are formed in the cavitation region. Furthermore, using this methodology and deriving the values for minimum streamers as a function of operation conditions, bearing geometry and lubricant properties, they also evaluate when cavitation should or should not appear. The pressure results are similar to those obtained using the classical lubrication methods.

Couto (2006) develops a bearing test rig to determine pressure field and visualisation of cavitation for statically loaded journal bearings, and, in a more general context, bearing behaviour for static, dynamic loading and assembly misalignments. In his experimental results, he noted particularly the effects of ventilation in the cavitation region, also observing separation effects. Immersion tests were performed, whose results indicated lower cavitation pressure for fully immersed bearings in comparison to a ventilated one. Numerical models presented very good agreement with the experimental results, giving confidence to progress on developing a fully coupled compressor bearing model.

Sahlin et al. (2007) modifies the Elrod algorithm to improve the determination of effects of lubricant compressibility in the full film region. It has been shown that different compressibility models can produce significantly different results in a hydrodynamic pressure range. It is reported that further physical dependence of

variables such as viscosity might be needed to improve the prediction of the cavitation region, fractional film content and pressure.

2.3 BUBBLY OILS

As observed in the previous section, the analysis of the lubrication problem has limited the analysis to the full-film region – even if solution is obtained for the full extent of the domain, it is assumed constant pressure to the cavitated region, giving no attention to the two-phase flow occurring in this region and understanding its nature.

Nevertheless, the use of terms related to two-phase flows and the release of gas can often be found in previous works studying cavitation. For instance, Jacobsson and Floberg (1957) use the expression "air expulsion pressure" in their work, which can be understood as the saturation pressure of the air dissolved in the oil. The variable $\lambda = \rho / \rho_c$ proposed by Elrod (1981) is also relating to liquid/gas two-phase flow occurring in the cavitated region, despite not making any assumptions regarding the gas phase involved. An initial step to advance in the study of such situations has been that where the gas released, or present in the lubricant fed to the bearing, remains in the form of dispersed bubbles with the oil throughout the flow, therefore creating a situation where bubbly oil lubrication is observed.

The presence of dispersed bubbles in the oil modifies the rheology of lubricant mixture in comparison to that of pure oil. Viscosity and density of lubricant are fundamental properties which influence working conditions of bearings. The density of the lubricant mixture, in the presence of gas, becomes more dependent on pressure and temperature, especially at high loads and speeds. The viscosity of the mixture increases in relation to the oil, which suggests that a higher load can be supported. Furthermore, conditions of film rupture and flow separation need to be revised, as well as film reformation. The effects associated to bubbles must also be considered – usually only surface tension is taken into account and viscous effects and inertia are neglected.

Lubrication in the presence of bubbles has been treated similarly to pure oil lubrication, but considering lubricant compressibility and the change in viscosity. The flow of the mixture is generally solved using homogeneous models, i.e., models in

which a single-phase pseudofluid is considered, and whose properties are based on averages of the properties of the fluids composing the mixture.

As in conventional two-phase flows treated by homogeneous models, the major difficulty in bubbly-oil lubrication lies upon the definition of a characteristic viscosity to the oil/gas mixture.

There are some contradicting reports on the effect of the viscosity of the mixtures in bearings, some considering that load carrying capacity is not significantly affected by changes in gas fraction, while other works verified a considerable change in load and pressure with bubbles dissolution. (Choi and Kim, 2002).

This conflict is resultant from the different models and equations used; some authors considered compressibility the most important effect in lubrication, in which case the load capacity is not significantly affected, while others believed that viscosity effects are dominant and rise in carrying capacity is observed. A better understanding of these effects is still necessary, and it will come from experimentation with confirmation in theoretical models. One objective of the present work is to contribute and advance on understanding of the effects of dissolved gases in the oil and how their release in the form of bubbles affects lubrication.

Relevant works of lubrication of bearings in the presence of bubbles, and where very different methodologies have been observed, are reviewed in the sequence.

Tønder (1977) analysed the effect of finely dispersed bubbles on the hydrodynamic lubrication of straight pivoted pad bearings. The lubricant is considered isoviscous, such that the effect of bubbles reflects only in a dependence of density with pressure. The gas is assumed ideal, and the flow is isothermal. The Reynolds equation is discretised by finite differences and the resultant linear system is solved iteratively. The author concluded that load is insignificantly affected by bubbles in comparison to the pure oil case, but load centre position is considerably shifted to downstream direction, and appreciably for small tilts. From a stability point-of-view, Tønder verified that start-up of bearing can be very difficult with bubbly lubricants due to the difficult of lifting.

Smith (1980) studied the influence of bubbles in fluid film lubrication of a steadily loaded plane-inclined slider bearing, with particular attention to surface tension effects. Considering that bubbles alter lubricant density, but assuming it isoviscous, the author concluded that load carrying capacity is virtually unaffected by the presence of

bubbles. However the centre of pressure can be considerably modified and the bearing tends to be more unstable. It is also suggested that another dimensionless parameter in addition to the Reynolds number is necessary to characterise the flow, and it should consider surface tension.

Kicinski (1983) studied isothermal lubrication using an air/oil emulsion as lubricant both in statically and dynamically loaded journal bearings. Solution for the Reynolds equation is performed by finite differences and no boundary conditions are used at the end of the positive pressure region. Air bubbles in the emulsion expand in the divergent region and suction of air from the boundaries is also possible – it is numerically modelled using suction coefficients. Air is considered a perfect gas and the density and viscosity of the emulsion vary with pressure. For a partial journal bearing (160º) under static load, he showed that the levels of negative pressure obtained are lower with the increase of air suction, being closer to the classical results for constant properties and Reynolds boundary conditions. The increase in bearing eccentricity also brings the solution closer to the classical results, even for considerably high degrees of aeration. In addition to that, for dynamic loads, he observes more stable properties in the system with higher degrees of aeration. It is mentioned however that results for higher degrees of aeration may be deviated from reality, as large bubbles tend to be forced out in the region of positive pressures.

Abdel-Latif et al. (1985) studied steady-state thermohydrodynamic behaviour of circular pad thrust bearings and developed a numerical methodology to solve governing equations. To solve the problem they used Reynolds equation, energy equation of the oil film and heat conduction equation of the bearing, assuming evenly dispersed bubbles. Variations in oil density and viscosity due to the presence of bubbles are considered, as well as pressure and temperature effects. Significant changes in load carrying capacity and friction losses were not observed. The bearing temperature rises a little for larger amounts of gas. In the same way as for previous works, the authors concluded that the bearing become more unstable as the bubble content increases, due to the downstream shift of the centre of pressure.

A series of works performed by Someya and collaborators have developed and explored a model for bubbly oil lubrication. Initially, Kawase and Someya (1985) studied circumferential pressure distribution in a dynamically loaded journal bearing, and investigated the influence of bubbles on the performance of isothermal bearings.

The oil film pressure was measured both in the journal and bearing and the results for a steady-state case were compared with two numerical models of bearing lubrication. The first considers an incompressible fluid composed of oil only and uses Reynolds condition on cavitation. The second model considers the lubricant a mixture of oil and uniformly dispersed bubbles. In this case, in addition to Reynolds equation to lubrication, another equation is necessary to determine the radius of bubbles along the bearing, since they are subjected to isothermal expansions and compressions; inertia and viscous effects of bubbles were neglected. Reynolds equation is solved using finite differences while the bubble radius equation uses a Newton-Raphson procedure. The two-phase model does not require a different boundary condition at cavitation since it is directly captured. In comparison to experimental results, the two-phase model showed better agreement, but also a larger positive pressure region. In addition to that, it reproduced negative pressures measured, which was not observed in the first model.

In the sequence, Natsumeda and Someya (1986) experimentally studied pressure distribution in a journal bearing under static and dynamic loading. In statically loaded journal bearings a sharp negative dent was observed just after minimum film thickness position, and the fluid film was kept near atmospheric pressure afterwards. Under dynamic loads, two distinct patterns of negative pressure were observed: one similar to the static load case (sharp dent), and the other with a considerable region of negative pressure, similar to the Sommerfeld condition. To explain these negative pressures, a numerical model is proposed treating the lubricant as an emulsion of oil and small dispersed bubbles. The lubrication equation is solved via finite differences while the equation for bubble radius is solved using a Runge-Kutta method. The relation between void fraction and radius of bubbles is known, as well as density and viscosity as a function of void fraction. The model presented a negative pressure dent, which is deeper and sharper as eccentricity increases (heavier loads). The model also predicts a region with negative pressures but close to atmospheric condition just after the negative dent. For some conditions, it is believed that film rupture can occur, but the model does not predict it since atmospheric pressure is the boundary condition at the bearing ends and air suction is ignored.

Still using this approach, Someya (2003) studied the development of negative pressures in the oil film of journal bearings and its influence in bearings performance, taking into account a bubbly oil. A constant mass of gas is considered to be

homogeneously dispersed in the oil in the form of spherical bubbles, all with the same radius. No evaporation, condensation or diffusion of gas occurs, and the bubbles can only expand or contract. These changes in bubble size are determined from the equation for bubble dynamics, where surface dilatational effects are taken into account. The solution for this equation determines bubble radius, and then void fraction can be determined. This enables the density of the homogeneous mixture to be calculated and used in the solution for the Reynolds equation. The viscosity of the mixture is determined by an empirical correlation. Testing bubble parameters, he concluded that maximum pressures are not affected by the presence of bubbles, as these are under strong compression in the positive pressure region. Compared with Reynolds solution for incompressible flow, for low loads there is an increase in bearing load capacity when negative pressures are developed, and the opposite occurs for heavier loads. The development of negative pressures in the film also tends to move outwards the locus center of the shaft. Someya also commented the careful treatment of the numerical solution, where there was a delicate dependence of the convergence with the under-relaxation parameter. Furthermore, Someya suggests that the magnitude of negative film pressure is limited to a value where rupture of the film occurs.

Feng and Hahn (1986) proposed density and viscosity models for homogeneous two-phase liquid mixtures to study cavitation in hydrodynamic dampers. They considered that the influence of oil in the gas phase is negligible due to its low vapour pressure and then correlations are developed as function of film pressure and known mole fraction of the noncondensable gas in relation to the liquid at the entrance. Ventilation is neglected, i.e., no extra gas is drawn from the ambient. The authors studied cases either where gas can re-dissolve in the oil or not, called collapse and noncollapse models respectively. It is believed that a real situation lies between the two extreme cases. The same is assumed in regard to isothermal and adiabatic conditions. The density of the mixture is determined analytically, while for the viscosity an analysis of the most commonly adopted correlations is performed. In the end, they suggested the Hayward correlation, which predicts an increase in viscosity with the increase of gas void fraction. Analysing the models, they concluded that noncollapse bubbles can have greater influence on density of the mixture for very low or very high pressures. They also pointed to the lack of data for viscosity behaviour with pressure for air/oil mixtures.

Zeidan and Vance (1989) investigated the cavitation phenomenon in squeeze film dampers, using high speed photography to verify the occurrence of vapour and gaseous cavitation. Pressure measurements pointed to a region in which values are almost constant, associated with the occurrence of gaseous cavitation. Furthermore, they concluded that at high speeds, after such occurrence the flow develops into a situation where two-phase homogeneous mixture of oil and gas is observed in the whole bearing, suggesting that such effect must be incorporated into a compressible lubrication model to evaluate more adequately the performance of squeeze film dampers.

Chamniprasart et al. (1993) extended the hydrodynamic lubrication theory to mixtures of newtonian liquid and ideal gases. Considering interaction between the mixture components, two coupled equations are obtained to the density of components. As opposed to the usual methods that propose a correlation for viscosity of the mixture as a function of void fraction, the proposed model does not require calculations for viscosity of the mixture, since its effect is a result of the solution of generalised Reynolds equations. Considering slip between air bubbles and the liquid, velocities for each phase are obtained from respective momentum equations. Conservation of mass for each component enables a pressure equation to be obtained, whose solution is possible if constitutive relations for partial pressure and density of each component are available. Two coupled equations for partial densities are then obtained, and these equations are finally solved to a finite isothermal journal bearing. Cavitation is only considered by the increase in void fraction, without a specific algorithm. It is verified that the amount of gas present in the fluid film affects considerably the pressure on the film, but bubble size only affects the extension of cavitated region.

Qi et al. (1997) studied experimentally the viscosity of bubbly oils, proposing its measurement with a rotary viscometer. After measurements of viscosity for a specific oil, a numerical model is proposed to reproduce the effect of bubbles. A modified Reynolds equation is derived and it considers variations in density and viscosity of bubbly oil with pressure. This equation is solved for a journal bearing, and its results are compared with the previously obtained experimental data. Differently from previous works, it is verified a reduction in load carrying capacity in the presence of bubbles, mainly for small eccentricities. However, reduction in friction force is confirmed, though it is negligible.

Nikolajsen (1999a) derived analytical models for density and viscosity of bubbly oils in fluid film bearings. Taking into account effects of film pressure, film geometry, aeration rate and bubble surface tension, it is confirmed the experimental evidence of higher viscosity of bubbly oils in comparison to pure oils. Density of the mixture considers the mass of gas dissolved, air-oil surface tension and mean bubble radius. Viscosity in turn presents two contributions: the first one tending to reduce lubricant viscosity due to the lower viscosity of the gas, while the second tends to increase it due to surface tension effects. After obtaining correlations for density and viscosity, simulations showed that a reduction in density occurs for increases in bubbles population, as well as for higher pressures and smaller bubble radius (but at constant air content). The viscosity of the bubbly oil was observed to be higher than that of pure oil for the entire range of parameters investigated, which leads to the conclusion of dominance of surface tension effects. Finally, as apparent properties for bubbles are already known, the Reynolds equation can be solved as usual and as increase in load carrying capacity is expected due to the increase in viscosity.

In the sequence, Nikolajsen (1999b) used the previous developed models to evaluate load carrying capacity of infinite journal bearings lubricated with aerated oil. Reynolds equation is solved replacing density and viscosity of pure oil for those apparent properties derived for aerated oil. Using half-Sommerfeld condition for cavitation, it is verified that surface tension effects can even duplicate load capacity, while compressibility effects seemed to be negligible. Based on these results, it is concluded that aeration of the oil can be a potential tool for controlling bearing dynamic behaviour.

Chun (2002) examined the influence of aerated oil on high-speed journal bearings with angular velocities between 20,000 and 80,000rpm. Density and viscosity models developed by Nikolajsen (1999a) are used, but Reynolds and energy equations additionally consider turbulent flows. Additional parameters are included, such as convection on bearing walls, mixing between recirculating and inlet oil and shaft misalignment. Results are obtained from a numerical solution using finite differences methodology, and they suggested that load capacity can be increased if higher aeration levels and smaller bubbles are used. The load capacity of journal bearings lubricated with aerated oil tends to increase considerably at higher degrees of misalignment due to

the surface tension effects in the region of the flow with higher shear rates. Power consumption however is not significantly affected by oil aeration.

Choi and Kim (2002) theoretically analysed the influence of evenly distributed air bubbles in lubricating oil on the performance of a steadily loaded journal bearing. A numerical model solves Reynolds equation for a homogeneous fluid considering Reynolds condition for cavitation, and it also solves an equation to determine bubble radius along the bearing. Assuming constant the mass of gas and that bubbles do not split or coalesce, the authors showed that load carrying capacity increases as smaller bubbles are fed into the flow and as surface tension increases. The increase in void fraction results in an increase in load up to a critical level, after which the load is reduced. This critical value is associated to the fact that compressibility effects became of the same order as those of surface tension.

Almqvist and Larsson (2002) investigated the possibility of solving the thermal elastohydrodynamic (EHL) contact problem using Navier-Stokes equations instead of the Reynolds equation. A commercial CFD software, CFX, is used. As cavitation cannot be solved using the common pressure boundary conditions at film rupture, they artificially modify the density when p_{cav} (cavitation pressure) is reached: a second order polynomial is used to interpolate density down to zero. The choice of the fit does not affect the solution, as pressures in the cavitated region are much smaller than those in the EHL contact. Although artificial, this solution does not require any modification to satisfy continuity, because pressure is a result of it. However, solutions had a very high computational cost due to the use of very small under-relaxation factor and slow convergence rate to avoid numerical instabilities.

Great contributors to the study of bubbly oil mixtures in squeeze film dampers are San Andrés and collaborators. Tao et al. (2000) proposed a continuum model to describe the motion of a bubbly oil in an open ended damper operating with circular centred orbits, comparing the results obtained using a robust finite difference procedure against a test rig with controlled air and oil mixture. The model considers a known composition of the mixture, such that the mass of gas is constant. However void fraction varies as pressure changes through the damper, being also affected by surface tension effects. The results agree with the experiments in pointing the reduction in damping as the amount of air increases, but concerns related to the viscosity correlation used are believed to be the source of difference. Diaz and San Andrés (2001) advance

the previous model by adding an empirical formula to estimate the amount of air entrained in a damper, which enables the authors to identify the likelihood of air entrainment in the bearing, when the operation significantly changes. San Andrés and Santiago (2004) derive damping and inertia force coefficients from a squeeze film damper test in several dynamic load conditions. The two-phase flow model previously developed is still used, and in this work assists in determining the effective damper length. Upon this appropriate estimation of effective length, good agreement is observed for damping force coefficients.

Simultaneously to the development of the present work, Ng (2007) performed a thorough investigation on the bubbly oil occurrence in squeeze film dampers. A homogeneous two-phase model is considered, now allowing gas to be released from the oil, in addition to pre-existing air bubbles. This work is one of the first to successfully investigate the viscosity of bubbly oils experimentally, using a modified cone-and-plate rheometer that could enclose the bubbly mixture. Additionally, a simplified oscillatory squeeze film experiment was performed to gain insight in the dynamic behaviour of the damper under bubbly oil lubrication. According to the results, both experimental and numerical, the bubble distribution strongly depends on supply pressure and operating frequency, affecting the damper by increasing stiffness and decreasing hydrodynamic inertia and damping effects. It is mentioned that further investigation should consider improving solubility correlations, restricted by the use of a general Henry's law.

2.4 OIL AND REFRIGERANT MIXTURES

A typical vapour compression refrigeration system is illustrated in figure 2.8. To increase the pressure of the refrigerant in the hot part of the cycle, a compressor is used. Ideally only refrigerant gas enters the compressor and leaves with a higher pressure and temperature. In the sequence, heat is removed in the condenser and the gas turns into liquid. Next, the liquid refrigerant flows through an expansion device, usually a capillary tube, reducing its pressure. Afterwards, the refrigerant reaches the evaporator, where it absorbs heat while returns to gas phase, and finally returns to the compressor, restarting the cycle. The lubricant oil is used only during compression,

reducing friction between moving components, cooling hot parts and sealing against refrigerant leakage.

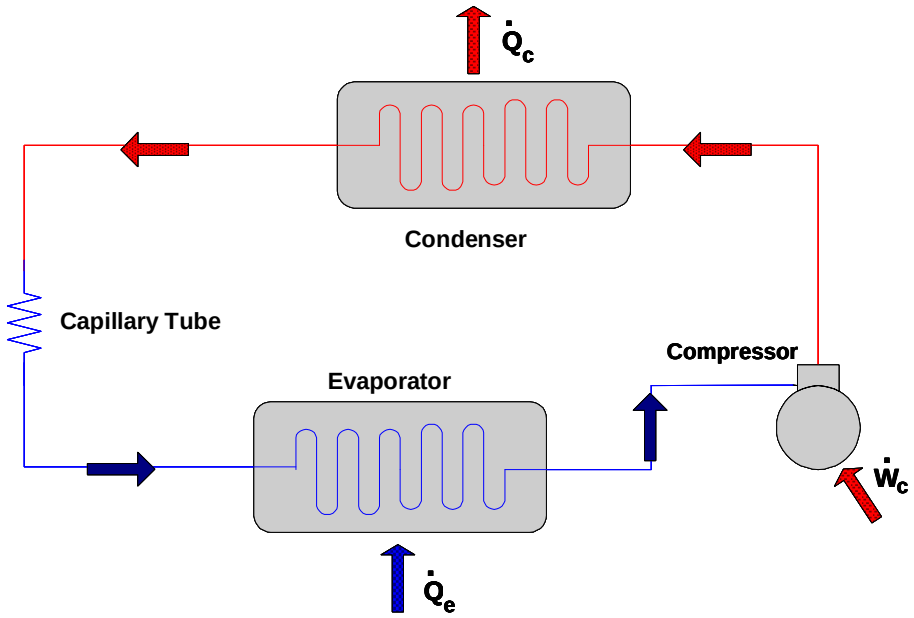

Figure 2.8. Diagram of a typical vapour compression refrigeration system.

The presence of two fluids inevitably leads to their interaction, and actually a mixture of refrigerant and oil, in several proportions, is observed along the circuit. This influences the performance of the whole system, including the compressor and its lubrication. Under these conditions, the refrigerant must have a good solubility in the oil to guarantee its return to the compressor – in which case, despite reducing system efficiency, avoids the harmful accumulation of oil outside the compressor. As an unfavourable aspect, the oil reduces condenser and evaporator efficiencies.

Therefore the choice of a pair refrigerant and lubricant is much more critical than simply defining a refrigerant capable of performing required heat exchanges of the circuit and an oil that lubricates adequately compressor moving parts (Grando, 2001). It is necessary to know, beyond refrigerant and oil characteristics and their expected performance, their physical properties and the behaviour of their mixture.

To perform its functions, it is desirable that the oil possess a high viscosity. On the other hand, fluidity is necessary to its return to the compressor. In addition to those, being the compressor hermetic, the oil must be durable as it will not be replaced during the compressor life cycle – the oil needs to present chemical stability in the presence of refrigerant, metals, motor insulation and other external contaminants. The stability of the oil/refrigerant mixture affects the cleanness of the system, since it is necessary to

avoid carbon deposits that promote wear and compressor failures. This reaffirms that a carefully decision has to be made when choosing the pair oil and refrigerant to meet the requirements of the refrigeration system.

There have not yet been performed studies relating mixture properties and compressor lubrication. However, several experimental works analysed the influence of a pressurised refrigerant atmosphere in the lubrication of components, which permits an overview of the mixing effects in compressor lubrication. Other works have also dedicated attention to characterise oil/refrigerant mixtures and their flow. Both of them are reviewed in the sequence.

2.4.1. Characterisation of Oil/Refrigerant Mixtures

Considering oil in a refrigerant environment under equilibrium conditions, refrigerant dissolves in the oil and creates a liquid mixture, with both phases in liquid state. As the vapour pressure of the oil is very small, the free gas phase can be assumed to be composed only of gas refrigerant. In saturation conditions and a mass basis, the amount of refrigerant dissolved in the oil for determined pressure and temperature conditions is defined as *solubility*, and it can be seen as the most important property to characterise an oil/refrigerant mixture. Figure 2.9 presents the solubility curve for a mixture of refrigerant R134a in the polyolester oil EMKARATE RL10H, which behaves as a typical oil and refrigerant mixture, increasing solubility with increasing pressure and decreasing temperature.

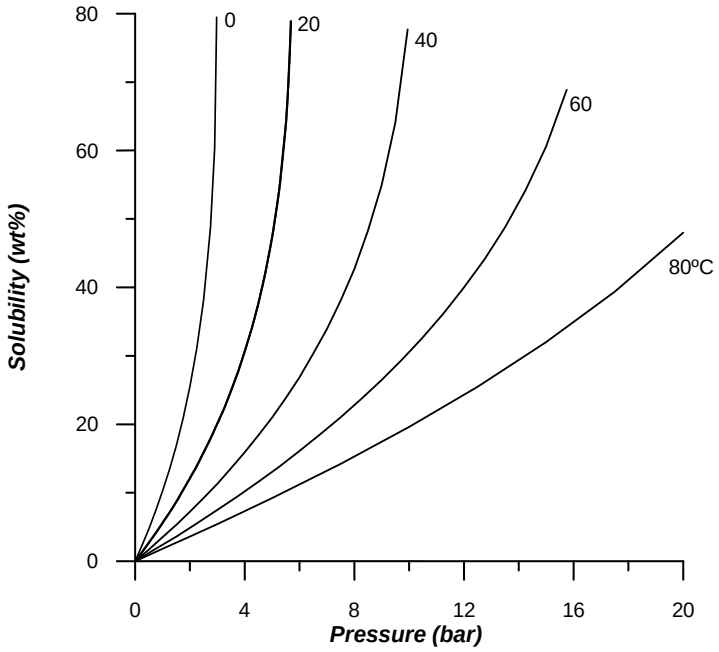

Figure 2.9. Solubility (mass fraction) of refrigerant R134a in polyolester oil EMKARATE RL10H.

If solubility is known, additional thermophysical properties of the mixture can be determined, such as density and viscosity. Alternatively, the mixture can contain only a fraction of the refrigerant dissolved in saturation conditions, when it is called a subsaturated mixture. Nevertheless, the properties can still be determined. Several works deal with determination of the thermophysical properties of these mixtures, such as Thome (1995), Conde (1996), Motta et al. (1998, 2000) and Mermond et al. (1999). They also need to take into account variation of properties of the base fluids with pressure and temperature. The gas phase, composed only of refrigerant, also need to have its properties determined. Appendices A and B present these properties in more details, as well as correlations to their determination. In a general way, the following behaviour can be observed:

- Viscosity of the mixture decreases with increasing temperature and also with increasing refrigerant mass fraction;
- Density of the mixture decreases with increasing temperature but increases with increasing mass fraction, as liquid refrigerant is usually heavier than the oil;
- Regarding gas properties, it is usually observed a decrease of density with the increase of temperature and decreasing pressure (compressibility effects), which is also observed for the viscosity. Not rarely these properties are neglected, as the density of the liquid is around 100 times bigger than the gas density, while for the viscosity this is of an order of a 1000 times.

An area where increasing attention has been given is the transient absorption of refrigerant in the oil, as opposed to the equilibrium condition only that is found in the previous literature. The research has been focused on understanding and modelling the mass diffusion mechanism, which assumes in principle very slow rates.

Yokozeki (2002) proposed a numerical model considering a one-dimension mass diffusion process, occurring due to the gradient of concentration in a flat bottom container filled with oil to a certain height. The model has been tested to determine the diffusion coefficient and solubility limit for dissolution in oil of both water vapour and refrigerants. The author indicates that the experimental data validates the model.

Silva (2004) explores experimentally and numerically the transient absorption of refrigerant in the oil using the conservation equations governing the phenomenon coupled with the thermodynamic equilibrium relationships, previously determined experimentally. The use of this procedure enables the properties to be determined for

any pressure, temperature or concentration. He also briefly explores the kinetics of the gas absorption in liquids.

Gessner and Barbosa Jr. (2006) studied the problem of absorption of refrigerant vapour in a stagnant layer of lubricant oil, describing the bulk motion of the solute in terms of apparent diffusion coefficients. It was studied both bi-component and multi-component mixtures. Comparing with the experimental literature data, binary pair diffusivities are in the order of typical molecular diffusivities of liquids. The results for multi-components agree with the literature, although slightly underpredictive. The authors acknowledge that further experimental and theoretical work is required to advance in the understanding of the problem.

In addition to determining the properties of the mixture, it is also desirable to have an understanding of the behaviour of the mixture under flowing conditions, which includes the existence of two-phases, the liquid oil/refrigerant mixture and the refrigerant gas phase. The gas phase usually appears under negative pressure gradients, where solubility decreases and then the excess of refrigerant is released in the form of bubbles. Until this moment, simpler geometries have been used in the study of the flow of oil/refrigerant mixtures. The following works have investigated this flow in small diameter circular pipes:

Lacerda et al. (2000) experimentally characterised the flow of the oil/refrigerant mixture, measuring pressure and temperature along the pipe and exploring aspects as changes in solubility, quality and void fraction throughout the flow. Furthermore, visualisation of the flow of a R12/SUNISO 1GS mineral oil was performed using a glass pipe. Dispersed bubbles were observed close to pipe entrance, while a great population occurs in an intermediary section. The spherical shape of the bubbles is an indication of homogeneous flow, with both phases mixed and with similar velocities. Next to the end of the duct, void fraction is high and aspects of foam formation are observed. Figure 2.10 presents a scheme of the flow and the visualisation for different positions along the tube. Poiate Jr. (2001) achieved similar conclusions for a test with the similar mixture, and Castro et al. (2004) studied this flow for a mixture of HFC134a with a synthetic oil.

Grando (2001) modelled the flow of the oil/refrigerant mixture in the small diameter pipe characterised by Lacerda et al. (2000), splitting it in two different regions: an initial one of bubbly two-phase flow, with smaller quantities of released gas, where

the mixture is treated by a homogeneous model with pseudo-properties based on averages of those from the mixture phases, and a second region of foam flow, where the gaseous phase is dominant and the fluid is treated as non-Newtonian. The main parameters of the flow are studied (pressure, temperature, mass fraction and void fraction), and the results are compared with experimental data from Lacerda et al. (2000), observing a good agreement. The model depends on correlations for the properties of the mixture, and some adjustment coefficients are still present due to the inaccuracy of some correlations, mainly when the uncertainty in the calculus of viscosity is acknowledged.

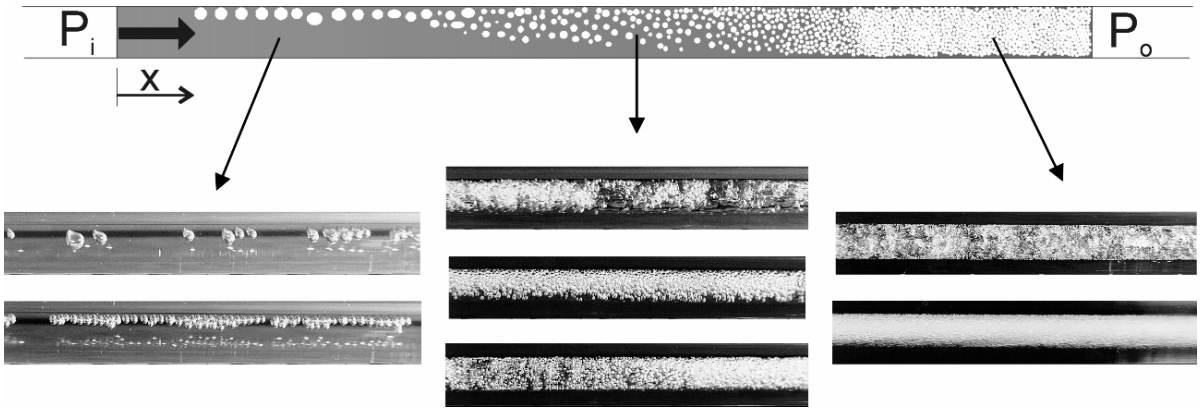

Figure 2.10. Visualisation of the oil/refrigerant mixture flow (Lacerda et al., 2000).

Barbosa Jr. et al. (2002, 2004) analysed the suitability of the available methodologies for predicting pressure drop due to friction in two-phase flows of the oil/refrigerant mixture. Several methods have been tested, and none of them predicts reasonably the pressure drop in the large range tested by Lacerda et al. (2000). The authors proposed then an adapted correlation which considers the relative content of oil in the mixture, the relative content of vapour and inertia effects, which leads to a 26% error (RMS) compared to experimental results. The main reasons for this deviation are attributed to the metastability on gas release, to the mass transfer, to the selective adsorption in central region and also to the foam formation at the end of the pipe.

2.4.2. Lubrication in a Refrigerant Environment

Two main areas are submitted to lubrication inside the reciprocating compressor: lubrication of cylinder, piston and rings (when available), and the lubrication of the crankshaft, which also comprises pins, bearings and guides. Some of these components can be observed in the mechanism represented in figure 2.11.

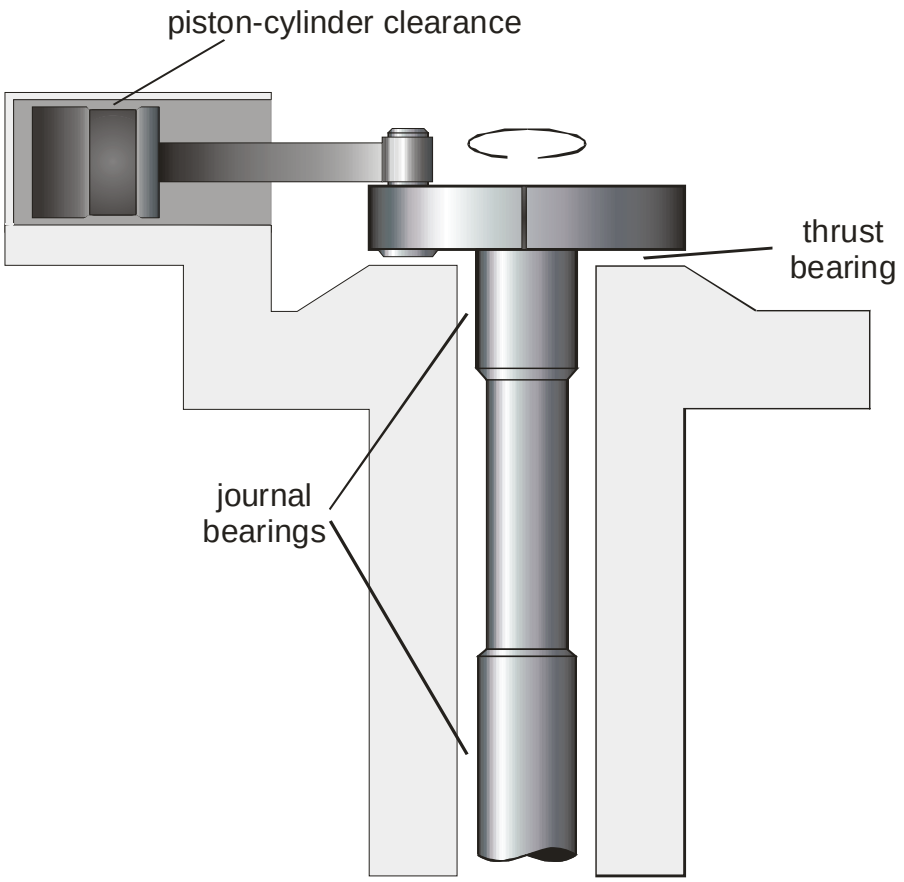

Figure 2.11. Piston and bearings present inside a reciprocating compressor.

The bearings and other components of the second group usually require larger amounts of lubricant, while cylinder lubrication has to be performed with the minimum lubricant capable to provide a strong lubricant film, minimizing friction and wear, sealing compression chamber and avoiding corrosion. Nevertheless, both sets have been designed to work in hydrodynamic lubrication regime, and suffer influence from the inevitable mixture occuring between oil and refrigerant.

Hydrodynamic lubrication, where a thin film is established between surfaces and where load is supported by pressure generation, is usually obtained in a well-designed system working in conditions of normal operation (steady-state). Nevertheless, during compressor start or stop, and during an overload or failure due to defective lubrication, boundary lubrication can occur and then contact between surface irregularities will be observed. A reasonable project must predict the occurrence of boundary lubrication.

Refrigerant dissolution in the oil provokes a reduction in lubricant viscosity, resulting in a lower capacity of the film between surfaces to support load, which can lead to contact between surfaces. Additionally, the decrease in viscosity can affect the leakage of gas through the piston-cylinder clearance, reducing pumping efficiency of

the compressor. On the other hand, the solubility of refrigerant in the oil tends to reduce equalisation pressure inside compressor shell when compressor is shut down, thus reducing starting torque and consequently the power required during compressor's initial operation. As a result, less quantity of copper is necessary in the motor, reducing compressor final price, since copper is one of the most expensive components of the electric motor.

The release of gas occurring when the film experiences negative pressure gradients is also another relevant factor. In critical situations, foaming can occur, which can increase power consumption due to the higher viscosity of the foams, or even failures in lubricant feed, leading to boundary lubrication and increasing wear.

Kruse and Schroeder (1984) discussed in details aspects related to the influence of oil in the various components of refrigeration systems, pointing positive and negative aspects. The work presents the basic requirements for the oil to a reasonable operation in the refrigeration system. It is recommended that the oil presents high surface tension to avoid foaming of the oil/refrigerant mixture, good thermal and chemical stability and viscosity enough high to keep a hydrodynamic lubrication during compressor operation. On the other hand, to permit the maximum return of oil from the system to the compressor and to produce the least impact on the remaining components, the oil must present high miscibility with the refrigerant such that a lower viscosity occurs. In extreme conditions, oil solubility is expected to be even higher to keep fluidity in a wide temperature range, very low water solubility and it should not split into paraffins.

Akei et al. (1996) experimentally investigated the effect of refrigerant in the film-forming capability of the lubricant through measurements of film thickness under pressurized refrigerant atmosphere. They tested mixtures of R12 and mineral oils as well as R134a with synthetic oils, polyalkylene glycol and polyol ester. Film thickness is evaluated by optical interferometry in an apparatus that contains a steel ball and a transparent disk. The speed of the ball and disk are monitored, as well as the oil temperature and the applied load. Elastohydrodynamic lubrication is observed, and it is verified that film-forming capability is highly affected by refrigerant pressure, since film thickness gradually decreases with the increase of the environment pressure due to a greater quantity of refrigerant dissolved in the oil and the consequent reduction in viscosity. On the other hand, an increase in oil temperature reduces refrigerant solubility in the oil and produces the opposite effect in relation to pressure increase.

When comparing the different mixtures, the authors concluded that pure mineral oils have superior film-forming capacity than synthethic oils, but this ability is reduced with refrigerant solubility and their behaviour become very similar. The performance of synthetic oils is almost identical. These results reinforce that the lubrication capacity of the mixture cannot be simply estimated from oil properties.

Na et al. (1997) have experimentally tested the behaviour of oils in compressors considering a rich refrigerant environment inside; miscibility and material compatibility tests are included aiming to develop a methodological way to proper selection of oils to improve durability and performance of compressors. Lubricity is determined by measuring friction force in a disc rotating over a pin or ball specimen under a refrigerant pressurized environment. Testing the system with mixtures of CFC-12 with mineral oils and of HFC-134a with polyalkylene glycol (PAG) and polyol ester (POE) synthethic oils, they concluded that refrigerant solubilty in the oil reduces viscosity and the friction coefficient. The increase in temperature also reduces friction due to reduction in oil viscosity, suggesting that lubricants with higher viscosities are needed to keep a hydrodynamic regime. Considering wear and extreme contact pressure conditions (elastohydrodynamic lubrication), PAG oil in HFC-134a environment is the most stable mixture, but ester oils present greater lubricity in start/stop situations (boundary lubrication). Despite this work provided good comparative results, the authors suggested that longer duration tests need to be performed.

Safari and Hadfield (1998) evaluated the influence new combinations of refrigerant and lubricant (alternatives to CFC-12 and mineral oils) have on the wear performance of domestic compressor refrigerators. They have tested during 500h a standard refrigeration cycle operating with HFC-134a and three synthetic oils completely miscible with the refrigerant and presenting distinct viscosities. After the test, the compressors were dismantled and the polished surfaces were analysed via Scanning Electron Microscopy (SEM) and Electron Surface Chemical Analysis (ESCA), with special attention given to the interfaces between piston, gudgeon pin and connecting rod. They verified that wear is more severe in the case of the lubricant with the lower viscosity, resulting in a surface roughness much smaller than that of the compressor running with the lubricant of higher viscosity. The latter also presents minimum plastic deformation. Nevertheless, with the higher viscosity oil the set presented bulging, which may be a result of cavitation – and which also can cause

vibration problems. But this work confirms that oils with higher viscosities present a greater capacity to maintain a lubricant film.

Ciantar et al. (1999) evaluated tribological characteristics related to the conforming contact between the die-cast aluminium alloy connecting rod and the hardened steel gudgeon pin of a reciprocating compressor. Testing three polyol ester synthethic lubricants distinguished by their viscosity in compressors working with HFC-134a, they concluded that the surface wear strongly depends on the viscosity of the lubricant/refrigerant combination used. For low viscosity oils a boundary lubrication regime was observed as well as severe wear, material transfer and friction. In addition to that, some oil decomposition was verified in the presence of steel and low temperatures, and the use of metal passivators is then suggested. In the higher viscosity combination, the absence of metallic contact signs is the indication that a permanent lubricant medium was present.

In the sequence, Ciantar et al. (2000) evaluated the performance of a new class of polyvinylether (PVE) lubricants in comparison to the polyol ester oils used in hermetic refrigerating compressors operating with HFC-134a refrigerant. Observations using scanning electron microscopy, energy-dispersive X-ray micro-analysis and X-ray photoelectron spectroscopy, among others, allowed to verify that the typical abrasive wear mechanisms occured for both of the lubricants tested. Therefore the anti-wear improvements atributed to the PVE, particularly the formation of a solidified film, have not been exhibited. In addition to that, the PVE seemed to be more chemically active on interfacing surfaces, particularly in that of aluminium, which resulted in more significant wear in the connecting rod. On the other hand, the wear on the steel pin was more significant with the POE oil. The authors also suggested that further investigation should be carried out to explain the mechanisms involved in the surface reactions of alluminium on the presence of PVE oil. A detailed description of these tests, adding also new oil-refrigerant combinations, was made by Garland and Hadfield (2005).

Fukui et al. (2000) tested the applicability of refrigeration lubricants with new chemical structures (fluorinated alkyl aryl ethers) in a HFC-134a environment. The polar structure of these oils suggests that the problems of poor stability and high moisture absorption observed with PAG and POE oils can be eliminated. Tests carried out showed that these oils have high miscibility with HFCs and high stability, as well as low moisture absorption, which could enable easy handling during production and

installation of refrigeration systems. Hydrolysis was observed to be smaller than that of the POE oils, leading to a more reliable operation. The new lubricants have lubricity as good as that of mineral oils. The authors considered the use of the new oils suitable for refrigeration systems; nevertheless, compressor operation tests were not carried out.

Further works have been carried out always reaching similar conclusions. E.g., Tuomas and Isaksson (2007) investigate film forming capability and wear for different oil compositions under distinct refrigerant environments. Using a capacitance method to monitor lubrication in a ball bearing experiment, they could initially verify the poorer lubrication conditions using a base POE oil with HFC-134a in comparison to a mineral oil and HCFC-22. However, they could overcome the difference with the use of additives, such as acid phosphate or phosphate ester, with the latter showing also similar wear levels as the mineral oil mixture.

From the previous reviewed works, it is evident the necessity of establishing correlations that consider the mixture of oil and refrigerant to calculate the properties of the fluid circulating through the refrigeration system, since interaction between oil and refrigerant alters significantly the operation of components. Additionally, it should be stressed that a good miscibility between oil and refrigerant is required to a satisfactory operation of the system, as well as good thermal and chemical stability is required to the oil to be durable. It is also verified that higher viscosity oils can maintain a hydrodynamic lubrication regime during most part of the cycle. On the other hand, their higher viscosity promotes a significant increase in power consumption due to friction on the piston.

2.5 PISTON LUBRICATION

The reciprocating movement of the piston inside the cylinder, induced by the connecting rod, determines how the gas will flow along the cycle in the equipment, which can be either an internal combustion engine or a compressor, or even others. In each cycle, there is at least one sub-cycle of suction and another of discharge/exhaust.

To enable an increase in efficiency during operation, it is necessary to achieve minimum gas leakage along the piston length. Thus the clearance between piston and

cylinder must be very small, promoting fluid sealing in the compression chamber, usually with the help of a lubricant. This can be performed with rings fixed to piston surface, as observed in the majority of internal combustion engines. This solution is normally adopted in larger sets and reflects in less power consumption due to friction. Additionally these sets can have maintenance or readjusting due to wear.

On the other hand, lubrication can be directly performed between piston and cylinder walls, in which case the clearances are much smaller than those of the previous case. This set is encountered in systems of smaller dimensions, usually hermetic, where the use of rings is almost impossible and maintenance is not an option, since the durability expected for the set is the same as the life-cycle of the product. An example of this configuration is the reciprocating compressor used in domestic refrigeration equipments, already presented in figure 1.1 and 2.11.

Even if the alternative motion is the only desired for the piston, the existence of the radial clearance leads to secondary movements, which in turn are fundamental in determining the gas leakage, friction power losses, wear and noise of the engine or compressor. Considering internal combustion engines, secondary movements also influence fuel and oil consumption as well as gas emissions.

Piston secondary movements in the piston-cylinder clearance occur due to the freedom of rotation about the wrist-pin joining connecting rod and piston, as well as due to clearances and misalignments resultant from the set assembly. To determine these movements it is necessary to perform the balance of the forces acting on the piston (dynamic equations). The main forces are schematically shown in figure 2.12.

Hydrodynamic force and viscous friction are determined after solving the problem of fluid film lubrication in piston-cylinder radial clearance. Generally a hydrodynamic lubrication regime is observed, but boundary lubrication can also occur due to the small velocities observed near bottom and top dead centres.

The complete study of piston lubrication inside the cylinder is of great importance to piston design, since it enables to determine the ideal clearance for operation. If the clearance is too small, great sealing is obtained but at the cost of enormous friction power losses. On the other hand, less power consumption occur in larger clearances but with a decrease in pumping efficiency due to greater gas leakage. Therefore, in addition to the optimisation of the clearance for an improved performance,

an accurate study can determine if piston movement is smooth and stable and whether it maintains constantly a minimum oil film separating piston and cylinder walls.

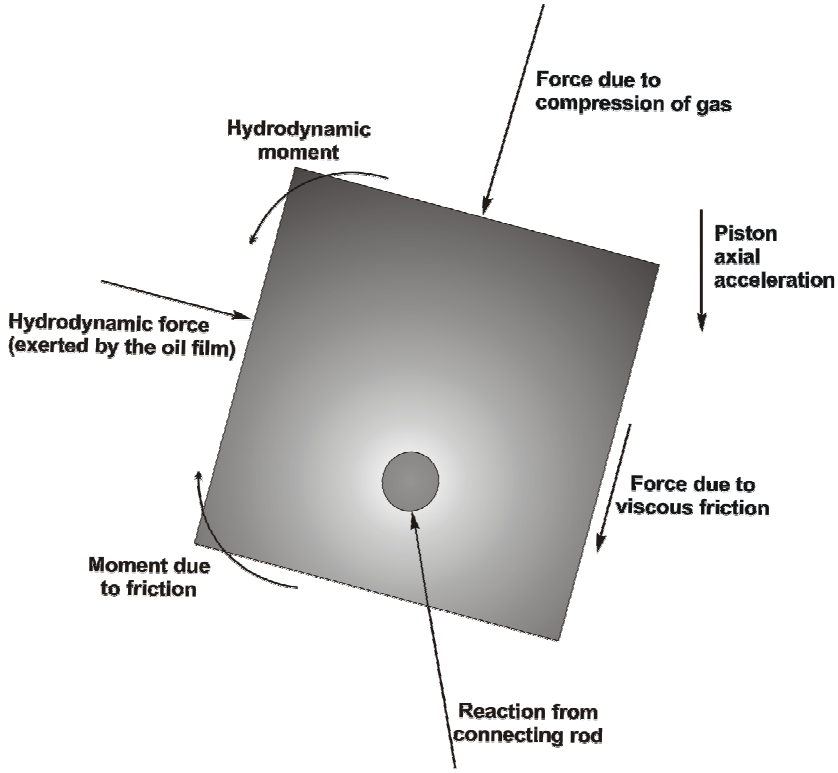

Figure 2.12. Main forces acting on the piston in reciprocating movement.

The impact between piston and cylinder was one of the first aspects considered in the study of their interaction, mainly because it is an important source of noise in the engine together with blow-up of combustion gases. The shock between piston and cylinder is one of the major responsibles for instabilities and lateral oscillations during the piston reciprocating motion.

Repaci (1987) developed a model for simulation of piston movement in a diesel engine, with particular attention to piston slap. Connecting rod-piston set is modelled as a double pendulum and presents two degrees of freedom when the crankshaft angular velocity is known. As the pressure curve in the compression chamber is also available, only the balance of forces and moments about the pin needs to be solved. These equations are integrated by a Runge-Kutta procedure at each time step when impact is not observed. Otherwise piston velocity is determined by dynamic equations of impact, as well as kinetic energy losses. The model allows changes in parameters of the motion (connecting rod-piston offset, gas pressure and lubricant viscosity) and is coherent with conclusions of previous experimental works.

Wlad and Weckas (1989) developed an experimental model to the interaction between cylinder-bore and piston-ring based on the measurement of oil film thickness between them and considering as main parameters ring velocity, cylinder temperature and bore-ring contact pressure. The latter is the hardest to obtain, being calculated from the solution of Reynolds equation for a parabolic ring. Simulations performed in the experiment were obtained in times considerably smaller than those performed in real engines, but their results were quite similar.

Gerges et al. (2002) have analysed the influence of lubrication on piston slap. The Reynolds equation is used to evaluate numerically the squeeze film effect on the impact. In addition to the damping effect of the oil, it was also verified that air bubbles, which mix in the oil during the impact, are also important and can significantly reduce impact force. A series of experimental results confirm the agreement of the proposed model, such that the transient behaviour of the impact force can be now determined.

Although piston slap is important, it is more relevant to this work the calculation of piston trajectory during reciprocating motion as well as the forces along the cycle. In this context, works studying piston lubrication are more important. Few works considering ringless pistons are available, since the majority of the works is dedicated to engine lubrication, mainly diesel engines. But piston-ring lubrication is also important as it considers cavitation and wear.

Miltsios et al. (1989) have used finite element methodology to solve governing equations for piston-ring lubrication and also have computed friction force in each ring. The model considers circular rings and a cylinder-bore of elliptical cross-section. The variation of oil film thickness with time is also necessary and the closing equation for the problem is the balance of forces, in which the applied load (available data) is in equilibrium with the hydrodynamic force on the rings. In regions near top dead centre (TDC) and bottom dead centre (BDC) film thickness severely decreases and the friction force is calculated differently, using a friction coefficient considering the film thickness and the surface roughness, characteristic of a mixed lubrication regime. Simulating a diesel engine with three piston rings, it is verified that the first ring (upper) presents hydrodynamic lubrication for almost the whole cycle, while the oil ring (lower) presents smaller film thicknesses and mixed lubrication during most of the cycle. The oil film thickness for the second ring (intermediate) is between the others. The authors also carried out an experiment with the same engine, measuring friction force. The

results from numerical and experimental tests were in good agreement during considerable part of the cycle.

Gommed and Etsion (1993) present a model for dynamical analysis of gas lubricated ringless pistons. The governing equation for lubrication considers a compressible fluid which behaves as an ideal gas. The energy equation is solved for the adiabatic case and, simultaneously with the isothermal solution, serves as the limit for the real thermal conditions of the gas. Piston and connecting rod dynamics complete the equation set. A computational program is developed and tested for a piston of a cryocooler compressor, and the inclusion of dynamics of connecting rod is important to the results. It is also shown that piston is more stable under isothermal conditions. The authors also suggested that additional research is necessary on the design parameters (geometry, dynamic properties and operation conditions) to determine their influence on piston stability.

Fernandes (1996) [Prata et al., 1998, 2000] have developed the first lubrication model with pure oil for the piston inside the cylinder in reciprocating compressors for refrigeration. The secondary motion of the piston is the rotation about the wrist-pin joining piston and connecting rod. The Reynolds equation is solved via finite volume methodology and the cavitation algorithm is used, while equations describing piston dynamics are solved with an iterative Newton-Raphson procedure. The lubricant is considered incompressible and isoviscous. The developed model is used to investigate the influence of several parameters such as wrist-pin position, dimension of the clearance and oil viscosity in piston stability. In addition to the pressure field and piston trajectory, power consumption due to friction is also calculated.

Ma et al. (1997) have developed a model for piston-ring lubrication considering circular and non-circular cylinder bores. The Reynolds equation is solved numerically using finite differences, and both fully-flooded and starvation conditions can be considered. In the latter, an algorithm that guarantees flow continuity is required, using one based on Jacobsson-Floberg conditions. The authors tested the influence of several parameters in lubrication, such as ring face profile, ring gap position and bore distortions, either for a single ring or for full ring pack. The variable ring profile can lead to a smaller power consumption compared to a uniform circular profile. Bore shape also has great influence on minimum film thickness: smaller thicknesses tend to be observed in deformed cylinders, due to failure of the ring to completely conform in

the bore. Friction force, however, does not reflect this strong dependence; in fact, friction force can even be smaller in regions far from the dead centres in distorted cylinders.

Han and Lee (1998) analysed piston-ring lubrication with three different boundary conditions: Reynolds condition and fully-flooded ring, starvation and modified Reynolds condition (with flow separation), and starvation and flow separation (Coyne and Elrod, 1970). All conditions respect conservation of mass, but present very different pressure profiles on the rings. Simulating piston lubrication from a diesel engine with these conditions, the authors concluded that the Coyne and Elrod condition should be preferably used. Due to starvation, they verified that effective ring width can be reduced to about 20-30% at some strokes, while it became almost the entire width near dead centres, indicating more severe conditions (dominance of the squeeze film effect), which also reflects in friction force. They still concluded that minimum film thickness decreases and friction force increases with lesser oil suppled, but this is observed mainly in mid-strokes.

Priest et al. (2000) have investigated sensitivity of mathematical models of piston ring dynamics and lubrication to cavitation boundary conditions. To this end they have applied several cavitation, flow separation and film reformation models to the analysis of a single compression ring from a diesel engine. For a ring defined by parabolic functions, pressure can be obtained analytically from Reynolds equation and the different boundary conditions are used to determine resulting integration constants. An iterative process is only necessary to determine minimum film thickness and squeeze film velocity, which is performed by using the closure equations from the balance of forces. To the several boundary conditions studied, significant differences were predicted in hydrodynamic pressure profiles, oil film thickness, oil flow and friction, and it is concluded that more research is necessary, mainly in works combining theoretical and experimental approaches to the problem. Nevertheless, the authors suggested that Reynolds cavitation and fluid film reformation may be applicable at high loads, while fluid film separation as proposed by Coyne and Elrod at low loads.

The model described in the previous paragraph is also used by Priest et al. (1999) in predictive wear modelling of piston rings in a diesel engine, using fluid film separation as boundary condition and including simulation of the wear of piston rings during engine work. The model has a predictive character and is the first

application of a model which considers simultaneously dynamics, lubrication and wear of piston rings. The model presented encouraging correlation between measured and simulated ring profiles after 120h of engine running, thus already enabling checks of film thickness and friction behaviour with ring wear, and also the problem of the oil-control ring performance. A more advanced model incorporating torsional twisting of the ring is suggested to be included. Extensive research, in both experimental and numerical fronts have been undertaken since, particularly focusing on understanding friction behaviour and also how to minimise it by improving fuel/lubricant properties (Mufti and Priest, 2004, 2005, and Smith et al., 2006).

Priest and Taylor (2000) also analysed how mathematical models of engine tribology are trying to treat the complexities resultant from the incorporation of surface topography. Among the pointed challenges, it is considered of superior importance the inclusion of improved surface profiles, consideration of surface roughness and mixed lubrication to reach better performance and durability of engines. The authors also give special attention to the understanding of lubricant rheology, wear modelling (including considerations of materials, failure, lubrication and thermal effects) and lubricant supply systems.

Dellis and Arcoumanis (2004) have modified a reciprocating test rig, including a charged-coupled device camera and a miniature pressure sensor. With this apparatus, they managed to visualise several and extremely varied transient cavitation patterns that are characteristic of the piston ring and cylinder linear film lubrication. It is confirmed that piston speed and load influence in the appearance and shape of cavities. Encouraged by these results, the authors believe that further efforts in modelling and understanding cavitation can be examined, and through a combined theoretical-experimental approach the level of understanding of piston ring lubrication can advance significantly.

2.6 SUMMARY

The review performed in this chapter focused on various issues related to two-phase lubrication, showing significant differences between a single phase flow and the lubrication considering the existence of a liquid/gas mixture. However, there have

been several assumptions regarding the modelling of bubbly oils, many of those for lack of knowledge on the behaviour of the oil/gas interaction – however much study has been devoted to the interaction between oil and refrigerant, where such flow also occurs. On the other hand, most of the lubrication studies for mechanical components have been based on single phase solutions, using cavitation assumptions for boundary conditions, which led to very distinct results.

In brief, from the revision performed in this chapter, among others, the following conclusions can be made,

- Considering cavitation, the release of gas is a factor leading to the distinct behaviour in the divergent region;
- For bubbly oil lubrication, homogeneous formulations have already been widely applied, but the release of gas was scarcely considered, and when it was, doubts were raised over the lack of knowledge of the oil/gas mixture;
- For the oil and refrigerant mixture, it has been observed that dissolution of refrigerant in the oil occurs, and release at lower pressures leads to a flow where gas bubbles can be finely dispersed in the liquid. Numerical models have been successful in reproducing this flow. There have been extensive studies to understand oil/refrigerant interaction;
- For bearing and piston lubrication models, it was verified that very different results were obtained using different boundary conditions, indicating the great sensitivity of the choice in the final results. It is likely that, if cavitation can be related to fluid behaviour, more universal conditions can be proposed, which could help in the correct choice being made.

In the light of these conclusions, further motivation is given to the study of a two-phase lubrication model where further attention can be given to the existing flow observed in the cavitated region, and particularly with better knowledge of properties and interaction such as is the case for the oil and refrigerant mixture. This will be the focus of the present work for the next chapters.

Chapter 3

A GENERAL TWO-PHASE LUBRICATION MODEL WITH RELEASE OF GAS

In this chapter, the governing equation for lubrication problems is presented. While detailing the most important factors that create load supporting capacity in a lubricated component, discussion is made on how this equation can consider the effect of the presence of gas in the lubricant oil, as a result of previous dissolution and later release under low pressure conditions. In the light of previous studies regarding the solubility of gases in the oil, the main parameters required to characterise an oil-gas mixture are presented. Finally, by coupling the mixture parameters to the governing equation using an appropriate two-phase flow formulation, a general two-phase lubrication model can be proposed and its solution methodology outlined.

3.1 REYNOLDS EQUATION

As the main objective of the problems to be considered in this work is to determine the pressure distribution due to fluid film lubrication, the phenomenon will be governed by the Reynolds equation. Following the analysis performed by Hamrock (1994), this equation is derived in the sequence.

3.1.1. Assumptions

Considering the geometry presented in figure 3.1, the following simplifications are adopted,

- Laminar flow;
- The dimension of the film thickness h is very small compared to the characteristic dimensions in the directions x and y;
- Constant pressure across the film;

- Viscous and pressure effects are dominant, i.e., fluid inertia and gravity effects are negligible compared to the influence of the shear flow;
- No slip between fluid and surfaces;
- Comparing with the velocity gradients across the film, the other velocity gradients are negligible.

Furthermore, assumptions to the fluid properties regarded as valid for most technological applications are made,

- Newtonian fluid;
- Viscosity and density of the fluid are constant across the film (but no restrictions are imposed in the other directions).

In some problems where thermal effects are of great significance, the assumption of constant viscosity in the *z* direction can be questioned. In these cases deriving a lubrication equation would be complicated. Nevertheless, for most applications, despite acknowledging the thermal effects on the viscous flow, the use of the average value of viscosity across the film is satisfactory.

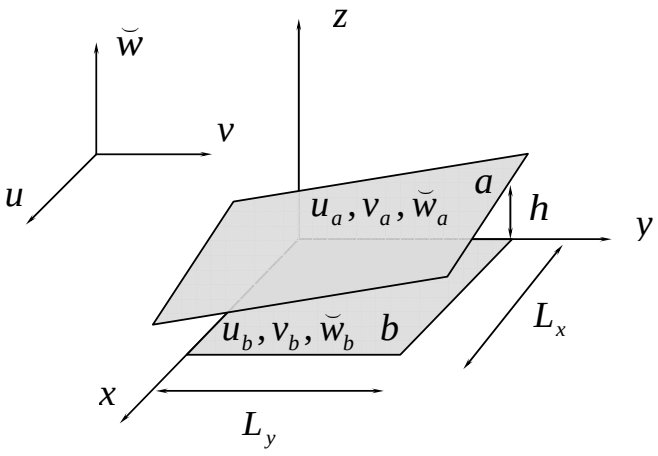

u_a, v_a, w_a : *x*, *y* and *z* velocities for surface *a*.
u_b, v_b, w_b : *x*, *y* and *z* velocities for surface *b*.
L_x : characteristic dimension in direction *x*.
L_y : characteristic dimension in direction *y*.
h : lubricant film thickness (*z* dimension).

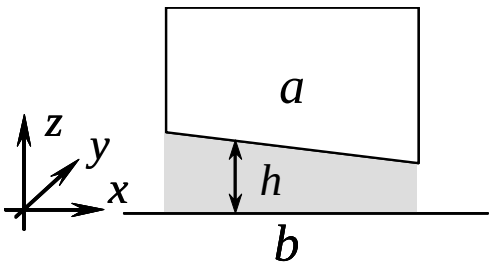

Figure 3.1. Geometry considered to derive Reynolds equation (*xz* plane in detail).

3.1.2. Mathematical Formulation

In the light of the previous assumptions, the Navier-Stokes equations are simplified to,

$$\frac{\partial p}{\partial x} = \frac{\partial}{\partial z}\left(\mu \frac{\partial u}{\partial z}\right) \tag{3.1.i}$$

$$\frac{\partial p}{\partial y} = \frac{\partial}{\partial z}\left(\mu \frac{\partial v}{\partial z}\right) \tag{3.1.ii}$$

From these equations, the velocity gradient can be identified,

$$\frac{\partial u}{\partial z} = \frac{z}{\mu}\frac{\partial p}{\partial x} + \frac{\tilde{A}}{\mu} \tag{3.2.i}$$

$$\frac{\partial v}{\partial z} = \frac{z}{\mu}\frac{\partial p}{\partial y} + \frac{\tilde{C}}{\mu} \tag{3.2.ii}$$

As a constant viscosity is assumed in the film thickness direction, a second integration is possible, giving the velocity profile,

$$u = \frac{z^2}{2\mu}\frac{\partial p}{\partial x} + \tilde{A}\frac{z}{\mu} + \tilde{B} \tag{3.3.i}$$

$$v = \frac{z^2}{2\mu}\frac{\partial p}{\partial y} + \tilde{C}\frac{z}{\mu} + \tilde{D} \tag{3.3.ii}$$

Still referring to figure 3.1, using the velocities u and v for each boundary, one can obtain for equations (3.2) and (3.3) respectively,

$$\frac{\partial u}{\partial z} = \left(\frac{2z-h}{\mu}\right)\frac{\partial p}{\partial x} - \frac{u_b - u_a}{h} \tag{3.4.i}$$

$$\frac{\partial v}{\partial z} = \left(\frac{2z-h}{\mu}\right)\frac{\partial p}{\partial y} - \frac{v_b - v_a}{h} \tag{3.4.ii}$$

and,

$$u = -z\left(\frac{h-z}{2\mu}\right)\frac{\partial p}{\partial x} + u_b\left(\frac{h-z}{h}\right) + u_a\frac{z}{h} \tag{3.5.i}$$

$$v = -z\left(\frac{h-z}{2\mu}\right)\frac{\partial p}{\partial y} + v_b\left(\frac{h-z}{h}\right) + v_a\frac{z}{h} \tag{3.5.ii}$$

A closure equation for the problem is obtained from the conservation of mass, whose integral form is given by,

$$\int_0^h \left[\frac{\partial \rho}{\partial t} + \frac{\partial}{\partial x}(\rho u) + \frac{\partial}{\partial y}(\rho v) + \frac{\partial}{\partial z}(\rho \breve{w})\right] dz = 0 \tag{3.6}$$

To solve this integral, it is beneficial to make use of the Lebnitz rule, given by,

$$\int_0^h \frac{\partial}{\partial x}[f(x,y,z)]dz = -f(x,y,h)\frac{\partial h}{\partial x} + \frac{\partial}{\partial x}\left[\int_0^h f(x,y,z)dz\right] \tag{3.7}$$

For the uniform properties across the lubricant film thickness,

$$\int_0^h \frac{\partial}{\partial x}(\rho u)dz = -(\rho u)\big|_{z=h}\frac{\partial h}{\partial x} + \frac{\partial}{\partial x}\left(\int_0^h \rho u dz\right) = -\rho u_a \frac{\partial h}{\partial x} + \frac{\partial}{\partial x}\left(\rho\int_0^h u dz\right) \tag{3.8.i}$$

$$\int_0^h \frac{\partial}{\partial y}(\rho v)dz = -(\rho v)\big|_{z=h}\frac{\partial h}{\partial y} + \frac{\partial}{\partial y}\left(\int_0^h \rho v dz\right) = -\rho v_a \frac{\partial h}{\partial y} + \frac{\partial}{\partial y}\left(\rho\int_0^h v dz\right) \tag{3.8.ii}$$

$$\int_0^h \frac{\partial}{\partial z}(\rho\breve{w})dz = \rho(\breve{w}_a - \breve{w}_b) \tag{3.8.iii}$$

The remaining integrals in equation (3.8) can be identified as the volumetric flow rate per unit width in directions x and y respectively. Making use of equation (3.5), they are calculated as,

$$q'_x = \int_0^h u dz = -\frac{h^3}{12\mu}\frac{\partial p}{\partial x} + \frac{u_b + u_a}{2}h \tag{3.9.i}$$

$$q'_y = \int_0^h v dz = -\frac{h^3}{12\mu}\frac{\partial p}{\partial y} + \frac{v_b + v_a}{2}h \tag{3.9.ii}$$

On the right-hand side of equations (3.9), the two terms are identified as the Poiseuille and Couette flows. The latter indicates the flow induced by the movement of the boundaries, while the former is the induced flow due to pressure gradients.

Returning the results from equations (3.8) and (3.9) into equation (3.7), the Reynolds equation is now defined as,

$$\begin{aligned} 0 = {} & \frac{\partial}{\partial x}\left(-\frac{\rho h^3}{12\mu}\frac{\partial p}{\partial x}\right) + \frac{\partial}{\partial y}\left(-\frac{\rho h^3}{12\mu}\frac{\partial p}{\partial y}\right) + \frac{\partial}{\partial x}\left[\rho h\frac{(u_a + u_b)}{2}\right] + \frac{\partial}{\partial y}\left[\rho h\frac{(v_a + v_b)}{2}\right] \\ & + \rho(\breve{w}_a - \breve{w}_b) - \rho u_a\frac{\partial h}{\partial x} - \rho v_a\frac{\partial h}{\partial y} + h\frac{\partial \rho}{\partial t} \end{aligned} \tag{3.10}$$

A number of different actions can be identified in the Reynolds equation. To a further understanding of these comprised effects, equation (3.10) can be considered for simplicity in the direction x only (e.g., a component with infinite width), which results after rearrangements,

$$\frac{\partial}{\partial x}\left(\frac{\rho h^3}{12\mu}\frac{\partial p}{\partial x}\right) = \frac{\partial}{\partial x}\left[\rho h\frac{(u_a + u_b)}{2}\right] + \rho\left(\breve{w}_a - \breve{w}_b - u_a\frac{\partial h}{\partial x}\right) + h\frac{\partial \rho}{\partial t} \tag{3.11}$$

On the left-hand side of equation (3.11), the Poiseuille term is identified. This term indicates the net flow rates resulting from the pressure induced in the lubricant film in response to the actions on the right, which can be divided as,

(i) Couette flow

$$\frac{\partial}{\partial x}\left[\rho h\frac{(u_a+u_b)}{2}\right]=\rho\frac{(u_a+u_b)}{2}\frac{\partial h}{\partial x}+h\frac{(u_a+u_b)}{2}\frac{\partial \rho}{\partial x}+\frac{\rho h}{2}\frac{\partial}{\partial x}(u_a+u_b) \tag{3.12}$$

Those terms indicate the net entraining flow rates due to surface velocities, distinguished in three different actions, as illustrated in figure 3.2. To compensate a reduction in film thickness in the sliding direction (**physical wedge**), a pressure flow is induced. Likewise, a reduction in density in the sliding direction requires an induced pressure gradient to conserve mass flow (**density wedge**). Alternatively, in bearings with elastic boundaries, a variation of sliding speeds within the length can be seen; if speed decreases with the flow, then positive pressure effects will be seen to expulse more fluid upwind (**elongation**).

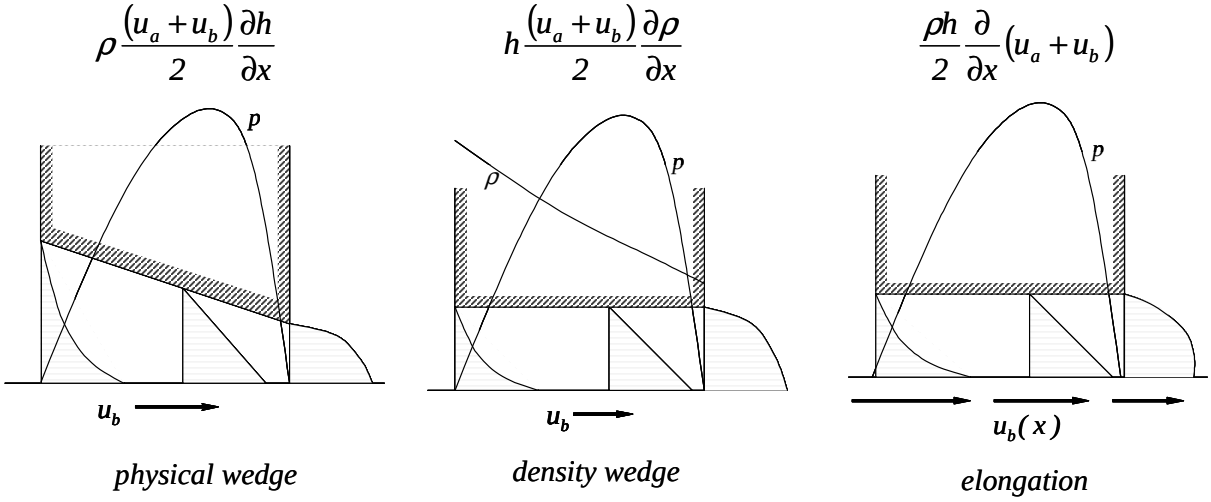

Figure 3.2. Couette flow actions identified in the Reynolds equation (Hamrock, 1994).

(ii) Squeeze film

$$\rho\left(\breve{w}_a-\breve{w}_b-u_a\frac{\partial h}{\partial x}\right)=\rho(\breve{w}_a-\breve{w}_b)-\rho u_a\frac{\partial h}{\partial x} \tag{3.13}$$

As a result of approaching surfaces, cushioning effects are predicted. Those can be of two types, as seen in figure 3.3. When the surfaces are pressed against each other, a very significant pressure effect is observed to eliminate fluid from the gap (**normal**

compression). Alternatively, positive pressures can be generated upon translation of inclined surfaces, when the local oil film thickness is reduced (**translational**).

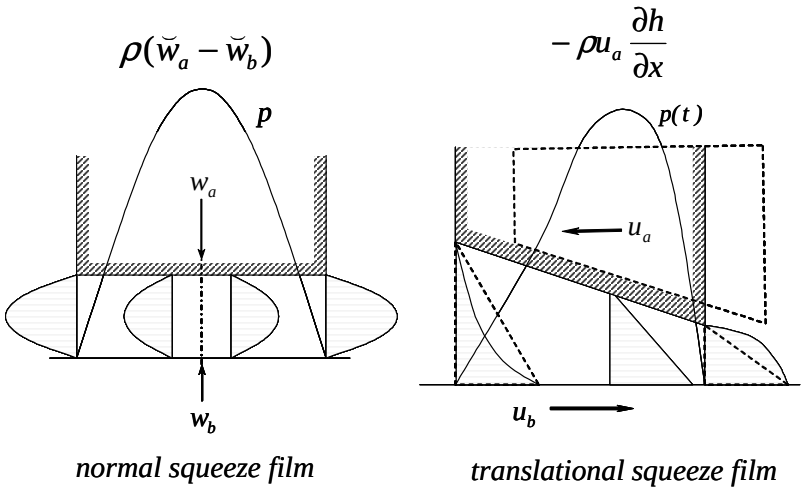

Figure 3.3. Squeeze film effects in the Reynolds equation (Hamrock, 1994).

(iii) Local fluid expansion

The remaining term in equation (3.11) is exemplified in figure 3.4, where the tendency of an expanding fluid to be eliminated from a stationary gap can be attributed to an induced Poiseuille flow.

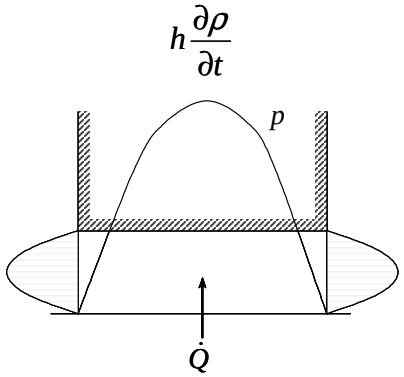

Figure 3.4. Local expansion mechanism for pressure generation (Hamrock, 1994).

3.1.3. Discussion

The majority of lubrication problems will rely upon the physical wedge and squeeze films to produce a pressure field and then support a load. Their effects are often more significant than the others remaining, when those are present. Furthermore, as their variations are related to geometric parameters, they are usually very convenient

and quick to provide solutions that are very representative for many problems. Besides, only a very basic knowledge of the lubricant properties will be required.

The dominance of these effects can be ultimately seen as one reason why lubrication solutions mainly focus only in the positive pressure region and, to some extent, why so few attempts were made to advance in the solution of the global lubrication problem, i.e., the solution of both full-film and cavitated regions.

However, it is misleading to believe that the Reynolds equation and the effects previously described cannot explain the behaviour in the cavitated region. For instance, consider the case presented in figure 3.5. Focusing attention to the divergent region, with the increase in distance between the surfaces, according to the physical wedge action negative pressures would be induced. On the other hand, and for whatever reason cavitation takes place (release of gas, ventilation or film rupture), one can conclude that the overall density of the fluid in any cross-section of the gap will decrease – which, according to the density wedge term, generates a positive pressure gradient. A similar example can be found in squeeze film dampers, when the separation of the surfaces will, on one hand induce a negative pressure field due to normal squeeze film and on the other hand have a positive pressure rising from the local expansion term when air bubbles are released (San Andrés, 2006).

Therefore, the low pressures usually observed in the cavitated region of a bearing can be explained by antagonistic actions described in the Reynolds equation, so that full film and cavitation solution can be achieved in a single equation.

Numerical assumptions have already been proposed to study the problem in its entirety, such as the Universal Equation proposed in Elrod's Algorithm (1980). There, a logical switch differentiates between the solution of the full-film region and the cavitation; however, some properties are said to have different meanings in each region.

In the present work, the proposal is that, by using the knowledge developed on the interaction between gas and oil, and particularly for oil and refrigerant mixtures, the solution for the entire lubrication problem can be performed with fewer assumptions on how the pressure profile should be calculated, but instead obtaining its conditions from the lubricant behaviour. Therefore, by considering the lubricant as a mixture of oil and a volatile substance, and tracking its changes throughout the flow, in particular the release of gas under saturation conditions, it is expected that the cavitation boundaries can be automatically captured and also that further insight into the behaviour in the

cavitated region can be gained. Furthermore, the assumptions made with other methodologies can be verified.

In addition to the lubricant mixture properties, a two-phase model formulation will be required to deal with the existence of two fluids in distinct phases.

3.2 TWO-PHASE FLOW CONSIDERATIONS AND THE PROPOSED EQUATION FOR THE GENERAL LUBRICATION MODEL

3.2.1. Physical Model

In this work, an oil-refrigerant mixture will commonly be assumed as the lubricant, but the description that follows can be seen in the general context of an oil-gas mixture, upon sufficient knowledge of its properties. The flow under consideration is schematically presented in figure 3.5.

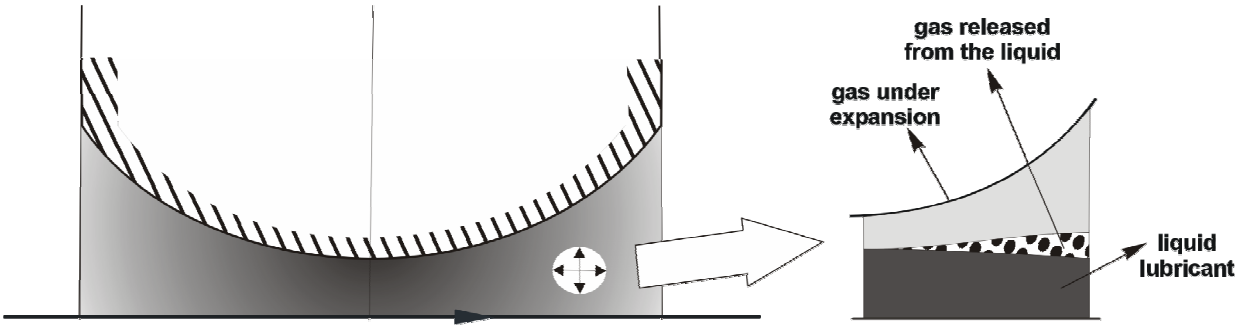

Figure 3.5. Lubricant flow through a convergent-divergent wedge.

In the convergent region, pressure increases due to the hydrodynamic wedge effect. Considering the liquid to be incompressible and with no free gas present in this region, the fluid properties remain constant.

However, in the divergent region, pressure decreases and eventually reaches the saturation pressure for the liquid oil-refrigerant mixture at the given temperature. At this point refrigerant is released from the liquid in the form of bubbles, flowing as a free gas. Two considerations are made at this stage: *(a)* as the oil vapour pressure is much lower than the mixture's saturation pressure, it is sensible to assume that no oil is present in the gas phase; *(b)* metastability of the mixture is negligible, so that instantaneous release of gas occur and the liquid mixture can be only saturated or subsaturated. As the fluid advances in the divergent region, the gap increases and there is further pressure reduction, such that free gas expands and new releases can take place.

An additional assumption is that the flow is isothermal, as the amount of gas released is usually small, such that the energy required for the change of phase can be neglected.

It is possible that the flow reaches upstream regions of higher pressures, e.g., as in the case of fluid recirculation in a 360º journal bearing. Therefore a region of pressure recovery can occur, by diffusion of momentum to the fluid. In this case, film pressure increases and some gas may conceivably redissolve in the oil. However, absorption usually occurs at a much slower rate than release, and the liquid may not be able to absorb the gas in the flow time available during the positive pressure region. Due to the unknown absorption rate, it is only possible at the present to identify the two limit thermodynamic situations:

- *Full-equilibrium*, where the gas is reabsorbed instantaneously, as happens during release;
- *Non-equilibrium*, where no gas is absorbed after being released, therefore potentially resulting in a two-phase flow throughout a positive pressure region.

Both hypotheses can be considered in the development of the model and should be tested. Before a choice can be made, additional research is required to rigorously evaluate the actual rates of absorption, particularly for the very quick times of flow observed in lubrication phenomena. As seen in chapter 2, a few workers have considered transient oil-refrigerant dissolution, however only at slow rates (Yokozeki, 2002, Silva, 2004, Gessner and Barbosa Jr., 2006). Quicker processes of gas absorption have been investigated in other areas, such as in liquid jets and carbon dioxide imprisonment in deep seawater (Cullen and Davidson, 1957, Tsuchiya et al., 1997).

When considering transient processes, either under steady load but out of equilibrium or under dynamic load, the only additional effect present is the squeeze film, which creates an additional pressure gradient, positive or negative. Under such circumstances, physical phenomena remain the same, with release of gas at saturation conditions. However, the position where saturation is reached may vary as pressure can be higher if the solid surfaces are approaching each other or lower if the surfaces are moving apart.

Finally, an important aspect regards the relative motion between the liquid phase and the gas bubbles along the flow. It has been observed in previous research of oil-refrigerant flow in pipes that the bubbles formed during outgassing present a very similar velocity to that of the liquid (Lacerda et al., 2000). This indicates that assuming

a homogeneous flow in modelling seems reasonable, following the same approach that has been adopted in previous bubbly-oil modelling (Kicinski, 1983, Smith, 1990, Someya, 2003). Therefore, due to good mixing and essentially the same velocity of gas and liquid, the two-phase flow can be modelled as a monophasic flow of an equivalent fluid, whose properties are based on averages from the constituent phases. An additional assumption is to neglect surface tension effects (Tao et al., 2000), such that pressure inside the bubbles can be assumed to be the same as that of the surrounding liquid. This assumption will however be tested in future chapters.

Having information on how the fluid behaves physically, the two-phase lubrication model can now be proposed, initially by appropriately characterising the mixture composition along the flow.

3.2.2. Preliminary definitions: homogeneous two-phase flow

Some parameters are necessary to characterise fractional compositions of liquid and gas in a two-phase flow. It is also needed to know the liquid lubricant, which in this case will be considered a binary mixture of oil and refrigerant, despite the several components present in the oil. Therefore, the fraction of liquid refrigerant present in the oil is required. The parameters that enable this characterisation are described in the sequence.

Refrigerant Mass Fraction: it is the amount of refrigerant dissolved in the liquid mixture, considered in a mass basis:

$$w_r = \frac{m_{lr}}{m_l} \tag{3.14}$$

where m_{lr} is the mass of liquid refrigerant and m_l is the total mass of liquid.

As previously defined in chapter 2, the maximum amount of refrigerant that can be dissolved in the oil for a defined condition of pressure and temperature is the *solubility*:

$$w_{sat} = w_{sat}(p,T) \tag{3.15}$$

Gas Quality: it is the ratio between the mass of gas and the total mass of the mixture. Quality can be written as a function of the mass fraction of the component at a specified point and the overall fluid composition, w_r and w_o, respectively, as follows,

$$\chi = \frac{w_o - w_r}{1 - w_r} \tag{3.16}$$

Void Fraction: ratio between the volume occupied by the gas and the total volume. Existing one uniform dimension, it equates to the ratio of cross-section areas,

$$\phi = \frac{\forall_g}{\forall_{tot}} = \frac{A_g dx}{A dx} = \frac{A_g}{A} \tag{3.17}$$

Considering the same velocity for both phases, then the void fraction of the mixture can be written explicitly as a function gas quality and the density of phases by,

$$\phi = \frac{1}{\left[1 + \left(\frac{1}{\chi} - 1\right)\frac{\rho_g}{\rho_l}\right]} \tag{3.18}$$

Apparent properties ($\bar{\rho}, \bar{\mu}$): Using the homogeneous model, the liquid/gas mixture is replaced by a monophasic pseudofluid. It is necessary then to define representative values of properties for the pseudofluid, which are called apparent properties. These properties are usually calculated from averages of the properties of the existing phases.

The apparent density can be determined from the usual thermodynamic definition, using gas quality and specific volume (Feng and Hahn, 1986, Carey, 1992),

$$\frac{1}{\bar{\rho}} = \bar{v} = \chi v_g + (1 - \chi) v_l \tag{3.19}$$

It can be shown that this definition is equivalent to,

$$\bar{\rho} = \phi \rho_g + (1 - \phi)\rho_l \tag{3.20}$$

However, the apparent viscosity does not have a precise definition. The only existing condition is that the proposed correlation must satisfy the limiting conditions determined in equation (3.21) (Carey, 1992),

$$\chi = 0 \rightarrow \bar{\mu} = \mu_l \quad \text{and} \quad \chi = 1 \rightarrow \bar{\mu} = \mu_g \tag{3.21}$$

Several correlations are proposed, sometimes not even respecting the condition imposed by equation (3.21), and usually the choice among them lies on testing and examining the suitability of, amongst others, factors such as geometry and the type of mixture; some models are more convenient than others for specific situations. The following correlations are often used in two-phase flow studies and will be tested in this work,

Cichitti $$\overline{\mu} = \chi\mu_g + (1-\chi)\mu_l \tag{3.22}$$

McAdams $$\overline{\mu} = \phi\mu_g + (1-\phi)\mu_l \tag{3.23}$$

Someya $$\frac{\overline{\mu}}{\mu_l} = 1 + 0.5062\phi + 9.044\phi^2 - 48.83\phi^3 + 60.13\phi^4 - 23.85\phi^5 \tag{3.24}$$

Hayward $$\overline{\mu} = (1 + 0.15\phi)\mu_l \tag{3.25}$$

Einstein $$\overline{\mu} = (1 + 2.5\phi)\mu_l \tag{3.26}$$

Correlations proposed in equations (3.22) and (3.23) are mentioned by Feng and Hahn (1986); equation (3.24) is adjusted and proposed by Someya (2003), and equations (3.25) and (3.26) are referenced in Cameron (1966) and Kicinski (1983). The two first correlations are commonly adopted in the study of two-phase flows in general, particularly those of pure refrigerants (Chang and Ro, 1996, Wongwises and Pirompak, 2001). The Hayward correlation is a usual suggestion in the study of bubbly oil lubrication, being used for small and medium values of void fraction (Cameron, 1966). The Einstein correlation was initially proposed in the study of sprays, but is often also considered in the study of liquid/gas two-phase flows (Cameron, 1966 and Drew, 1983). In the study of oil/refrigerant mixtures, Grando (2001) adopted the Cichitti correlation (3.22) when studying the flow of the mixture in horizontal pipes.

3.2.3. Governing equation for the two-phase lubrication problem

With the mixture completely characterised by thermodynamic correlations, which in turn enable the physical properties density and viscosity to be calculated, considering gas and liquid phases, the two-phase lubrication model can now be

proposed. The common hypotheses adopted to derive the lubrication equation in section 3.1 remain valid, such that, by including the apparent properties as characteristic density and viscosity of the lubricant in equation (3.10), the general two-phase lubrication equation is given by,

$$0=\frac{\partial}{\partial x}\left(-\frac{\bar{\rho}h^3}{12\bar{\mu}}\frac{\partial p}{\partial x}\right)+\frac{\partial}{\partial y}\left(-\frac{\bar{\rho}h^3}{12\bar{\mu}}\frac{\partial p}{\partial y}\right)+\frac{\partial}{\partial x}\left[\bar{\rho}h\frac{\left(u_a+u_b\right)}{2}\right]+\frac{\partial}{\partial y}\left[\bar{\rho}h\frac{\left(v_a+v_b\right)}{2}\right] + \bar{\rho}\left(\breve{w}_a-\breve{w}_b\right)-\bar{\rho}u_a\frac{\partial h}{\partial x}-\bar{\rho}v_a\frac{\partial h}{\partial y}+h\frac{\partial\bar{\rho}}{\partial t} \tag{3.27}$$

In order to obtain a more concise form for the equation, the time derivative of film thickness can be identified as,

$$\frac{\partial h}{\partial t}=\breve{w}_a-\breve{w}_b-u_a\frac{\partial h}{\partial x}-v_a\frac{\partial h}{\partial y} \tag{3.28}$$

Therefore, equation (3.27) can be rewritten as,

$$\frac{\partial}{\partial x}\left(\frac{\bar{\rho}h^3}{12\bar{\mu}}\frac{\partial p}{\partial x}\right)+\frac{\partial}{\partial y}\left(\frac{\bar{\rho}h^3}{12\bar{\mu}}\frac{\partial p}{\partial y}\right)=\frac{\partial}{\partial x}\left[\bar{\rho}h\frac{\left(u_a+u_b\right)}{2}\right]+\frac{\partial}{\partial y}\left[\bar{\rho}h\frac{\left(v_a+v_b\right)}{2}\right]+\frac{\partial}{\partial t}\left(\bar{\rho}h\right) \tag{3.29}$$

As a characteristic of the homogeneous formulation, a single equation is still achieved, which simplifies the two-phase flow problem solution. The effects present in equation (3.27) or (3.29) remain the same as in the original Reynolds equation (3.10), but further work is required to characterise the fluid, and additional simplifications for physical properties, that are very common in conventional lubrication problems, are now less likely. Furthermore, by defining cavitation pressure as the onset of release of gas, it can be automatically identified by the saturation pressure of the lubricant liquid mixture.

3.3 OVERVIEW OF THE SOLUTION METHODOLOGY

In lubrication problems, only a few and very simplified cases can be solved analytically. Considering equation (3.29), and particularly the existence of areas of compressible flow, there is an interdependence between the pressure field and the homogeneous properties of the fluid, which add in complexity even for a simple

geometry. Therefore, numerical methodologies have to be applied. In the present work, the finite volume methodology (Patankar, 1980) is utilised. The solution domain will be divided in control volumes, in which the governing equation is integrated. The procedure applied to a two-dimensional domain is presented in figure 3.6, detailing also a generic control volume,

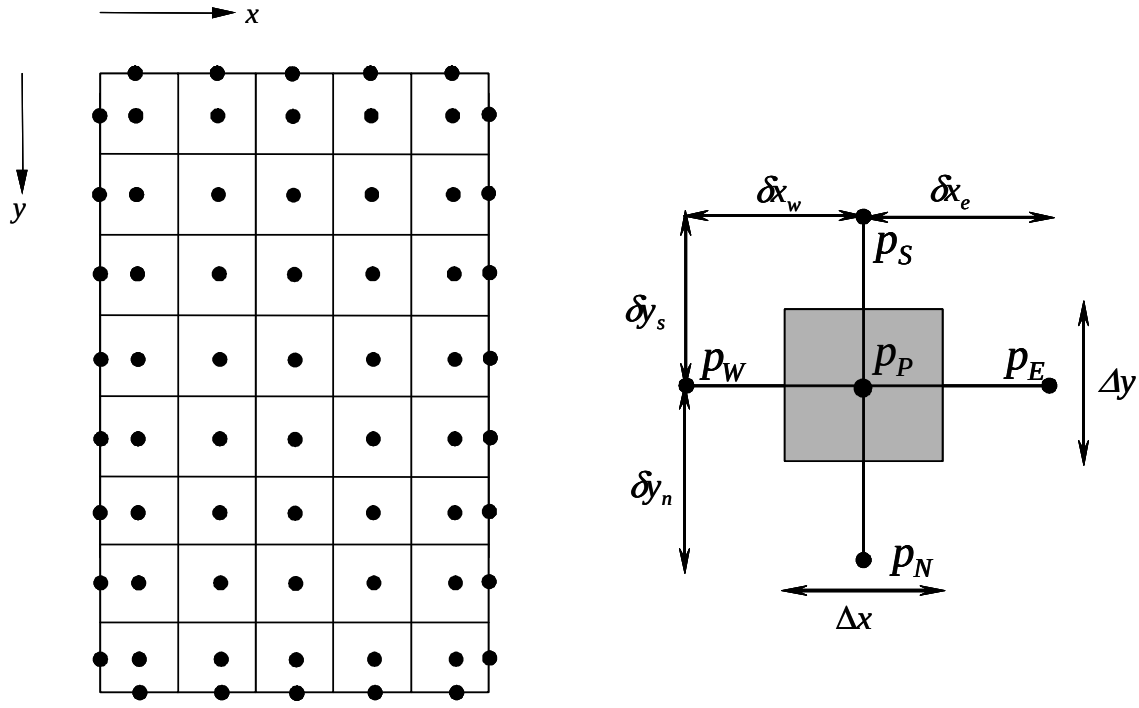

Figure 3.6. Discretisation of the solution domain via finite volume methodology.

The next step is to integrate the governing equation in the generic control volume. Considering equation (3.29) for a defined time step, one has,

$$\int_s^n \int_w^e \frac{\partial}{\partial x}\left(\frac{\overline{\rho}h^3}{12\overline{\mu}}\frac{\partial p}{\partial x}\right)dxdy + \int_s^n \int_w^e \frac{\partial}{\partial y}\left(\frac{\overline{\rho}h^3}{12\overline{\mu}}\frac{\partial p}{\partial y}\right)dxdy = \tag{3.30}$$
$$= \int_s^n \int_w^e \left[\frac{\partial}{\partial x}\left(\overline{\rho}h\frac{U}{2}\right) + \frac{\partial}{\partial y}\left(\overline{\rho}h\frac{V}{2}\right) + \frac{\partial}{\partial t}\left(\overline{\rho}h\right)\right]dxdy$$

where $U=(u_a+u_b)/2$ and $V=(v_a+v_b)/2$.

Resolving the integrals, assuming rigid surfaces so that U and V are constants, results,

$$\left[\left(\frac{\overline{\rho}h^3}{12\overline{\mu}}\frac{\partial p}{\partial x}\right)_e - \left(\frac{\overline{\rho}h^3}{12\overline{\mu}}\frac{\partial p}{\partial x}\right)_w\right]\Delta y + \left[\left(\frac{\overline{\rho}h^3}{12\overline{\mu}}\frac{\partial p}{\partial y}\right)_n - \left(\frac{\overline{\rho}h^3}{12\overline{\mu}}\frac{\partial p}{\partial y}\right)_s\right]\Delta x = \tag{3.31}$$
$$= \frac{U}{2}\Delta y\left[\left(\overline{\rho}h\right)_e - \left(\overline{\rho}h\right)_w\right] + \frac{V}{2}\Delta x\left[\left(\overline{\rho}h\right)_n - \left(\overline{\rho}h\right)_s\right] + \left.\frac{\Delta\left(\overline{\rho}h\right)}{\Delta t}\right|_P \Delta x\Delta y$$

Additionally, considering properties constant along the film thickness, this equation can be expressed as,

$$\left.\frac{\overline{\rho}_e h_e^3}{12\overline{\mu}_e}\frac{\partial p}{\partial x}\right|_e \Delta y - \left.\frac{\overline{\rho}_w h_w^3}{12\overline{\mu}_w}\frac{\partial p}{\partial x}\right|_w \Delta y + \left.\frac{\overline{\rho}_n h_n^3}{12\overline{\mu}_n}\frac{\partial p}{\partial y}\right|_n \Delta x - \left.\frac{\overline{\rho}_s h_s^3}{12\overline{\mu}_s}\frac{\partial p}{\partial y}\right|_s \Delta x = \tag{3.32}$$
$$= \frac{U}{2}\Delta y\left(\overline{\rho}_e h_e - \overline{\rho}_w h_w\right) + \frac{V}{2}\Delta x\left(\overline{\rho}_n h_n - \overline{\rho}_s h_s\right) + \left.\frac{\Delta\left(\overline{\rho}h\right)}{\Delta t}\right|_P \Delta x\Delta y$$

where the temporal derivative for $\overline{\rho}h$ at the point *P* is assumed given in the process.

The physical properties are required at the start of the numerical process. In this case, as they may depend on pressure, they can be provided from an initial guess or calculated from an initially guessed pressure field, and corrected as the process progresses. Furthermore, as pressures are calculated in the nodal points of the volume, properties at the boundaries are not known. However, as the boundary is chosen in the midline between two points, one reasonable approximation is,

$$\overline{\rho}_e = \frac{\overline{\rho}_E + \overline{\rho}_P}{2} \tag{3.33}$$

and similarly for the other boundaries.

For the lubrication problem, it seems that the approximation for the convective terms of the governing equation (i.e., terms including velocity components) is not as significant as in usual fluid dynamics problems, where the use of *upwind* approximations for the convective terms is very important in preparing the discretised set of equations (Patankar, 1980). Nevertheless, to be coherent with the methodology, for the left (bottom) side of the equation the approximations will be,

$$\overline{\rho}_e = \overline{\rho}_E \text{ and } \overline{\rho}_w = \overline{\rho}_P \tag{3.34}$$

and again similarly for the approximations in the *y* direction.

The film thickness is unlikely to follow this procedure, as usually it can be calculated analytically for any position of domain from the geometrical properties.

The derivatives for pressure also required calculation. Assuming linear variation of the pressure between two consecutive points, the pressure derivative is given by,

$$\left.\frac{\partial p}{\partial x}\right|_e = \frac{p_E - p_P}{x_E - x_P} = \frac{p_E - p_P}{\delta x_e} \tag{3.35}$$

and similarly for the remainder derivatives at different positions.

Using this equation in the finite volume methodology, an approximation of second order ($\Delta x^2, \Delta y^2$) occurs (Roache, 1998). Replacing now in equation (3.32) the derivatives and physical properties estimations, the following algebraic equation can be written,

$$-\left(\frac{\overline{\rho}_e h_e^3}{12\overline{\mu}_e}\frac{\Delta y}{\delta x_e}+\frac{\overline{\rho}_w h_w^3}{12\overline{\mu}_w}\frac{\Delta y}{\delta x_w}+\frac{\overline{\rho}_n h_n^3}{12\overline{\mu}_n}\frac{\Delta x}{\delta y_n}+\frac{\overline{\rho}_s h_s^3}{12\overline{\mu}_s}\frac{\Delta x}{\delta y_s}\right)p_P + \tag{3.36}$$
$$+\left(\frac{\overline{\rho}_e h_e^3}{12\overline{\mu}_e}\frac{\Delta y}{\delta x_e}\right)p_E+\left(\frac{\overline{\rho}_w h_w^3}{12\overline{\mu}_w}\frac{\Delta y}{\delta x_w}\right)p_W+\left(\frac{\overline{\rho}_n h_n^3}{12\overline{\mu}_n}\frac{\Delta x}{\delta y_n}\right)p_N+\left(\frac{\overline{\rho}_s h_s^3}{12\overline{\mu}_s}\frac{\Delta x}{\delta y_s}\right)p_S=$$
$$=\frac{U\Delta y}{2}\left(\overline{\rho}_E h_e-\overline{\rho}_P h_w\right)+\frac{V\Delta x}{2}\left(\overline{\rho}_N h_n-\overline{\rho}_P h_s\right)+\left.\frac{\Delta(\overline{\rho}h)}{\Delta t}\right|_P \Delta x\Delta y$$

Therefore, the pressure at position *P* is related to the neighbouring position *E*, *W*, *N* and *S*. Obtaining one equation for every internal point, a set of algebraic equations will result. Equation (3.36) can be rewritten in a more convenient form as,

$$A_p p_P = A_e p_E + A_w p_W + A_n p_N + A_s p_S + S \tag{3.37}$$

where,

$$A_e=\frac{\overline{\rho}_e h_e^3}{\overline{\mu}_e}\frac{\Delta y}{\delta x_e} \qquad A_w=\frac{\overline{\rho}_w h_w^3}{\overline{\mu}_w}\frac{\Delta y}{\delta x_w}$$

$$A_n=\frac{\overline{\rho}_n h_n^3}{\overline{\mu}_n}\frac{\Delta x}{\delta y_n} \qquad A_s=\frac{\overline{\rho}_s h_s^3}{\overline{\mu}_s}\frac{\Delta x}{\delta y_s}$$

$$A_p = A_e + A_w + A_n + A_s$$

$$S=-12\left[\frac{U\Delta y}{2}\left(\overline{\rho}_E h_e-\overline{\rho}_P h_w\right)+\frac{V\Delta x}{2}\left(\overline{\rho}_N h_n-\overline{\rho}_P h_s\right)+\left.\frac{\Delta(\overline{\rho}h)}{\Delta t}\right|_P \Delta x\Delta y\right]$$

This set of equations can be organised in the form of a linear system and then be solved simultaneously to obtain the pressure field. The boundary conditions are also incorporated in the equations, only for the points in the vicinity of a domain boundary.

The transient term present in the source term *S* of the equation above is given for any time. How to obtain it can be complicated, but this discussion will be made only when necessary in the next chapters.

It should now be remembered that interdependence exists between fluid properties and the pressure field. Therefore, their values need to be updated after obtaining the pressure field. Furthermore, for the new set of properties, a new pressure

field will result from the solution of the set of equations (3.37), thus characterising an iterative process where successive corrections are needed.

The iterative process should be repeated until variations of fluid properties and film pressure are smaller than a desired tolerance – which is considered the converged solution. In this problem, pressure and density are the variables presenting significant variations, while viscosity presents smaller variations, as it will be discussed in later chapters. Numerically, the convergence criterion proposed is,

$$\max\left(\left|\frac{p_i^k - p_i^{k-1}}{p_{ref}}\right|, \left|\frac{\overline{\rho}_i^k - \overline{\rho}_i^{k-1}}{\overline{\rho}_{ref}}\right|\right) < tol \tag{3.38}$$

where *i* is the index for the nodal points, *k* and *k-1* are respectively the current and the previous iterations, and *ref* is the index to indicate the chosen reference properties, which are initially known. The predefined tolerance is specified by *tol*.

A problem that arises from the iterative method is that properties, especially the density of the refrigerant gas, are non-linear and very sensitive to pressure variations. Minor variations in pressure can produce considerable variations in properties, which then promote new changes in pressure, resulting in an unstable numerical process. To overcome numerical instabilities, under-relaxation factors are included, in order that corrections between two successive iterations are made as described in equations (3.39) and (3.40),

$$p_i^k = \beta_p \, p_i^k\big|_{calc} + (1-\beta_p) p_i^{k-1} \tag{3.39}$$

$$\overline{\rho}_i^k = \beta_\rho \, \overline{\rho}_i^k\big|_{calc} + (1-\beta_\rho) \overline{\rho}_i^{k-1} \tag{3.40}$$

where β_p and β_ρ are the under-relaxation factors for pressure and density, respectively, while *calc* means the value for property actually calculated, which is only partially updated in the iterative process.

The choice of the under-relaxation factors depend on geometry and flow conditions, and inevitably requires testing and optimisation. This will be discussed in future chapters as well.

To sum up the procedure, at a given point, the solution for the two-phase flow searches for the pair of pressure-void fraction that completely fills the clearance. Thus, for a given value of pressure, one looks for the volume of gas necessary to fill the

clearance and then the void fraction can be obtained. With this new value, properties change and a new pressure field is calculated. This iterative process must be repeated until the determined void fraction becomes coherent with the pressure calculated at the point.

The solution of the problem can be briefly described as follows,

1. Known all initial and reference conditions, a pressure field is estimated in the fluid film (input data for geometry, e.g., film thickness *h*, and estimated pressure *p*);

2. With the arbitrary pressure field, fluid properties along the film are determined. When $p < p_{sat}(w_{ref})$, release of gas occurs and the size of bubbles is changed by two effects: expansion due to pressure drop and also gas release.

3. With the readjusted values of properties, the pressure field is recalculated using equation (3.37) and the result is compared with the previous pressure field;

4. Steps 2 and 3 are repeated until convergence is reached.

This procedure provides the pressure field throughout the lubricated component without using hypotheses about the pressure behaviour in the middle of the film, that is, without adopting any cavitation criterion.

Some difficulties that might be present in this solution are the definition of apparent viscosity for the pseudofluid and considerations of surface tension. To the second, it is necessary to determine the solution of an additional equation to find gas pressure, which in turn is used to determine properties of the mixture. Considerations about absorption of the gas under positive pressure gradients will also affect the control of the iterative process and ultimately the solution of the problem.

Another concern is whether the liquid lubricant has enough refrigerant to evaporate and fill the clearance. In this case there is a tendency to pressure drop further than the saturation, which can occur for instance in a sealed bearing. If the bearing is communicated with the environment, gas can enter from the surroundings to fill the clearance, and this may need to be taken into account. Nevertheless, due to the high expansion that gases can have, just minimum quantities of gas should suffice to fill the clearance.

Given the number of uncertainties involving the appropriate characterisation of the mixture behaviour throughout the flow, it was decided in this work to pursue this understanding by initially solving problems of simplified geometry and, as further

knowledge into the mixture behaviour is obtained, geometry assumptions can be relaxed and gradually the complexity of the problems can be increased. Therefore further discussion on the matters regarding the numerical solution, and particularly the mixture behaviour, will continue to be discussed through the following chapters.

3.4 USUAL METHODOLOGIES IN THE LIGHT OF THE TWO-PHASE MODEL

The proposal for the generalised two-phase lubrication equation intends to advance the understanding of the flow in the cavitated region, and to provide a tool that enables the analysis of the lubrication problem in its entire domain. Nevertheless, it is important that it can be comparable to the commonly adopted solution methodologies, so that conclusions can be made on when the added complexity of the new methodology is essential to an accurate solution of the problem, and when a representative solution can still be obtained from simpler methodologies, upon awareness of their assumptions.

To conclude this chapter, a brief comparison is made between the two-phase flow approach and the solution provided by the cavitation algorithm, described in the literature review. The purpose is to indicate that the single phase methodology is a simplified case of the two-phase flow one, and to identify the assumptions adopted in terms of fluid properties, so that they can be later verified.

The cavitation algorithm (Christopherson, 1942) assumes incompressible and single phase fluid flow. For instance, in a simplified steady-state and uni-dimensional case, with fixed sliding speed, the equation to solve is reduced from equation (3.10) to,

$$\frac{\partial}{\partial x}\left(h^3 \frac{\partial p}{\partial x} \right) = 6\mu U \frac{\partial h}{\partial x} \tag{3.41}$$

By using a discrete numerical methodology to solve equation (3.41), and considering $p_{cav}=0$, the cavitation algorithm states that, for every step of the iteration,

$$\text{if } p<p_{cav}=0, \text{ then } p=p_{cav}=0 \tag{3.42}$$

which, as described with some surprise by Parkins (1985), leads to the converged pressure field resulting in that expected for a solution using the Reynolds boundary conditions.

Now, considering the two-phase lubrication equation, for the similar geometry assumptions, equation (3.29) is rewritten as,

$$\frac{\partial}{\partial x}\left(\frac{\overline{\rho}h^3}{\overline{\mu}}\frac{\partial p}{\partial x}\right)=6U\frac{\partial}{\partial x}\left(\overline{\rho}h\right) \tag{3.43}$$

First, assuming negligible properties for the gas phase, i.e., $\rho_g \approx 0$ and $\mu_g \approx 0$, equations (3.20) and (3.22) become,

$$\overline{\rho}=\phi\rho_g+(1-\phi)\rho_l \xrightarrow{\rho_g \approx 0} (1-\phi)\rho_l \tag{3.44}$$

$$\overline{\mu}=\chi\mu_g+(1-\chi)\mu_l \xrightarrow{\mu_g \approx 0} (1-\chi)\mu_l \tag{3.45}$$

Furthermore,

$$\rho_l = constant \tag{3.46}$$

$$(1-\chi)\mu_l \approx constant \approx \mu \tag{3.47}$$

Considering these assumptions, equation (3.30) is rewritten as,

$$\rho_l\frac{\partial}{\partial x}\left((1-\phi)h^3\frac{\partial p}{\partial x}\right)=6\rho_l\mu U\frac{\partial}{\partial x}\left[(1-\phi)h\right] \tag{3.48}$$

from where it can be concluded that such approach is independent of the liquid lubricant density. Therefore,

$$\frac{\partial}{\partial x}\left((1-\phi)h^3\frac{\partial p}{\partial x}\right)=6\mu U\frac{\partial}{\partial x}\left[(1-\phi)h\right] \tag{3.49}$$

The above equation reinforces the idea of searching for the paired pressure-void fraction in the solution of a two-phase lubrication problem.

Now, assume $p_{cav}=0$ and only liquid is present outside the cavitation region. For the cavitation region, it is considered in the model that the mixture cannot be supersaturated, i.e., with excess of gas dissolved below the saturation pressure (constant p_{cav} in this case where gas density assumed zero). Furthermore, the gas will occupy any further space above the lubricant film thickness in the onset of cavitation (h_{cav}). Thus,

$$p > p_{cav} \rightarrow \phi = 1 \tag{3.50.i}$$

$$p \leq p_{cav} \rightarrow p = p_{cav} = 0 \rightarrow \phi \equiv \frac{\forall_g}{\forall_t} \equiv 1-\frac{h_{cav}}{h} \tag{3.50.ii}$$

Using this information, equation (3.43) can be rewritten for two instances,

$$\frac{\partial}{\partial x}\left(h^3 \frac{\partial p}{\partial x}\right) = 6\mu U \frac{\partial h}{\partial x}, \text{ for } p > p_{cav} \tag{3.51.i}$$

$$\frac{\partial}{\partial x}\left[\left(1-1+\frac{h_{cav}}{h}\right)h^3 \frac{\partial p}{\partial x}\right] = 6\mu U \frac{\partial}{\partial x}\left[\left(1-1+\frac{h_{cav}}{h}\right)h\right] = 0, \text{ cavitation} \tag{3.51.ii}$$

Equation (3.51.i) is identical to (3.41), while from equation (3.51.ii) it can be concluded that the pressure gradient is zero for the cavitation region, as indicated also by the Reynolds boundary conditions.

Therefore, it can be demonstrated using the two-phase flow how the cavitation algorithm results in the Reynolds boundary condition, and further, that this is valid for the specific condition of zero gas density and negligible influence of gas on the lubricant film viscosity throughout the bearing.

It can be shown that similar conclusions will be obtained for the Elrod algorithm (1980) in the cavitated region, although further elaboration would be required in the full-film domain.

In the next chapters, by using appropriate data for the gas phase, which is available when an oil-refrigerant mixture is studied, it will be possible to infer the adequacy of the so commonly used assumptions described above.

3.5 SUMMARY

In this chapter, the general equation and model proposal to solve two-phase lubrication problems in this work were presented. After reviewing the Reynolds equation and its main parameters and describing the physical aspects of the problem to solve, the requirements to characterise two-phase flows were presented, so that the modified Reynolds equation for the two-phase lubrication model could be stated.

The methodology of finite volumes, which will be used to solve numerically the target problems of this work, was described in details.

Finally, it was proved that the methodology defined as the Cavitation Algorithm could be understood as a simplified case of the two-phase model here proposed.

Chapter 4

TWO-PHASE FLOW SOLUTION FOR AN INFINITE PARTIAL JOURNAL BEARING

This chapter presents the first geometry selected to be solved with the two-phase lubrication methodology, and how it will be approached. Firstly the problem is physically described, discussing simplifications and assumptions. Based on this characterisation, the governing equation is simplified from the general two-phase lubrication equation, pointing the requirements for its numerical solution and the parameters of interest that can be obtained. With the methodology fully defined, initial steps of the solution discuss a calibration of the model, i.e., the physical and numerical adjustments necessary to its appropriate and viable implementation. Finally, the numerical methodology proposed to solve the mathematical problem is evaluated for a number of cases, advancing in its physical understanding.

4.1 INTRODUCTION

With the limited experience in operating with the proposed two-phase flow approach for lubrication problems, possibly the choice for a simplified geometry is recommended, such that good steps can be made in understanding the methodology while the geometry does not pose a challenge – therefore the choice for an 180^{o} partial journal bearing. Nevertheless, a brief description of the case in study and a proper list of the assumptions adopted is required beforehand. On that basis, the specific case can be simplified from the general proposal and the physical model is posed.

There will still be questions on how to operate the model that could not be defined in the modelling stage, such as the choice for the specific viscosity correlation. Additionally, the numerical parameters of the model need to be tested so that their operation is understood and optimised in the sequence to ensure simulation conditions

close to optimal ones or, at least, that convergence is achieved respecting conservation equations. These all can be done only after the choice of the two-phase mixture – to this problem, a mixture of mineral oil SUNISO 1GS and refrigerant R12 was chosen. Despite the phase-out of R12 and other CFCs from new refrigeration systems, this mixture has its properties well characterised and it was previously studied with a similar model in its two-phase flow in pipes (Grando, 2001), which is helpful to the present development.

Having the model adjusted, a comparison of the results with those using Reynolds boundary conditions can provide verification of the coherence of the model. This should be the best reference at present, given that experimental results are not available, despite the simple geometry. Furthermore, based on the knowledge of the applicability of the Reynolds model, this will enable to observe in which conditions the assumptions adopted in Reynolds are verified and when significant differences are observed.

With this initial understanding of the model and its verification against classical lubrication theory, the phenomenology of the flow can be explored and described in more details, providing an understanding on how the release of gas occurs and how this modifies lubrication of the bearing.

4.1.1. Specific objectives

- To obtain a structured methodology to numerically solve the two-phase lubrication problem for the infinite partial journal bearing;
- To investigate effect of thermodynamic equilibrium and non-equilibrium of the mixture flow on the bearing performance;
- To define an equation for the homogeneous two-phase viscosity, among the choices researched in the literature – criteria for judgement include the appropriate representation of the cavitation region where two-phase flow occurs and also friction considerations;
- Investigate the methodology proposed against the solution provided by the classical approach in lubrication, considering the Reynolds boundary conditions;

4.2 MODEL DEVELOPMENT

4.2.1. Physical Considerations

The case in study is a partial journal bearing, where a rotating shaft is separated from a support by a lubricant film. The support is an arc of circle of extension $\Delta\theta_{pjb}$, where lubricant is supplied in one side as a liquid oil-refrigerant mixture and completely eliminated in the other side to ensure continuity. Constant load is applied on the shaft in such a way that its centre assumes an eccentric position in relation to the centre of the support (bearing), as shown in figure 4.1.

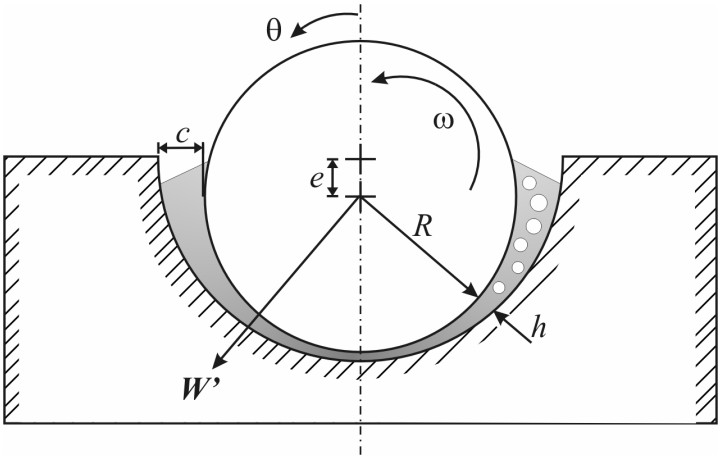

Figure 4.1. Geometry of the partial journal bearing and applied load.

The following assumptions are made to simplify the problem:

1. Radial clearance *c* is much smaller than shaft radius:

- pressure in the radial direction can be considered constant;
- radial clearance is fully filled with oil (no starvation);
- entrance effects are negligible;

2. Pressure and viscous forces are dominant in the flow;

3. Shaft and bearing are very long, and a unidimensional flow can be assumed;

4. Constant load applied; furthermore, steady-state conditions;

5. Isothermal flow;

6. Negligible metastability of the liquid mixture: instantaneous gas release;

Simplifications 1-2 assumed above are commonly adopted in the solution of lubrication problems and to some extent already assumed in the model derivation in the previous chapter. The third hypothesis is assumed in order to study the problem in a simpler geometry – reducing complexity is also the purpose of assumptions 4 and 5, but they are more related to the limitation of phenomena occurring with the lubricant mixture. The sixth consideration is commonly assumed when studying oil and refrigerant mixtures and was also taken as an assumption when deriving the model.

Briefly recapitulating the physical behaviour of the mixture, also described in chapter 3, for the partial journal bearing the main characteristics of the flow will be,

- In the convergent region, pressure increases due to the hydrodynamic wedge effect and the fluid is a liquid mixture that can be deemed incompressible, remaining with constant properties;
- In the divergent region, pressure will fall and eventually reach the saturation pressure of the liquid mixture, when gas will be released and flow as bubbles well mixed with the liquid mixture. The gas is composed by refrigerant only;
- Near the end of the bearing, pressure can conceivably be higher than those observed in the two-phase film and pressure recovery may be observed. The rate of gas dissolution in the mixture, if any, is not know and should be investigated;

4.2.2. Mathematical Considerations

Taking advantage of the shape of the journal bearing presented in figure 4.1, the most suitable coordinate system to use is the cylindrical, $r\theta y$, whose centre is located at the centre of the shaft and anti-clockwise rotations are considered positive. The bearing and the journal have a radius difference given by the radial clearance *c*, and during operation their centres are eccentric, which is characterised by the dimensional eccentricity *e*. These two characteristics enable to identify at any position the film thickness, *h*. Due to the very small dimension of the radial clearance, curvature effects are negligible, and the polar system can be related with a conventional Cartesian coordinate system, *xyz*, in order that the film can be studied unwrapped (Hamrock, 1994). This will also enable to consider a single radial characteristic, which can be the radius of the shaft, *R*. The shaft also presents a tangential velocity *U* due to rotation.

Despite the hypothesis of an infinite bearing, a width L may be considered to the bearing to characterise better parameters such as load and friction. It must respect however, the geometry ratio to which infinite bearing can be assumed, that is, *L/D>2* (Hamrock, 1994).

In the light of the assumptions previously described, equation (3.29) can be strongly simplified, given that,

- $\frac{\partial \rho}{\partial t} = 0$, $\frac{\partial h}{\partial t} = 0$ for the steady state condition;
- unidimensional: $\frac{\partial}{\partial y}(.) = 0$;
- rotating shaft: $u_a = U$;
- stationary bush: $u_b = 0$;

Therefore resulting in,

$$\frac{\partial}{\partial x}\left(\frac{\overline{\rho} h^3}{12\overline{\mu}}\frac{\partial p}{\partial x}\right) = \frac{\partial}{\partial x}\left(\frac{\overline{\rho} h U}{2}\right) \tag{4.1}$$

As the radial clearance is much smaller than the journal radius, the film can be linearised and the curvature effects neglected, such that,

$$\begin{aligned} dx &= R d\theta \\ x &= R\theta \end{aligned} \tag{4.2}$$

Furthermore, using the dimensionless eccentricity ration ε, the film thickness for the journal bearing can be derived as (Hamrock, 1994),

$$h = c(1 + \varepsilon \cos\theta) \tag{4.3}$$

Finally, the equation for the two-phase flow along the partial journal bearing can be written as,

$$\frac{\partial}{\partial \theta}\left(\frac{\overline{\rho} h^3}{\overline{\mu}}\frac{\partial p}{\partial \theta}\right) = 6UR\frac{\partial}{\partial \theta}(\overline{\rho} h) \tag{4.4}$$

This equation is valid for the whole extension of the lubricant film, and, upon knowledge of entrance and exit conditions, the boundary conditions described in equation (4.5) can be applied to obtain its solution,

$$\begin{aligned} \theta &= \theta_i, \;\; p = p_i \\ \theta &= \theta_o, \;\; p = p_o \end{aligned} \tag{4.5}$$

where θ_i corresponds to the inlet position of the bearing, where a pressure p_i exists, while θ_o is the outlet position of the bearing at a pressure p_o, which often is equal to the entrance pressure.

The properties for the liquid mixture and for the refrigerant gas are required to determine the apparent properties used in equation (4.4). Those are specific for the mixture chosen, commonly being determined by empirical correlations. Appendices A and B present properties for the oil/refrigerant mixtures R12/SUNISO 1GS and R134a/EMKARATE RL10H, respectively.

Having determined the pressure profile, other performance variables can be calculated. The load capacity per unit length is given by,

$$W' = \sqrt{W_1'^2 + W_2'^2} \tag{4.6}$$

where W_1' and W_2' are components of the load in the direction of the line of centres and the perpendicular to it, as observed in figure 4.2 ,

$$W_1' = -\int_{\theta_i}^{\theta_o} p(\theta) R \cos\theta d\theta \tag{4.7.i}$$

$$W_2' = \int_{\theta_i}^{\theta_o} p(\theta) R \sin\theta d\theta \tag{4.7.ii}$$

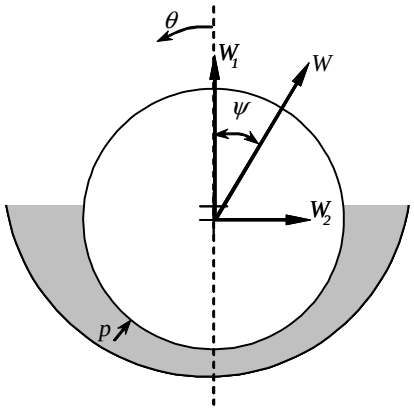

Figure 4.2. Hydrodynamic force acting on the bearing and its components.

In addition to that, the *attitude angle* ψ, defined as the angle between the load line and the line of centres is calculated according to equation (4.8),

$$\tan\psi = \frac{W_2'}{W_1'} \tag{4.8}$$

Another important parameter that can be determined from the pressure field is the *friction torque*, given by,

$$T_f' = \int_{\theta_i}^{\theta_o} \tau_{r\theta} R^2 d\theta \tag{4.9}$$

where the shear stress can be derived from the velocity equation (3.5.i). Simplifying for the journal bearing conditions, and considering the homogeneous pseudofluid Newtonian, results,

$$\tau_{r\theta} = \bar{\mu}\frac{du}{dz} = \left(\frac{2z-h}{2R}\right)\frac{dp}{d\theta} + \bar{\mu}\frac{U}{h} \tag{4.10}$$

It should be now remembered that, for the coordinate system adopted, the bush is at $z=0$ while the shaft is at $z=h$. The friction torque will be considered at the shaft ($z=h$).

From the actual torque, the magnitude of the *friction force* vector can be derived,

$$F_f' = \frac{T_f'}{R} = \int_{\theta_i}^{\theta_o}\left(\frac{h}{2R}\frac{dp}{d\theta} + \bar{\mu}\frac{U}{h}\right)Rd\theta \tag{4.11}$$

It should be noticed here that friction force is calculated using the same expression throughout the bearing. This result is different from the usual methodology (Pinkus and Sternlicht, 1969), which considers film rupture and suggests friction to be taken as,

$$F_f^* = \int_{\theta_i}^{\theta_{cav}}\left(\frac{h}{2R}\frac{dp}{d\theta} + \mu_i\frac{U}{h}\right)Rd\theta + \int_{\theta_{cav}}^{\theta_o}(1-\phi_a)\mu_i\frac{U}{h}Rd\theta \tag{4.12}$$

where the viscosity is considered constant and equal to that at the entrance, and ϕ_a is the fraction of the film filled by gas cavities around which the oil flows in streams. The shear stress in the gas is assumed to be negligible. Furthermore, ϕ_a can be considered as the void fraction of the ruptured film and calculated by,

$$\phi_a = \frac{h-h_{cav}}{h}, \text{ for } \theta \geq \theta_{cav} \tag{4.13}$$

In a homogeneous flow, equation (4.12) is not applicable, since a common velocity and good mixing between phases are assumed. The effect of gas is introduced via the homogeneous viscosity. The difference in the results using these two equations for friction is discussed in more detail later.

From the friction torque, the viscous power consumption can be also calculated,

$$Pot' = T_f' \omega \tag{4.14}$$

Finally, the circumferential mass flow rate at any cross section of the bearing can also be checked,

$$q_\theta = \int_A \bar{\rho} u dz = -\frac{\bar{\rho} h^3}{12 \bar{\mu} R} \frac{dp}{d\theta} + \frac{\bar{\rho} U h}{2} \tag{4.15}$$

The variables previously described will be used to evaluate bearing behaviour and to compare the results of the model with other approaches. The mass flow rate also enables to verify the conservation of mass.

4.2.3. Numerical Methodology

Equation (4.4) will be solved numerically as indicated in section 3.3. However, either by simplifying equation (3.36) or restarting the discretisation from the governing equation of the problem, a much simplified algebraic equation is obtained. The governing equation (4.4) will be integrated in the unidimensional control volume indicated in figure 4.3,

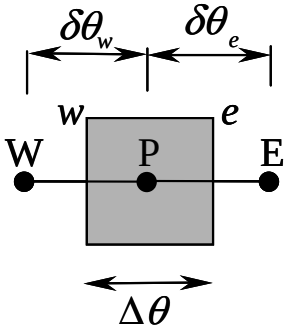

Figure 4.3. Unidimensional control volume used to integrate the governing equation.

Therefore,

$$\int_w^e \frac{\partial}{\partial \theta} \left(\frac{\bar{\rho} h^3}{\bar{\mu}} \frac{\partial p}{\partial \theta} \right) d\theta = \int_w^e 6UR \frac{\partial}{\partial \theta} (\bar{\rho} h) d\theta \tag{4.16}$$

After integration, a set of algebraic equations as indicated by equation (4.17) results,

$$A_p p_P = A_e p_E + A_w p_W + S \tag{4.17}$$

where,

$$A_e = \frac{\overline{\rho}_e h_e^3}{\overline{\mu}_e \delta\theta_e} \qquad A_w = \frac{\overline{\rho}_w h_w^3}{\overline{\mu}_w \delta\theta_w}$$

$$A_p = A_e + A_w \qquad S = -6UR\left(\overline{\rho}_E h_e - \overline{\rho}_P h_w\right)$$

The algebraic set of equations resulting from the discretization is iteratively solved, until the tolerance stipulated according to equation (3.38) is reached. Furthermore, relaxations indicated by equations (3.39-40) are likely to be required.

After obtaining the converged solution for pressure, the additional characteristics of bearing operation can be numerically calculated, again using the variables calculated in discrete points of the domain.

For the load carrying capacity, departing from equations (4.7) results,

$$W_1' = -\int_{\theta_i}^{\theta_o} p(\theta) R\cos\theta d\theta = -\sum_{i=2}^{n_\theta - 1} p_i \cos\theta_i R\Delta\theta_i \tag{4.18.i}$$

$$W_2' = \int_{\theta_i}^{\theta_o} p(\theta) R\sin\theta d\theta = \sum_{i=2}^{n_\theta - 1} p_i \sin\theta_i R\Delta\theta_i \tag{4.18.ii}$$

where the index $i=2$ to $n_\theta-1$ indicates a sum of the differential values in the inner points.

The friction force is numerically calculated as,

$$F_f' = \int_{\theta_i}^{\theta_o} \tau_{r\theta} R d\theta = \sum_{j=1/2}^{n_\theta - 1/2} \left(\frac{h_j}{2} \left.\frac{dp}{d\theta}\right|_j + \frac{\overline{\mu}_j U}{h_j} \right) R\Delta\theta \tag{4.19}$$

where the fractional index j indicates calculation in volume boundaries (e.g., e, w) due to the approximation used for the pressure derivative.

Additionally, the mass flow rate is calculated for every volume boundary using,

$$q_\theta = -\frac{\overline{\rho}_j h_j^3}{12\overline{\mu}_j R} \left.\frac{dp}{d\theta}\right|_j + \frac{\overline{\rho}_j h_j U}{2} \tag{4.20}$$

At this point, the numerical methodology is complete to enable further investigation. The solution procedure can be explained according to the algorithm presented in figure 4.4.

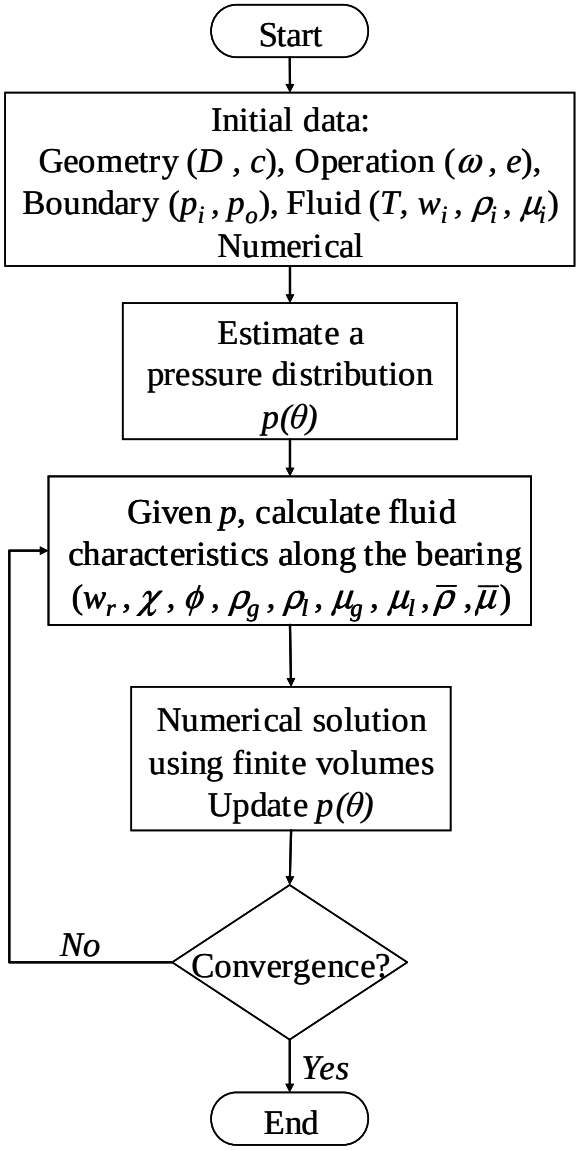

Figure 4.4. Solution procedure for the partial journal bearing problem.

The solution having converged, performance parameters of the bearing can be calculated, such as load, friction, mass flow rate and others. This is also included in the numerical methodology, which was implemented for this work using a code written for the software *Matlab*.

Finally, it should be remembered that, some questions remain open. For instance, occasional absorptions may occur in the bearing and their influence has to be considered, as well as the most suitable correlation for homogeneous viscosity between those presented in equations (3.22) to (3.26). These need to be adjusted in the model based on preliminary tests. This is presented in the sequence, and the solutions provided by simulations with the adjusted model will be explored thereafter.

4.3 ADJUSTMENTS TO THE THERMOPHYSICAL PROPERTIES OF THE MIXTURE

Having defined the mixture to use, refrigerant R12 and mineral oil SUNISO 1GS, correlations to determine properties are chosen and included in the two-phase lubrication model. For the mixture in study, these correlations are presented in Appendix A. The model depends on the precision of these data to provide a realistic result. Although some discussion of the correlations used have been performed by Lacerda (2000) and Grando (2001), this will not be repeated here. No experimental results are available for comparison at this moment, and the same properties will be adopted to obtain verification results using Reynolds condition. Using the correlations, the problem of determining properties of the constituent phases for the two-phase mixture is resolved.

Nevertheless, as discussed in chapter 3, a correlation for homogeneous viscosity needs to be determined from the alternatives proposed, which will require testing and comparison between their results. In addition to that, the absorption of refrigerant gas by the liquid mixture under positive pressure gradients is not well understood, and its importance has to be examined before a decision is made. This is discussed in the following sections.

4.3.1. Absorption of gas refrigerant by the liquid mixture

Several works studying the flow of refrigerants have pointed to a metastable condition in the release of gas from the liquid (Meyer and Dunn, 1998), although the vast majority simply neglects it obtaining very similar results (Wongwises and Pirompak, 2001). The same has been assumed in the study of oil and refrigerant mixtures, despite some tendency of metastability observed by Lacerda et al. (2000).

Regarding absorption, however, its existence is acknowledged, although the phenomenon tends to reach equilibrium via very slow processes. In his experiment, Lacerda (2000) mentioned that considerably long times were required to achieve equilibrium of the oil and refrigerant mixture. Furthermore, in an attempt to ensure saturation at the entrance, release of gas through a reduction in pressure was induced, which also pointed to the difficulty of dealing with absorption. No precise method is available to determine the time required to the absorption of the gas by the liquid.

Furthermore, it has not yet been studied the behaviour of the mixture when experiencing sudden changes in pressure.

To evaluate the influence of the reabsorption of gas near the bearing exit, simulations comparing the equilibrium and non-equilibrium assumptions are performed, respectively representing the situations where absorption is instantaneous and where the absorption can be neglected, i.e., the two extreme cases among which the actual situation may lie.

A first comparison considers a journal bearing with a large clearance combined with low eccentricity, which corresponds to a situation of lower bearing load. Results are shown in figure 4.5. It is observed a pressure recovery very close to the end of the bearing, communicating the higher ambient pressure to the cavitated film with subambient pressures (figure 4.5a). Mass fraction then recovers if absorption is considered (figure 4.5b). As pressure increases in this region, density increases and void fraction decreases due to gas compression or refrigerant absorption (figures 4.5c-d). This phenomenon is much more significant in the case where absorption occurs, when the fluid returns to the entrance conditions (entrance and outlet pressure are considered the same, in this case more realistic). The length of recovery region is small, especially for the case with absorption. It is however highly unlikely that such an absorption can completely occur in this small length and at this speed. Despite this difference, in terms of load carrying capacity and friction force, differences are very small, which results from the similarity of the pressure profile in the convergent region. Results for those variables are presented in table 4.1, where differences smaller than 1% are observed.

Table 4.1. Results for load and friction for the different conditions regarding absorption.

	W (N)	Ψ (º)	F_f (N)
Non-equilibrium	120.24	34.13	2.05
Equilibrium	120.55	34.45	2.05
Difference (%)	0.26	0.93	0.10

($D = 20mm, c = 100\mu m, \varepsilon = 0.6, \omega = 60Hz, p_i = p_o = 100kPa, T = 40^oC, w_i = w_{sat} = 4.07\%, L = 100mm$)

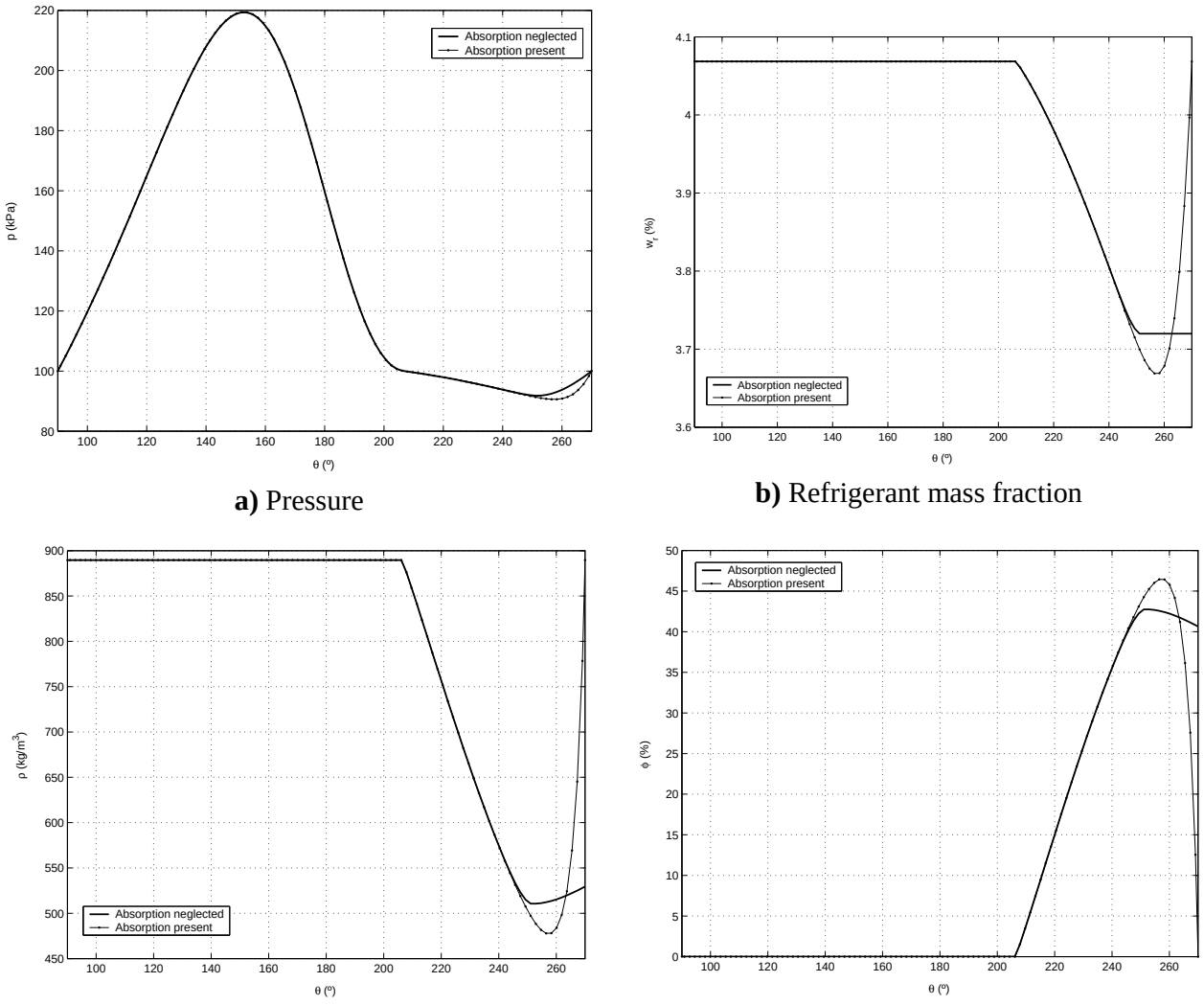

a) Pressure

b) Refrigerant mass fraction

c) Apparent density

d) Void fraction

Figure 4.5. Influence of absorption of refrigerant gas near the outlet in the behaviour of the fluid. ($D = 20mm, c = 100\mu m, \varepsilon = 0.6, \omega = 60Hz, p_i = p_o = 100kPa, T = 40^o C, w_i = w_{sat} = 4.07\%, L = 100mm$)

To verify the higher load case, another simulation is studied, now closer to usual application of the bearings. Results for pressure, cavitated pressure, solubility and density can be seen in figure 4.6a-d, respectively. The apparent density provides identical interpretation to the void fraction effects, which reaches a maximum close to 70% prior to the pressure recovery region. A mesh refinement was necessary to the detail the solution of the simulation considering absorption near the outlet. For better visualisation, the majority of the results show exclusively the cavitated region, given that only minor differences were noticed.

It can be concluded from the second case, which is closer to real bearing working conditions, that outlet absorption effects are negligible in terms of operation. This is also confirmed observing the values for load and friction in table 4.2. It should be noticed however that not only absorption is less important, but also the cavitation

region has less influence due to the higher level of pressures in the convergent region. Furthermore, as pressure recovery is concentrated nearer the end of the bearing, the rate of absorption is expected to be higher than before, which is not expected.

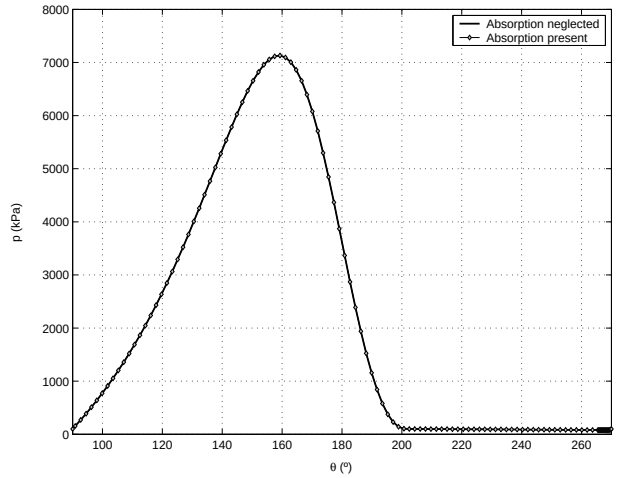

a) Pressure

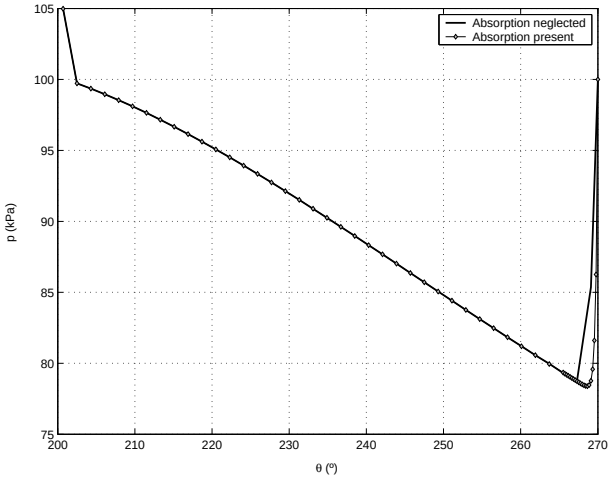

b) Pressure in the cavitated region

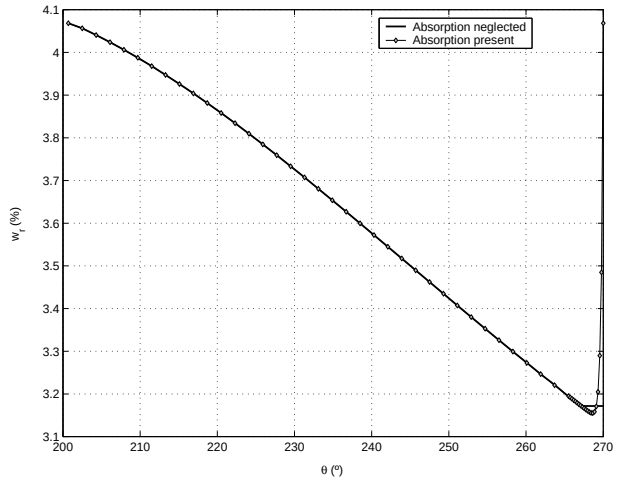

c) Refrigerant mass fraction – cavitated region

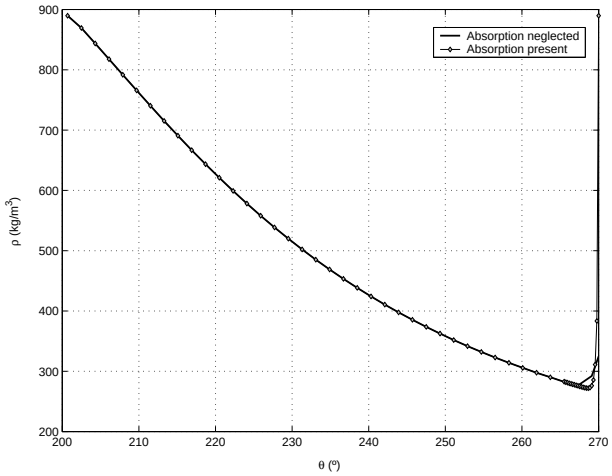

d) Apparent density – cavitated region

Figure 4.6. Influence of refrigerant absorption in the behaviour of fluid along the bearing – heavy load. ($D = 20mm, c = 20\mu m, \varepsilon = 0.75, \omega = 60Hz, p_i = p_o = 100kPa, T = 40^oC, w_i = w_{sat} = 4.07\%, L = 100mm$)

Table 4.2. Results for load and friction for the different absorption conditions – heavy load

	W (N)	*Ψ (º)*	*F_f (N)*
Non-equilibrium	6209.2	29.046	14.49
Equilibrium	6209.2	29.047	14.49
Difference (%)	0.001	0.004	0.0007

From the previous results, and considering this initial application of the model, absorption will not be considered in further simulations, i.e., gas can be released from the liquid when pressure falls below saturation, but no gas is reabsorbed afterwards when the saturation pressure is exceeded. This will limit the study to situations where bearings are fed only with liquid lubricant. This restriction is expected to be relaxed in the next developments of this work.

4.3.2. Study of the correlation for the homogeneous viscosity

To provide an adequate solution to a specific problem, the homogeneous model requires a suitable correlation for the apparent (homogeneous) viscosity. To achieve this objective, a number of correlations has been proposed, usually fitted for specific problems through comparison with experimental results. This leads to controversy in the definition of two-phase homogeneous correlation for distinct fields of engineering, such as in heat transfer problems, transport lines for oil and gas, among others.

The same problem has been observed in lubrication, despite the small number of studies adopting two-phase models. There is an additional problem in lubrication: as gases and volatile liquids can dissolve considerably in the oil, the viscosity of the liquid phase also varies considerably, usually decreasing when compared to the pure oil. Neither the variation of the liquid phase viscosity or in which condition it was measured have received significant attention. Therefore, some authors believe that viscosity decreases with the release of gas (Kicinski, 1983, Qi et al., 1997), which probably means a comparison with pure oil viscosity. Others, however (Nikolajsen, 1999, Choi and Kim, 2002), suggest that viscosity increases with the release of gas, which is likely to occur when it is compared to the original liquid lubricant mixture (not pure oil). The distribution and shape of the free gas phase may also influence in the choice of the correlation. All these aspects require further investigation, and clarification about their influence can only be achieved with experimental testing.

Not having this information available, the five correlations proposed in chapter 3, equations (3.22) to (3.26) were tested and compared in this work; they were also checked with the analytical results obtained using Reynolds condition (Pinkus and Sternlicht, 1961). To interpret the results, evaluation considered variables such as pressure, density and viscosity, and performance parameters of the bearings, such as the load capacity and the friction force. Tests performed are exemplified in figures 4.7a-c

and 4.8a-c, where two different clearances were considered, respectively *100μm* and *40μm*. The case of a lower applied load (larger clearance) is studied to provide better distinction between the correlations. Results are shown for two-phase flow simulations using correlations of Cichitti, equation (3.22), McAdams (3.23), Someya (3.24), Hayward (3.25) and Einstein (3.26), with pressures also shown for the solution using the analytical Reynolds condition. To exemplify the difference of considering constant liquid viscosity, a test with a modified Hayward correlation is also presented. In this case, the apparent viscosity is defined by,

Hayward mod. $$\bar{\mu} = (1 + 0.15\phi)\mu_e \tag{4.21}$$

where μ_e *(Pa.s)* is the liquid viscosity at the entrance of the bearing (constant).

In figure 4.7a, it is seen that Someya and McAdams, averaged by void fraction, promote considerable reduction in viscosity. Actually, Someya correlation presents a strange behaviour, which indicates that it was adjusted to work only in lower fractions of gas. On the other hand, Einstein produces a huge increase. Hayward correlations and Cichitti show more reasonable variations. Differences between Hayward and Hayward modified are small; when the increase in base (liquid) viscosity is not considered, the second is closer to the Cichitti result.

In figure 4.7b, for the pressure along the bearing, correlations predicting higher viscosities reach lower pressures and have a smaller extension to the pressure recovery region. This can be analysed using Navier-Stokes equation (3.1.i), where the balance of viscous and pressure forces is stated. As viscosity increases, there is a tendency of increasing viscous force, which is then balanced by higher pressure force resulting from bigger pressure gradients – moving pressure recovery closer to the end (further discussion of this effect will be presented in section 4.5). The viscosity effects however do not create any difference in pressures in the convergent region (single phase flow). Again, the effect is not important in pressure results for the cavitated region (195-240^o), despite big differences in density and viscosity. Therefore, the effect of viscosity correlation can be considered isolated at the pressure recovery region. For this reason, it can be stated that *density* is the most important property in the cavitated region instead of *viscosity*, which is more important in the full-film region.

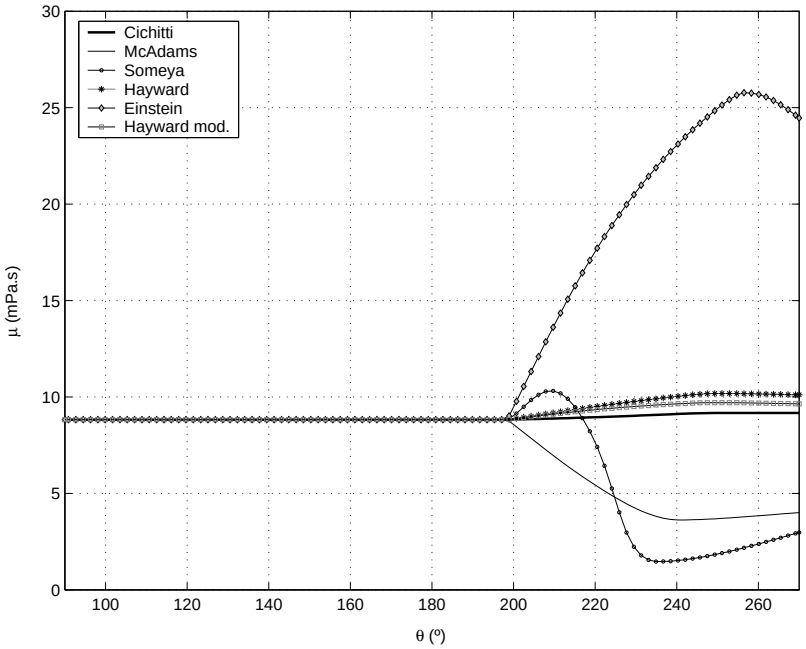

a) Apparent viscosity

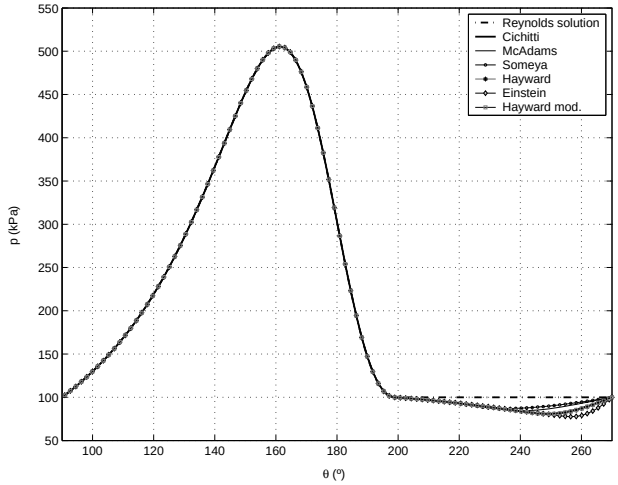

b) Pressure

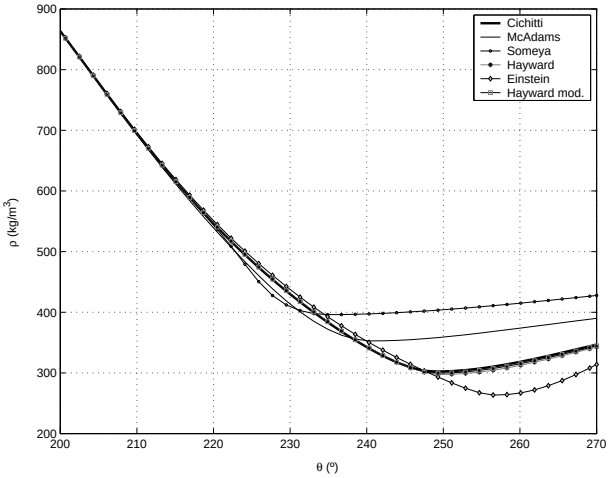

c) Apparent density – cavitated region

Figure 4.7. Influence of viscosity correlation in the behaviour of fluid along the bearing – light load. ($D = 20mm, c = 100\mu m, \varepsilon = 0.80, \omega = 60Hz, p_i = p_o = 100kPa, T = 40^oC, w_i = w_{sat} = 4.07\%, L = 100mm$)

The effect of viscosity correlation will then present significant influence only for the friction force, as shown in table 4.3. While load carrying capacity and attitude angle are practically constant, friction force varies more than 40% in comparison to the friction force predicted by the analytical solution considering Reynolds boundary conditions (Pinkus and Sternlicht, 1961) and assuming striated flow in cavitation. As in this condition the importance of friction is reduced by the presence of streamers, not surprisingly correlations predicting lower viscosities present better agreement. If the comparison is performed to a friction force calculated using Reynolds solution but considering a full-film occupies the whole thickness, Hayward and Cichitti results are

the closest ones. Analytical solution for pressure and correlations for the analytical forces are derived by Pinkus and Sternlicht (1961). Unfortunately, for a firm and definite conclusion, only experimental results can show which result is closest in a real situation.

Table 4.3 – Results for load and friction for the different viscosity correlations – light load

	W (N)	$W/W_{Reynolds}$	ψ (^{o})	$\psi/\psi_{Reynolds}$	F_f (N)	$F_f/F_{f\ Reynolds}$	$F_f/F_{fReynolds}^{full-film}$
Reynolds	*333.8*	*1*	*27.4*	*1*	*3.04*	*1*	*0.8981*
Cichitti	*334.0*	*1.0006*	*29.5*	*1.0746*	*3.44*	*1.1328*	*1.0173*
McAdams	*333.8*	*0.9988*	*29.1*	*1.0623*	*3.09*	*1.0175*	*0.9138*
Someya	*333.2*	*0.9984*	*28.9*	*1.0541*	*3.13*	*1.0293*	*0.9244*
Hayward	*334.0*	*1.0008*	*29.5*	*1.0758*	*3.50*	*1.1518*	*1.0344*
Einstein	*334.6*	*1.0026*	*29.8*	*1.0846*	*4.35*	*1.4314*	*1.2854*
Hay Mod.	*334.0*	*1.0007*	*29.5*	*1.0752*	*3.48*	*1.1445*	*1.0278*

($D = 20mm, c = 100\mu m, \varepsilon = 0.80, \omega = 60Hz, p_i = p_o = 100kPa, T = 40^oC, w_i = w_{sat} = 4.07\%, L = 100mm$)

A second simulation, closer to practical applications (moderately loaded bearing, $c=40\mu m$) is presented in figures 4.8a-c and table 4.4. As shown respectively in figures 4.8b-c, differences in pressure and density are less significant than those in the first simulation, where $c=100\mu m$. Apart from the Someya correlation, differences are noticed only in the last 15^o of the bearing. Pressures could be taken as identical, despite the big differences in viscosity seen in figure 4.4a. Again, higher viscosities are predicted for Einstein correlation, lower for McAdams, Hayward and Cichitti showed closer results, and Someya repeats the strange behaviour.

From these results, it can be concluded that, apart from the friction force and the viscosity itself, all other results for the bearing would not be significantly affected by the correlation chosen. A definite answer would depend on measurement of the apparent viscosity or perhaps friction force, both unavailable at the moment.

The choice for this work is then taken based on related works and previous experiences. Reasonable variations of viscosity are expected to be around those

obtained using Cichitti and Hayward, especially considering a constant viscosity for the liquid in the second. Hayward is the most commonly used in lubrication (Feng and Hahn, 1986). However, Grando (2001) used Cichitti correlation in a pipe flow study with the oil and refrigerant mixture, obtaining good agreement with experimental data from Lacerda (2000). Additionally, Cichitti obeys the conditions recommended by equation (3.21) for pure liquid and gas, while Hayward fails in it. Therefore, Cichitti correlation will be adopted for further simulations in this work. Nevertheless, it should be stressed that a comparison with experimental results is necessary to a definite conclusion, providing both pressure and friction results accurately.

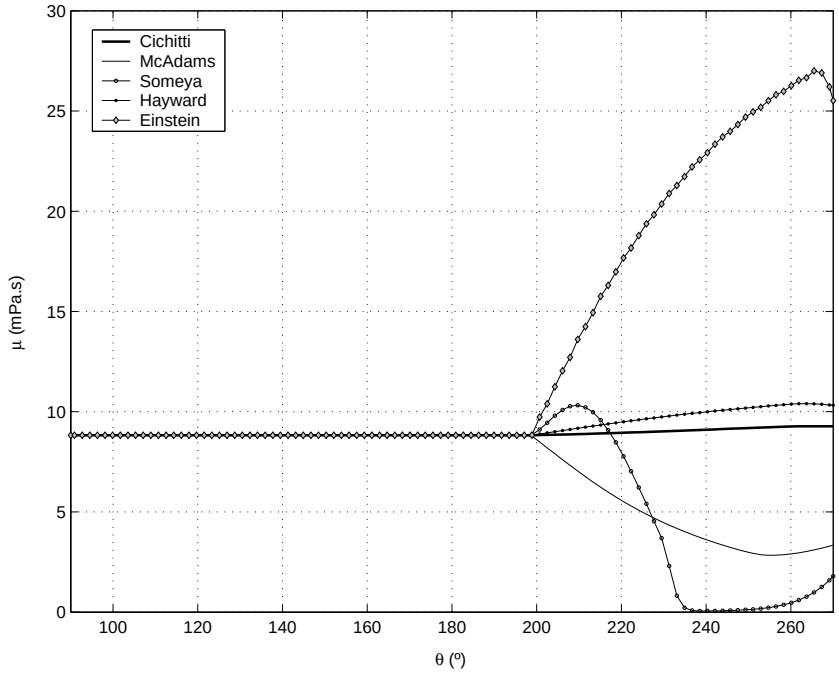

a) Apparent viscosity

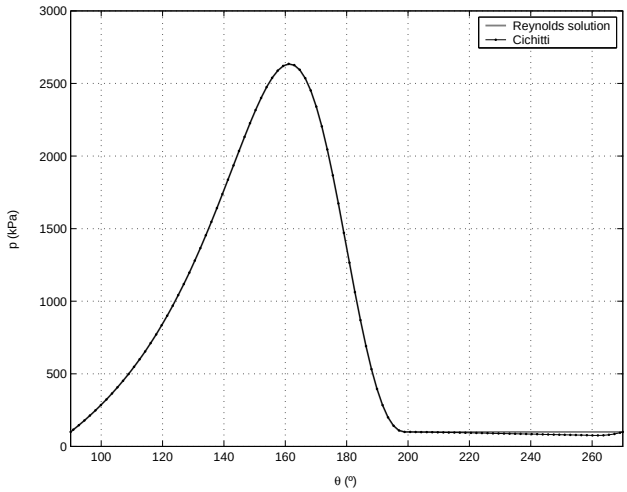

b) Pressure

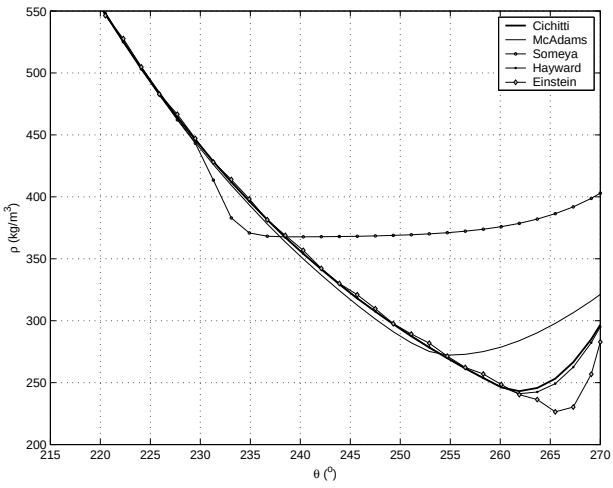

c) Apparent density – cavitated region

Figure 4.8. Influence of viscosity correlation in the behaviour of fluid in the bearing – moderate load. ($D = 20mm, c = 40\mu m, \varepsilon = 0.80, \omega = 60Hz, p_i = p_o = 100kPa, T = 40^o C, w_i = w_{sat} = 4.07\%, L = 100mm$)

Table 4.4 – Results for load and friction for the different viscosity correlations – moderate load

	W (N)	$W/W_{Reynolds}$	ψ (^{o})	$\psi/\psi_{Reynolds}$	F_f (N)	$F_f/F_{f\ Reynolds}$	$F_f/F^{full-film}_{fReynolds}$
Reynolds	*2086.0*	*1*	*27.4*	*1*	*7.60*	*1*	*0.8981*
Cichitti	*2088.1*	*1.0010*	*27.8*	*1.0142*	*8.53*	*1.1220*	*1.0076*
McAdams	*2087.5*	*1.0007*	*27.8*	*1.0130*	*7.65*	*1.0060*	*0.9034*
Someya	*2087.1*	*1.0005*	*27.7*	*1.0104*	*7.68*	*1.0102*	*0.9072*
Hayward	*2088.1*	*1.0010*	*27.8*	*1.0143*	*8.67*	*1.1409*	*1.0246*
Einstein	*2088.4*	*1.0011*	*27.8*	*1.0149*	*10.78*	*1.4183*	*1.2737*

($D = 20mm, c = 40\mu m, \varepsilon = 0.80, \omega = 60Hz,\ p_i = p_o = 100kPa, T = 40^oC, w_i = w_{sat} = 4.07\%, L = 100mm$)

4.4 PARAMETERS OF THE NUMERICAL METHODOLOGY

To implement the numerical methodology presented in section 3.3, a series of control parameters is required, such as the number of discrete points to use (n_θ, mesh), the tolerance required in the iterative method, the initial guess and the under-relaxation factors, βp and $\beta\rho$, to be used. These parameters contribute to the stability of the method and the precision of the solution.

Regarding the mesh, tests indicated that a discretisation using 102 points (100 uniformly distributed internal points) proved to give enough precision to predict smooth variation of the properties throughout the solution domain. Comparing with more refined meshes, 300 and 500 internal points, the improvement of the result was not significant, while the computational time presented a considerable increase. In some cases, for heavier loads (smaller clearances, higher eccentricities and velocities), the pressure recovery region is very small; a local refinement is then recommended close to the end of the bearing, to communicate the back pressure smoothly and to enable prediction of the pressure recovery region. In this case, there is not a considerable increase in the number of points (around 10%), and the computational time remains similar or can even be reduced due to a more stable convergence. Despite the

non-uniform grid, the nodal points are still positioned in the centre of the volume. Table 4.5 presents the comparison between different simulations, each of them using two distinct meshes. It will be noticed in case 2 that different tolerances were also considered, however without major influence in the results. For the third case, the mesh of 119 points indicates a refinement in the two last points in a mesh of 102, including new points and reducing the distance between them from the initial $\Delta\theta$ to $\Delta\theta/8$.

In the same table, results are presented to assist in defining the tolerance (relative error) of the iterative process (*tol*). The maximum error is achieved systematically for the pressure field, and it can be seen that the increase in tolerance from the order of 10^{-5} to 10^{-7} or smaller demands considerable increase in the computational effort without major improvements in the results, particularly for higher pressures. Therefore, a tolerance of 10^{-6} was defined throughout the simulations, ensuring satisfactory precision and reasonable computational effort.

Table 4.5. Comparison of simulations using different number of points and different tolerances

Case	*Points*	*max(p)*	*min(p)*	*W (N)*	*F_f (N)*	*min(ρ)*	*max(μ)*	*tol*	*time(s)*	*iter*
1	***102***	*741.35*	*85.46*	*598.02*	*3.17*	*369.30*	*9.09*	*9.9e-9*	*109.8*	*733*
1	***502***	*741.44*	*85.48*	*597.68*	*3.17*	*369.63*	*9.08*	*9.9e-9*	*659.3*	*966*
2	*102*	*7130.2*	*78.74*	*6209.1*	*14.49*	*275.89*	*9.21*	***1.2e-5***	*208.0*	*1500*
2	***102***	*7130.3*	*78.79*	*6209.2*	*14.49*	*276.38*	*9.21*	***8.1e-7***	*294.3*	*2500*
2	***302***	*7128.2*	*79.05*	*6209.2*	*14.49*	*279.33*	*9.20*	*3.2e-8*	*5600*	*9999*
3	***102***	*16028*	*64.73*	*11898*	*20.82*	*163.46*	*9.48*	*4.3e-5*	*195.4*	*1500*
3	***119***	*16028*	*65.40*	*11898*	*20.82*	*167.36*	*9.46*	***3.7e-5***	*201.4*	*1500*
3	*119*	*16028*	*65.99*	*11899*	*20.82*	*170.86*	*9.45*	***7.7e-7***	*613.4*	*4500*

Case 1:
$D = 20mm, c = 40\mu m, \varepsilon = 0.70, \omega = 30Hz, p_i = p_o = 100kPa, T = 40^oC, w_i = 4.07\%, L = 100mm$

Case 2:
$D = 20mm, c = 20\mu m, \varepsilon = 0.75, \omega = 60Hz, p_i = p_o = 100kPa, T = 40^oC, w_i = 4.07\%, L = 100mm$

Case 3:
$D = 20mm, c = 20\mu m, \varepsilon = 0.85, \omega = 60Hz, p_i = p_o = 100kPa, T = 40^oC, w_i = 4.07\%, L = 100mm$

The most important numerical parameter, however, is the under-relaxation factor for pressure, β_p. Relaxation for properties (β_ρ) seemed to be of small significance, such

that the control of pressure relaxation exclusively is simpler and more effective. Pressure relaxation was previously defined by equation (3.39) as,

$$p_i^k = \beta_p \, p_i^k\big|_{calc} + (1-\beta_p) p_i^{k-1} \tag{3.39}$$

The determination of the value for the under-relaxation factor, however, is not an easy task. From testing, it was observed that the values for the factor had to be very small, updating pressure slowly. Failing to do so promoted an unstable oscillatory process, not uncommonly remaining far from the expected tolerance. Smaller relaxation, on the other hand, reduced the convergence rate. An optimal value then exists, as presented in figure 4.9.

An additional challenge is that the value proved to be case dependent; further tests indicated that relaxation seems to decrease with the increase of clearance, eccentricity, velocity and viscosity. For instance, while $\beta_\rho=0.055$ was defined for $c=100\mu m$ in figure 4.9, for $c=15\mu m$ one had to use $\beta_\rho=0.0015$, also requiring an increase in the number of iterations.

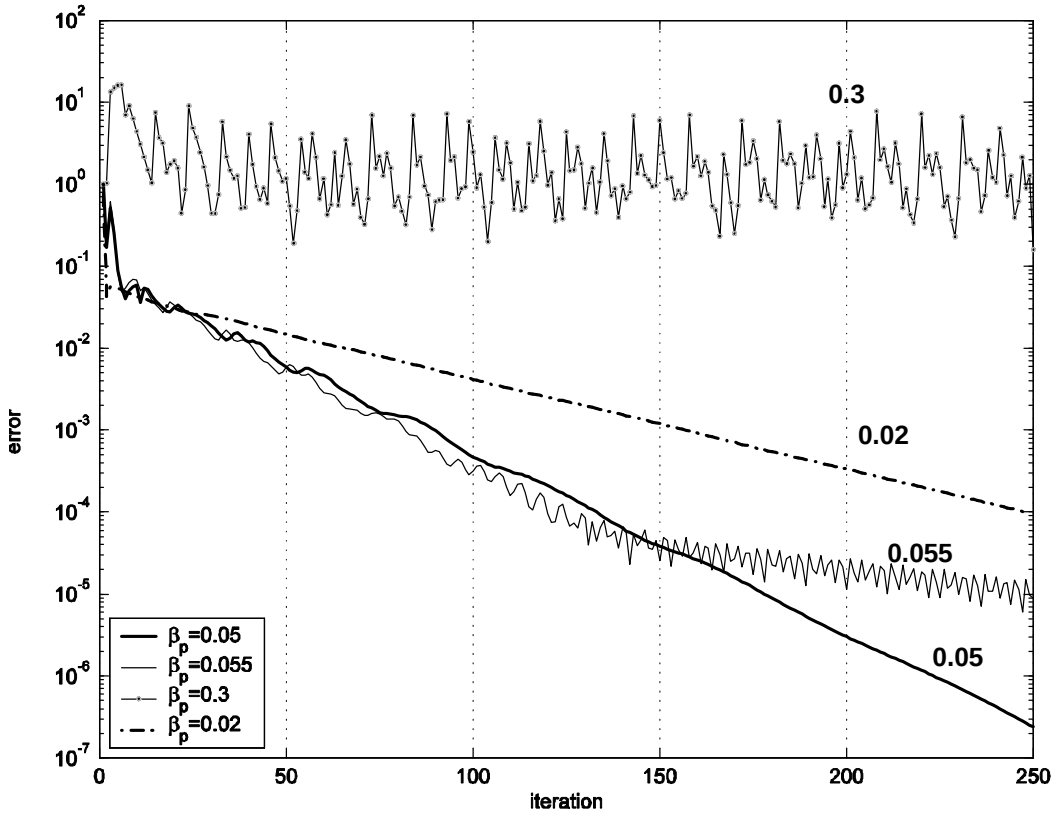

Figure 4.9. Influence of under-relaxation in pressure in the convergence of the solution. ($D = 20mm, c = 100\mu m, \varepsilon = 0.80, \omega = 60Hz, p_i = p_o = 100kPa, T = 40^oC, w_i = w_{sat} = 4.07\%, L = 100mm$)

As a result of the strong relaxation required, for every iteration a typical correction as that presented in figure 4.10 is observed; in an intermediate iterative step, with properties calculated from the pressure obtained in a previous iteration, a new pressure profile is calculated. This solution tries to bring the previous field in the direction of the converged solution at every point, which, despite indicating the self-correcting characteristic of the method, produces a high degree of oscillation. Using the relaxation factor, the solution is then updated in a lower oscillatory level. This is repeated until convergence, when both calculated and relaxed solutions have very similar and non-oscillatory profiles.

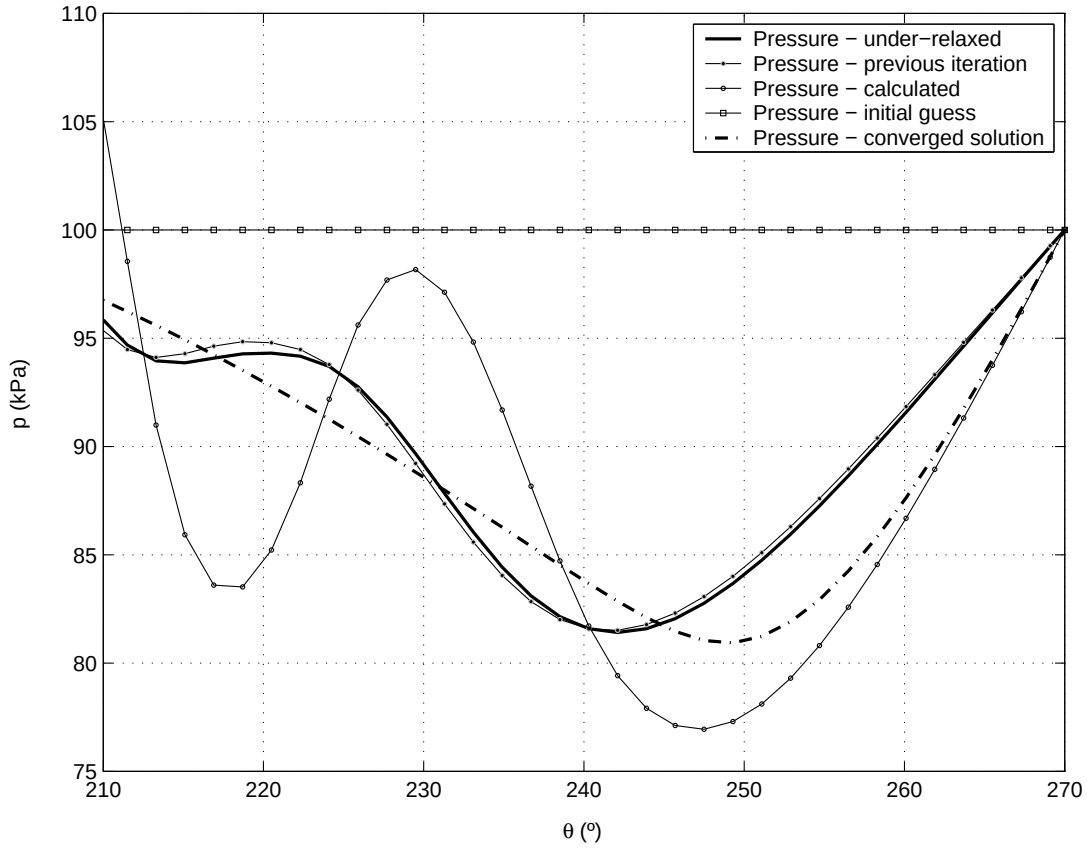

Figure 4.10. Correction of the pressure field using under-relaxation – cavitated region.
($D = 20mm, c = 100\mu m, \varepsilon = 0.80, \omega = 60Hz, p_i = p_o = 100kPa, T = 40^oC, w_i = w_{sat} = 4.07\%, L = 100mm$)

Figures 4.11a-b present the evolution of the pressure solution and the calculated density throughout the iterative process, using the optimum relaxation factor β_ρ=0.055. Initial conditions considered half-Sommerfeld solution for pressure and constant density. Here, the oscillatory corrective behaviour described in figure 4.10 can also be observed, despite the use of relaxation. Visually, from iteration 50 of a total of 250 the profiles are already very similar and of hard distinction.

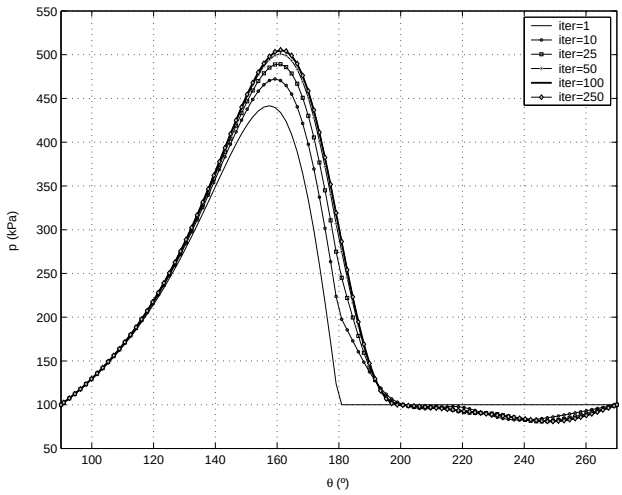

a) Pressure (relaxed)

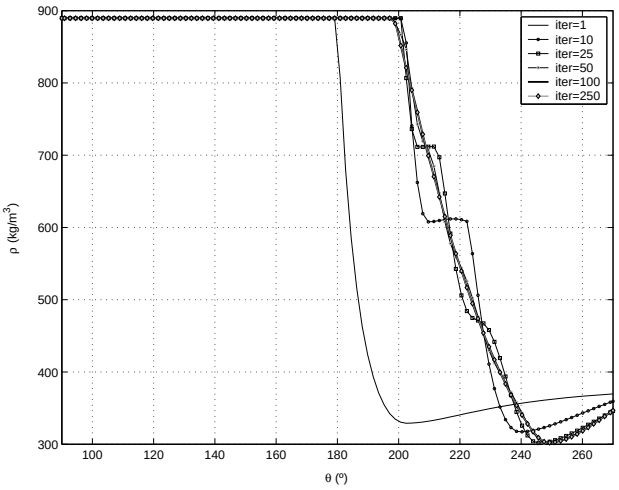

b) Apparent density

Figure 4.11. Evolution of pressure and density within the iterative process.
($D = 20mm, c = 40\mu m, \varepsilon = 0.80, \omega = 60Hz, p_i = p_o = 100kPa, T = 40^oC, w_i = w_{sat} = 4.07\%, L = 100mm$)

Despite the similarity of the pressure profiles already in the 50th iteration, the process is continued for a longer time after that to satisfy the conservation of mass. This is presented in figures 4.12a-b to the mass flow rate and the flow difference between two consecutive nodal points.

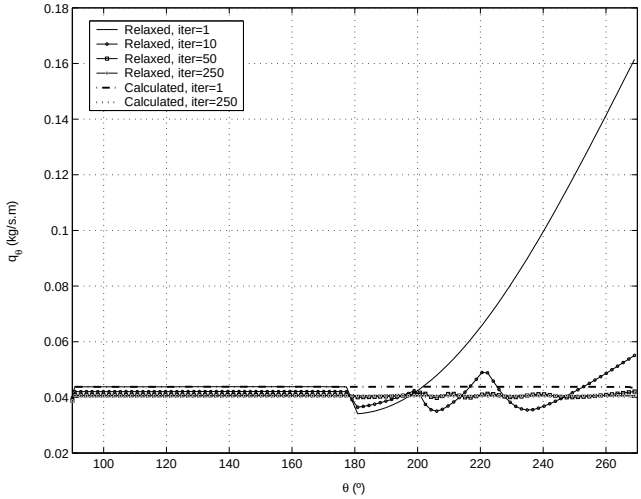

a) Circumferential mass flow rate

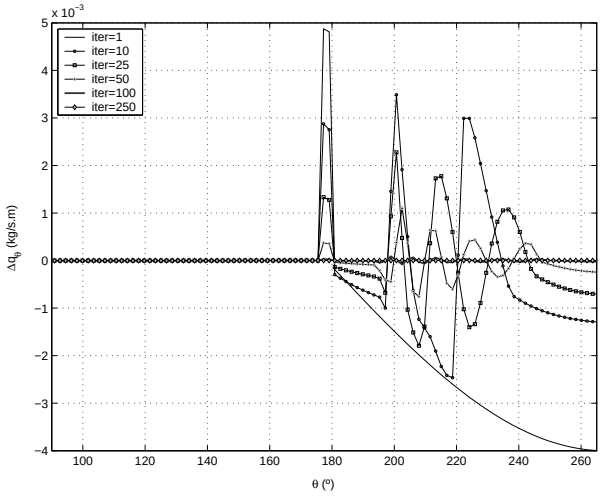

b) Difference of flow between consecutive points

Figure 4.12. Conservation of mass within the iterative process.
($D = 20mm, c = 40\mu m, \varepsilon = 0.80, \omega = 60Hz, p_i = p_o = 100kPa, T = 40^oC, w_i = w_{sat} = 4.07\%, L = 100mm$)

In figure 4.12, it is observed that for the initial iteration the conservation of mass is far from being conserved. However, as a consequence of the calculation using the Reynolds equation, a mass-conserving solution is obtained for every iterative step. The use of relaxation, however, destroys this conservative solution when averaging results with those from previous iteration, and conservation of mass has to be improved with

the evolution of the iterative process. This can be better observed in figure 4.12b for the difference of flow between consecutive points. In these figures, it can also be observed that the oscillations are only seen for the cavitated region, therefore indicating that the numerical effort is related with the solution of the two-phase flow.

The numerical effort can be reduced using a better estimative for pressure and void fraction (affecting density), such as the pressure profile from Reynolds solution and a void fraction estimated from the film thickness, shown in equation (4.13) as,

$$\phi_a = \frac{h - h_{cav}}{h}, \text{ for } \theta \geq \theta_{cav} \tag{4.13}$$

An initial estimative for density can be given from the above result as,

$$\overline{\rho} = (1 - \phi_R)\rho_e \tag{4.22}$$

This improves considerably convergence. For the above simulation, under the same conditions, same level of error is achieved in 201 iterations instead of 250 – and the potential of improvement is more significant is cases of higher applied loads. This initial guess is adopted for the simulations, but one should bear in mind that obtaining Reynolds solution for more complex problems also requires some computational effort and may not compensate the 20% gain in effort observed in the two-phase unidimensional problem.

Despite the attempts to accelerate convergence and the use of optimal parameters, the computational effort is still big compared to the conventional methodologies, particularly for higher eccentricity and clearances. This was also reported by Someya (2003), therefore indicating a cost for the two-phase solution. The challenge that remains is to create a uniform convergent method instead of the oscillatory one, which then enables relaxation to be significantly reduced.

4.5 COMPARISON WITH SOLUTION USING THE REYNOLDS BOUNDARY CONDITION

The usual hydrodynamic lubrication problem for journal bearings considers constant properties along the full-film region and solves cavitation using Reynolds

boundary conditions, as given by equation (2.4). Pinkus and Sternlicht (1961) present the analytical solution for the case of a partial journal bearing. Dowson and Taylor (1979) suggest that these boundary conditions provide a good approximation for heavier loads along the bearing, while the result is deviated from reality for lightly loaded bearings

These observations are also confirmed when the two-phase model proposed here was compared with Reynolds solution. Figures 4.13 to 4.15 present dimensionless pressure profiles for different eccentricities, $\varepsilon=0.2$, $\varepsilon=0.5$ and $\varepsilon=0.85$, respectively. The dimensionless pressure is defined here as,

$$p^* = \frac{(p - p_e)c^2}{6\mu_e UR} \tag{4.23}$$

Four different clearances were considered in the simulations using two-phase methodology: *c=20, 100, 250 and 1000μm.* From the first to the last, the load acting on the bearing dramatically decreases. For the Reynolds condition, dimensionless results do not depend on the clearance.

For all the three figures, the larger clearance presents a results very different from the heavily and moderately loaded bearings (*c=20, 100μm*). Although a non-symmetric profile occurs, the results are closer to Sommerfeld solution as clearance increases, especially for the lower eccentricity ($\varepsilon=0.2$, figure 4.13). The position of pressure recovery also moves towards the centre of the bearing (180^o), which means that back pressure influences a longer region of the bearing as clearance increases.

From figures 4.14 and 4.15, it can be seen that as eccentricity increases (and so does the load), pressure profiles come closer to the ones predicted by Reynolds condition, even for larger clearances. Nevertheless, it would still be a reasonable approximation only for the smaller values (*c=20, 100μm*), which are also those closer to practical applications. Also, the case for *1000μm* should be seen as an exaggeration of the test, given that at such larger clearances, assumptions such as the negligible circumferential effects are probably questionable.

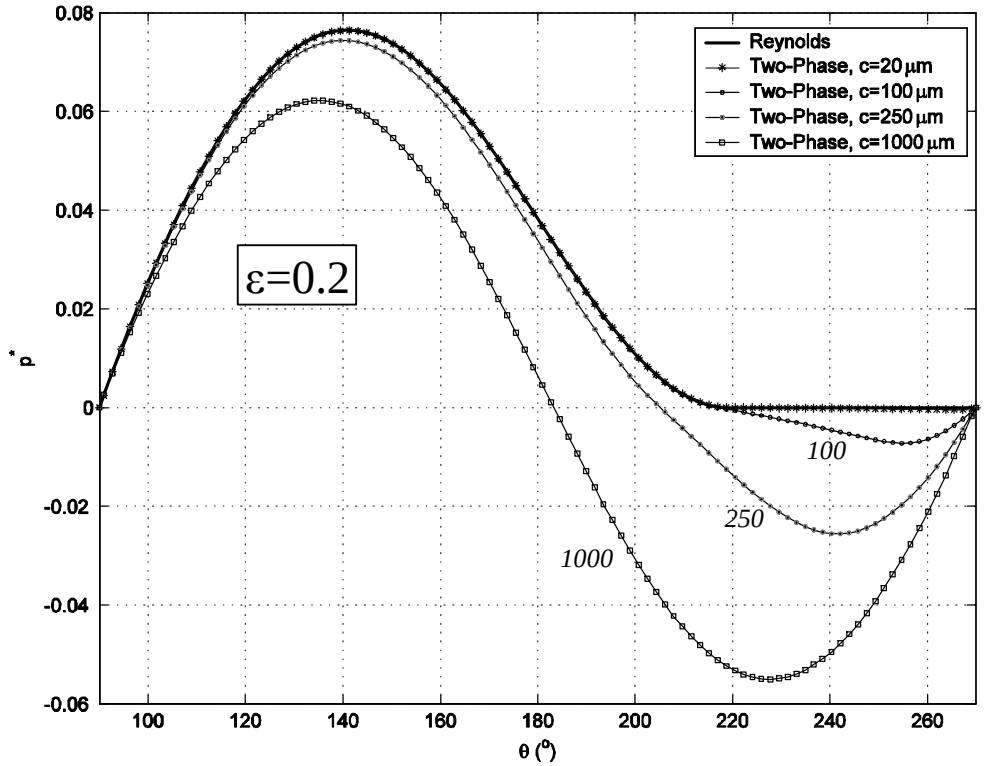

Figure 4.13. Comparison between Reynolds results and the two-phase method for different clearances.
($D = 20mm,\ \omega = 60Hz,\ p_i = p_o = 100kPa, T = 40^oC, w_i = w_{sat} = 4.07\%,\ L = 100mm$)

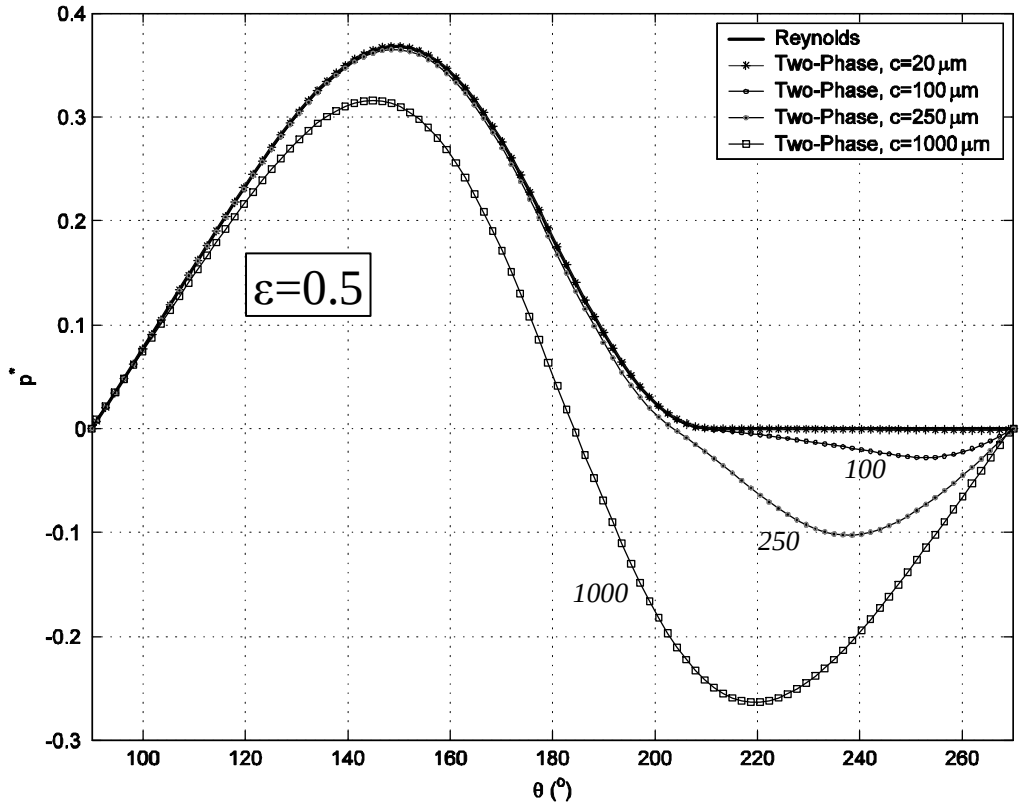

Figure 4.14. Comparison between Reynolds results and the two-phase method for different clearances.
($D = 20mm,\ \omega = 60Hz,\ p_i = p_o = 100kPa, T = 40^oC, w_i = w_{sat} = 4.07\%,\ L = 100mm$)

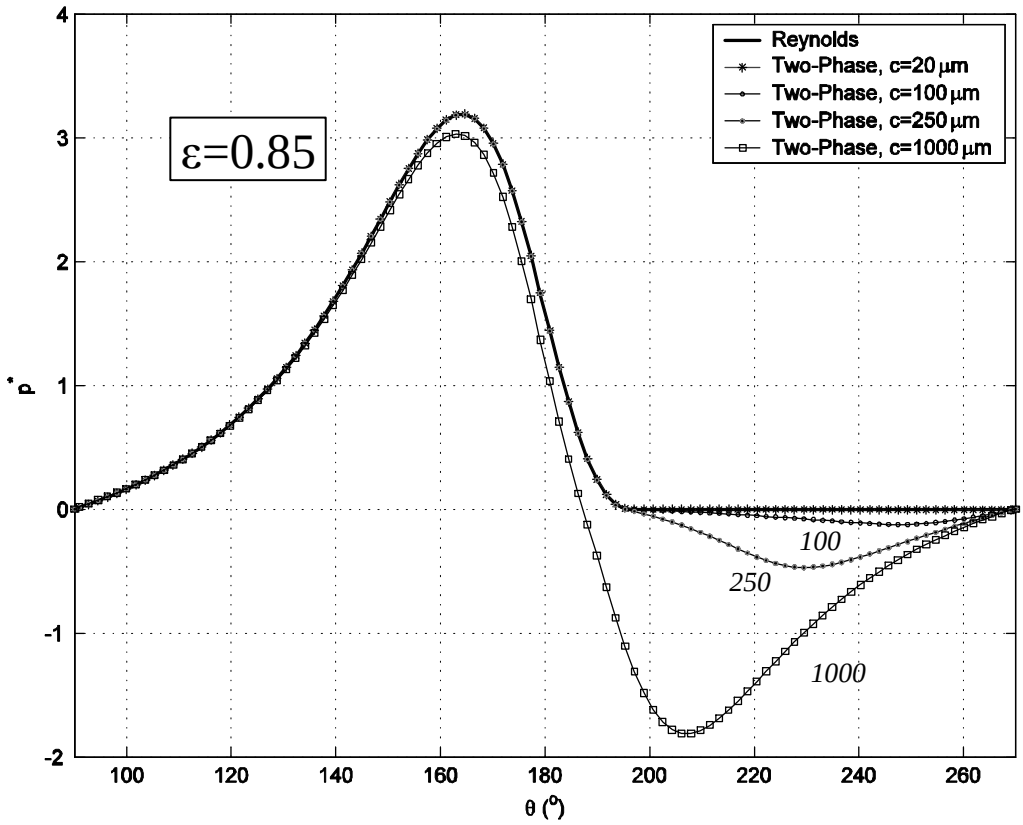

Figure 4.15. Comparison between Reynolds results and the two-phase method for different clearances. ($D = 20mm,\ \omega = 60Hz,\ p_i = p_o = 100kPa, T = 40^o C,\ w_i = w_{sat} = 4.07\%,\ L = 100mm$)

In addition to the pressure profiles, other parameters were used to compare the different solutions and geometries, in order to characterise the performance of the bearing. These were the *Sommerfeld number* and the *attitude angle*, related to the load capacity of the bearing, the *friction factor*, and the *cavitation angle*. The cavitation angle is defined for the two-phase model as the position where the release of gas starts. The Sommerfeld number and the friction factor are respectively defined by,

$$\Delta = \frac{Wc^2}{6\mu_e UR^2} \tag{4.24}$$

$$f = \frac{F_f}{W} \tag{4.25}$$

The results for these four parameters with the variation of eccentricity are presented in figures 4.16a-d. The friction factor (4.16c) was multiplied by the factor *R/c* to take into account the aspect ratio. It can be observed for all the results that, with the increase in clearance, increasing distinction occurs between two-phase results and

Reynolds conditions throughout the eccentricity domain. For the smallest clearance, *c=20μm*, results are almost identical to those from the Reynolds solution.

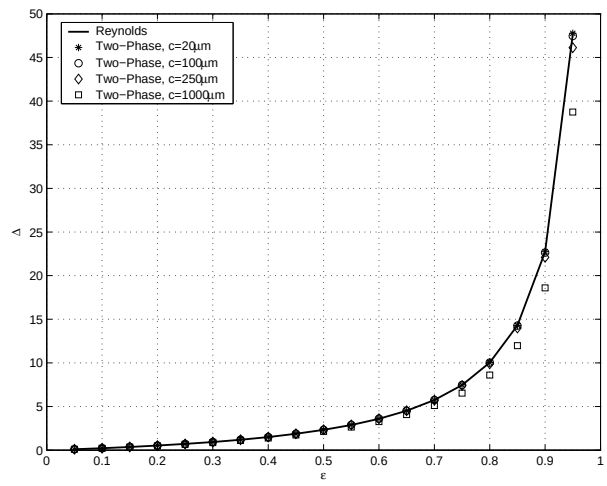

a) Sommerfeld number

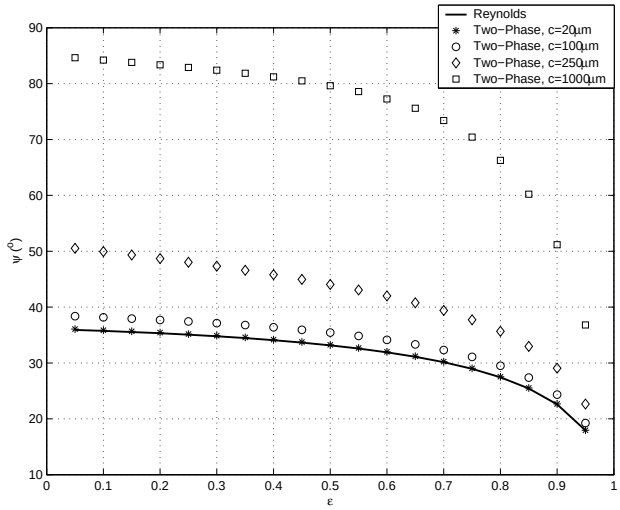

b) Attitude angle

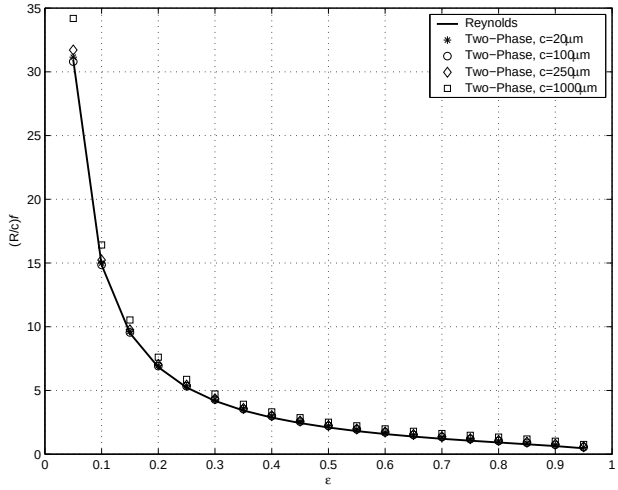

c) Friction factor

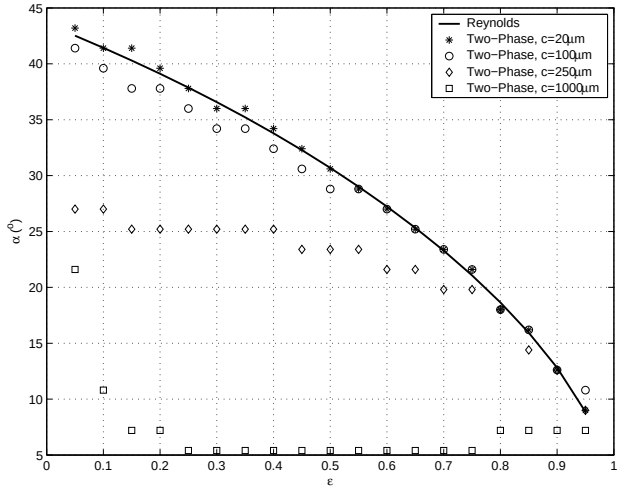

d) Cavitation angle

Figure 4.16. Performance parameters for Reynolds solution and two-phase flow method. ($D = 20mm, \omega = 60Hz,\ p_i = p_o = 100kPa, T = 40^oC, w_i = w_{sat} = 4.07\%, L = 100mm$)

The attitude angle (figure 4.16b) moves from the values predicted using Reynolds condition to close to 90^o in the case of *c=1000μm* and smaller eccentricities, which shows that, at lower loads, the results approach the Sommerfeld solution ($\psi=90^o$). As the eccentricity increases, results approach the Reynolds solution again. However, a significant difference can still be noticed for load and friction in larger clearances.

An interesting result is obtained for the cavitation angle, figure 4.16d. The results for *c=20* and *100 μm* are all very close to the Reynolds values, while for *c=250* and *1000 μm* for most of the eccentricities cavitation angle remains the same and far

below the values for smaller clearances. This points to the idea that, for such lower loads, separation of the flow may take place in the divergent region of the bearing, as the behaviour in this region has little influence in the positive pressure region. In this case, it would be more effective to compare the results obtained with those using separation conditions. Nevertheless, it should be stressed that, for such large clearances, even the hypotheses adopted to derive Reynolds equation are questionable, for instance, to neglect curvature and the importance of inertia terms are no longer valid approximations. These effects should be included in the model in order to be proposed to better predict solutions in a wider range of clearances.

To sum up, it can be concluded that a good agreement between the model and Reynolds conditions is achieved for smaller clearances, which are usually characteristic of bearing operation. Under these conditions, heavily and moderated loads occur and the Reynolds conditions are acknowledged as good approximations, being widely used. For larger clearances, results diverge from the one using Reynolds and approach that from Sommerfeld. Despite reproducing an expected behaviour, it cannot be affirmed that those results are still close to the real situation; this would require comparison with other cavitation conditions and the inclusion of effects not considered at present. Nevertheless, the capacity of the model to predict different behaviours is positive, especially considering the wide range of conditions a bearing can experience during dynamic loading.

4.6 EVALUATION OF NUMERICAL RESULTS

In order to analyse in details the behaviour of the infinite 180^o partial journal bearing lubricated with the oil/refrigerant mixture R12/SUNISO 1GS, a simulation was performed using the following conditions:

$$D = 20mm,\ (L = 100mm), c = 40\mu m, \varepsilon = 0.70, \omega = 30Hz\ (1800rpm),$$
$$p_i = p_o = 100kPa, T = 40^o C, w_i = w_{sat} = 4.07\%$$

The load in these conditions is slightly smaller than in usual operation, being considered moderate ($W=597.7N$), but it was chosen to enable observation of both convergent and divergent region in details. Under these conditions, the pressure profile

obtained in the simulation is shown in figure 4.17. The profile obtained with Reynolds condition is also presented for comparison purposes.

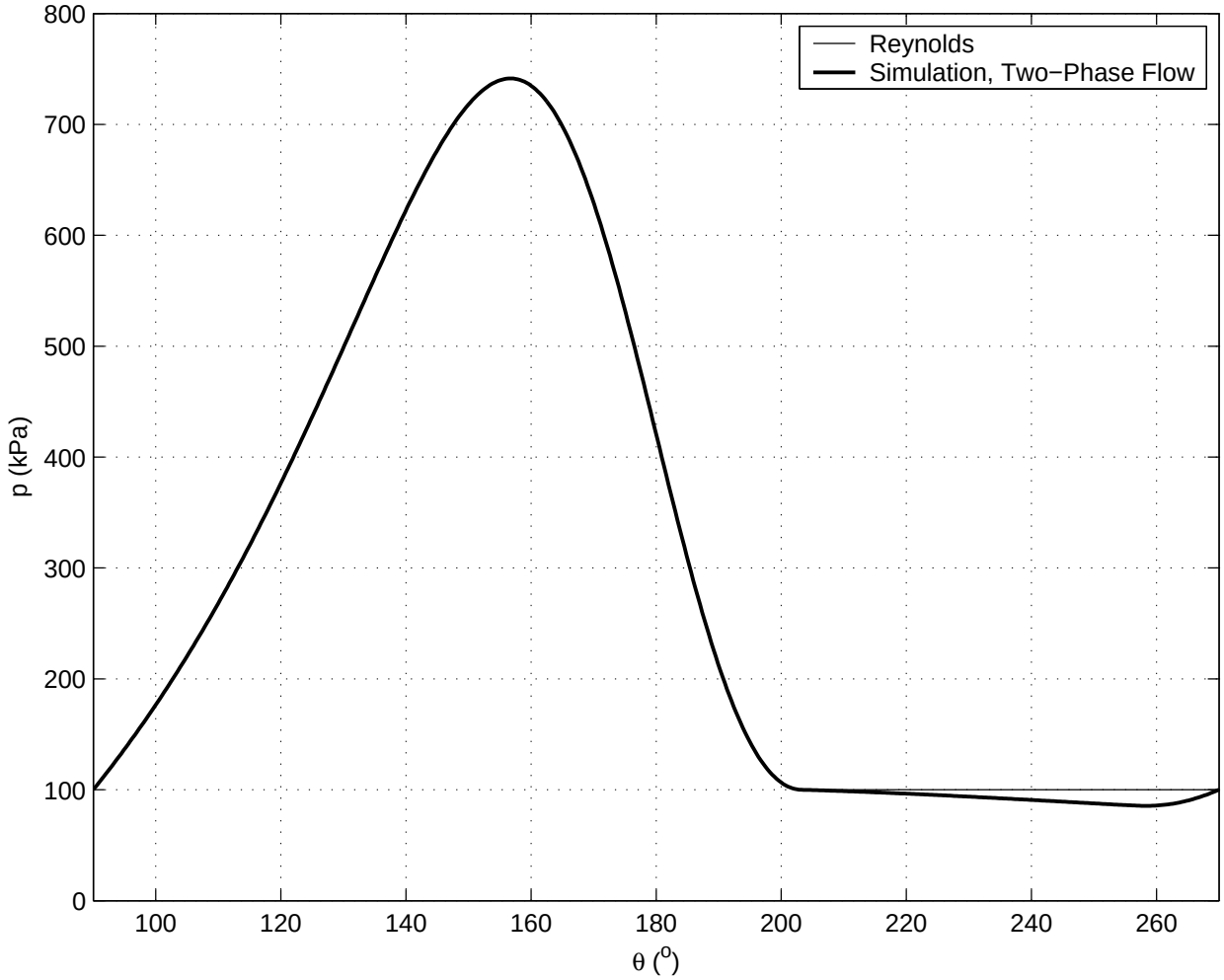

Figure 4.17. Pressure profile in the bearing, using Reynolds condition and the two-phase model. ($D = 20mm, c = 40\mu m, \varepsilon = 0.70, \omega = 60Hz, p_i = p_o = 100kPa, T = 40^oC, w_i = w_{sat} = 4.07\%, L = 100mm$)

In the convergent region, fluid is forced to flow into smaller areas and pressure increases. Later, as the film thickness starts to increase, velocity is reduced and pressure sharply decreases, until reaching a position close to $\theta \cong 200^o$; before this point, the lubricant remains exclusively an oil/refrigerant liquid mixture. From $\theta \cong 200^o$ onwards, slower rates of pressure decrease are observed. In this region, pressure falls to values below saturation of the liquid mixture and gas is released, starting a two-phase flow. As the film thickness continues to increase, pressure decreases, the released gas expands and additional releases are also observed, remaining now the liquid mixture saturated. Close to the end of the bearing, $\theta \cong 260^o$, pressure recovers and reaches the ambient levels at the exit of the bearing. At that point, the fluid is a mixture of liquid (oil and refrigerant) and gas (pure refrigerant).

The behaviour of the liquid lubricant mixture can be observed in figures 4.18a-b, where refrigerant solubility in the oil and the actual refrigerant mass fraction are presented. In the region where pressure increases, between *0* and 158^o, refrigerant solubility increases, but the liquid remain at the same composition as no gas is available to be absorbed. The liquid is therefore subsaturated. From $\theta \cong 160^o$, pressure decreases and so does solubility, then re-approaching the saturation value of the liquid mixture. This value is reached at $\theta=202^o$, and the mixture is again saturated. From this point, as pressure continues to decrease, gas is released in order to keep the mixture saturated, followed by a reduction in the amount of the refrigerant dissolved in the oil. Close to the outlet, $\theta=260^o$, pressure increases again, but as was assumed that no absorption occurs, the fluid at the exit is composed of gas and a subsaturated liquid.

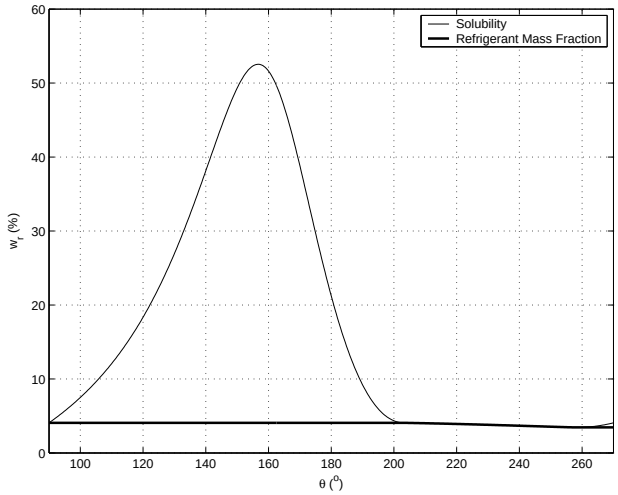

a) Comparison between solubility and mass fraction

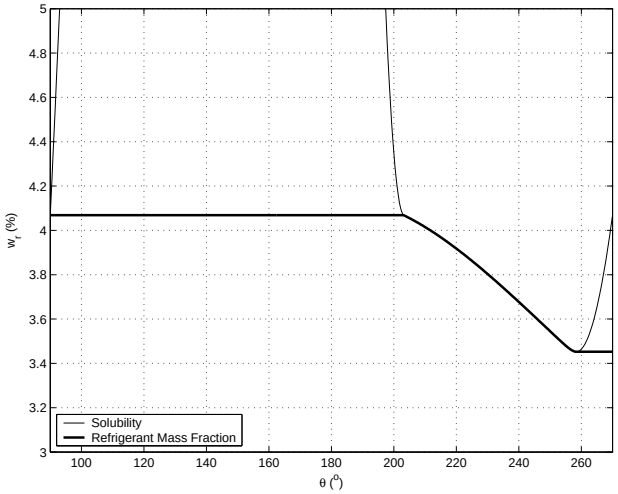

b) Detail on refrigerant mass fraction

Figure 4.18. Behaviour of solubility and mass fraction of refrigerant in the liquid along the bearing.
$(D = 20mm, c = 40\mu m, \varepsilon = 0.70, \omega = 60Hz,\ p_i = p_o = 100kPa, T = 40^o C, w_i = w_{sat} = 4.07\%,\ L = 100mm)$

The release of gas and the increase in the presence of this phase results in the increase of the refrigerant gas quality in the two-phase region, as shown in figure 4.19a. It shall be observed that the mass of refrigerant released is very small, below *1%* throughout the bearing. Nevertheless, due to the very low density of the gas, this small mass of gas occupies a great volume of the space between shaft and bush, corresponding at the end to levels close to 60% in volume. This is concluded from the void fraction presented in figure 4.19b. In this figure, it is also shown the estimated void fraction obtained from the Reynolds solution using equation (4.13). Their equality during most of the two-phase region confirms that it is the release of gas and its expansion that enables the fluid to fill the space between shaft and bush.

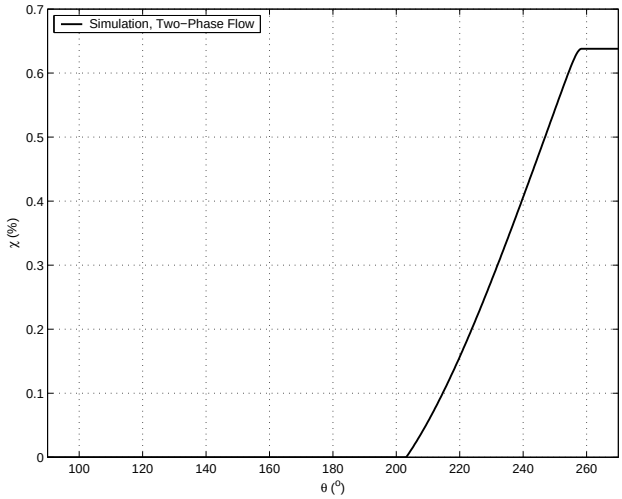

a) Refrigerant gas quality

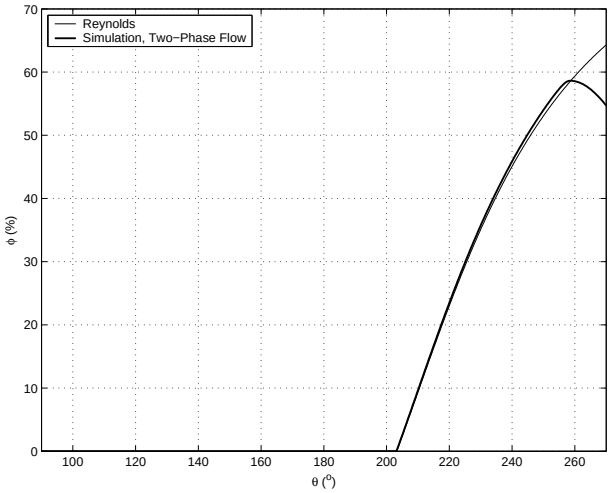

b) Void fraction

Figure 4.19. Behaviour of the gas phase along the bearing: gas quality and void fraction.
($D = 20mm, c = 40\mu m, \varepsilon = 0.70, \omega = 60Hz,\ p_i = p_o = 100kPa, T = 40^oC, w_i = w_{sat} = 4.07\%,\ L = 100mm$)

The release of gas and consequent increase in void fraction promotes the reduction of the apparent density of the fluid, presented in figure 4.20. The figure shows also the density of the liquid and the gas, with the latter about 100 times smaller than the former. It can be seen that variation of density of phase properties is very small compared to the variation of the apparent density. Nevertheless, it is important to consider the changes in component properties with density – for instance, the reduction in void fraction and the increase in density close to the end of the bearing are due to the compressibility of the gas, whose density increases in the pressure recovery region.

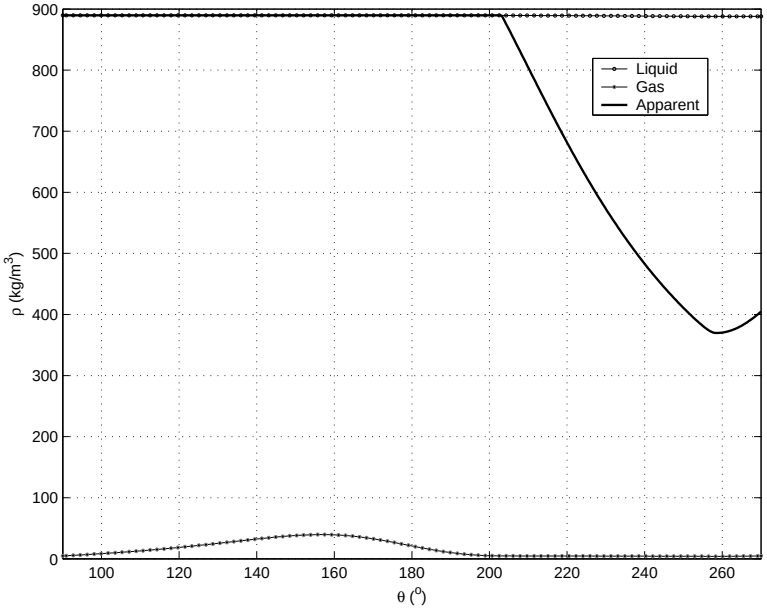

Figure 4.20. Density of the two-phase mixture and of the phases along the bearing.
($D = 20mm, c = 40\mu m, \varepsilon = 0.70, \omega = 60Hz,\ p_i = p_o = 100kPa, T = 40^oC, w_i = w_{sat} = 4.07\%,\ L = 100mm$)

Despite the variation of fluid density and film thickness along the bearing, mass flow remains constant, as expected. This can be observed in figure 4.21, where the total mass flow rate, calculated from equation (4.15), and its components, Couette and Poiseuille are presented.

$$q_\theta = q_{Couette} + q_{Poiseuille} = \frac{\overline{\rho} U h}{2} + \left(-\frac{\overline{\rho} h^3}{12 \overline{\mu} R} \frac{dp}{d\theta} \right) \tag{4.15}$$

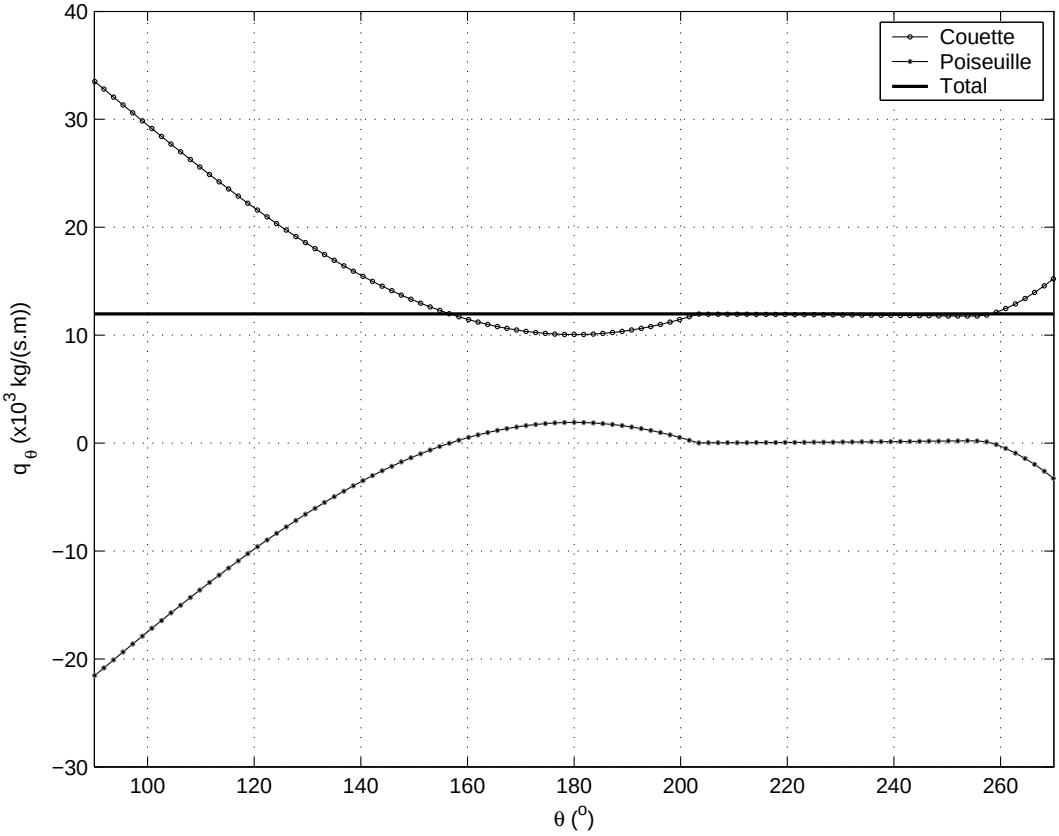

Figure 4.21. Mass flow rate along the bearing and its components, Couette and Poiseuille.
($D = 20mm, c = 40\mu m, \varepsilon = 0.70, \omega = 60Hz, p_i = p_o = 100kPa, T = 40^o C, w_i = w_{sat} = 4.07\%, L = 100mm$)

In the single phase region, density is constant and the Couette term decreases as film thickness decreases. The Poiseuille term is an induced flow resisting to the tendency of more fluid flowing at the entrance than in the central region, where the flowing area is smaller. In the region between maximum pressure ($\theta \cong 160^o$) and cavitation ($\theta \cong 200^o$), the pressure gradient induces more fluid to flow in the direction of the exit, adding to the fluid being carried by the journal rotation. In the sequence, at the cavitated region, Poiseuille flow is almost inexistent as pressure gradients are very small. The Couette flow remains then almost constant, indicating that the apparent density of the homogeneous fluid decreases at the same rate as film thickness increases.

Close to the end of the bearing, in the pressure recovery region, the Couette flow increases as both density and film thickness increases. The positive pressure gradient then promotes a resisting flow opposing to the increase in the amount of fluid being carried by shaft rotation. As a result, mean velocity of the fluid in the transversal section will reduce.

An equivalent manner to express that the invariance of the mass flow rate is,

$$q_\theta = \bar{\rho} h u_{mean} = constant \tag{4.25}$$

where u_{mean} is the mean velocity calculated in any cross section as,

$$u_{mean} = \frac{1}{h}\int_0^h u dz = \frac{U}{2} - \frac{h^3}{12\bar{\mu}R}\frac{\partial p}{\partial \theta} \tag{4.26}$$

The result for the mean velocity along the bearing is presented in figure 4.22. In the single phase region ($\bar{\rho} = constant$), it can be observed that initially mean velocity increases in order to accommodate the reduction in film thickness, and in the sequence it starts to decrease to accommodate the increase in the flow area. When cavitation occurs, changes in the mean velocity are very small, as the increase of film thickness is followed by a release of gas and consequent reduction in homogeneous density. Close to the bearing exit, back pressure is communicated to the fluid by diffusion of momentum, and again the mean velocity decreases.

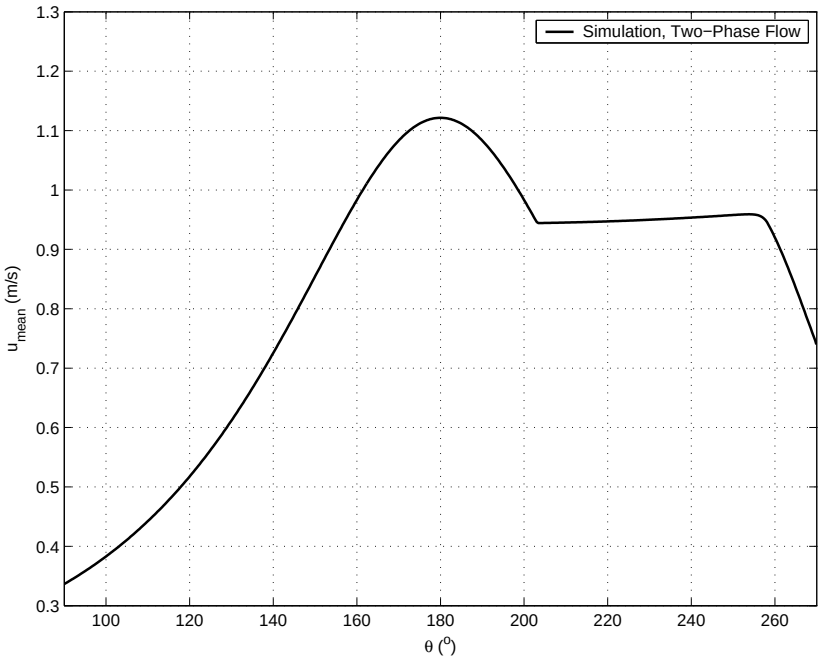

Figure 4.22. Mean velocity of the flow along the bearing.
($D = 20mm, c = 40\mu m, \varepsilon = 0.70, \omega = 60Hz, p_i = p_o = 100kPa, T = 40^o C, w_i = w_{sat} = 4.07\%, L = 100mm$)

The behaviour of velocity along the flow can be also characterised by velocity profiles in cross-sectional areas along the flow, as shown in figure 4.23a. For a defined section, the velocity profile can be calculated from equation (3.5.i), which for the current problem results in,

$$u(z) = \frac{Uz}{h} - \frac{z(h-z)}{2\bar{\mu}R}\frac{\partial p}{\partial \theta} \tag{4.27}$$

The gradient pressure inducing the Poiseuille flow in the previous equation is presented in figure 4.23b, and it is compared to the pressure gradient resultant from the analytical solution using Reynolds condition.

In the initial region of the monophasic flow ($\theta=120^o$), a negative pressure gradient exists and reduces the velocity in comparison to a pure Couette flow, such as the one for $\theta=155^o$, where the pressure gradient is zero. In the sequence, with the pressure increasingly negative, velocity increases and reaches a maximum at $\theta=180^o$. The pressure gradient then decreases in absolute value and reach very small values at cavitation ($\theta=200^o$), remaining almost constant in this region, producing velocity profiles similar to the one at $\theta=210^o$. Later, with pressure recovery, opposing Poiseuille flow increases and the profile again returns to lower values.

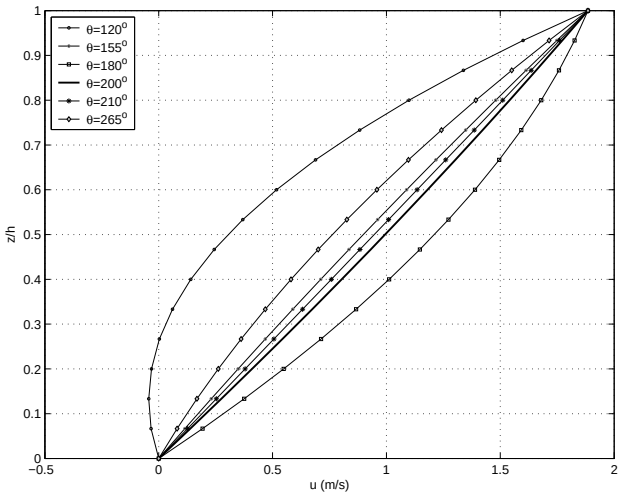

a) Velocity profiles at some positions in the bearing

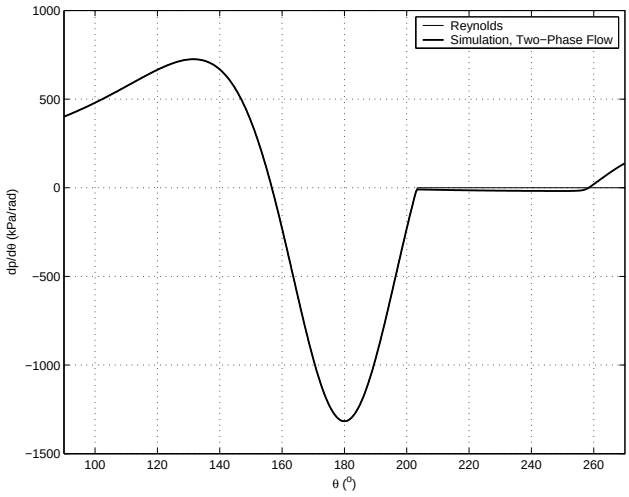

b) Pressure gradient along the bearing

Figure 4.23. Velocity profiles and the pressure gradient along the bearing.
($D = 20mm, c = 40\mu m, \varepsilon = 0.70, \omega = 60Hz, p_i = p_o = 100kPa, T = 40^o C, w_i = w_{sat} = 4.07\%, L = 100mm$)

At this point, observing the velocity profiles, a comparison with the usual boundary conditions adopted in lubrication problems can be discussed. To this end, it is shown in figure 4.24 the velocity derivative at the bush ($z=0$). In the monophasic region, it can be observed the acceleration of the flow until the minimum film thickness

position, $\theta=180^o$. In the sequence, deceleration occurs until the onset of gas release. In this region, although an almost constant velocity profile is observed, as film thickness increases, the derivative at the wall decreases, though in a lower rate. In the pressure recovery region, the gradient again gains more significance. In the present case, it is kept above zero for all the divergent region, which should exclude the possibility of separation of the flow, whose condition of occurrence is $\partial u/\partial z=0$ in the divergent region. However, the pressure recovery region can move towards the centre of the bearing, as previously observed in figures 4.13 to 4.15 for larger clearances. In these cases, the more significant gradient of the recovery region in comparison to the cavitated region will cause further reduction in $\partial u/\partial z$, such that it could reach zero. This again points to the separation of the flow in lower loads. For higher loads, as the gradient is positive, separation is unlikely to occur and it is confirmed that behaviour is expected to be more similar to the one described by Reynolds conditions.

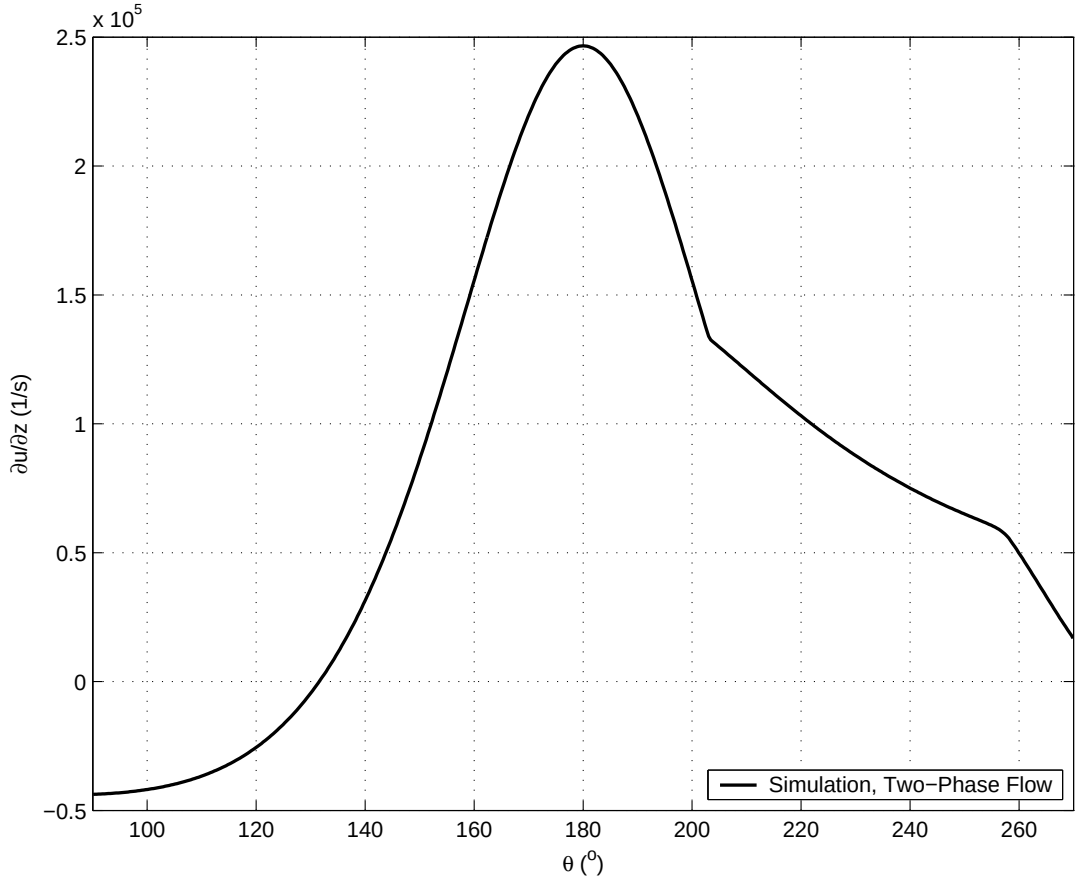

Figure 4.24. Velocity gradient at the bearing wall ($z=0$).
($D=20mm, c=40\mu m, \varepsilon=0.70, \omega=60Hz, p_i=p_o=100kPa, T=40^oC, w_i=w_{sat}=4.07\%, L=100mm$)

The velocity gradient at the walls is also important to determine the friction force acting on the bearing. However, it is also important to know the behaviour of

viscosity along the flow to determine friction. The apparent viscosity of the fluid, equation (3.22), is presented in figure 4.25, where the viscosity of the oil/refrigerant liquid mixture is also shown. Despite the presence of a low viscosity second phase, viscosity increases with the presence of gas. This occurs because less refrigerant is dissolved in the oil, and the viscosity of the liquid moves closer to the viscosity of the pure oil (μ_{oil}=*11.33mPa.s* at *40°C*). But one should also observe that the apparent viscosity is lower than the liquid phase viscosity, which is now due to the presence of gas. It reduces the fraction of liquid present in the two-phase mixture as well as contributes to the homogeneous viscosity with its lower one (μ_{gas}=*12.44μPa.s* at *100kPa, 40°C*), smaller than the liquid viscosity in an order of 1000. Nonetheless, the increase of viscosity in the two-phase region represents only 3% of change, such that the assumption of constant viscosity would not be a bad first approximation.

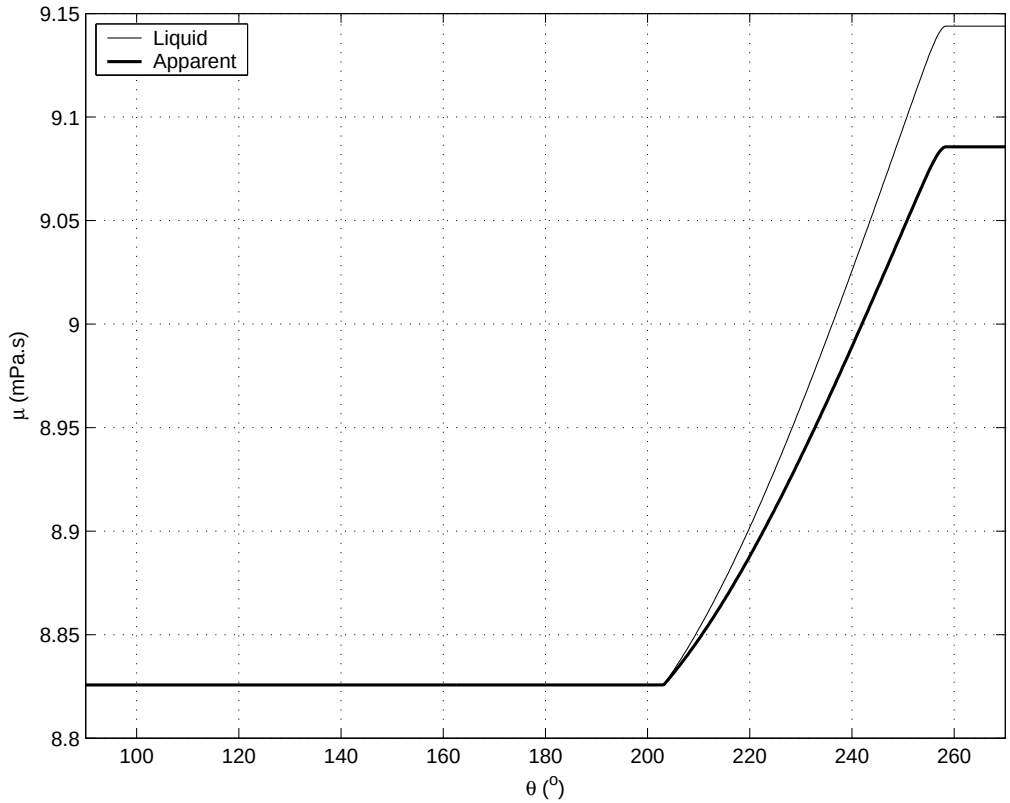

Figure 4.25. Apparent and liquid viscosity along the bearing.
($D = 20mm, c = 40\mu m, \varepsilon = 0.70, \omega = 60Hz, p_i = p_o = 100kPa, T = 40^o C, w_i = w_{sat} = 4.07\%, L = 100mm$)

The influence of viscosity on friction can be observed in the results of the accumulated friction force along the bearing, presented in figure 4.26a and detailed in figure 4.26b. In these figures, four different results for friction force are calculated and compared. The present solution is compared with the friction considering only viscous effects (constant viscosity). These results are also

compared with analytical results for Reynolds condition, either considering a distributed film in the two-phase region as well as a complete separation of liquid and gas (striated flow). As only liquid is present in the first region, differences in the results will occur only in the cavitated region. The Reynolds solution considering striated flow has a total friction force about 10% smaller than the other cases, where a film filling completely the space between bearing and journal is considered. The results, in these cases, are very similar; accumulated Reynolds friction force is higher in the cavitated region, but at the end is slightly smaller as further contribution of the positive pressure gradient at recovery region occurs for two-phase simulations. The biggest friction force is predicted by the present model, but results for constant viscosity are very similar, which reinforces the negligibility of changes in viscosity.

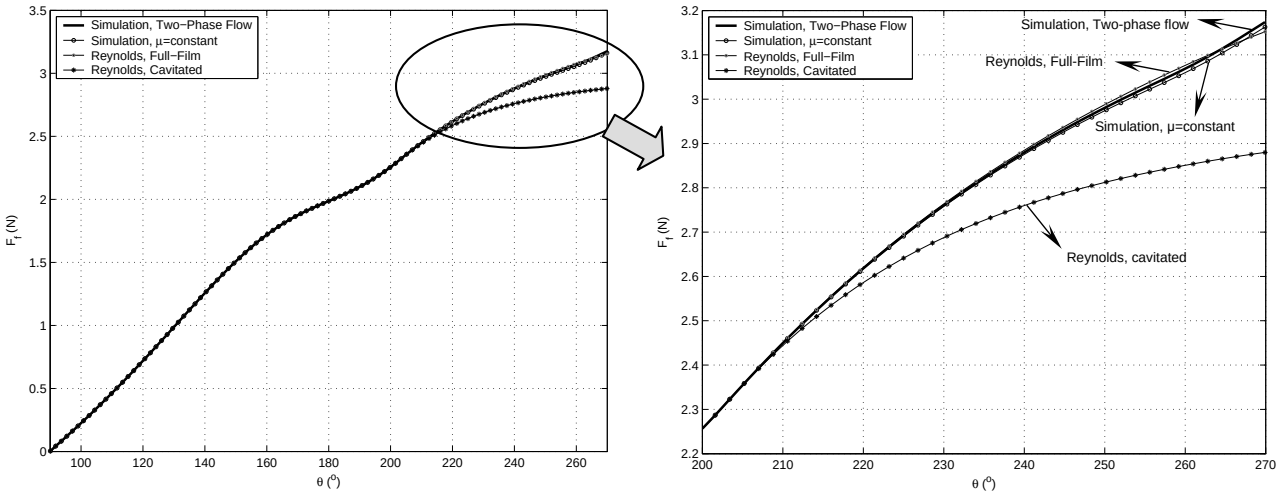

a) Comparison between four different procedures

b) Cavitation region in details

Figure 4.26. Accummulated friction force along the bearing.
($D = 20mm, c = 40\mu m, \varepsilon = 0.70, \omega = 60Hz, p_i = p_o = 100kPa, T = 40^o C, w_i = w_{sat} = 4.07\%, L = 100mm$)

4.7 SUMMARY

The two-phase numerical solution for a 180º infinite partial journal bearing subject to a steady load was performed. The lubricant considered was a mixture of CFC R12 and a mineral oil SUNISO 1GS, from which the refrigerant gas release under saturation conditions could be numerically modelled. For the problem, boundary

conditions used were only the pressures at the entrance and exit of the bearing, assuming that no flow was directly returned through the bearing.

The main conclusions regarding the examination of the model were,

- Three distinct regions can be identified in the bearing: the positive pressure region, in the convergent area, where very high pressures are usually observed, and where only liquid exists; the cavitation region, in the divergent portion of the bearing, where release and expansion of gas occurs and the pressures are below ambient; and the pressure recovery region, where the back pressure is communicated to the fluid and the release of gas is interrupted, resulting in a positive pressure gradient and the reduction of the mean velocity of the flow, which still presents two phases;
- In the convergent pressure region, the model has a very similar behaviour to that predicted by the solution using Reynolds boundary conditions. In this region, viscosity is the most important property. The mixture presents higher viscosities at lower pressures, temperatures and mass fractions, and under these conditions it will be able to achieve higher pressures in the bearing; in addition to that, the reduction of clearance and the increase in velocity or eccentricity also produce higher pressures;
- In the cavitated region, geometric (operational) influence occurs only due to eccentricity. Furthermore, viscosity is not the most important property, but density instead;
- The viscosity presents some influence again in the pressure recovery region, as well as the velocity of the shaft and the clearance. The extension of the pressure recovery region tends to be smaller as viscosity and velocity increases, or with the reduction of the radial clearance. Under these conditions, viscous forces are greater, and a stronger pressure gradient is required in the balance of forces. The recovery region, also depends on the behaviour of the fluid in the cavitated region, particularly the levels of pressure achieved during the release of gas;
- Under higher clearances, the results obtained by the two-phase model deviates from those obtained using Reynolds conditions. This is positive, as it is known that Reynolds conditions are not appropriate for this light load situation. On the other hand, before any conclusion is made, it is necessary to consider other

effects in the model, such as fluid inertia – especially because separation conditions are likely to occur. Nevertheless, the model has potential to predict solutions in a wider range of situations than Reynolds conditions do;

- The numerical method requires considerable computational effort, which is particularly connected to the solution of the cavitated region. Although in moderate load conditions the time required is equivalent to the one using the cavitation algorithm, effort has to be made in the direction of providing smoother pressure profiles during intermediate steps of the iterative process, then considerably improving convergence;

Most of the objectives stated at the beginning of the chapter were covered. However, the refrigerant absorption has shown no significant influence for the partial bearing and requires an alternative problem to be investigated. The viscosity correlation was chosen in the light of previous studies with the mixture, but for a firm decision it would be required experimental results, out of the scope of this work.

Chapter 5

PARAMETRIC ANALYSIS AND THE BEHAVIOUR FOR DIFFERENT OIL-REFRIGERANT MIXTURES

The proposed two-phase model can be used to explore the influence of the main parameters on bearing operation and mixture conditions. To this end, operation and geometry parameters are studied, and the results focus on understanding how the mixture is affected and ultimately the performance variables of the bearing, as a characteristic of its operation. Additionally, the behaviour of different mixtures is evaluated, observing the differences between them in the same component and evaluating the influence this can have in a refrigeration system.

5.1 INTRODUCTION

Having the model adjusted, and with increased confidence through its verification against classical lubrication theory, the phenomenology of the flow can be further explored. Studying parameters such as eccentricity, clearance and velocity, as well as factors affecting mixture conditions, such as entrance pressure, refrigerant mass fraction and the fluid temperature, it is possible to evaluate which are the important factors controlling the operation of the component, and also how to condition the mixture appropriately.

Finally, an example is considered, where the mixture of R12 and mineral oil is compared with its most common replacement nowadays, the refrigerant R134a and a synthethic polyol ester oil, observing their differences in the two-phase flow and what impact this can have in their operation in a refrigeration system.

5.1.1. Specific objectives

- To evaluate the effect of the main operation and mixture parameters in the bearing operation;
- To clarify, in the light of the two-phase flow solution, the distinct behaviour for different oil-refrigerant mixtures.

5.2 PARAMETRIC ANALYSIS

Having chosen the methodologies to deal with the physical behaviour of the mixture in the flow, understanding the model operation and also having compared it to the usual Reynolds solution, conditions affecting bearing operation and performance can have their importance evaluated using the two-phase model. These conditions comprise bearing characteristics – clearance (geometry), shaft velocity and eccentricity (operation), and also fluid conditions at the entrance of the flow, such as entrance pressure, refrigerant mass fraction and fluid temperature. The latter conditions reflect in fluid properties, where viscosity and density are of direct interest to the lubrication problem. Solubility can also promote changes in bearing operation. Simulations were carried out varying one parameter at once, keeping the geometry of the bearing constant for all simulations (apart from the clearance test). The fixed parameters for all the simulation will therefore be diameter and width of the bearing (the last one could be neglected), as well as the angular extension of the bearing, assumed 180º throughout the chapter. Conditions were set closer to real operation conditions for a typical bearing under moderate/heavy loads, which also brings results closer to Reynolds. Regarding the correlations for lubricant properties, there is a limitation for operating temperatures.

5.2.1. Variables investigated and expected influence of the parameters

In order to characterise the lubrication of the bearing, the pressure profile is calculated. The use of the dimensionless pressure defined in equation (4.23) can also be helpful on defining whether the variation of the parameters can follow a general rule as observed for the classical solution. The behaviour of the fluid along the bearing is also

evaluated using two-phase characteristic properties, solubility, apparent density and its most influencing variable void fraction, viscosity and the property controlling its changes, gas quality.

The use of common performance parameters is also important. Among those, load, attitude angle, cavitation angle, friction force, friction coefficient and the mass flow rate will be evaluated. As variations are not very big for fluid conditions, dimensional variables were preferred. The maximum gauge pressure can also be seen as a performance parameter, while the minimum gauge pressure can be seen as a measure of the influence of gas release on bearing performance.

A theoretical background from fluid mechanics and the analytical results for the partial journal bearing using Reynolds conditions can provide useful information to evaluate results obtained with the two-phase model in the sequence, particularly through a dimensional analysis.

To this end, consider initially Navier-Stokes for the problem, as before,

$$\frac{\partial p}{\partial x} = \frac{\partial}{\partial z}\left(\mu \frac{\partial u}{\partial z}\right) \tag{3.5.i}$$

The term in the left hand side represents the pressure forces, which balances the viscous forces represented in the right hand side. The latter can also be seen as the diffusion of momentum. Considering equation (3.5.i), taking as characteristic values for bearings the clearance c for the dimension, shaft speed U for velocity and μ for the viscosity, results,

$$\frac{\Delta p}{\Delta x} \propto \mu \frac{U}{c^2} \tag{5.1}$$

From this equation, it is expected higher viscous forces for higher velocities and viscosities and also for smaller clearances. Under these conditions, more significant pressure gradients shall also occur to the balance of forces.

In chapter 3, equation (3.5) was combined with conservation of mass to determine Reynolds equation. For constant properties and considering the Reynolds boundary conditions, an analytical solution can be obtained for pressure in the bearing and then for the performance parameters. Pinkus and Sternlicht (1961) give details of this derivation.

For the pressure profile, the solution is given by,

$$p^* = \frac{(\gamma - \gamma_e) - \varepsilon(\sin\gamma - \sin\gamma_e)}{(1-\varepsilon^2)^{3/2}} - \\ -\frac{(1-\varepsilon^2)}{(1-\varepsilon\cos\gamma_m)}\left[\frac{(\gamma-\gamma_e) - 2\varepsilon(\sin\gamma - \sin\gamma_e) + \frac{\varepsilon}{2}(\gamma-\gamma_e) + \frac{\varepsilon^2}{4}(\sin 2\gamma - \sin 2\gamma_e)}{(1-\varepsilon^2)^{5/2}}\right] \tag{5.2}$$

where γ is the Sommerfeld variable defined by,

$$1 + \varepsilon\cos\theta = \frac{1-\varepsilon^2}{1-\varepsilon\cos\gamma} \tag{5.3}$$

From equation (5.2), it can be concluded that,

$$p^* = \frac{(p - p_e)c^2}{6\mu UR} = f(\varepsilon) \tag{5.4}$$

alternatively,

$$p \propto \mu\frac{U}{c^2} f(\varepsilon) \tag{5.5}$$

The dependency with the eccentricity is more complex than that with other parameters, as even the maximum pressure angle depends on it. Nevertheless, as the most independent and influential parameter, only recognising a dependence is sufficient for the purpose of this work.

The cavitation angle is calculated from,

$$\cos(\pi + \alpha) = \frac{\cos(\pi + \beta) - \varepsilon}{1 - \varepsilon\cos(\pi + \beta)} \tag{5.6}$$

where,

$$\cos\beta = \frac{\left[\sin\beta + \sin\gamma_e - \frac{\varepsilon}{2}(\sin\beta\cos\beta - (\pi + \beta - \gamma_e) + 2\cos\beta\sin\gamma_e + \sin\gamma_e\cos\gamma_e)\right]}{(\pi + \beta - \gamma_e)} \tag{5.7}$$

which is clearly a function only of eccentricity (ε) for a fixed arc of partial journal bearing.

For the hydrodynamic load, one has,

$$W_1 = \frac{6\mu U R^2 L}{c^2}\frac{\varepsilon}{\left(1-\varepsilon^2\right)}\frac{\left(1+\cos 2\gamma_e + 4\cos\beta\cos\gamma_e + 2\cos^2\beta\right)}{4\left(1+\varepsilon\cos\beta\right)} \tag{5.8}$$

$$W_2 = \frac{6\mu U R^2 L}{c^2}\frac{1}{\left(1-\varepsilon^2\right)^{1/2}}\frac{\cos\beta(\pi+\beta-\gamma_e)-\sin\beta-\sin\gamma_e}{\left(1+\varepsilon\cos\beta\right)} \tag{5.9}$$

$$W = \sqrt{W_1^2 + W_2^2} \tag{5.10}$$

resulting,

$$W \propto \mu\frac{U}{c^2} f(\varepsilon) \tag{5.11}$$

From this, the attitude angle is,

$$\psi = a\tan\left(\frac{W_2}{W_1}\right) = a\tan\left[\frac{4\left(1-\varepsilon^2\right)^{1/2}}{\varepsilon}\frac{\cos\beta(\pi+\beta-\gamma_e)-\sin\beta-\sin\gamma_e}{1+\cos 2\gamma_e + 4\cos\beta\cos\gamma_e + 2\cos^2\beta}\right] \tag{5.12}$$

also a function of eccentricity only.

An additional calculation is the friction force, given by,

$$F_f = \frac{\mu U R L}{c\left(1-\varepsilon^2\right)^{1/2}}\left\{\left(\gamma_f - \gamma_e\right) + 3\left[\left(\pi+\beta-\gamma_e\right) - \frac{\left(\pi+\beta-\gamma_e\right)+\varepsilon\left(\sin\beta+\sin\gamma_e\right)}{\left(1+\varepsilon\cos\beta\right)}\right]\right\} \tag{5.13}$$

The friction force will therefore depend on,

$$F_f \propto \mu\frac{U}{c} f(\varepsilon) \tag{5.14}$$

For the friction factor, defined initially in equation (4.25),

$$f = \frac{F_f}{W} \propto c \tag{5.15}$$

The mass flow rate analytically calculated is,

$$q_\theta = \frac{\rho U h}{2} - \frac{6\rho U h^3}{c^2}\left[\frac{1}{\left(1+\varepsilon\cos\theta\right)^2} - \frac{\left(1+\varepsilon\cos\theta_m\right)}{\left(1+\varepsilon\cos\theta\right)^3}\right] \tag{5.16}$$

from where,

$$q_\theta \propto f(\varepsilon)\rho U c \tag{5.17}$$

Finally, for the maximum pressure, $p_{max}=max(p-p_e)$, the dependencies of pressure in equation (5.4) are also observed. For the minimum pressure, $p_{min}=|min(p-p_e)|$, no relation with the analytical solution is available, as the cavitated region is not solved. It will depend on mixture factors, to which properties are also not constant.

In the sequence, parameters will be tested for the two-phase model. As the results are expected to be close to Reynolds conditions, the dependencies here derived might be observed in the parameters varied, but differences due to the solution of the cavitated region and the occurrence of pressure recovery may produce some deviations in results.

5.2.2. Influence of clearance

The reduction in clearance produces a considerable increase in pressure in the convergent region, as already predicted by the analytical solution using Reynolds. This can be observed in figure 5.1a, where results are presented for simulations of six different clearances, ranging from *5* to *80μm*. However, not significant difference is noticed in the cavitated region, where the pressures are very similar until the point where pressure recovery starts, as shown in figure 5.1b.

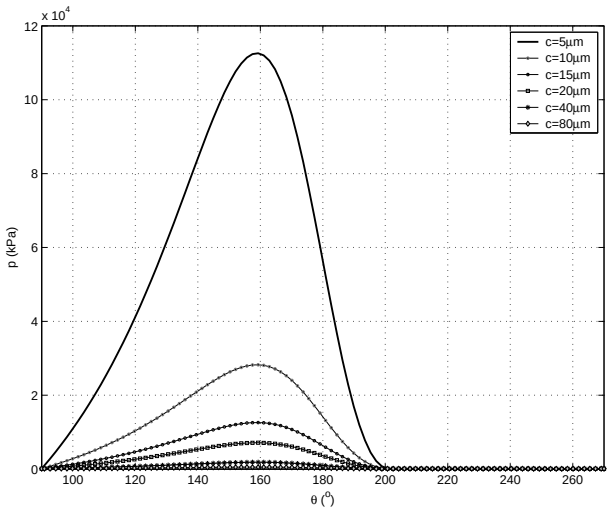

a) Full domain of the bearing

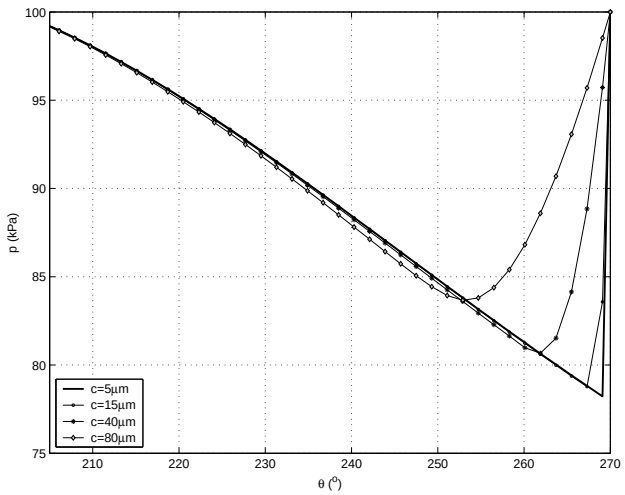

b) Cavitation region in details

Figure 5.1. Pressure results for different clearances.
($D=20mm, \varepsilon=0.75, \omega=60Hz, p_i=p_o=100kPa, T=40^oC, w_i=w_{sat}=4.07\%, L=100mm$)

Observing the results for the dimensionless pressure (figures 5.2a-b), curves are identical for the convergent region, but higher amplitudes of pressure occur for larger clearances in the cavitated region. This suggests that the "negative" (subambient) pressures are independent on clearance for a fixed eccentricity, and also points to the better approximation of Reynolds equation for heavier loads (smaller clearances).

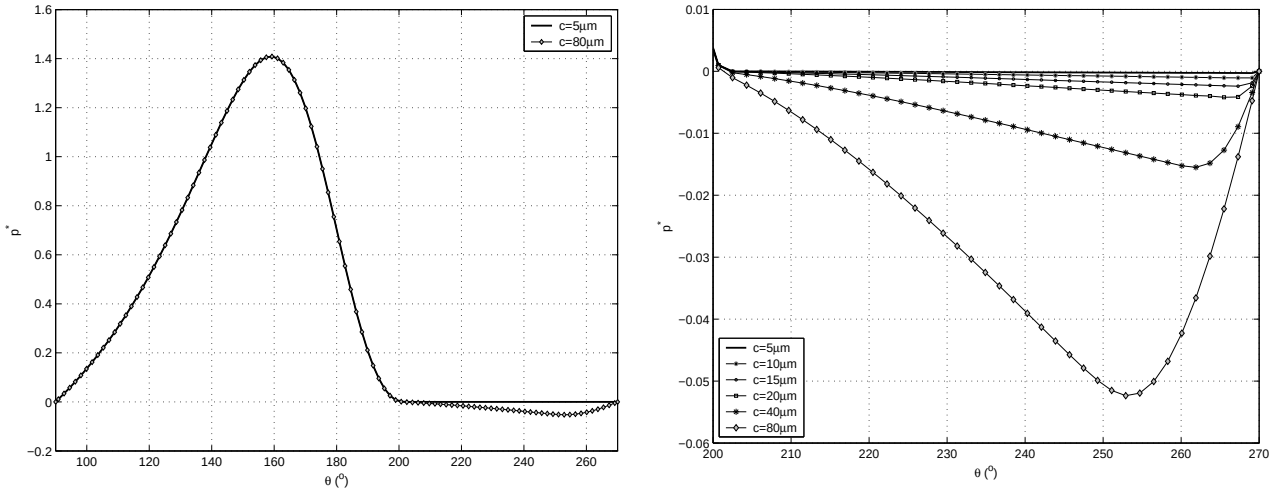

a) Full domain of the bearing **b)** Cavitation region in details

Figure 5.2. Dimensionless pressure results for different clearances.
($D = 20mm, \varepsilon = 0.75, \omega = 60Hz, p_i = p_o = 100kPa, T = 40^o C, w_i = w_{sat} = 4.07\%, L = 100mm$)

In the previous figures it is observed that pressure recovery, or simply the point inside the bearing affected by back pressure, is closer to the end for smaller clearances. Referring to equation (5.1), it can be concluded that viscous effects are more significant in these cases, such that for a similar difference of pressure, a lower length of the bearing is required to balance pressure force at the outlet position.

This later recovery of pressure implies in a longer length for the cavitated region, occurring then more release of gas for larger clearances, as observed in figure 5.3 for the mass fraction, where some clearances were suppressed for clarity purposes. Also in this figure, one can observe that the release of gas starts in a same point for all the clearances, and releases are very similar until pressure recovery starts, whereafter mass fraction remains the same.

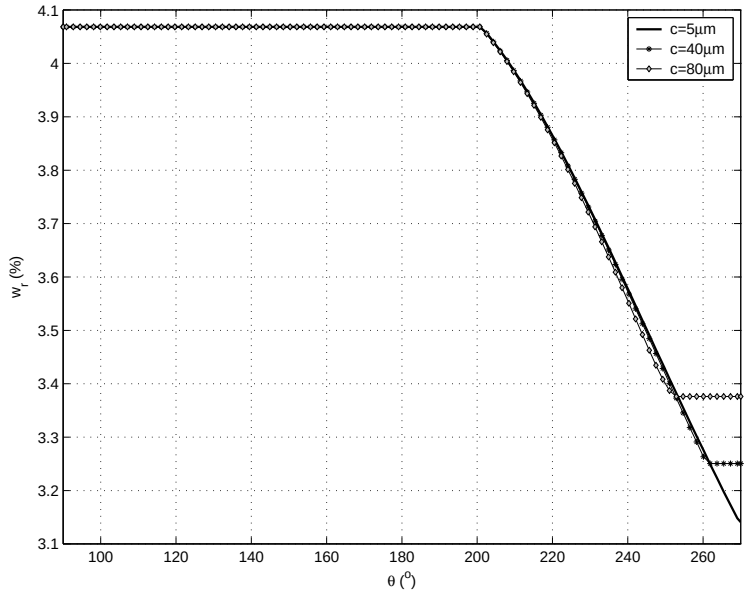

Figure 5.3. Refrigerant mass fraction along the bearing – results for different clearances. ($D = 20mm, \varepsilon = 0.75, \omega = 60Hz, p_i = p_o = 100kPa, T = 40^oC, w_i = w_{sat} = 4.07\%, L = 100mm$)

Being the starting point of gas release the same, suggestions that it is only a function of eccentricity follows development in section 5.2.1. Therefore, geometry to be filled has the same aspect ratio for all clearances, requiring proportionally the same amount of gas from the liquid. This is observed in figures 5.4a-b, respectively for the apparent density and void fraction of the two-phase mixture, identical for the different clearances in most of the bearing length. This would mean that, given the mixture, a certain amount of gas would be released in order to achieve void fraction presented in figure 5.4b, then filling the space in the divergent region of the bearing. Figure 5.4c shows void fraction detailed in the recovery region. If the back pressure was lower, release would still be occurring until the end of bearing. However, as the fluid leaves the bearing at a higher pressure, this is accommodated inside the bearing through diffusion of momentum. In this case, as more fluid was released for the smallest clearance, higher void fraction occurs for the fluid at the end.

Viscosity is also affected by the release of gas, as presented in figure 5.5a. For $c=5\mu m$, where the highest load is observed, an increase of 4.5% in viscosity occurs, while 3.4% is observed for $c=80\mu m$. The behaviour of viscosity is determined by the quality, presented in figure 5.5b. Less than 1% of gas in a mass basis is released from the liquid. Figure 5.5c shows the quality at the final region of the bearing. Higher releases are confirmed for smaller clearances, and a flat region is always present due to the pressure recovery at the end.

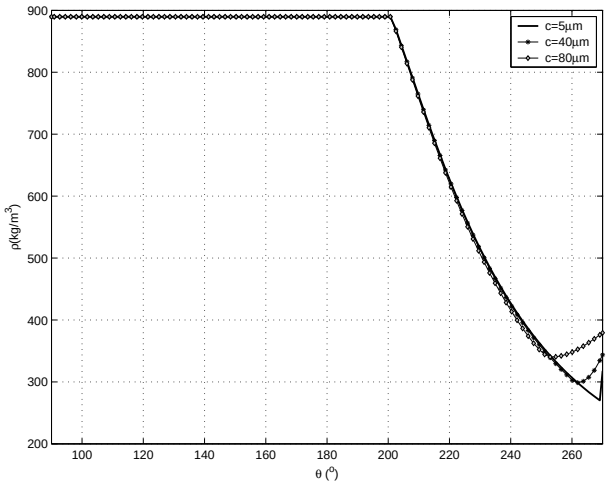

a) Apparent density

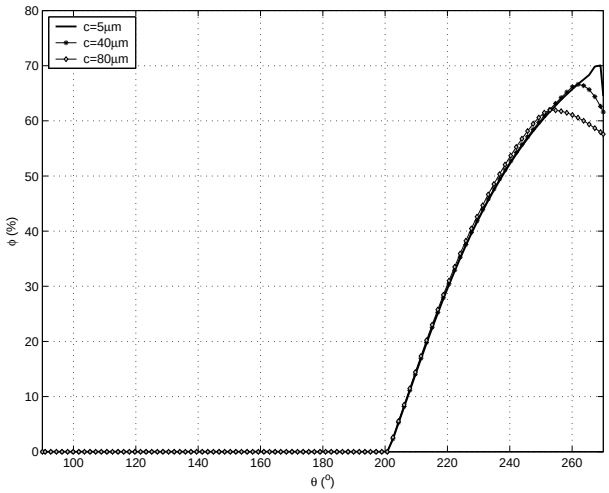

b) Void fraction

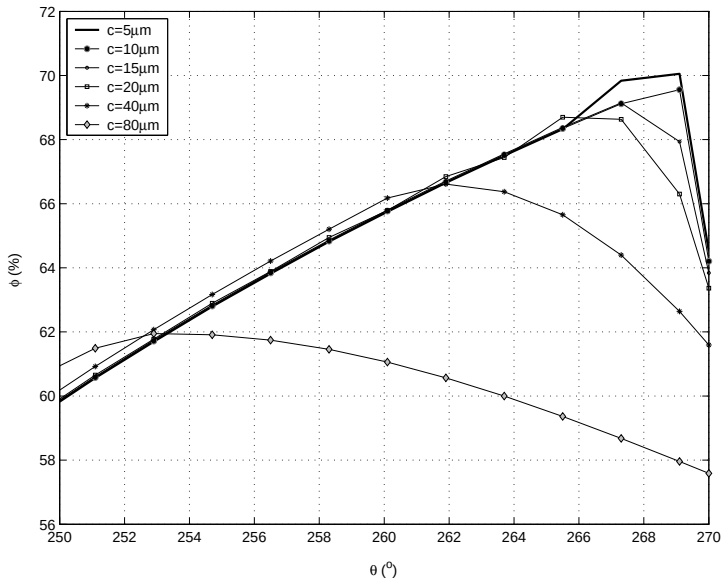

c) Void fraction at the end of cavitation region and during pressure recovery

Figure 5.4. Density and void fraction of the mixture for different clearances.
($D = 20mm, \varepsilon = 0.75, \omega = 60Hz,\ p_i = p_o = 100kPa, T = 40^o C, w_i = w_{sat} = 4.07\%,\ L = 100mm$)

Finally, performance variables of the bearing are presented in figure 5.6. They are compared to the medium value of the clearance tested ($c=20\mu m$) in a log-log graphic. As predicted in section 5.2.1, load carrying capacity and maximum pressure present the most significant variations. Friction force is also greater for smaller clearances, but the friction coefficient increases with clearance, as a result of the stronger dependency of load than friction force. It is linear with clearance, and so is the mass flow rate. On the other hand, attitude and cavitation angle present negligible variations, indicating no dependence with clearance. Minimum pressure also presents very small variations, which is only due to the earlier recovery of pressure for larger clearances. Table 5.1 present the absolute values for the properties plotted in figure 5.6.

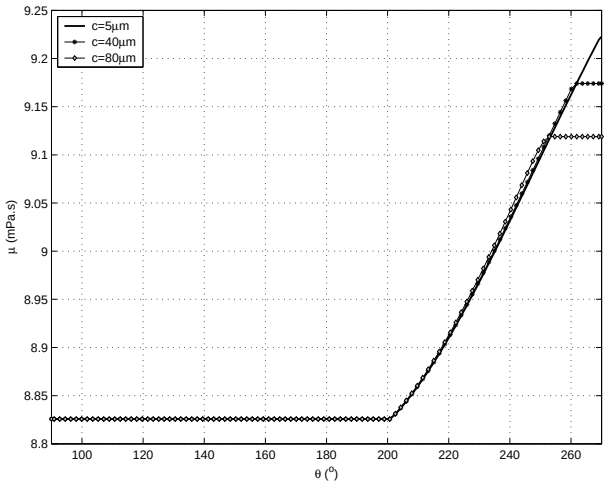

a) Apparent viscosity

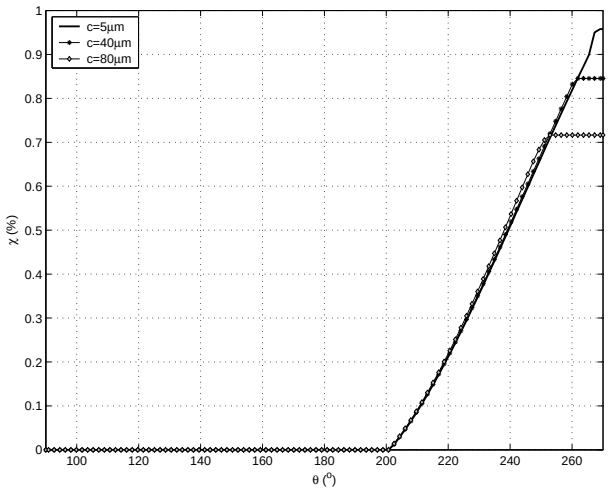

b) Gas quality

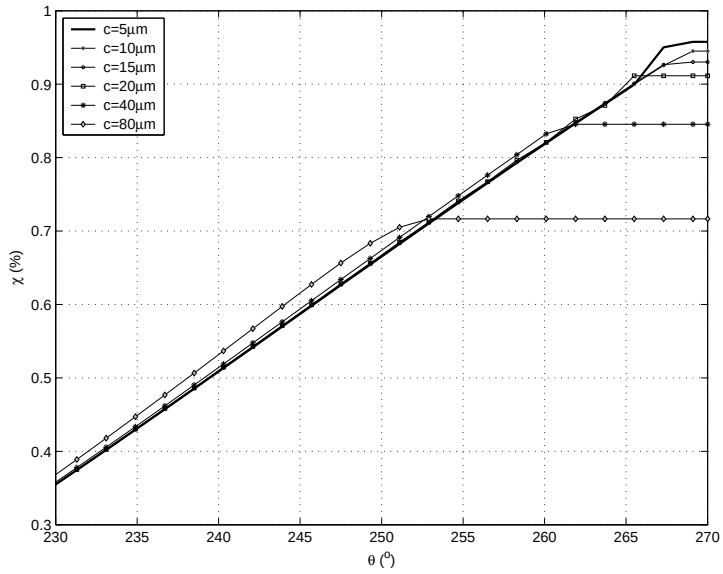

c) Quality at the end of cavitation region and during pressure recovery

Figure 5.5. Apparent viscosity and gas quality of the mixture for different clearances.
($D = 20mm, \varepsilon = 0.75, \omega = 60Hz, p_i = p_o = 100kPa, T = 40^oC, w_i = w_{sat} = 4.07\%, L = 100mm$)

Table 5.1. Results for performance variables for different clearances.

	W (kN)	ψ (°)	α (°)	F_f (N)	$f.10^3$	q_θ (g/s.m)	p_{max} (MPa)	p_{min} (kPa)
c=5μm	*96.00*	*29.6*	*21.6*	*57.80*	*0.60*	*2.50*	*109.63*	*21.80*
c=10μm	*24.82*	*29.0*	*21.6*	*28.96*	*1.17*	*5.03*	*28.11*	*21.22*
c=15μm	*11.04*	*29.0*	*21.6*	*19.31*	*1.75*	*7.55*	*12.50*	*21.22*
c=20μm	*6.21*	*29.0*	*21.6*	*14.49*	*2.33*	*10.06*	*7.03*	*20.65*
c=40μm	*1.55*	*29.3*	*21.6*	*7.26*	*4.67*	*20.13*	*1.76*	*19.32*
c=80μm	*0.39*	*30.4*	*21.6*	*3.65*	*9.38*	*40.26*	*0.44*	*16.33*

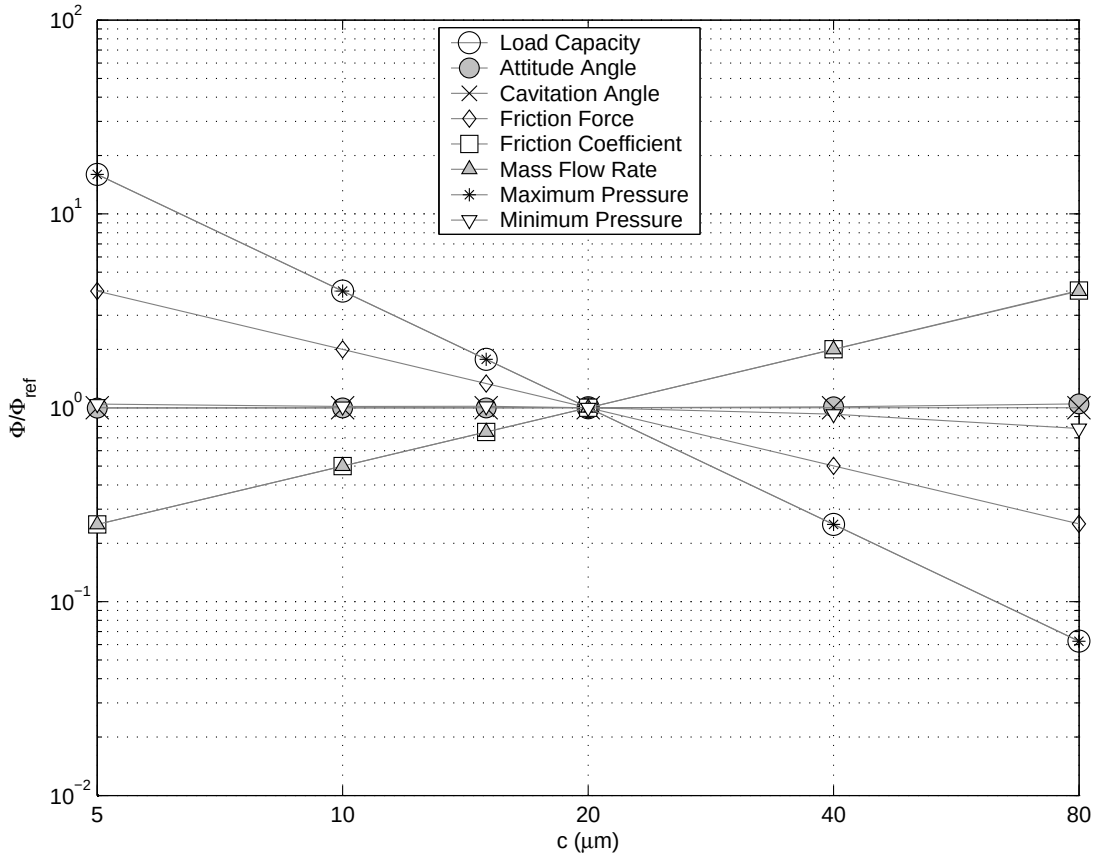

Figure 5.6. Variations of performance variables in relation to the medium clearance value (log-log).
($D = 20mm, \varepsilon = 0.75, \omega = 60Hz,\ p_i = p_o = 100kPa, T = 40^o C, w_i = w_{sat} = 4.07\%,\ L = 100mm$)

5.2.3. Influence of shaft velocity

Six different velocities of rotation for the shaft were tested, in equal variations from 15Hz (900rpm) to 90Hz (5400rpm). With the increase of rotational speed of the journal, a linear increase is observed for pressure at every position in the convergent region of the bearing. However, in the same way as observed for clearance, pressures are very similar in the cavitated region, differing only in the recovery region, which occurs later for higher velocities. This is observed in figures 5.7a-b. Considering dimensionless pressures, figure 5.7c-d, similar behaviour occurs in the convergent region, while in the divergent region the amplitude of negative pressures increases as velocity decreases. This behaviour points for an independence of the pressures in the cavitated region with velocity. Either in figure 5.7b and 5.7d, it is seen that the release of gas starts practically is the same point for all the six velocities tested.

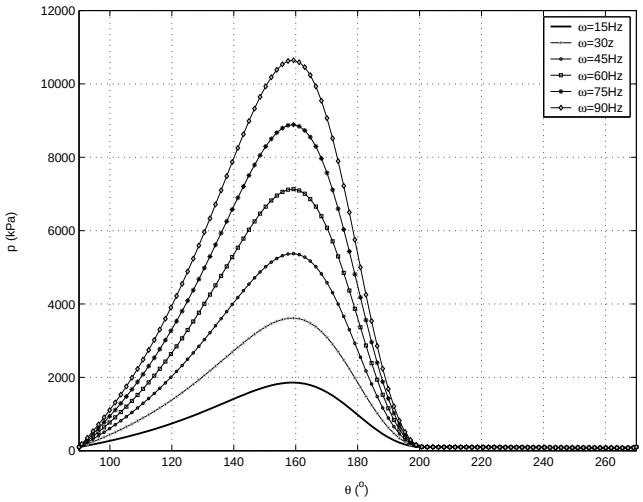

a) Full domain of the bearing

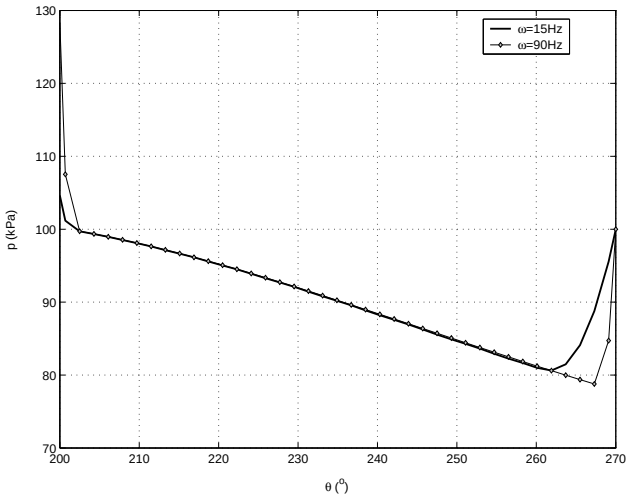

b) Cavitation region in details

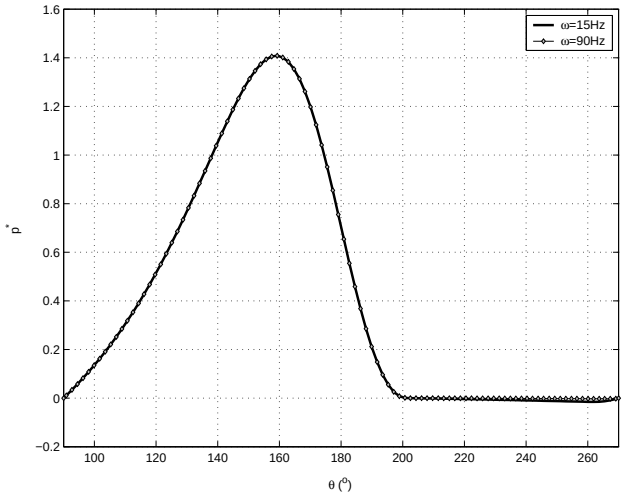

c) Dimensionless - Full domain of the bearing

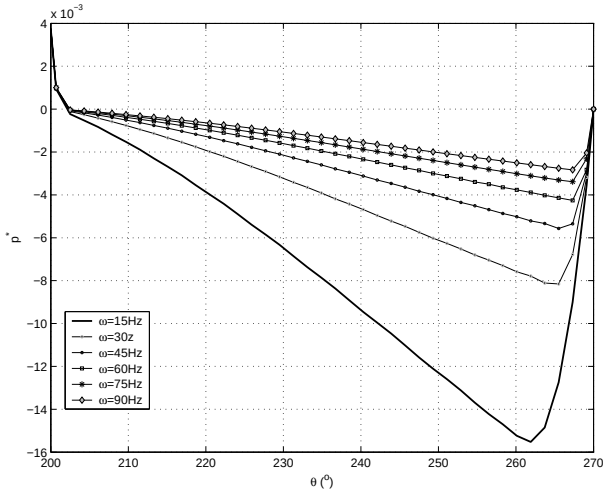

d) Dimensionless - Cavitation region in details

Figure 5.7. Pressure results for different velocities of the shaft.
($D = 20mm,\ c = 20\mu m,\ \varepsilon = 0.75,\ p_i = p_o = 100kPa, T = 40^oC, w_i = w_{sat} = 4.07\%,\ L = 100mm$)

The similarity of the behaviour in the divergent region can also be concluded from figures 5.8 and 5.9a-b, presenting respectively the refrigerant mass fraction, apparent density and void fraction. Smaller mass fractions are observed at the bearing outlet for the higher velocities, which is due to the smaller extension of the pressure recovery region. Void fraction reaches values up to 70%, which produces a reduction in the apparent density to less than a third of that at the entrance. The reduction of void fraction due to the increase of pressure at the end of the bearing and consequent compression of the gas is seen in figure 5.9c – the region presented contains only 7 points of the 102 of the discretisation, giving the sharp variations. Refined meshes would result in smoother profiles, but would not change results.

As the behaviour of the fluid in the divergent region does not depend on velocity as it happened with clearance, figures 5.10a-b, respectively viscosity and gas quality,

give an idea of the similarity between the different conditions, and also of those with the results of clearance. The mass of gas released is less than 1% (figure 5.10b), and changes in viscosity are around 4%. Figure 5.10c presents differences in the behaviour of the fluid close to the exit of the bearing for the different velocities. It is seen that at 15Hz about 10^o are used for pressure recovery, while a little less than 3^o is required for 75 and 90Hz.

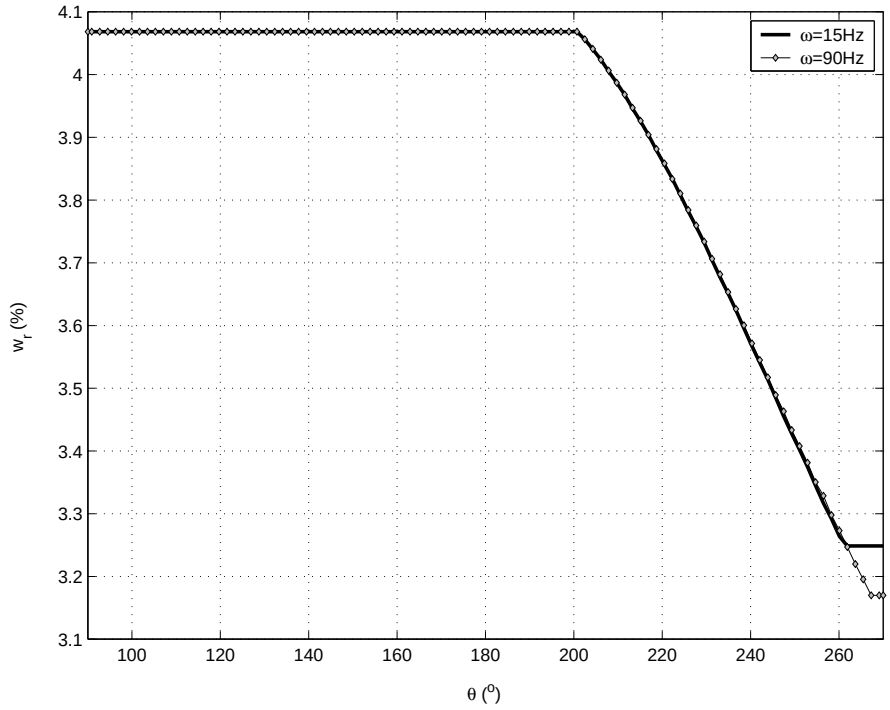

Figure 5.8. Refrigerant mass fraction along the bearing – results for different velocities.
$(D = 20mm,\ c = 20\mu m,\ \varepsilon = 0.75,\ p_e = p_o = 100kPa, T_e = 40^o C, w_e = w_{sat} = 4.07\%,\ L = 100mm)$

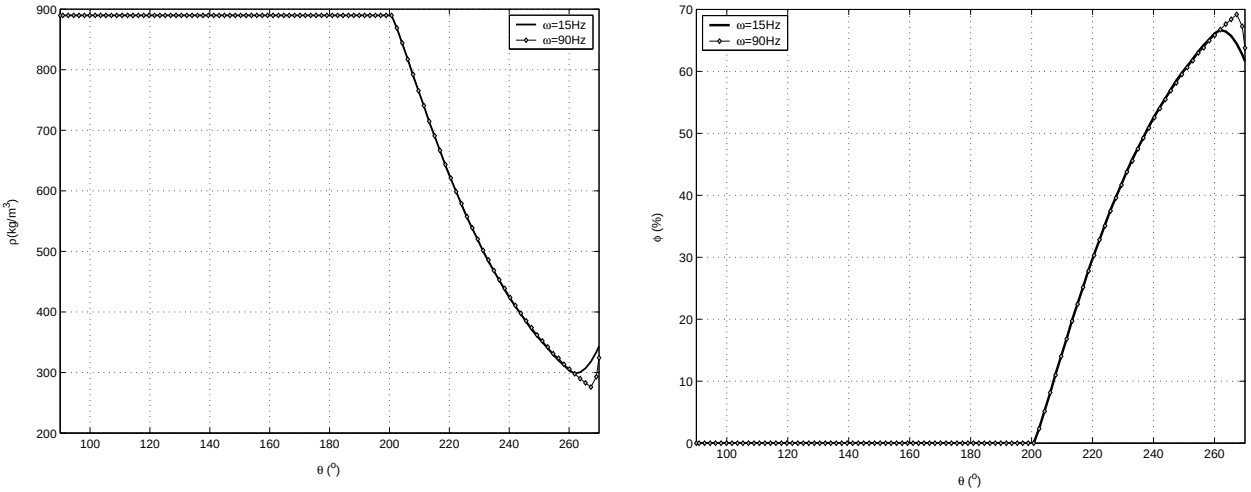

a) Apparent density **b)** Void fraction

Figure 5.9. Density and void fraction of the mixture for different velocities.
$(D = 20mm,\ c = 20\mu m,\ \varepsilon = 0.75,\ p_i = p_o = 100kPa, T = 40^o C, w_i = w_{sat} = 4.07\%,\ L = 100mm)$

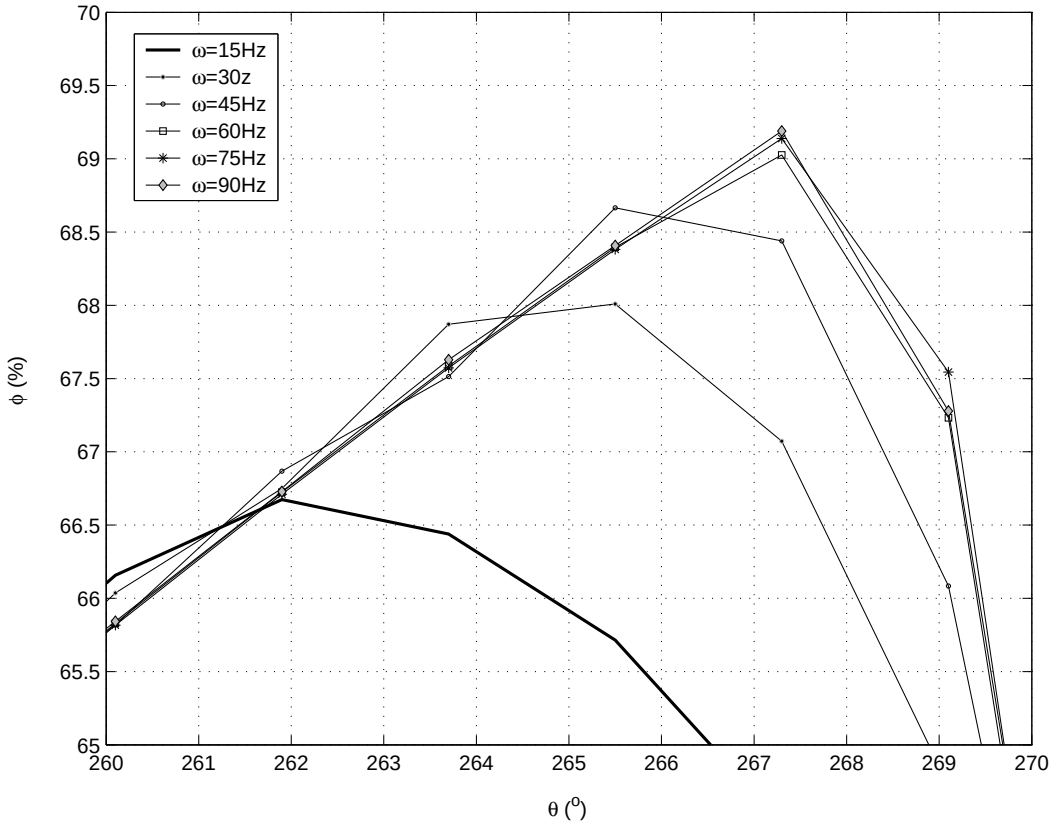

c) Void fraction at the end of cavitation region and during pressure recovery

Figure 5.9. Density and void fraction of the mixture for different velocities.
($D = 20mm,\ c = 20\mu m,\ \varepsilon = 0.75,\ p_i = p_o = 100kPa, T = 40^oC, w_i = w_{sat} = 4.07\%,\ L = 100mm$)

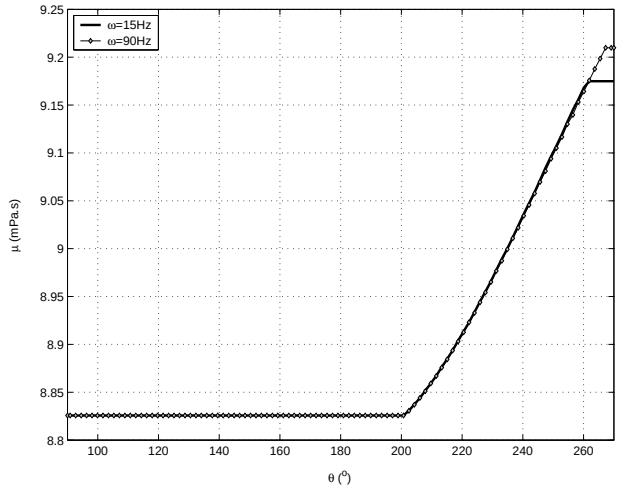

a) Apparent viscosity

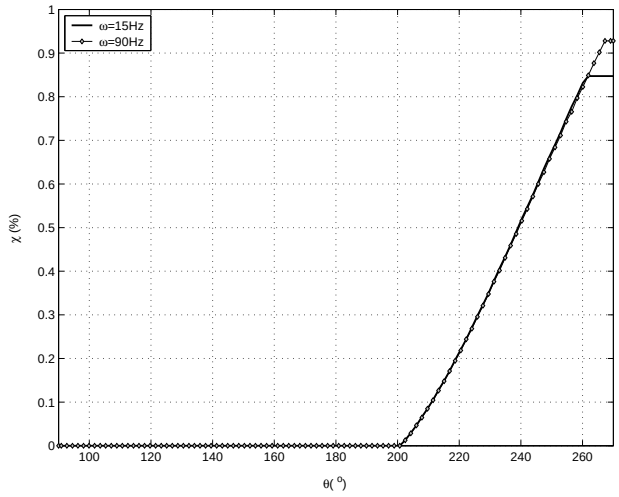

b) Gas quality

Figure 5.10. Viscosity and quality of the mixture for different journal velocities.
($D = 20mm,\ c = 20\mu m,\ \varepsilon = 0.75,\ p_i = p_o = 100kPa, T = 40^oC, w_i = w_{sat} = 4.07\%,\ L = 100mm$)

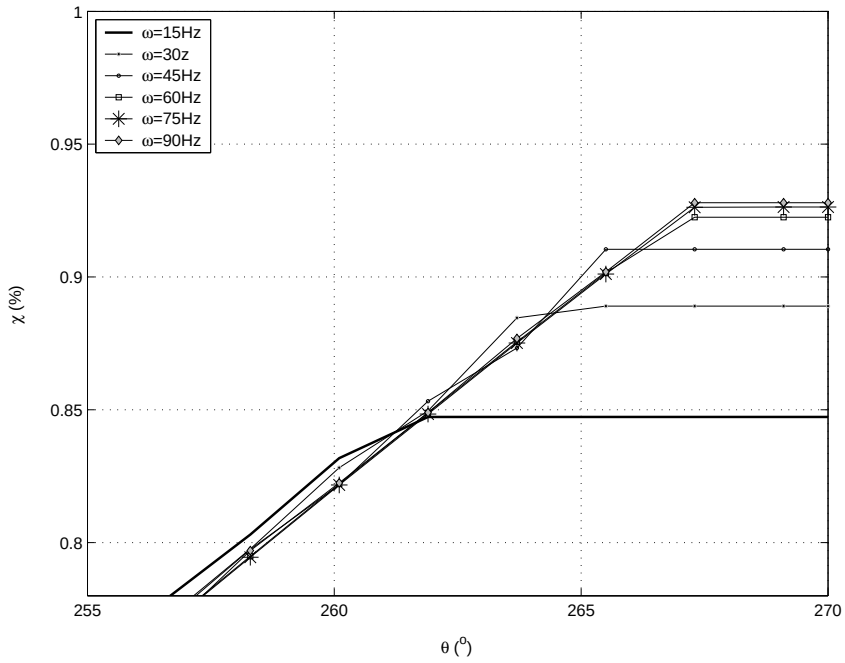

c) Quality at the end of cavitation region and during pressure recovery

Figure 5.10. Viscosity and quality of the mixture for different journal velocities.
($D = 20mm,\ c = 20\mu m,\ \varepsilon = 0.75,\ p_i = p_o = 100kPa, T = 40^oC, w_i = w_{sat} = 4.07\%,\ L = 100mm$)

Figure 5.11 shows the variation of main bearing characteristics with shaft velocity. Load, friction force, mass flow rate and maximum pressure increase linearly with speed, while no significant changes are observed for attitude and cavitation angle, friction coefficient, and minimum pressure. Actually, for the minimum pressure a very smooth increase is observed, which reproduces the later pressure recovery for higher speeds. Table 5.2 presents the absolute values for the properties analysed in relation to the reference values.

Table 5.2. Results for performance variables for different shaft velocities.

	W (kN)	ψ (°)	α (°)	F_f (N)	$f.10^3$	q_θ (g/s.m)	p_{max} (MPa)	p_{min} (kPa)
ω=15Hz	1.55	29.3	21.6	3.63	2.33	2.52	1.76	19.37
ω=30Hz	3.10	29.1	21.6	7.25	2.33	5.03	3.52	20.35
ω=45Hz	4.66	29.1	21.6	10.87	2.33	7.55	5.72	20.85
ω=60Hz	6.21	29.0	21.6	14.49	2.33	10.06	7.03	21.26
ω=75Hz	7.76	29.0	21.6	18.11	2.33	12.58	8.79	21.13
ω=90Hz	9.31	29.0	21.6	21.73	2.33	15.10	10.54	21.22

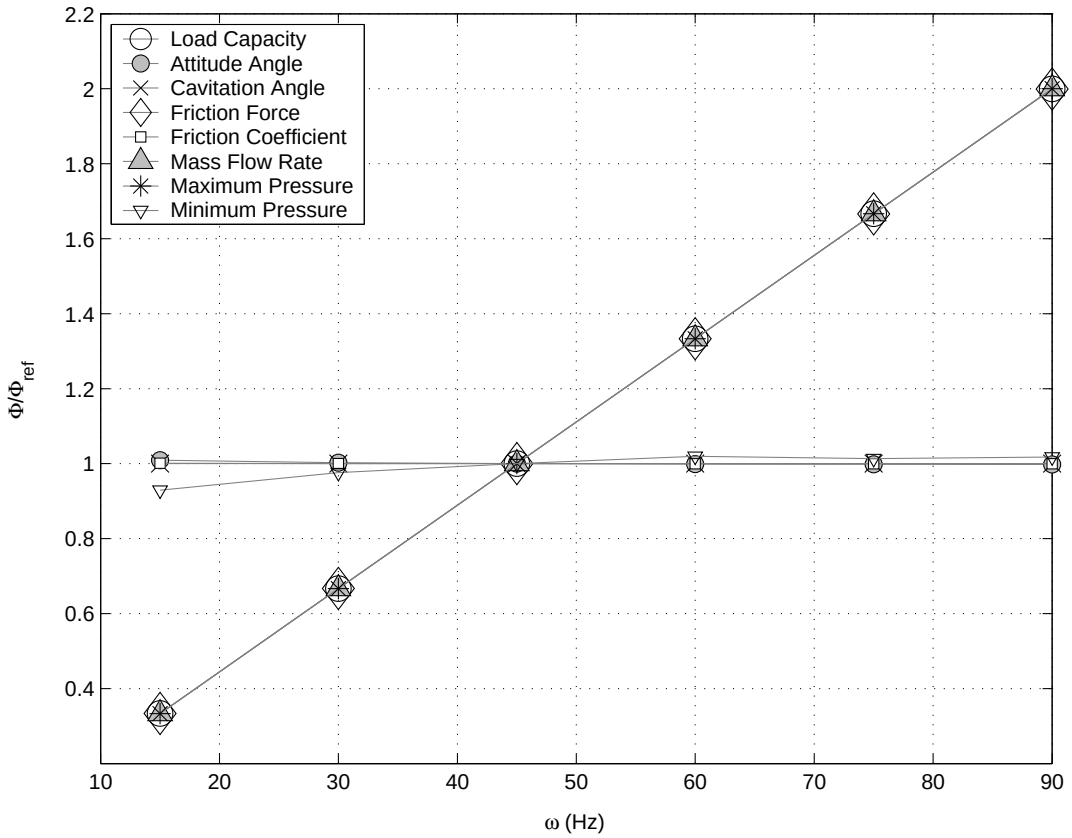

Figure 5.11. Variations of performance variables of the bearing with velocity in relation to ω=45Hz. ($D = 20mm,\ c = 20\mu m,\ \varepsilon = 0.75,\ p_i = p_o = 100kPa, T = 40^oC, w_i = w_{sat} = 4.07\%,\ L = 100mm$)

5.2.4. Influence of eccentricity

From previous sections, it has been observed that eccentricity is the parameter capable of producing more significant changes in a greater number of variables. Tests were performed here using eccentricities between 0.05 and 0.95, keeping all other variables constant. Under different eccentricities, the profiles of film thickness change considerably, as is seen in figure 5.12 (for clarity, not all eccentricities are shown).

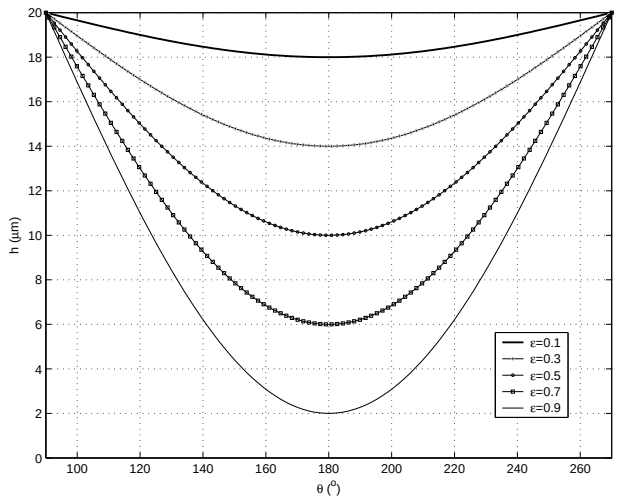

Figure 5.12. Variation of film thickness along the bearing for different eccentricities ($c = 20\mu m$).

Differently from the previous cases, the ratio between minimum film thickness and clearance varies, which influences considerably the behaviour of the lubricant film along the bearing. The pressure profile is significantly modified with the variation of eccentricity, as shown in figures 5.13a-b. For higher eccentricities, a very high level of pressure is achieved (*~30MPa* for $\varepsilon=0.9$), and the more severe changes in film thickness induce cavitation to start earlier, moving to the centre of the bearing (5.13a). As the release of gas starts earlier, a greater amount of gas will be required to fill the volume in divergent region which the liquid is not capable to do, then reflecting in lower pressures in the cavitated region (5.13b). The same behaviour is observed in figures 5.14a-b, as the dimensionless pressure depends on eccentricity as does the absolute pressure.

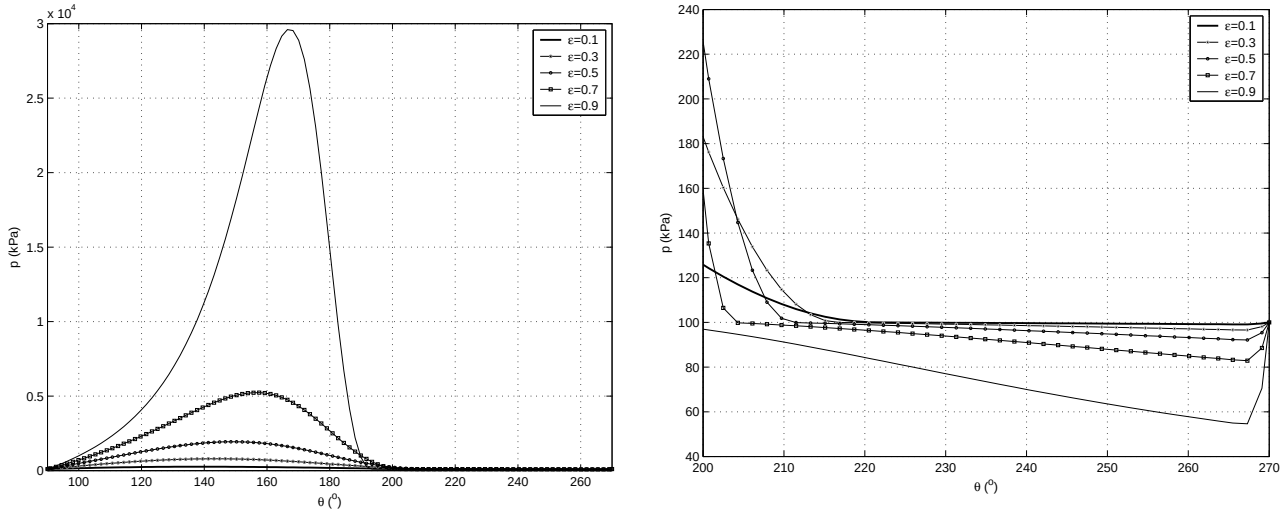

a) Full domain of the bearing **b)** Cavitation region in details

Figure 5.13. Pressure results for different eccentricities.
($D = 20mm, c = 20\mu m,\ \omega = 60Hz,\ p_i = p_o = 100kPa, T = 40^oC, w_i = w_{sat} = 4.07\%,\ L = 100mm$)

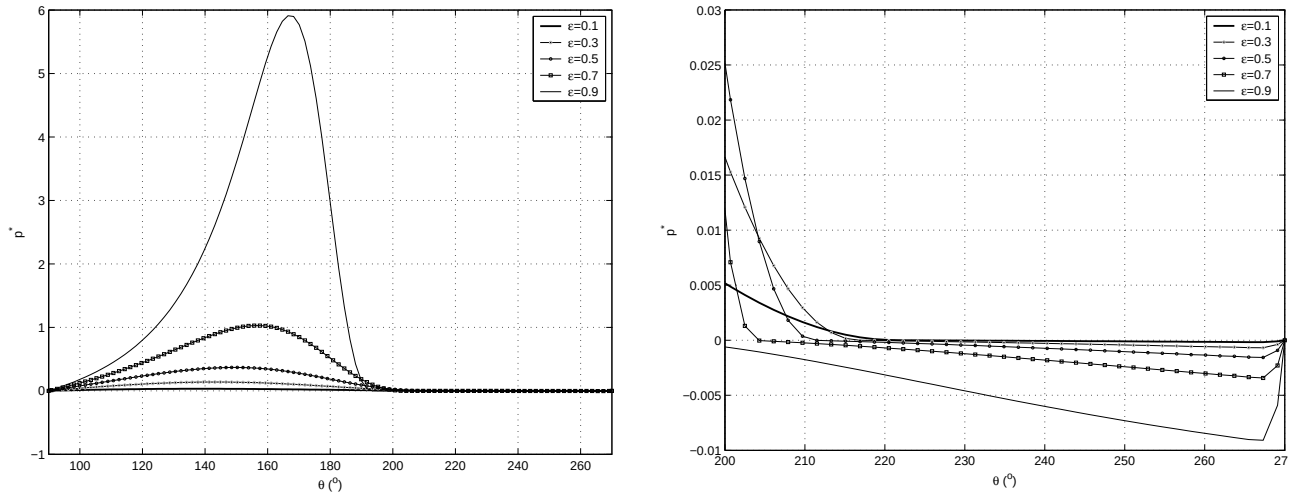

a) Full domain of the bearing **b)** Cavitation region in details

Figure 5.14. Dimensionless pressure results for different eccentricities.
($D = 20mm, c = 20\mu m,\ \omega = 60Hz,\ p_i = p_o = 100kPa, T = 40^oC, w_i = w_{sat} = 4.07\%,\ L = 100mm$)

In figure 5.14b, it can be noticed that pressure recovery occurs in a similar position for all the cases presented, therefore having weak correlation with eccentricity. This is also seen for the refrigerant mass fraction in figure 5.15 where it is also observed the necessity of releasing more gas at higher eccentricities. While for an eccentricity of *0.5* mass fraction reduces from *4.1* to *3.75%*, for $\varepsilon=0.9$ it goes down to *2.2%*, thus having greater mass of free gas.

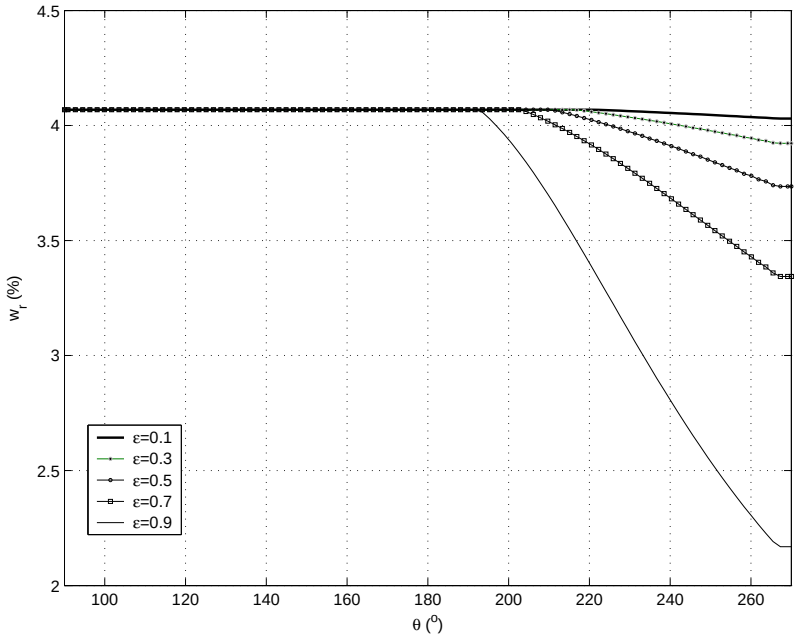

Figure 5.15. Refrigerant mass fraction along the bearing for different eccentricities.
($D = 20mm, c = 20\mu m,\ \omega = 60Hz,\ p_i = p_o = 100kPa, T = 40^o C, w_i = w_{sat} = 4.07\%,\ L = 100mm$)

The release of gas reduces the apparent density, as shown in figure 5.16a; the proportion in which it decreases is determined by void fraction, presented in figure 5.16b; it reaches more than *85%* for $\varepsilon=0.9$, while is limited to around *20%* for $\varepsilon=0.3$. It is interesting to note that the rate of increase gradually reduces as void fraction increases; this can be understood as the lower relative importance of new gas releases at higher void fractions, since a considerable amount of gas is already available in these conditions.

The earlier release of gas observed in higher eccentricities also induces more significant changes in the homogeneous viscosity, presented in figure 5.17a. This is due to the increasing mass of gas refrigerant free from the liquid, characterised in figure 5.17b by gas quality. The gas participates with *2%* of the total fluid mass at $\theta=260^o$ and $\varepsilon=0.9$, which brings the liquid mixture viscosity closer to oil viscosity, increasing homogeneous viscosity in about *10%*. For $\varepsilon=0.7$, the mass of gas contributes with

about *0.8%* of the total mass, and this produces a change in viscosity of less than *3.5%*. For even lower eccentricities, variations in viscosity can practically be disconsidered.

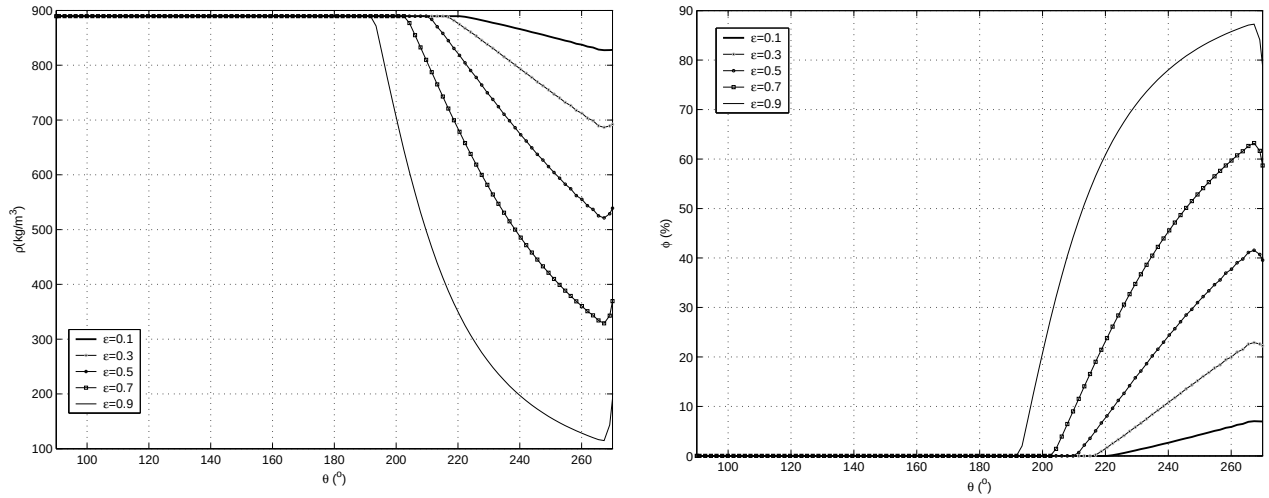

a) Apparent density **b)** Void fraction

Figure 5.16. Density and void fraction of the mixture along the bearing for different eccentricities.
($D = 20mm, c = 20\mu m,\ \omega = 60Hz,\ p_i = p_o = 100kPa, T = 40^oC, w_i = w_{sat} = 4.07\%,\ L = 100mm$)

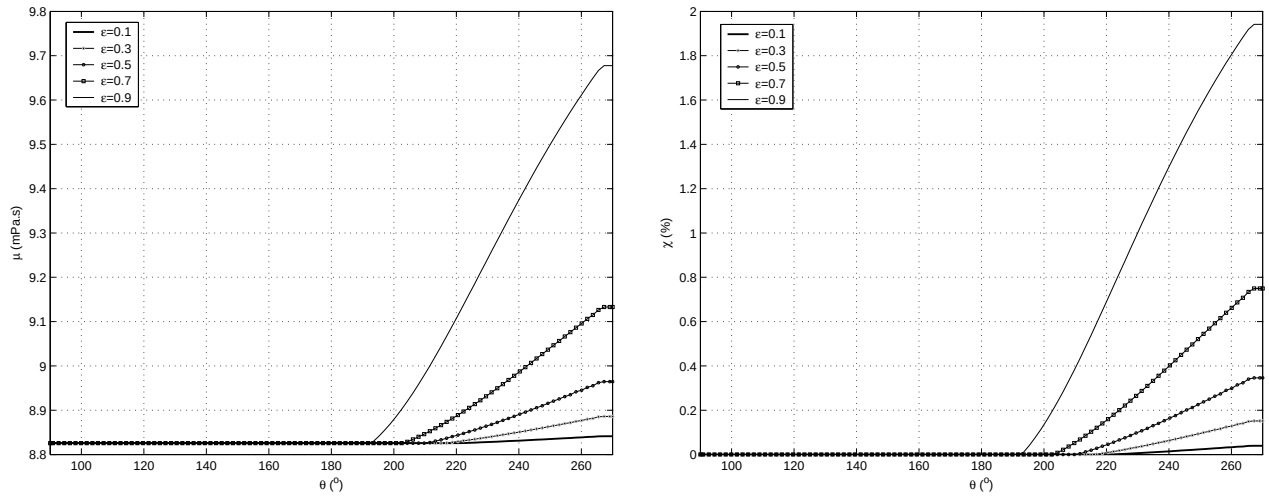

a) Apparent viscosity **b)** Gas quality

Figure 5.17. Viscosity and quality of the mixture for different eccentricities.
($D = 20mm, c = 20\mu m,\ \omega = 60Hz,\ p_i = p_o = 100kPa, T = 40^oC, w_i = w_{sat} = 4.07\%,\ L = 100mm$)

In regard to performance variables, all are influenced by eccentricity, tough in different levels. This is presented in figure 5.18, using a logarithmic scale for the *y*-axis. Load capacity and maximum pressure are the most influenced ones, and monotonically increases with eccentricity. The minimum pressure is also greater for higher eccentricities, as more gas needs to be released in these conditions. The decrease in attitude angle with eccentricity, observing a higher decrease rate at higher eccentricities, indicates that line of centres and the load line come closer, with the load approaching the vertical line at $\theta=180^o$. In a higher rate than that of the attitude angle,

cavitation angle decreases with eccentricity, bringing the release of gas closer to the centre line. In an opposite way, friction force increases with eccentricity, especially for higher values. However, as this rate of increase is lower than the rate of increase of load, friction coefficient monotonically decreases with eccentricity. The same is observed for the mass flow rate, as the restriction to the flow increases with eccentricity. The absolute values for the performance parameters are presented in table 5.3.

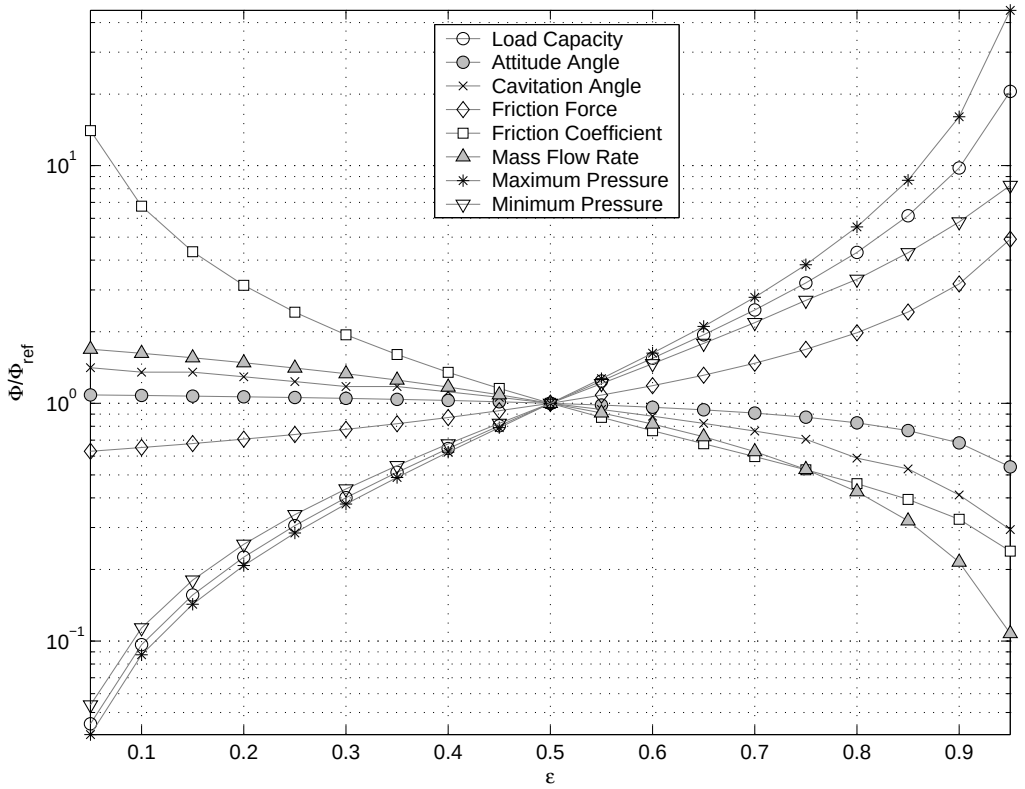

Figure 5.18. Variations of performance variables with eccentricity in relation to medium value ($D = 20mm, c = 20\mu m,\ \omega = 60Hz,\ p_i = p_o = 100kPa, T = 40^o C, w_i = w_{sat} = 4.07\%,\ L = 100mm$)

Table 5.3. Results for performance variables for different shaft velocities.

	W (kN)	ψ (^{o})	α (^{o})	F_f (N)	$f.10^3$	q_θ (g/s.m)	p_{max} (MPa)	p_{min} (kPa)
ε=0.1	0.19	35.9	41.4	5.60	29.98	31.02	0.16	0.89
ε=0.2	0.44	35.4	39.6	6.07	13.93	28.33	0.38	2.00
ε=0.3	0.77	34.9	36.0	6.68	8.62	25.46	0.69	3.41
ε=0.4	1.25	34.2	34.2	7.49	6.00	22.38	1.14	5.28
ε=0.5	1.94	33.2	30.6	8.59	4.44	19.12	1.84	7.82
ε=0.6	2.99	32.0	27.0	10.19	3.40	15.64	2.98	11.488
ε=0.7	4.78	30.2	23.4	12.66	2.65	11.97	5.13	17.10
ε=0.8	8.35	27.5	18.0	17.03	2.04	8.11	10.14	26.02
ε=0.9	18.92	22.7	12.6	27.31	1.44	4.10	29.50	45.36

5.2.5. Influence of entrance pressure

Considering a saturated mixture, variations on the entrance pressure will produce changes in refrigerant mass fraction and this will consequently affect all other fluid properties, therefore reflecting in lubrication performance. Simulations were performed for 6 different levels of entrance pressure, from *20kPa* to *300kPa*, representing conditions ranging from a relative vacuum to a pressurised environment. The back pressure is also set to the entrance value.

Results for absolute pressure are presented in figures 5.19a-b, where it can be seen that the highest and lowest levels of pressure are achieved in the low entrance pressure condition, while the amplitude of pressures is the smallest for the highest entrance pressure.

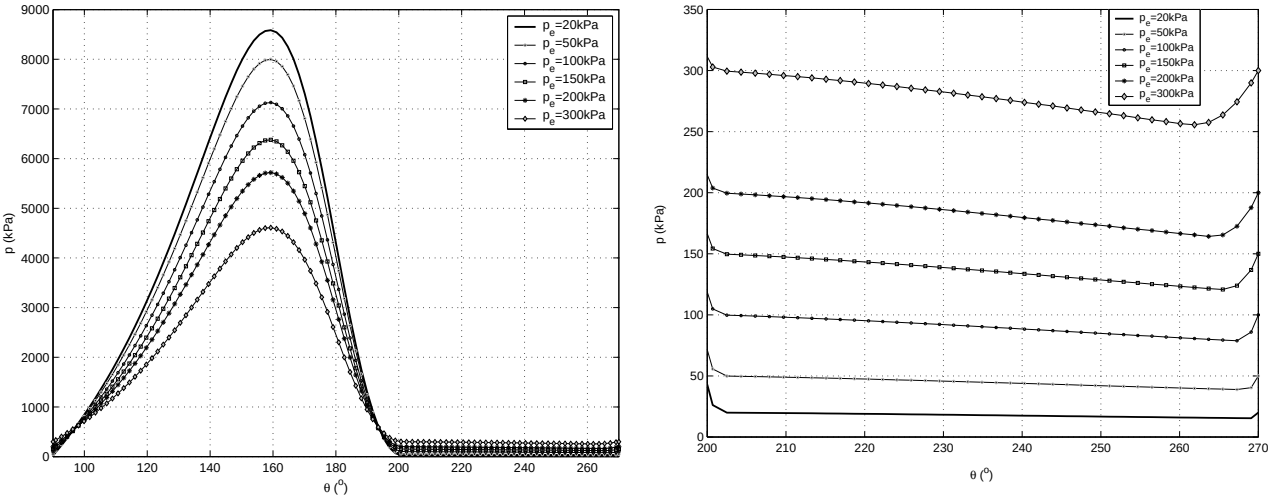

a) Full domain of the bearing **b)** Cavitation region in details

Figure 5.19. Pressure profile for different entrance pressures.
($D = 20mm, c = 20\mu m, \varepsilon = 0.75,\ \omega = 60Hz, T = 40^{o}C, w_i = w_{sat},\ L = 100mm$)

To a better comparison, relative (gauge) pressures should be considered. Those are presented in figures 5.20a-b. In this case, highest levels of pressure are still achieved for lower entrance pressures, but the decrease in pressure is greater for higher entrance pressure, reaching a depression of *45kPa* for p_e*=300kPa* against less than *5kPa* for p_e*=20kPa*. In figure 5.20b, it can be also observed the later pressure recovery for the lowest entrance pressure.

Further conclusions can be taken from the dimensionless pressures presented in figure 5.21a-b. In figure 5.21a, it is seen that results for the several conditions are very similar. As geometry is the same, the only condition producing changes for the different simulations is viscosity. Therefore, it is expected that saturated liquid

mixtures at lower entrance pressures present higher viscosity. Furthermore, as the lowest entrance pressure is the closest to Reynolds condition, it might also have the highest load.

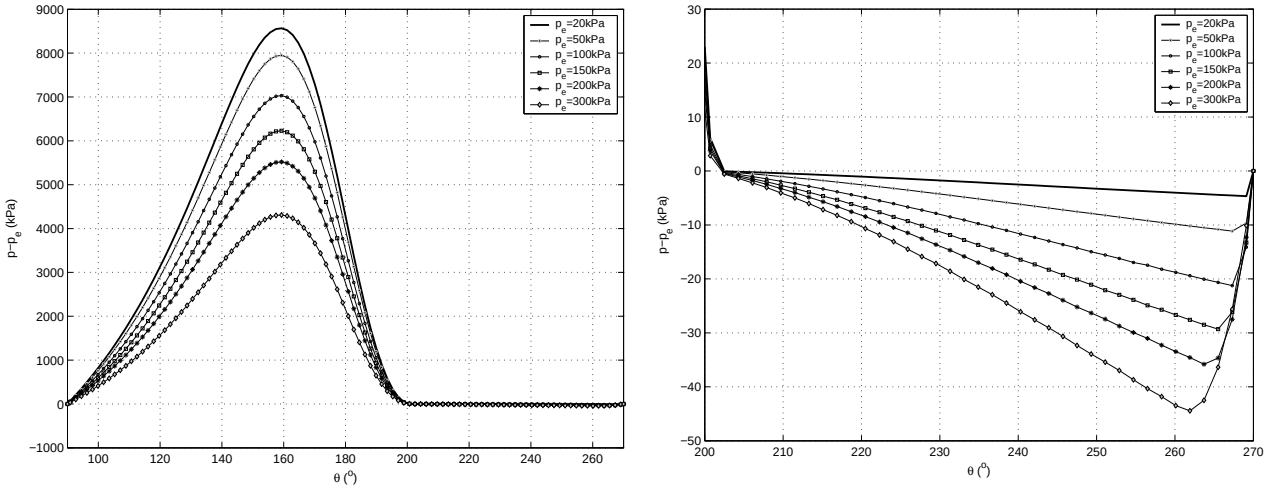

a) Full domain of the bearing **b)** Cavitation region in details

Figure 5.20. Gauge pressure for different entrance pressures.
($D = 20mm, c = 20\mu m, \varepsilon = 0.75,\ \omega = 60Hz, T = 40^{o}C, w_i = w_{sat},\ L = 100mm$)

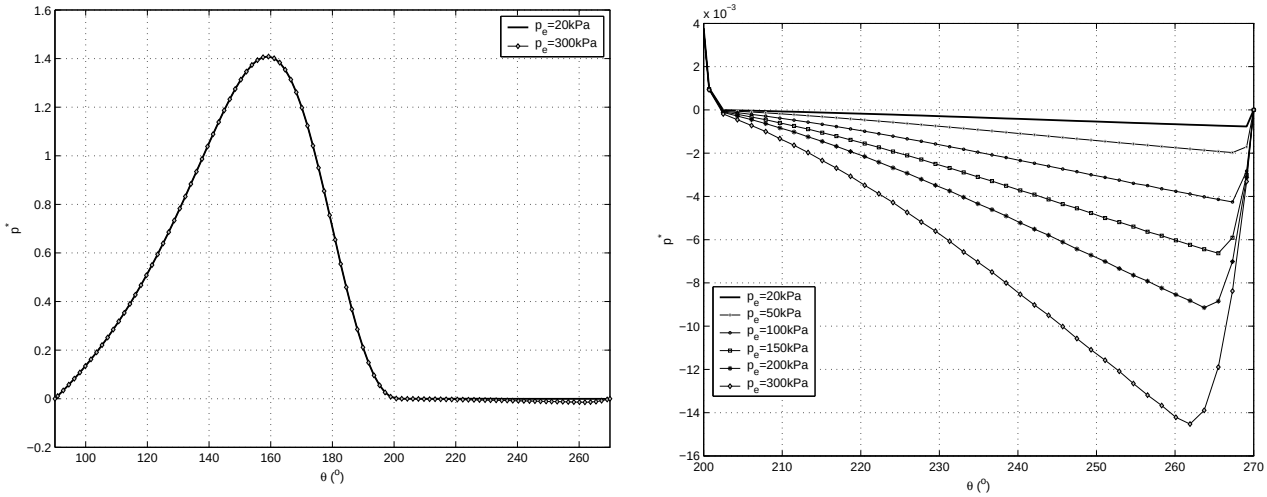

a) Full domain of the bearing **b)** Cavitation region in details

Figure 5.21. Dimensionless pressure results for different ambient pressures.
($D = 20mm, c = 20\mu m, \varepsilon = 0.75,\ \omega = 60Hz, T = 40^{o}C, w_i = w_{sat},\ L = 100mm$)

Figure 5.22 presents the refrigerant mass fraction of the liquid mixture for the different cases. It can be seen that, at the same temperature, more refrigerant is dissolved in the oil for higher pressures. For instance, solubility it is almost 14% at 300kPa while less than 1% for 20kPa. It is also observed from figure 5.22 that more gas is released from the liquid at higher entrance pressures.

In spite of the different mass fractions, density and void fraction are very similar for the different conditions, as shown respectively in figures 5.23a and b. In

figure 5.23a, it is seen that liquid mixture is heavier at higher pressures; this occurs because the liquid refrigerant is heavier than the oil, and more refrigerant is dissolved in the oil as pressures increases. Nevertheless, the behaviour is very similar in the two-phase region: density starts to decrease at the same point and curves are very close throughout the cavitated region. Density differs only in the pressure recovery region, which starts earlier for higher entrance pressures. In figure 5.23b, void fraction shows an almost identical profile for the extreme cases. As in any case the release of gas starts at the same point ($\theta \cong 200^o$), the proportional volume of the fluid film to be filled is equal; therefore, void fraction is required to be equal. Differences are observed only in the pressure recovery region, presented in figure 5.23c.

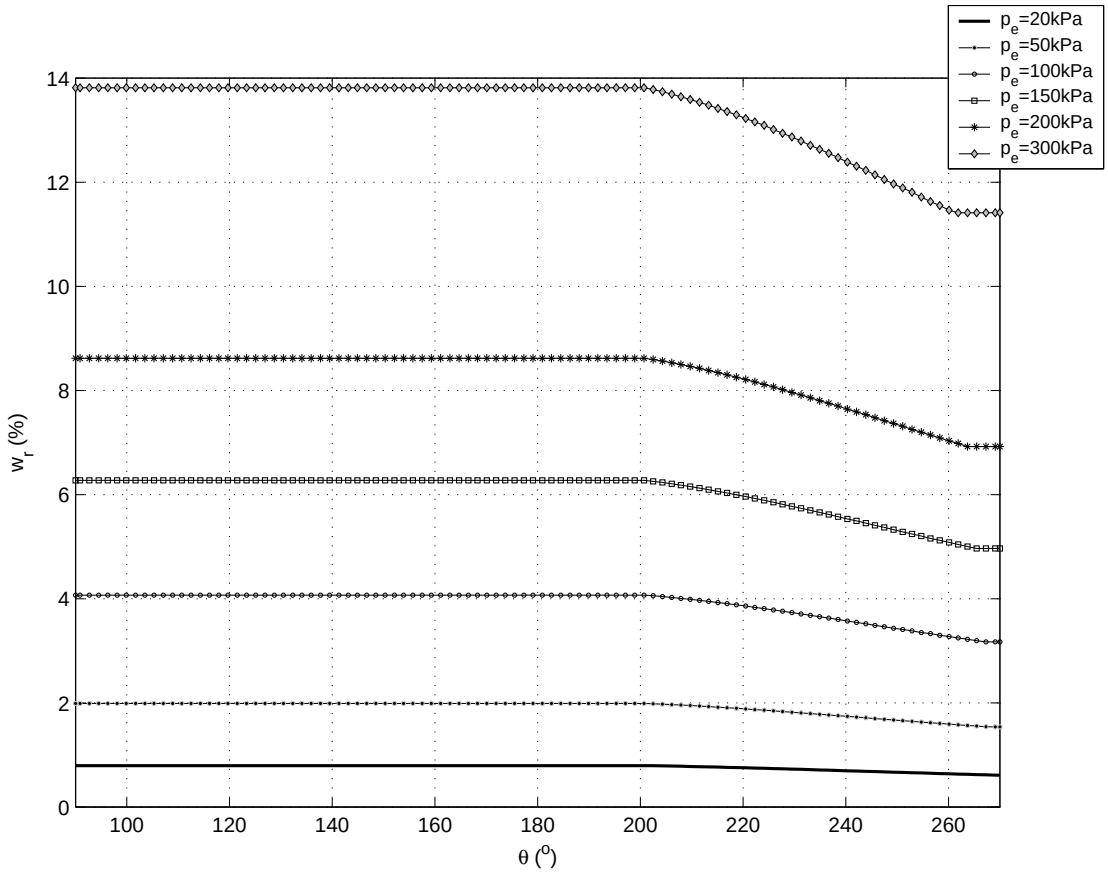

Figure 5.22. Behaviour of refrigerant mass fraction for different entrance pressures.
($D = 20mm, c = 20\mu m, \varepsilon = 0.75,\ \omega = 60Hz, T = 40^o C, w_i = w_{sat},\ L = 100mm$)

The results presented in figure 5.23 indicate that behaviour of void fraction and consequently changes in density are not determined by fluid properties, but by geometry instead – or, more precisely, eccentricity, the factor practically determining cavitation angle. This means that, for a given geometry, regardless the mixture, the fluid will release the amount of gas necessary to achieve the void fraction geometrically required. Densities, averaged by the similar void fraction, will present similar behaviour. It

should be stressed however that this does not mean the same apparent density, as it also depends on liquid and gas phase densities, which are specific for each mixture.

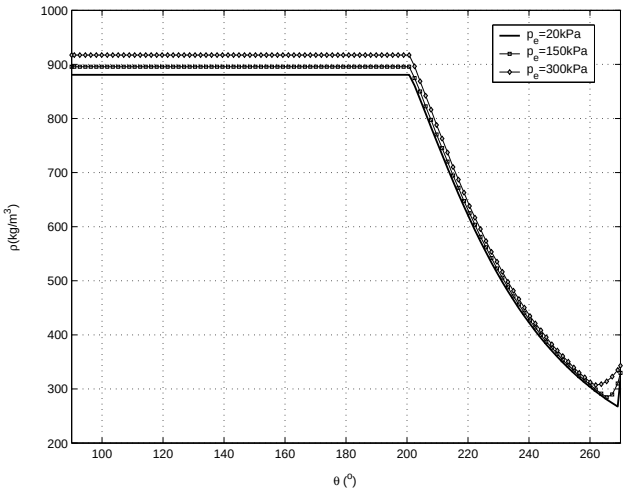

a) Apparent density

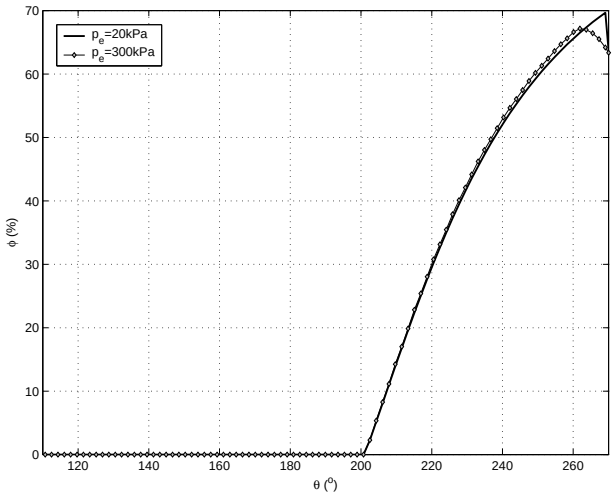

b) Void fraction

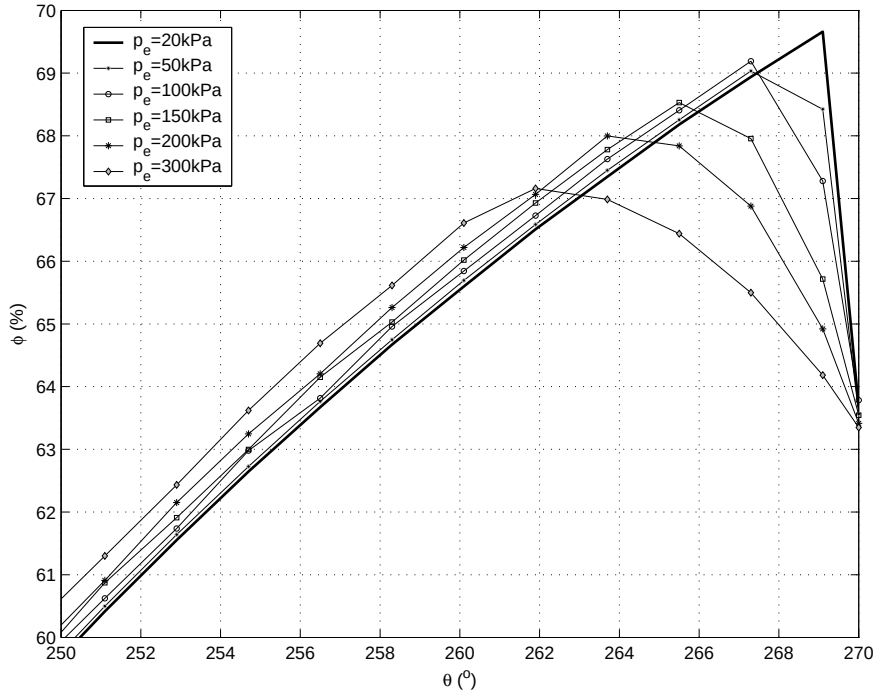

c) Void fraction at the end of cavitation region and during pressure recovery

Figure 5.23. Density and void fraction of the mixture for different entrance pressures. ($D = 20mm, c = 20\mu m, \varepsilon = 0.75,\ \omega = 60Hz, T = 40^{o}C, w_i = w_{sat},\ L = 100mm$)

Differently from void fraction (and density to some extent), other properties will not necessarily have similar results. In fact, they tend to present considerable differences in order to achieve the requirements imposed by void fraction. This was already observed from figure 5.22 with mass fraction, but it is confirmed in figure 5.24a-b, for viscosity and quality. The viscosity of the liquid mixture at the entrance for p_e*=20kPa* is almost twice that for p_e*=300kPa*, which reflects in the higher pressures

seen in figure 5.20a. With the release of gas, the viscosity variations gradually increase with the higher entrance pressure, due to the higher fraction of refrigerant released from the oil, as quality confirms in figure 5.24b. The mass of gas released is less than 0.5% for p_e*=50kPa,* while for p_e*=300kPa* gas eventually reaches 3.75% of the mass of the two-phase mixture.

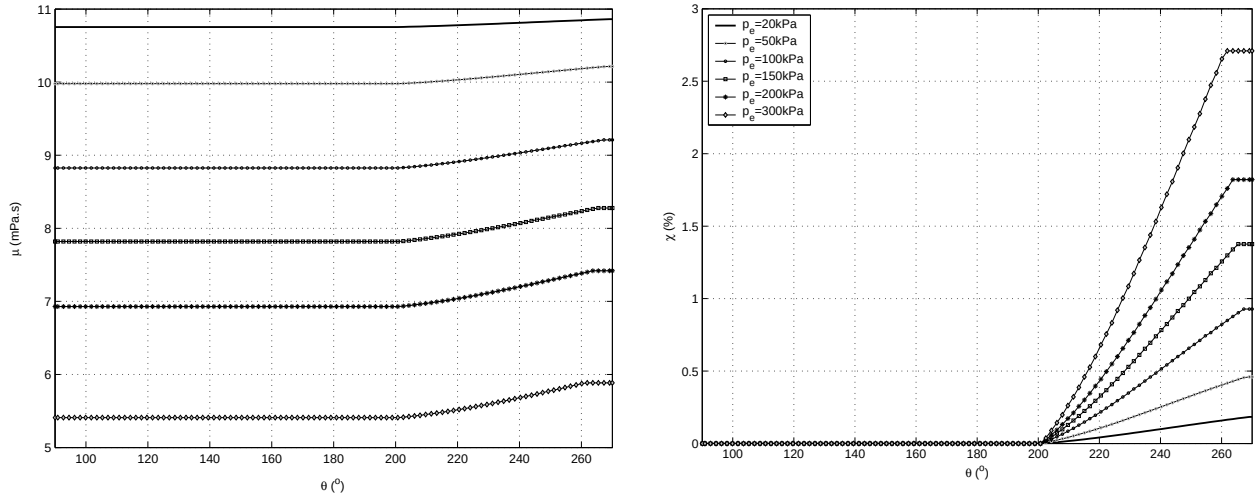

a) Apparent viscosity **b)** Gas quality

Figure 5.24. Viscosity and quality for different entrance pressures. (both figures follows 5.24b legend)
($D = 20mm, c = 20\mu m, \varepsilon = 0.75,\ \omega = 60Hz, T = 40^{o}C, w_i = w_{sat},\ L = 100mm$)

To explain the greater release of gas at higher entrance pressures, the density of the gas needs to be considered. Due to compressibility, it increases with pressure. Therefore, to fill the same volume (geometrically determined), more gas is required to be released at higher pressures – which reflects in the higher quality for the same void fraction.

In regard to performance variables, presented in figure 5.25, variations occur basically due to changes in liquid viscosity. Load capacity, friction force and maximum pressure vary linearly with viscosity; as liquid viscosity decreases with the increase in entrance pressure, these variables will decrease with increasing p_e. On the other hand, attitude and cavitation angles, friction coefficient and mass flow rate do not depend on viscosity and are almost constant with entrance pressure changes – mass flow rate presents a small increase due to the increase of liquid density with pressure as a result of increasing refrigerant solubility. Minimum pressure increases considerably with entrance pressure as more gas is required in that situation. Table 5.4 presents data the plotted in figure 5.25.

Table 5.4. Results for performance variables for the different entrance pressures.

	W (kN)	ψ (^{o})	α (^{o})	F_f (N)	$f.10^3$	q_θ (g/s.m)	p_{max} (MPa)	p_{min} (kPa)
p_e=20kPa	7.56	29.0	21.6	17.59	2.32	9.96	8.57	4.66
p_e=50kPa	7.02	29.0	21.6	16.34	2.33	10.00	7.95	11.14
p_e=100kPa	6.21	29.0	21.6	14.49	2.33	10.06	7.03	21.26
p_e=150kPa	5.50	29.1	21.6	12.86	2.34	10.13	6.23	29.30
p_e=200kPa	4.88	29.2	21.6	11.41	2.34	10.21	5.52	35.82
p_e=300kPa	3.81	29.3	21.6	8.94	2.35	10.38	4.31	44.44

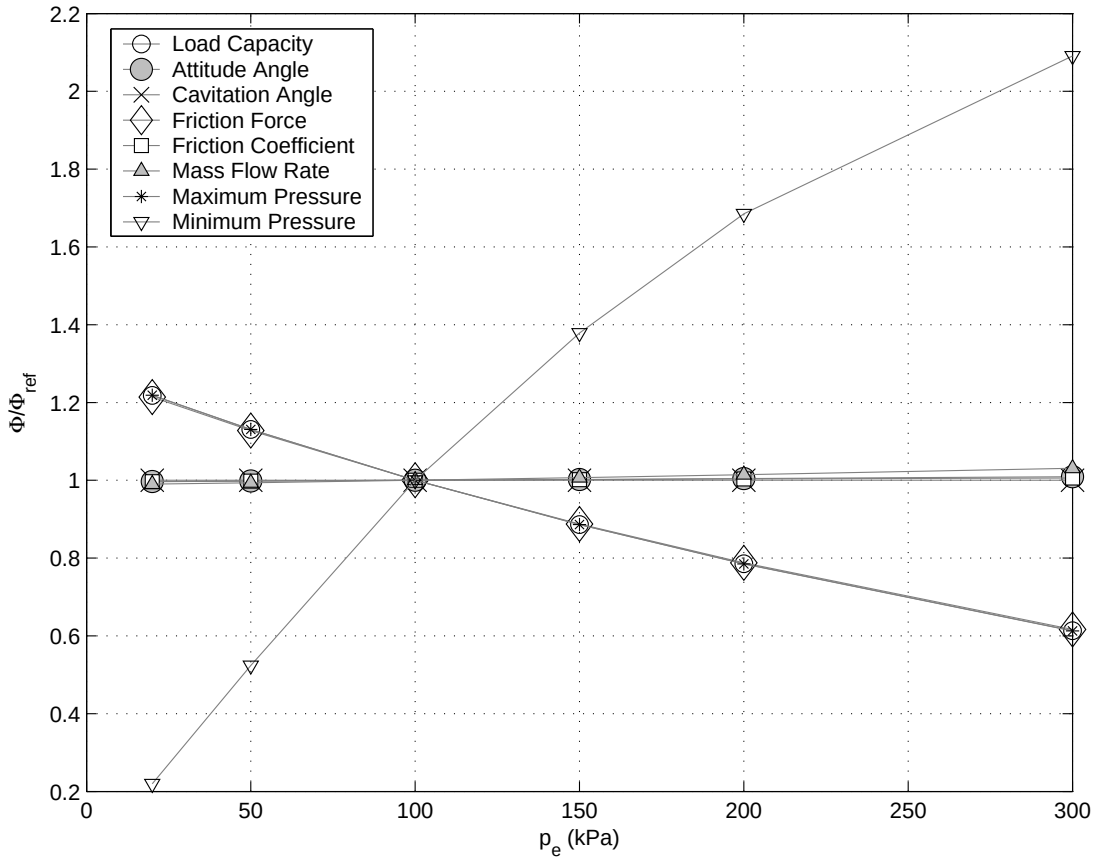

Figure 5.25. Variations of performance variables with pressure in relation to p_e=100kPa
($D = 20mm, c = 20\mu m, \varepsilon = 0.75,\ \omega = 60Hz, T = 40^oC, w_i = w_{sat},\ L = 100mm$)

5.2.6. Influence of refrigerant mass fraction at the entrance

In some situations, it may not be possible to have a saturated mixture at the entrance of the bearing. This can either result from a mixture kept at lower pressure conditions, not enough time to reach equilibrium with the ambient or other causes. When these cases are considered, a subsaturated mixture will enter the bearing. This mixture has different properties than a saturated one, and this reflects on bearing

lubrication. Tests were performed here considering 6 different mass fractions at the entrance, ranging from 70% of the saturation concentration to a saturated mixture. Remaining all the other variables constant, results obtained for the pressure profile are those presented in figures 5.26a-b.

It can be seen from figure 5.26a that higher levels of pressure occur for the lowest fractions – indicating its higher viscosity as less refrigerant is dissolved. In the cavitated region, figure 5.26b, lower levels of pressure are observed for the lowest mass fraction, which also has the lowest saturation pressure. However, the pressure drop in the cavitated region is smaller for lower mass fractions is comparison to the saturation condition (15kPa to $w_e=0.7w_{sat}$ and 20kPa to $w_e=w_{sat}$).

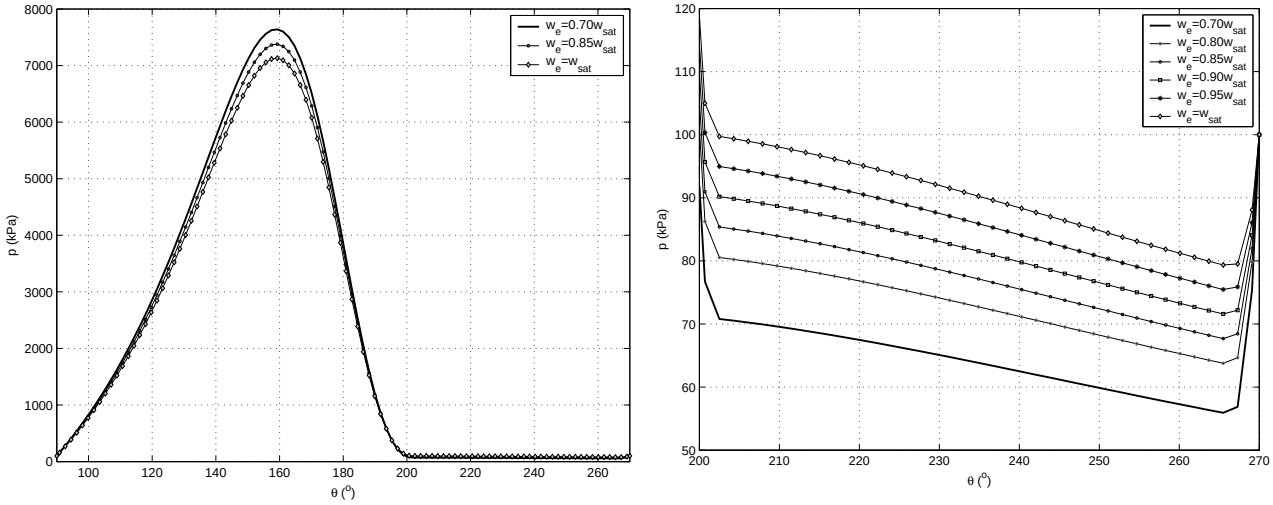

a) Full domain of the bearing **b)** Cavitation region in details

Figure 5.26. Pressure profile for different refrigerant mass fractions at the entrance.
($D=20mm, c=20\mu m, \varepsilon=0.75,\ \omega=60Hz,\ p_i=p_o=100kPa,\ T=40^oC, L=100mm$)

Dimensionless pressures are also plotted for the problem in figure 5.27, where close similarities are observed for all the mass fractions tested in the positive pressure region. For instance, from figure 5.27a, maximum pressure and cavitation position are the same – which points towards their geometry dependency only. In figure 5.27b, no significant differences are observed in the pressure recovery position, despite the higher pressure gradient for the lower mass fraction (which in turn requires a stronger recovery than that the higher mass fractions).

The behaviour of mass fraction at the entrance and throughout the flow is presented in figure 5.28. Despite the different mass fractions, the release of gas starts at the same position, $\theta\cong 202^o$, but a greater release is observed for higher mass fractions (0.9% for w_{sat} against 0.65% for $0.95w_{sat}$). Considering however the release

for a same pressure drop, lower fractions present slightly greater specific releases (eg, for a $\Delta p=10kPa$, $\Delta w_r=0.4\%$ between $202\text{-}235^o$ for $w_e=w_{sat}$, while $\Delta w_r=0.3\%$ occurs for $w_e=0.8w_{sat}$ between $202\text{-}245^o$). This occurs due to the increase of the rate of solubility with pressure. However, this is not a dominant effect in the flow.

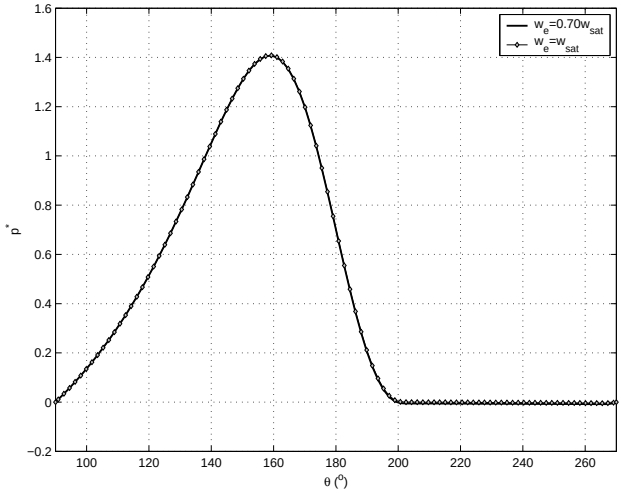

a) Full domain of the bearing

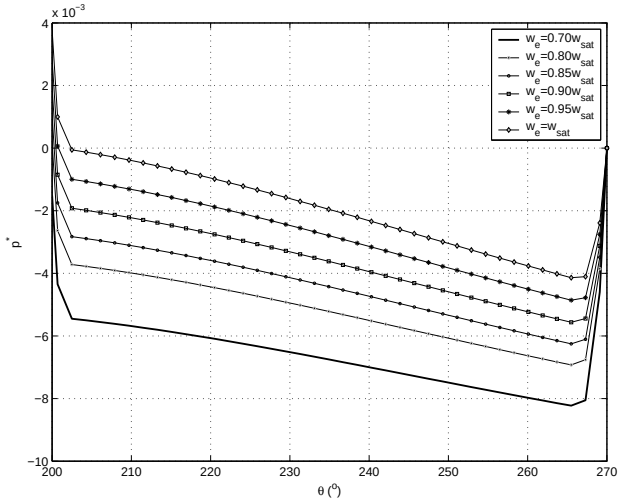

b) Cavitation region in details

Figure 5.27. Dimensionless pressure results for different refrigerant mass fractions at the entrance. ($D=20mm, c=20\mu m, \varepsilon=0.75,\ \omega=60Hz,\ p_i=p_o=100kPa,\ T=40^oC, L=100mm$)

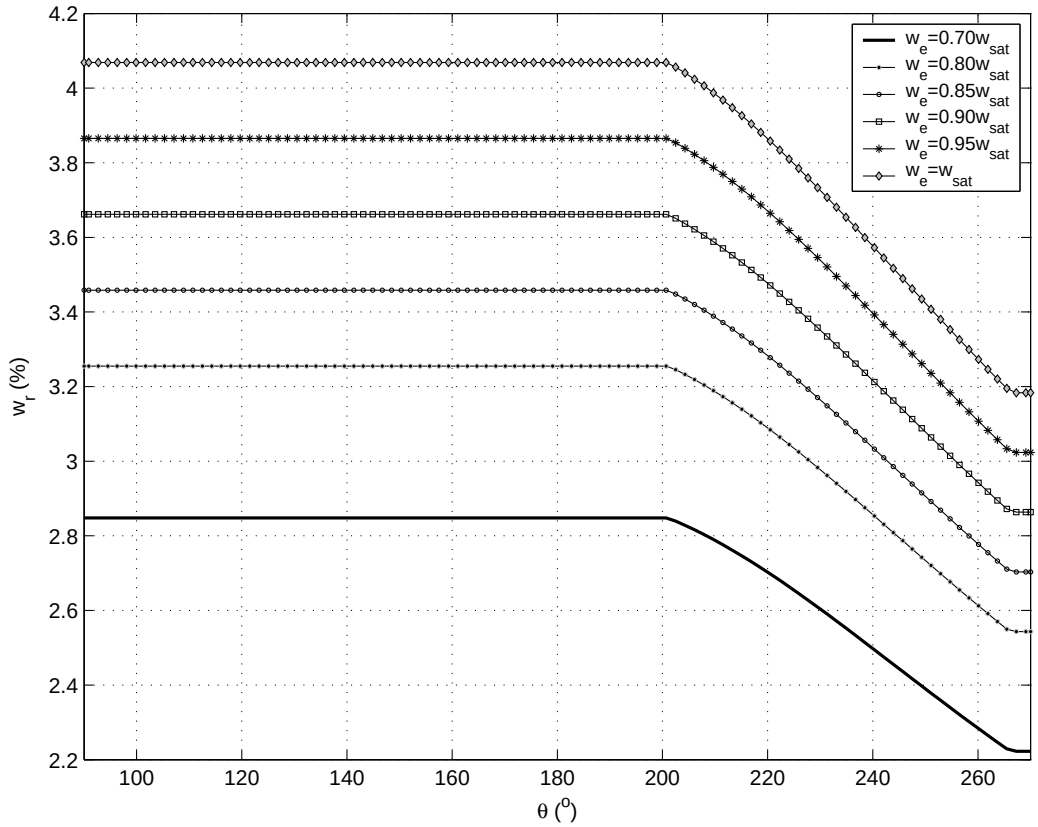

Figure 5.28. Behaviour of refrigerant mass fraction for distinct conditions at the entrance. ($D=20mm, c=20\mu m, \varepsilon=0.75,\ \omega=60Hz,\ p_i=p_o=100kPa,\ T=40^oC, L=100mm$)

As for the entrance pressure, the different mass fractions at the entrance do not change density and void fraction profiles, which are very similar for all cases. This is observed in figures 5.29a-b; the minimal difference in density seen in figure 5.29a is caused by the greater amount of refrigerant dissolved in the oil at saturation, which then increases liquid density due to the higher proportion of liquid refrigerant. The release of gas reduces the apparent density of the fluid in equivalent rates to those of the increase in void fraction. Again, as the eccentricity is the same and only liquid is present in the convergent region (incompressible flow), the cavitation position will not depend on the fluid and the same volume is required to fill the divergent region.

Figure 5.29c shows for the recovery pressure region more details of the void fraction. No significant changes are observed for the point where pressure recovery starts. From previous results, it could be expected a later recovery for the situation with lower mass fraction at the entrance due to its higher viscosity. On the other hand, the fluid presents a lower cavitation pressure under this condition, and a greater gradient of pressure will occur at the end so that outlet pressure is reached. Figure 5.26b confirms the existence of this gradient and its increase with reduction in mass fraction. Therefore, it can be concluded that for a lower viscosity a smaller pressure recovery is required, while for higher viscosities this increase compensates the higher recovery required, keeping in similar lengths for the pressure build-up at the end, as predicted by equation (5.1). Finally, as the gas suffers more compression due to the higher gradient, void fraction next to the exit will be smaller for lower mass fractions.

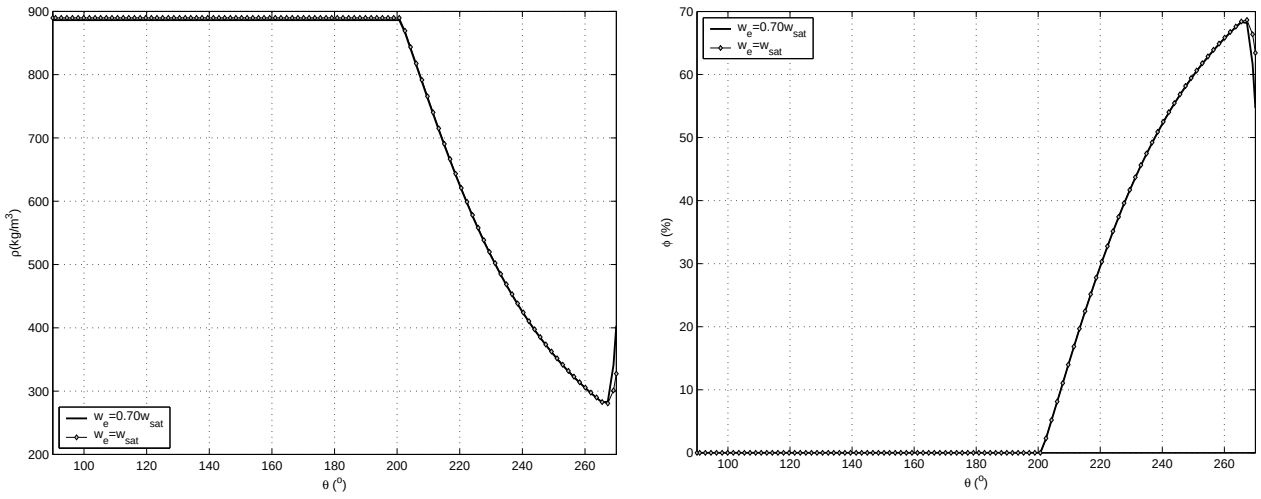

a) Apparent density **b)** Void fraction

Figure 5.29. Behaviour of density and void fraction for different mass fractions at the entrance. ($D = 20mm, c = 20\mu m, \varepsilon = 0.75,\ \omega = 60Hz,\ p_i = p_o = 100kPa,\ T = 40^oC, L = 100mm$)

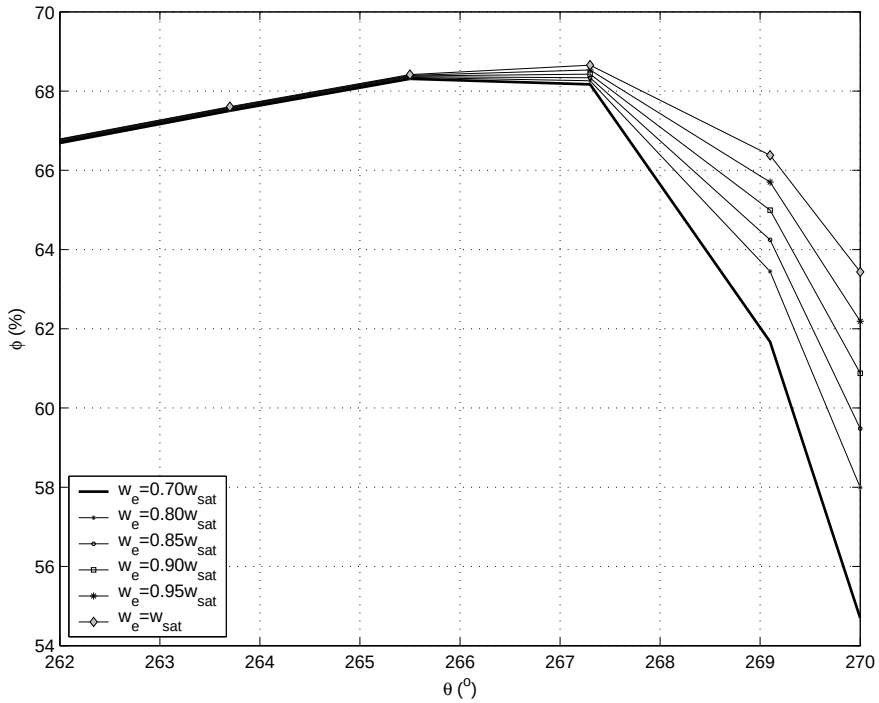

c) Void fraction at the cavitation region and during pressure recovery

Figure 5.29. Behaviour of density and void fraction for different mass fractions at the entrance. ($D = 20mm, c = 20\mu m, \varepsilon = 0.75,\ \omega = 60Hz,\ p_i = p_o = 100kPa,\ T = 40^oC, L = 100mm$)

The different viscosities for different fluid conditions are presented in figure 5.30a. The fluid with lower entrance mass fraction has the higher viscosity (9.475mPa.s), while the saturated one has the lowest (8.825mPa.s). With the release of gas, viscosity increases due to the changes in liquid viscosity – variation is more significant for the saturated fluid in comparison to the subsaturated ones, which is explained by the greater release of gas. Figure 5.30b characterises gas quality – 0.9% of the mass is released gas for saturation conditions at the entrance, while 0.65% is observed for a fluid entering the bearing with $w_e=0.7w_{sat}$. The greater mass of gas in the saturation condition can be explained by the gas density: cavitation starts at 100kPa, where the density of the gas is higher than that of the mixture at $w_e=0.7w_{sat}$, whose cavitation starts for 71kPa and in which pressures remain always below the values observed for the mixture saturated at the entrance. Under these lower pressures, the mass of gas required to achieve the same void fraction is smaller, thus ending the fluid with a lower quality. Furthermore, it will produce a smaller pressure drop due to release of gas.

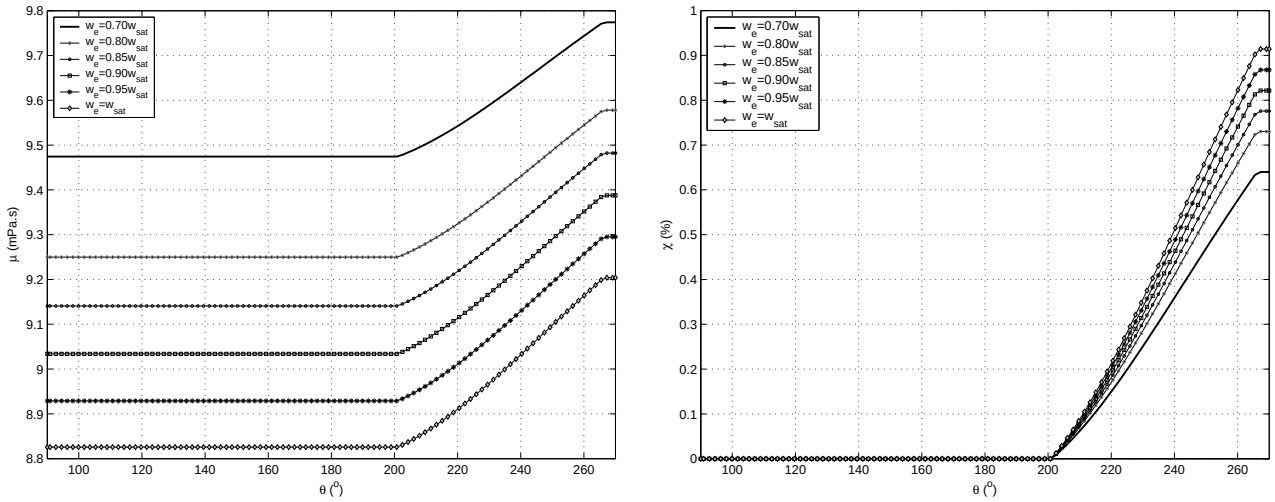

a) Apparent viscosity **b)** Gas quality

Figure 5.30. Viscosity and quality for the different mass fraction conditions at entrance. ($D = 20mm, c = 20\mu m, \varepsilon = 0.75,\ \omega = 60Hz,\ p_i = p_o = 100kPa,\ T = 40^oC, L = 100mm$)

The performance variables of the bearing are affected by changes in entrance mass fraction in a very similar way as observed for the entrance pressures, with increases proportional to the viscosity for load, maximum pressure and friction. Apart from minimum pressure, other variables present negligible variation. Figure 5.31 presents the results for the performance variables in comparison to the values for $w_e=0.85w_{sat}$, suppressing minimum pressure as its variations are more significant. This occurs because cavitation pressures are different, producing more significant effect than the pressure drop caused by release of gas. Results for minimum pressure and the other variables are presented in table 5.5, where p_{cav} was also included to a better interpretation of p_{min}.

Table 5.5. Results for performance variables for the different entrance mass fractions.

	W (kN)	ψ (°)	α (°)	F_f (N)	$f.10^3$	q_θ (g/s.m)	p_{max} (MPa)	p_{min} (kPa)	p_{cav} (kPa)
$w_e=0.7w_{sat}$	6.65	29.3	21.6	15.55	2.34	10.03	7.54	44.08	70.8
$w_e=0.8w_{sat}$	6.50	29.2	21.6	15.19	2.34	10.04	7.36	36.23	80.6
$w_e=0.85w_{sat}$	6.42	29.2	21.6	15.01	2.34	10.05	7.28	32.87	85.4
$w_e=0.9w_{sat}$	6.35	29.2	21.6	14.83	2.34	10.05	7.19	28.97	90.2
$w_e=0.95w_{sat}$	6.28	29.1	21.6	14.66	2.33	10.06	7.11	25.10	95.0
$w_e=w_{sat}$	6.21	29.0	21.6	14.49	2.33	10.06	7.03	21.26	100.0

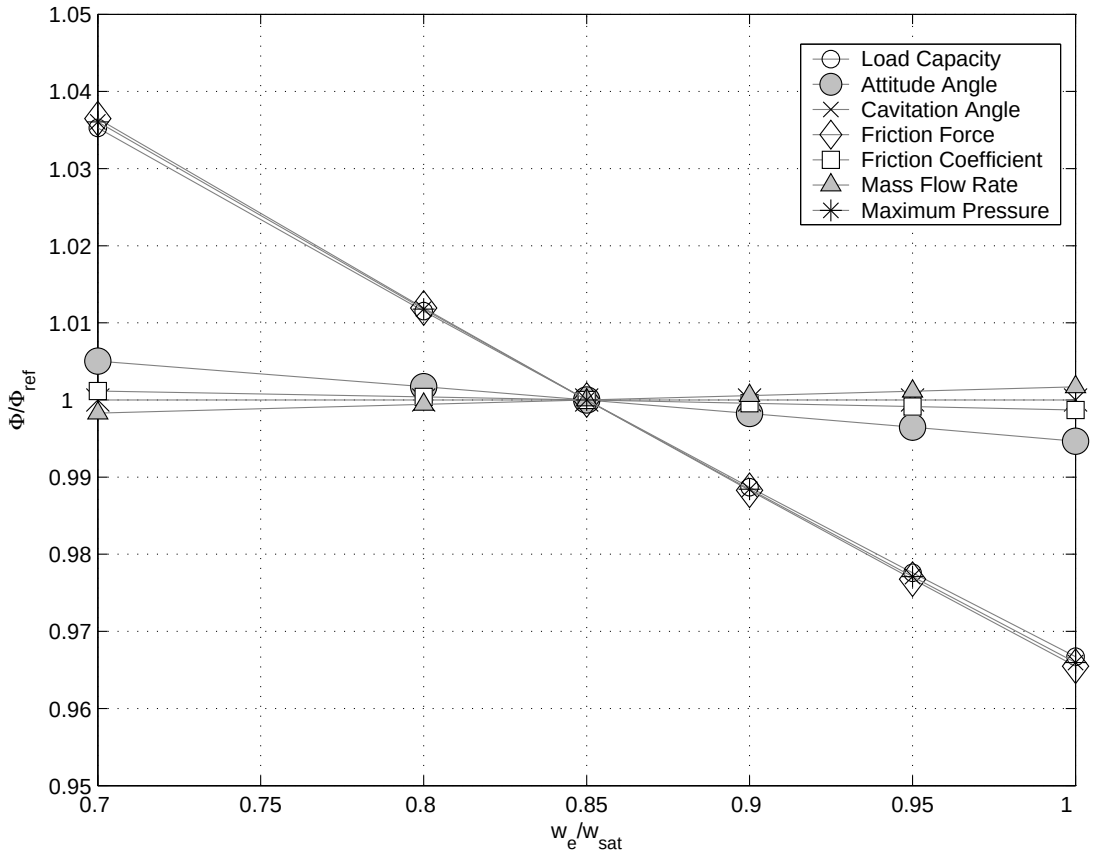

Figure 5.31. Variations of performance variables with entrance mass fraction relative to $w_e=0.85w_{sat}$. ($D=20mm, c=20\mu m, \varepsilon=0.75,\ \omega=60Hz, p_e=p_o=100kPa,\ T_e=40^oC, L=100mm$)

5.2.7. Influence of fluid temperature

Fluid temperature is important to determine the viscosity of the oil. In the case of the oil/refrigerant mixture, it also produces changes in solubility, creating two opposite effects influencing lubricant properties, and particularly viscosity: reduction of the oil viscosity with the increase in temperature and reduction of refrigerant solubility with the increase in temperature, which in turn tends to increase the viscosity of the mixture. To evaluate how these effects influence bearing lubrication, 6 simulations were performed varying temperature between 10^oC to 60^oC. The mixture was considered saturated at the entrance, and the other variables were kept constant.

Figure 5.32a-b shows the pressure profile generated on the bearing. It is observed higher levels of pressure occur in the convergent region for lower temperatures. In the cavitated region, lower levels of pressure occur in higher temperatures, which also present longer regions of pressure recovery.

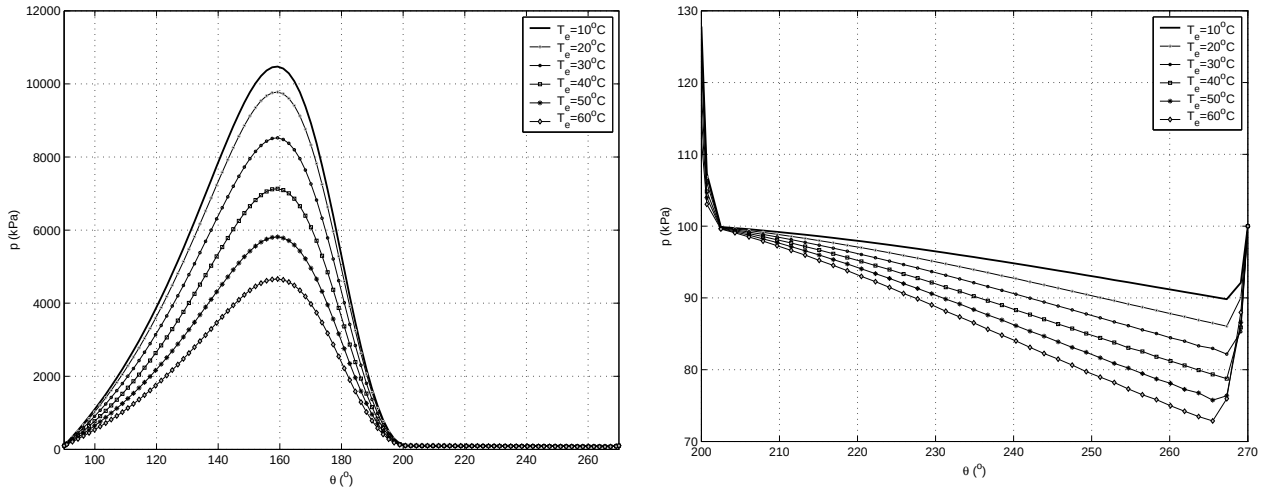

a) Full domain of the bearing **b)** Cavitation region in details

Figure 5.32. Pressure profile for different temperatures.
($D = 20mm, c = 20\mu m,\ \varepsilon = 0.75, \omega = 60Hz,\ p_i = p_o = 100kPa, w_i = w_{sat},\ L = 100mm$)

Figure 5.33a for dimensionless pressure reinforces the idea that position for maximum pressure and cavitation are geometry dependent only, as all the results produce a very similar curve, with distinctions only in the cavitated region. Amplifying this region in figure 5.33b, the behaviour observed in figure 5.32b is repeated, showing that pressures in cavitated region depend on more variables than geometry and viscosity. As negative pressures have lower magnitude, solutions for lower temperatures are also closer to Reynolds solution.

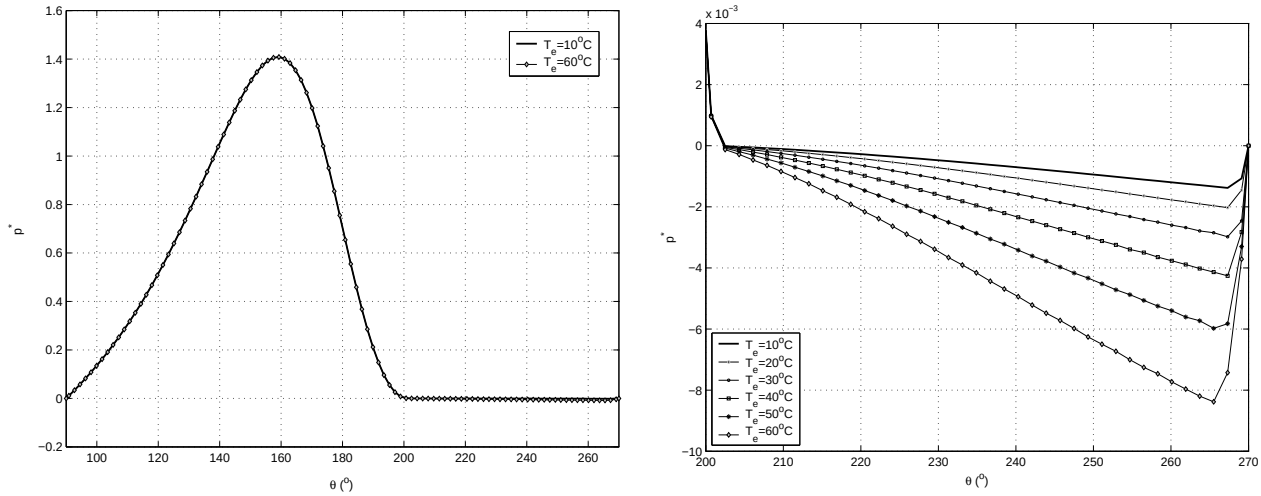

a) Full domain of the bearing **b)** Cavitation region in details

Figure 5.33. Dimensionless pressure results for different temperatures.
($D = 20mm, c = 20\mu m,\ \varepsilon = 0.75, \omega = 60Hz,\ p_i = p_o = 100kPa, w_i = w_{sat},\ L = 100mm$)

To achieve the results for pressure, the refrigerant mass fraction in the mixture behaves according to figure 5.34. The solubility is higher for lower temperatures, reaching a refrigerant concentration of *9.3%* for 10^oC while only *2.8%* is dissolved in

the oil at 60^oC. In the two-phase region, the mixture of higher mass fraction (lower temperature) presents greater releases, despite the lower pressure drop. This means that, at lower temperatures, solubility is more sensitive to pressure variations than it is on higher temperatures.

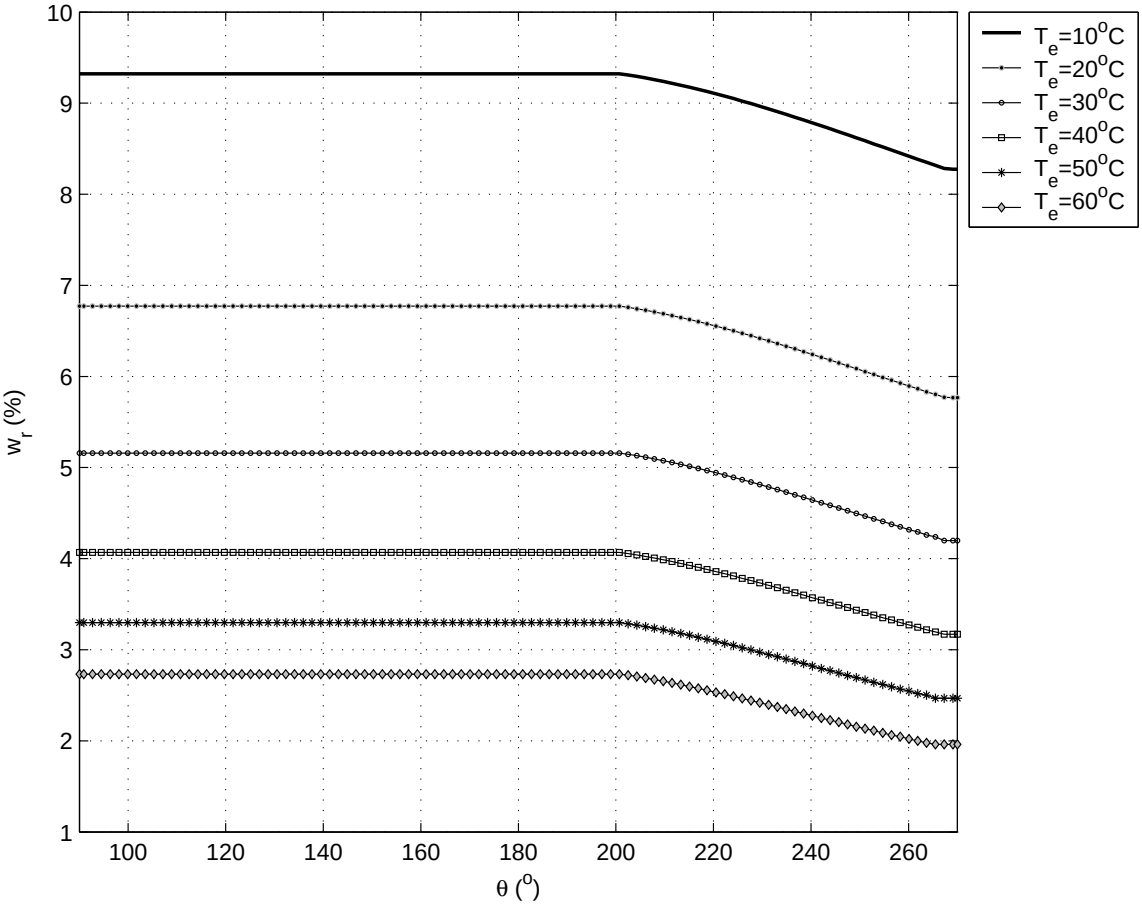

Figure 5.34. Behaviour of refrigerant mass fraction for different temperatures.
$(D = 20mm, c = 20\mu m,\ \varepsilon = 0.75, \omega = 60Hz,\ p_i = p_o = 100kPa, w_i = w_{sat},\ L = 100mm)$

Despite the different pressure changes and refrigerant mass fraction, the behaviour of density is similar for the different temperatures, as shown in figure 5.35a. The higher density at lower temperatures is observed for two reasons: the higher density of the oil and the higher solubility of the refrigerant, heavier than the oil. The rate of decrease of apparent density due to the increase in the volume of free gas is similar for the different temperatures. As observed in the previous cases, this is due to the geometrically determined void fraction, practically the same for all situations, as seen in figure 5.35b. Exception occurs only for the pressure recovery region, presented in figure 5.35c. For lower temperatures, a later recovery is observed. This points to the higher viscosity of the mixture in such conditions, which is also expected from the higher pressures observed in the convergent region. Furthermore, as the pressure drop is

smaller at lower temperatures, a lower pressure gradient is required to return to ambient pressure, resulting in a higher void fraction at the end. On the other hand, at higher temperatures, recovery starts earlier and final void fraction is smaller. The differences between the temperatures, however, are small.

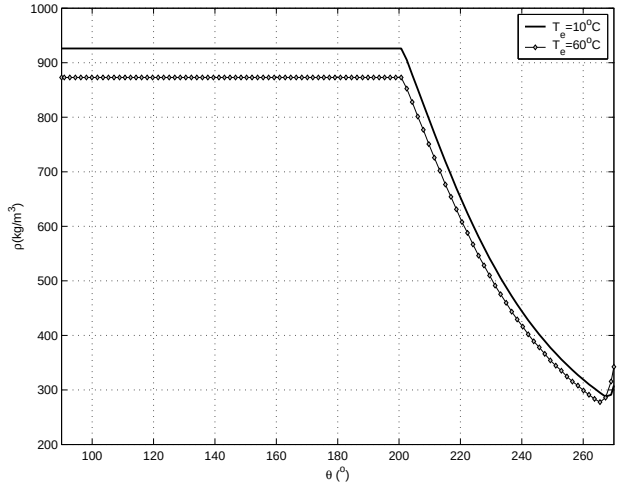

a) Apparent density

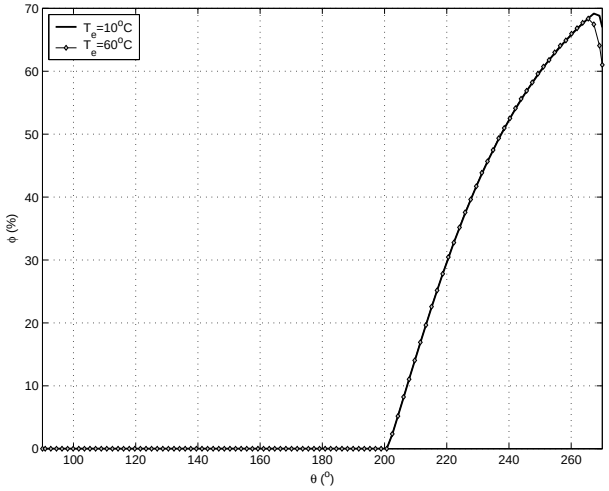

b) Void fraction

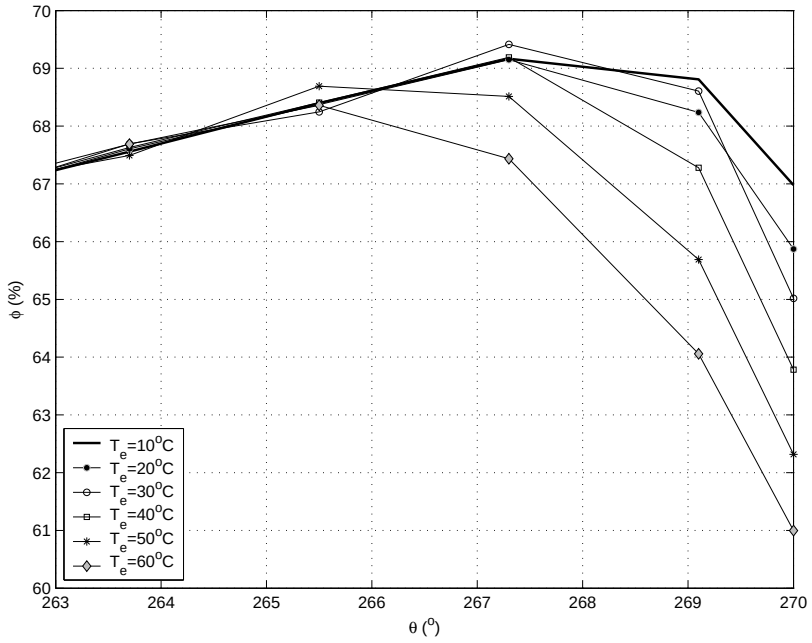

c) Void fraction at the end of cavitation region and during pressure recovery

Figure 5.35. Density and void fraction of the mixture for different temperatures.
($D = 20mm, c = 20\mu m,\ \varepsilon = 0.75, \omega = 60Hz,\ p_i = p_o = 100kPa, w_i = w_{sat},\ L = 100mm$)

Confirming the expectation created from the previous results, apparent viscosity is presented in figure 5.36a, where higher viscosities occur for lower temperatures, with significant variations with temperature: despite the higher solubility observed for lower temperatures, the liquid viscosity at 10°C is more than twice that for 60°C. This shows that increase of oil viscosity with reduction of temperature is dominant in comparison to

the tendency of decreasing viscosity as solubility increases at lower temperatures. In regard to the more significant variation in two-phase viscosity at lower temperatures, mention is made to gas quality, presented in figure 5.36b. The quality decreases with the increase of temperature. Having in mind that a same void fraction has to be achieved, more gas will be released when gas density is smaller – which occurs for lower temperatures, thus reflecting higher qualities.

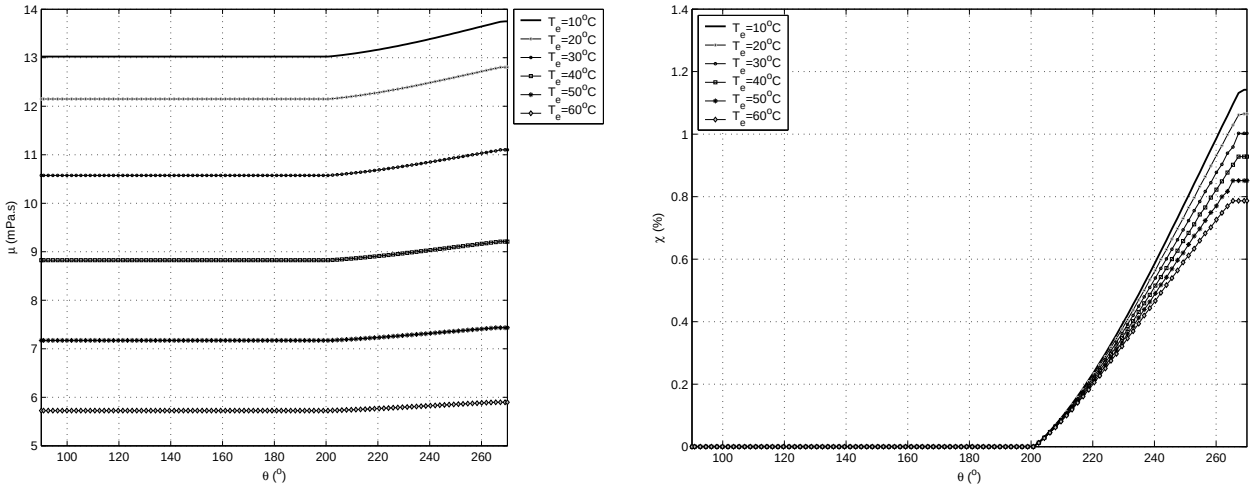

a) Apparent viscosity **b)** Gas quality

Figure 5.36. Viscosity and quality for different fluid temperatures.
$(D = 20mm, c = 20\mu m,\ \varepsilon = 0.75, \omega = 60Hz,\ p_i = p_o = 100kPa, w_i = w_{sat},\ L = 100mm)$

The influence of these fluid changes in the performance of the bearing is described by table 5.6 and figure 5.37; the latter presents variables in relative values to those at 30°C. Load capacity, friction force and maximum pressure, which vary linearly with viscosity, decreases with the increase in temperature. Here, a non-linear increase in viscosity between 10 and 15°C is observed. Attitude and cavitation angles and the friction coefficient, independent of density and viscosity, remain practically constant. The mass flow rate, however, decreases with temperature due to the decrease in liquid density. Finally, the minimum pressure increases with temperature, showing a different behaviour than observed for the two previous mixture variables. Despite the greater release of gas for lower temperatures, a smaller pressure drop is required. This is due to the sensitivity of solubility with temperature: at the same saturation pressure, a much smaller pressure drop is required to release the same amount (mass) of refrigerant in lower temperatures – then reflecting in minimum pressure.

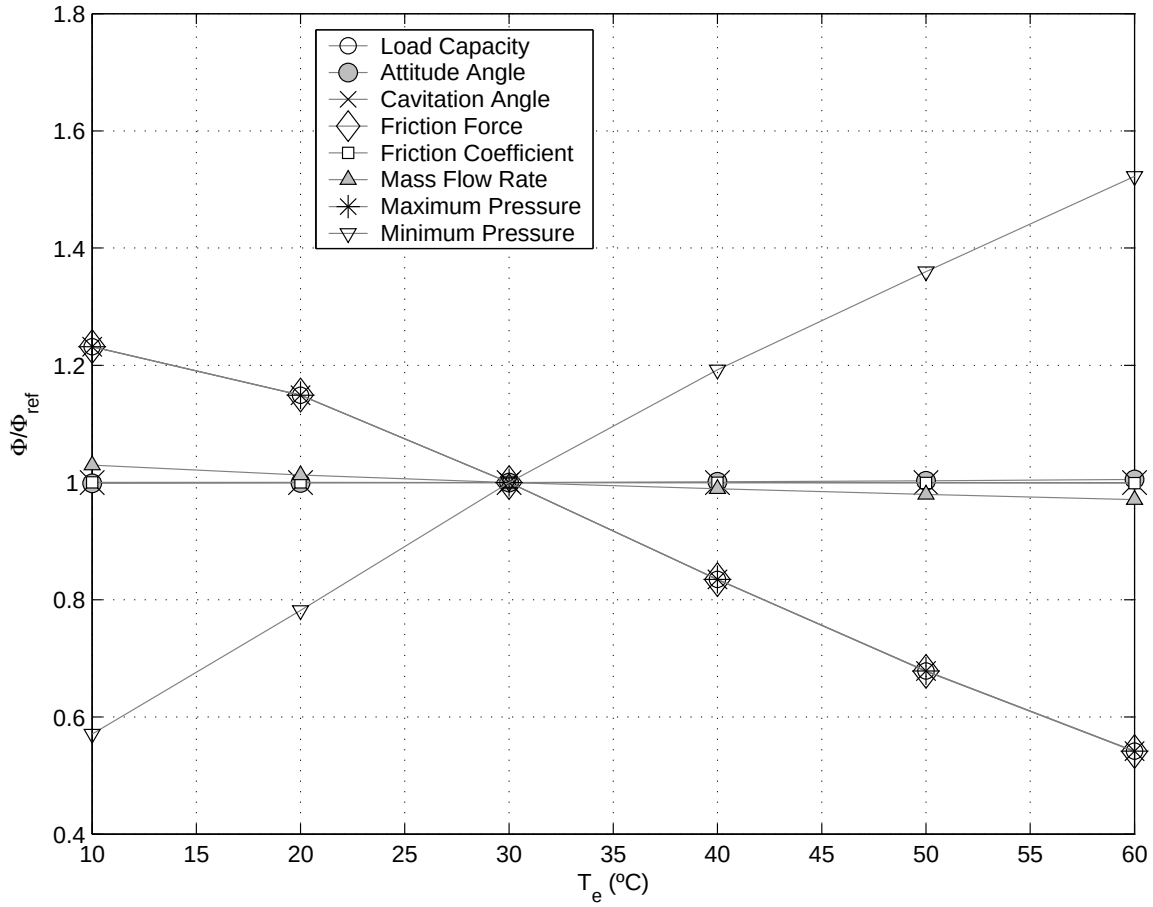

Figure 5.37. Variations of performance variables with temperature relative to T_e=30^{o}C. ($D = 20mm, c = 20\mu m,\ \varepsilon = 0.75, \omega = 60Hz,\ p_i = p_o = 100kPa, w_i = w_{sat},\ L = 100mm$)

Table 5.6. Results for performance variables for different fluid temperatures.

	W (kN)	***ψ (°)***	***α (°)***	***F_f (N)***	***f.10^3***	***q_θ (g/s.m)***	***p_{max} (MPa)***	***p_{min} (kPa)***
T_e=10^{o}C	*9.16*	*29.0*	*21.6*	*21.38*	*2.34*	*10.48*	*10.37*	*10.18*
T_e=20^{o}C	*8.54*	*29.0*	*21.6*	*19.95*	*2.34*	*10.30*	*9.68*	*13.94*
T_e=30^{o}C	*7.44*	*29.0*	*21.6*	*17.36*	*2.33*	*10.17*	*8.42*	*17.83*
T_e=40^{o}C	*6.21*	*29.0*	*21.6*	*14.49*	*2.33*	*10.06*	*7.03*	*21.26*
T_e=50^{o}C	*5.05*	*29.1*	*21.6*	*11.77*	*2.33*	*9.97*	*5.71*	*24.24*
T_e=60^{o}C	*4.03*	*29.2*	*21.6*	*9.40*	*2.33*	*9.88*	*4.56*	*27.14*

A final point to be mentioned is that the release of gas from the liquid, as in a usual change of phase, requires energy – and probably the most easily available source of energy to enable this release is the liquid mixture itself, which points to a non-isothermal condition. Therefore, the study of the flow under adiabatic conditions is recommended, in which case the use of the energy equation will be required.

5.2.8. Closure

From the parametric tests previously performed, it could be clearly observed a greater approximation between the results of the model and those from Reynolds solution when the load on the bearing increases, either resulting from smaller clearances, faster rotation of the shaft or higher viscosities. Nevertheless, in a general way, the results for all the parameters tested presented behaviour similar to the one expected from the classical lubrication analysis.

The results showed that clearance, velocity, eccentricity and liquid viscosity are the most important properties in the convergent region. On the other hand, apart from the eccentricity, these properties have no influence in the divergent region, where the behaviour is mostly determined by the density of the gas refrigerant. As the fluid is considered incompressible in the convergent region, the cavitation position is exclusively determined by the eccentricity, leading to a same profile of void fraction in the cavitated region, regardless the properties of the mixture.

Table 5.7 summarises the influence of the parameters tested in the main characteristics of the bearing and in the fluid behaviour along the flow. In addition to the parameters presented throughout the text, the length of pressure recovery region is also included ($d\theta_{rec}$), as well as the variation of mixture properties along the flow (dw_r, $d\rho$, $d\mu$).

Table 5.7. Influence of the parameters tested on the main variables of bearing and mixture.

	Bearing parameters									*Fluid properties*							
	p_{max}	p_{min}	$d\theta_{rec}$	W	ψ	α	F_f	f	q_θ	w_r	dw_r	ρ	$d\rho$	ϕ	μ	$d\mu$	χ
$\uparrow c$	↓	−	↑	↓	−	−	↓	↑	↑	−	−	−	−	−	−	−	−
$\uparrow \omega$	↑	−	↓	↑	−	−	↑	−	↑	−	−	−	−	−	−	−	−
$\uparrow \varepsilon$	↑	↑	−	↑	↓	↓	↑	↓	↓	−	↑	−	↑	↑	−	↑	↑
$\uparrow p_e$	↓	↑	↑	↓	−	−	↓	−	−	↑	↑	↑	−	−	↓	↑	↑
$\uparrow w_e$	↓	↑*	−	↓	−	−	↓	−	−	↑	↑	↑	−	−	↓	↑	↑
$\uparrow T_e$	↓	↑	↑	↓	−	−	↓	−	−	↓	↓	↓	−	−	↓	↓	↓

↑ (increase), ↓ (decrease), − (practically constant).

* p_{min} increases, but it is not the pressure drop in this case. In fact, $\downarrow[p_{cav} - min(p)]$.

5.3. COMPARISON BETWEEN DIFFERENT MIXTURES

One of the motivators for this study is the necessity to compare the performance of the refrigerants HFC and their synthetic lubricants to the widely used in the past CFC and mineral oils mixtures, which are being banned due to its pollutant characteristics. Although effort has been done to obtain similar characteristics to the mixtures, some differences are observed, particularly regarding solubility – which was seen to have influence in the performance of the system. Among others, one of the major concerns is the blockage of flow in the capillary tube that happens with polyolester synthetic oils; questions such as the leakage of refrigerant through the piston skirt are also important, influencing in compressor efficiency.

The difference between the lubrication using two of these mixtures is explored in the sequence, using the proposed model for partial journal bearings. To compare with the results previously obtained for R12 and SUNISO 1GS mineral oil, the mixture of R134a and EMKARATE RL10H polyoester oil was chosen. Correlations for properties of the mixture were obtained similarly to those for R12/SUNISO 1GS, and they are detailed in Appendix B. Based on these correlations, observing the general behaviour of the mixtures, the following characteristics can be identified from the comparison between their properties:

- For fixed temperature and pressure, solubility of R12 in the mineral oil is greater than that of R134a in the synthetic oil. Variations of solubility with pressure are also more significant for the mixture of R12 and SUNISO 1GS;
- SUNISO 1GS has a lower density than EMKARATE RL10H. On the other hand, R12 is heavier than R134a in both liquid and gas phases. However, the liquid mixture of R134a and EMKARATE RL10H is still heavier;
- Viscosity of the liquid mixture R12/1GS is more sensitive to variations in refrigerant mass fraction, while R134a/RL10H is more sensitive to temperature (which reflects significantly the behaviour of the oil);

Aware of the difference in behaviour between mixtures, a particular case was chosen to compare operational differences of the bearing using each mixture. These results are explored in the sequence.

5.3.1. Comparison between the two different mixtures for the same operation condition

To detail the difference in performance between the two mixtures, a particular case simulated to the mixture R12 and mineral oil is compared to two equivalent situations for the mixture R134a and synthetic oil: first, keeping the same eccentricity as in the situation using R12/1GS, while the second considers the same load applied in the bearing. These three simulations are indicated in figure 5.38, where the load curves for the mixtures are presented. The arrow indicates how the eccentricity for the mixture of R134a/RL10H was determined in the second simulation. In the case studied, the load supported by a bearing lubricated with a mixture of R12 and SUNISO 1GS operating at $\varepsilon=0.8$ requires an eccentricity of $\varepsilon=0.827$ when the lubricant is a mixture of R134a and EMKARATE RL10H.

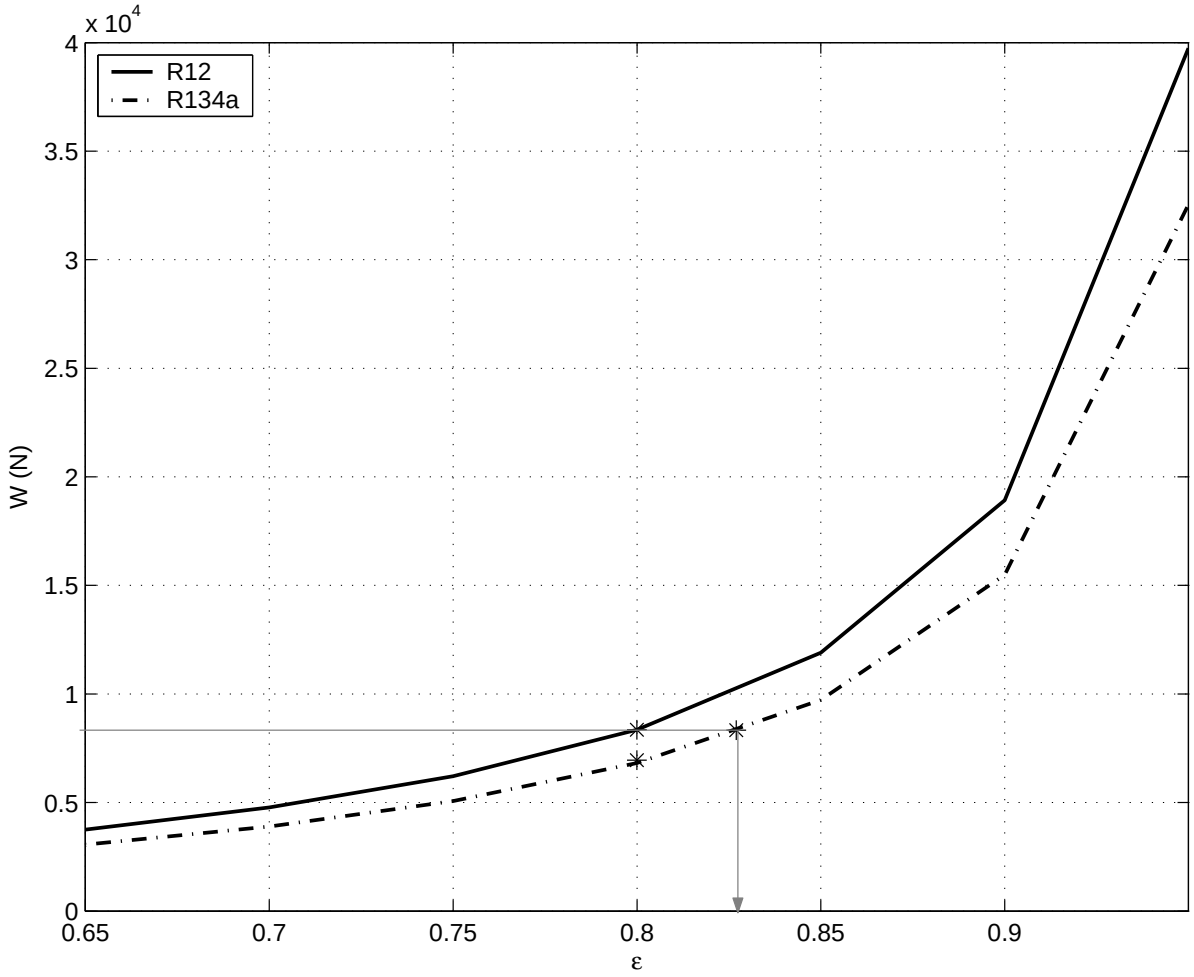

Figure 5.38. Load curve for the different lubricant mixtures.
($D = 20mm, c = 20\mu m,\ \omega = 60Hz,\ p_i = p_o = 100kPa, T = 40^o C, w_i = w_{sat},\ L = 100mm$)

The differences in properties between the three simulation conditions lead to the different pressure profiles seen in figure 5.39a. Considering the same eccentricity, pressures for the system operating with R134a are lower than in the one operating in a R12 environment. When the eccentricity increases in the bearing operating with R134a/RL10H, maximum pressure exceeds the value for R12/1GS, and is also moving closer to the centre of the bearing. The pressure in the initial region, however, remains below the values for the R12/1GS mixture. In the cavitated region, figure 5.39b, very similar pressure drops are verified at the same eccentricity for the different mixtures. On the other hand, pressure falls more significantly for the case of higher eccentricity, as a result of the additional release of gas required, since cavitation started earlier in this case.

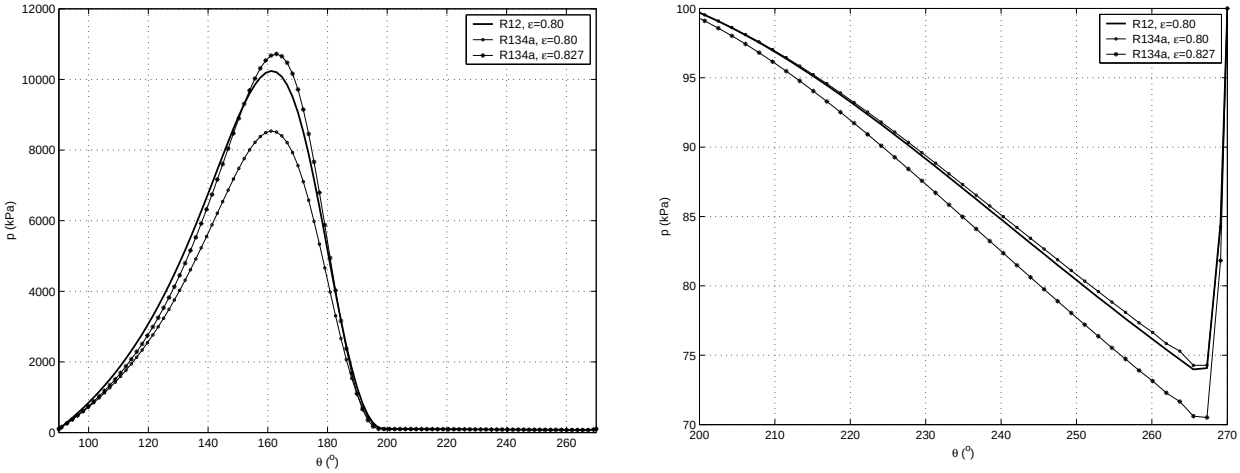

a) Pressure **b)** Cavitated region

Figure 5.39. Pressure profile for the three distinct simulations.
($D = 20mm, c = 20\mu m,\ \omega = 60Hz,\ p_i = p_o = 100kPa, T = 40^o C, w_i = w_{sat},\ L = 100mm$)

Under the pressure conditions developed, refrigerant mass fraction behaves according to figure 5.40. Mass fraction is lower for R134a/RL10H due to the lower solubility at same conditions of pressure and temperature. In the cavitation region, mass fraction decreases with the release of gas, and a lower rate is observed for the R134a/RL10H mixture in comparison to R12/1GS. It is reduced more significantly for R12/1GS than for R134a/RL10H in both cases. This result, combined with the negative pressures observed in figure 5.39b, confirms that the mixture of R12/1GS is more sensitive to pressure variations.

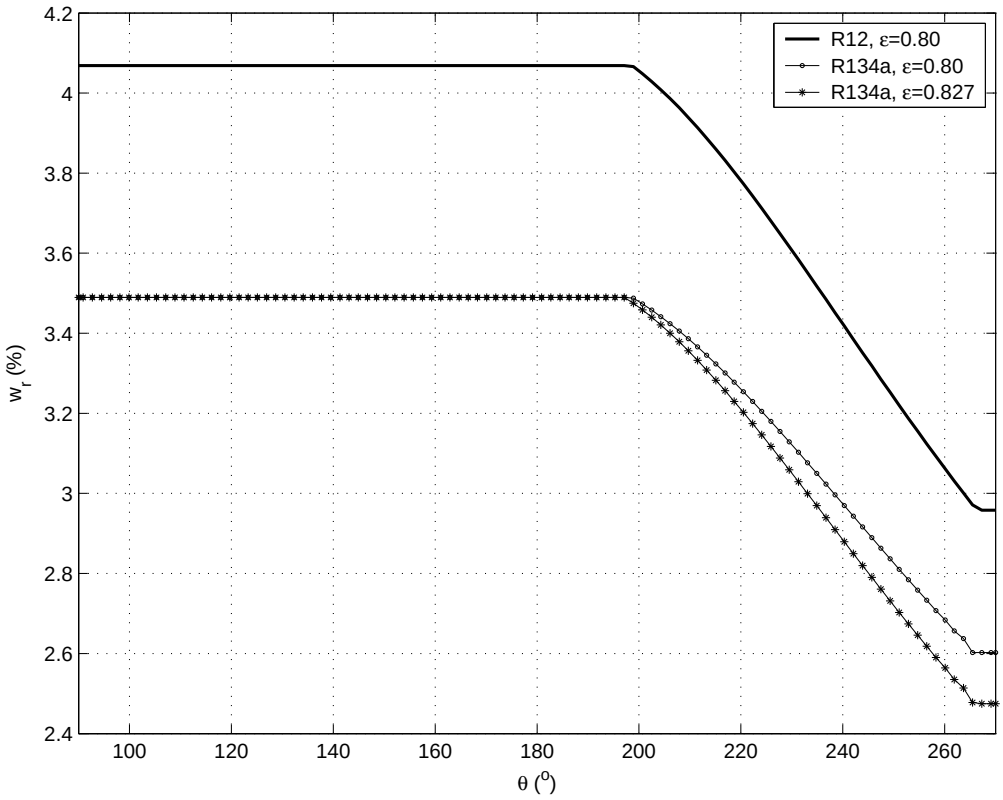

Figure 5.40. Refrigerant mass fraction along the bearing for the three distinct simulations. ($D = 20mm, c = 20\mu m,\ \omega = 60Hz,\ p_i = p_o = 100kPa, T = 40^o C, w_i = w_{sat},\ L = 100mm$)

The release of gas modifies the apparent density according to figure 5.41a. Despite the higher density of the liquid mixture R134a/RL10H, the rate of decrease in density is similar for the cases with same eccentricity. For the simulation using a higher eccentricity, a stronger decrease is observed and a lower density is reached before pressure recovery. The different behaviour observed in density can be better analysed for the void fraction, figure 5.41b. Identical values occur for the same eccentricity, as void fraction is determined by geometry. When the higher eccentricity is considered, release of gas starts earlier and higher values of void fraction are observed throughout the two-phase region. From the final region, where void fraction decreases as the gas is compressed, one can conclude that no significant differences exist in the length of the pressure recovery region. It starts earlier for the R134a/RL10H mixture, which is expected from a mixture of lower viscosity, but the differences between the three cases are negligible.

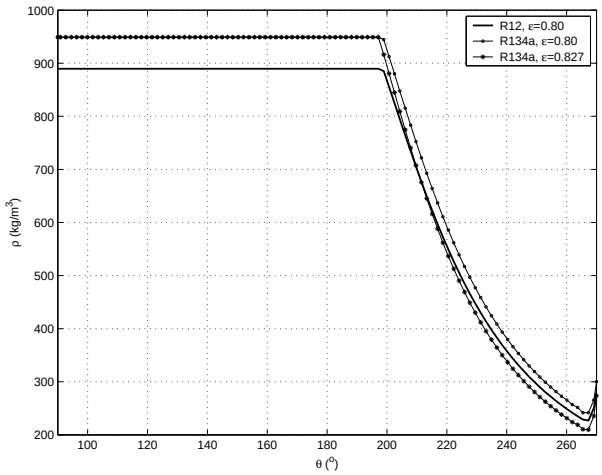

a) Density

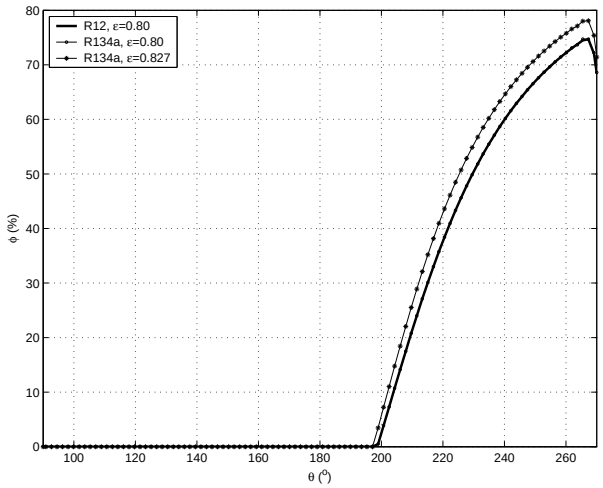

b) Void fraction

Figure 5.41. Density and correspondent void fraction along the bearing for the three simulations.
($D = 20mm, c = 20\mu m,\ \omega = 60Hz,\ p_i = p_o = 100kPa, T = 40^o C, w_i = w_{sat},\ L = 100mm$)

The lower viscosity of the mixture of refrigerant R134a and polyolester oil is verified in figure 5.42a. This lower viscosity explains the lower pressures obtained with R134a/RL10H in the bearing. Another aspect to observe is that variations in viscosity for the R12/1GS mixture are much more significant than those for R134a/RL10H. This is in part explained by the greater release of gas observed for R12/1GS, as confirmed by the gas quality presented in figure 5.42b. However, changes in viscosity are more significant than those is mass fraction, which points to the fact that viscosity of the mixture R12/SUNISO 1GS is more sensitive to variations in mixture composition than the mixture R134a/EMKARATE RL10H is.

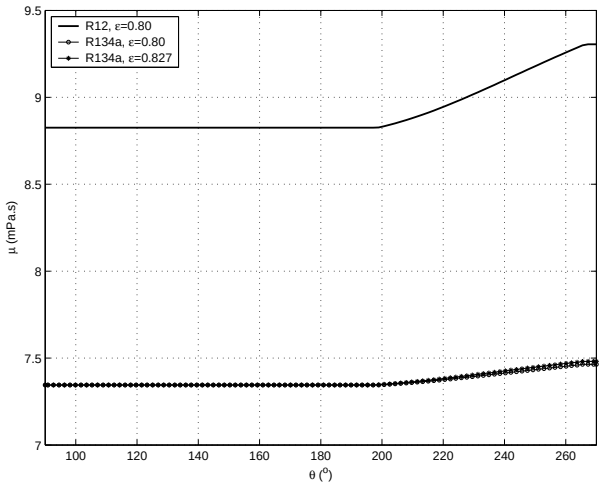

a) Apparent viscosity

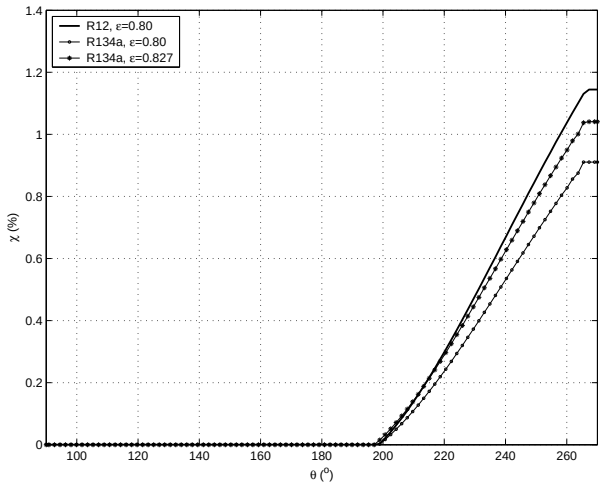

b) Quality

Figure 5.42. Viscosity and gas quality for the three distinct simulations.
($D = 20mm, c = 20\mu m,\ \omega = 60Hz,\ p_i = p_o = 100kPa, T = 40^o C, w_i = w_{sat},\ L = 100mm$)

As a consequence of the lower viscosity of the mixture R134a/RL10H, friction force in both cases is smaller than that calculated for the operation using R12/1GS. The friction curve for both mixtures is presented in figure 5.43. For the same eccentricity, it is observed that friction force reduces in the same proportion as viscosity does. As the ratio between friction force for R134a and R12 is the same as the ratio of liquid viscosities at the entrance (*0.84*), the linear dependence of friction force with viscosity is confirmed. Regarding the case of higher eccentricity, the lower values for viscosity guarantees smaller viscous effects, giving then some advantage for the R134a under this particular operation condition. However, it should be understood that this is not exclusively an advantage of the mixture. In fact, the viscosity of the pure oil is lower in the second case (at 40°C, $\mu_{1GS}=11.33mPa.s$ and $\mu_{RL10H}=8.10mPa.s$). Considering now the mixing of refrigerant, one can observe that R12 has a more significant effect, reducing the viscosity of the lubricant more than R134a does.

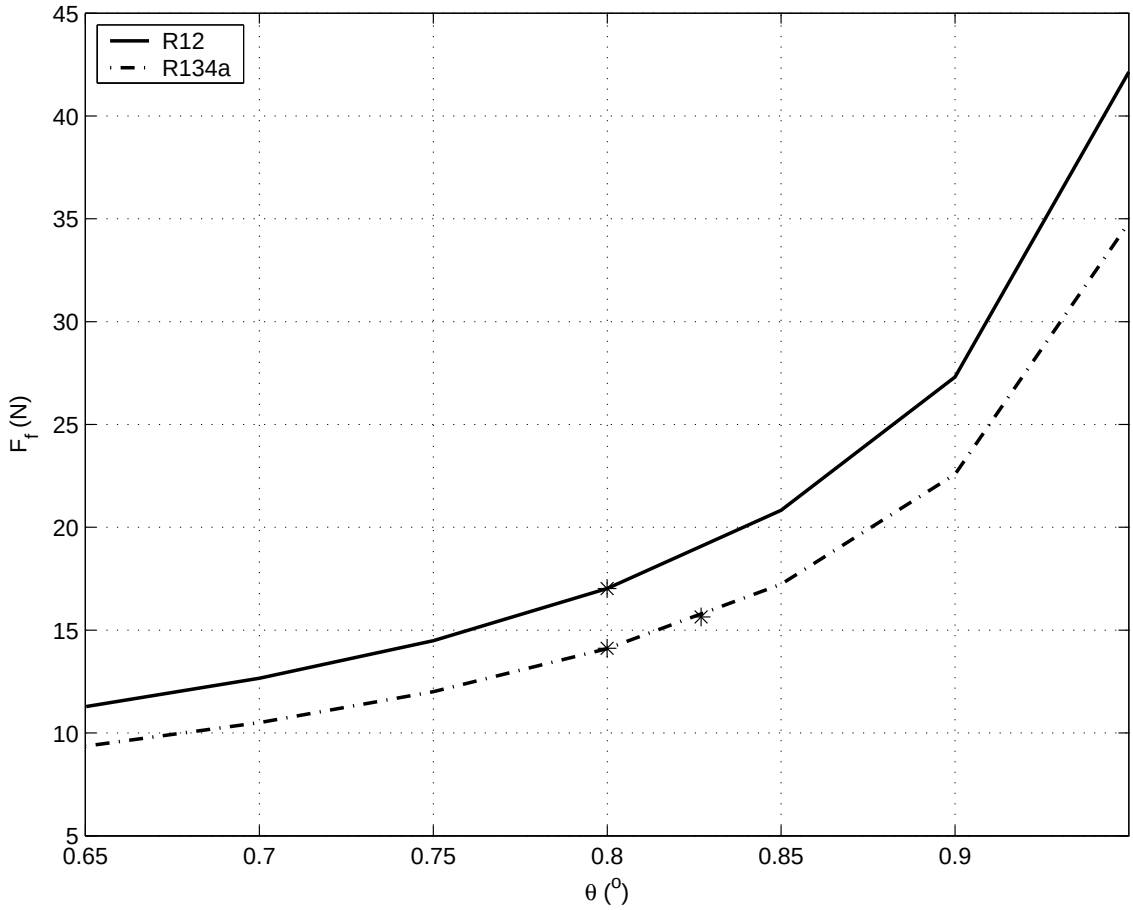

Figure 5.43. Friction curve for the different lubricant mixtures.

$(D = 20mm, c = 20\mu m,\ \omega = 60Hz,\ p_i = p_o = 100kPa, T = 40^o C, w_i = w_{sat},\ L = 100mm)$

Additionally, it should be stressed that the example given above not necessarily represents the general behaviour along all the range of parameters, which can lead to

different results. For instance, if the entrance pressure is increased, solubility of both mixtures will increase and come closer to each other and higher friction can be obtained for the R134a at the same eccentricity. This will certainly occur in lower temperatures, regardless of solubility, as the viscosity of the synthetic oil is more influenced by temperature than the mineral oil used with R12, therefore considerably increasing friction for the R134a/RL10H mixture.

5.4. SUMMARY

An extensive parametric analysis was performed to the case of a 180º infinite partial journal bearing subject to a steady load. The lubricant considered was initially a mixture of CFC R12 and a mineral oil SUNISO 1GS. As main observations from this stage,

- The model, while considering a liquid mixture at the entrance, presented results in very good agreement with the classical theory predictions developed at the beginning of the chapter;
- In the pressure generation region, geometrical and operation parameters are more important, such as clearance, velocity and eccentricity. Additionally, viscosity is the dominant fluid property;
- The cavitated region is dominated by the density of the gas, and the mixture can by numerous ways result in similar conditioning. Lower pressure drops will occur under lower densities of the gas, the dominant effect, but some compensation can arise from the higher sensitivity of the mixture solubility to pressure; however, in the comparison between two distinct mixtures, similar pressure drop was observed due to the equivalence between the effects: while R134a is lighter than R12 gas, the mixture with the second can release more refrigerant for the same pressure drop.

Chapter 6

INFINITE WIDTH JOURNAL BEARINGS

Significant understanding was obtained in regard to the two-phase flow model by studying the partial journal bearing. This gives confidence to advance in complexity from that geometry, from which the immediate next step is that of an enclosed 360^o bearing. For the new geometry, the fluid will recirculate in the domain, which is a convenient situation to evaluate the thermodynamic assumptions regarding the absorption of refrigerant under positive pressure gradients, which will be the main item of discussion in this chapter. Also, as a result of the recirculation, the solution for the problem is in principle transient, and the consideration regarding this process is also included. Finally, discussion about several model assumptions is undertaken, including a brief note in comparison to available experimental data from the literature.

6.1 INTRODUCTION

The recirculation of fluid that is observed in a closed journal bearing creates the appropriate geometry for comparing the different assumptions regarding the re-absorption of refrigerant, which was not possible in the case for a partial journal bearing, where actually the differences could be deemed negligible.

For the present problem, the mixture chosen is that of refrigerant HFC-134a with a synthetic polyolester oil ICI EMKARATE RL10H, already introduced in the last chapter, and more commonly used presently than the CFC-12/mineral oil mixture also investigated previously. It will be valuable to re-evaluate the influence of mixture parameters on bearing behaviour, particularly for the non-equilibrium case, which has not yet been performed. The results against the classical solution using Reynolds boundary conditions can be further checked, to verify whether the agreement previously observed still holds.

Finally, with the variety of works undertaken in lubrication, it is desirable to compare the results from the present methodology against alternative proposals, which may assist in indicating the applicability of the model, its weaknesses, and also guidelines for future investigation.

6.1.1. Specific objectives

- To extend the methodology for partial journal bearing and numerically solve the two-phase lubrication problem for the infinite long journal bearing;
- To investigate how thermodynamic equilibrium and non-equilibrium of the mixture flow affect bearing behaviour;
- Review the proposed methodology proposed against the solution Reynolds boundary conditions, for both equilibrium and non-equilibrium assumptions;
- To evaluate the suitability of some model assumptions, such as the isothermal condition and the surface tension effects.
- To investigate how the solution provided by the model compares against literature data available for journal bearings;

6.2 MODEL DEVELOPMENT

6.2.1. Physical Considerations

The geometry considered is that of an infinitely long journal bearing, with a shaft that rotates at constant angular speed and is subjected to an external load, indicated in figure 6.1. The bearing is initially filled with an oil-refrigerant mixture of known composition. For simplicity, the bearing is considered in its steady-state equilibrium position, but for a transient situation the only amendment to consider is the additional pressure offset induced by the squeeze film.

The bearing presents a convergent-divergent geometry as a result of the eccentricity between shaft and bush centres. In the convergent region, pressure increases mainly due to the wedge effect. So long as only liquid is present in this region, fluid properties will remain constant. When the flow enters the divergent region, pressure falls and eventually reaches the saturation pressure for the liquid

oil-refrigerant mixture at the given temperature, as also observed for the partial journal bearings. Release of gas takes place and a two-phase flow is observed in the cavitated region.

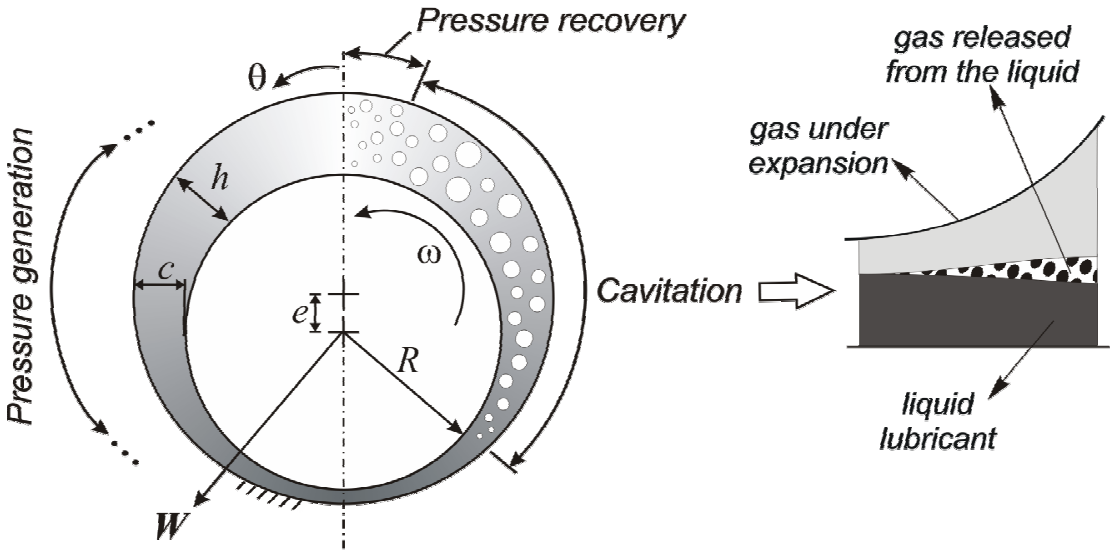

Figure 6.1. Geometry for the infinite journal bearing and detail of the lubricant behaviour.

As the flow once again approaches the convergent region of the bearing, the higher pressures upstream are communicated to the fluid by diffusion of momentum. Consequently the fluid will experience a region of pressure recovery before recirculating into the convergent area. In this case, film pressure increases and gas can redissolve in the oil. However, as the rate of absorption is unknown, and usually expected slow, the liquid may not be able to absorb the gas in the flow time available during the positive pressure region. Due to this unknown absorption rate, it is only possible at the present to determine the two limit thermodynamic situations discussed in chapter 3,

- *Full-equilibrium*, where the gas is reabsorbed instantaneously, as it happens during release;
- *Non-equilibrium*, where no gas is absorbed after being released, therefore resulting in a two-phase flow throughout the whole bearing, including the positive pressure region. This situation is similar to a bubbly oil flow, and leads to a transient problem even for constant loads, as the fluid properties vary continuously at all bearing positions from the initial condition until reaching equilibrium.

These situations will be evaluated for the journal bearing and behaviour differences discussed in the results.

Similarly to chapter 4, the assumptions made to simplify the problem are:

1. Radial clearance *c* is much smaller than shaft radius:

- pressure in the radial direction can be considered constant;
- radial clearance is fully filled with oil;
- entrance effects are negligible;

2. Pressure and viscous forces are dominant in the flow;

3. Shaft and bearing are very long, and a unidimensional flow can be assumed;

4. Constant load applied;

5. Isothermal flow;

6. Negligible metastability of the liquid mixture: instantaneous gas release;

The only change in comparison to the previous chapter is that even for a constant load applied, in principle steady-state conditions cannot be guaranteed, particularly for the expected bubbly oil flow that can potentially happen under non-equilibrium conditions.

6.2.2. Mathematical Considerations

To solve the lubrication problem, it is adopted the convenient cylindrical coordinate system, $r\theta y$, centred at the shaft centre and positive for anti-clockwise rotations.

Additional assumptions regarding the geometry can follow those performed for the partial journal bearing, i.e., radial clearance *c* between shaft and bearing, and eccentricity *e* between their centres. The oil film thickness *h* can be calculated as a result, as given previously,

$$h = c(1+\varepsilon \cos\theta) \tag{4.3}$$

The shaft rotates at an angular speed ω, which results in a tangential velocity *U* for a shaft with radius *R*; the radius, much bigger than the clearance, enables a coordinate transformation $x = R\theta$ (film unwrapped).

Furthermore, the following assumptions can be stated,

- unidimensional: $\frac{\partial}{\partial y}(.) = 0$;

- rotating shaft: $u_a = U$;
- stationary bush: $u_b = 0$;

Therefore, equation (3.29) is simplified to,

$$\frac{1}{R^2}\frac{\partial}{\partial\theta}\left(\frac{\overline{\rho}h^3}{12\overline{\mu}}\frac{\partial p}{\partial\theta}\right) = \frac{1}{R}\frac{\partial}{\partial\theta}\left(\frac{\overline{\rho}hU}{2}\right) + \frac{\partial}{\partial t}\left(\overline{\rho}h\right) \tag{6.1}$$

In considering the homogeneous properties for the solution, distinction has to be made for the two different thermodynamic states to be evaluated, as this will result in different properties for the lubricant.

As previously defined in chapter 3, the characterisation of the oil-refrigerant mixture is given initially by the refrigerant mass fraction,

$$w_r = \frac{m_{lr}}{m_l} \tag{3.14}$$

To verify the condition in which the mixture is, the mass fraction is checked against the solubility, $w_{sat}(p,T)$.

When gas is released in an isothermal process, pressure decreases and so does the mass fraction to maintain the mixture saturated. Therefore,

$$w = w_{sat}, \text{ for } p<p_r \tag{6.2}$$

where p_r and p are the pressures in two consecutive positions of the bearing, which in this case gives $dp/d\theta<0$.

When the opposite is observed, i.e., a positive pressure gradient, absorption can potentially occur. However two different conditions are considered here. Under thermodynamic equilibrium, gas is absorbed in the liquid for as long as there is availability, such that,

$$w^{(eq)} = w_{sat} \leq w_o, \text{ for } p>p_r \tag{6.3.i}$$

Alternatively, if non-equilibrium is considered, refrigerant never returns to the liquid mixture once released. Therefore,

$$w^{(ne)} = w_r, \text{ for } p>p_r \tag{6.3.ii}$$

where w_r is the mass fraction at the position immediately before the location considered.

A convenient way of generalising the information for the mass fraction is to use a potential equation, based in electric circuit analogy. Equation (6.4) can be used to calculate the mass fraction,

$$w = w_r + \kappa \cdot \Delta t \cdot \left(w_{sat} - w_r \right) \tag{6.4}$$

where κ is the absorption/release coefficient and Δt the time step considered.

From equation (6.4), it can be seen that $\kappa \cdot \Delta t = 0$ under non-equilibrium and for equilibrium conditions $\kappa \cdot \Delta t = 1$.

With these considerations, equation (6.1) can be solved for the full domain of the bearing at any time step. By doing so, the solution for pressure is mass conservative. For boundary conditions, a circular condition is observed, such that, if the pressure at a reference position for the full journal bearing is also known, the following boundary conditions can be written,

$$\begin{aligned} &p = p_{ref} \quad \text{for } \theta = \theta_{ref} \\ &p(\theta = 0) = p(\theta = 2\pi) \end{aligned} \tag{6.5}$$

where θ_{ref} is the reference position in the bearing where the absolute pressure is known.

The position of the reference angular position has to be given in relation to a fixed coordinate system, which is not the case for the system presented in figure 6.1. To overcome this issue, a new coordinate system is defined, considering the vertical line passing through the centre of the shaft, as indicated in figure 6.2.

The properties for the liquid mixture and for the refrigerant gas are required to determine the apparent properties, then used for the lubrication equation – the correlations used for the mixture R134a/EMKARATE RL10H are available in Appendix B.

Once the solution for the pressure profile is achieved, the hydrodynamic force acting on the bearing can be calculated, and per unit length it is given by,

$$F_h' = \sqrt{F_\varepsilon'^2 + F_\xi'^2} \tag{6.6}$$

where F_ε' and F_ξ' are the force components in the direction of the line of centres and the perpendicular to it, as observed in figure 6.2,

$$F'_{\varepsilon} = -\int_{0}^{2\pi} p(\theta) R \cos\theta d\theta \tag{6.7.i}$$

$$F'_{\xi} = \int_{0}^{2\pi} p(\theta) R \sin\theta d\theta \tag{6.7.ii}$$

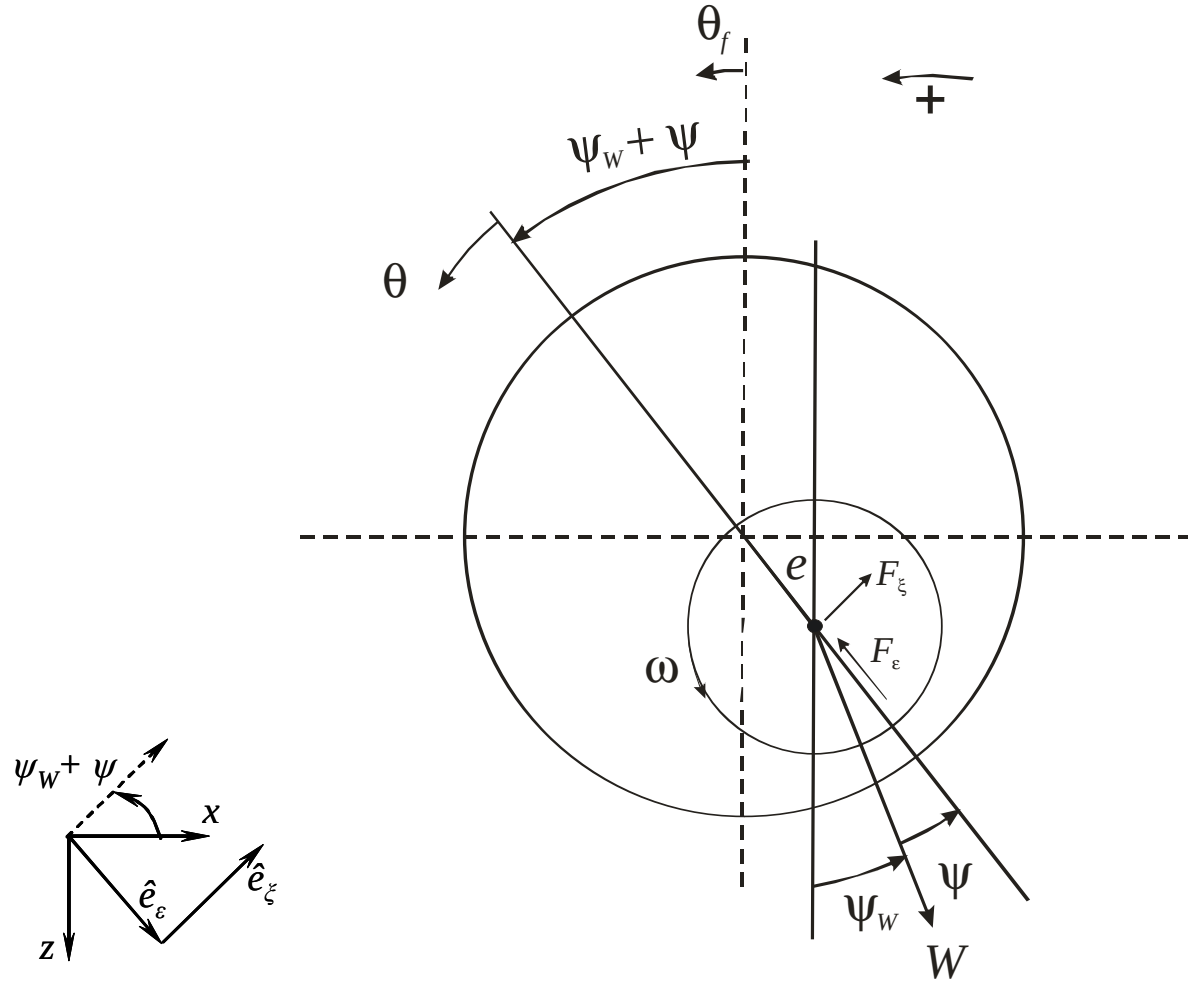

Figure 6.2. Relation between fixed and moving coordinate systems, θ_f and θ respectively, and the balance of forces acting on the shaft.

And the friction force on the shaft is calculated as,

$$F'_f = \int_{0}^{2\pi} \left(\frac{h}{2R} \frac{dp}{d\theta} + \bar{\mu} \frac{U}{h} \right) R d\theta \tag{6.8}$$

As a reminder, equation (6.8) considers friction for the full length of the bearing, to be coherent with the assumptions of the homogeneous model. This is different from the approach used in usual methodologies, as discussed in chapter 4 and presented in equation (4.12).

To solve the governing equation for the problem, (6.1), it is required the squeeze film term, $\partial(\bar{\rho}h)/\partial t$ for the time step considered. Moreover, to determine the transient behaviour of the bearing, the solution for shaft dynamics is required.

To this end, a balance of forces in the shaft is performed. The fixed reference system is of help to track the shaft trajectory, but considering the axes ε and ξ for the balance,

$$m \cdot a_\varepsilon = W \cos\psi - F_\varepsilon \tag{6.9.i}$$

$$m \cdot a_\xi = -W \sin\psi + F_\xi \tag{6.9.ii}$$

where a_ε and a_ξ are the accelerations for the shaft in the respective coordinates.

To determine these accelerations, the relationships between the Cartesian fixed and the moving polar coordinate system are evoked,

$$\vec{r} = x\hat{i} + z\hat{k} = r\hat{e}_\varepsilon \tag{6.10}$$

where $\hat{i}$, $\hat{k}$, $\hat{e}_\varepsilon$ are the unit direction vectors for the coordinate systems.

Considering also $\hat{e}_\xi$ normal to $\hat{e}_\varepsilon$, one has,

$$\hat{e}_\varepsilon = \sin(\psi_W + \psi)\hat{i} + \cos(\psi_W + \psi)\hat{k} \tag{6.11.i}$$

$$\hat{e}_\xi = \cos(\psi_W + \psi)\hat{i} - \sin(\psi_W + \psi)\hat{k} \tag{6.11.ii}$$

from where the following derivatives can be worked out,

$$\frac{d\hat{e}_\varepsilon}{d\varepsilon} = 0,\ \frac{d\hat{e}_\xi}{d\varepsilon} = 0,\ \frac{d\hat{e}_\varepsilon}{d\xi} = \hat{e}_\xi,\ \frac{d\hat{e}_\xi}{d\xi} = -\hat{e}_\varepsilon \tag{6.12}$$

which gives, for $e=c\varepsilon$,

$$\vec{v} = \frac{d\vec{r}}{dt} = c\dot{\varepsilon}\,\hat{e}_\varepsilon + c\varepsilon(\dot{\psi}_W + \dot{\psi})\,\hat{e}_\xi \tag{6.13}$$

and,

$$\vec{a} = \frac{d^2\vec{r}}{dt^2} = c\left[\ddot{\varepsilon} - \varepsilon(\dot{\psi}_W + \dot{\psi})^2\right]\hat{e}_\varepsilon + c\left[\varepsilon(\ddot{\psi}_W + \ddot{\psi}) + 2\dot{\varepsilon}(\dot{\psi}_W + \dot{\psi})\right]\hat{e}_\xi \tag{6.14}$$

where $\dot{\varepsilon}$, $\ddot{\varepsilon}$ are respectively once and twice derivatives of eccentricity with time, and similarly for ψ and ψ_W.

Replacing the derived accelerations in equations (6.9), results the balance of forces for the shaft,

$$mc\left[\ddot{\varepsilon} - \varepsilon\left(\dot{\psi}_W + \dot{\psi}\right)^2\right] = W\cos\psi - F_\varepsilon \tag{6.15.i}$$

$$mc\left[\varepsilon\left(\ddot{\psi}_W + \ddot{\psi}\right) + 2\dot{\varepsilon}\left(\dot{\psi}_W + \dot{\psi}\right)\right] = -W\sin\psi + F_\xi \tag{6.15.ii}$$

Therefore, the simultaneous solution of Reynolds equation (6.1) and shaft dynamics equations (6.15) enables both pressure and journal trajectory to be determined at every time step.

Naturally, analytical solutions are very difficult to obtain, such that a numerical methodology is proposed in the next section.

6.2.3. Numerical Methodology

Equation (6.1) is discretised as indicated in section 3.3, but for the simplified unidimensional control volume already discussed in chapter 4 and reproduced here as figure 6.3,

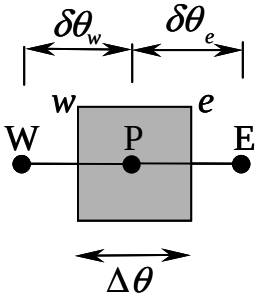

Figure 6.3. Unidimensional control volume used to integrate the Reynolds equation.

Therefore,

$$\int_w^e \frac{\partial}{\partial\theta}\left(\frac{\overline{\rho}h^3}{\overline{\mu}}\frac{\partial p}{\partial\theta}\right)d\theta = \int_w^e \left[6UR\frac{\partial}{\partial\theta}\left(\overline{\rho}h\right) + 12\frac{\partial}{\partial t}\left(\overline{\rho}h\right)\right]d\theta \tag{6.16}$$

resulting in,

$$A_p p_P = A_e p_E + A_w p_W + S \tag{6.17}$$

where, considering indexes *t* and *t-1* for two consecutive time steps,

$$A_e = \frac{\overline{\rho}_e h_e^3}{\overline{\mu}_e \delta\theta_e} \qquad A_w = \frac{\overline{\rho}_w h_w^3}{\overline{\mu}_w \delta\theta_w}$$

$$A_p = A_e + A_w \qquad S = -6UR\left(\overline{\rho}_E h_e - \overline{\rho}_P h_w\right) - 12\frac{\Delta\theta}{\Delta t}\left(\overline{\rho}_P^t h_P^t - \overline{\rho}_P^{t-1} h_P^{t-1}\right)$$

In addition to solving the pressure, equations (6.15) are used to calculate the shaft acceleration. From there, and with load conditions W, ψ_W and its derivatives known for the time t, accelerations are given by,

$$\ddot{\varepsilon}^t = \varepsilon^t\left(\dot{\psi}_W^t + \dot{\psi}^t\right)^2 + \frac{1}{mc}\left(W\cos\psi^t - F_\varepsilon\right) \tag{6.18}$$

and,

$$\ddot{\psi}^t = -\ddot{\psi}_W^t - \frac{1}{\varepsilon^t}\left[2\dot{\varepsilon}^t\left(\dot{\psi}_w^t + \dot{\psi}^t\right) + \frac{1}{mc}\left(W\sin\psi^t - F_\xi\right)\right] \tag{6.19}$$

The conditions for the next time step, $t+\Delta t$, are then calculated using an Euler marching scheme,

$$\dot{\varepsilon}^{t+\Delta t} = \dot{\varepsilon}^t + \ddot{\varepsilon}^t \cdot \Delta t \tag{6.20}$$

$$\dot{\psi}^{t+\Delta t} = \dot{\psi}^t + \ddot{\psi}^t \cdot \Delta t \tag{6.21}$$

and,

$$\varepsilon^{t+\Delta t} = \varepsilon^t + \dot{\varepsilon}^{t+\Delta t} \cdot \Delta t \tag{6.22}$$

$$\psi^{t+\Delta t} = \psi^t + \dot{\psi}^{t+\Delta t} \cdot \Delta t \tag{6.23}$$

When the values for eccentricity ratio and attitude angle are available, the time step is advanced by one and the solution for pressure proceeds in the new time. The process is repeated until a permanent condition is obtained, either the equilibrium position of the shaft or a defined orbit, depending on the case studied. The algorithm for the solution of the transient problem is illustrated in figure 6.4.

The numerical code developed in *Matlab* for the problem solved in chapter 4 was expanded to now solve the transient problem. Considerations for the numerical parameters there discussed remain valid for the present problem.

It should be stressed that the computational effort for solving the complete transient problem is significantly greater than for the steady-state solution previously studied. However, in many cases, this final solution is exactly what is being looked for. For thermodynamic equilibrium, the steady-state solution is easily obtained by following the procedures from chapter 4. However, for the non-equilibrium condition,

given the continuous release of gas, assumptions have to be made to obtain a simpler solution. This is discussed in the course of the results.

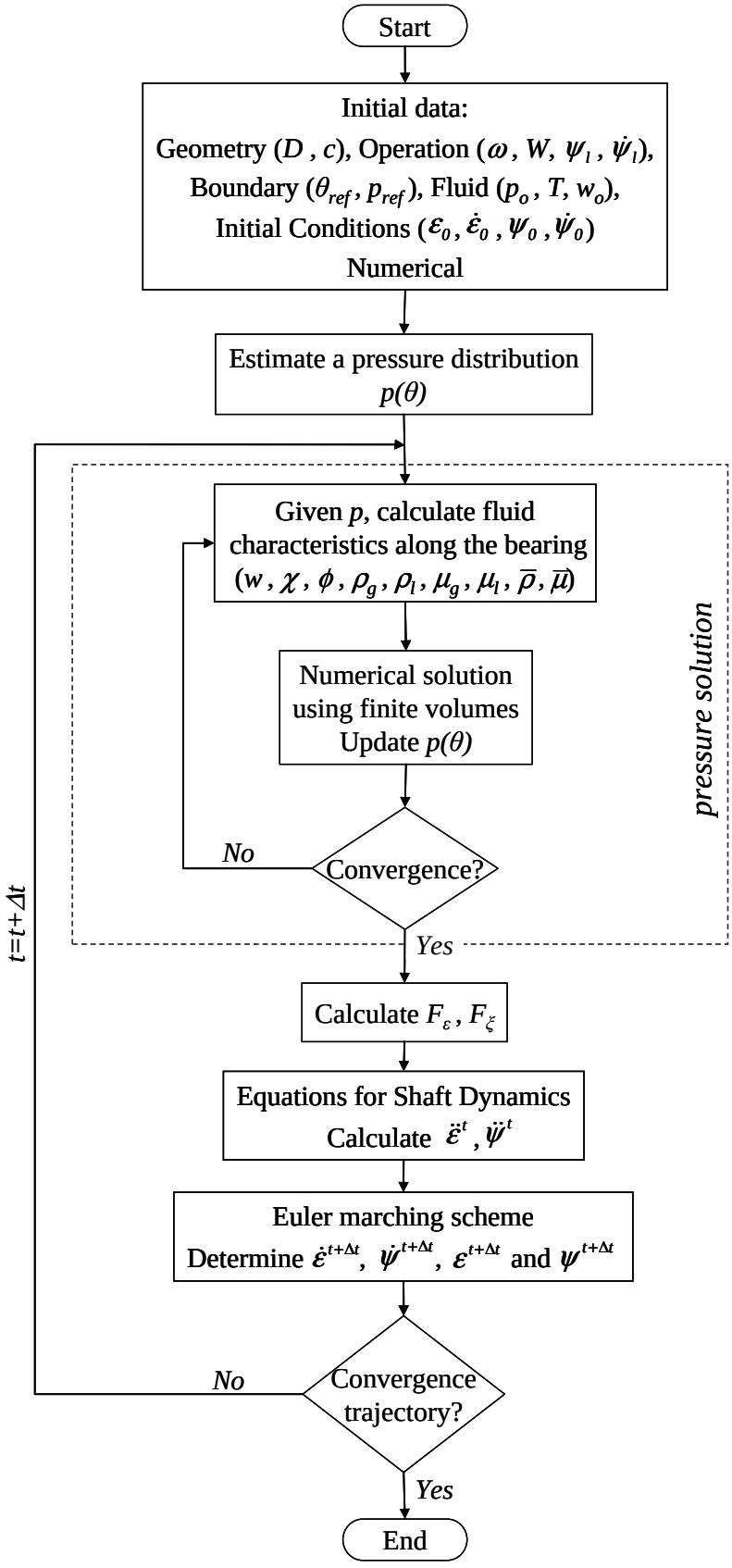

Figure 6.4. Solution procedure for the transient journal bearing problem.

6.3 RESULTS AND DISCUSSION

The methodology previously developed has been explored to differentiate the bearing behaviour for the two extreme thermodynamic conditions regarding the reabsorption of gas into the liquid. The mixture chosen for the analysis in this chapter is a widely used combination in the refrigeration industry, composed of the HFC refrigerant R134a and a synthetic, polyolester oil EMKARATE RL10H, whose properties are presented and discussed in the Appendix B.

6.3.1. Bearing behaviour for the two extreme thermodynamic conditions

As the targeted investigation of this chapter, the comparison between equilibrium and non-equilibrium conditions is first performed. For the numerical solution, 100 internal points were used in the discretisation and a time step of 1ms was adopted. The simulation considered a saturated oil-refrigerant mixture in the initial condition, a constant vertical load applied in the centre of the shaft, and remaining values for geometry and operation conditions defined as,

$$D=20mm,\ c=20\mu m,\ \omega=30Hz=1800rpm,\ W=48kN/m$$

$$p_{ref}=200kPa \text{ at } \theta_f=45^o,\ T=40^oC,\ w_o=w_{sat}=7.13\%$$

The steady-state solution is of interest here, and the results for pressure are plotted in figure 6.5. In this figure is also present, for reference, a solution considering the Reynolds boundary conditions via the cavitation algorithm, in which constant viscosity was assumed equal to that at the reference position.

As for partial journal bearings, a good similarity exists between pressures calculated using the two-phase flow approach considering full thermodynamic equilibrium and those using Reynolds boundary conditions, which is expected under moderate and heavier loads. For the two-phase model however, pressure decreases as the local clearance between shaft and bush increases, so that sub-ambient pressures exist, although presenting much lower levels than those observed of maximum pressure. This is detailed in the magnified area of the graph.

Still considering equilibrium conditions, sub-ambient pressures lead to the release of gas, which moderates the reduction in pressure in the cavitated region. Close to the maximum film thickness, diffusion of momentum communicates the existence of

the higher pressure region and results in pressure recovery being automatically determined by the two-phase model in a similar manner as to the cavitation region.

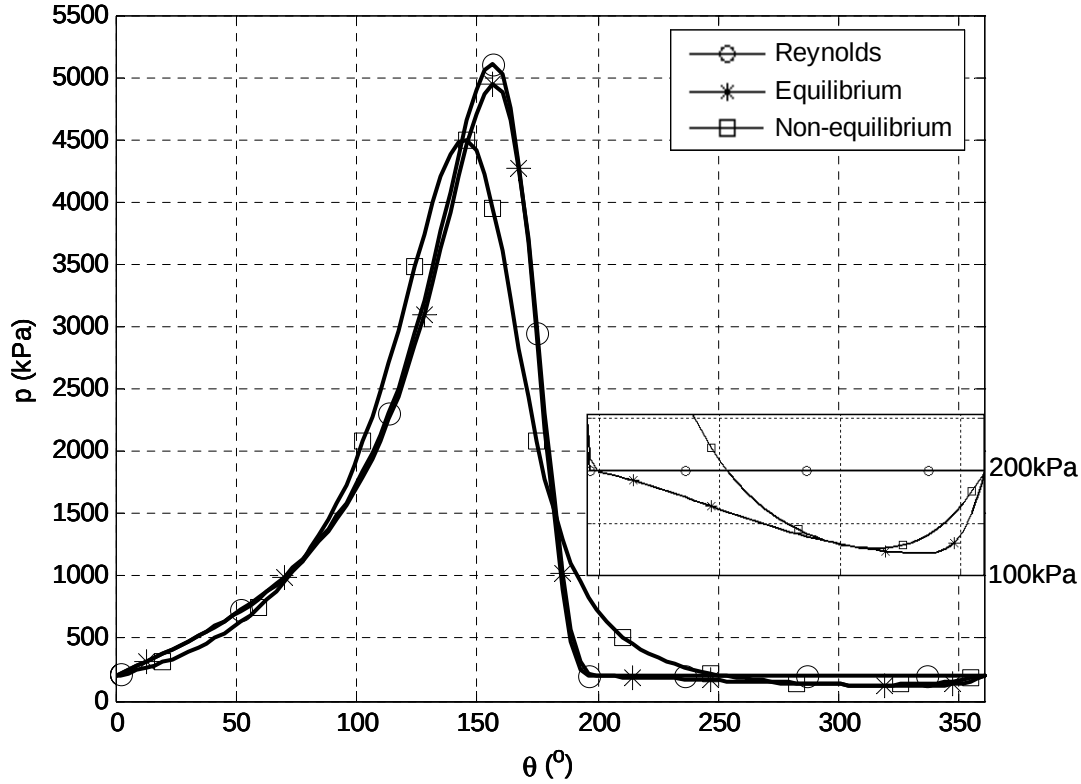

Figure 6.5. Pressure results considering steady-state conditions and different methodologies

On the other hand, under non-equilibrium conditions for the mixture, where gas is present throughout the bearing, lower maximum pressure is observed as well as a longer positive pressure region compared to the results obtained for equilibrium and also for the Reynolds conditions. This indicates that the bearing supports the same load under lower eccentricity, thus potentially reducing friction force. The calculated friction force is indicated in Table 6.1, also compared to the result for the conventional methodology (F_f^*). Resultant eccentricity and attitude angle for each case studied are also given, where the very different positioning of the bearing for the non-equilibrium condition is worth of note.

Table 6.1. Summary of results for position and friction for the different simulations.

	ε	$\psi\ (^o)$	$F_f'\ (N/m)$	$F_f^*\ (N/m)$
Reynolds	*0.81*	*41*	*93.7*	*80.9*
Equilibrium	*0.80*	*42*	*93.6*	-
Non-equilibrium	*0.77*	*25*	*87.5*	-

The different behaviour observed for the pressure profile in the non-equilibrium case can be explained by compressibility effects, as shown in figure 6.6a in terms of the homogeneous density. For comparison, an estimated density is presented for the classical solution using Reynolds boundary conditions, defined as $\overline{\rho}_R = \phi_a \cdot \rho_l$, where the estimated void fraction is calculated as defined in equation (4.13).

The density for the Reynolds solution presents a discontinuity, considering that the values for the angles 0º and 360º should be the same – and reflects the non-conservative character of this boundary condition for film reformation. This can be interpreted as an instantaneous film reformation at 360º or alternatively as the gas content required by the variation of geometry after cavitation. However, as the value for density is not used for the solution and therefore does not affect the result provided by the classical solution, this density value can be used as a useful estimate to compare with those obtained with the two-phase solutions.

For the two-phase model assuming thermodynamic equilibrium, liquid only is present in the convergent region and as the flow reaches the cavitated region, gas is released and density decreases in response to the release and subsequent gas expansion. Similarity is again evident with the estimated results using Reynolds conditions, distinguished only in the pressure recovery region where gas returns to the liquid. Such agreement points to the importance of geometry in determining cavitation. The density results also permit estimation of the volume fraction of the gas, reaching a maximum of 85% close to 360º.

Considering non-equilibrium, gas is present throughout the bearing, and its compressibility enables the fluid to adapt in a smoother way to the geometry changes, which is the density wedge effect. Therefore, the density wedge assists the physical wedge effect in generating pressure, which explains the lower eccentricity presented in this case. Considering the cavitated region, as more gas is available from the beginning of the divergent region, a lower rate of change in density is observed when compared to that of the equilibrium solution, being similar only at higher aeration levels.

The behaviour of the absolute homogeneous viscosity for the different simulations performed is presented in figure 6.6b. It can be observed that despite the low viscosity of the gas, the viscosity of the two-phase mixture actually increases. This can be explained by the increase in the viscosity of the liquid: with the release of refrigerant as gas, the mass fraction of the oil in the liquid mixture increases, therefore

increasing the viscosity of the liquid given the higher viscosity of the oil compared to the liquid refrigerant. Nevertheless, it should be noted that the change in viscosity is small compared to that in density, as the latter depends on the volume fraction ($\phi_{max}\approx 85\%$) while the former depends on the mass of gas ($\chi_{max}\approx 3\%$). In the non-equilibrium case, the higher viscosity points to a greater release of gas. Furthermore, the constant behaviour throughout the bearing shows that variation of gas viscosity can be assumed negligible.

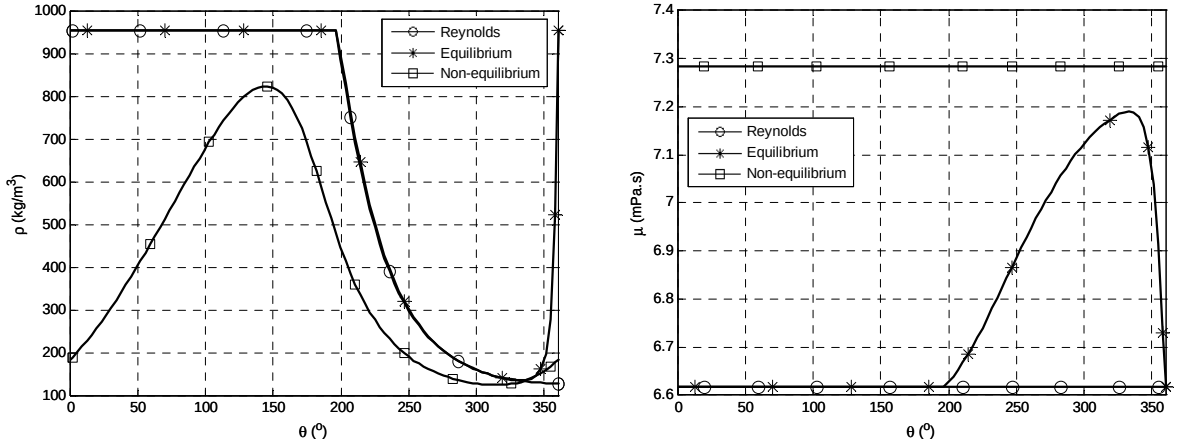

a) Density **b)** Viscosity

Figure 6.6. Homogeneous properties along the journal bearing

6.3.2. Influence of initial mass fraction on bearing performance

Given the variation that the mixture properties can experience, it is worthwhile evaluating how different initial mixture conditions affect the performance of the journal bearing. To this end parametric tests were performed considering mixture of different mass fractions at the initial condition. This effect could also be obtained through pressure and temperature, which affect directly the solubility – such that these tests can be seen in a wider context as influence of mixture properties on bearing behaviour. Evaluating separately equilibrium and non-equilibrium conditions, the parametric tests considered mass fractions varying from 0.8 to 1.2 times the solubility at the initial pressure and temperature, using additionally the following data,

$D=20mm$, $c=20\mu m$, $\omega=60Hz$, $\varepsilon=0.8$, $p_{ref}=200kPa$ at $\theta=0^o$, $T=40^oC$, $w_o=w_{sat}=7.13\%$

For equilibrium conditions, presented in figure 6.7a, the results are aligned with those presented in chapter 5. The release of gas starts at the same angular location along the fluid film, indicating the geometry influence in determining the onset of cavitation. However, as saturation pressure differs among the mixtures, so does the

cavitation pressure, with lower value observed for the lower mass fraction. Furthermore, as the density of the gas decreases with pressure, the pressure drop is smaller for the mixture with the lower mass fraction. These results reinforce the conclusions that viscosity influences the positive pressure region, whereas the gas density is the most important property in the cavitated region.

The influence of fluid properties in the bearing performance variables is presented in figure 6.7b. It can be seen that variables such as the load capacity, friction force and maximum pressure vary at the same rate as the viscosity. This may seem unclear for mixtures above w_{sat} – however, at this condition some gas is available at the start, and is readily absorbed in the liquid once pressure increases, thus reducing viscosity. On the other hand, variables such as the friction coefficient and mass flow rate do not depend on viscosity and remain practically constant regardless the mixture conditions. Those results are also expected in the classical solution for journal bearings (Pinkus and Sternlicht, 1961). The attitude angle, however, varies more than expected, indicating some influence of the fluid behaviour in cavitation, not predicted in the classical solution.

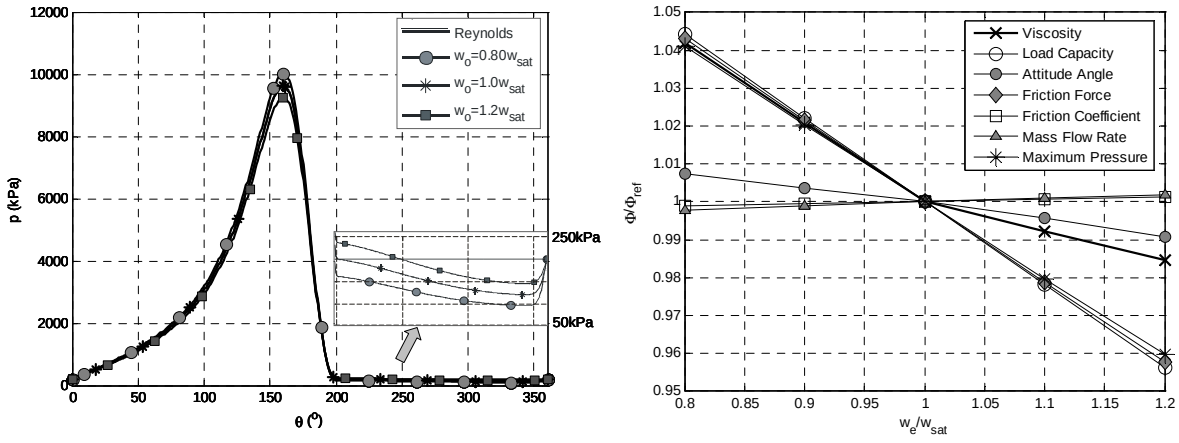

a) Pressure results **b)** Performance variables

(μ_{sat}=6.62mPa.s, W_{sat}=95kN/m, $F_{f,sat}$=183N/m, ψ_{sat}=42º, f_{sat}=0.0019, $q_{\theta,sat}$=89g/(s.m), $p_{max,sat}$=9.64MPa)

Figure 6.7. Variation of bearing operation with the initial mass fraction – equilibrium conditions

Despite the differences in the pressure profile previously seen, similar conclusions can be drawn for simulations considering the non-equilibrium hypothesis, as shown for pressure results in figure 6.8a. Viscosity remains the decisive property in the convergent region, resulting in higher pressures for mixtures of higher viscosity, i.e. lower mass fractions. Additionally, as observed in the magnified area of figure 6.8a,

comparing to mixtures of higher overall mass fraction, lower pressures are observed for the lower mass fraction mixtures in the cavitated region, which points to a smaller mass of free gas.

However the performance variables are affected more significantly than those observed for the equilibrium case, as observed in figure 6.8b. While maximum pressure and load capacity expectedly vary linearly with the viscosity of the lubricant mixture, friction force varies more significantly than viscosity, which could be related to the extended length of the positive pressure profile. Thus viscosity is likely to influence friction through Couette and Poiseuille flows through the whole bearing. The friction coefficient reflects the distinct behaviour for load capacity and friction, decreasing as the mass fraction increases. The mass flow rate is also reduced with increasing mass fraction, which can be explained by the density of the fluid – as less mass of gas is released, more refrigerant is dissolved in the liquid, therefore increasing the apparent density.

The attitude angle is the variable presenting greater deviation with the initial mixture mass fraction, which is one indication of the reasons why severe numerical instability is observed during simulations for non-equilibrium conditions.

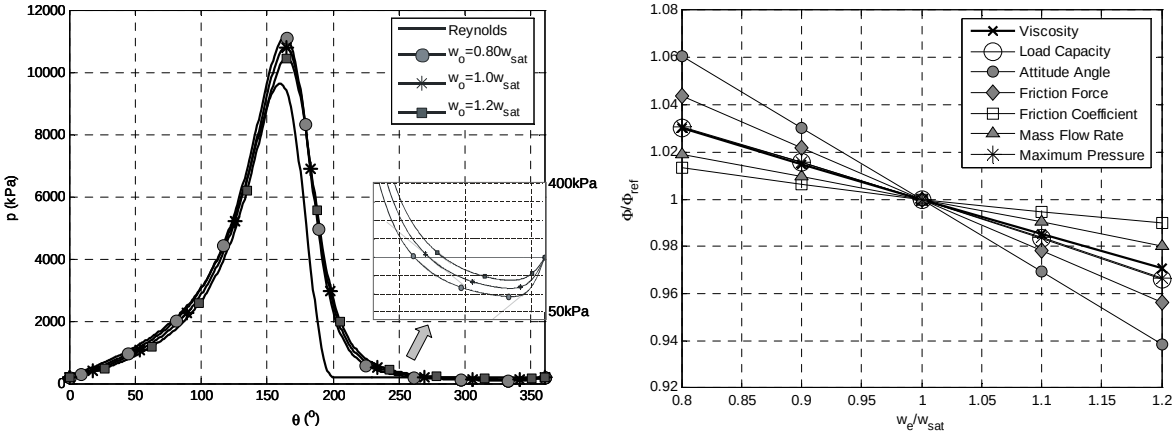

a) Pressure results **b)** Performance variables

(μ_{sat}=6.62mPa.s, W_{sat}=95kN/m, $F_{f,sat}$=183N/m, ψ_{sat}=42º, f_{sat}=0.0019, $q_{\theta,sat}$=89g/(s.m), $p_{max,sat}$=9.64MPa)

Figure 6.8. Variation of bearing operation with the initial mass fraction – non-equilibrium

As the previous results indicated, considerable difference exists between equilibrium and non-equilibrium assumptions in the modelling, requiring further analysis to determine the exact rate of absorption and consequently predict more accurately the behaviour of the bearing. Although results for the equilibrium condition

agree well with the classical solution considering Reynolds boundary conditions, the time required for absorption should be investigated. For instance, considering the case presented in Figure 6.6, reabsorption takes place in the last 25º of the bearing, corresponding to a flow time of 2ms, seeming unrealistic given the effort usually required to dissolve the refrigerant in the oil (Lacerda et al., 2002). On the other hand, for the refrigerant gas to sustain such high pressures as observed in the positive region of the flow can also be proven unlikely, such that an intermediate situation between the extreme thermodynamic conditions should be considered in future investigations.

6.3.3. Considerations about the transient solution – non-equilibrium

The solution for the bearing assuming thermodynamic equilibrium for absorption presents similar results as those for the solution considering Reynolds boundary conditions. Furthermore, as any gas released is reabsorbed completely as soon as pressure increases, then it is possible to use a solution similar to that for partial journal bearings only to determine the steady-state solution of a problem.

However, the situation is not so simple for the non-equilibrium solutions. As the gas released is not reabsorbed, then the solution for the problem is always transient, which naturally is more time consuming.

An example of trajectory calculated for a mildly loaded bearing in which non-equilibrium conditions were assumed is presented in figure 6.9. The figures also indicate the solution for Reynolds boundary conditions using the cavitation algorithm, and the solution considering half-Sommerfeld pressure profiles.

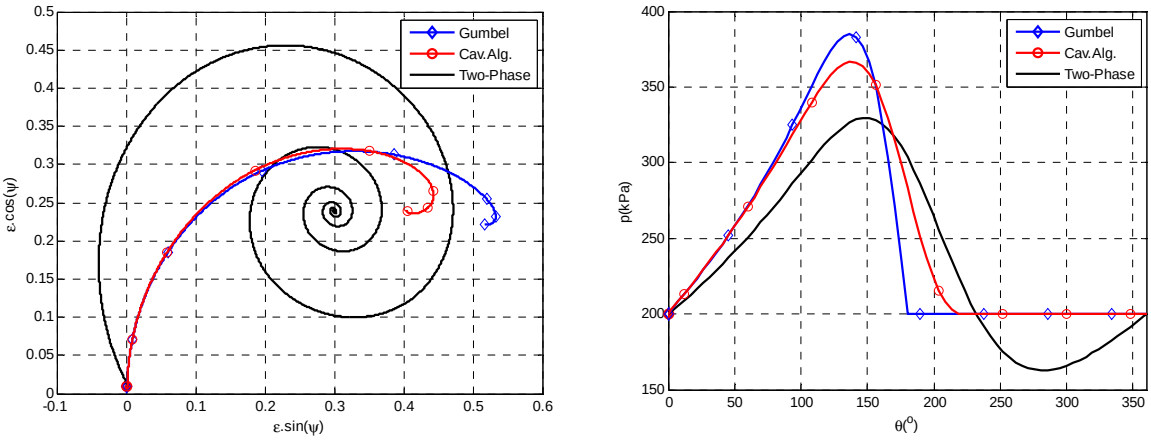

a) Trajectory **b)** Converged pressure

(μ=6.62mPa.s, W=300N/m, ω=3000rpm, D=70mm, c=250μm, p_e=200kPa, T_e=40^{o}C, w_o=w_{sat}=7.13%)

Figure 6.9. Dynamic solution for a journal bearing

Considering steel as the material of the shaft, it is still clear that inertia is negligible for the problem considered, as can be observed by the smooth trajectory for both single-phase solutions. However, there is a significant oscillation for the solution where gas is present, which requires more computational time and not uncommonly convergence problems.

The instability for this situation is indeed due to the presence of bubbles in the oil. As often reported for squeeze film dampers (e.g., Tao et al., 2000), the presence of bubbles increases the stiffness of the system and reduces its damping, which are both observed in figure 6.9. The increased stiffness enables the bearing to support more load at lower eccentricity, however the reduced damping of the system promotes significant oscillation until equilibrium is reached. That is actually one limitation of application of the bubbly oil journal bearing, given that it may be difficult to undergo transient processes, despite its higher load capacity.

The solution for the bearing considering non-equilibrium mixture for the bearing will therefore be time-consuming, and it may also depend on the initial condition given, which should not be expected in usual conditions. Those factors have to be taken into account when considering the feasibility of this specific two-phase solution.

6.4 FURTHER INVESTIGATION ON THE MODEL ASSUMPTIONS

Amongst the model assumptions proposed in chapter 3, some were subjected to further investigation. Here, attention will be given to the isothermal assumption and also the surface tension effects. Later in the chapter, in an opportunity to qualitatively evaluate the results of the model in the light of experimental results available from the literature, aspects such as the metastability of the mixture during release, and also the influence of the ventilation are analysed.

6.4.1. Adiabatic versus Isothermal Solution

In chapter 3, when developing the model, the flow was assumed isothermal. This hypothesis can be questioned having in mind that the release of gas requires energy to occur, usually removed from the bulk liquid lubricant, thus reducing its temperature (Grando, 2001).

In the study of the oil-refrigerant flow in straight horizontal pipes, Grando (2001) included the solution of the energy equation in the analysis and often reported temperature drops in the order of more than 10°C. Typical results of the pipe flow simulation are reported here in figures 6.10a-d. The mixture considered is that of refrigerant R12 and mineral oil SUNISO 1GS.

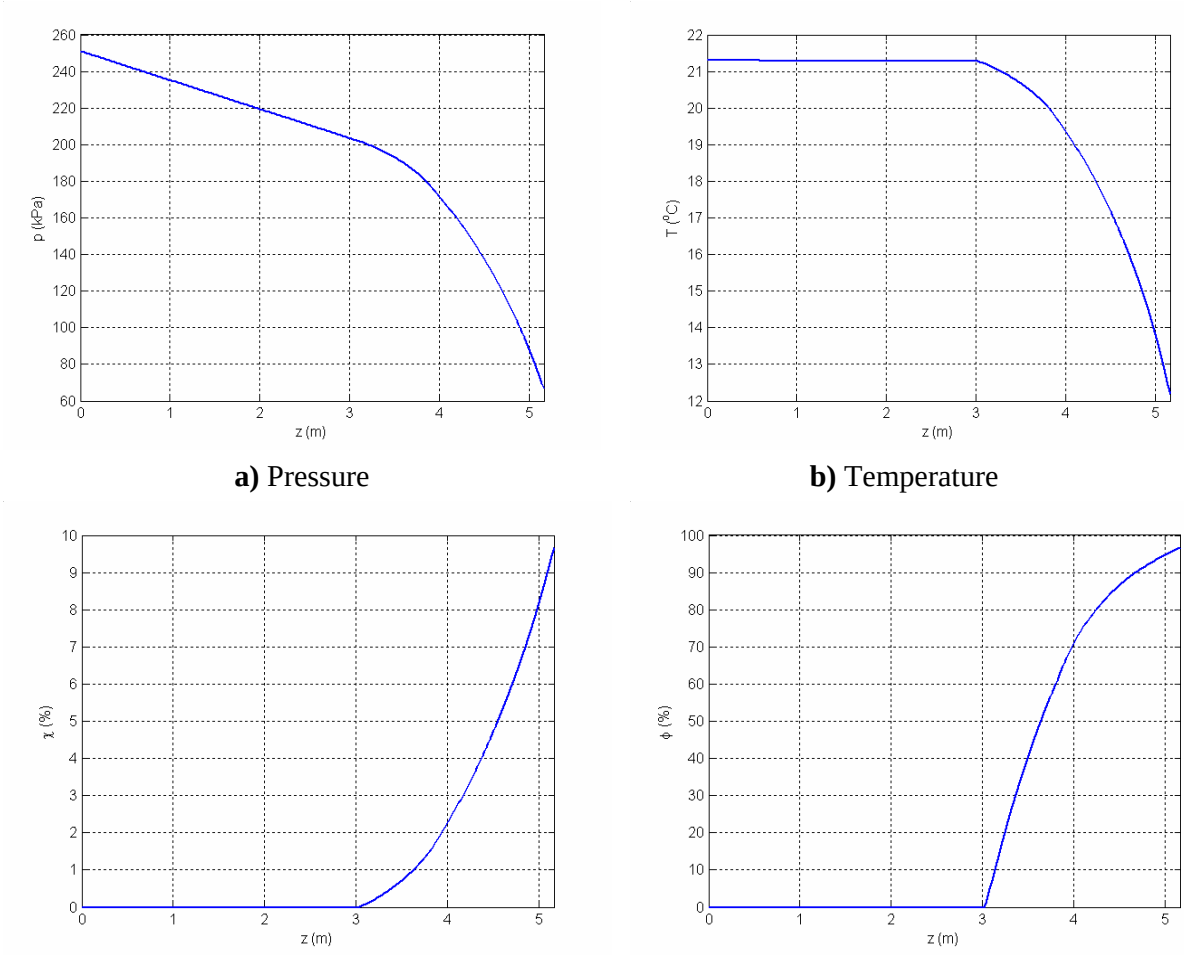

a) Pressure **b)** Temperature

c) Gas quality **d)** Void fraction

(mass flow rate=11.475kg/h, D=2.9mm, we=0.76wsat=14.75%)

Figure 6.10. Solution for oil-refrigerant flow along a straight horizontal pipe (Grando, 2001)

For the bearing problem, using a simplified derivation for the energy equation, extracted from the aforementioned work, the temperature drop exclusively due to the release of gas from the liquid can be calculated by,

$$\Delta T = \frac{h_{lg}\Delta\chi}{c_{po}} \tag{6.24}$$

where h_{lg} is the enthalpy difference between the gas and liquid phases, $\Delta\chi$ the quality variation, and c_{po} the specific heat for the oil.

Having the temperature difference, the temperature at each position can be determined through the numerical solution. The procedure from figure 6.4 remains the same, only now considering a variable temperature when calculating the lubricant properties.

The solution for a bearing using thermodynamic equilibrium conditions for absorption is presented in figure 6.11, including also the solution for an isothermal flow. Note that, for the non-equilibrium problem, once gas is released from the lubricant, as it does not return to the liquid, a uniform temperature should be expected in the steady-state condition.

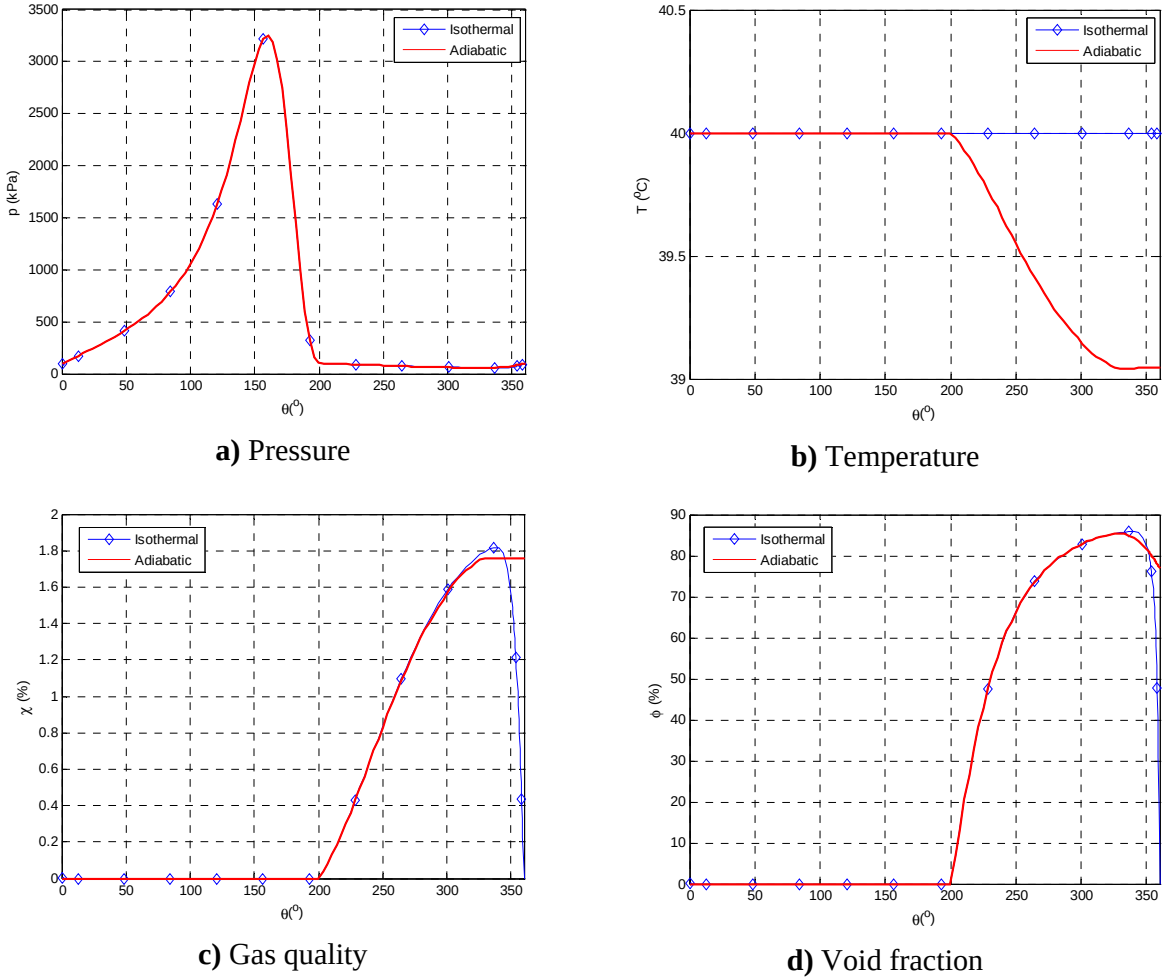

a) Pressure **b)** Temperature

c) Gas quality **d)** Void fraction

(D=20mm, c=40μm, ω=60Hz, ε=0.8, p_{ref} =200kPa at θ=0º, T=40ºC, w_o=w_{sat}=7.13%)

Figure 6.11. Adiabatic and isothermal solution for the journal bearing.

From the results, not a significant difference can be observed. The pressure profiles are almost perfectly overlaid while the decrease in temperature is observed in the order of less than 1°C. The load capacity is 3195.4N for the isothermal case against 3196.8N for the adiabatic case, while friction force is respectively 12.27N and 12.30N.

In evaluating the reasons for such small temperature drop, it is observed that a very small quantity of gas is actually released, with quality smaller than 2% - as the energy required for degassing is related with quality from equation (6.24), it results in a negligible contribution.

In the pipe flow, for instance, the quality of the released gas at the exit is about 10%, this requiring a larger energy input from the liquid to enable further degassing.

In the light of the previous results, it can be concluded that the isothermal assumption is satisfactory for the practical problems considered. It should be noted that this applies only to the fluid mixture effects, with no conclusion over the bearing thermo-hydrodynamic problem, as this was not into consideration in the present study.

6.4.2. Surface Tension considerations

The great majority of the literature for two-phase lubrication considers models in which the bubble dynamics is governed by surface tension effects (e.g. Smith, 1980, Someya, 2003). In the present model, such effect was not considered.

For comparison purposes, a simplified analysis with inert bubbles will consider:

- Ideal gas;
- Spherical shape, bubbles of radius r;
- Constant mass of gas;
- Liquid with constant surface tension;
- Instantaneous expansion and compression;

From the first two assumptions, it can be written,

$$p_g \forall_g = m_g RT \tag{6.25}$$

$$\forall_g = \frac{4}{3}\pi r^3 \tag{6.26}$$

It can be concluded from the two equations above that,

$$p_g r^3 = constant \tag{6.27}$$

The Rayleigh-Plesset equation (Smith, 1980) can now be evoked,

$$p_g = p_l + 2\frac{\sigma}{r} \tag{6.28}$$

where σ is the surface tension (N/m).

Combining now equations (6.27) and (6.28), assuming that one reference condition is known and defining $\bar{r} = r / r_0$, it can be shown that,

$$\bar{r}^3 + \frac{2\sigma}{r_0 p_l}\bar{r}^2 - \left(\frac{p_{l0}}{p_l} + \frac{2\sigma}{r_0}\right) = 0 \tag{6.29}$$

A second consideration relates to the void fraction, which was previously defined as

$$\phi = \frac{\forall_g}{\forall_{tot}} = \frac{\forall_g}{\forall_g + \forall_l} \tag{3.17}$$

which, for a void fraction known at a reference condition, can be rearranged as,

$$\forall_l = \forall_g\left(\frac{1}{\phi} - 1\right) = \forall_{g0}\left(\frac{1}{\phi_0} - 1\right) \tag{6.30}$$

for a constant number of bubbles, equation (6.30) can be rewritten with the help of equation (6.26),

$$\phi = \frac{\phi_0 \bar{r}^3}{1 - \phi_0 + \phi_0 \bar{r}^3} \tag{6.31}$$

This result is identical to that obtained by Someya (2003), and for a set of known initial conditions r_0, ϕ_0 and p_{l0} enables void fraction and bubble radius to be calculated for any other film pressure.

To use this information in the two-phase lubrication model, now the void fraction has to be used to determine the value of the homogeneous density, in a simplified form as,

$$\bar{\rho} \approx \rho_l(1 - \phi) \tag{6.32}$$

For the homogeneous viscosity, as previously concluded in this work as not a bad initial approximation, one can use,

$$\bar{\mu} \approx \mu_l \tag{6.33}$$

With these set of equations, the solution for equation (3.29) can be obtained, with a very similar procedure as for the two-phase model,

1. Provide initial data, including operation and geometry for the bearing, and for the bubbles r_0 and ϕ_0;

2. Estimate a pressure field;
3. Calculate for the bubbles $\bar{r}(\theta)$, r, ϕ and $\bar{\rho}$;
4. Solve Reynolds equation (3.29) and update *p*;
5. Repeat steps 3 and 4 to convergence.

To illustrate the differences, a simulation considering gas at the entrance of a partial journal bearing was investigated calculating the properties of the mixture using three different methods: spherical bubbles (considering surface tension), expansion of gas already available, and further release of gas in the cavitated region. For simplicity and also to enable a solution where the initial condition is exactly the same, a partial journal bearing was elected. Results are shown in figure 6.12a-d.

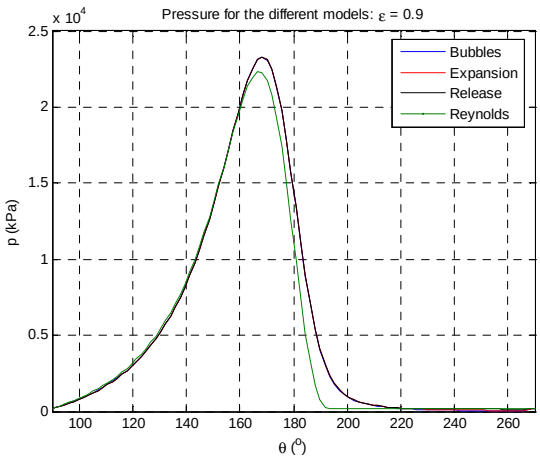

a) Pressure

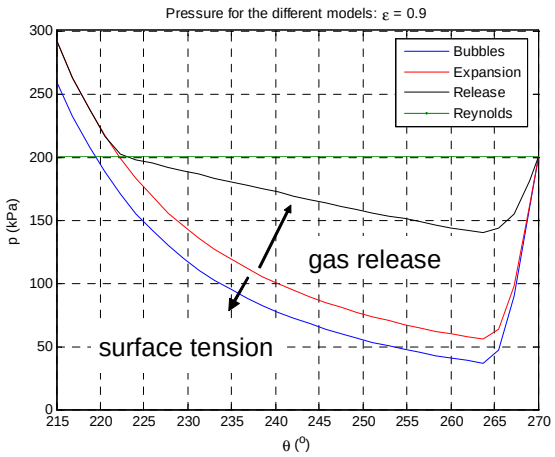

b) Detail of the cavitated region

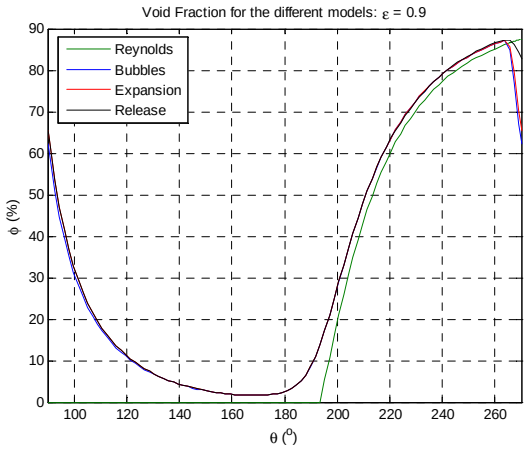

c) Void Fraction

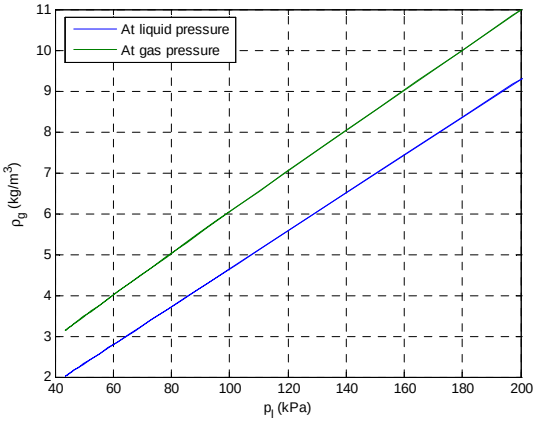

d) Density for the gas (R134a)

(D=20mm, c=20μm, ω=60Hz, ε=0.9, p_e =200kPa, T=40ºC, w_o=1.2w_{sat}=8.55%, r_0 =1.0μm)

Figure 6.12. Solution considering different treatment for the released gas from the mixture.

In this high eccentricity case, it can be seen that the differences in the positive pressure area are negligible (figure 6.12a). On the other hand, as seen in figure 6.12b, detailing in the cavitation region, it can be noticed that while the release of gas moves the result closer to the Reynolds condition, for the case where surface tension is considered, pressures are lower. By observing the similarity between the results for void fraction (figure 6.12c), it can be concluded that lower pressures were required to fill the clearance in the cavitated region. This results from the higher pressures in the bubbles, such that gas density in higher (figure 6.12d). Therefore, there is an influence of surface tension and it should be considered in future models – however this still needs to enable the release of gas, requiring a more elaborate derivation than the one performed in this section.

Another aspect to be considered for this example is that, for a gas such as R134a, at the maximum pressure achieved in the example, it would likely be in a liquid state instead – and even more considering the surface tension effects. This situation can lead to damage of the bearing, if the bubbles implode at such high pressure.

Therefore, inert solutions may be deviating from the actual behaviour of the mixture, and additional developments of the model, considering or not surface tension, should be considered.

6.4.3. Qualitative discussion against experimental results from literature

Couto (2006) in his investigation of cavitation for journal bearings discussed the importance of ventilation during the phenomenon. One evaluation involved an immersion test; in this test, the bearing was surrounded by contention plates that accumulated lubricant until the full immersion of the bearing. The lubricant (silicon oil) was evacuated at the beginning of the test to reduce the influence of the gases and humidity. The circumferential pressure results for the sequence of the test are shown in figures 6.13 to 6.17; the sequence started with the bearing open to the ambient, being gradually immersed, and later the bearing emerges back. Additional oil column pressure at full immersion does not exceed 0.05bar. Couto (2006) obtained the theoretical results using the adaptative mesh methodology (Prata and Ferreira, 1990).

At the beginning of the test, subambient pressures are observed in the bearing, with a striated flow observed in similar experiments performed in the same work. However, as the bearing is immersed, instead of a profile tending to the Sommerfeld

solution, as expected in the work, it actually develops towards the Reynolds boundary conditions, as shown in figure 6.16.

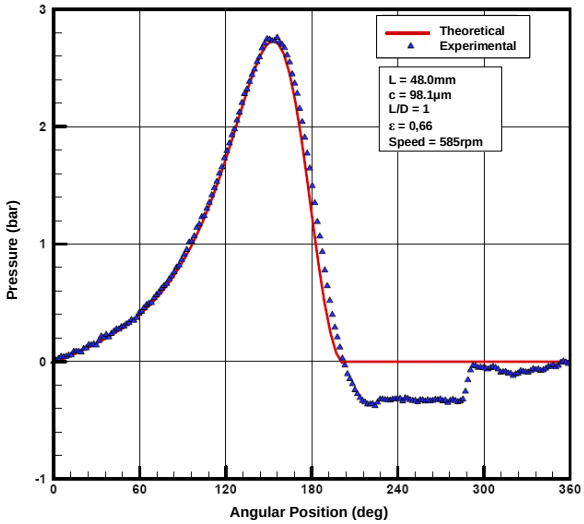

Figure 6.13. Circumferential pressure prior to the immersion test (Couto, 2006).

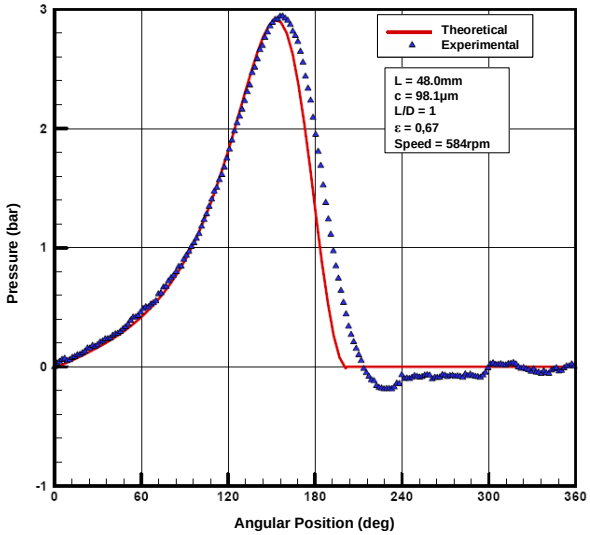

Figure 6.14. Circumferential pressure at the beginning of the immersion (Couto, 2006).

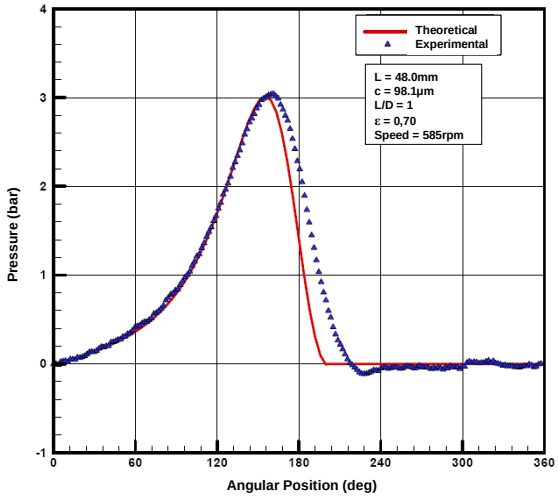

Figure 6.15. Circumferential pressure with bearing partially immersed (Couto, 2006).

In the light of the two-phase model developed in the present work, figure 6.16 presents pressure results that are very similar to those where only release of gas is observed, and from a saturated mixture. Also coherent with the two-phase model results, a small region of pressure recovery seems to be identifiable also close to the position where the bearing is fed (~300^{o}), although this is observed more clearly for the other figures.

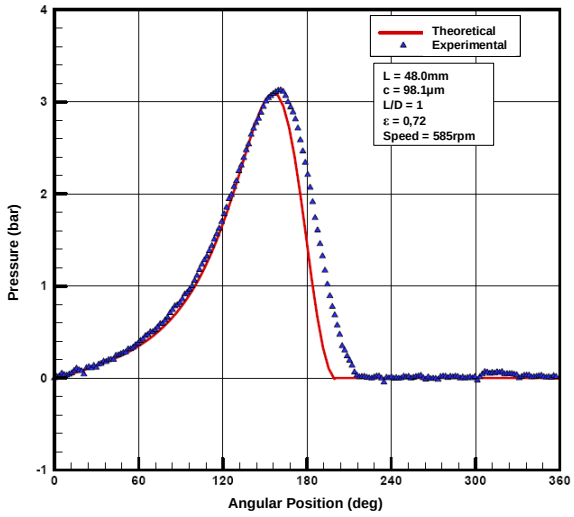

Figure 6.16. Circumferential pressure for the fully immersed bearing (Couto, 2006).

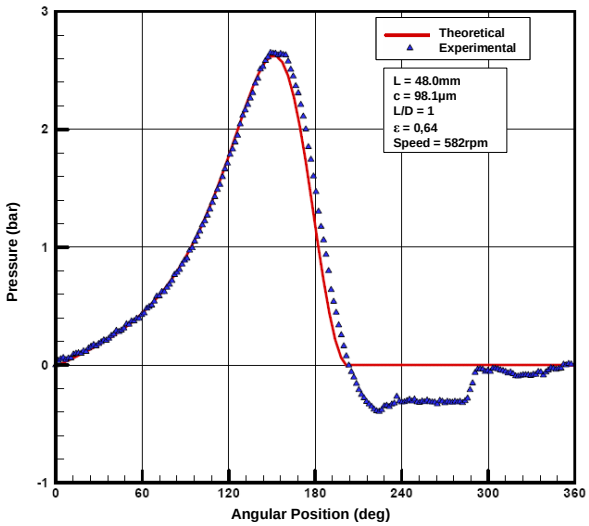

Figure 6.17. Circumferential pressure when immersion is ceased (Couto, 2006).

In the present work, modelling ventilation was under consideration for occasions, but it was believed that under such conditions the pressure in the cavitation region should become closer to the atmospheric, and not further away.

To rationalise this result in the context of the present work, reference is made to figure 6.7a, where mixtures with three different mass fractions were considered. Similar conclusions can also be drawn from the parametric analysis in chapter 5.

It is observed that, for the mixture with lower mass fraction, further pressure drops are required to start the release of gas (in that case, coinciding in each case with the own saturation pressure).

Understanding the additional pressure drop as a difficulty of the fluid to releasing gas, in figure 6.17, it could be understood that, in the presence of abundant air from the surroundings, extra difficulty is posed to the fluid to release its own dissolved gas, i.e., degassing occurs later under metastable conditions. The pressure increase, seen just after the pressure drop and before the flat pressure region (which again could be associated with degassing), may correspond to the release of gas from its unstable equilibrium, and not being as smooth a process as that seen in figure 6.16, could lead to a separation of the flow.

This explanation is by no means a definite answer to the issue, but serves well to enlighten the discussion on the basis of the two-phase flow model here developed. As the important factor to be raised, is the need to study release under metastable conditions, which could clarify the issue. This is also an observation from the flow of oil-refrigerant mixtures, as reported by Lacerda (2000).

6.5 SUMMARY

The two-phase numerical solution for an infinite width full journal bearing was proposed, and in sequence solved for a constant vertical load applied on the shaft. The lubricant considered was a mixture of synthetic polyolester oil ICI EMKARATE RL10H and refrigerant HFC R134a, from where gas release under saturation conditions. The problem increases in complexity now with a closed bearing, where fluid recirculates, and has to be solved for transient conditions, which then also required the analysis of equations for the shaft dynamics. For the lubrication equation, boundary conditions used were only the pressures at a reference fixed position and to fulfill the circular condition for the unwrapped film. The main investigation from the model perspective was in regarding to the absorption of gas under positive pressure gradients, but further assumptions of the model were also elaborated.

The main conclusions regarding the examination of the model were,

- When absorption of refrigerant occurs under thermodynamic equilibrium, then liquid only should circulate in the positive pressure region of the bearing and cavitation occurs in the divergent portion, in pretty much the same manner as previously discussed for the partial journal bearing problem. The solution again agrees with the Reynolds boundary condition under moderate and heavier loads.
- The situation is significantly different when non-equilibrium conditions are considered for the bearing, thus not allowing any absorption of gas. The presence of gas in the convergent region induces a density wedge effect in this area such that the bearing can support heavier loads with a lower eccentricity in comparison to the equilibrium case, therefore potentially reducing friction. The zero gradient conditions stated by the Reynolds condition is not as good an approximation as it is for the equilibrium case.
- However, under transient conditions the behaviour of the bearing tends to be very unstable, such that concerns with its integrity can possibly be raised. This behaviour is coherent with observations on bubbly oils in squeeze film dampers.
- The amount of gas released under cavitation is very small, such that temperature effects associated with it are negligible and the assumption of isothermal conditions of the mixture is acceptable.
- Considerations of surface tension lead to further decrease of pressure in the cavitated region, mainly as a result of the higher gas pressure, reflected in the gas density, requiring further pressure decrease to fill the divergent gap of the bearing. However higher pressures in the convergent region should also be investigated.
- Experimental results from the literature indicated that lower film pressures are observed under ventilated conditions. In the light of the results for the two-phase model, this could correspond to more difficulty for the fluid to release gas, such that metastable conditions can be present and should be investigated.

The objectives stated at the beginning of the chapter were covered, although it already appears as suggestion for future work the inclusion of surface tension effects. Additionally, more knowledge of the mixture is required to define the appropriate conditions for absorption.

Chapter 7

TWO-PHASE RINGLESS PISTON LUBRICATION

The two-phase lubrication problem is now applied to the problem with the highest degree of complexity in this work. A transient, two-dimensional solution is required to characterise the piston movement inside the cylinder in refrigeration compressors. The trajectory for the piston along the cycle is obtained and important design parameters such as power consumption and refrigerant leakage can be calculated. In this chapter a comparison against current methodologies is also made, but in this case to understand whether their assumptions are suitable for the solution of the problem.

7.1 INTRODUCTION

The clearance existing between piston and cylinder gives rise to secondary movements of the piston in addition to the main effort of pumping refrigerant through the circuit. The secondary movements have great importance on performance and reliability of the hermetic reciprocating compressor used in refrigeration, as it influences the friction power losses, the gas leakage through the clearance, wear and noise, among others. In the design of the compressor, it is acknowledged that many parameters influence piston behaviour, such that the development of a numerical tool to analyse piston dynamics would prove useful for engineering design, enabling the optimisation of the relevant parameters and ensuring smooth operation of the piston.

Currently there are models available (e.g., Fernandes, 1996), but uncertainties in their boundary conditions for the pressure equation restrict their use. Therefore, by comparing the existing models against the two-phase flow model, it should be possible to identify their suitability or inadequacy for the problem.

The use of the two-phase methodology will enable for the first time to explore the transient and in-cylinder mixture conditions for this problem, such that a new insight into the lubrication of the ringless piston used is refrigeration is expected.

For the present problem, the mixture chosen is that of refrigerant HFC-134a with a synthetic polyolester oil ICI EMKARATE RL10H, already introduced in the last chapter, and more commonly used in compressors nowadays.

7.1.1. Specific objectives

- To develop a two-phase lubrication model and apply it to the solution of the piston lubrication;
- To compare the proposed model against current methodologies;
- To investigate the gas leakage in the piston-cylinder clearance as a result of the dissolution of refrigerant in the oil.

7.2 MODEL DEVELOPMENT

7.2.1. Physical Considerations

A typical piston-cylinder assembly for hermetic reciprocating compressors is presented in figure 7.1. The piston is performing an alternative axial movement, driven by the uniform rotation of the crankshaft, together with the connecting rod. A full cycle occurs for each 360º of crankshaft movement, where $\tau=0^o$ corresponds to the position of the piston near the bottom dead centre. An offset d avoids complete alignment between cylinder axis and crankshaft centre, and this way assists the compressor during start up.

The compressor is hermetic and its environment pressure (shell pressure) is p_{suc}, which is also the pressure at the bottom of the piston. In the compression chamber, at the top of the piston, pressure is given by p_{cyl}, and corresponds to the pressure imposed to refrigerant gas during the compression cycle. This pressure varies with the crankshaft angle τ, and can be obtained experimentally or from numerical simulations of the thermodynamic cycle of the refrigerant inside the cylinder. A typical pressure field on the top of the piston as a function of the crankshaft angle is also shown in figure 7.1, along with the environment pressure p_{suc}, which will be assumed constant throughout

the cycle. In fact, due to the mechanical response of suction and discharge valves, the environment (shell) pressure also oscillates, but in negligible levels compared to p_{cyl}.

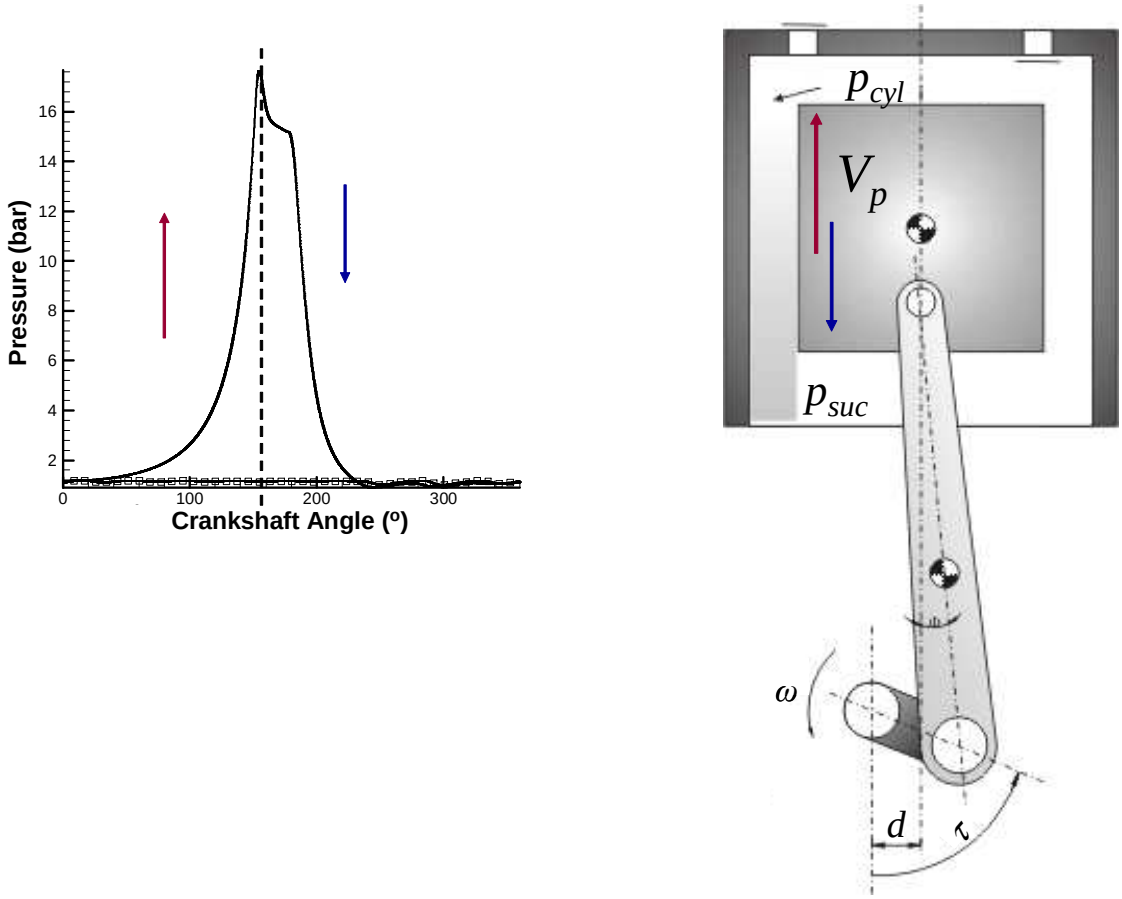

Figure 7.1. Geometry of the piston assembly in the compressor and detail of acting pressures.

A complete fluid film exists within the clearance either during the upstroke or downstroke movement. For the first, lubricant is carried to the chamber due to the piston movement. The lubricant present inside the cylinder interacts with the refrigerant being compressed. During the downstroke, the lubricant is brought out of the cylinder with the piston axial motion. Through this process refrigerant that has been dissolved into the oil escapes from the cylinder, reducing pumping efficiency. Such lubricant feeding conditions occur due to the compressor assembly, which uses a very small piston-cylinder clearance to sealing the compression chamber. Additionally, compressor operation also ensures that lubricant is abundantly splashed at cylinder walls, piston base and the wrist-pin. Furthermore, for the downstroke condition, small droplets of oil that have been also carried into the cylinder during the suction of refrigerant from the shell environment assures that fully flooded lubrication can be assumed (Fernandes, 1996).

Given the interaction between oil and refrigerant inside the hermetic compressor, refrigerant dissolution occurs and it can be released as bubbles at any time when the saturation pressure is reached. As already mentioned in chapter 6, determination of the dissolved refrigerant is difficult, and in the present work estimates will be made in intermediate conditions between the equilibrium and non-equilibrium assumptions. Also, the oil splashed at the bottom of the piston remains in contact with the pressurised refrigerant environment for long time, such that equilibrium can assumed and a mixture saturated at p_{suc} is observed.

The lubricant film responds hydrodynamically to the imbalance of the other forces acting on the piston and influences the rotation and translation of the component in its secondary motion. A convenient way to characterise the secondary movement is in the coordinate system where eccentricities at top and bottom of the piston are calculated, from which all the others can be determined if a rigid piston is assumed. Positioning of these eccentricities (e_t and e_b) is presented in figure 7.2. All the movements are assumed to occur in the plane perpendicular to the gudgeon pin axis.

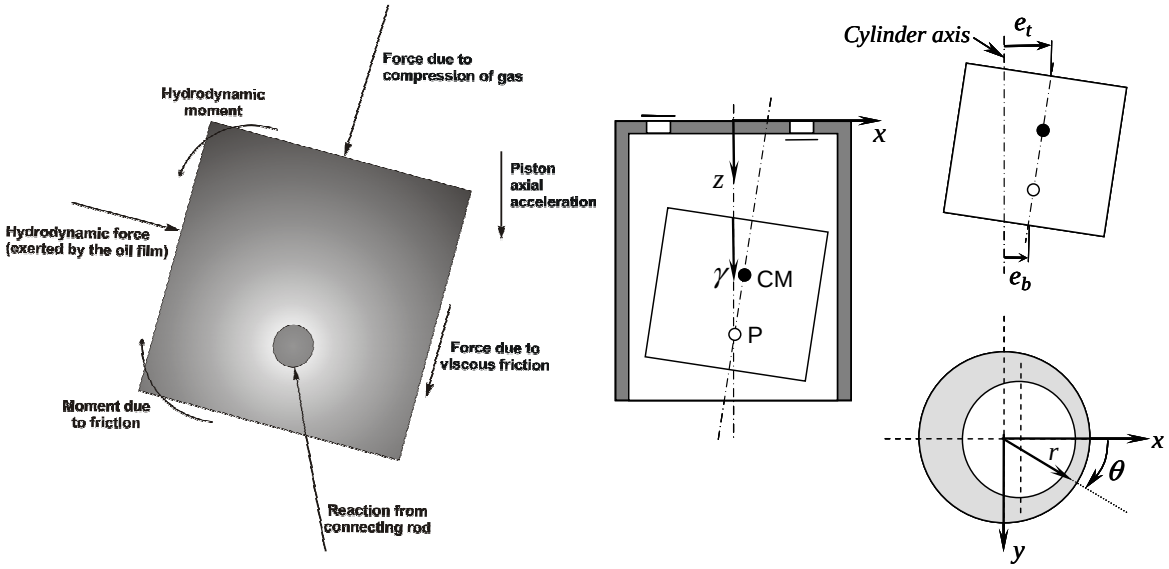

Figure 7.2. Forces acting on the piston and coordinate systems of reference to the problem

Figure 7.2 also shows the coordinate systems adopted in the solution of the problem. The balance of forces is calculated in a Cartesian system *xyz*. The vertical axis z coincides with the cylinder axis and *x* indicates the other direction of movement. Furthermore, a cylindrical system $r\theta\gamma$ positioned at the top of the piston is useful to determine hydrodynamic film pressures throughout the radial clearance. This system moves with the piston, therefore with axial velocity V_P.

Finally, the assumptions to simplify the problem are,

1. Radial clearance *c* is much smaller than piston radius:

- pressure in the radial direction can be considered constant;
- radial clearance is fully filled with lubricant;
- entrance effects are negligible;

2. Radial clearance *c* is small is comparison to piston length:

- radial accelerations are much smaller than the axial one, such that axial velocities and accelerations are the same for any point on piston surface;

3. Piston and cylinder are rigid and wear is neglected;

4. Pressure and viscous forces are dominant in the flow;

5. Isothermal flow;

6. Negligible metastability of the liquid mixture: instantaneous gas release;

In comparison to previous problems, the unidimensional conditions and constant load have been removed.

7.2.2. Mathematical Considerations

Regarding the oil-refrigerant mixture lubricating the piston, the interaction occurring inside the compression chamber has to be modelled. The overall fluid composition, w_o, varies with the piston position. When lubricant flows into the cylinder, the saturation value for the mixture is the shell pressure, p_{suc}. For the downstroke movement, w_o can be estimated from the pressure inside the cylinder. However, as the piston moves at considerable speeds, the refrigerant may not be able to dissolve to its maximum in the oil, and the precise value is not known. As previously described in chapter 6, by making use of a potential equation, it can be estimated as,

$$w = w_r + \kappa \cdot \Delta t \cdot \left(w_{sat} - w_r \right) \tag{6.4}$$

where κ is the absorption/release coefficient and Δt the time step considered, w and w_r mass fraction in two consecutive time steps for a given position.

For the lubricant film thickness, the convenient coordinates $r\theta\gamma$ enable to write,

$$h = c\left(1 - \varepsilon \cos\theta\right) \tag{7.1}$$

where c is the piston-cylinder clearance and ε the eccentricity at any given position.

Additionally, given the rigid piston shape, the eccentricity can always be related to that for top and bottom of the piston, resulting,

$$h = c\left[1 - \left(\varepsilon_t - \frac{\xi R}{L}\left(\varepsilon_t - \varepsilon_b\right)\right)\cos\theta\right] \tag{7.2}$$

where ε_t and ε_b are the dimensionless eccentricities for top and bottom respectively, R and L dimensions of the piston, and the ξ=z/R for convenience.

For the geometry considered, and assuming that the translational velocity of the piston V_P is much greater than the radial components, Reynolds equation (3.29) is simplified to,

$$\frac{\partial}{\partial\theta}\left(\frac{\overline{\rho}h^3}{12\overline{\mu}R^2}\frac{\partial p}{\partial\theta}\right) + \frac{\partial}{\partial\xi}\left(\frac{\overline{\rho}h^3}{12\overline{\mu}R^2}\frac{\partial p}{\partial\xi}\right) = \frac{V_P}{2R}\frac{\partial(\overline{\rho}h)}{\partial\xi} - \frac{\partial(\overline{\rho}h)}{\partial t} \tag{7.3}$$

where the following boundary conditions apply,

$$\begin{aligned} &\xi = 0 \rightarrow p = p_{cyl} \\ &\xi = \frac{R}{L} \rightarrow p = p_{suc} \\ &p(\theta = 0) = p(\theta = 2\pi) \end{aligned} \tag{7.4}$$

where no intermediate boundary conditions are required for the cavitation of the film as it is automatically determined from the release of gas. In conventional single-phase methodologies, these boundary conditions are also respected, but additional assumptions on the behaviour of pressure for intermediate positions are required.

When determining the pressure field across the lubricant film, at the same time the balance of forces and moments in the piston must be satisfied. The main forces acting on the piston are the gas force, the connecting rod force, inertia effects, friction force and the hydrodynamic force due to the lubricant film. Friction and hydrodynamic forces can also produce momentum around the wrist-pin, as seen in figure 7.2. The balance of forces is then written as,

$$\sum F_z = F_g + F_f + F_{rz} = mA_P \tag{7.5}$$

$$\sum F_x = F_h + F_{rx} = mc\omega^2\left(\ddot{\varepsilon}_t - z_{CM}\frac{\ddot{\varepsilon}_t - \ddot{\varepsilon}_b}{L}\right) \tag{7.6}$$

$$\sum M_{pin} = M_h + M_f = I_P c\omega^2 \frac{\ddot{\varepsilon}_t - \ddot{\varepsilon}_b}{L} \tag{7.7}$$

with forces and moments acting on the piston related to lubricant film hydrodynamic force and viscous friction.

For the hydrodynamic efforts,

$$F_h = -\int_0^L \int_0^{2\pi} p(\theta,\xi) R^2 \cos\theta d\theta d\xi \tag{7.8}$$

$$M_h = -\int_0^L \int_0^{2\pi} p(\theta,\xi)(z_P - R\xi) R^2 \cos\theta d\theta d\xi \tag{7.9}$$

and for the friction forces and moments,

$$F_f = -\int_0^L \int_0^{2\pi} \left(\frac{h}{2R}\frac{\partial p}{\partial \xi} + \mu \frac{V_P}{h} \right) R^2 d\theta d\xi \tag{7.10}$$

$$M_f = -\int_0^L \int_0^{2\pi} \left(\frac{h}{2R}\frac{\partial p}{\partial \xi} + \mu \frac{V_P}{h} \right) R^3 \cos\theta d\theta d\xi \tag{7.11}$$

As the pressure for cylinder and suction are given, the force of gas is calculated,

$$F_g = \pi R^2 \left(p_{cyl} - p_{suc} \right) \tag{7.12}$$

The balance of forces in the connecting rod and reactions in the crankshaft are also required. They are determined analytically from the geometrical relationships of the system. Details of those manipulations can found in Prata et al. (2000), together with derivations for piston velocity and acceleration.

In the present formulation, it was assumed a rigid and aligned movement in the *y*-direction. In addition to depend of the connecting rod bending and the inclination of the main shaft supported by the journal bearings (figure 2.11), assembly clearances and misalignments are also very important and should be included. Couto (2006) discusses the modelling in which such direction can be appropriately considered, i.e., one in which solution for the several components of the compressor lubricating system are solved simultaneously and where the different boundary conditions are coupled, such that, among others, the transversal movement (*y*) of the piston can be characterised.

The solution of the problem consists in resolving simultaneously equations (7.3), (7.6) and (7.7), therefore determining pressure and piston dynamics for a given crankshaft angle τ. A solution procedure to solve this problem is required, as presented in the section 7.2.3.

7.2.3. Numerical Methodology

Equation (7.3) is discretised as indicated in section 3.3, but for control volumes indicated in figure 7.3, which differs from the general deduction due to the circular conditions in the vertical corners,

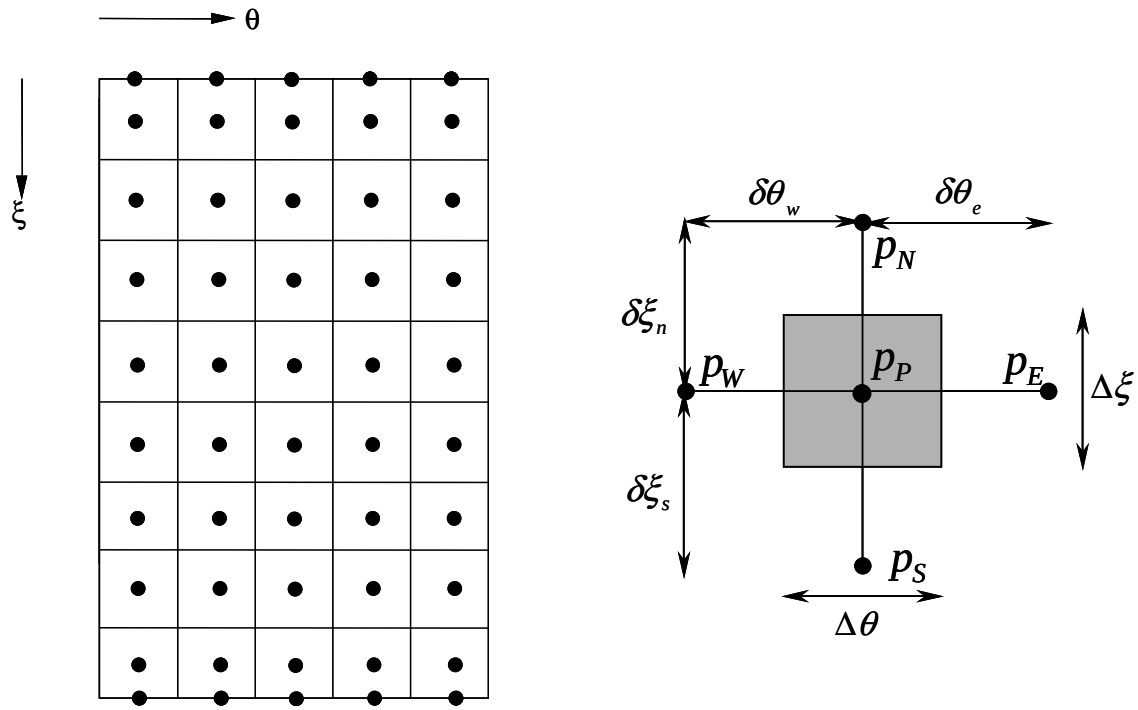

Figure 7.3. Discretised domain for the piston-cylinder lubricant film.

Therefore,

$$\int_s^n \int_w^e \frac{\partial}{\partial\theta}\left(\frac{\overline{\rho}h^3}{12\overline{\mu}R^2}\frac{\partial p}{\partial\theta}\right)d\theta d\xi + \int_s^n \int_w^e \frac{\partial}{\partial\xi}\left(\frac{\overline{\rho}h^3}{12\overline{\mu}R^2}\frac{\partial p}{\partial\xi}\right)d\theta d\xi = \tag{7.13}$$

$$= \int_s^n \int_w^e \left[\frac{V_P}{2R}\frac{\partial(\overline{\rho}h)}{\partial\xi} - \frac{\partial(\overline{\rho}h)}{\partial t}\right]d\theta d\xi$$

resulting in equation (7.14) as follows,

$$A_p p_P = A_e p_E + A_w p_W + A_n p_N + A_s p_S + S \tag{7.14}$$

where,

$$A_e = \frac{\overline{\rho}_e h_e^3}{\overline{\mu}_e}\frac{\Delta\xi}{\delta\theta_e} \qquad A_w = \frac{\overline{\rho}_w h_w^3}{\overline{\mu}_w}\frac{\Delta\xi}{\delta\theta_w}$$

$$A_n = \frac{\overline{\rho}_n h_n^3}{\overline{\mu}_n}\frac{\Delta\theta}{\delta\xi_n} \qquad A_s = \frac{\overline{\rho}_s h_s^3}{\overline{\mu}_s}\frac{\Delta\theta}{\delta\xi_s}$$

$$A_p = A_e + A_w + A_n + A_s$$

$$S = -12\left[\frac{V_P \Delta\theta}{2R}\left(\overline{\rho}_N h_n - \overline{\rho}_P h_s\right) - \left.\frac{\Delta(\overline{\rho}h)}{\Delta t}\right|_P \Delta\theta\Delta\xi\right]$$

As one equation is obtained for each internal point, a linear system comprising the set of algebraic equation is obtained, which can be organised into a linear system and solved by a variety of methods, directly on interatively; in this methodology it is solved by the TDMA algorithm (Patankar, 1980). When the linear system is solved, pressure values for the discrete points are determined.

Additionally, piston velocities for the secondary movement must be determined; these velocities are implicit in the time derivative of $\overline{\rho}h$ in equation (7.14). To this end, Fernandes (1996) used a Newton-Raphson iterative procedure to solve differential equations (7.6) and (7.7), which is explained as follows.

For a dimensionless time $\tau + \Delta\tau$, departing from an estimated value for velocities, dynamics equations can be written as,

$$R_1\left(\dot{\varepsilon}_t, \dot{\varepsilon}_b\right) = F_h\left(\dot{\varepsilon}_t, \dot{\varepsilon}_b\right)^{\tau+\Delta\tau} - F_r\left(\dot{\varepsilon}_t, \dot{\varepsilon}_b\right)^{\tau+\Delta\tau} - mc\omega^2\left(\ddot{\varepsilon}_t^{\tau+\Delta\tau} - z_{CM}\frac{\ddot{\varepsilon}_t^{\tau+\Delta\tau} - \ddot{\varepsilon}_b^{\tau+\Delta\tau}}{L}\right) \tag{7.15}$$

$$R_2\left(\dot{\varepsilon}_t, \dot{\varepsilon}_b\right) = M_h\left(\dot{\varepsilon}_t, \dot{\varepsilon}_b\right)^{\tau+\Delta\tau} + M_f\left(\dot{\varepsilon}_t, \dot{\varepsilon}_b\right)^{\tau+\Delta\tau} - I_P c\omega^2\left(\frac{\ddot{\varepsilon}_t^{\tau+\Delta\tau} - \ddot{\varepsilon}_b^{\tau+\Delta\tau}}{L}\right) \tag{7.16}$$

where R_1 and R_2 are residuals that must be brought to zero in the converged solution; F_h, M_x and M_f are obtained by numerical integration.

Accelerations are numerically calculated by,

$$\ddot{\varepsilon}_t^{\tau+\Delta\tau} = \frac{\dot{\varepsilon}_t^{\tau+\Delta\tau} - \dot{\varepsilon}_t^{\tau}}{\Delta\tau} \tag{7.17}$$

$$\ddot{\varepsilon}_b^{\tau+\Delta\tau} = \frac{\dot{\varepsilon}_b^{\tau+\Delta\tau} - \dot{\varepsilon}_b^{\tau}}{\Delta\tau} \tag{7.18}$$

In the Newton-Raphson method, increments $\Delta\dot{\varepsilon}_t$ and $\Delta\dot{\varepsilon}_b$ must be found so that residuals are brought to zero. Therefore,

$$\begin{bmatrix} R_1 \\ R_2 \end{bmatrix} = \begin{bmatrix} \frac{\partial R_1}{\partial \dot{\varepsilon}_t} & \frac{\partial R_1}{\partial \dot{\varepsilon}_b} \\ \frac{\partial R_2}{\partial \dot{\varepsilon}_t} & \frac{\partial R_1}{\partial \dot{\varepsilon}_b} \end{bmatrix} \begin{bmatrix} \Delta\dot{\varepsilon}_t \\ \Delta\dot{\varepsilon}_b \end{bmatrix} \tag{7.19}$$

where the derivatives appearing in the linear system are numerically calculated.

$$\frac{\partial R_n}{\partial \dot{\varepsilon}_i} = \frac{R_n\left(\dot{\varepsilon}_i - \delta\dot{\varepsilon}_i, \dot{\varepsilon}_j\right) - R_n\left(\dot{\varepsilon}_i, \dot{\varepsilon}_j\right)}{\delta\dot{\varepsilon}_i}, \qquad n=1,\ 2 \text{ and } i, j=t,\ b \tag{7.20}$$

The pressure field needs to be solved again to the increment δ, and in the sequence forces and moments are calculated to obtain the derivatives for numerical residuals. This procedure then requires considerable computational effort.

After residuals are solved, velocities of the secondary motion can be determined. In a similar manner to the full journal bearing problem, acceleration and position can be derived, for the top of the piston as well as for the bottom, according to equations (7.21) and (7.22),

$$\varepsilon_t^{\tau+\Delta\tau} = \varepsilon_t^{\tau} + \dot{\varepsilon}_t^{\tau+\Delta\tau} \cdot \Delta\tau \text{ and } \varepsilon_b^{\tau+\Delta\tau} = \varepsilon_b^{\tau} + \dot{\varepsilon}_b^{\tau+\Delta\tau} \cdot \Delta\tau \tag{7.21}$$

and for accelerations,

$$\ddot{\varepsilon}_t^{\tau+\Delta\tau} = \frac{\dot{\varepsilon}_t^{\tau+\Delta\tau} - \dot{\varepsilon}_t^{\tau}}{\Delta\tau} \text{ and } \ddot{\varepsilon}_b^{\tau+\Delta\tau} = \frac{\dot{\varepsilon}_b^{\tau+\Delta\tau} - \dot{\varepsilon}_b^{\tau}}{\Delta\tau} \tag{7.22}$$

Using these values, time is advanced in a time step to $\tau+\Delta\tau$ and an iterative process is used to search for the correct values for radial velocities that satisfy the balance of forces. For the initial step, the system departs from defined initial conditions,

$$\varepsilon_t^0, \varepsilon_b^0, \dot{\varepsilon}_t^0, \text{and } \dot{\varepsilon}_b^0 \text{ for } \tau = 0 \tag{7.23}$$

The solution methodology is illustrated according to figure 7.4,

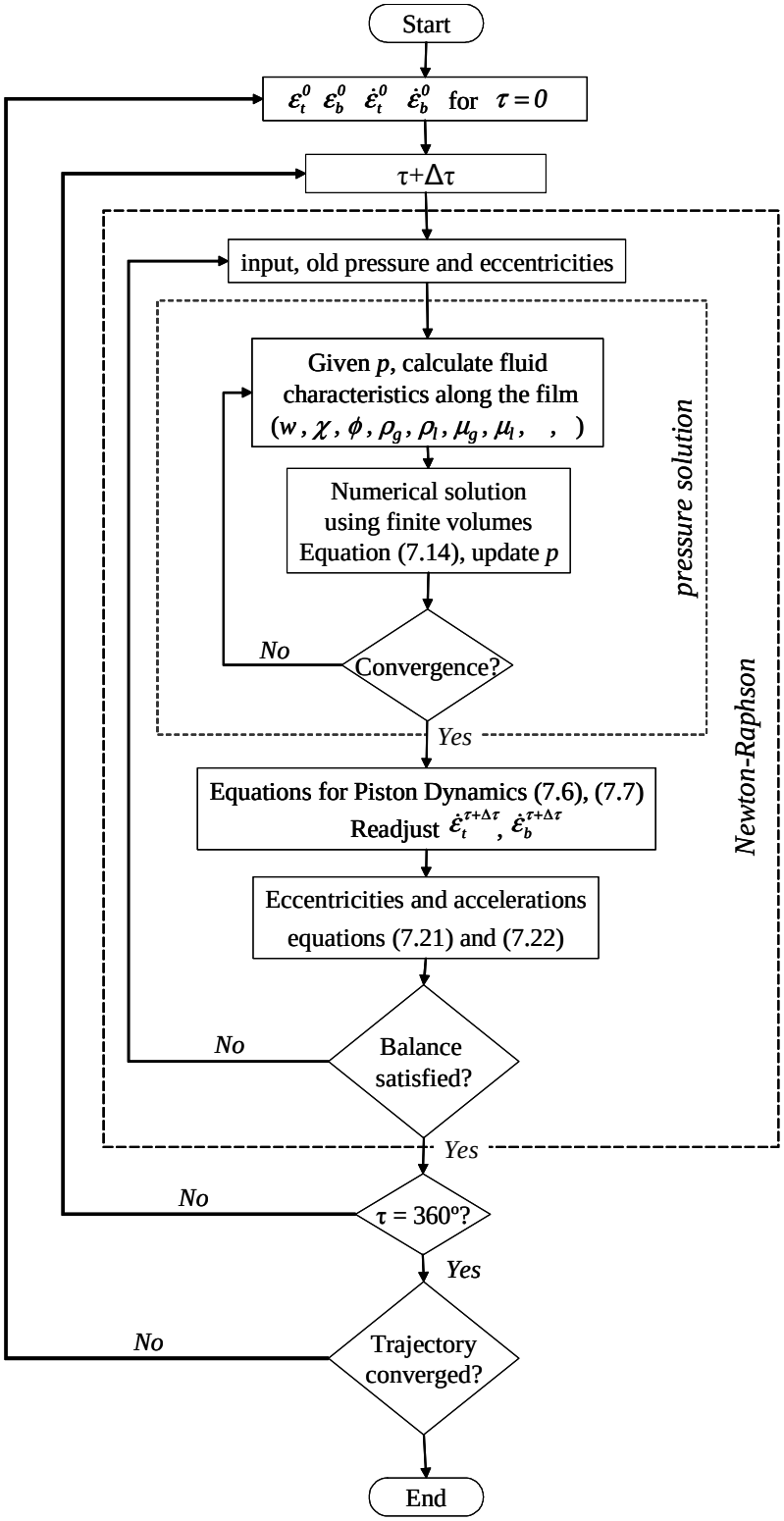

Figure 7.4. Solution procedure for the transient journal bearing problem.

7.3 RESULTS AND DISCUSSION

The proposed methodology has been used to simulate dynamics for a pre-defined piston-cylinder system, assumed running with the combination of fluids HFC R134a and polyolester oil EMKARATE RL10H. For simplicity, the lubricant is assumed to be at constant temperature. Relevant compressor data required for the simulation is presented in Table 7.1, as well as the parameters defined for the numerical simulation.

Table 7.1. Geometry and numerical data used in the simulations for the piston-cylinder clearance

	Parameter	Value
Geometry	R (mm)	10.5
	L (mm)	21.0
	c (μm)	5.0
	z_P (mm)	12.08
	z_{CM} (mm)	9.53
	C_{BP} (mm)	25.54
	C_{MP} (mm)	36.47
	d (mm)	2.0
	ω (rad/s)	370
	m (g)	34.6
	m_b (g)	24.2
	I_P (kg·m^2)	$0.287 \cdot 10^{-5}$
	p_{suc} (kPa)	238.50
	T (ºC)	60
Numerical	Mesh (θ, ξ)	18x30
	$\Delta\tau$ (º)	5
	Tolerance (p)	$1 \cdot 10^{-6}$
	Tolerance (ε_i)	$1 \cdot 10^{-4}$

Additionally, pressure in the cylinder as a function of the crankshaft angle is given by the compressor manufacturer (Ussyk, 1984), and is plotted in figure 7.5.

Regarding the absorption of refrigerant in the oil, equation (6.4), two different absorption conditions were tested: the first simulated a low absorption

condition ($\kappa \cdot \Delta t = 0.05$), while the second ($\kappa \cdot \Delta t = 0.50$) indicates easy dissolution of the refrigerant in the oil even at fast transients (the time step was fixed during simulations). The latter dissolves twice as much refrigerant as the former, which indicates a lower viscosity of the lubricant in such conditions, as well as a higher potential to release gas under negative pressure gradients, related to a higher saturation pressure. However, at lower coefficient of absorption refrigerant dissolves for a longer time. The behaviour of the refrigerant dissolution in the oil for the two mixtures is plotted in figure 7.6. There it can be noted that the values are just attributed to the lubricant film in the clearance when the piston starts descending.

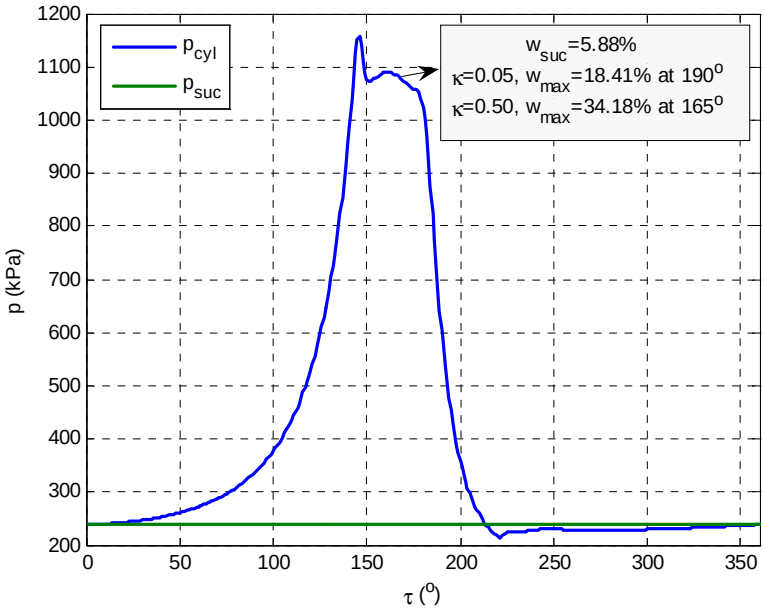

Figure 7.5. Pressure in the cylinder and mixture conditions along the cycle.

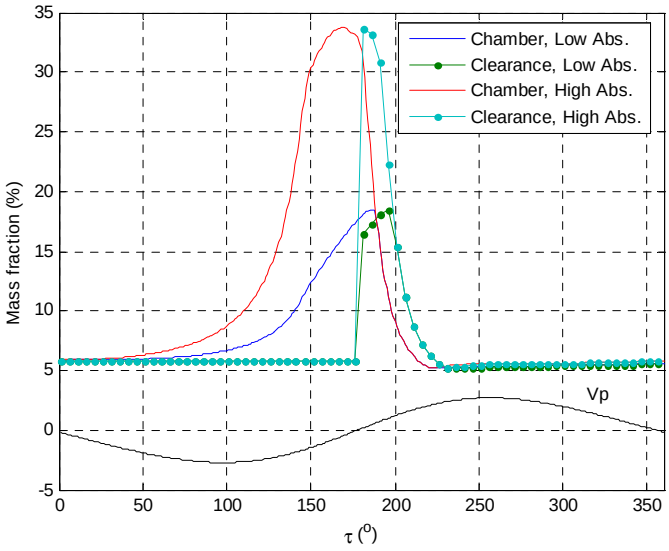

Figure 7.6. Transient mixture conditions in the cylinder and in the clearance.

As indicated in the objectives, the results for the two-phase model are compared to those obtained using classical methodologies, for a single-phase fluid. Different cavitation criteria are used, as indicated in table 7.2 along with the test conditions for the two-phase model.

Table 7.2. Different boundary conditions explored

Fluid	Case	Cavitation criterion	μ (mPa.s)
Oil	Oil NCav	None (Sommerfeld)	4.9481
	Oil Cav	Linear between p_{cyl} and p_{suc}	
	Oil Cav_{min}	Constant, minimum between p_{cyl} and p_{suc}	
Oil and Refrigerant saturated at p_{suc}	OR NCav	None (Sommerfeld)	4.2514
	OR Cav	Linear variation between p_{cyl} and p_{suc}	
	OR Cav_{min}	Constant, minimum between p_{cyl} and p_{suc}	
Oil and refrigerant Two-phase	$2p_{05}$	Automatically determined from w_{sat}	Variable
	$2p_{05}$		

The three different cavitation criteria are graphically indicated in figure 7.7, and can be briefly described as follows,

- *NCav*: in this case, no cavitation pressure is assumed, i.e., the pressure is always that determined by the solution of the linear system. This criterion in nothing else than the Sommerfeld condition;
- *Cav:* the cavitation pressure is assumed to vary linearly along the length of the piston, starting from the cylinder pressure at the top (p_{cyl}) and reaching the shell pressure at the bottom of the piston (p_{suc}). Whenever the pressure calculated from a given position is less than the cavitation pressure at that position, the former value is replaced by the latter;

- *Cavmin:* the minimum value between cylinder and shell pressures is considered as a constant value for the cavitation pressure. When the value calculated is smaller that this minimum value, it is updated to the cavitation pressure;

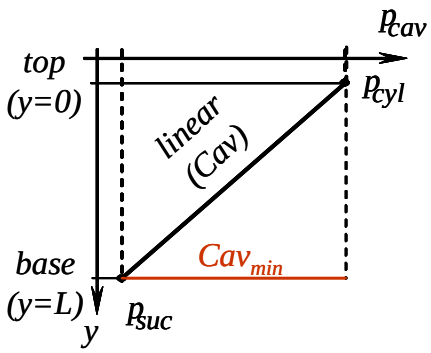

Figure 7.7. Illustrative indication of the defined cavitation conditions.

Figure 7.8 presents the eccentricity for the top and bottom of the piston as a function of the crankshaft angle. The cavitation criteria adopted showed to be crucial in determining the trajectory. Higher eccentricities are observed when cavitation is not considered, while the top of the piston moves closer to the cylinder axis when cavitation criteria are adopted. The two-phase model results were similar to those neglecting cavitation. An increase in the eccentricity at the top is observed for the mixture absorbing a less amount of refrigerant (OR $2p_{05}$). It can also be noticed a greater amplitude of the movements for the results where cavitation criteria were adopted, indicating additional effort from the piston to balance the forces along the cycle. Along with the more inclined condition in which the piston moves, a hydrodynamic wedge effect is expected in order to balance the forces. On the other hand, the two-phase model has predicted a more stable motion, as also observed for the non-cavitated solution. An interesting result is that the difference between the single phase solution using the viscosity of the oil (Oil) and that for the oil-refrigerant (OR) showed not significant. It seems that, given the higher friction for the oil, a slightly stronger conrod reaction occurs, but this is duly compensated due to the higher hydrodynamic force that the oil film gives in comparison to the oil-refrigerant mixture of lower viscosity (figure 7.10). Therefore, and to improve clarity in the figures, the analysis will be limited hereafter to oil only, leaving the single phase OR behind.

The behaviour of the piston is explained if figure 7.8 and 7.9 are analysed simultaneously. Greater amplitude of the movements is seen for the results where the cavitation criteria were adopted, indicating additional effort from the piston to balance

the forces along the cycle due to lack of sustentation. Along with the more inclined condition in which the piston moves, a hydrodynamic wedge effect is expected in order to balance the forces. On the other hand, the two-phase model has predicted a more stable motion, as well as the non-cavitated solution. For the piston lubricated with the less absorbent mixture, inclination slightly increases at the top dead centre region.

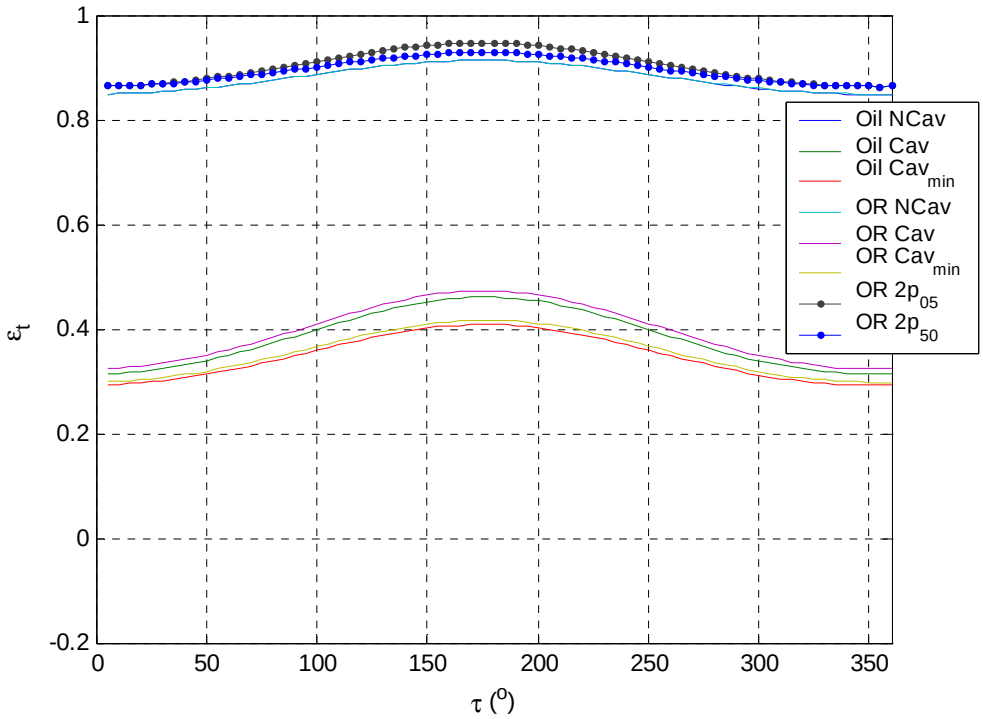

Figure 7.8. Eccentricities at the top of the piston.

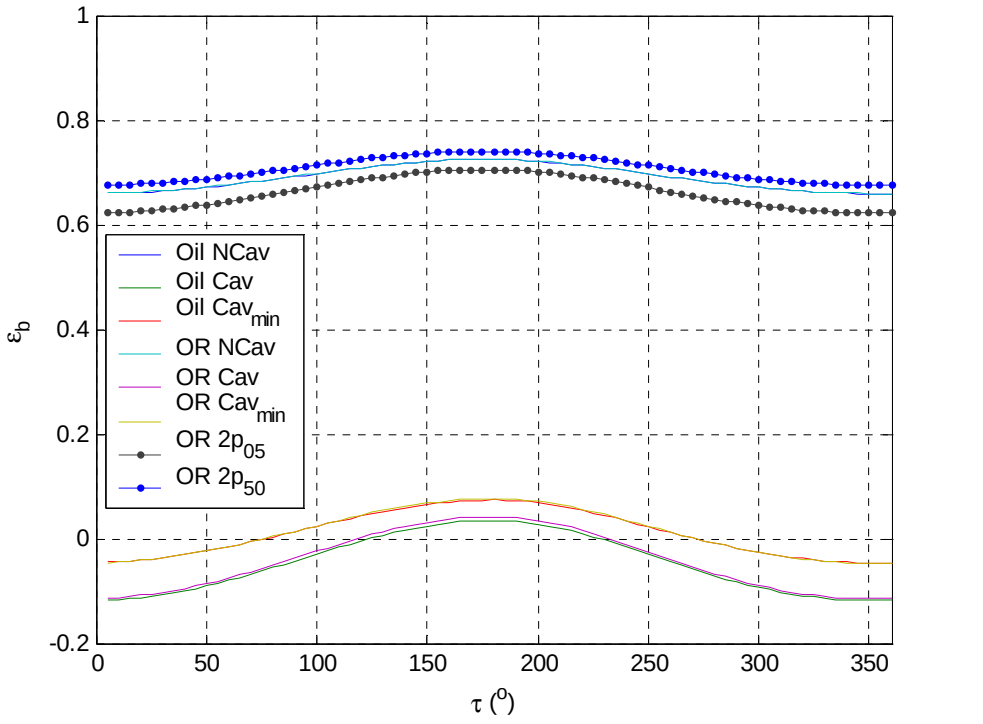

Figure 7.9. Eccentricities at the bottom of the piston.

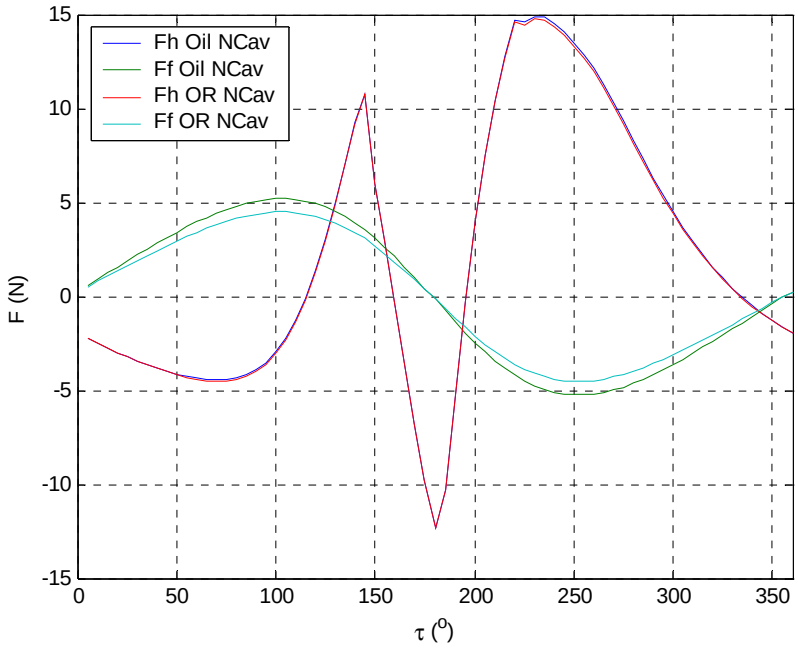

Figure 7.10. Hydrodynamic and friction force for the non-cavitated case, oil and oil-refrigerant.

To evaluate deeper the differences in eccentricity, an analysis of pressure profiles along the piston trajectory was made. The behaviour for the two-phase mixture is also characterised by plotting void fraction as well. In figure 7.11, the profiles for circumferential positions $\theta=10^o$ and $\theta=190^o$ positions are presented for a crankshaft angle $\tau=120^o$. Such circumferential positions are chosen among the discretised points for being the closest to thrust and anti-thrust surfaces of the piston, respectively. At this time, the piston is moving upwards. Due to the high axial velocity, a significant wedge effect develops in the anti-thrust surface of piston, and hydrodynamic forces acts pushing the piston against the wall at $\theta=10^o$.

The two-phase flow model presents limited difference in this region, as the lubricant flows against a positive pressure gradient. Therefore, no release of gas takes place in the upward movement of the piston, as seen in figure 7.12.

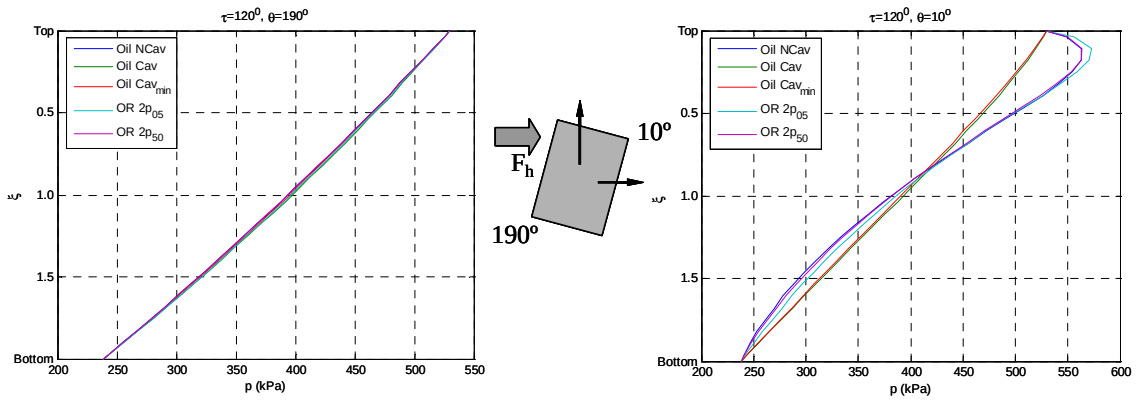

Figure 7.11. Pressures for two opposite sides of the piston at $\tau=120^o$

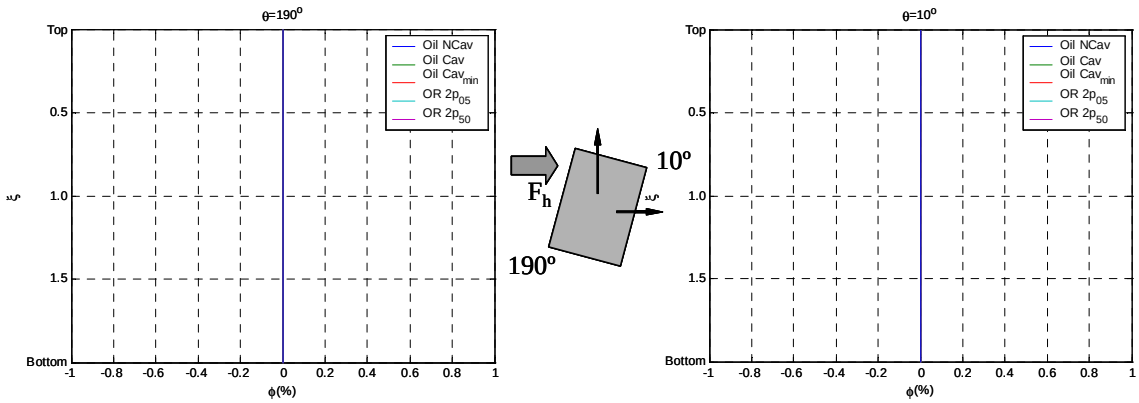

Figure 7.12. Null void fraction for both sides of the piston at $\tau=120^o$

A different picture is seen for the piston returning to the bottom dead centre. Initially a negative pressure gradient develops and a divergent gap exists for the flow along the minimum film thickness region ($\theta= 0^o$). Such a situation can be seen in figure 7.13, for a crankshaft angle of 240^o. The squeeze film compensates the decreasing pressure in the left hand side of the bearing. On the other side, the squeeze film overcomes the positive pressure effects and, as the fluid reaches the divergent region, pressure decreases and refrigerant is released from the oil, triggering a two-phase flow where, to accommodate changes in geometry, further expansion of the gas occurs. As the shell pressure at the bottom of the piston is communicated, pressure recovery also takes place. The effect of gas expansion is clear when comparing the results with those for a non-cavitated condition. On the other hand, when a cavitation criterion is applied, the behaviour is exactly the opposite. The low pressures cause the rupture of the film, and a squeeze film effect provokes increase in pressure at θ=190º, eventually resulting in the same effect on the piston.

On figure 7.14, the release of gas can be seen on the right hand side of the bearing, while the left hand side remains as a full film.

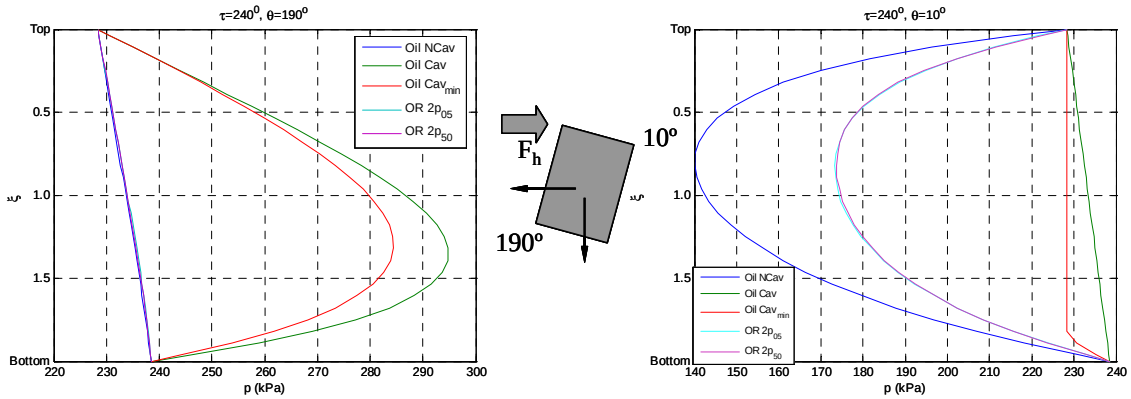

Figure 7.13. Pressures for two opposite sides of the piston at $\tau=240^o$

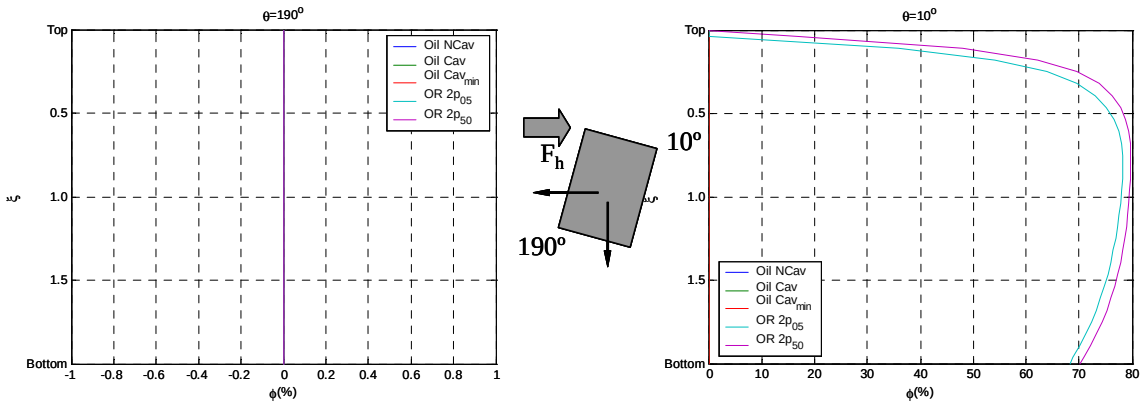

Figure 7.14. Void fraction for both sides of the piston at $\tau=240^o$

As an important parameter for piston design, power consumption was also determined. After calculating the friction force using equation (7.24), power loss can be calculated as,

$$Pot = F_f \cdot V_P \tag{7.24}$$

Values are presented in figure 7.15, where it can be observed that lower values are obtained when cavitation is numerically enforced, as the cavitated points are as usual removed from calculation (negligible shear stress). Here, viscosity plays a major role and when the oil-refrigerant is considered as the lubricant, lower values are obtained. Results for the two-phase flow model are closer to that for the oil-refrigerant lubricant when cavitation is neglected, although slightly higher. This results from the increase in the lubricant viscosity when gas is released from the lubricant - despite the presence of lower viscosity gas, the liquid mixture is now richer in oil, whose effect is dominant for the two-phase viscosity. Minimal differences occur for the different mixture conditions, with higher friction for the mixture with more refrigerant dissolved.

Table 7.3. Cycle averaged values for power consumption due to viscous friction

Case	*Pot* (W)
Oil NCav	6.904
Oil Cav	4.249
Oil Cav_{min}	4.240
OR NCav	5.941
OR Cav	3.663
OR Cav_{min}	3.652
$2p_{05}$	5.960
$2p_{50}$	6.189

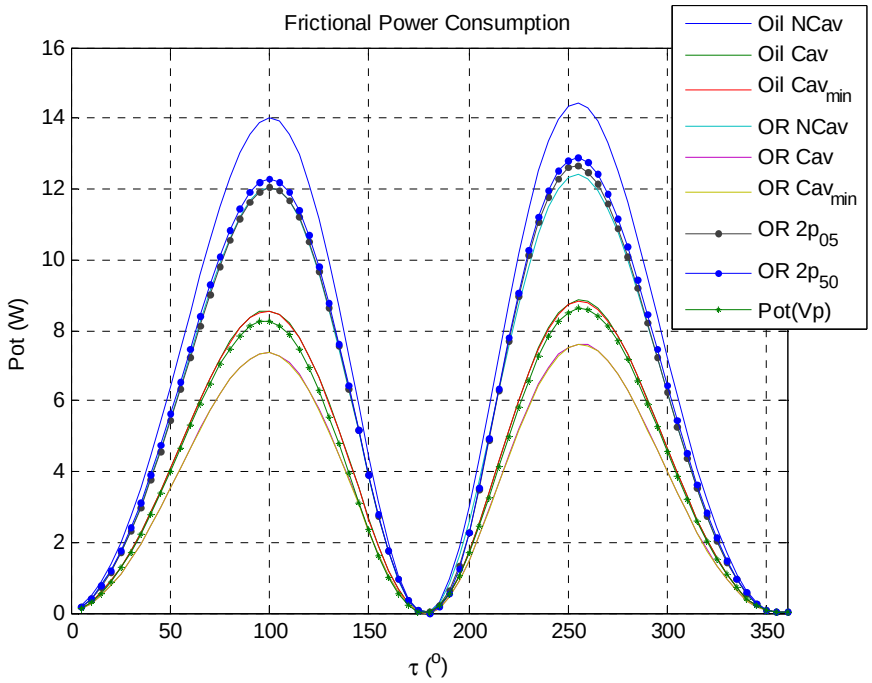

Figure 7.15. Power consumption due to viscous friction as a function of the crankshaft angle.

Another contribution expected from this work is to estimate the leakage of refrigerant flowing with the oil through the piston skirt, which can be estimated the pressure profile determined. At the bottom of the piston, it is calculated as,

$$q_{bottom} = \int_0^{2\pi} \left(-\frac{h^3}{12\bar{\mu}R}\frac{\partial p}{\partial \xi} + V_P \frac{h}{2} \right)\Bigg|_{z=L} Rd\theta \qquad (7.25)$$

Figure 7.16 presents results for flow rate. The main effect has been proved to be the piston axial movement (*qVp*), with only small differences between the cases, which indicates the sealing capacity promoted by the small clearance. This value is significant for any of the single phase simulations.

However, an opportunity arises to estimate the leakage of refrigerant as gas from the two-phase model, estimating such leakage from equation (3.18) with the void fraction of the liquid-gas lubricant leaving the piston skirt. Refrigerant flow starts a little before *180º*, when the piston changes direction; the presence of gas naturally increases the volumetric flow rate. The release of gas can also be concluded from figure 7.17, where the void fraction for the lubricant mixture is plotted. Additional refinements will be required as the Poiseuille term is conceivably important for that region. Nevertheless, it can be seen that maximum leakage occurs for the lowest piston velocities, as no resistence is imposed against the pressure gradient and the mixture

presents a high mass fraction. Thereafter, gas leakage gradually reduces as pressures in the cylinder start to decrease, reducing the amount of refrigerant dissolved.

Surprisingly, the mixture with a lower mass fraction presents a higher leakage than the one capable of absorbing more refrigerant, as can be seen in the detail in figure 7.16. While the mixture with a higher coefficient of absorption has too much refrigerant dissolved from the start and refrigerant is released as soon as cylinder pressure decreases. On the other hand, the mixture with lower coefficient of absorption can still absorb refrigerant; despite pressure drop, levels are high and the refrigerant remains dissolving in the oil, therefore being carried out of the compression chamber – this situation was already observed in figure 7.6.

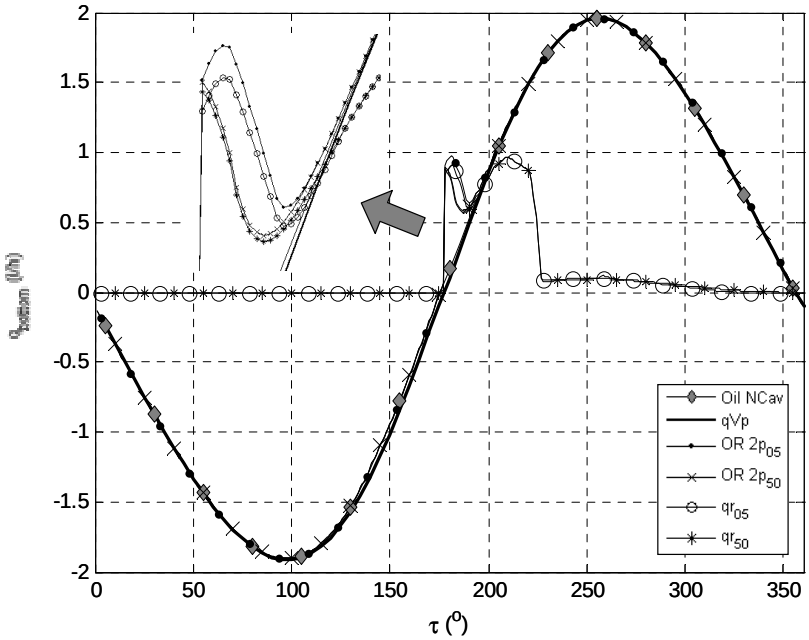

Figure 7.16. Volumetric flow rate and participation of gas refrigerant for each two-phase case

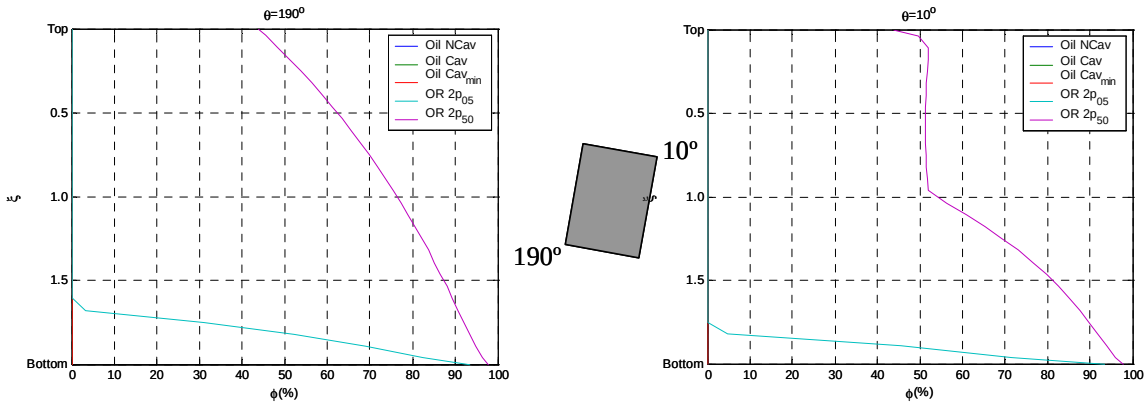

Figure 7.17. Void fraction for both sides of the piston at *τ=180º*

It should be stressed that the results intend to show the prediction capability of the model, although significant advances are required to the precise determination of the oil-refrigerant mixture inside the cylinder, thereby improving the understanding of the refrigerant release during suction.

7.4 SUMMARY

The final case studied in this work was the target problem of the ringless piston lubrication. This is to date the first attempt of using variables properties in the liquid film lubrication for the problem, and it could be seen that release of gas indeed occurs during the alternative movement of the piston inside the cylinder. The lubricant mixture of synthetic polyolester oil ICI EMKARATE RL10H and refrigerant HFC R134a was used, and due to the dissolution of refrigerant properties vary and release can occur under saturation conditions. The main conclusions are,

- The two-phase model presented a good agreement in comparison to solution where cavitation is not considered, and significant discrepancy was shown against the solutions using cavitation boundary conditions for the piston. Therefore, the controversy regarding the use of cavitation conditions is highlighted.
- The models using cavitation also calculate much lower values for viscous friction, while agreement is observed between the two-phase model and non-cavitated solutions for single-phase oil-refrigerant. Using oil as the lubricant would lead to exaggerated values.
- The two-phase model was used to estimate the amount of refrigerant leaking as it flows with the oil through the clearance. Results showed that the occurrence of this is more likely at the TDC, when the pressure is high and the piston is changing direction.
- The influence of the coefficient of absorption has not proven very significant in the simulations performed, although a surprising result indicated that a mixture with lower rate of absorption can potentially lead to more gas leakage from the cylinder. Nevertheless, further study is essential to better quantify the absorption of refrigerant in the quick transients of operation.

Chapter 8

CONCLUSIONS

8.1 OVERVIEW

The present work has proposed an alternative numerical model to simulate hydrodynamic lubrication, using a homogeneous two-phase model. This has been used to solve both full-film and cavitated regions using Reynolds equation, avoiding the use of intermediate boundary conditions.

The lubricant is considered a mixture in which refrigerant is dissolved in an oil, usually provided to the components in the liquid phase. However, due to the gradients experienced throughout the flow, the mixture can release gas when saturation conditions are reached. The liquid mixture can potentially reabsorb gas when positive pressure gradients are encountered, but the treatment of absorption requires further consideration.

The flow of gas and liquid is treated by a homogeneous model, which considers good mixing and the same velocity for both phases. In addition to that, non-Newtonian effects are neglected, such that a pseudofluid is used as an alternative to the two existing phases. Its properties are conveniently defined based on averages of the liquid and gas phases. Each phase has its properties calculated by empirical correlations, thus defining characteristics of the liquid (oil and refrigerant), gas (refrigerant only), and also defining the solubility of the refrigerant in the oil.

The pseudofluid is used in Reynolds equation, discretised and solved using the finite volume methodology. Despite considering the problem to be isothermal, properties still vary as a function of pressure. This requires an iterative process for the solution of pressure, updating values for density and viscosity in each iterative step.

Initially the model was used to study a steadily loaded infinite partial journal bearing, where conditions at both inlet and exit are known. By starting from a simpler geometry, the model can be numerically adjusted and its functioning explored, investigating from aspects such as the lubrication behaviour through a varied range of

geometries to a thorough analysis of the influence of both operation and fluid parameters in the lubricated component.

The geometries analysed have complexity increased gradually, and a full journal bearing is evaluated after the partial bearing. The main purpose of this investigation was to improve understanding on the reabsorption of gas in the bearing when positive pressure gradients are experienced. The two extreme thermodynamic conditions are explored. The situation where instantaneous absorption is allowed and the extreme where no gas can be readmitted in the liquid showed a significant difference in lubrication behaviour. The behaviour of the mixture under non-equilibrium conditions requires the problem to be always solved for transient conditions.

The final problem considered was the ringless piston lubrication in alternative movement inside a refrigeration compressor. Transient loads were now considered that depend on the operation of the compressor. Transient conditions are also considered for the lubricant mixture fed to the piston-cylinder clearance, which can also be related to the leakage of gas from the cylinder. The two-phase methodology here was compared against current proposals to solve the piston movement, either considering pure oil lubrication as well as lubricant such as the oil and refrigerant mixture.

8.2 MAIN FINDINGS

- The two-phase model can identify automatically three regions of distinct behaviour in the lubricated component: *the positive pressure region*, in the convergent area, where very high pressures are usually observed, and where liquid is the dominant phase; *the cavitated region*, usually in the divergent portion of the component, where release and expansion of gas occurs and the pressures are below ambient; and *the pressure recovery region*, where back pressures are communicated to the fluid and the release of gas is interrupted, resulting in a positive pressure gradient and the reduction of the mean velocity of the flow, which still presents two-phases;
- For liquid only present in the convergent pressure region, the model has a very similar behaviour to that predicted by the solution using Reynolds boundary

conditions. In this region, viscosity is the most important. The mixture presents higher viscosities at lower pressures, temperatures and mass fractions, and under these conditions it will enable the achievement of higher pressures. In addition, the reduction of clearance and the increase in velocity or eccentricity also produce higher pressures;

- In the cavitated region, geometric influence occurs only due to eccentricity. Furthermore, viscosity is not the most important property, but density instead. Lower pressure drops will occur under lower densities of the gas and with more sensitivity of the mixture solubility to pressure, the first being usually dominant.
- The viscosity presents some influence again in the pressure recovery region. The extent of the pressure recovery region tends to be smaller as viscosity and velocity increases, or with the reduction of the radial clearance. Under these conditions, viscous forces are greater, and a stronger pressure gradient is required in the balance of forces. The recovery region, however, also depends on the behaviour of the fluid in the cavitated region, with particular importance to the levels of pressure achieved during the release of gas;
- With larger clearances, the results obtained by the two-phase model deviates from those obtained using Reynolds conditions. Knowing that the Reynolds boundary conditions do not predict satisfactorily bearing behaviour in situations of light loads, this is an indication that the two-phase model can capture different cavitation occurrences depending on the prevailing conditions. On the other hand, before any conclusion is made, it is necessary to consider other effects in the model, such as fluid inertia – especially because separation conditions are likely to occur.
- If gas is present in the convergent region, which is a characteristic accounted by the model when considering thermodynamic non-equilibrium, the behaviour of the lubricated component can be significantly affected. Viscosity is still the most relevant property in the positive pressure region, but due to the presence of gas and a resulting density wedge effect, the extension of this region increases and it can potentially support a similar load with potentially less friction than a bearing with liquid only in the positive region.
- On the other hand, the presence of gas in the positive region causes the bearing to be extremely unstable under transient conditions. This conclusion is in line

with observations of higher stiffness and lower damping for squeeze film dampers lubricated with bubbly oils.

- The attitude angle of a bearing lubricated with a bubbly oil mixture varies significantly with the lubricant condition, with a more distinct behaviour than observed in the classical lubrication theory and reflected in the tests with a lubricant mixture in which gas is absorbed under positive pressure gradients.
- Surface tension effects tend to reduce further the pressure in the cavitated region, as a result of the higher pressure inside the bubble and consequently lower density, requiring further expansion to accommodate the film thickness variations. On the other hand, and particular for gas refrigerant, the higher pressures observed in the convergent region indicate a likelihood that the gas should redissolve in the liquid mixture or even implode, a factor which would just be exacerbated by the surface tension effects and requires further investigation.
- The quantities of refrigerant usually released in the cavitated region to fill the clearance are very small – as a result of that, the isothermal assumption is valid.
- In the parametric analysis for partial bearings, it was observed that subsaturated mixtures present a lower cavitation pressure than a saturated one, despite the similar position in which cavitation occurs. In evaluating experimental results available from the literature, similar behaviour was observed in the presence of ventilation. This may indicate that in such conditions metastability of the mixture is relevant.
- When the two-phase model is considered for the piston lubrication, it shows a significant discrepancy in results against methodologies that assume a cavitation criteria for the piston. On the other hand, the two-phase model agrees well with solutions not adopting any cavitation criterion for the clearance. Therefore, in the light of the two-phase model, current cavitation proposals for the ringless piston problem are unsuitable.
- The solution for the piston using the two-phase flow model indicated the occurrence of cavitation for a period when the piston returns from the top dead centre and starts the suction cycle. Assumptions have to be made in regard to the absorption of gas refrigerant by the oil in the compression chamber. A

mixture with a lower rate of absorption has actually shown lower friction and higher gas leakage, which is believed to have a relationship with the longer period in which refrigerant is being absorbed after TDC.

- It is concluded that in conditions where the interaction of refrigerant and oil occurs, using pure oil as lubricant can led to erroneous results. Furthermore, different oil-refrigerant mixtures can respond differently in lubrication, reinforcing the need to understand appropriately the interaction between the phase components in order to accurately solve the lubrication problem of interest.

In the light of these findings, it can be seen that, in addition to proposing a two-phase model for lubrication taking into account the properties of the lubricant mixture, significant insight was gained into the advantages of using such an approach, as well as many of the difficulties inherent to it. By solving problems for bearings and pistons, additional information was provided regarding the modelling and understanding of these tribological entities. Furthermore, by exploring oil and refrigerant mixtures in practical applications, much use could be done from the information already available for this mixture, as well as a number of recommendations for future studies can be read through the text. Therefore, the objectives of this research project were achieved.

8.3 INNOVATIVE ASPECTS OF THE WORK

As discussed in chapter 2, this work aimed to utilise relevant information from previous research and propose a model that worked in the intersection of these areas.

As such, the work provided a unique contribution to the field by,

- Proposing a model that considers simultaneously the dissolution of a low viscosity liquid in the oil, affecting then the bulk lubricant properties, and its release in the form of bubbles from the oil, relating it to the phenomenon of cavitation;
- Incorporating for the first time the effect of the interactions of a complex mixture such as the oil and refrigerant in the behaviour of lubricated components in which they operate;

- Thoroughly investigating how the factors that affect this mixture can influence the lubrication of a component such as the journal bearing and ringless piston, identifying the main contributors for effects that should be controlled for improved operation.
- Comparing the new methodology with the existing approaches, providing further assurance of when such methodologies can provide a satisfactory solution and when the more refined development is recommended.

8.4 RECOMMENDATIONS FOR FUTURE RESEARCH AND WORK

As a new proposal for the study of lubricated components in the refrigeration sector, and despite mentioning several times the amount of research already performed for the oil and refrigerant mixture given its importance in this sector, at this final stage many recommendations point to the need to study specific aspects of the interaction not fully dominated. Among those,

- *Further understanding of the absorption of refrigerant in the oil under transient conditions*: For several times in the work, assumptions were made in trying to cover the investigation options when knowledge of this behaviour was unavailable. By the significant difference shown in the results for the thermodynamic assumptions of equilibrium and non-equilibrium, it is imperative for a more precise solution that the behaviour of the mixture under fast transients is better understood. This development will inevitably occur, but it seems first necessary to understand the dissolution of refrigerant in the oil under quasi-static conditions, as currently pursued by Gessner and Barbosa Jr (2006), among others.
- *Metastability effects during the release of gas:* the observation from Couto (2006) that higher subambient pressures occurred for a ventilated bearing in comparison with an immersed one point out that metastability can be a factor in the release of gas from oils in the cavitation region. The problem of dealing with metastability has already been mentioned in the study of oil and refrigerant mixtures (Lacerda, 2000, and Grando, 2001), not only for rich oil mixtures, but also for mixtures where oil is a contaminant. To advance the work developed

here in considering additional sources of gas in the cavitation region, clarity regarding this phenomenon will be quite important.

- *Study of different mixtures*: From the refrigeration point-of-view, mixture such as the ones studied in this work were and are still of great importance. However, with new equipment already using CO_2 as refrigerant, as having this gas as more inert in comparison to the usual refrigerants, it is likely that relevant information will arise. And a great opportunity to finally link developments in the refrigeration sector with other areas of tribology, which undoubtedly lack in the knowledge of properties when compared to the developments on refrigeration. Potentially studying mixtures of CO_2 and oil will give an important step in further understanding the dissolution of atmospheric air in oils, therefore providing additional and relevant information for many of the bubbly oil proposal existing nowadays.

From the two-phase model here proposed, the focus has to be in carry on advancing in the complexity of its applications and also of the phenomena it considers. It is relevant then that,

- *Model finite bearings considering the effect of ventilation*: Although previously mentioned that further information about the fluid mixture could assist in providing a better explanation of how ventilation and release of gas interact in the cavitated region, the fact that most applications use more realistic componets like this means that it requires urgent consideration.
- *Incorporate surface tension effects, further study on the shape and size of bubbles, as well as its growth and collapse*: a step were release of gas and surface tension effects are dealt with simultaneously is not yet available for lubrication problems, and has to be considered for the cavitated region. It has also been reported in this work that there is the chance of bubble collapse under the very high pressures in the convergent region, which could be one consideration for such study.
- *Better estimates of the friction force*: This work indicated that the current viscosity correlations simply cannot provide a single an accurate choice for the viscosity of the mixture, and as a result appropriately calculate the friction force. Further investigation into the mixture behaviour in the divergent region will provide additional information for this problem, but it is fundamental that

experimental works better consider the investigation of friction force in addition to the pressure profile.

- *Application of the model to the full compressor lubrication*: With the understanding gained from this work in the behaviour of the oil and refrigerant mixture in lubrication, then improved boundary conditions can be defined for a fully coupled compressor lubrication model, in which all the lubricated components of the compressor, in its different regimes, can be solved simultaneously.
- *Investigate additional lubrication regimes for the oil-refrigerant lubrication and consider wear models:* As seen for the solution considering non-equilibrium conditions for the mixture in the bearing, very unstable trajectories can occur, which are then likely to induce extreme situation where boundary lubrication can be seen. While the influence of the refrigerant environment in compressor lubrication has been experimentally investigated, as described in chapter 2, wear models are still scarce for the lubrication in refrigeration and should be pursued.
- *Improve numerical methodology*: The numerical method requires a considerable computational effort, which is particularly connected to the solution of the cavitated region. Although in moderate load conditions the time required is equivalent to the one using the cavitation algorithm, effort has to be made in the direction of providing smoother pressure profiles during intermediate steps of the iterative process, which would improve considerably convergence and may be fundamental to the wider application of the developed model.

REFERENCES

ABDEL-LATIF, L.A., PEIKEN, H., BENNER, J. **Thermohydrodynamic Analysis of Thrust-Bearing with Circular Pads Running on Bubbly Oil (BTHD-Theory).** Journal of Tribology, Transactions of the ASME, Vol.107, No.4, p.527-537, 1985.

AKEI, M., MIZUHARA, K., TAKI, T., YAMAMOTO, T. **Evaluation of Film-forming Capability of Refrigeration Lubricants in Pressurized Refrigerant Atmosphere.** Wear, Vol.196, p.180-187, 1996.

ALMQVIST, T., LARSSON, R. **The Navier-Stokes Approach for Thermal EHL Line Contact Solutions.** Tribology International, Vol.35, p.163-170, March 2002.

BARBOSA JR., J.R., LACERDA, V.T., PRATA, A.T. **Prediction of Pressure Drop in Refrigerant-Lubricant Oil Flows with Refrigerant Outgassing in Small Diameter Tubes.** Proceeding of IX Brazilian Congress in Thermal Sciences and Engineering, ENCIT 2002, Caxambú/MG, Paper CIT02-0774, 11p., 2002.

BARBOSA JR., J.R., LACERDA, V.T., PRATA, A.T. **Prediction of Pressure Drop in Refrigerant-Lubricant Oil Flows with Refrigerant Outgassing in Small Diameter Tubes.** International Journal of Refrigeration, Vol.27, p.129-139, March 2004.

CAMERON, A. **The Principles of Lubrication.** London: Longmans, 1966.

CAREY, V.P. **Liquid-Vapor Change Phenomena:** an introduction to the thermophysics of vaporization and condensation processes in heat transfer equipment. Bristol: Taylor and Francis, 1992. 645p.

CASTRO, H.O.S., GASCHE, J.L., CONTI W.P. **Foam Flow of Oil-Refrigerant R134a mixture in a Small Diameter Tube**. Proc, 10th International Refrigeration and Air Conditioning Conference at Purdue, Paper R171, 2004.

CHANG, S.D., RO, S.T. **Pressure Drop of Pure HFC Refrigerants and their Mixtures Flowing in Capillary Tubes**. International Journal of Multiphase Flow, Vol. 22, No. 3, pp.551-561, 1996.

CHOI, S., KIM, K.W. **Analysis of Bubbly Lubrication in Journal Bearings.** JSME International Journal, Series C, Vol.45, No.3, p.802-808, 2002.

CIANTAR, C., HADFIELD, M., SMITH, A.M., SWALLOW, A. **The Influence of Lubricant Viscosity on the Wear of Hermetic Compressor Components in HFC-134a Environments.** Wear, Vol.236, p.1-8, 1999.

CIANTAR, C., HADFIELD, M., SWALLOW, A., SMITH, A.M. **The Influence of POE and PVE Lubricant Blends within Hermetic Compressors Operating with Components in HFC-134a Refrigerant.** Wear, Vol.241, p.53-64, 2000.

CONDE, M.R. **Estimation of Thermophysical Properties of Lubricating Oils and Their Solutions with Refrigerants: An Appraisal of Existing Methods**. Applied Thermal Engineering, Vol. 16, No. 1, p.51-61, 1996.

COUTO, P.R.C. **Experimental Investigation of Hydrodynamic Journal Bearings with Aplication in Refrigeration Hermetic Compressors.** PhD Thesis (Mechanical Engineering)-Department of Mechanical Engineering, Federal University of Santa Catarina, Florianópolis, Brazil. 2004. *(In Portuguese)*.

COYNE, J.C., ELROD JR., H.G. **Conditions for the Rupture of a Lubricating Film. Part I: Theoretical Model.** Journal of Lubrication Technology, Transactions of the ASME, Vol.92, No.3, p.451-456, July 1970.

CHRISTPOPHERSON, D.G. **A new mathematical method for the solution of film lubrication problems.** Journal and Proceedings of the Institution of Mechanical Engineers, Vol.46, p.126-135, January 1942.

CULLEN, E.J., DAVIDSON, J.F. **Absorption of gases in liquid jets.** Trans. Faraday Soc. 52 (1957) 113.

DELLIS, P., ARCOUMANIS, C. **Cavitation development in the lubricant film of a reciprocating piston-ring assembly.** Proc. IMechE, Journal of Engineering Tribology, Vol.218, p.157-171, 2004.

DIAZ, S, SAN ANDRÉS. **A Model for Squeeze Film Dampers with Air Entrainment and Validation with Experiments.** Journal of Tribology, Vol.123, January, p.125-133, 2001.

DOWSON, D., TAYLOR, C.M. **Cavitation in Bearings.** Annual Review of Fluid Mechanics, Vol.11, p.35-66, 1979.

DREW, D.A. **Mathematical Modeling of Two-Phase Flow**. Annual Review of Fluid Mechanics, Vol. 15, p.261-291, 1983.

ELROD, H.G. **A Cavitation Algorithm.** Journal of Lubrication Technology, Transactions of the ASME, Vol.103, No.3, p.350-354, July 1981.

FENG, N.S., HAHN, E.J. **Density and Viscosity Models for Two-Phase Homogeneous Hydrodynamic Damper Fluids.** ASLE Transactions, Vol.29, No.3, p.361-369, July 1986.

FUKUI, H., SANECHIKA, K.I., IKEDA, M. **Novel Refrigeration Lubricants for Use with HFC Refrigerants.** Tribology International, Vol.33, p.707-713, 2000.

GARLAND, N.P., HADFIELD, M. **Environmental Implications of Hydrocarbon Refrigerants applied to the Hermetic Compressor.** Materials and Design, Vol.26, p.578-586, 2006.

GESSNER, T.R., BARBOSA JR., J.R. **Modeling absorption of pure refrigerants and refrigerant mixtures in lubricant oil.** Int. Journal Refrigeration, Vol.29, p.773-780, 2006.

GRANDO, F.P. **Computacional Modelling of the Two-Phase Flow with Foam Formation of na Oil-Refrigerant Mixture in Straight Horizontal Pipes.** Dissertation (Master in Mechanical Engineering)-Department of Mechanical Engineering, Federal University of Santa Catarina, Florianópolis, Brazil, 2001. 131p. (*In Portuguese)*

JACOBSSON, B., FLOBERG, L. **The Infinite Journal Bearing Considering Vaporization.** Transactions of the Charlmers University of Technology, No.189, 1957.

KICINSKI, J. **Effect of the Aeration of a Lubricating Oil Film and its Space- and Time-Related Compression on the Static and Dynamic Characteristics of Journal Bearings.** Wear, Vol. 91, p.65-87, October 1983.

HAMROCK, B.J. **Fundamentals of Fluid Film Lubrication.** New York: McGraw-Hill, 1994. 690p.

HAN, D.C., LEE, J.S. **Analysis of the Piston Ring Lubrication with a New Boundary Condition.** Tribology International, Vol.31, No.12, p.753-760, 1998.

INGHAM, D.B., RITCHIE, J.A., TAYLOR, C.M. **The Use of the Boundary Element Method for Determining Flow Separation at a Corner.** Engineering Analysis with Boundary Elements, Vol.10, p.199-208, 1992.

KAWASE, T., SOMEYA, T. **An Investigation into the Oil Film Pressure Distribution in Dynamically Loaded Journal Bearing.** Proceedings of the 4th European Tribology Congress, Vol.II, No.5.2.3, 10p., 1997.

KRUSE, H.H., SCHROEDER, M. **Fundamentals of Lubrication in Refrigerating Systems and Heat Pumps.** ASHRAE Transactions, Vol.90, Part 2B, p.763-783, 1984.

LACERDA, V.T. **Experimental Characterisation of the Two-Phase Flw of an Oil-Refrigerant Mixture in Small Diameter Pipes.** Dissertation (Master in Mechanical Engineering)-Department of Mechanical Engineering, Federal University of Santa Catarina, Florianópolis, Brazil. 2000. 165p. (*In Portuguese)*

LACERDA, V.T., PRATA, A.T., FAGOTTI, F. **Experimental Characterization of Oil-Refrigerant Two-Phase Flow**. Proceedings of the ASME, Advanced Energy Systems Division, Vol. 40, p.101-109, 2000.

LEMAÎTRE, F., BERKER, A. **Non-Newtonian Cavitation Analysis in Journal Bearings.** Journal of Non-Newtonian Fluid Mechanics, Vol.59, p.31-48, 1995.

MA, M.T., SHERRINGTON, I., SMITH, E.H., GRICE, N. **Development of a Detailed Model for Piston-Ring Lubrication in IC Engines with Circular and Non-circular Bores.** Tribology International, Vol. 30, No.11, p.779-788, 1997.

MANKE, A.L. **Uma Metodologia de Cálculo para a Simulação de Mancais Radiais Submetidos a Carregamento Dinâmico.** 1991. 170p. Dissertation (Master in Mechanical Engineering)-Department of Mechanical Engineering, Federal University of Santa Catarina, Florianópolis, Brazil.

MCLINDEN, M.O., KLEIN, S.A, LEMMON, E.W., PESKIN, A.W. **REFPROP: Thermodynamic and Transport Properties of Refrigerants and Refrigerant Mixtures.** Version 6.0. Washington (DC): NIST, 1998.

MCMULLAN, J.T. **Refrigeration and the environment – issues and strategies for the future.** International Journal of Refrigeration, v.25, 2002; pp.89-99

MERMOND, Y., FEIDT, M., MARVILLET, C. **Propriétés Thermodynamiques et Physiques des Mélanges de Fluides Frigorigènes et d'Huiles.** International Journal of Refrigeration, Vol. 22, p.569-579, November 1999.

MEYER, J.J., DUNN, W.E. **New Insights into the Behavior of the Metastable Region of an Operating Capillary Tube.** HVAC&R Research, Vol. 4, No. 1, pp. 105-115, January 1998.

MERMOND, Y., FEIDT, M., MARVILLET, C. **Propriétés Thermodynamiques et Physiques des Mélanges de Fluides Frigorigènes et d'Huiles.** International Journal of Refrigeration, Vol. 22, p.569-579, November 1999.

MILTSIOS, G.K., PATTERSON, D.J., PAPANASTASIOU, T.C. **Solution of the Lubrication Problem and Calculation of the Friction Force on the Piston Rings.** Journal of Tribology, Transactions of the ASME, Vol.111, No.4, p.635-641, October 1989.

MOTTA, S.Y., MARQUES, R.P., BRAGA, S.L., PARISE, J.A.R. **Misturas Refrigerante-Óleo Lubrificante: Pressão e Temperatura de Saturação.** Revista de Ciência e Engenharia, Vol.7, No. 2, p.70-78, 1998.

MOTTA, S.Y., MARQUES, R.P., BRAGA, S.L., PARISE, J.A.R. **Misturas Refrigerante-Óleo Lubrificante: Propriedades Termodinâmicas.** Revista de Ciência e Engenharia, Vol. 9, No.1, p.52-61, 2000.

MUFTI, R.A., PRIEST, M. **Experimental and Theoretical Study of Instantaneous Piston Assembly Friction in a Gasoline Engine.** Proc.of the ASME/STLE International Joint Tribology Conference, ITJC 2004, p907-921, 2004.

MUFTI, R.A., PRIEST, M. **Experimental Evaluation of Piston-Assembly Friction under Motored and Fired Conditions in a Gasoline Engine.** Journal of Tribology, Vol.127, No.4, October, p.826-836, 2005.

NA, B.C., CHUN, K.J., HAN, D.C. **A Tribological Study of Refrigeration Oils under HFC-134a Environment.** Tribology International, Vol.30, No.9, p.707-716, 1997.

NATSUMEDA, S., SOMEYA, T. **Negative Pressures in Statically and Dynamically Loaded Journal Bearings.** Proceedings of the 13th Leeds-Lyon Syimposion on Tribology, England, p.65-72, 1986.

NG, W.S. **Bubbly Oil Properties and their Effects on Squeeze Film Damper Dynamic Performance.** Ph.D Thesis, School of Mechanical Engineering, University of Leeds, 2007.

NIKOLAJSEN, J.L. **Viscosity and Density Models for Aerated Oil in Fluid-Film Bearings.** Tribology Transactions, Vol.42, No.1, p.186-191, 1999a.

NIKOLAJSEN, J.L. **The Effect of Aerated Oil on the Load Capacity of a Plain Journal Bearing.** Tribology Transactions, Vol.42, No.1, p.58-62, 1999b.

NOSOV, V.R., GOMEZ-MANCILLA, J. **On the Appearance of Lubricant Film Rupture in Cylindrical Journal Bearings.** Tribology Transactions, Vol.47, p.233-238, April 2004.

PARKINS, D.W. **Conference Report: Cavitation in Fluid Films: 17 October 1984, Cranfield Institute of Technology, UK.** Tribology International, Vol.18, No.1, p.50-51, 1985.

PATANKAR, S.V. **Numerical Heat Transfer and Fluid Flow.** New York: Hemisphere Publishing Corp, 1980. 197p.

PINKUS, O., STERNLICHT, B. **Theory of Hydrodynamic Lubrication.** New York: McGraw-Hill, 1961. 465p.

POIATE, E.J. **Estudo Experimental do Escoamento Bifásico de Misturas Óleo Refrigerante Usadas em Compressores de Refrigeracao.** Dissertation (Master in Mechanical Engineering)-Department of Mechanical Engineering, Universidade Estadual Paulista, Ilha Solteira, 2001.

PRATA, A.T. **Lubrificação Hidrodinâmica de Mancais Radiais.** Monograph, Department of Mechanical Engineering, Federal University of Santa Catarina, Florianópolis, Brazil, 1992.

PRATA, A.T., FERNANDES, J.R.S., FAGOTTI, F. **Piston Lubrication Model for Reciprocating Compressors.** Proceedings of the ASME Advanced Energy Systems Division, Vol.38, p.325-332, 1998.

PRATA, A.T., FERNANDES, J.R.S., FAGOTTI, F. **Dynamic Analysis of Piston Secondary Motion for Small Reciprocating Compressors.** Journal of Tribology, Transactions of the ASME, Vol.122, No.4, p.752-760, October 2000.

PRATA, A.T., FERREIRA, R.T.S. **The Accuracy of Short Bearing Theory in Presence of Cavitation.** Journal of Tribology, Transactions of the ASME, Vol.112, No.4, p.650-654, October 1990.

PRIEST, M., DOWSON, D., TAYLOR, C.M. **Predictive Wear Modelling of Lubricated Piston Rings in a Diesel Engine.** Wear, Vol.231, p.89-101, 1999.

PRIEST, M., DOWSON, D., TAYLOR, C.M. **Theoretical Modelling of Cavitation in Piston Ring Lubrication.** Proceedings of the Institution of Mechanical Engineers, Vol.214, Part.C, No.3, p.435-447, 2000.

PRIEST, M., TAYLOR, C.M. **Automobile Engine Tribology – Approaching the Surface.** Wear, Vol.241, p.193-203, 2000.

QI, A., YINSHENG, Z., YONGXIN, Q. **Study on the Viscosity Properties of Bubbly Oil and the Static Characteristics of Journal Bearing Lubricated with Bubbly Oil.** Wear, Vol. 213, p.159-164, 1997.

REPÀCI, A. **Non-linear Modelling of the Piston Slap Phenomenon in an Alternative Internal Combustion Engine.** Mathematical Modelling, Vol.8, p.366-367, 1987.

RAPOSELLI, E., D'AGOSTINO, L. **A Modified Isenthalpic Model of Cavitation in Plane Journal Bearings.** Proceedings of the Fourth International Symposium on Cavitation – CAV2001, Pasadena, California, USA, 20-23 June 2001, paper B5.003. 8pp., 2001. (http://cav2001.library.caltech.edu).

ROACHE, P.J. **Fundamentals of Computational Fluid Dynamics.** Albuquerque: Hermosa, 1998. 648p.

ROWE, W.B., CHONG, F.S. **A Computational Algorithm for Cavitating Bearings.** Tribology International, Vol.117, No.5, p.243-250, October 1984.

SAN ANDRÉS, L. **Cavitation in Liquid Film Bearings.** Lecture Notes, Texas A&M University, 2006 (online).

SAN ANDRÉS, L., SANTIAGO, O. **Forced Response of a Squeeze Film Damper and Identification of Force Coefficients from Large Orbital Motions.** Journal of Tribology, Vol.126, April, p.292-300, 2004.

SAFARI, S., HADFIELD, M. **Wear Behaviour of the Piston/Gudgeon Pin in a Hermetic Compressor with Replacement CFC Refrigerants.** Wear, Vol.219, p.8-15, 1998.

SAHLIN, F., ALMQVIST, A, LARSSON, R., GLAVATSHIV, S. **A cavitation algorithm for arbitrary lubricant compressibility.** Tribology International, Vol.40, p.1294-1300, 2007.

SANTOS, E.V. **Carregamento Dinâmico de Mancais Radiais com Cavitação do Filme de Óleo.** Dissertation (Master in Mechanical Engineering)-Department of Mechanical Engineering, Federal University of Santa Catarina, Florianópolis, Brazil. 1995. 100p. (In Portuguese).

SILVA, A. **Kinetics and Dynamics of the Gas Absorption by Lubricant Oil.** PhD Thesis (Mechanical Engineering)-Department of Mechanical Engineering, Federal University of Santa Catarina, Florianópolis, Brazil. 2004. *(In Portuguese)*

SMITH, E.H. **The Influence of Surface Tension on Bearings Lubricated with Bubbly Oil.** Journal of Lubrication Technology, Transactions of the ASME, Vol.102, No.1, p.91-96, January 1990.

SMITH, O, PRIEST, M., TAYLOR, R.I., PRICE, R., CANTLAY, A., COY, R.C. **Simulated Fuel Dilution and Friction Modifier Effects on Piston Ring Friction.** Proc. IMEchE, Journal of Engineering Tribology, Vol.220, No.3, p181-189, 2006.

SOMEYA, T. **On the Development of Negative Pressure in Oil-Film and the Characteristics of Journal Bearing.** Meccanica, Vol.38, p.643-658, December 2003.

TAO, L., DIAZ, S., SAN ANDRÉS, L, RAJAGOPAL, K.R. **Analysis of Squeeze Film Dampers Operating with Bubbly Lubricants.** Journal of Tribology, Vol.122, January, p.205-210, 2000.

THOME, J.R. **Comprehensive Thermodynamic Approach to Modeling Refrigerant-Lubricant Oil Mixtures**. HVAC&R Research, Vol. 1, No. 2, p.110-126, April 1995.

TØNDER, K. **Effect of Gas Bubbles on Behavior of Isothermal Michell Bearings.** Journal of Lubrication Technology, Transactions of the ASME, Vol.99, No.3, p.354-358, July 1977.

TSUCHIYA, K, MIKASA, H., SAITO, T. **Absorption dynamics of CO2 bubbles in a pressurized liquid flowing downward and its simulation in seawater.** Chemical Engineering Science, Vol.52, No.21-22, p.4119-4126, 1997.

TUOMAS, R., ISAKSSON, O. **The effect of additives on the lubrication of rolling element bearings in a refrigerant environment.** Int. Journal of Refrigeration, Vol.30, p.28-36, 2007.

USSYK, M.S. **Simulação Numérica do Desempenho de Compressores Herméticos Alternativos.** Dissertation (Master in Mechanical Engineering)-Department of

Mechanical Engineering, Federal University of Santa Catarina, Florianópolis, Brazil. 1984. 120p. (In Portuguese).

VIJAYARAGHAVAN, D., KEITH JR, T.G. **Effect of Cavitation on the Performance of a Grooved Misaligned Journal Bearing.** Wear, Vol.134, p.377-397, 1989.

VIJAYARAGHAVAN, D., KEITH JR., T.G. **An Efficient, Robust, and Time Accurate Numerical Scheme Applied to a Cavitation Algorithm.** Journal of Lubrication Technology, Transactions of the ASME, Vol.112, No.1, p.44-51, January 1990.

VINCENT, B. MASPEYROT, P., FRENE, J. **Cavitation in Dynamically Loaded Journal Bearings Using Mobility Method.** Wear, Vol.193, p.155-162, 1996.

VINCENT, B. MASPEYROT, P., FRENE, J. **Cavitation in Non-circular Journal Bearings.** Wear, Vol.207, p.122-127, 1997.

WLAD, P., WECLAS, M. **Modeling of Piston-Ring and Cylinder-Bore Interaction and Wear in Internal Combustion Engines.** Mechanics Research Communications, Vol.16, No.5, p.273-278, 1989.

WONGWISES, S., PIROMPAK, W. **Flow Characteristics of Pure Refrigerants and Refrigerant Mixtures in Adiabatic Capillary Tubes.** Applied Thermal Engineering, Vol.21, pp. 845-861, 2001.

YOKOZEKI, A. **Time-dependent behavior of gas absorption in lubricant oil.** Int. Journal of Refrigeration, Vol.25, p.695-704, 2002.

YOUNG, F.R. **Cavitation**. London: McGraw-Hill, 1989, p.230.

YU, Q., KEITH JR, T.G. **Prediction of Cavitation in Journal Bearings Using a Boundary Element Method.** Journal of Tribology, Transactions of the ASME, Vol.117, No.3, p.411-421, July 1995.

ZEIDAN, F.Y., VANCE, J.M. **Cavitation Leading to a Two Phase Fluid in a Squeeze Film Damper.** Tribology Transactions, Vol.32, No.1, p.100-104, 1989.

Appendix A

PROPERTIES OF THE MIXTURE R12 AND MINERAL OIL

The properties adopted to the study of the mixture of refrigerant R12 and mineral oil SUNISO 1GS are the same developed by Lacerda (2000), where a detailed discussion about the methodology to calculate the properties can be found. Properties for the liquid mixture of oil and refrigerant were obtained from manufacturer data (Witco), provided by the Brazilian Compressor Company (EMBRACO), and also from tests directly performed in the company. Properties for the refrigerant R12 are calculated from numerical fits applied to data obtained using the software *REFPROP*.

A.1. SOLUBILITY

An empirical correlation is used to the calculus of the solubility of the refrigerant R12 in the mineral oil SUNISO 1GS. This equation was obtained by adjusting a curve using data from a pressure-temperature-solubility diagram obtained from the oil producer (Witco).

The equation was adjusted in the interval between $0 < p < 3bar$ and $20 < T < 120^{o} C$. Results are extrapolated for use under 20ºC, without considerable errors in the predicted values.

The adjusted correlation is given by:

$$w_{sat} = \frac{a_1 + b_1 T + c_1 p + d_1 T^2 + e_1 p^2 + f_1 Tp}{a_2 + b_2 T + c_2 p + d_2 T^2 + e_2 p^2 + f_2 Tp} \tag{A.1}$$

$a_1 = 0.00914975$ $\quad$ $a_2 = 1.0$

$b_1 = -0.00027718$ $\quad$ $b_2 = 0.03051147$

$c_1 = 0.098930906$ $\quad$ $c_2 = -0.22346262$

$$d_1 = 1.52029 \cdot 10^{-6} \qquad d_2 = 0.000223492$$

$$e_1 = -0.00138089 \qquad e_2 = -0.00149545$$

$$f_1 = -1.088 \cdot 10^{-6} \qquad f_2 = 0.001392493$$

where,

$w_{sat}(kg_{ref} / kg_{mist})$ = refrigerant solubility in the oil;

$p(bar)$ = absolute pressure;

$T(^{o}C)$ = temperature;

Table A.1 and figure A.1 present characteristic data for solubility as function of pressure and temperature, in which equation (A.1) has been used:

Table A.1. Mass solubility of refrigerant R12 in SUNISO 1GS mineral oil.

Solubility $w_{sat}(\%)$		$p(kPa)$					
		50	*100*	*150*	*200*	*250*	*300*
$T(^{o}C)$	*0*	*6.6*	*13.8*	*23.3*	*35.8*	*57.4*	*92.8*
	10	*4.6*	*9.3*	*15.0*	*22.0*	*30.9*	*42.4*
	20	*3.3*	*6.8*	*10.6*	*15.1*	*20.2*	*26.2*
	30	*2.5*	*5.2*	*8.0*	*11.1*	*14.6*	*18.4*

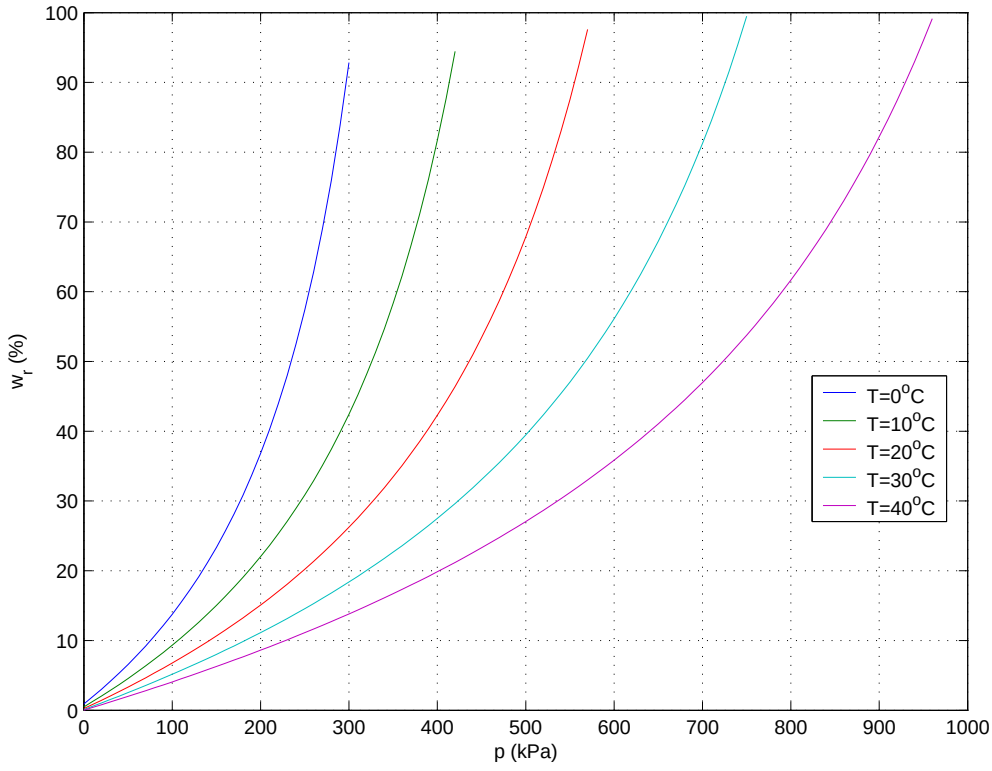

Figure A.1. Mass solubility of refrigerant R12 in SUNISO 1GS mineral oil.

A.2. DENSITY

The density of the liquid is calculated by the additive law for mixtures; however, since the behaviour is not perfectly ideal, a correction factor is applied to the equation,

$$\rho_l = \frac{1}{A}\frac{\rho_{oil}}{1 + w\left(\frac{\rho_{oil}}{\rho_{lr}} - 1\right)} \tag{A.2}$$

The correction factor *A* is given by:

$$A = \frac{a + bT + cT^2 + dw + ew^2 + fw^3}{1 + gT + hT^2 + iw + jw^2} \tag{A.3}$$

$a = 0.999650597$ $\quad f = 8.06502 \cdot 10^{-8}$

$b = -0.01811382$ $\quad g = -0.01811257$

$c = 8.82352 \cdot 10^{-5}$ $\quad h = 8.81506 \cdot 10^{-5}$

$d = 0.004534102$ $\quad i = 0.004733494$

$e = -5.5197 \cdot 10^{-5}$ $\quad j = -4.9138 \cdot 10^{-5}$

When calculating *A*, mass fraction *w* is given in %, and the temperature in *ºC*.

The densities for the oil and the liquid refrigerant are respectively,

$$\rho_{oil}\left(kg/m^3\right) = 902.0 - 0.6T \text{ , } T(^oC) \tag{A.4}$$

$$\rho_{lr}\left(kg/m^3\right) = 1396.314 - 3.28742T + 2.29105 \cdot 10^{-3}T^2 - 1.05736 \cdot 10^{-4}T^3 \text{ , } T(^oC) \tag{A.5}$$

Equation for oil density was adjusted between $20 < T < 120^o C$ whilst the liquid refrigerant was adjusted between $0 < T < 70^o C$.

Table A.2 presents values for oil and liquid refrigerant densities as a function of temperature. Table A.3 and figure A.2 present typical values for density of the mixture as function of refrigerant mass fraction and temperature. Both oil and refrigerant densities are also present in figure A.2.

Table A.2. Densities for the SUNISO 1GS mineral oil and for the liquid refrigerant R12.

$T(^oC)$	0	10	20	30
$\rho_{oil}(kg/m^3)$	902.0	896.0	890.0	884.0
$\rho_{lr}(kg/m^3)$	1396.3	1363.6	1330.6	1296.9

Table A.3. Density for a liquid mixture of SUNISO 1GS mineral oil and refrigerant R12.

Density of the Liquid $\rho_l(kg/m^3)$		*w(%)*					
		5	10	15	20	25	30
$T(^oC)$	0	918.6	935.4	952.9	971.1	990.0	1009.6
	10	912.0	928.2	945.0	962.4	980.5	999.2
	20	905.5	921.0	937.0	953.7	970.9	988.8
	30	898.8	913.6	953.7	944.7	961.1	978.0

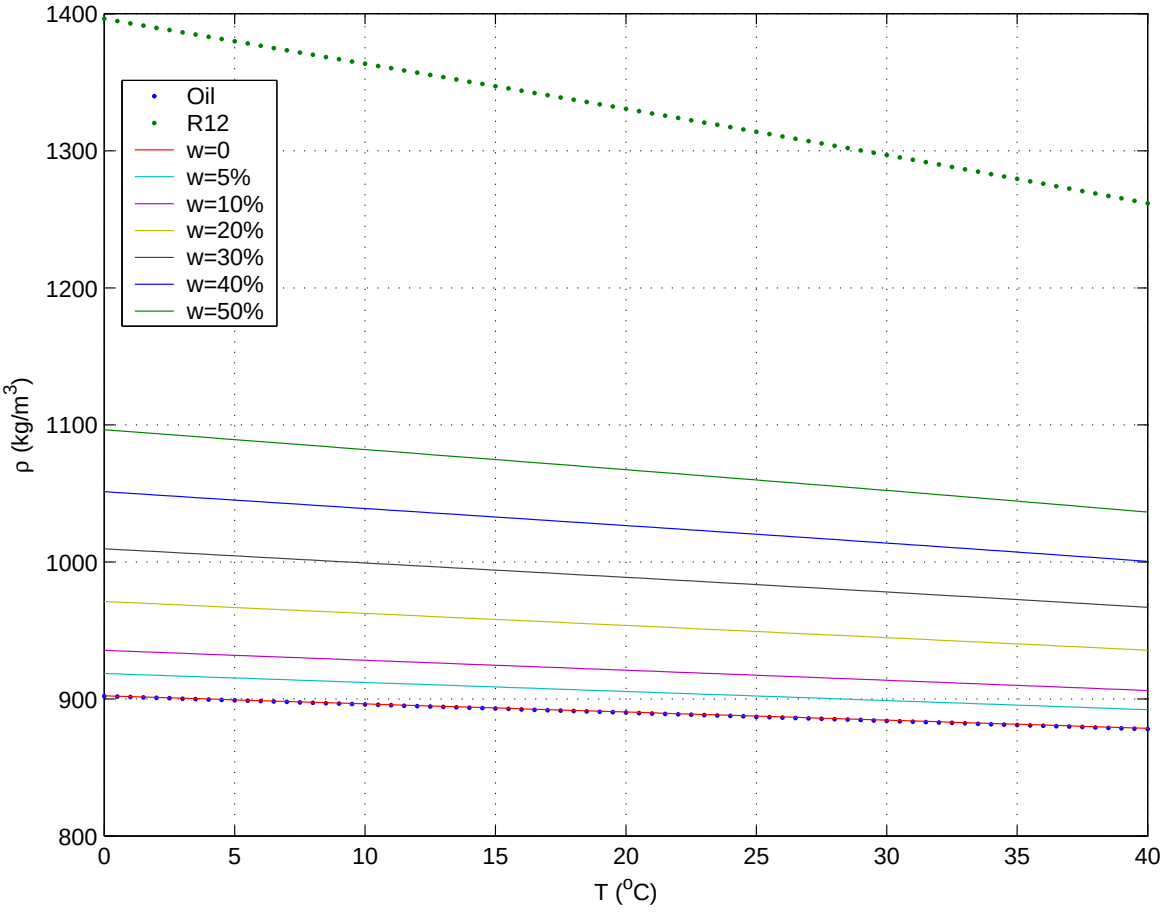

Figure A.2. Density for the R12/SUNISO 1GS liquid mixture at different mass fractions.

A.3. VISCOSITY

Dynamic viscosity was adjusted from data provided by the oil producer (Witco), in a temperature range of $20 < T < 100^{o} C$, and it is given by the following correlation:

$$\mu_l(cP) = 10^{(f_1 + f_2 T)}$$
$$\mu_l(Pa.s) = \mu_l(cP) \cdot 10^{-3} \tag{A.6}$$

$$f_1 = 1.526652699 - 0.03990154 w + 0.00733838 w^2 - 9.0446 \cdot 10^{-6} w^3$$

$$f_2 = -0.01181413 + 0.000277629 w - 3.4171 \cdot 10^{-6} w^2 - 1.875 \cdot 10^{-7} w^3 + 4.45984 \cdot 10^{-9} w$$

where $w(\%)$, $T(^{o} C)$.

Characteristic values for the viscosity of the liquid mixture calculated via equation (A.6) are present in table A.4 and figure A.3.

Table A.4. Dynamic viscosity for liquid mixture SUNISO 1GS mineral oil and refrigerant R12.

Viscosity of the Liquid $\mu_l(mPa \cdot s)$		*w(%)*					
		5	*10*	*15*	*20*	*25*	*30*
$T(^{o} C)$	*0*	*22.1*	*15.6*	*11.6*	*8.9*	*7.0*	*5.6*
	10	*17.3*	*12.5*	*9.4*	*7.3*	*5.8*	*4.6*
	20	*13.6*	*10.0*	*7.7*	*6.0*	*4.8*	*3.8*
	30	*10.7*	*8.0*	*6.3*	*5.0*	*4.0*	*3.2*

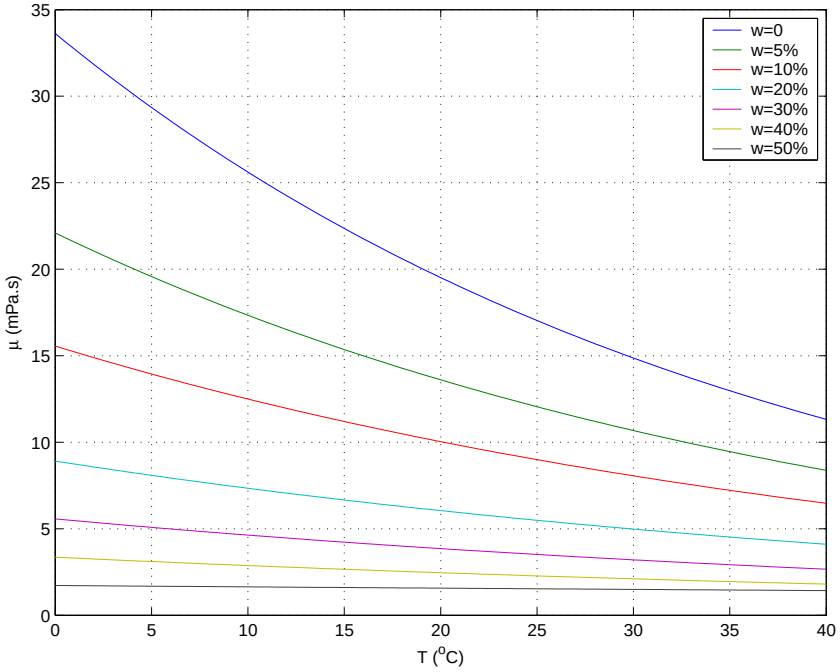

Figure A.3. Dynamic viscosity for R12/SUNISO 1GS liquid mixturefor different mass fractions.

A.4. SURFACE TENSION

Barbosa Jr. et al. (2004) proposed a procedure to estimate surface tension of the oil and refrigerant mixtures, which is based on the work of Sprow and Prausnitz (1967). Treating the oil as a pure substance is a simplification adopted. Although this hypothesis may be exaggerated, at least an order of magnitude can be obtained to the surface tension of the mixture.

To the oil and refrigerant mixture, the surface tension will be given by:

$$\sigma_l \left(N/m \right) = \hat{x}_{oil}\sigma_{oil} + \hat{x}_{lr}\sigma_{lr} - \frac{A}{2RT}\left(\sigma_{oil} - \sigma_{lr}\right)^2 \hat{x}_{oil}\hat{x}_{lr} \tag{A.7}$$

where,

$$A = \frac{1}{2}\left[\left(\frac{M_{oil}}{\rho_{oil}} \right)^{2/3} + \left(\frac{M_{lr}}{\rho_{lr}} \right)^{2/3} \right] N_0^{1/3} \tag{A.7a}$$

$\hat{x}_i$ = molar fraction, component *i* (*kmol/kmol*); σ_i = surface tension, component *i* (*N/m*);

M_i = molecular mass, component *i* (*kg/kmol*); ρ_i = density, component *i* (kg/m^3);

$R = 8314{,}1\ J/(kmol K)$; $N_0 = 6{,}023 \cdot 10^{26}\ kmol^{-1}$;

Considering pure substances, surface tension can be calculated by:

$$\sigma\left(mN/m \right) = p_c^{2/3} T_c^{2/3} Q \left(1 - T_r\right)^{11/9} \tag{A.8}$$

where,

$$Q = 0{,}1196\left[1 + \frac{T_{b,r}\, ln\left(p_c / 1{,}01325 \right)}{1 - T_{b,r}} \right] - 0{,}279 \tag{A.8a}$$

p_c = critical pressure (*bar*); T_c = critical temperature (*K*);

$T_r = \dfrac{T(K)}{T_c}$ = reduced temperature;

$T_{b,r} = \dfrac{T_b(K)}{T_c}$ = normal boiling temperature at atmospheric pressure (reduced);

The critical values, normal boiling point and the molecular mass for the oil and for the refrigerant are presented in table A.5.

Table A.5. Parameters of SUNISO 1GS oil and refrigerant R12 to calculate surface tension.

Substance (Reference)	$p_c(bar)$	$T_c(K)$	$T_b(K)$	$M(kg/kmol)$
Oil SUNISO 1GS (Barbosa Jr., 2004)	*17.22*	*647.75*	*433.64*	*251*
Refrigerant R12 (REFPROP)	*41.36*	*385.12*	*243.40*	*120.91*

Table A.6 presents some characteristic values for surface tension of the oil and refrigerant as a function of temperature,

Table A.6. Surface tension for the mineral oil SUNISO 1GS and for the refrigerant R12 liquid.

$T(^oC)$	*0*	*10*	*20*	*30*
$\sigma_{oil}(mN/m)$	*15.56*	*15.06*	*14.55*	*14.05*
$\sigma_{lr}(mN/m)$	*11.58*	*10.33*	*9.11*	*7.91*

The surface tension for the liquid mixture of SUNISO 1GS mineral oil and refrigerant R12 has been calculated as a function of refrigerant mass fraction and temperature, and the results are presented in figure A.4 and table A.7,

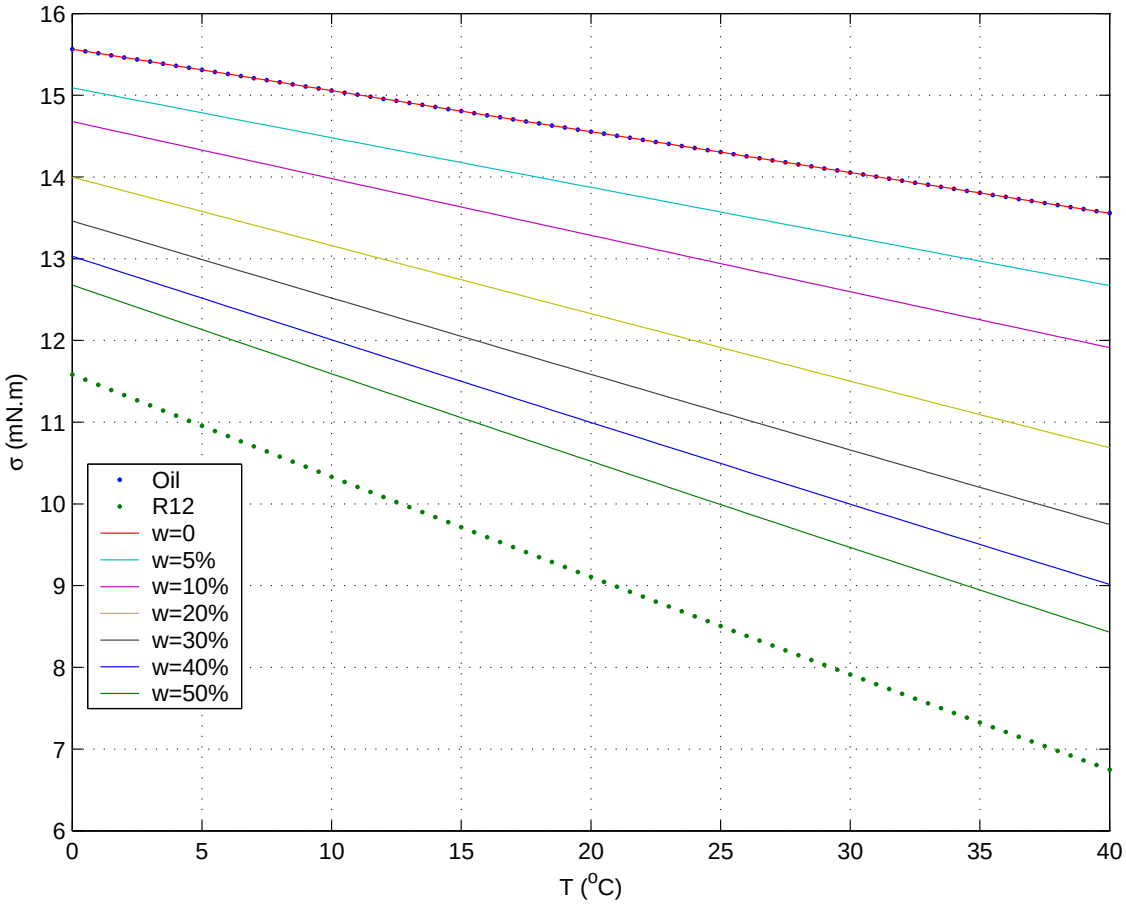

Figure A.4. Surface tension for liquid mixture at different refrigerant mass fractions.

Table A.7. Surface tension for liquid mixture of SUNISO 1GS mineral oil and refrigerant R12.

Surface Tension $\sigma_l(mN/m)$		*w(%)*					
		5	*10*	*15*	*20*	*25*	*30*
$T(^oC)$	*0*	*15.09*	*14.68*	*14.32*	*14.00*	*13.71*	*13.46*
	10	*14.48*	*13.98*	*13.54*	*13.16*	*12.82*	*12.52*
	20	*13.87*	*13.28*	*12.78*	*12.33*	*11.93*	*11.58*
	30	*13.27*	*12.60*	*12.01*	*11.50*	*11.06*	*10.66*

A.5. REFRIGERANT PROPERTIES IN THE GAS PHASE

Density and viscosity of the refrigerant R12 were adjusted for pressures and temperatures respectively between $0{,}5 < p < 7bar$ and $-10 < T < 30^oC$, and can be represented by the equations in the sequence:

$$\rho_g(kg/m^3) = \frac{-4.2936\cdot10^{-4} + 5.9619\cdot10^{-4}T - 2.2594\cdot10^{-5}T^2 - 5.3237\,p - 0.25614\,p^2}{1 + 3.7908\cdot10^{-3}T - 5.0975\cdot10^{-6}T^2 - 0.072791\,p + 6.6012\cdot10^{-4}\,p^2} \quad \text{(A.9)}$$

$$\mu_g(cP) = \frac{0.01083615 + 1.0571\cdot10^{-4}T + 2.6707\cdot10^{-7}T^2 - 1.857\cdot10^{-4}\,p + 1.4031\cdot10^{-6}\,p^2}{1 + 6.00450\cdot10^{-3}T + 2.4519\cdot10^{-6}T^2 - 0.0140206\,p} \quad \text{(A.10)}$$

where *T(ºC)* and *p(bar).*

Table A.8 and figures A.5 and A.6 present characteristic values obtained with the previous equations for density and viscosity of the refrigerant R12 in the gas phase.

Table A.8. Numerical data for density and viscosity of the refrigerant R12 gas.

T=0ºC						
$p(kPa)$	*50*	*100*	*150*	*200*	*250*	*300*
$\rho_g(kg/m^3)$	*2.7*	*5.5*	*8.3*	*11.2*	*14.2*	*17.4*
$\mu_g(\mu Pa\cdot s)$	*10.82*	*10.80*	*10.78*	*10.77*	*10.76*	*10.74*

T=10ºC						
$p(kPa)$	50	100	150	200	250	300
$\rho_g(kg/m^3)$	2.6	5.2	8.0	10.8	13.6	16.6
$\mu_g(\mu Pa \cdot s)$	11.23	11.22	11.20	11.19	11.18	11.17
T=20ºC						
$p(kPa)$	50	100	150	200	250	300
$\rho_g(kg/m^3)$	2.5	5.1	7.7	10.3	13.1	15.9
$\mu_g(\mu Pa \cdot s)$	11.63	11.63	11.62	11.61	11.60	11.60
T=30ºC						
$p(kPa)$	50	100	150	200	250	300
$\rho_g(kg/m^3)$	2.4	4.9	7.4	10.0	12.6	15.2
$\mu_g(\mu Pa \cdot s)$	12.04	12.04	12.03	12.03	12.02	12.02

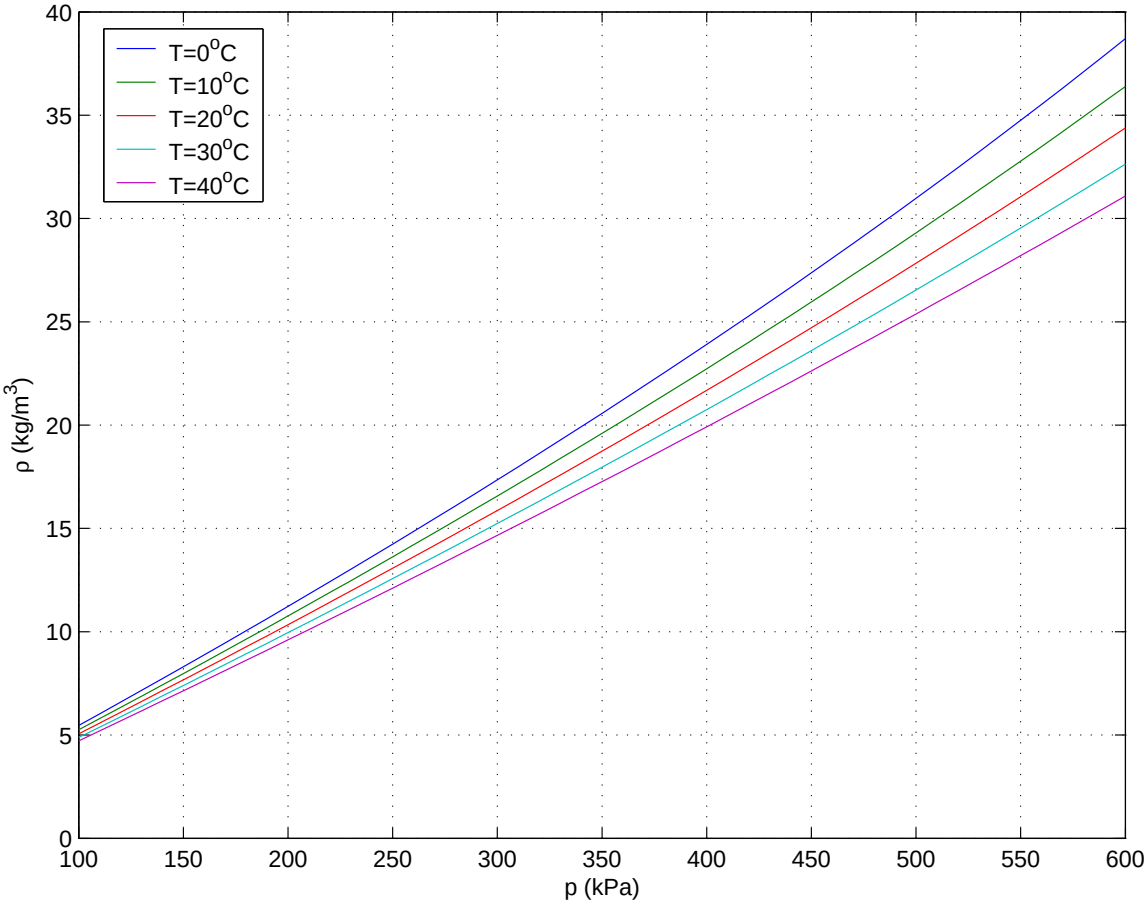

Figure A.5. Density for the refrigerant R12 gas as a function of pressure and temperature.

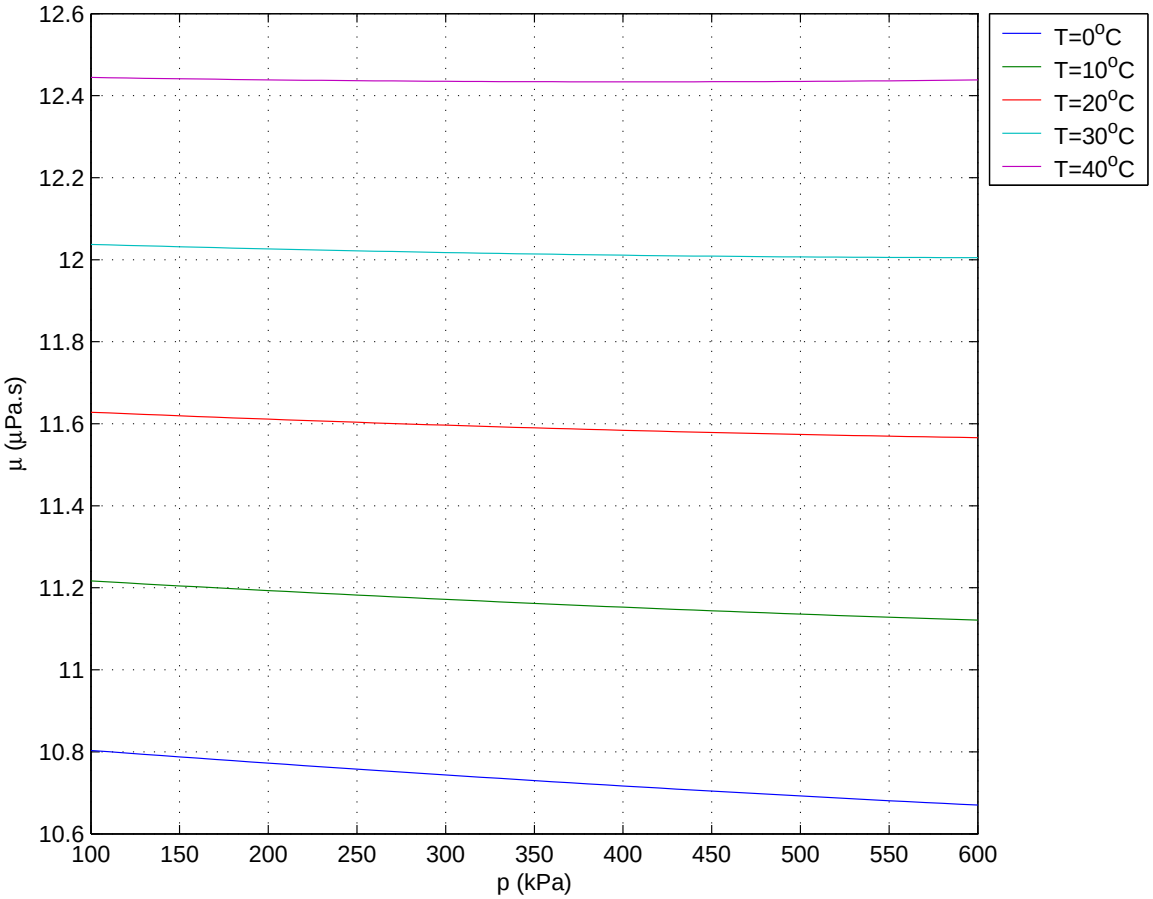

Figure A.6. Viscosity of the refrigerant R12 gas as a function of pressure and temperature.

Appendix B

PROPERTIES OF THE MIXTURE R134A AND POLYOLESTER OIL

The procedure to obtain properties for the mixture R134a and polyolester oil followed that from the previous case, for the mixture R12 and mineral oil. Solubility and viscosity results were calculated using a numerical fit base on data from the manufacturer (ICI), provided by EMBRACO, as well as for the oil density. Refrigerant properties were calculated from data provided by the software REFPROP.

B.1. SOLUBILITY

The correlation for the solubility of the refrigerant R134a in the synthetic oil EMKARATE RL10H was determined empirically, adjusting a curve from data obtained from a pressure-temperature-solubility diagram provided by the oil supplier (ICI).

Application range is $0 < p < 1000kPa$ and $0 < T < 60^{o}C$, and the correlation for the refrigerant solubility is given by:

$$w_{sat} = \frac{a_1 + b_1 p + c_1 T + d_1 p^2 + e_1 T^2 + f_1 Tp}{a_2 + b_2 p + c_2 T + d_2 p^2 + e_2 T^2 + f_2 Tp} \tag{B.1}$$

$a_1 = 0.68247268$ $a_2 = 1.0$

$b_1 = 0.0700619$ $b_2 = -0.00313147$

$c_1 = 0.06991081$ $e_2 = 0.00136449$

$d_1 = -0.00012087$ $f_2 = -6.40745705 \cdot 10^{-5}$

$e_1 = -0,00171566$ $e_2 = 0,00136449$

$$f_1 = 0{,}00241240 \qquad f_2 = -6{,}40745705 \cdot 10^{-5}$$

where,

$w_{sat}(kg_{ref} / kg_{mist})$ = refrigerant solubility in the oil;

$p(bar)$ = absolute pressure;

$T(^{o}C)$ = temperature

Characteristic values for refrigerant solubility in the oil for different values of pressure and temperature can be seen in table B.1 and figure B.1.

Table B.1. Mass solubility of refrigerant R134a in the ester oil EMKARATE RL10H.

Solubility $w_{sat}(\%)$		$p(kPa)$					
		50	*100*	*150*	*200*	*250*	*300*
$T(^{o}C)$	*0*	*4.6*	*9.3*	*15.3*	*23.7*	*37.6*	*69.6*
	10	*3.9*	*7.4*	*11.5*	*16.4*	*22.6*	*30.8*
	20	*3.0*	*5.7*	*8.6*	*11.8*	*15.4*	*19.6*
	30	*2.3*	*4.4*	*6.6*	*9.0*	*11.5*	*14.3*

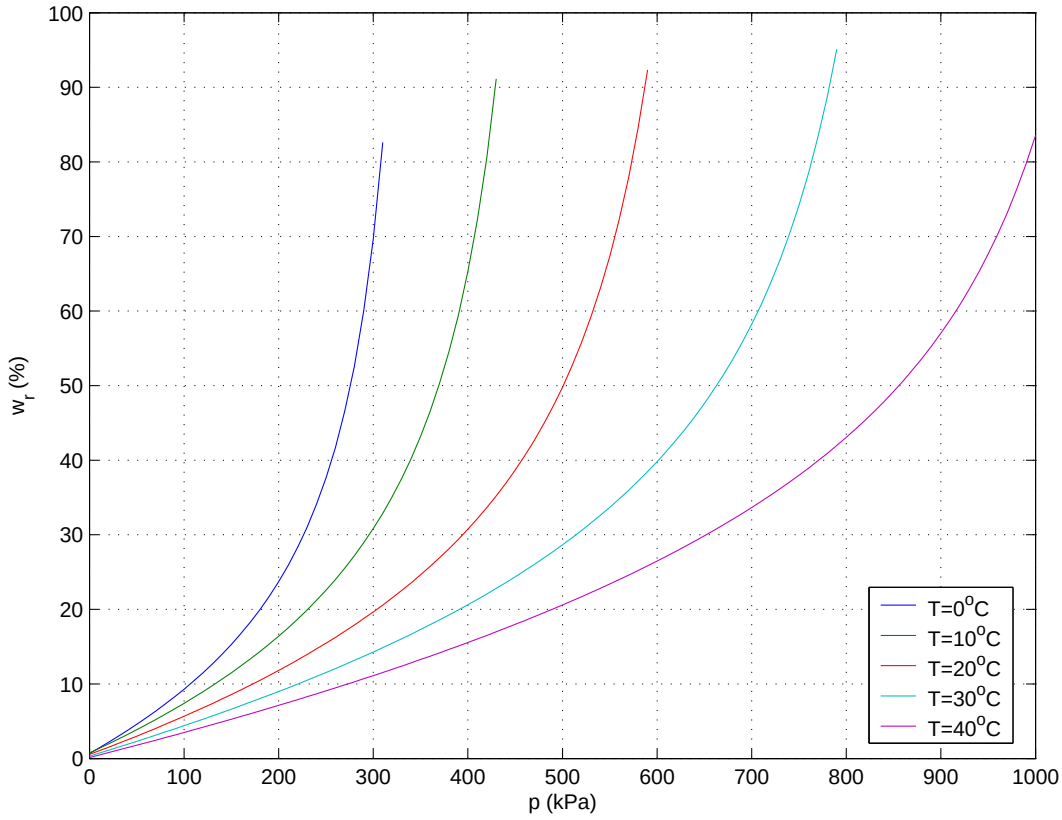

Figure B.1. Mass solubility of refrigerant R134a in the polyolester oil EMKARATE RL10H.

B.2. DENSITY

The density of the mixture is calculated by the additive law of mixtures, considering an ideal mixture. It might happen that a correction factor is needed in this calculation, but this value was not found in the literature reviewed.

$$\rho_l = \frac{\rho_{oil}}{1 + w\left(\frac{\rho_{oil}}{\rho_{lr}} - 1\right)} \tag{B.2}$$

The densities of the oil and of the liquid refrigerant are, respectively,

$$\rho_{oil}\left(kg/m^3\right) = 966.43636 - 0.57391608T - 0.00024475524T^2 \tag{B.3}$$

$$\rho_{lr}\left(kg/m^3\right) = 1294.679 - 3.22131T - 1.23398 \cdot 10^{-2} T^2 \tag{B.4}$$

The oil was adjusted between $20 < T < 120^o C$ while the refrigerant was adjusted for $-5 < T < 50^o C$.

Table B.2 presents results for the density of the ester oil and for the refrigerant R134a liquid as a function of temperature, while typical values for the density of the mixture as a function of temperature and refrigerant mass fraction are found in table B.3. Additionally, figure B.2 presents these results in the form of a graphic.

Table B.2. Densities for polyolester oil EMKARATE RL10H and for liquid refrigerant R134a.

$T(^oC)$	0	10	20	30
$\rho_{oil}(kg/m^3)$	966.4	960.7	954.9	949.0
$\rho_{lr}(kg/m^3)$	1294.8	1261.0	1225.3	1187.5

Table B.3. Density of the liquid mixture of EMKARATE RL10H polyolester and HFC R134a.

Density of the Liquid $\rho_l(kg/m^3)$		*w(%)*					
		5	10	15	20	25	30
$T(^o C)$	0	978.8	991.6	1004.7	1018.1	1031.9	1046.0
	10	972.2	984.1	996.3	1008.7	1021.5	1034.6
	20	965.5	976.4	987.6	999.0	1010.6	1022.6
	30	958.6	968.4	978.5	988.7	999.2	1009.8

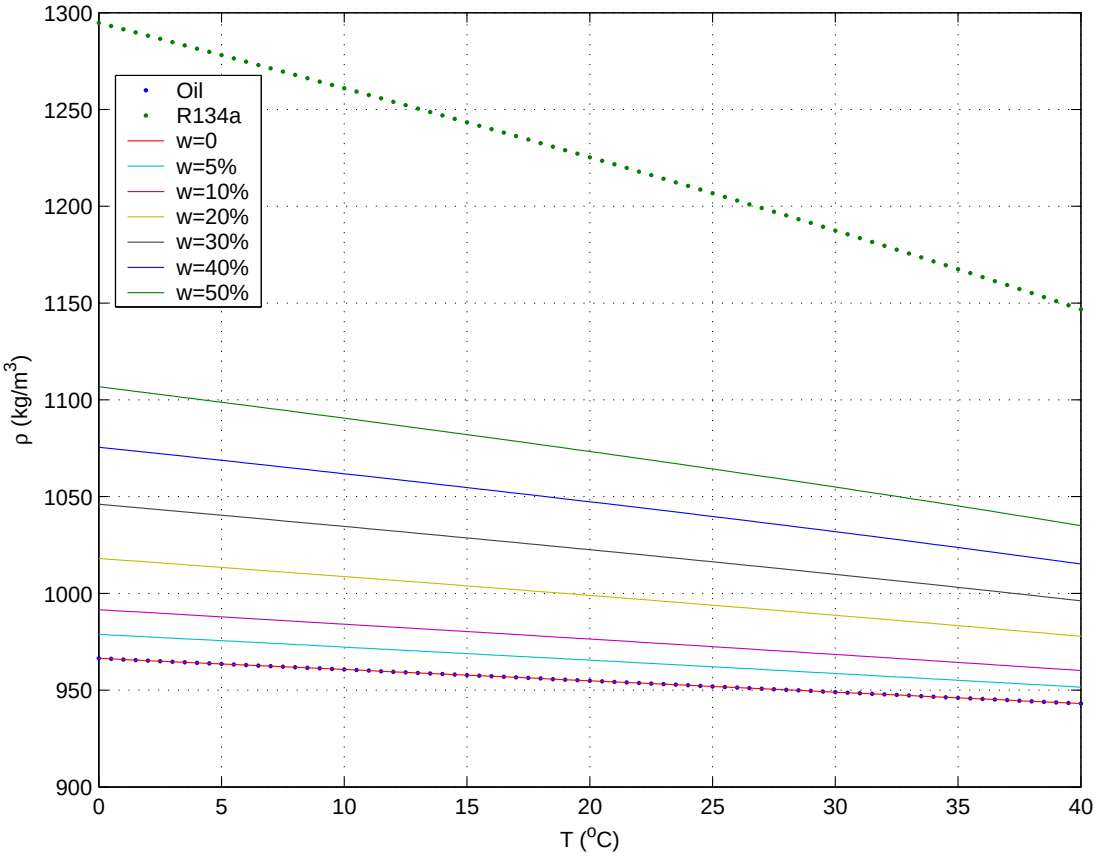

Figure B.2. Density of liquid mixture oil EMKARATE RL10H and refrigerant R134a.

B.3. VISCOSITY

Cinematic viscosity was adjusted from data provided by the producer (ICI) in a temperature range of $0 < T < 60^{o}C$, $0 < w < 50\%$, and it is given by the following equation, to $\nu(cSt)$:

$$\nu = \frac{a_1 + b_1 T + c_1 w + d_1 T^2 + e_1 w^2 + f_1 T w}{a_2 + b_2 T + c_2 w + d_2 T^2 + e_2 w^2 + f_2 T w} \tag{B.5}$$

$$a_1 = 38.31853120 \qquad a_2 = 1.0$$

$$b_1 = 0.03581164 \qquad b_2 = 0.05188487$$

$$c_1 = -0.55465145 \qquad c_2 = 0.02747679$$

$$d_1 = -6.02449153 \cdot 10^{-5} \qquad d_2 = 9.61400978 \cdot 10^{-4}$$

$$e_1 = 7.67717272 \cdot 10^{-4} \qquad e_2 = 4.40945724 \cdot 10^{-4}$$

$$f_1 = -2.82836964 \cdot 10^{-4} \qquad f_2 = 1.10699073 \cdot 10^{-3}$$

where $w(\%)$, $T(^{o}C)$.

The absolute viscosity can be obtained by multiplying kinematic viscosity and the density of the mixture. Therefore,

$$\mu = \rho\nu \text{ , and } \nu(m/s^2) = \nu(cSt)\cdot 10^6 \tag{B.6}$$

Table B.4 presents characteristic values for the viscosity of the mixture. These are also the values adopted in the program. Figure B.3 sketches the behaviour of the viscosity in terms of temperature and refrigerant mass fraction.

Table B.4. Absolute viscosity for mixture EMKARATE RL10H and refrigerant R134a.

Viscosity of the Liquid $\mu_l(mPa\cdot s)$		*w(%)*					
		5	*10*	*15*	*20*	*25*	*30*
$T(^oC)$	*0*	*30.3*	*24.7*	*20.0*	*16.2*	*13.1*	*10.5*
	10	*19.2*	*16.0*	*13.2*	*11.0*	*9.0*	*7.4*
	20	*13.0*	*11.0*	*9.3*	*7.8*	*6.5*	*5.4*
	30	*9.4*	*8.0*	*6.8*	*5.8*	*4.9*	*4.1*

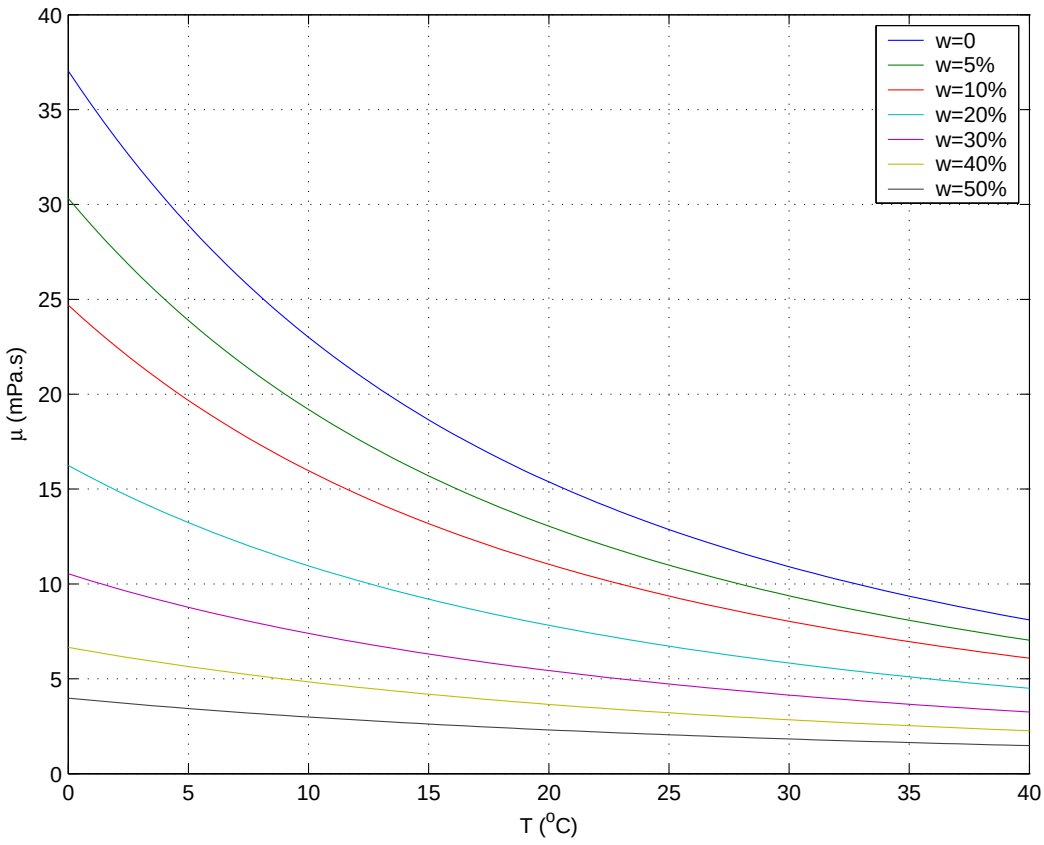

Figure B.3 – Absolute viscosity of the liquid mixture of R134a and oil EMKARATE RL10H.

B.4. REFRIGERANT PROPERTIES IN THE GAS PHASE

For the refrigerant R134a, density and viscosity were adjusted in the interval $25 < p < 400kPa$ and $-5 < T < 40^{o}C$, and can be represented respectively by equations (B.7) and (B.8):

$$\rho_g(kg/m^3) = \frac{a_1 + b_1 p + c_1 T + d_1 p^2 + e_1 T^2 + f_1 Tp}{a_2 + b_2 p + c_2 T + d_2 p^2 + e_2 T^2 + f_2 Tp} \qquad \text{(B.7)}$$

$a_1 = -3.76767 \cdot 10^{-5}$ $\quad$ $a_2 = 1.0$

$b_1 = 0.04493$ $\quad$ $b_2 = -9.03844 \cdot 10^{-4}$

$c_1 = -6.44683 \cdot 10^{-5}$ $\quad$ $c_2 = 0.01415$

$d_1 = -2.83514 \cdot 10^{-5}$ $\quad$ $d_2 = 9.37849 \cdot 10^{-8}$

$e_1 = 3.0247 \cdot 10^{-6}$ $\quad$ $e_2 = 3.98492 \cdot 10^{-5}$

$f_1 = 4.72793 \cdot 10^{-4}$ $\quad$ $f_2 = -2.38858 \cdot 10^{-6}$

$$\mu_g(Pa \cdot s) = \frac{10.8186 - 0.0026\,p + 0.1451T + 3.7658 \cdot 10^{-4} T^2 - 2.0170 \cdot 10^{-7} p^3}{1 - 2.1278 \cdot 10^{-4}\,p - 7.7520 \cdot 10^{-9}\,p^2 + 0.00967T} \qquad \text{(B.8)}$$

where *T(ºC)* and *p(kPa).*

Table B.5 presents values for density and viscosity of the refrigerant gas as function of pressure and temperature, which can also be seen in figures B.4 and B.5.

Table B.5. Characteristic values for density and viscosity of the refrigerant R134a gas.

T=0ºC						
$p(kPa)$	*50*	*100*	*150*	*200*	*250*	*300*
$\rho_g(kg/m^3)$	*2.3*	*4.6*	*7.0*	*9.5*	*12.1*	*14.8*
$\mu_g(\mu Pa \cdot s)$	*10.80*	*10.79*	*10.77*	*10.76*	*10.74*	*10.73*

T=10ºC						
$p(kPa)$	50	100	150	200	250	300
$\rho_g(kg/m^3)$	2.2	4.4	6.8	9.1	11.6	14.1
$\mu_g(\mu Pa \cdot s)$	11.21	11.20	11.19	11.18	11.17	11.17
T=20ºC						
$p(kPa)$	50	100	150	200	250	300
$\rho_g(kg/m^3)$	2.1	4.3	6.5	8.8	11.1	13.5
$\mu_g(\mu Pa \cdot s)$	11.61	11.61	11.61	11.60	11.60	11.59
T=30ºC						
$p(kPa)$	50	100	150	200	250	300
$\rho_g(kg/m^3)$	2.0	4.1	6.2	8.4	10.6	12.9
$\mu_g(\mu Pa \cdot s)$	12.01	12.01	12.01	12.01	12.01	12.01

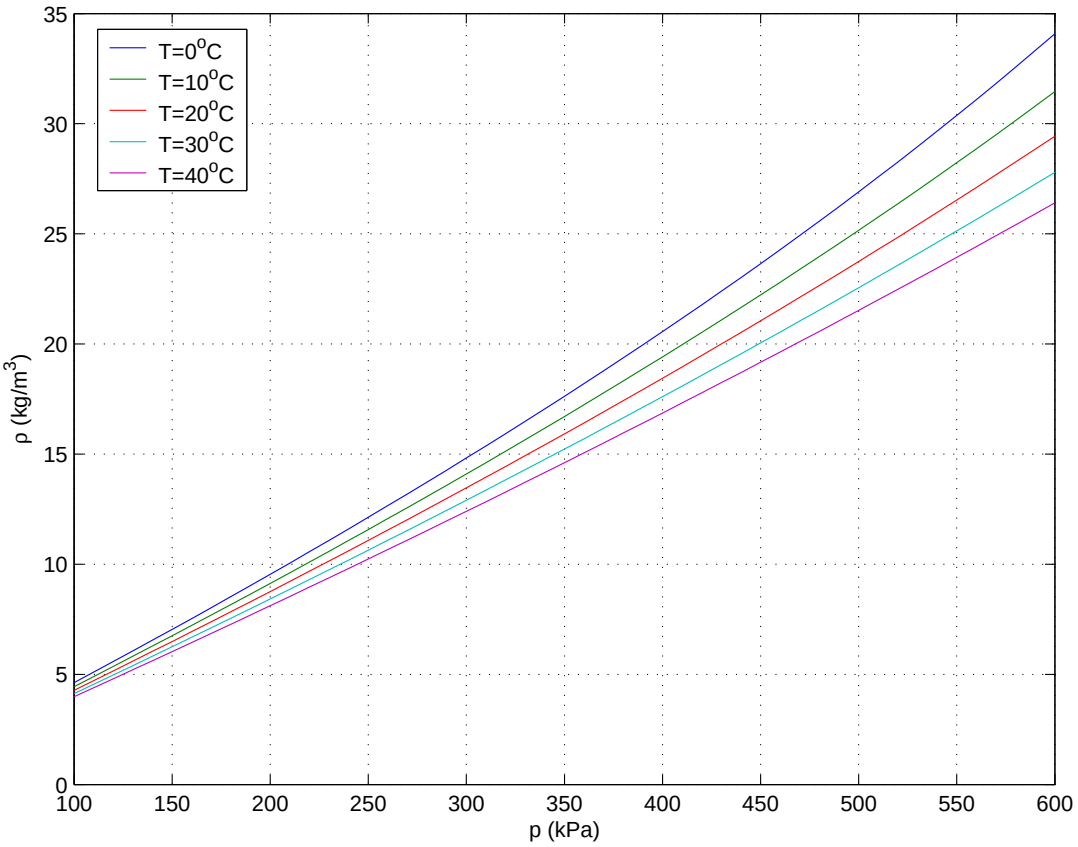

Figure B.4. Density of the refrigerant R134a gas as a function of pressure for various temperatures.

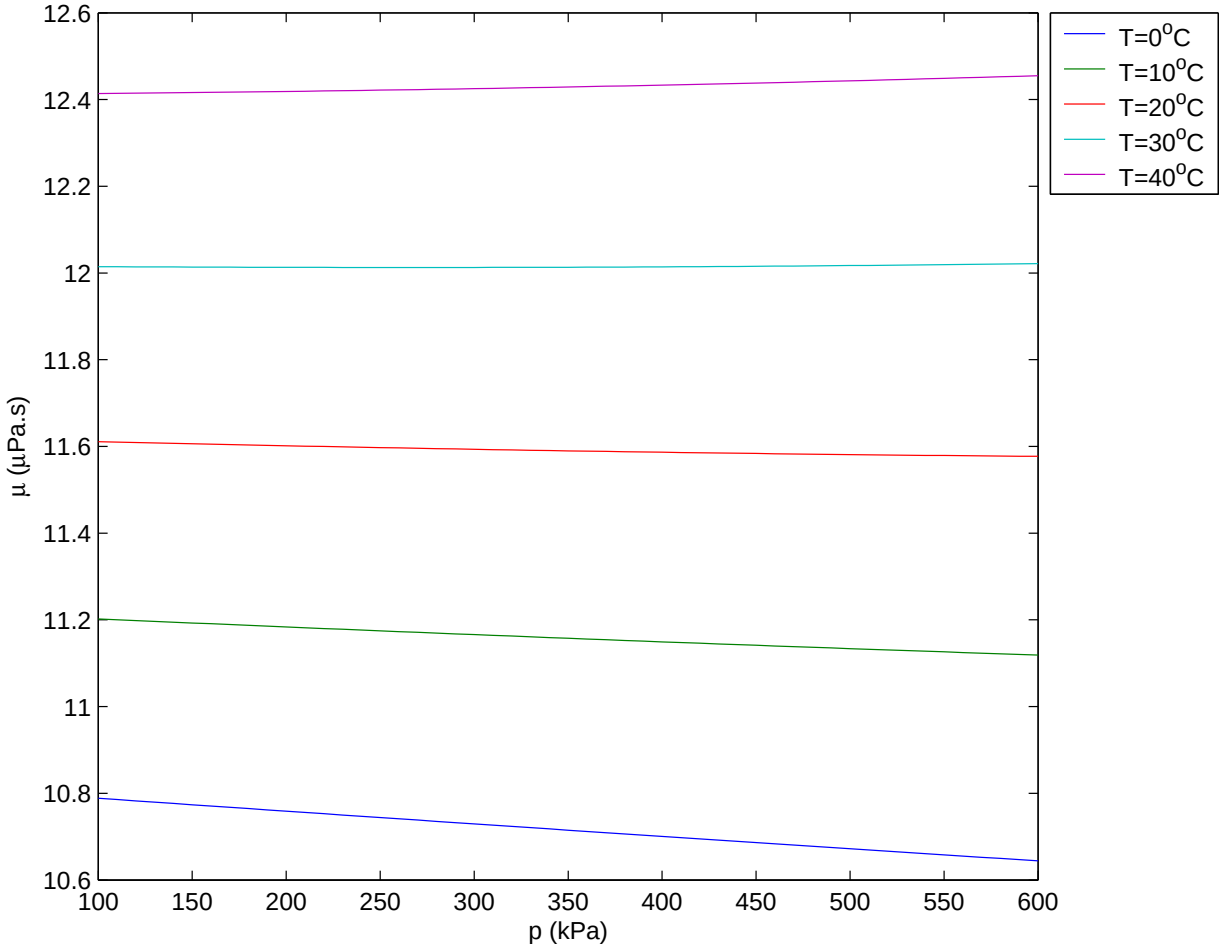

Figure B.5. Viscosity of the refrigerant R134a gas as a function of pressure for various temperatures.

Appendix C

RESEARCH PAPERS WRITTEN

Copies of the following papers are included in this appendix:

- Grando, F.P., Priest, M. and Prata, A.T. **Lubrication in Refrigeration Systems: Performance of Journal Bearings Lubricated with Oil and Refrigerant Mixtures**. Life Cycle Tribology, Proc. 31st Leeds-Lyon Symposium on Tribology, Leeds 2004, Tribology and Interface Engineering Series, Elsevier, Amsterdam, 2005, pp.481-491.
- Grando, F.P., Priest, M. and Prata, A.T. **A Two-Phase Flow Approach to Cavitation Modelling in Journal Bearings**. Tribology Letters, v.21, n.3, 2006, pp.233-244.
- Grando, F.P., Priest, M. and Prata, A.T. **Lubrication in Refrigeration Systems: Numerical Model for Piston Dynamics considering Oil-Refrigerant Interaction**. Proc. IMechE, Part J, Journal of Engineering Tribology, v.220, n.3, 2006, pp.245-258.

Lubrication in Refrigeration Systems: Performance of Journal Bearings Lubricated with Oil and Refrigerant Mixtures

F. P. Grando[a,b], M. Priest[a], A. T. Prata[b]

[a] Institute of Tribology, School of Mechanical Engineering, The University of Leeds, LS2 9JT, Leeds, UK

[b] Department of Mechanical Engineering, Federal University of Santa Catarina, 88040-900, Florianopolis, Brazil

The phasing out of chlorofluorocarbon refrigerants (CFCs) from refrigeration systems for environmental reasons has stimulated the study of oil and refrigerant mixtures, as different oils are required to work with the replacement refrigerants, especially hydrofluorocarbons (HFCs). Considering lubrication of the compressor present in most refrigeration systems, several experimental studies have investigated aspects such as film-forming capability and wear performance presented by oils working in pressurised refrigerant environments. However, there is little published research on how lubricant properties are affected by the solubility of refrigerant in rich oil-phase mixtures and their application to the design of components.

In this context, this work studies lubrication with an oil and refrigerant mixture as the lubricant. Initially, a steadily loaded partial journal bearing is analysed, where the lubricant is characterised through correlations for solubility, density and viscosity. The methodology presented eliminates the use of intermediate boundary conditions in determining cavitation. Alternatively, the release of refrigerant gas from the lubricant mixture when saturation pressure is reached in the divergent region of the bearing is considered directly, with a two-phase flow thereafter. Results comparing this alternative treatment of cavitation with the Reynolds condition are presented and discussed. Furthermore, the differences in the performance of the bearing lubricated with the oil-refrigerant mixture instead of pure oil are analysed. It is observed that, under the same operating conditions, a reduction in the load carrying capacity occurs for the lubricant mixture due to its lower viscosity.

1. INTRODUCTION

The refrigeration industry has been experiencing a series of major challenges in the last two decades. Under the regulations imposed by the Montreal Protocol in 1987, the well-established working fluids CFC (chlorofuorocarbon) have been banned due to their detrimental environmental impact, especially their ozone depletion potential [1]. Therefore, the use of alternative refrigerants was required, such as HFCs, hydrofluorocarbons, and HCs, hydrocarbons. This also induced a change in the lubricants used, where oils such as polyol esters and alkylbenzenes replaced mineral oils in many cases. Furthermore, being responsible for about 10% of the world energy demand [1], there has been considerable pressure for increases in energy efficiency – where compressor energy performance plays an important role along with cycle and thermodynamic efficiency of the system [2]. For these reasons, significant impulse was given to the study of the inevitable interaction between the refrigerant fluid and the lubricant oil in refrigeration systems using mechanical compression of vapour. Such a system is schematically presented in Figure 1, along with the effects of the oil and refrigerant interaction in the main components [3].

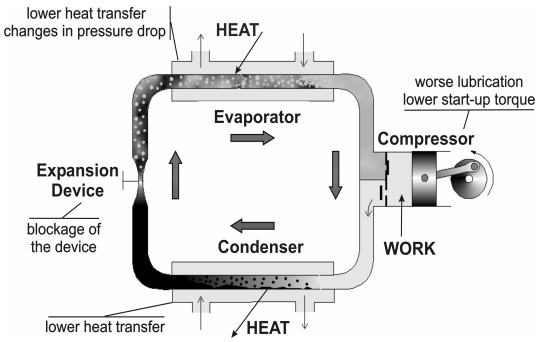

Figure 1. Schematic model of a refrigeration system and the effects of oil-refrigerant interaction

As reviewed by Motta et al. [4], much of the work has been devoted to studies where the oil is treated as a contaminant, considering mixtures with a rich-refrigerant phase and being mainly focused on the influence of the mixture in the heat transfer processes occurring in the system [5,6].

With regard to compressor lubrication, where a rich-oil phase prevails, a series of experimental studies have dealt with lubricant performance in a pressurised refrigerant environment. It was observed that a considerable reduction in film forming capability occurs as the environment pressure increases [7,8]. The study of wear performance also showed that combinations of lubricant and refrigerant with lower viscosities are subjected to more severe conditions and even boundary lubrication [9,10]. The results of these studies highlight effects such as the reduction of lubricant viscosity with refrigerant solubility and the increase in solubility with pressure.

As previous research shows, compressor lubrication cannot be simply estimated from oil properties. Nevertheless, the numerical approaches currently used for the design of components still consider such a condition [11,12], and improvements are therefore required.

In order to develop more accurate methodologies to study lubrication of compressor parts, the first step was the determination of the properties of liquid mixtures of oil and refrigerant, especially solubility and viscosity. Despite considerable effort, general rules have not yet been achieved, and correlations for properties are in the main empirical [13,14].

A series of other effects can also be observed in addition to changes in liquid properties. The fluid can experience significant negative pressure gradients in the system and refrigerant can be released in the form of bubbles as solubility decreases, giving raise to a flow where liquid-vapour phase change occurs, commonly defined as a *flashing flow*. In order to understand flashing flow, it has been studied initially in the simpler geometry of a straight, horizontal, constant diameter pipe. Experimental tests showed for different mixtures that considerable outgassing occurs with the decrease of pressure along the flow, even observing foaming characteristics when larger amounts of gas are released [15,16]. In the light of these findings, the first numerical models were proposed by Grando and Prata [17] and Barbosa Jr. et al. [18], both obtaining good agreement with experimental results from Lacerda et al. [15]. Such developments are useful to the analysis of lubrication and leakage processes inside the compressor. The amount of gas released in the flow can be related to the leakage of refrigerant, which consequently influences pumping efficiency.

Concerning compressor lubrication, with the knowledge of mixture properties and flashing flows, a new proposal to study cavitation is possible. How to model this phenomenon is not completely clear, as conditions in which it occurs are difficult to identify in situations such as dynamic loading in bearings and in the clearance between the ringless piston and the cylinder. Using conventional methodologies, in which intermediate boundary conditions are defined, results are very sensitive to the assumed boundary conditions, as shown by Priest et al. [19] when studying piston ring lubrication. Attempting to overcome this difficulty, the present work proposes the analysis of lubrication using a two-phase flow approach and considering an oil and refrigerant mixture as the lubricant. The model is applied to the simplified conditions occurring in a partial journal bearing, where inlet and outlet pressures can be identified.

2. NOMENCLATURE

c	radial clearance of the bearing [m]
D	diameter of the shaft [m]
e	eccentricity [m]
$F_f^{'}$	friction force per unit length [N/m]
F_f^{*}	friction force per unit length for a ruptured film [N/m]
h	lubricant film thickness ($=c+e\cos(\theta)$) [m]
m_l	total mass of liquid (oil+refrigerant) [kg]
m_{lr}	mass of liquid refrigerant [kg]
p	absolute pressure [Pa]
R	shaft radius [m]
T	temperature [^oC]
U	tangential velocity of the shaft ($=2\pi\omega R$) [m/s]
w_i	overall refrigerant mass fraction at inlet [-]
w_r	refrigerant mass fraction [-]
w_{sat}	refrigerant solubility in the oil [-]
$W^{'}$	applied load per unit length [N/m]
$W_1^{'}$	load component along the line of centres [N/m]
$W_2^{'}$	load component, perpendicular to $W_1^{'}$ [N/m]

Greek symbols

ε eccentricity ratio (=*e/c*) [-]
θ angular coordinate of the bearing [^{o}, *rad*]
λ ratio between mass fraction and solubility [-]
μ dynamic viscosity [*Pa.s*]
$\overline{\mu}$ homogeneous viscosity, equation (6) [*Pa.s*]
ρ density [kg/m^3]
$\overline{\rho}$ homogeneous density, equation (5) [kg/m^3]
ϕ void fraction, equation (4) [-]
ϕ_a estimated void fraction, analytical solution [-]
χ quality, equation (3) [-]
ω angular velocity of the shaft [*Hz*]

Subscripts

cav cavitation position
g gas phase
i inlet position
l liquid phase
o outlet position

3. MODEL DEVELOPMENT

3.1. Physical Modelling

The case under study is a 180º infinitely long partial journal bearing subject to a steady load. The applied load is such that the line of centres between shaft and bearing remains aligned with the vertical, corresponding to a symmetric convergent/divergent gap as presented in Figure 2. The lubricant is supplied in one side as a liquid oil-refrigerant mixture and completely removed at the other side to ensure continuity.

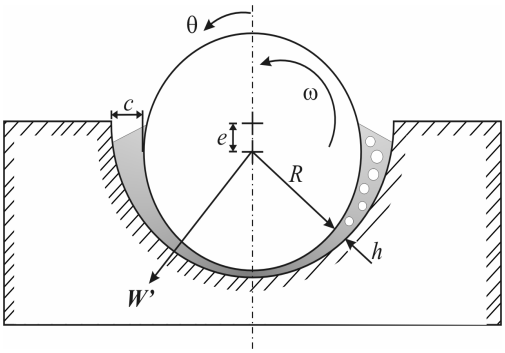

Figure 2. Geometry of the problem

In the convergent region, pressure increases due to the hydrodynamic wedge effect. Considering the liquid to be incompressible and with no free gas present in this region, the fluid properties remain constant. However, in the divergent region, pressure decreases and at the point where the saturation pressure of the mixture is reached, refrigerant will be released from the liquid and will flow as a free gas. As the oil vapour pressure is low, no oil is present in the gas phase. Additionally, considering metastability to be negligible, instantaneous releases occur and the liquid mixture can only be saturated or subsaturated. As the fluid advances in the divergent region, the gap increases and there is further pressure reduction, such that free gas expands and new releases can take place. This situation is schematically presented in Figure 3. No ventilation from the surroundings is considered, as the bearing is infinite.

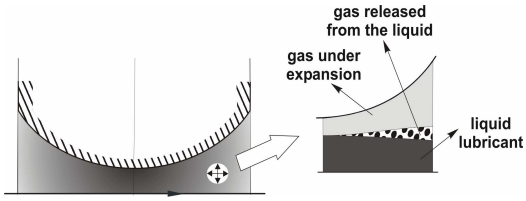

Figure 3. Flow behaviour in the divergent region

From observations in the previous flashing flow research in pipes [15], the bubbles formed with the release of gas flow with a velocity very similar to the liquid, such that a homogeneous flow can be assumed. Therefore, due to good mixing and essentially the same velocity of gas and liquid, the two-phase flow can be modelled as a monophasic flow of an equivalent fluid, whose properties are based on averages from the constituent phases. Other authors have also adopted this approach in the study of bubbly oil lubrication, where non-condensable gases are considered [20,21].

Close to the end of the bearing, ambient pressure at the outlet is communicated to the fluid. As the pressure in the fluid film can be lower than the ambient, pressure recovery may occur. In this case, film pressure increases and some gas may conceivably redissolve in the oil. However, absorption is expected to be much slower than the release of refrigerant, and the liquid may not have sufficient time to reabsorb the gas. In this work, absorption will not be considered at the outlet, such that at this position a flow of gas and subsaturated liquid will be observed. With the advance in studies of absorption, this hypothesis will be reviewed. At present it is impossible to determine the rate in

which refrigerant will return to the liquid mixture, such that further research into the transient behaviour of absorption is required. Yokozeki [22] and Silva [23] have performed preliminary studies considering slow process rates and are referenced as a motivating starting point.

These assumptions concerning the fluid behaviour are included in addition to the common hypotheses adopted for journal bearings [24], such that the lubrication equation remains valid for the mathematical model presented.

3.2. Mathematical Modelling

To characterise fractional composition of refrigerant and oil in the liquid mixture, as well as the proportion of liquid and gas in the two-phase flow, a series of parameters are needed, defined as follows.

Refrigerant mass fraction: the amount of refrigerant dissolved in the liquid mixture, on a mass basis, defined by equation (1),

$$w_r = \frac{m_{lr}}{m_l} \tag{1}$$

The maximum quantity of refrigerant that can be dissolved in the liquid for a specific condition of pressure and temperature is defined as the *solubility*,

$$w_{sat} = w_{sat}(p,T) \tag{2}$$

Quality: the ratio between the mass of gas and the total mass of the mixture within a cross-sectional area of the flow. In terms of the refrigerant mass fraction, it can related to the overall fluid composition at the entrance, thus being given by,

$$\chi = \frac{w_i - w_r}{1 - w_r} \tag{3}$$

Void fraction: ratio between the gas volume and the total volume within a section of the flow. In the homogeneous model, for identical velocities of both phases, it is calculated by equation (4),

$$\phi = \frac{1}{\left(1 + \left(\frac{1}{\chi} - 1\right)\frac{\rho_g}{\rho_l}\right)} \tag{4}$$

Having defined these parameters, the liquid-gas mixture can be replaced in the homogeneous model by a monophasic pseudofluid, whose density and viscosity are given by [25],

$$\bar{\rho} = \phi\rho_g + (1-\phi)\rho_l \tag{5}$$

and,

$$\bar{\mu} = \chi\mu_g + (1-\chi)\mu_l \tag{6}$$

Based on these definitions and assuming steady-state, one-dimensional and isothermal conditions, with pressure and viscous forces dominant, the flow is governed by the Reynolds equation, where the homogeneous properties are considered as presented in equation (7).

$$\frac{\partial}{\partial\theta}\left(\frac{\bar{\rho}h^3}{\bar{\mu}}\frac{\partial p}{\partial\theta}\right) = 6UR\frac{\partial}{\partial\theta}(\bar{\rho}h) \tag{7}$$

The governing equation is valid for the whole angular extent of the bearing, which also indicates that the solution respects conservation of mass. Furthermore, as inlet and outlet pressures are known, the following boundary conditions apply,

$$\begin{aligned} &\theta = \theta_i,\ p = p_i \\ &\theta = \theta_o, p = p_o \end{aligned} \tag{8}$$

Equation (7) is then numerically solved using finite volume methodology [26]. As fluid properties vary along the bearing, additionally depending on pressure, an iterative process is required. The procedure adopted is described in Figure 4.

Having determined the pressure profile, other performance variables can be calculated. The load capacity per unit length is given by,

$$W' = \sqrt{W'^2_1 + W'^2_2} \tag{9}$$

where,

$$W'_1 = -\int_{\theta_i}^{\theta_o} p(\theta)R\cos\theta d\theta \tag{10.i}$$

$$W'_2 = \int_{\theta_i}^{\theta_o} p(\theta)R\sin\theta d\theta \tag{10.ii}$$

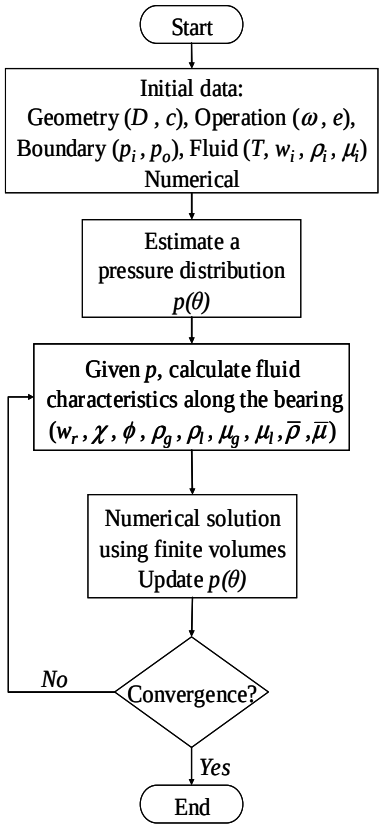

Figure 4. Solution procedure

The friction force on the shaft is calculated as,

$$F_f^{'} = \int_{\theta_i}^{\theta_o} \left(\frac{h}{2R}\frac{dp}{d\theta} + \bar{\mu}\frac{U}{h} \right) R d\theta \tag{11}$$

It should be noticed here that friction force is calculated using the same expression throughout the bearing. This result is different from the usual methodology [24], which considers film rupture and suggests friction to be taken as,

$$F_f^{*} = \int_{\theta_i}^{\theta_{cav}} \left(\frac{h}{2R}\frac{dp}{d\theta} + \mu_i\frac{U}{h} \right) R d\theta + \int_{\theta_{cav}}^{\theta_o} (1-\phi_a)\mu_i\frac{U}{h} R d\theta \tag{12}$$

where the viscosity is considered constant and equal to that at the entrance, and ϕ_a is the fraction of the film filled by gas cavities around which the oil flows in streams. The shear stress in the gas is assumed to be negligible. Furthermore, ϕ_a can be considered as the void fraction of the ruptured film and calculated by,

$$\phi_a = \frac{h - h_{cav}}{h}, \text{ for } \theta \geq \theta_{cav} \tag{13}$$

In a homogeneous flow, equation (12) is not applicable, since a common velocity and good mixing between phases are assumed. The effect of gas is introduced via the homogeneous viscosity. The difference in the results using these two equations for friction is discussed in more detail later.

4. RESULTS AND DISCUSSION

The model has been applied to a mixture of the HFC refrigerant R134a and a polyol ester oil (ICI EMKARATE RL10H), whose properties were provided by the oil manufacturer and adjusted using curve fitting. In addition, gas properties for R134a were calculated using the software REFPROP [27]. The correlations adopted are presented in the Appendix, and further details of the properties can be found in Silva [23].

Having defined the mixture, characteristic values for geometry and operating parameters were chosen for the partial journal bearing to approximate compressor operational conditions, as follows,

D=20mm, c=20μm, ω=60Hz=3600rpm, ε=0.8,
p_i=p_o=200kPa, T=40ºC, w_i=w_{sat}=7.13%

To solve the problem numerically, the domain was discretized into 100 regularly distributed internal points. Pressure results are presented in Figure 5. The result of the two-phase model is compared with the analytical solution considering Reynolds boundary conditions [24], where viscosity is considered constant and equal to that at the inlet of the bearing. Analytical results are presented both for the saturated condition and pure oil, with the same eccentricity. Due to the higher viscosity, the bearing lubricated with pure oil reaches considerably higher pressures. This confirms the reduction in load capacity observed with the solubility of the refrigerant in the oil.

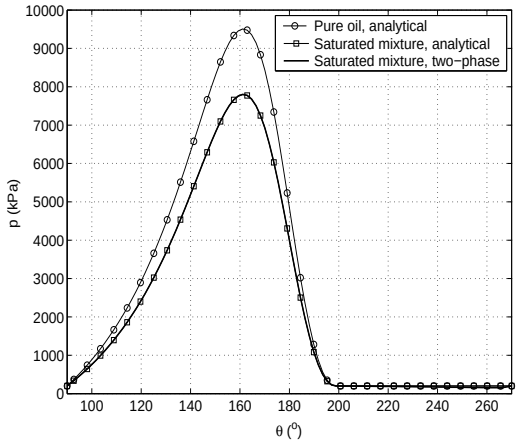

Figure 5. Pressure results for the partial journal bearing

In Figure 5, very good agreement is observed between the two-phase model and the analytical solution when the same fluid conditions are considered at the entrance. However, differences are observed when detailing the cavitation region in Figure 6, where it can be seen that pressure decreases as the film thickness increases for the two-phase model. Close to the end of the bearing, ambient pressure is communicated to the fluid by diffusion of momentum, resulting in pressure recovery. It should be noticed that the levels of pressure in the cavitated region are small compared to the maximum pressure. Therefore, in this particular case, where the bearing is heavily loaded, it is confirmed that Reynolds condition provides a good approximation [28]. However, additional tests using the model under light loads (e.g. higher clearances and smaller eccentricities) showed results moving gradually from Reynolds towards Sommerfeld conditions.

The reduction in pressure in the cavitated region is moderated by the release of gas from the liquid mixture, which is represented in Figure 7 by the refrigerant mass fraction in the liquid mixture. In the convergent region, despite the increase in pressure, mass fraction remains the same as no free gas is available to be absorbed. In the divergent region, pressure decreases and at $\theta \approx 200^o$ the mixture returns to the initial saturated condition. After this point, as solubility decreases with pressure, release of gas occurs in order that the mixture remains saturated. In the final 10^o, with pressure recovery, solubility increases but by assumption gas is not absorbed, and the mixture is now subsaturated. However, as this region is extremely small, no significant difference in the bearing behaviour would be observed if absorption occurred.

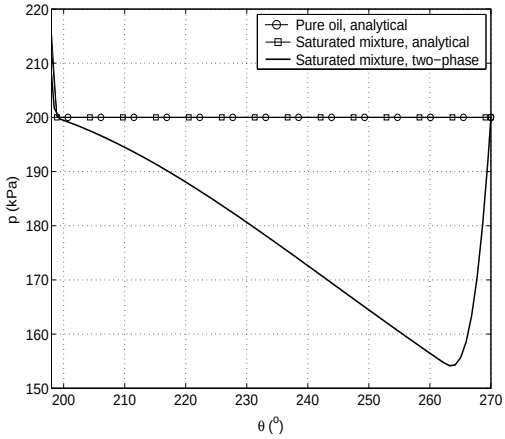

Figure 6. Detail of pressure in the cavitated region

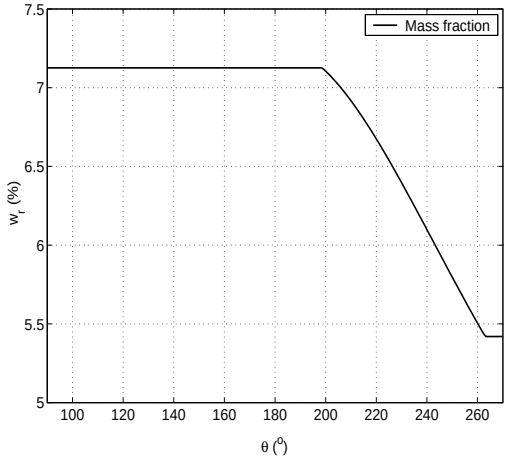

Figure 7. Mass fraction of the liquid mixture along the bearing

An estimate of quality from mass fraction after equation (3) shows that less than 2% gas is present at the exit, indicating that a very small amount of gas is required to fill the clearance in the divergent region. Despite the small quantity of gas released, its low density means that void fraction reaches values above 70%, as presented in Figure 8. This figure also presents the estimate of void fraction from the analytical solution, given by equation (13).

Apart from the pressure recovery region, good agreement is observed between the two curves in Figure 8. This occurs particularly because the flow in the convergent region is assumed incompressible, having no gas present. From this similarity, one can conclude that void fraction is basically determined by geometrical factors if only liquid is present at the entrance.

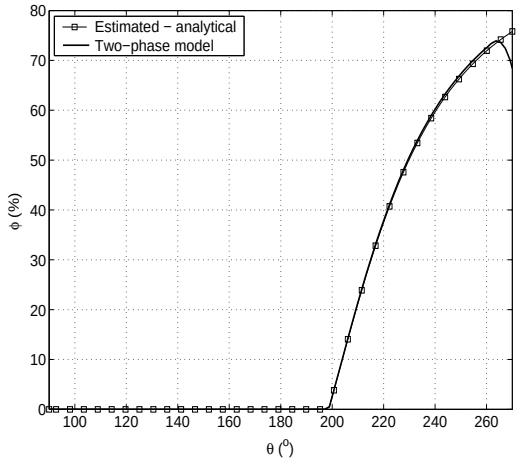

Figure 8. Void fraction for the two-phase flow

The same behaviour observed for void fraction occurs for the homogenous density, presented in Figure 9 along with the liquid density. While the latter is almost constant throughout the bearing, the homogeneous density varies significantly in the cavitated region, such that the two-phase mixture completely fills the space between shaft and bearing. The large magnitude of variation is due to the low density of the refrigerant gas, which is below $10kg/m^3$ in this test condition, while the density of the liquid is approximately $950kg/m^3$. Although less significant than the effects of outgassing, variations also occur due to the changes in gas density with pressure. This is clearly seen at the end of the bearing, when homogeneous density increases as the gas is compressed.

The changes experienced by the fluid along the flow also promote changes in viscosity, as Figure 10 presents for the liquid and homogeneous viscosities. For the latter, despite the increasing presence of a very low viscosity phase ($\mu_g \approx 12.5 \mu Pa.s$), viscosity actually increases, which reflects the change in liquid viscosity with the reduction in its refrigerant mass fraction. Nevertheless, the variation is not greatly significant (≈3.5%) so the assumption of a constant viscosity would not be a bad first approximation for practical purposes.

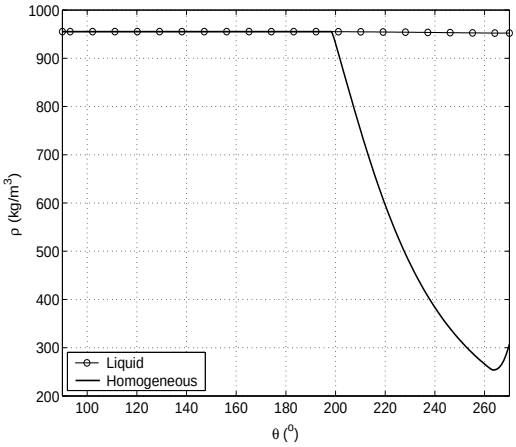

Figure 9. Liquid and homogeneous density along the bearing

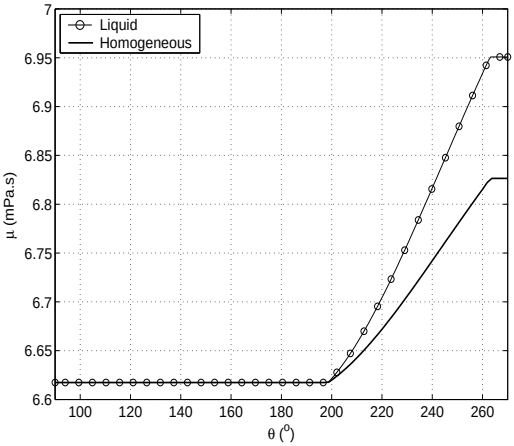

Figure 10. Liquid and homogeneous viscosity

For the three different simulations previously presented, load and friction were calculated and the results are presented in Table 1. Considering the saturated mixture, good agreement between the two-phase model and the analytical solution is confirmed by results for load capacity and friction force F_f', computed neglecting film rupture (it should be noticed that this is not the typical result for the analytical solution). The small differences observed are related to the negative pressures in the divergent region.

However, the load capacity and friction force are 22% bigger if pure oil is used as lubricant. This is

simply due to the higher viscosity of the oil compared to the mixture.

When film rupture is considered to calculate friction, F_f^*, as just the liquid flow is responsible for viscous effects in the cavitated region, a significant reduction is observed *(≈10%*), as shown in Table 1. Theoretically, film rupture would occur in pure oil, where no gas is available to be released and F_f^* is appropriate. However, for an oil and refrigerant mixture, with the release of gas in bubbles that remain imprisoned in the middle of the lubricant film [15], rupture or film separation are not expected and F_f' should be used. Nevertheless, even if pure oil is considered, equation (11) is pragmatically adopted in situations where the cavitation boundary is not easily identifiable, such as in a ringless piston [11,12]. A similar procedure, calculating F_f', was also used by Qi et al. [20] in the study of bubbly oil lubrication.

Table 1. Results for load and friction

	Pure oil μ_i*=8.10mPa.s*	*Saturated mixture* μ_i*=6.62mPa.s*	
	Analytic	*Analytic*	*Two-phase*
W' *(kN/m)*	*76.64*	*62.56*	*62.62*
F_f' *(N/m)*	*155.48*	*126.93*	*127.52*
F_f^* *(N/m)*	*139.63*	*113.99*	-

Using the same methodology, a wider range of eccentricities and mass fractions were evaluated using both the analytical solution and the two-phase model. Results for load capacity and friction force are presented respectively in Figures 11 and 12. Friction force is calculated assuming film rupture in the analytical solution, while in the two-phase model it is calculated without rupture. Different levels of refrigerant dissolution are considered. To characterise them, the ratio between refrigerant mass fraction and solubility at the inlet (λ_i) is used, ranging from *0* (pure oil) to *1* (saturated mixture).

It can be observed from Figure 11 that as more refrigerant is dissolved in the oil, viscosity is gradually reduced and this adversely affects load capacity. To illustrate the change in performance for a particular load, lines 1-1' and 2-2' are considered. For the first case (1-1'), a bearing expected to work with pure oil at ε*=0.65* (*W'=34.5kN/m*) would actually be operating at ε*=0.69* for a saturated oil/refrigerant mixture; for the second case, the *110kN/m* supported by pure oil at ε*=0.85* would shift to ε*=0.875* for the mixture. These changes are small compared to the changes in viscosity, but indicate the potential variations that can occur under conditions such as dynamic loading. For instance, during gas compression, pressure increases and more refrigerant can dissolve in the oil, amplifying the effects previously described. They would be even more evident in other mixtures with higher solubilities, such as refrigerant R12 and mineral oil, as experimentally observed by Akei et al. [7].

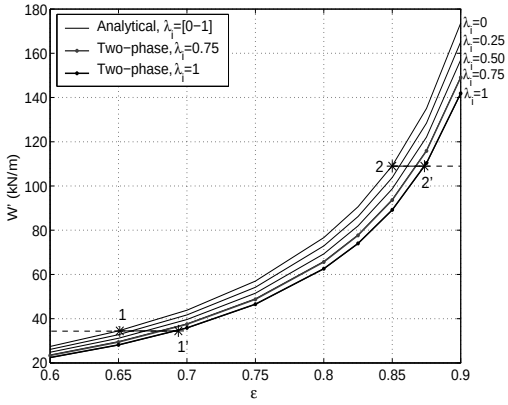

Figure 11. Load capacity for different fluid conditions and eccentricities

For the friction results in Figure 12, analytical results consider the hypothesis of film rupture (more suitable for pure oil) while the two-phase model remains consistent with the assumption of a homogeneous flow. Analysing the two examples, at low eccentricity, 1-1', friction reduces due to reduction in viscosity. However friction force is greater in the two-phase model at higher eccentricities, 2-2', as geometric effects outweigh the reduction in viscosity. This reinforces the necessity to consider fluid conditions in operation to optimise the design of refrigeration compressors.

The good agreement between the two-phase model and the Reynolds solution obtained in the previous results is encouraging, showing that variations of fluid properties considered so far can reproduce a series of phenomena occurring in a bearing. However, the model is intended for more complex conditions, such as dynamic loading and bubbly lubrication, where significant differences with current methodologies are expected. This requires additional studies regarding absorption

under the strong positive pressure gradients occurring in the convergent region when gas is present at the inlet. Furthermore, as surface tension is also affected by mixing conditions, bubble dynamics along the extent of the bearing also need to be considered. All these developments must be validated by experimental studies, especially for the fast transient behaviour of oil and refrigerant mixtures. The generality of the model must also be verified by testing more mixture combinations.

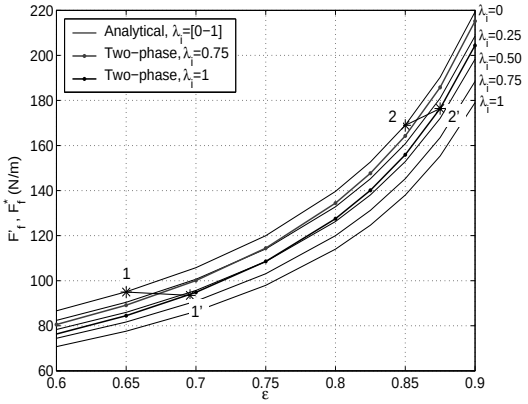

Figure 12. Friction force for different fluid conditions as a function of eccentricity

5. CONCLUSIONS

The effect of refrigerant dissolution in oil on the performance of journal bearings has been evaluated using a homogeneous two-phase flow approach. The model considers cavitation through refrigerant outgassing from a liquid mixture under saturation conditions, and no intermediate boundary conditions are required in solving the lubrication equation. A partial journal bearing was chosen for the tests due to its simplified geometry and well-defined inlet and outlet pressure conditions.

For a case where the bearing is heavily loaded, the model agrees very well with the analytical results considering Reynolds boundary conditions with a saturated mixture. Assuming only liquid is present in the convergent region, the cavitation position and the void fraction are also similar and can be seen as geometrically determined. However, sub-ambient pressures are observed in the cavitated region. The level of these pressures is related to the density of the gas released. A pressure recovery region to the outlet pressure is also identified, which is related to the diffusion of momentum.

Comparing the results of an oil and refrigerant mixture to those considering pure oil, a considerable reduction in load capacity is observed with the mixture, which is a consequence of the reduction in viscosity due to refrigerant dissolution. This also leads to different working conditions under the same applied load, with higher eccentricities for the mixture case. The differences are expected to be bigger if gas is present in the convergent region. This, however, requires detailed knowledge and a model for the absorption of the refrigerant by the oil, which have not yet been established.

ACKNOWLEDGEMENTS

This research is supported by the Programme Alβan, the European Union Programme of High Level Scholarships for Latin America, identification number E03D22219BR. Assistance from the Brazilian Compressor Company EMBRACO SA is duly acknowledged. Thanks also to Prof. Richard Coy of the University of Leeds and Dr. Jader Barbosa Jr. of the Federal University of Santa Catarina for the useful discussions.

REFERENCES

[1] McMullan J.T. Refrigeration and the environment – issues and strategies for the future. International Journal of Refrigeration, 2002; 25:89-99.

[2] Possamai F.C., Todescat M.L. A review of compressors energy performance. Proceedings of the 17th International Compressor Engineering Conference at Purdue, 2004; Paper C046.

[3] Cavallini A., Del Col D., Doretti L., Longo G.A., Rossetto L. Heat transfer and pressure drop during condensation of refrigerants inside horizontal enhanced tubes. International Journal of Refrigeration, 2000; 23:4-25.

[4] Motta S.F.Y., Braga S.L., Parise J.A.R. Experimental study of adiabatic capillary tubes: critical flow of refrigerant/oil mixtures. HVAC&R Research, 2001; 7(4):331-344.

[5] Spauschus H.O., Speaker L.M. A review of viscosity data for oil-refrigerant solutions. ASHRAE Transactions, 1987; 93(2):667-681.

[6] Hewitt N.J., McMullan J.T. Refrigerant-oil solubility and its effects on system performance. Proceedings of the 19th ICR,

International Congress of Refrigeration, 1995; IVa:290-296.
[7] Akei M., Mizuhara K., Taki T., Yamamoto T. Evaluation of film-forming capability of refrigeration lubricants in pressurized refrigerant atmosphere. Wear, 1996; 196:180-187.
[8] Na B.C., Chun K.J., Han D.C. A tribological study of refrigeration oils under HFC-134a environment. Tribology International, 1997; 30(9):707-716.
[9] Safari S., Hadfield M. Wear behaviour of the piston/gudgeon pin in a hermetic compressor with replacement CFC refrigerants. Wear, 1998; 219:8-15.
[10] Ciantar C., Hadfield M., Smith A.M., Swallow A. The influence of lubricant viscosity on the wear of hermetic compressor components in HFC-134a environments. Wear, 1999; 236:1-8.
[11] Prata A.T., Fernandes J.R.S., Fagotti F. Dynamic analysis of piston secondary motion for small reciprocating compressors. Journal of Tribology, 2000; 122:752-760.
[12] Kim T.J., Han J.S. Comparison of the dynamic behavior and lubrication characteristics of a reciprocating compressor crankshaft in both finite and short bearing models. Tribology Transactions, 2004; 47(1):61-69.
[13] Grebner J.J., Crawford R.R. Measurement of pressure-temperature-concentration relations for mixtures of R12/mineral oil and R134a/synthetic oil. ASRHAE Transactions, 1993; 99(1):380-386.
[14] Mermond Y., Feidt M., Marvillet C. Thermodynamic and physical properties of mixtures of refrigerants and oils. International Journal of Refrigeration, 1999; 22:569-579 [*In French*].
[15] Lacerda V.T., Prata A.T., Fagotti F. Experimental characterisation of oil-refrigerant two-phase flow. Proceedings of the ASME – Advanced Energy Systems Division, 2000; 40:101-109.
[16] Castro H.O.S., Gasche J.L., Conti W.P. Foam flow of oil-refrigerant R134a mixture in a small diameter tube. Proceedings of the 10th International Refrigeration and Air Conditioning Conference at Purdue, 2004; Paper R171.
[17] Grando F.P., Prata A.T. Computational modeling of oil-refrigerant two-phase flow with foam formation in straight horizontal pipes. Proceedings of the 2nd International Conference on Heat Transfer, Fluid Mechanics and Thermodynamics – HEFAT, 2003; Paper GF2.
[18] Barbosa Jr. J.R., Lacerda V.T., Prata A.T. Prediction of pressure drop in refrigerant-lubricant oil flows with high contents of oil and refrigerant outgassing in small diameter tubes. International Journal of Refrigeration, 2004; 27:129-139.
[19] Priest M., Dowson D., Taylor C.M. Theoretical modelling of cavitation in piston ring lubrication. Proceedings of the Institution of Mechanical Engineers, Part C, 2000; 214(3):435-447.
[20] Qi A., Yinsheng Z., Yongxin Q. Study on the viscosity properties of bubbly oil and the static characteristics of journal bearing lubricated with bubbly oil. Wear, 1997; 213:159-164.
[21] Someya T. On the development of negative pressure in oil-film and the characteristics of journal bearing. Meccanica, 2003; 38:643-658.
[22] Yokozeki A. Time-dependent behavior of gas absorption in lubricant oil. International Journal of Refrigeration, 2002; 25:695-704.
[23] Silva A. Kinetics and dynamics of gas absorption by lubricant oil. DEng thesis, Federal University of Santa Catarina, Florianopolis, Brazil, 2004 [*In Portuguese*].
[24] Pinkus O., Sternlicht B. Theory of hydrodynamic lubrication. New York: McGraw-Hill, 1961.
[25] Carey V.P. Liquid-vapor phase-change phenomena. New York: Hemisphere, 1992.
[26] Patankar S.V. Numerical heat transfer and fluid flow. New York: McGraw-Hill, 1980.
[27] McLinden M.O., Klein S.A., Lemmon E.W., Peskin A.W. REFPROP – Thermodynamic and transport properties of refrigerants and refrigerant mixtures, version 6.0. Washington(DC): NIST, 1998.
[28] Dowson D., Taylor C.M. Cavitation in bearings. Annual Review of Fluid Mechanics, 1979; 11:35-66.

APPENDIX: Calculation of physical properties

As previously described in the text, empiricism is the most common procedure in determining physical properties for oil-refrigerant mixtures, very often

adjusting curves from experimental data that has been made available. In this work, properties for the mixture of refrigerant R134a and oil ICI EMKARATE RL10H were calculated using mainly data provided in graphical form by the oil manufacturer. For pure refrigerant, data were obtained from the software REFPROP [27]. This Appendix presents the numerical correlations adopted to calculate the physical properties required. For further discussion on the properties of the fluids and the behaviour of this specific mixture, reference is made to Silva [23].

A.1. Solubility

The solubility of R134a in the polyol ester oil ICI EMKARATE RL10H was provided by the oil manufacturer in a diagram and adjusted by curve fitting for the interval $0<p<1000kPa$ and $0<T<60ºC$ as,

$$w_{sat} = \frac{a_1 + b_1 p + c_1 T + d_1 p^2 + e_1 T^2 + f_1 Tp}{a_2 + b_2 p + c_2 T + d_2 p^2 + e_2 T^2 + f_2 Tp} \qquad \text{(A1)}$$

where a_1=0.6825, b_1=0.0701, c_1=0.0699, d_1=-1.2087x10^{-4}, e_1=-1.7157x10^{-3}, f_1=2.4124x10^{-3}, a_2=1.0, b_2=-3.1315x10^{-3}, c_2=0.0503, d_2=1.0541x10^{-6}, e_2=1.3645x10^{-3}, f_2=-6.4074x10^{-5}.

A.2. Density

The density for the mixture R134a-EMKARATE RL10H is calculated using the additive law of mixtures. Considering an ideal mixture, the result is presented in equation (A2),

$$\rho_l = \frac{\rho_{oil}}{1 + w_r\left(\frac{\rho_{oil}}{\rho_{lr}} - 1\right)} \qquad \text{(A2)}$$

where ρ_l is the density of the liquid mixture, ρ_{oil} the density of the pure oil, ρ_{lr} the density of the liquid refrigerant, and w_r is the refrigerant mass fraction.

The oil density, provided by the manufacturer and adjusted in the range $20<T<120ºC$ is given by,

$$\rho_{oil} = a_3 + b_3 T + c_3 T^2 \qquad \text{(A3)}$$

where a_3=966.4364, b_3=-0.5739, c_3=-2.4476x10^{-4}, and ρ_{oil} the density in kg/m^3.

The density of the liquid refrigerant is obtained from the software REFPROP [27] and validated for the interval $-5<T<50ºC$ as follows,

$$\rho_{lr} = a_4 + b_4 T + c_4 T^2 \qquad \text{(A4)}$$

where a_4=1294.6790, b_4=-3.2213, c_4=-0.0123, and ρ_{lr} the density in kg/m^3.

A.3. Viscosity

The viscosity of the liquid mixture R134a and the polyol ester oil was provided by the oil manufacturer and the following fit is proposed for the interval $0<T<60ºC$ and $0<w_r<1$,

$$\mu_l = \frac{a_5 + b_5 T + c_5 w_r + d_5 T^2 + e_5 w_r^2 + f_5 T w_r}{a_6 + b_6 T + c_6 w_r + d_6 T^2 + e_6 w_r^2 + f_6 T w_r} \qquad \text{(A5)}$$

where a_5=0.0371, b_5=9.1603x10^{-5}, c_5=-0.0800, d_5=-2.7390x10^{-7}, e_5=-0.0435, f_5=-6.0485x10^{-5}, a_6=1.0, b_6=0.0531, c_6=2.2309, d_6=1.1656x10^{-3}, e_6=-0.3053, f_6=0.0334; and μ_l the viscosity ($Pa.s$).

A.4. Properties for the refrigerant in gas phase

The properties of the gas were obtained using the software REFPROP [27], and for the interval $0<p<1600kPa$ and $0<T<60ºC$ the following fits are proposed for density ρ_g (kg/m^3) and viscosity μ_g ($Pa.s$), respectively,

$$\rho_g = \frac{a_7 + b_7 p + c_7 T + d_7 p^2 + e_7 T^2 + f_7 Tp}{a_8 + b_8 p + c_8 T + d_8 p^2 + e_8 T^2 + f_8 Tp} \qquad \text{(A6)}$$

where a_7=4.2473x10^{-3}, b_7=-1.9077x10^{-4}, c_7=0.0448, d_7=3.4605x10^{-5}, e_7=-2.4624x10^{-5}, f_7=5.3830x10^{-4}, a_8=1.0, b_8=0.0155, c_8=-8.2500x10^{-4}, d_8=4.5680x10^{-5}, e_8=6.9326x10^{-8}, f_8=-2.1388x10^{-6}.

$$\mu_g = \frac{a_9 + b_9 p + c_9 T + d_9 T^2 + e_9 p^3}{a_{10} + b_{10} p + c_{10} p^2 + d_{10} T} x10^{-6} \qquad \text{(A7)}$$

where a_9=10.8186, b_9=-2.6052x10^{-3}, c_9=0.1451, d_9 = 3.7658x10^{-4}, e_9 = -2.0170x10^{-7}, a_9 = 1.0, b_{10}=-2.1278x10^{-4}, c_{10}=-7.752x10^{-9}, d_{10}=9.6695x10^{-3}.

Tribology Letters, Vol. 21, No. 3, March 2006 (© 2006)
DOI: 10.1007/s11249-006-9027-6

A two-phase flow approach to cavitation modelling in journal bearings

F.P. Grando[a,b,*], M. Priest[a] and A.T. Prata[b]

[a]*Institute of Tribology, School of Mechanical Engineering, The University of Leeds, Leeds LS2 9JT, UK*
[b]*Department of Mechanical Engineering, Federal University of Santa Catarina, Florianopolis 88040-900, Brazil*

Received 4 November 2005; accepted 12 January 2006; published online 6 May 2006

Cavitation has been extensively treated in numerical models for lubrication using boundary conditions in the pressure equation, and several criteria are available. However, an inappropriate choice can lead to imprecise results, thus having serious implications for performance prediction. This work proposes the numerical solution for lubrication analysing the changes suffered by the lubricant along a journal bearing, considering the release of gas from the liquid and the existence of a two-phase flow. Results obtained are compared with those using the Reynolds, or Swift-Steiber, boundary condition. The influence of fluid properties on the main parameters of bearing operation is also discussed.

KEY WORDS: cavitation, journal bearings, two-phase flow, oil–refrigerant mixture

Notation

c	radial clearance of the bearing [m]
D	diameter of the shaft [m]
e	eccentricity [m]
f	friction coefficient ($=F_f/W$) [-]
F'_f	friction force per unit length [N/m]
F^*_f	friction force per unit length for a ruptured film [N/m]
F'_h	hydrodynamic force per unit length [N/m]
F'_ε	hydrodynamic component along the line of centres [N/m]
F'_ξ	hydrodynamic component, perpendicular to F'_ε [N/m]
h	lubricant film thickness ($=c+e\cos(\theta)$) [m]
m	mass of the shaft [kg]
m_l	total mass of liquid (oil + refrigerant) [kg]
m_{lr}	mass of liquid refrigerant [kg]
p	absolute pressure [Pa]
q_θ	mass flow rate per unit length [kg/(s m)]
R	shaft radius [m]
t	time [s]
T	temperature [°C]
U	tangential velocity of the shaft ($=2\pi\omega R$) [m/s]
w	refrigerant mass fraction [-]
w_o	overall refrigerant mass fraction [-]
w_{sat}	refrigerant solubility in the oil [-]
W'	applied load per unit length [N/m]

Greek symbols

Δt	time step [s]
ε	eccentricity ratio ($=e/c$) [-]
$\dot{\varepsilon}$	velocity of the shaft in the eccentricity direction [s^{-1}]
$\ddot{\varepsilon}$	acceleration of the shaft in the eccentricity direction [s^{-2}]
θ	angular coordinate based in the line of centres [°, rad]
θ_f	fixed angular coordinate of the bearing [°, rad]
μ	dynamic viscosity [Pa s]
$\bar{\mu}$	homogeneous dynamic viscosity, equation (8) [Pa s]
ρ	density [kg/m^3]
$\bar{\rho}$	homogeneous density, equation (7) [kg/m^3]
ρ_R	estimated homogeneous density for the classical solution, equation (23) [kg/m^3]
ϕ	void fraction, equation (6) [-]
χ	quality, equation (5) [-]
ψ	attitude angle [°, rad]
$\dot{\psi}$	shaft velocity in the attitude angle direction [s^{-1}]
$\ddot{\psi}$	shaft acceleration in the attitude angle direction [s^{-2}]
ψ_W	angle between the applied load and the vertical [°, rad]
$\dot{\psi}_W$	first order time derivative of the load angle [s^{-1}]
$\ddot{\psi}_W$	second order time derivative of load angles [s^{-2}]
ω	angular velocity of the shaft [Hz]

Subscripts

cav	cavitation position
g	gas phase
l	liquid phase
o	overall, initial condition
r	position immediately after the location considered
ref	reference, boundary position

Superscripts

(eq)	equilibrium
(ne)	non-equilibrium
t	current time step
$t+\Delta t$	next time step

*To whom correspondence should be addressed.
E-mail: menfpgr@leeds.ac.uk

1. Introduction

The disruption of a continuous liquid lubricant film, defined as cavitation, is very common is convergent–divergent geometries, such as found in journal bearings. For a very long time this phenomenon has been associated with the interaction of the oil and gases present in the working environment [1]. Many researchers explicitly mention terms referring to the solubility between oil and ambient gases, such as "air expulsion pressure" [2] and more commonly "saturation pressure" [3]. The saturation pressure is reached in the divergent region as pressure decreases, so that gases are released from the oil and break the continuity of the liquid film, leading to cavitation.

Nevertheless, the acknowledgement of this oil–gas interaction has not often been considered in developing numerical models to determine the cavitated region in practical problems. Instead, the approach has often been the use of boundary conditions to reproduce situations where film rupture, separation and reformation are believed to occur [3], therefore avoiding the solution of the existence of a two-phase flow in the cavitated region. Furthermore, the analysis remains limited to the full-film region. A detailed discussion on the most common conditions in which cavitation occurs can be found in [3]. Their implementation in boundary conditions for the lubrication equation has been made with many different models, many of which described in [4].

This approach has been widely used in the solution of practical problems, and has produced satisfactory results in many cases [1]. However, it may represent a difficulty in several other situations, three of which described as follows,

(i) *Cavitation pressure easily determined but difficult to determine how it occurs:* this situation can be exemplified by piston ring lubrication. In this case, the cavitation pressure is the ambient pressure at the bottom of the ring, but either separation or rupture of the film may occur. Priest *et al.* [5] tested different boundary conditions to determine cavitation and showed that results can vary significantly.
(ii) *Cavitation pressure is unknown:* in some cases, the pressure in which cavitation occurs may vary with time or space. For instance, in a ringless piston, considerable pressure gradient exists from top to bottom, maintained by a lubricant film in the piston-cylinder clearance. If cavitation exists at an intermediate position of piston length, the value of pressure for which it occurs is not clear.
(iii) *Bubbly oils:* If cavitation is defined as the emergence of gas dissolved in the oil, a conceptual difficulty arises when studying a situation where free gas already exists throughout the bearing. Using the commonly adopted boundary conditions, such as Reynolds, may lead to unrealistic results, particularly as the fluid is now compressible. Such a situation is commonly observed in squeeze film dampers [6].

Many of these problems had their solution attempted still using the approach based on boundary conditions. A powerful tool in this case is the well-known Elrod algorithm [7], which ensures conservation of mass and handles cavitation automatically, despite basing its definitions in usual intermediate boundary conditions for cavitaton. Solutions were obtained for either vapour [8] or gaseous cavitation [9], nevertheless without properly solving a two-phase flow, which may result from the difficulty of defining a compressibility factor for the two-phase solution as opposed to the one assumed for liquid only.

A great step was given by Kumar and Booker [10], modifying the Elrod algorithm [7] and including many ideas of two-phase flows. However, it still uses cavitation pressure as an adjustable parameter of the model and not as a property of the lubricant mixture, which represents a barrier to some of the difficulties previously listed.

To overcome these difficulties, the idea is to study the behaviour of the lubricant in the cavitated region, which inevitably requires the solution of a two-phase flow. This work proposes to model a two-phase flow in a journal bearing, analysing the behaviour of the fluid mixture along the flow, evaluating the dissolution of the gas in the oil and the interaction between liquid and gas phases, thereby changing lubricant properties.

2. Literature review

The first attempts to use two-phase flow models in lubrication considered thrust bearings. Tønder [11] analysed the effect of finely dispersed air bubbles in hydrodynamic lubrication of straight pivot pads. A compressible solution assuming a homogeneous two-phase flow was proposed to determine pressure variation in an isoviscous lubricant film containing a constant mass of gas distributed in the form of bubbles. Additional developments included surface tension effects in bubbles [12] but conclusions still pointed to few changes in load capacity and considerable shift in the load centre.

Further research has considered the solution for journal bearings where the isoviscous assumption was relaxed, usually replaced by empirical correlations for viscosity. Kicinski [13] used a homogeneous two-phase flow model to solve steady-state and dynamic problems involving partial and full journal bearings. Intermediate boundary conditions for pressure were not required and the model included estimates for the effect of air suction from the surroundings in the negative pressure region, defined as ventilation. Similarity with the results obtained using classical solutions, such as Reynolds boundary conditions, were obtained for simulations where a lower content of air in emulsion with the oil was considered, combined with a greater intake of air from the surroundings.

One of the widest tested models was proposed by Someya and collaborators [14–16], where a two-phase flow model has been used to solve journal bearing problems and compared with experimental results. Considering a constant mass of gas, this model included the solution for bubble dynamics and accounted for viscosity increases due to the compression of the gas. An empirical correlation based on the volume content of the gas was used to determine the mixture viscosity. It was shown that the model could reproduce both the negative

pressures observed experimentally and the larger positive pressure region when compared to incompressible fluid solutions.

Similar models have been developed and especially applied to squeeze film damper modelling. Tao *et al*. [6], using a two-phase flow model considering constant mass of gas and assuming surface tension to be negligible, demonstrated a dramatic reduction in damping force with the increase in aeration levels. They also mentioned the difficulty in determining the effective viscosity of the lubricant.

Bubbly-oil formulations, considering non-condensable gases, have promoted significant development in modelling journal bearings lubricated with aerated oil. However, interaction between oil and gas can be more significant. The gas can be dissolved in the oil and depending on the rate of decompression, it can be released in the form of bubbles. In such cases, the complexity of the problem increases as the local amount of free gas is not known and one must rely on thermodynamic calculations to determine the local gas fraction [17].

Information regarding such calculations is extremely scarce. For an oil–air mixture, Feng and Hahn [18] were one of the few authors to propose correlations for properties. Nevertheless, one area has received significant attention and considerable data is available: studying oil and refrigerant mixtures for the refrigeration industry. Due to environmental pressures, a series of recent major challenges have required the replacement of CFCs (chlorofluorocarbons) with alternative refrigerants, which include HFCs (hydrofluorocarbons), HCs (hydrocarbons) and CO_2. This has also perpetuated a change in the lubricants used, including synthetic oils such as POEs (polyol esters) and alkylbenzenes. To evaluate appropriate combinations of oil and refrigerant, considerable research has been done to determine properties of the mixture, particularly solubility, density, viscosity and enthalpy [19]. This mixture is of interest to lubrication studies, as it has already been shown that the interaction between the oil and refrigerant affects significantly the lubrication of the compressor present in refrigeration systems [20,21].

The present authors have previously proposed a preliminary model to study partial journal bearings, where the difference between modelling considering pure oil or oil–refrigerant as the lubricant was discussed [22]. Due to the availability of correlations for properties, the oil–refrigerant mixture will again be considered in the present work, which advances the modelling of two-phase lubrication in solving the problem of a full journal bearing.

3. Problem formulation

3.1. Physical modelling

The geometry considered is that of an infinitely long journal bearing, with a shaft that rotates at constant angular speed and is subjected to an external load. The bearing is initially filled with an oil–refrigerant mixture of known composition.

In the first instance, the physical analysis is undertaken for a steadily loaded journal bearing in its equilibrium position, but it can be easily extended to more complex situations, as detailed later. A liquid oil–refrigerant mixture is assumed at the start.

Due to the eccentricity between shaft and bush centres, the bearing will present a convergent–divergent geometry. In the convergent region, pressure increases due to the wedge effect. As long as only liquid is present in this region, fluid properties will remain constant. When the flow enters the divergent region, pressure falls and eventually reaches the saturation pressure for the liquid oil–refrigerant mixture at the given temperature.

At this point refrigerant is released from the liquid in the form of bubbles, flowing as a free gas. It is assumed that no oil is present in the gas phase due to its low vapour pressure. Furthermore, release occurs as soon as the saturation pressure is reached, and the liquid mixture can be only saturated or subsaturated. As the fluid advances further into the divergent region, free gas expands and new releases from the liquid take place. This situation is schematically presented in figure 1, along with the geometry of the problem. An additional assumption is that the flow is isothermal, as the amount of gas released is usually small, so that the energy required for the change of phase can be neglected.

As the flow once again approaches the convergent region of the bearing, the higher pressures upstream are communicated to the fluid by diffusion of momentum. Consequently the fluid will experience a region of pressure recovery before recirculating into the convergent area. In this case, film pressure increases and gas can be redissolved in the oil. However, absorption usually occurs at a much slower rate than release, and the liquid may not be able to absorb the gas in the flow time available during the positive pressure region. Due to the unknown absorption rate, it is only possible at the present to determine the two limit thermodynamic situations:

- *Full-equilibrium*, where the gas is reabsorbed instantaneously, as happens during release;
- *Non-equilibrium*, where no gas is absorbed after being released, therefore resulting in a two-phase flow throughout the whole bearing, including the positive pressure region. This situation has been observed in the literature [23] and leads to a transient problem even for constant loads, as the fluid properties vary continuously at all bearing positions from the initial condition until reaching equilibrium.

Additional research is required to rigorously evaluate the actual rates of absorption, particularly for the very quick times of flow observed in lubrication phenomena.

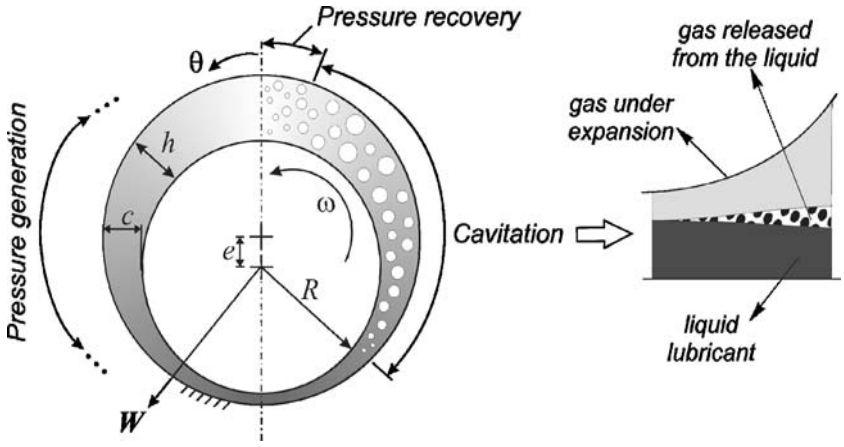

Figure 1. Geometry of the problem and detail of the gas release and film expansion in the cavitated region.

A few workers [24,25] have considered transient oil–refrigerant dissolution, however only at slow rates. Quicker processes of gas absorption have been investigated in other areas, such as in liquid jets and carbon dioxide imprisonment in deep seawater [26,27].

When considering transient processes in the bearing, either under steady load but out of equilibrium or under dynamic load, the only additional effect present is the squeeze film, which creates an additional pressure gradient, positive or negative. Under such circumstances, physical phenomena remain the same, with release of gas at saturation conditions. However, the position where saturation is reached may vary as pressure can be higher if the solid surfaces are approaching each other or lower if the surfaces are moving apart.

Another relevant aspect regards the relative motion between the liquid phase and the gas bubbles along the bearing. It has been observed in previous research of oil–refrigerant flow in pipes that the bubbles formed during outgassing present a very similar velocity to that of the liquid [28]. This indicates that assuming a homogeneous flow in modelling seems reasonable, following the same approach that has been adopted in previous bubbly-oil modelling [11–16]. Additionally, as surface tension effects can be neglected [6], pressure inside the bubbles can be assumed to be the same as that of the surrounding liquid.

Having information on how the fluid behaves physically, the lubrication of the journal bearing can be modelled. The common hypotheses adopted to derive the lubrication equation for journal bearings [29] are valid for the mathematical model presented here as the geometry of the bearing is entirely conventional.

3.2. Mathematical modelling

It is necessary to characterise the lubricant mixture in order to solve the lubrication problem. Therefore, to determine the fractional composition of oil and refrigerant in the liquid mixture and also the amount of liquid and gas in the two-phase flow, a series of parameters is needed. Regarding the liquid mixture, these are defined as follows

Refrigerant mass fraction. the amount of refrigerant dissolved in the liquid mixture, on a mass basis, defined by equation (1),

$$w = \frac{m_{\mathrm{lr}}}{m_{\mathrm{l}}} \tag{1}$$

At thermodynamic equilibrium, the maximum quantity of refrigerant that can be dissolved in the liquid for a given condition of pressure and temperature is defined as *solubility*,

$$w_{\mathrm{sat}} = w_{\mathrm{sat}}(p, T) \tag{2}$$

Refrigerant mass fraction is the parameter related to the release and absorption of gas from the liquid, and therefore depends on the thermodynamic situation considered.

For the release of gas in an isothermal process, pressure decreases and to maintain a saturated mixture so does the mass fraction. Thus,

$$w = w_{\mathrm{sat}}, \quad \text{for } p < p_{\mathrm{r}} \tag{3}$$

where p is the pressure at the current bearing position and p_{r} at the previous position, i.e., $\mathrm{d}p/\mathrm{d}\theta < 0$.

Considering absorption, however, two distinct situations are tested. Under thermodynamic equilibrium, as long as refrigerant is available as gas it can be absorbed in the liquid when pressure increases, i.e.,

$$w^{(\mathrm{eq})} = w_{\mathrm{sat}} \leq w_{\mathrm{o}}, \text{ for } p > p_{\mathrm{r}} (\text{ie.}, \mathrm{d}p/\mathrm{d}\theta > 0) \tag{4a}$$

where w_{o} is the overall refrigerant concentration (maximum available in the mixture).

If non-equilibrium is considered instead, refrigerant never returns to the liquid mixture once released. Therefore,

$$w^{(\mathrm{ne})} = w_{\mathrm{r}}, \quad \text{for } p > p_{\mathrm{r}} (\mathrm{d}p/\mathrm{d}\theta > 0) \tag{4b}$$

where w_r is the mass fraction at the position immediately before the location considered.

Having defined mass fraction, the proportion of liquid and gas in the two-phase flow can be characterised by the following parameters,

Quality: the ratio between the mass of gas and the total mass of the mixture within a cross-sectional area of the flow. In terms of the refrigerant mass fraction, it can related to the overall fluid composition, thus being given by

$$\chi = \frac{w_o - w}{1 - w} \tag{5}$$

Void fraction:. ratio between the gas volume and the total volume within a section of the flow, sometimes also known as the *aeration ratio*. In the homogeneous model, for identical velocities of both phases, it is calculated by equation (6),

$$\phi = \frac{1}{\left(1 + \left(\frac{1}{\chi} - 1\right)\frac{\rho_g}{\rho_l}\right)} \tag{6}$$

Given these parameters, the liquid–gas mixture is replaced in the homogeneous model by a monophasic pseudofluid, whose density and dynamic viscosity are given by [30],

$$\bar{\rho} = \phi\rho_g + (1 - \phi)\rho_l \tag{7}$$

and,

$$\bar{\mu} = \chi\mu_g + (1 - \chi)\mu_l \tag{8}$$

The correlation for density can be derived analytically from thermodynamic considerations. Homogeneous dynamic viscosity, however, does not have a precise definition and is chosen from several correlations available. Recently, analytical expressions taking into account the aeration rate and surface tension effects have been proposed [31].

Based on the two-phase flow definitions [30] and assuming one-dimensional conditions for a long bearing, with pressure and viscous forces dominant, the flow is governed by the Reynolds equation, where the homogeneous properties are considered as presented in equation (9),

$$\frac{1}{R^2}\frac{\partial}{\partial\theta}\left(\frac{\bar{\rho}h^3}{12\bar{\mu}}\frac{\partial p}{\partial\theta}\right) = \frac{1}{R}\frac{\partial}{\partial\theta}\left(\frac{\bar{\rho}Uh}{2}\right) + \frac{\partial}{\partial\theta}(\bar{\rho}h) \tag{9}$$

The governing equation is valid during a time step for the whole angular extent of the bearing, which also indicates that the solution respects conservation of mass. Furthermore, the solution requires calculation of absolute pressures so that lubricant properties can be updated. In this case, considering the pressure known at a reference position θ_{ref} in the full journal bearing, the following boundary conditions apply,

$$\begin{aligned} &p = p_{ref} \text{ for } \theta = \theta_{ref} \\ &p(\theta = 0) = p(\theta = 2\pi) \end{aligned} \tag{10}$$

For each time step, the numerical integration of equation (9) is performed numerically using finite volume methodology [32]. As fluid properties vary along the bearing due to pressure dependence, an iterative process needs to be adopted until convergence is achieved for pressure and fluid properties.

The conservation of mass can be checked by calculating the mass flow rate at any position in the fluid film according to equation (11),

$$q_\theta = \int_A \bar{\rho}u\,\mathrm{d}z = -\frac{\bar{\rho}h^3}{12\bar{\mu}R}\frac{\mathrm{d}p}{\mathrm{d}\theta} + \frac{\bar{\rho}Uh}{2} \tag{11}$$

Once a converged solution is achieved for the pressure field, the hydrodynamic force acting on the bearing can be calculated, and per unit length is given by

$$F'_h = \sqrt{F'^2_\varepsilon + F'^2_\xi} \tag{12a}$$

where,

$$F'_\varepsilon = -\int_0^{2\pi} p(\theta)R\cos\theta\,\mathrm{d}\theta \tag{12b}$$

$$F'_\xi = -\int_0^{2\pi} p(\theta)R\sin\theta\,\mathrm{d}\theta \tag{12c}$$

Additionally, the friction force on the shaft is calculated as

$$F'_f = -\int_0^{2\pi}\left(\frac{h}{2R}\frac{\mathrm{d}p}{\mathrm{d}\theta} + \bar{\mu}\frac{U}{h}\right)R\,\mathrm{d}\theta \tag{13}$$

Equation (13) differs from the equation usually adopted in the usual methodology [29], since friction is calculated using the same expression throughout the bearing, which results from the hypothesis of a homogeneous flow that assumes uniform mixing between phases and introduces gas effects through the homogeneous viscosity correlation. The more usual methodology instead considers film rupture and suggests friction to be taken as

$$F^*_f = \int_0^{\theta_{cav}}\left(\frac{h}{2R}\frac{\mathrm{d}p}{\mathrm{d}\theta} + \mu_{ref}\frac{U}{h}\right)R\,\mathrm{d}\theta + \int_{\theta_{cav}}^{2\pi}\left(\frac{h_{cav}}{h}\right)\mu_{ref}\frac{U}{h}R\,\mathrm{d}\theta \tag{14}$$

where μ_{ref} is the dynamic viscosity at the reference position of the bearing.

When considering the classical single-phase methodology [29] in the results to be explored, friction will be calculated using both approaches, that is, using equations (13) and (14), so that the difference can be evaluated. Additional discussion on the differences in the results of these equations can be found in [22].

To solve Reynolds equation (9), it is necessary to know the squeeze film term, $\partial(\bar{\rho}h)/\partial t$, for the time step considered. Furthermore, to determine the transient behaviour of the bearing, the solution for shaft dynamics is required. To this end, a balance of forces in the shaft is performed and a fixed reference needs to be considered in addition to the usual coordinate system passing through the line of centres of the shaft and bearing to track the shaft trajectory. The forces acting on the shaft and the reference coordinate systems employed here as presented in figure 2.

After appropriate algebraic manipulation, the balance of forces on the shaft can be written as [33]

$$mc\left[\ddot{\varepsilon} - \varepsilon\left(\dot{\psi}_W + \dot{\psi}\right)^2\right] = W\cos\psi - F_\varepsilon \qquad (15)$$

and

$$mc\left[2\dot{\varepsilon}\left(\dot{\psi}_W + \dot{\psi}\right) + \varepsilon\left(\ddot{\psi}_W + \ddot{\psi}\right)\right] = F_\xi - W\sin\psi \qquad (16)$$

From equations (15) and (16), for given load conditions as well as the shaft position and velocity at the time step t, accelerations can be determined,

$$\ddot{\varepsilon}^t = \varepsilon^t\left(\dot{\psi}_W^t + \dot{\psi}^t\right)^2 + \frac{1}{mc}(W\cos\psi^t - F_\varepsilon) \qquad (17)$$

and

$$\ddot{\psi}^t = -\ddot{\psi}_W^t - \frac{1}{\varepsilon^t}\left[2\dot{\varepsilon}^t\left(\dot{\psi}_W^t + \dot{\psi}^t\right) + \frac{1}{mc}(W\sin\psi^t - F_\xi)\right] \qquad (18)$$

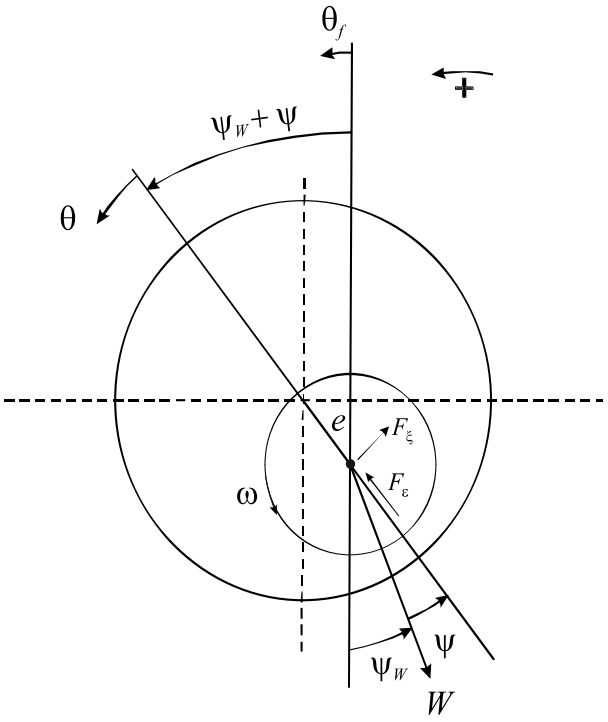

Figure 2. Balance of forces acting on the shaft and relation between fixed and moving coordinate systems, θ_f and θ, respectively.

The conditions for the next time step, $t+\Delta t$, are then calculated using an Euler marching scheme,

$$\dot{\varepsilon}^{t+\Delta t} = \dot{\varepsilon}^t + \ddot{\varepsilon}^t \cdot \Delta t \qquad (19)$$

$$\dot{\psi}^{t+\Delta t} = \dot{\psi}^t + \ddot{\psi}^t \cdot \Delta t \qquad (20)$$

and,

$$\varepsilon^{t+\Delta t} = \varepsilon^t + \dot{\varepsilon}^{t+\Delta t} \cdot \Delta t \qquad (21)$$

$$\psi^{t+\Delta t} = \psi^t + \dot{\psi}^{t+\Delta t} \cdot \Delta t \qquad (22)$$

Finally, with the new values for eccentricity ratio and attitude angle, a new pressure profile can be calculated using equation (9), in a marching process that continues until the equilibrium condition for the shaft is reached, which is a defined position in the case of a constant load or a defined orbit in the case of a dynamic load.

Figure 3 graphically describes the algorithm procedure to solve the transient problem.

4. Results and discussion

The methodology developed has been used to evaluate the difference between the classical solution and the two-phase flow approach, either considering equilibrium or non-equilibrium conditions during gas absorption. To this end, a mixture of the refrigerant HFC-134a and polyol ester oil ICI EMKARATE RL10H was chosen, with properties provided by the oil manufacturer and adjusted by curve fitting. In addition, gas properties were required and obtained from the software REFPROP [34]. The correlations adopted are presented in the Appendix A.

The first simulation considered a saturated oil–refrigerant mixture in the initial condition lubricating a bearing with a constant vertical load applied in the shaft centre. Although the potentialities of the model aim future application for dynamic loads, initially a steadily loaded bearing will be considered to evaluate the differences between the different thermodynamic assumptions for the mixture, which nevertheless will require a transient solution, particularly for the non-equilibrium case. Values for geometry and operating conditions are as follows

$$D = 20\,\text{mm},\ c = 20\,\mu\text{m},\ \omega = 30\,\text{Hz} = 1800\,\text{rpm},$$
$$W = 48\,\text{kN/m},\quad p_{\text{ref}} = 200\,\text{kPa}\quad at\quad \theta_f = 45^\circ,$$
$$T = 40\,^\circ\text{C},\ w_o = w_{\text{sat}} = 7.13\%$$

The numerical solution of the problem was discretized into 100 regularly distributed volumes and a time step of 1 ms. Initial conditions for ε_0, $\dot{\varepsilon}_0$, ψ_0 and $\dot{\psi}_0$ are all taken as 0.01. The solution for steady-state operating conditions permits comparison of the behaviour for two-phase solutions versus that considering Reynolds boundary conditions, where constant viscosity is

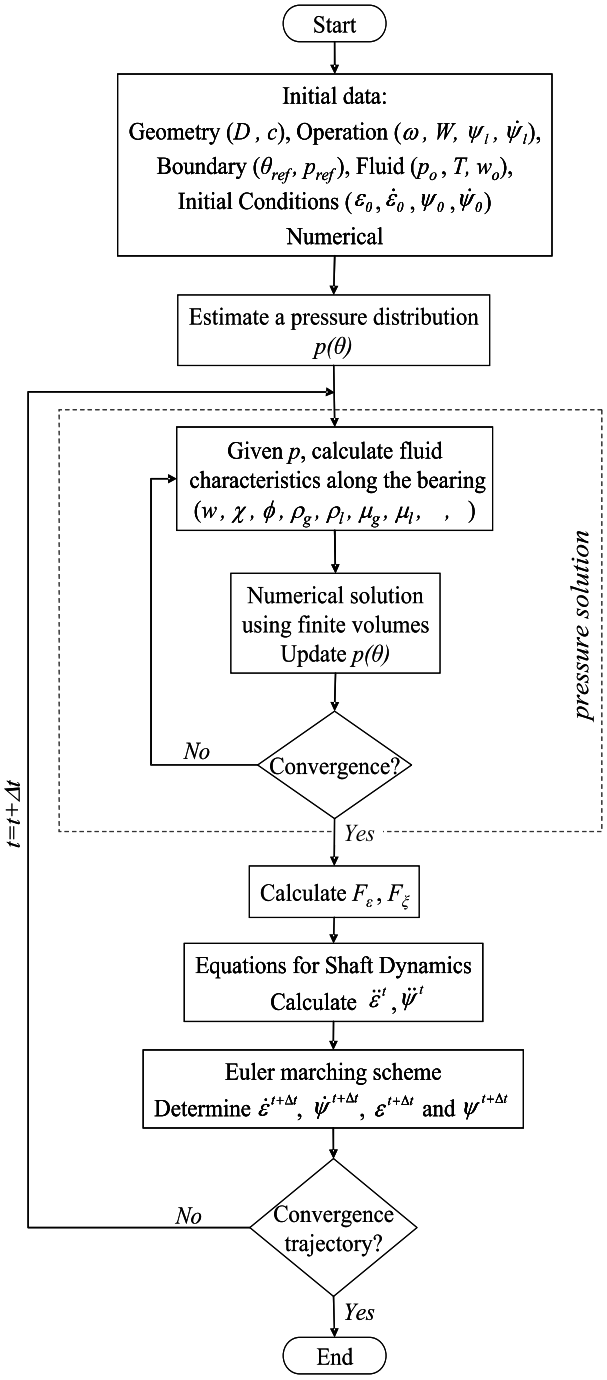

Figure 3. Algorithm employed for the solution procedure.

assumed and obtained using the cavitation algorithm [35]. Results for pressure are presented in figure 4.

As can be seen, good similarity exists between pressures calculated using the two-phase flow approach considering full thermodynamic equilibrium and those using Reynolds boundary conditions, which is expected under moderate and heavier loads. The differences appear only in the cavitated region, as detailed in the magnified area of the graph. For the two-phase model, pressure decreases as the film thickness increases, so that sub-ambient pressures exist. However, when comparing their values with the reference pressure, their magnitude is much lower than those observed for the maximum pressure in the convergent region. Under equilibrium

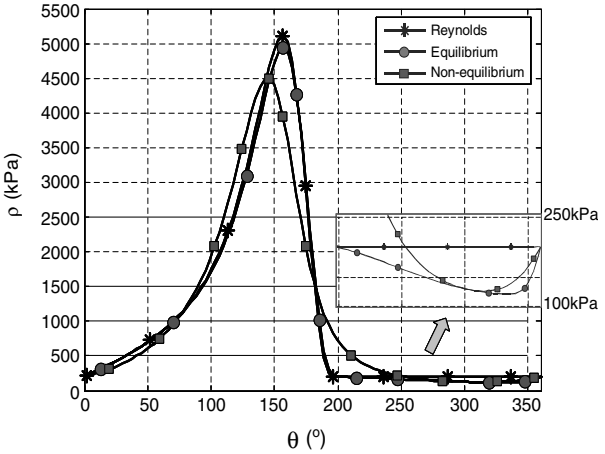

Figure 4. Steady-state pressure results for the different methodologies.

conditions, sub-ambient pressures lead to the release of gas, which in turn moderates the reduction in pressure. Close to the maximum film thickness, diffusion of momentum communicates the existence of the higher pressure region and results in pressure recovery being automatically determined by the two-phase model in a similar manner to the cavitation region.

However, as observed in figure 4, under non-equilibrium conditions for the mixture, where gas is present throughout the bearing, lower maximum pressure and a longer positive pressure region occur, indicating that the bearing supports the same load at lower eccentricity, thus potentially reducing friction force, as shown in table 1. Also note in table 1 the difference in attitude angle, due to the different profile of the pressure field.

The different behaviour observed for the pressure profile in the non-equilibrium case can be explained by compressibility effects, as shown in figure 5 in terms of the homogeneous density. For comparison, an estimated density is presented for the classical solution using Reynolds boundary conditions, defined as

$$\bar{\rho}_{\mathrm{R}} = \rho_{\mathrm{l,ref}}, \quad \text{for } \theta \leqslant \theta_{\mathrm{cav}}$$
$$\bar{\rho}_{\mathrm{R}} = \rho_{\mathrm{l,ref}}\left(\frac{h_{\mathrm{cav}}}{h}\right), \quad \text{for } \theta \geqslant \theta_{\mathrm{cav}} \tag{23}$$

Equation (23) will result in a discontinuity when reflecting that the values for the angles 0° and 360° should be the same. This can be interpreted as an instantaneous film reformation at 360° or alternatively as the gas content required by the variation of geometry

Table 1.
Results for shaft position and friction for the different simulations.

	ε	ψ (°)	F'_{f} (N/m)	F^*_{f} (N/m)
Reynolds	0.81	41	93.7	80.9
Equilibrium	0.80	42	93.6	–
Non-equilibrium	0.77	25	87.5	–

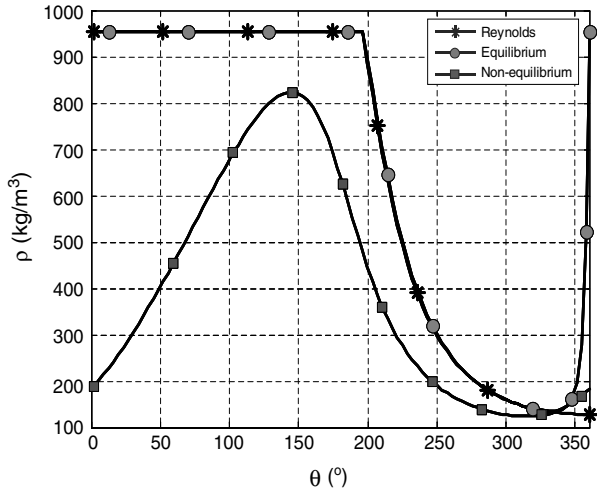

Figure 5. Homogeneous density along the bearing.

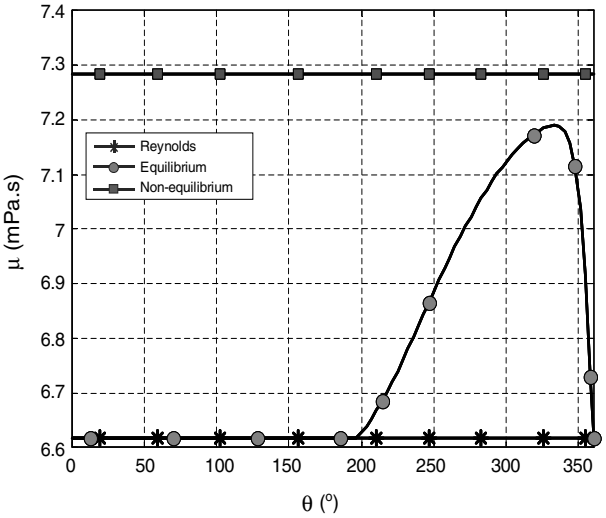

Figure 6. Viscosity of the two-phase mixture along the bearing.

after cavitation. However, as the value for density is not used for the solution and therefore does not affect the result provided by the classical solution, this density value can be used as an useful estimate to compare with those obtained with the two-phase solutions.

For the two-phase model assuming thermodynamic equilibrium, liquid only is present in the convergent region and as the flow reaches the cavitated region, gas is released and density decreases in response to the release and subsequent gas expansion. Similarity is again evident with the estimated results using Reynolds conditions, distinguished only in the pressure recovery region where gas returns to the liquid. Such agreement points to the importance of geometry in determining cavitation. The density results also permit estimation of the volume fraction of the gas, reaching a maximum of 85% close to 360°.

Considering non-equilibrium, gas is present throughout the bearing, and its compressibility enables the fluid to adapt in a smoother way to the geometry changes, which is called the density wedge [33]. Therefore, the density wedge assists the physical wedge effect in generating pressure, which explains the lower eccentricity presented in this case. Considering the cavitated region, as more gas is available from the beginning of the divergent region, a lower rate of change in density is observed when compared to that of the equilibrium solution, being similar only at higher aeration levels.

The behaviour of the absolute homogeneous viscosity for the different simulations performed is presented in figure 6. It can be observed that despite the low viscosity of the gas, the viscosity of the two-phase mixture actually increases. This can be explained by the increase in the viscosity of the liquid: with the release of refrigerant as gas, the mass fraction of the oil in the liquid mixture increases, therefore increasing the viscosity of the liquid given the higher viscosity of the oil compared to the liquid refrigerant. Nevertheless, it should be noted that the change in viscosity is small compared to that in density, as the latter depends on the volume fraction ($\phi_{max} \approx 85\%$) while the former depends on the mass of gas ($\chi_{max} \approx 3\%$). In the non-equilibrium case, the higher viscosity points to a greater release of gas. Furthermore, the constant behaviour throughout the bearing shows that variation of gas viscosity can be assumed negligible.

Given the potentially large property variations, it is interesting to evaluate how different initial mixture conditions affect the performance of the journal bearing. To this end, parametric tests were performed considering a mixture with different mass fractions at the initial condition. This effect could also be obtained through pressure and temperature, which affect directly the solubility.

Evaluating separately equilibrium and non-equilibrium conditions, the parametric tests considered mass fractions varying from 0.8 to 1.2 of the solubility at the initial pressure and temperature, using additionally the following data,

$$D = 20\,\text{mm},\ c = 20\,\mu\text{m},\ \omega = 60\,\text{Hz} = 3600\,\text{rpm},\ \varepsilon = 0.8,$$
$$p_{ref} = 200\,\text{kPa}\ \text{ at }\ \theta = 0^\circ,\ T = 40\,^\circ\text{C},\ w_o = w_{sat} = 7.13\%$$

Figure 7 presents the pressure results for equilibrium conditions, including, for comparison, the simulation using Reynolds boundary conditions. It is shown that higher pressures are obtained for the lower mass fraction ($0.8w_{sat}$), reflecting its higher viscosity. The release of gas starts at the same angular location along the fluid film, indicating the geometry influence in determining the onset of cavitation. However, as saturation pressure differs among the mixtures, so does the cavitation pressure, and a lower value occurs for the lower mass fraction. Furthermore, as the density of the gas decreases with pressure, the pressure drop is smaller for the mixture with the lower mass fraction. These results point to the influence of viscosity in the positive pressure region, whereas the gas density is the most important property in the cavitated region.

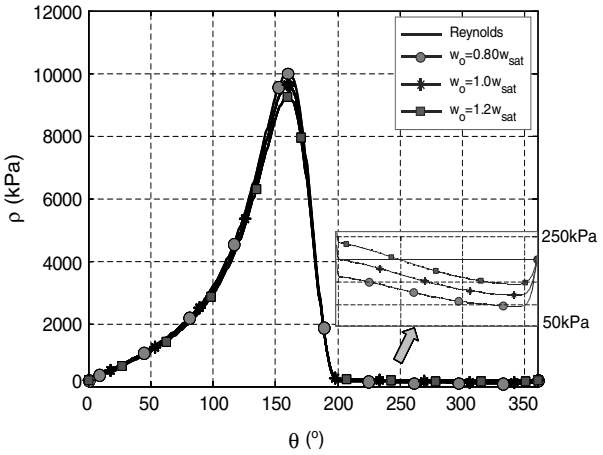

Figure 7. Pressure profiles for mixtures with different initial mass fractions. Simulations considering thermodynamic equilibrium.

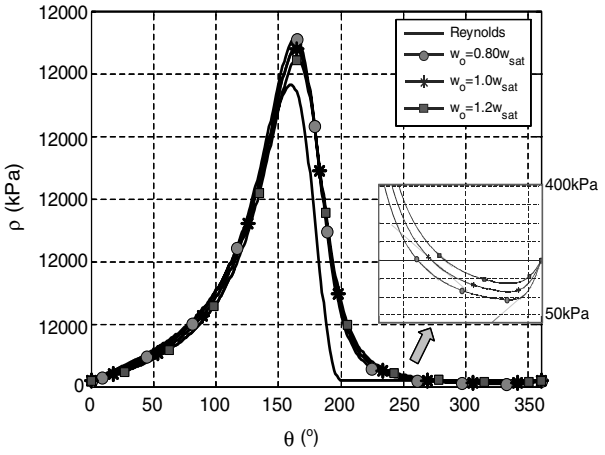

Figure 9. Pressure profiles for mixtures with different initial mass fractions. Simulations considering thermodynamic non-equilibrium.

The influence of fluid properties on a range of performance variables is presented in figure 8. It can be seen that variables such as the load capacity, friction force and maximum pressure vary at the same rate as the viscosity. This may seem unclear for mixtures above w_{sat}, however at this condition some gas is available at the start and is readily absorbed in the liquid once pressure increases, thus reducing viscosity. On the other hand, variables such as the friction coefficient and mass flow rate do not depend on viscosity and remain practically constant regardless of mixture conditions. Such results are also expected in the classical solution for journal bearings [29]. The attitude angle, however, varies more than expected, indicating some influence of the fluid behaviour in cavitation not predicted in the classical solution.

Similar conclusions can be drawn for simulations considering the non-equilibrium hypothesis, as shown for pressure results in figure 9. Despite the shift in the pressure profile due to compressibility effects, viscosity remains the decisive property in the convergent region, resulting in higher pressures for mixtures of higher viscosity, i.e., lower mass fractions. Additionally, as observed in the magnified area of figure 9, comparing to mixtures of higher overall mass fraction, lower pressures are observed for the lower mass fraction mixtures in the cavitated region, which points to a smaller mass of gas released.

However, the performance variables presented in figure 10 for the non-equilibrium case are affected more significantly than those observed for the equilibrium case. Maximum pressure and load capacity vary linearly with the viscosity of the lubricant mixture, as expected. But friction force varies more significantly than viscosity, which could be related to the greater extent of the pressure profile into the divergent region. In this case, viscosity influences friction through Couette and Poiseuille flows in the whole bearing,

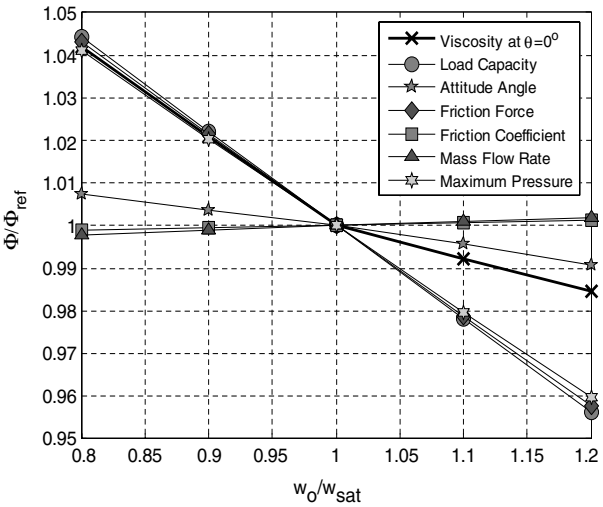

Figure 8. Variation of performance variables with the initial mass fraction under equilibrium conditions.

($\mu_{sat} = 6.62\,\text{mPa.s}$, $W_{sat} = 95\,\text{kN/m}$, $F_{f,sat} = 183\,\text{N/m}$, $\psi_{sat} = 42°$, $f_{sat} = 0.0019$, $q_{\theta,sat} = 89g/(s.m)$, $p_{max,sat} = 9.64\,\text{MPa}$)

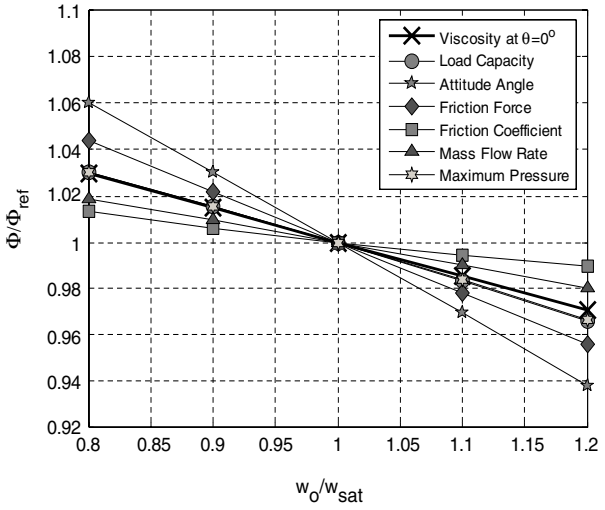

Figure 10. Variation of performance variables with the initial mass fraction under non-equilibrium conditions.

($\mu_{sat} = 7.00\,\text{mPa.s}$, $W_{sat} = 111\,\text{kN/m}$, $F_{f,sat} = 183\,\text{N/m}$, $\psi_{sat} = 31°$, $f_{sat} = 0.0017$, $q_{\theta,sat} = 80\,\text{g/(s m)}$, $p_{max,sat} = 10.80\,\text{MPa}$)

which is different to the equilibrium condition that presents a flat pressure region beyond around 200°, as seen in figure 7.

The friction coefficient reflects the distinct behaviour for load capacity and friction, decreasing as the mass fraction increases. The mass flow rate also reduces with increasing mass fraction, what can be explained by the density of the fluid. As a lower mass of gas is released, the liquid retains more liquid refrigerant in solution, therefore increasing the apparent density.

For the non-equilibrium case, the variable presenting greater variation is the attitude angle, which points to the effects observed in the pressure profile. Reaching the highest and lowest pressures, the fluid with lowest mass fraction presents the greatest angle, which would eventually reach the value for a symmetric pressure profile (90°) in a limit situation. The greater variation in the attitude angle is one of the factors to be investigated further in order to explain numerical instability observed during simulations for non-equilibrium conditions.

As the previous results presented, considerable differences exist between equilibrium and non-equilibrium assumptions in the modelling. Therefore, further analysis is required to determine the exact rate of absorption and consequently predict more accurately the behaviour of the bearing under dynamic conditions. Although results for the equilibrium condition agree well with the classical solution considering Reynolds boundary conditions, the time required for the absorption process should be investigated. For instance, considering the case presented in figures 4–6, reabsorption takes place in the last 25° of the bearing, corresponding to a flow time of 2 ms, which seems unrealistic when compared to the effort usually required to dissolve the refrigerant in the oil [28].

5. Conclusions

A homogeneous two-phase flow approach has been proposed to evaluate the performance of journal bearings. An oil and refrigerant mixture was considered but the model is general and can be used to study bubbly oils and other mixtures of oil and volatile liquids. The model considers cavitation through outgassing from a liquid mixture under saturation conditions, and no intermediate boundary conditions are required in solving the lubrication equation. Additionally, a region of pressure recovery is automatically identified near the convergent region. The absorption of gas that can occur under positive pressure gradients has been studied under equilibrium and non-equilibrium thermodynamic conditions.

For a case of a moderately loaded bearing under equilibrium conditions, the model agrees well with the results provided by the classical solution considering Reynolds boundary conditions. Usually only liquid will be present in the convergent region of the fluid film and in this case cavitation can be seen as geometrically determined. In the cavitated region, however, sub-ambient pressures are observed and their level can be related to the saturation pressure of the mixture and especially to the density of the gas. Viscosity does not have an important role in this region, in contrast to the positive pressure region where it plays a major role.

Under non-equilibrium conditions, the behaviour of the bearing is significantly altered. Gas is present along all the bearing and its compressibility improves the accommodation of geometry changes. As a result, the pressure profile spreads across a wider extent of the bearing and a specific load can be supported with lower eccentricities when compared to the equilibrium condition, potentially reducing friction. With the aeration levels obtained in the simulations, clearly adopting the zero pressure gradient boundary condition would lead to considerably imprecise results.

Due to the difference in the behaviour obtained using the two limit thermodynamic situations, additional investigation should focus on determining the real rate of absorption, enabling more accurate prediction of the behaviour of journal bearings as well as other mechanical components. In this case, a model for the absorption of the refrigerant by the oil is required, particularly for very rapid transients, which has not yet been established.

Acknowledgments

This research is supported by the Programme Alβan, the European Union Programme of High Level Scholarships for Latin America, identification number E03D22219BR. Assistance from the Brazilian Compressor Company EMBRACO SA is duly acknowledged.

Appendix A: Calculation of physical properties

Empiricism is the most common procedure to determine physical properties for oil–refrigerant mixtures, very often adjusting curves from experimental data that has been made available. In this work, properties for the mixture of refrigerant R134a and oil ICI EMKARATE RL10H were calculated using mainly data provided in graphical form by the oil manufacturer. For pure refrigerant, data were obtained from the software REFPROP [34]. This appendix presents the numerical correlations adopted to calculate the physical properties required. For further discussion on the properties of the fluids and the behaviour of this specific mixture, reference is made to Silva [36].

A.1. Solubility

The solubility of R134a in the polyol ester oil ICI EMKARATE RL10H was provided by the oil

manufacturer in a diagram and adjusted by curve fitting for the interval $0 < p < 1000$ kPa and $0 < T < 60$ °C as,

$$w_{sat} = \frac{a_1 + b_1 p + c_1 T + d_1 p^2 + e_1 T^2 + f_1 Tp}{a_2 + b_2 p + c_2 T + d_2 p^2 + e_2 T^2 + f_2 Tp} \quad (A.1)$$

where $a_1 = 0.6825$, $b_1 = 0.0701$, $c_1 = 0.0699$, $d_1 = -1.2087 \times 10^{-4}$, $e_1 = -1.7157 \times 10^{-3}$, $f_1 = 2.4124 \times 10^{-3}$, $a_2 = 1.0$, $b_2 = -3.1315 \times 10^{-3}$, $c_2 = 0.0503$, $d_2 = 1.0541 \times 10^{-6}$, $e_2 = 1.3645 \times 10^{-3}$, $f_2 = -6.4074 \times 10^{-5}$.

A.2. Density

The density for the mixture R134a-EMKARATE RL10H is calculated using the additive law of mixtures. Considering an ideal mixture, the result is presented in equation (A2),

$$\rho_l = \frac{\rho_{oil}}{1 + w_r\left(\frac{\rho_{oil}}{\rho_{lr}} - 1\right)} \quad (A.2)$$

where ρ_l is the density of the liquid mixture, ρ_{oil} the density of the pure oil, ρ_{lr} the density of the liquid refrigerant, and w_r is the refrigerant mass fraction.

The oil density, provided by the manufacturer and adjusted in the range $20 < T < 120$ °C is given by

$$\rho_{oil} = a_3 + b_3 T + c_3 T^2 \quad (A.3)$$

where $a_3 = 966.4364$, $b_3 = -0.5739$, $c_3 = -2.447 \times 10^{-4}$, and ρ_{oil} the density in kg/m^3.

The density of the liquid refrigerant is obtained from the software REFPROP [34] and validated for the interval $-5 < T < 50$ °C as follows

$$\rho_{lr} = a_4 + b_4 T + c_4 T^2 \quad (A.4)$$

where $a_4 = 1294.6790$, $b_4 = -3.2213$, $c_4 = -0.0123$, and ρ_{lr} the density in kg/m^3.

A.3. Dynamic viscosity

The viscosity of the liquid mixture R134a and the polyol ester oil was provided by the oil manufacturer and the following fit is proposed for the interval $0 < T < 60$ °C and $0 < w_r < 1$,

$$\mu_l = \frac{a_5 + b_5 T + c_5 w_r + d_5 T^2 + e_5 w_r^2 + f_5 T w_r}{a_6 + b_6 T + c_6 w_r + d_6 T^2 + e_6 w_r^2 + f_6 T w_r} \quad (A.5)$$

where $a_5 = 0.0371$, $b_5 = 9.1603 \times 10^{-5}$, $c_5 = -0.0800$, $d_5 = -2.7390 \times 10^{-7}$, $e_5 = -0.0435$, $f_5 = -6.0485 \times 10^{-5}$, $a_6 = 1.0$, $b_6 = 0.0531$, $c_6 = 2.2309$, $d_6 = 1.1656 \times 10^{-3}$, $e_6 = -0.3053$, $f_6 = 0.0334$; and μ_l the viscosity (Pa s).

A.4. Properties for the refrigerant in gas phase

The properties of the gas were obtained using the software REFPROP [34], and for the interval $0 < p < 1600$ kPa and $0 < T < 60$ °C the following fits are proposed for density ρ_g (kg/m^3) and viscosity μ_g (Pa s), respectively,

$$\rho_g = \frac{a_7 + b_7 p + c_7 T + d_7 p^2 + e_7 T^2 + f_7 Tp}{a_8 + b_8 p + c_8 T + d_8 p^2 + e_8 T^2 + f_8 Tp} \quad (A.6)$$

where $a_7 = 4.2473 \times 10^{-3}$, $b_7 = -1.9077 \times 10^{-4}$, $c_7 = 0.0448$, $d_7 = 3.4605 \times 10^{-5}$, $e_7 = -2.4624 \times 10^{-5}$, $f_7 = 5.3830 \times 10^{-4}$, $a_8 = 1.0$, $b_8 = 0.0155$, $c_8 = -8.2500 \times 10^{-4}$, $d_8 = 4.5680 \times 10^{-5}$, $e_8 = 6.9326 \times 10^{-8}$, $f_8 = -2.1388 \times 10^{-6}$.

$$\mu_g = \frac{a_9 + b_9 p + c_9 T + d_9 T^2 + e_9 p^3}{a_{10} + b_{10} p + c_{10} p^2 + d_{10} T} \times 10^{-6} \quad (A.7)$$

where $a_9 = 10.8186$, $b_9 = -2.6052 \times 10^{-3}$, $c_9 = 0.1451$, $d_9 = 3.7658 \times 10^{-4}$, $e_9 = -2.0170 \times 10^{-7}$, $a_9 = 1.0$, $b_{10} = -2.1278 \times 10^{-4}$, $c_{10} = -7.752 \times 10^{-9}$, $d_{10} = 9.6695 \times 10^{-3}$.

References

[1] C.M. Taylor, J. Mech. Eng. Sci. 15 (1973) 237.
[2] B. Jacobsson and L. Floberg, Trans. Chalmers Univ. Tech. 189 (1957).
[3] D. Dowson and C.M. Taylor, Ann. Rev. Fluid Mech. 11 (1979) 35.
[4] M. Priest, R.I. Taylor, D. Dowson and C.M. Taylor, Proc. 22nd Leeds-Lyon Symp. Tribology 1995, Tribology Series 31. Elsevier, Amsterdam (1996), p. 441.
[5] M. Priest, D. Dowson and C.M. Taylor, Proc. IMechE C 214 (2000) 435.
[6] L. Tao, S. Diaz, L. San Andrés and K.R. Rajagopal, J. Tribol. 122 (2000) 205.
[7] H.G. Elrod, J. Lub. Technol. 103 (1981) 350.
[8] D.E. Brewe, J. Tribol. 108 (1986) 628.
[9] G. Talmage and M. Carpino, Tribol. Trans. 45 (2002) 310.
[10] A. Kumar and J.F. Booker, J. Tribol. 113 (1991) 276.
[11] K. Tønder, J. Lub. Technol. 99 (1977) 354.
[12] E.H. Smith, J. Lub. Technol. 102 (1990) 91.
[13] J. Kicinski, Wear 91 (1983) 65.
[14] S. Natsumeda and T. Someya, Proc. 13th Leed-Lyon Symp. Tribology (1986) 65.
[15] T. Kawase and T. Someya, Proc. 4th European Tribology Cong. (1987).
[16] T. Someya, Meccanica 38 (2003) 643.
[17] J.R. Barbosa Jr., V.T. Lacerda and A.T. Prata, Int. J. Ref. 27 (2004) 129.
[18] N.S. Feng and E.J. Hahn, ASLE Trans. 29 (1986) 361.
[19] S.F.Y. Motta, S.L. Braga and J.A.R. Parise, HVAC&R Res. 7 (2001) 331.
[20] B.C. Na, K.J. Chun and D.C. Han, Tribol. Int. 30 (1997) 707.
[21] C. Ciantar, M. Hadfield, A.M. Smith and A. Swallow, Wear 236 (1999) 1.
[22] F.P. Grando, M. Priest and A.T. Prata, Proc. 31st Leeds-Lyon Symp. Tribology 2004, Tribology and Interface Eng. Series. Elsevier, Amsterdam (2005), p. 481.
[23] F.Y. Zeidan and J.M. Vance, Tribol. Trans. 32 (1989) 100.
[24] A. Yokozeki, Int. J. Ref. 25 (2002) 695.
[25] A. Prata, F. Grando, A. Silva and J. Barbosa Jr. Proc. Int. Compressor Conf. at Purdue (2004) C071.
[26] E.J. Cullen and J.F. Davidson, Trans. Faraday Soc. 52 (1957) 113.
[27] K. Tsuchiya, H. Mikasa and T. Saito, Chem. Eng. Sci. 52 (1997) 4119.

[28] V.T. Lacerda, A.T. Prata and F. Fagotti, Proc. ASME Adv. Eng. Sys. Div. 40 (2000) 101.
[29] O. Pinkus and B. Sternlicht, *Theory of Hydrodynamic Lubrication* (McGraw-Hill, New York, 1961).
[30] V.P. Carey, *Liquid-Vapor Phase Change Phenomena* (Hemisphere, New York, 1992).
[31] J. Nikolajsen, Tribol. Trans. 42 (1999) 186.
[32] S.V. Patankar, *Numerical Heat Transfer and Fluid Flow* (McGraw-Hill, New York, 1980).
[33] B.J. Hamrock, *Fundamentals of Fluid Film Lubrication* (McGraw-Hill, New York, 1994).
[34] M.O. McLinden, S.A. Klein, E.W. Lemmon and A.W. Peskin, *REFPROP Version 6.0* (NIST, Washington DC, 1998).
[35] D.W. Parkins, Tribol. Int. 18 (1985) 50.
[36] A. Silva, Kynetics and Dynamics of Gas Absorption by Lubricant Oil. Deng Thesis, Fed. Univ. of Santa Catarina, Florianopolis, Brazil (2004).

Lubrication in refrigeration systems: numerical model for piston dynamics considering oil–refrigerant interaction

F P Grando[1,2], **M Priest**[1*], and **A T Prata**[2]
[1]Institute of Tribology, School of Mechanical Engineering, The University of Leeds, Leeds, UK
[2]Department of Mechanical Engineering, Federal University of Santa Catarina, Florianopolis, Brazil

The manuscript was received on 7 September 2005 and was accepted after revision for publication on 7 November 2005.

DOI: 10.1243/13506501JET147

Abstract: Piston dynamics plays a fundamental role in several processes related to the operation of hermetic reciprocating compressors used in refrigeration. For example, the refrigerant leakage through the radial clearance between piston and cylinder, which reduces compressor pumping efficiency, and also the viscous friction associated with the lubricant film in the radial clearance, which is related to energy consumption. It is important to optimize such variables, ensuring at the same time smooth operation of the piston in its reciprocating motion, minimizing wear and increasing lifetime.

In this context, numerical models studying piston dynamics provide a useful tool for engineering design. These models usually consider an oil film filling the piston–cylinder clearance and operating in the hydrodynamic regime. Determining cavitation conditions occurring along the ringless piston represents an additional difficulty in modelling. As refrigerant is present in the compressor environment, it inevitably interacts with the oil, changing lubricant characteristics. The refrigerant can dissolve in the oil at higher pressures, reducing viscosity, and can be released at lower pressures, leading to a two-phase flow.

This work explores how the interaction of oil and refrigerant affects piston dynamics, using a numerical model that considers as the lubricant a mixture of oil and refrigerant with variable properties. Comparing the results with simulations where pure oil is considered as the lubricant and a cavitation criterion is adopted, significant differences were observed in predicting piston trajectory and power consumption along the cycle.

Keywords: piston dynamics, oil–refrigerant mixture, two-phase flow, cavitation

1 INTRODUCTION

The tribological behaviour of the piston inside the cylinder bore has been recognized as an important factor influencing the performance of reciprocating machines. In addition to the main oscillatory movement performed by the piston, its behaviour also depends on small translations and rotations that can occur in the radial direction, where a clearance exists. These small movements are a consequence of the imbalance among the several forces and moments acting on the piston while it goes up and down during operation, shown in Fig. 1.

Given the importance of the oscillatory motions for the performance and reliability of reciprocating machines, all the major concerns in designing these systems, such as the gas leakage, frictional power loss, noise and wear, are tightly related to piston dynamics and lubrication, which also depend on the radial clearance. The dimension of this clearance involves a compromise between gas leakage and friction loss. If the radial clearance is too small, there will be considerable friction loss. On the other hand, larger clearances cannot prevent gas leakage.

Additionally, any contact between piston and cylinder has to be avoided, thus guaranteeing a

Corresponding author: Institute of Tribology, School of Mechanical Engineering, University of Leeds, Woodhouse Lane, Leeds LS2 9JT, UK. email: m.priest@leeds.ac.uk

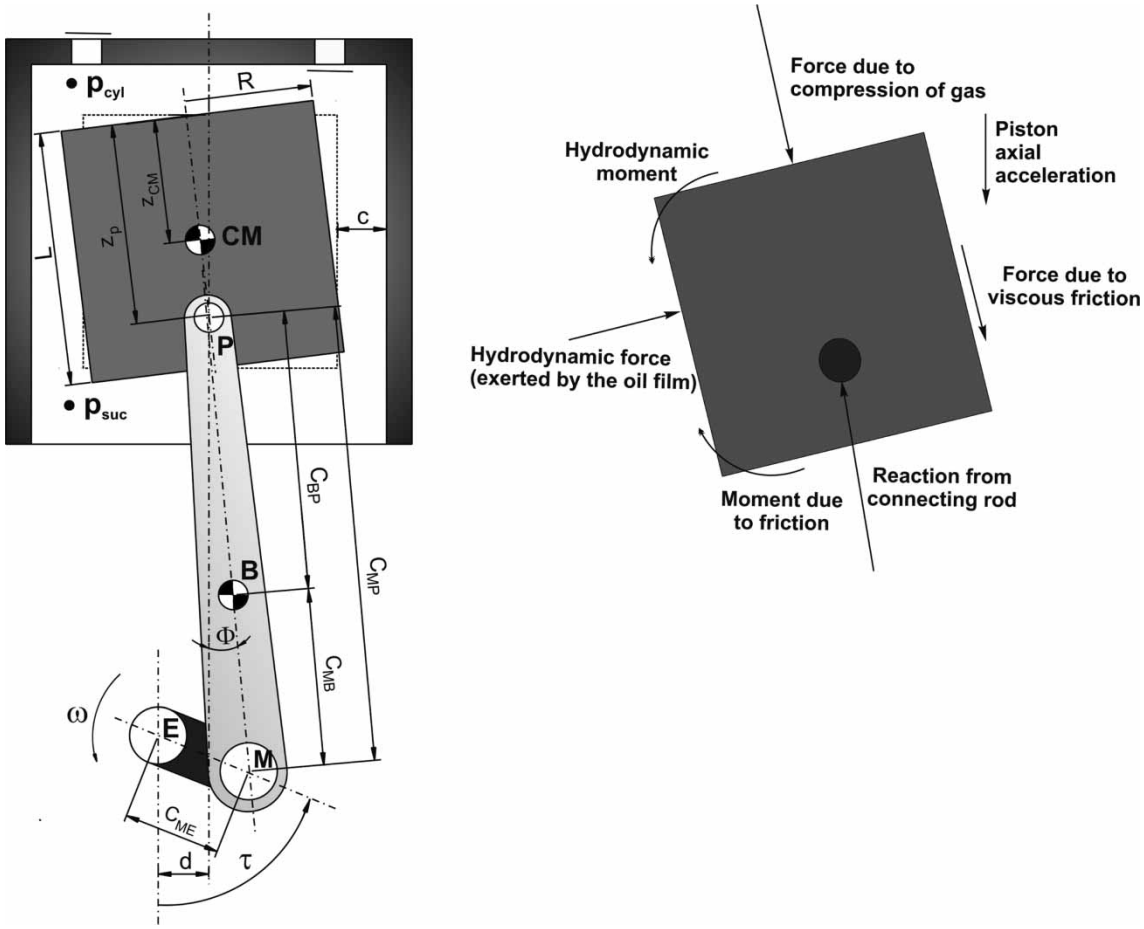

Fig. 1 Details of the piston–cylinder system and the main forces acting on the piston

stable motion and a reasonable piston life. Therefore, a thin fluid film between piston and cylinder should be maintained all times, which aims to ensure a hydrodynamic lubrication regime. However, boundary lubrication often occurs at top and bottom dead centres, as well as during starting and stopping. Such condition is crucial in studying piston ring lubrication, but is also observed for piston skirts, whether rings are present or not.

For those reasons, lubrication plays a fundamental role in performing the dynamic analysis of pistons in reciprocating motion. Several authors have been working towards this purpose. The first scientific investigations concerning piston dynamics started during the 1950s in Germany and in Britain, both from theoretical and experimental points of view [**1**], mainly dealing with diesel engines.

Repàci [**1**] developed a numerical model to simulate the behaviour of a piston in a diesel engine. Pressure was obtained analytically and two equations were used to determine piston velocity and acceleration: the balance of forces along the direction perpendicular to the connecting rod, and the moment equation around the wrist pin. Both equations were integrated by a Runge–Kutta method. His main attention was the impact of the piston against the cylinder bore, which is commonly called piston slap, and a good agreement with experimental results from the literature was reported.

Zhu *et al.* [**2**, **3**] have also confirmed the importance of the radial clearance and oil viscosity to the radial motion of the piston and its power consumption. They developed a numerical model for piston motion, lubrication, and friction in mixed lubrication. The proposed model was applied to an automotive engine and showed that hydrodynamic lubrication can improve piston life by reducing its wear and also reduces frictional loss.

Chittenden and Priest [**4**] proposed a model to calculate numerically the translation of the piston and its rotation around the gudgeon pin, considering the axial forces due to gas compression and connecting rod action, the inertia of the piston and the hydrodynamic forces of the lubricant film, considering the possibility of contact between piston and cylinder. Using the predictions of this model, Gamble *et al.* [**5**] calculated piston ring pack gas flow, dynamics and lubrication, showing significant

influence of piston motion on gas flow and inter-ring pressures. These changes can potentially affect oil film thickness, friction, wear and oil transport and degradation during engine operation. Further research also confirmed that the proposed numerical model presents better agreement with experimental results compared with the friction calculated, considering only axial piston movement along the cylinder axis [**6**].

Concerning small reciprocating compressors used in refrigeration, Prata *et al.* [**7**] developed the first model describing piston trajectory during its oscillatory movement inside the cylinder in a hermetic reciprocating compressor. Pressure was obtained via a finite volume solution of Reynolds equation, and the piston dynamics was solved using a Newton–Raphson procedure, obtaining radial velocities at the top and at the bottom of the piston.

Rigola *et al.* [**8**] included a similar numerical model in the simulation of thermal and fluid dynamic behaviour of hermetic reciprocating compressors. With additional information from experimental results for the compressor (motor torque and system pressures), preliminary results of forces and moments in the piston, connecting rod, and crankshaft were obtained.

Given the small clearances characteristic of this system, further research analysed the hypothesis of non-deformation of piston and cylinder [**9**]. Under severe conditions, results indicated that flexibility of the structure can produce variations of around 10 per cent in the initial system clearance and should be considered.

Despite the additional developments in the numerical modelling of the piston dynamics, there is still controversy regarding the cavitation criterion to be considered and the determination of gas leakage through the clearance. One possible reason for this is that all the previous works have not considered the interaction between the oil and the environment in which it operates, i.e., the solubility between oil and refrigerant in the case of refrigeration compressors.

The hermetic compressor environment is pressurized by the presence of refrigerant in the gas phase inside the shell, where the oil sump is located. In addition, refrigerant is being compressed inside the cylinder, whose walls present a thin lubricant film. Inevitably interaction occurs between oil and refrigerant, affecting system operation. A series of experimental studies have dealt with the performance of lubricant in a pressurized refrigerant environment. Considerable reduction in film forming capability was observed as the environment pressure increases [**10**, **11**]. The study of wear performance also showed that combinations of lubricant and refrigerant with lower viscosities are subjected to more severe conditions and even boundary lubrication [**12**, **13**]. The results of these studies highlight effects such as the reduction of lubricant viscosity with refrigerant solubility and the increase in solubility with pressure.

Other effects can also be observed in addition to changes in liquid properties. Under significant negative pressure gradients, refrigerant can be released in the form of bubbles as solubility decreases, giving raise to a flashing flow, where liquid–vapour phase change occurs. Experimental tests in straight horizontal pipes have shown that considerable outgassing occurs with the decrease of pressure along the flow, and even foaming characteristics can be seen when larger amounts of gas are released [**14**, **15**]. In the light of these findings, the first numerical models were proposed by Grando and Prata [**16**] and Barbosa *et al.* [**17**], both obtaining good agreement with experimental results from Lacerda *et al.* [**14**].

Such developments are useful to the analysis of lubrication and leakage processes inside the compressor. The amount of gas released in the flow can be related to the leakage of refrigerant, which consequently influences pumping efficiency. The understanding of mixture properties and flashing flows creates an appropriate opportunity to advance in the study of cavitation. This phenomenon has long been associated with the interaction of the oil, and gases present in the working environment. Many researchers explicitly mention terms referring to the solubility between oil and ambient gases, commonly attributing the break of liquid film continuity to the release of gas when the 'saturation pressure' is reached [**18**]. This situation can be identified for the compressor operation when refrigerant is released from the oil, representing an alternative to the usual methodologies that use intermediate boundary conditions to model cavitation.

The current authors have proposed a numerical two-phase model considering cavitation from the release of gas and explored it in the study of partial journal bearings, where the difference between modelling considering pure oil or oil–refrigerant as the lubricant was discussed [**19**]. The model was also applied to long journal bearings. Under the presence of gas, it was seen that classical boundary conditions used to determine cavitation produced results significantly different than those obtained using the two-phase methodology [**20**].

The present work continues to explore the model proposed, introducing, for the first time, the two-phase methodology to study the problem of piston dynamics in the refrigeration compressor. To determine the secondary motion of the piston, the analysis of the thin lubricant film considers the behaviour of the fluid mixture along the flow, evaluating the dissolution of the gas in the oil and the interaction

between liquid and gas phases, thereby changing lubricant properties. Differences compared with the methodologies considering constant properties and common cavitation criteria are highlighted.

2 PROBLEM FORMULATION

A typical piston–cylinder system for small reciprocating compressors is presented in Fig. 1. The piston (length L and a constant radius R throughout the length) is driven in a reciprocating motion by the action of a crankshaft on the connecting rod. Apart from the presence of intermediate recesses, this profile is a good approximation of a piston for domestic refrigeration compressors and also attends the aims of this preliminary work. A full cycle occurs for each 360° of rotation of the crankshaft, assumed to start at $\tau = 0°$ when the piston is near the bottom dead centre. An offset d exists between the cylinder axis and the crankshaft centre.

The piston is subjected to a gas force due to the pressure difference between the compression chamber and the shell. While the pressure inside the cylinder (p_{cyl}) varies with the movement, the compression suction pressure (the pressure in the compressor shell, p_{suc}) is assumed constant.

A complete fluid film exists within the clearance either during the upstroke or downstroke movement. For the first, lubricant is carried to the chamber due to the piston movement. The lubricant present inside the cylinder interacts with the refrigerant being compressed. During the downstroke, the lubricant is now brought out of the cylinder with the piston axial motion. Through this process, refrigerant that has been dissolved into the oil escapes from the cylinder, reducing pumping efficiency. Such lubricant feeding conditions occur because of the compressor assembly, which uses a small piston–cylinder clearance to sealing the compression chamber. In addition, compressor operation also ensures that lubricant is abundantly splashed at cylinder walls, piston base, and the gudgeon pin. Furthermore, for the downstroke condition, small droplets of oil that have been also carried into the cylinder during the suction of refrigerant from the shell environment assures that fully flooded lubrication can be assumed [**7**].

At any time during the cycle, refrigerant is dissolved to a certain amount in the oil and can potentially be released in the form of bubbles when the saturation pressure is reached. Determination of the dissolved refrigerant is a difficult task, especially as the process undergoes a rapid transient. Despite some preliminary research on the transient absorption of refrigerant in the oil [**21**, **22**], this issue is not completely resolved and different absorption estimates are tested in this work. It is additionally assumed that the oil splashed at the bottom of the piston is in equilibrium with the refrigerant present in the shell, therefore resulting in a saturated mixture at p_{suc}.

The lubricant film responds hydrodynamically to the imbalance of the other forces acting on the piston and influences the rotation and translation of the component in its secondary motion. To characterize this movement, several coordinate systems could be used. A very convenient one is that where eccentricities at top and bottom of the piston are calculated, from which all the others can be determined if a rigid piston is assumed. Positioning of these eccentricities (e_t and e_b) is presented in Fig. 2. All the movements are assumed to occur in the plane perpendicular to the wrist pin axis.

Figure 2 also shows the coordinate systems adopted in the solution of the problem. A Cartesian system xyz is used to calculate the balance of forces. The vertical axis z coincides with the cylinder axis and x indicates the other direction of movement. In addition, a cylindrical system $r\theta\gamma$ positioned at the top of the piston is convenient to calculate hydrodynamic film pressures throughout the radial clearance. This system moves with the axial velocity of the piston, V_P.

In this context, with simultaneous solution of the pressure in the lubricant film and the balance of forces in the component, the piston trajectory throughout the cycle can be characterized.

2.1 Mathematical modelling

For the piston–cylinder system, most of the basic assumptions adopted in hydrodynamic lubrication

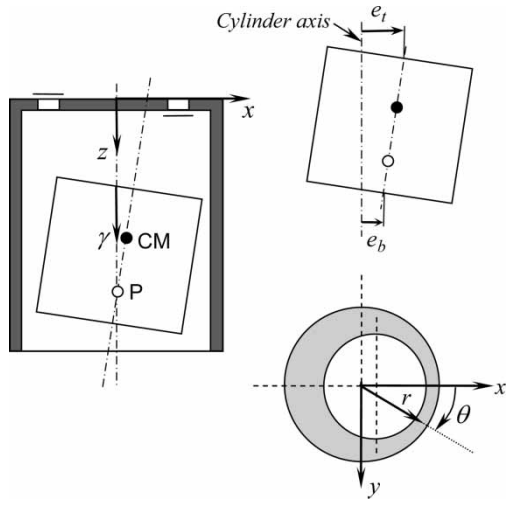

Fig. 2 Coordinate systems and variables used to characterise the secondary movement

problems remain valid [**23**], such as the negligible variation of pressure in the radial direction and laminar flow.

However, the problem now considers the variation of fluid properties due to the interaction of oil and refrigerant, and particularly the two-phase flow occurring when gas is released. To characterize fractional composition of refrigerant and oil in the liquid mixture, as well as the proportion of liquid and gas in the two-phase flow, a series of parameters are needed, defined as follows.

Refrigerant mass fraction: the amount of refrigerant dissolved in the liquid mixture, on a mass basis, defined by equation (1)

$$w = \frac{m_{\mathrm{lr}}}{m_{\mathrm{l}}} \tag{1}$$

The maximum quantity of refrigerant that can be dissolved in the liquid for a specific condition of pressure and temperature is defined as the solubility

$$w_{\mathrm{sat}} = w_{\mathrm{sat}}(p, T) \tag{2}$$

Quality: the ratio between the mass of gas and the total mass of the mixture within a cross-sectional area of the flow. In terms of the refrigerant mass fraction, it can be related to the overall fluid composition at a given instant, thus being given by

$$\chi = \frac{w_{\mathrm{o}} - w}{\mathrm{I} - w} \tag{3}$$

The overall fluid composition, w_{o}, varies with the piston position. When lubricant flows into the cylinder, it is the saturation value for the mixture at the shell pressure, p_{suc}. For the downstroke movement, w_{o} can be estimated from the pressure inside the cylinder. However, as the piston moves at considerable speeds, the refrigerant may not be able to dissolve to its maximum in the oil. As the precise value is not known, intermediate values will be estimated from the mass fraction at the previous time (w_{r}) according to equation (4)

$$w_{\mathrm{o}} = w_{\mathrm{r}} + \kappa[w_{\mathrm{sat}}(p_{\mathrm{cyl}}, T) - w_{\mathrm{r}}] \tag{4}$$

Additional assumptions are required regarding release and absorption of gas in the flow within the clearance that determines the refrigerant mass fraction w_{r}. In this case, it is considered that the gas is released instantaneously when the saturation pressure is reached. However, the gas is not reabsorbed in the liquid if film pressure increases. Further discussion of this assumption can be found in reference [**19**, **20**].

In addition to the mass-related parameters, the ratio between the gas volume and the total volume within a section of the flow is also required. This is defined as the void fraction, which for identical velocities of both phases is determined by

$$\phi = \frac{1}{(1 + ((1/\chi) - 1)\rho_{\mathrm{g}}/\rho_{\mathrm{l}})} \tag{5}$$

As previous research shows [**14**, **15**], assuming similar velocities is a reasonable approach for the two-phase flow of oil and refrigerant mixtures. For this particular condition, a homogeneous two-phase flow model can be adopted, where the liquid–gas mixture can be replaced by a monophasic pseudofluid, whose density and viscosity are given by reference [**24**]

$$\bar{\rho} = \phi\rho_{\mathrm{g}} + (1 - \phi)\rho_{\mathrm{l}} \tag{6}$$

and

$$\bar{\mu} = \chi\mu_{\mathrm{g}} + (1 - \chi)\mu_{\mathrm{l}} \tag{7}$$

Having defined the characteristics of the lubricant, the governing equation for the lubrication of the piston–cylinder clearance can be written. Considering pressure and viscous forces to be dominant, the flow is governed by the Reynolds equation, where the homogeneous properties are considered as presented in equation (8)

$$\frac{\partial}{\partial\theta}\left(\frac{\bar{\rho}h^3}{12\bar{\mu}R^2}\frac{\partial p}{\partial\theta}\right) + \frac{\partial}{\partial\xi}\left(\frac{\bar{\rho}h^3}{12\bar{\mu}R^2}\frac{\partial p}{\partial\xi}\right) = \frac{V_p}{2R}\frac{\partial(\bar{\rho}h)}{\partial\xi} - \frac{\partial(\bar{\rho}h)}{\partial t} \tag{8}$$

For a given time, if the position and velocities resulting from the piston secondary motion are known, the governing equation can be solved considering the following boundary conditions

$$\begin{aligned} &\xi = 0 \longrightarrow p = p_{\mathrm{cyl}} \\ &\xi = \frac{R}{L} \longrightarrow p = p_{\mathrm{suc}} \\ &p(\theta = 0) = p(\theta = 2\pi) \end{aligned} \tag{9}$$

where no intermediate boundary conditions are required for the cavitation of the film as it is automatically determined from the release of gas. In conventional single-phase methodologies, these boundary conditions are also respected, but

additional assumptions on the behaviour of pressure for intermediate positions are required.

When determining the pressure field across the lubricant film, at the same time the balance of forces and moments in the piston must be satisfied. The main forces acting on the piston are the gas force, the connecting rod force, inertia effects, friction force, and the hydrodynamic force due to the lubricant film. Friction and hydrodynamic forces can also produce momentum around the wrist pin.

From the scheme previously shown in Fig. 1, the following equations can be written for the piston

$$\sum F_z = F_g + F_f + F_{rz} = mA_p \tag{10}$$

$$\sum F_x = F_h + F_{rx} = mc\omega^2\left(\ddot{\varepsilon}_t - z_{CM}\frac{\ddot{\varepsilon}_t\ddot{\varepsilon}_b}{L}\right) \tag{11}$$

$$\sum M_{pin} = M_h + M_f = I_P c\omega^2\frac{\ddot{\varepsilon}_t - \ddot{\varepsilon}_b}{L} \tag{12}$$

The forces and moments acting on the piston related to the hydrodynamic force due to the lubricant film and to the viscous frictional force can be determined from the pressure profile as follows

$$F_h = -\int_0^L\int_0^{2\pi} p(\theta,\xi)R^2\cos\theta\,\mathrm{d}\theta\,\mathrm{d}\xi \tag{13}$$

$$M_h = \int_0^L\int_0^L p(\theta,\xi)(z_p - R\xi)R^2\cos\theta\,\mathrm{d}\theta\,\mathrm{d}\xi \tag{14}$$

and

$$F_f = -\int_0^L\int_0^{2\pi}\left(\frac{h}{2R}\frac{\partial p}{\partial\xi} + \mu\frac{V_p}{h}\right)R^2\,\mathrm{d}\theta\,\mathrm{d}\xi \tag{15}$$

$$M_f = -\int_0^L\int_0^{2\pi}\left(\frac{h}{2R}\frac{\partial p}{\partial\xi} + \mu\frac{V_P}{h}\right)R^3\cos\theta\,\mathrm{d}\theta\,\mathrm{d}\xi \tag{16}$$

The force of gas can be easily calculated by

$$F_g = \pi R^2(p_{cyl} - p_{suc}) \tag{17}$$

Connecting rod forces are obtained from the respective balance of forces and moments in this component. These equations also consider the reactions in the crankshaft, which can be determined analytically from the geometry of the system. Analytical expressions for piston acceleration and velocity are derived similarly. Details of these manipulations can be found in Prata *et al.* [**7**].

As previously stated, for a given time, if the characteristics of the secondary movement of the piston are known, equations (8) and (10) to (12) are satisfied. However, the inverse problem is the one of interest, so that piston conditions are not initially known. Therefore, a solution procedure to solve simultaneously pressure and dynamics is required. Details of the methodology adopted in this work are presented subsequently.

2.2 Solution methodology

From the input of connecting rod dynamics, equation (10) can be used to determine F_{rx}. Therefore, for each crankshaft angle τ, piston trajectory can be determined from equations (11) and (12) that implicitly depend on ε_t and ε_b. In these equations, however, knowledge of the pressure profile is required to determine forces and moments related to the hydrodynamic fluid film.

To this end, solution starts from initial estimates for piston eccentricities and velocities for the initial crankshaft angle

$$\varepsilon_t^0,\ \varepsilon_t^0,\ \dot{\varepsilon}_t^0,\ \dot{\varepsilon}_t^0 \quad \text{for } \tau = 0 \tag{18}$$

As the piston presents a periodical trajectory, the converged solution does not depend on the initial guess.

Using these values, time is advanced in a time step to $\tau + \Delta\tau$ and an iterative process is used to search for the correct values for radial velocities that satisfy the balance of forces. In this work, a Newton–Raphson procedure is adopted [**8**]. Piston eccentricities and accelerations are determined from

$$\varepsilon_t^{\tau+\Delta\tau} = \varepsilon_t^\tau + \dot{\varepsilon}_t^{\tau+\Delta\tau}\cdot\Delta\tau, \quad \varepsilon_b^{\tau+\Delta\tau} = \varepsilon_b^\tau + \dot{\varepsilon}_t^{\tau+\Delta\tau}\cdot\Delta\tau \tag{19}$$

$$\ddot{\varepsilon}_t^{\tau+\Delta\tau} = \frac{\dot{\varepsilon}_\tau^{\tau+\Delta\tau} - \dot{\varepsilon}_t^\tau}{\Delta\tau}, \quad \ddot{\varepsilon}_b^{\tau+\Delta\tau} = \frac{\dot{\Delta}_b^{\tau+\Delta\tau} - \dot{\varepsilon}_b^\tau}{\Delta\tau} \tag{20}$$

To determine the forces acting on the piston, pressure is solved from Reynolds equation (8), with the film thickness calculated with values for ε_t and ε_b. Then, the equation is numerically integrated using a finite volumes approach [**25**], where the whole extent of the lubricant film is discretized. It should be noted that the density and viscosity depend on pressure, so that an iterative process is also required to solve the pressure field.

When a converged solution is obtained for $\tau + \Delta\tau$, another advance in the time step is performed and the procedure is repeated, marching in time until a periodical solution is found for the whole cycle.

The solution algorithm is schematically represented in Fig. 3.

3 RESULTS AND DISCUSSION

The proposed methodology has been used to simulate dynamics for a pre-defined piston–cylinder

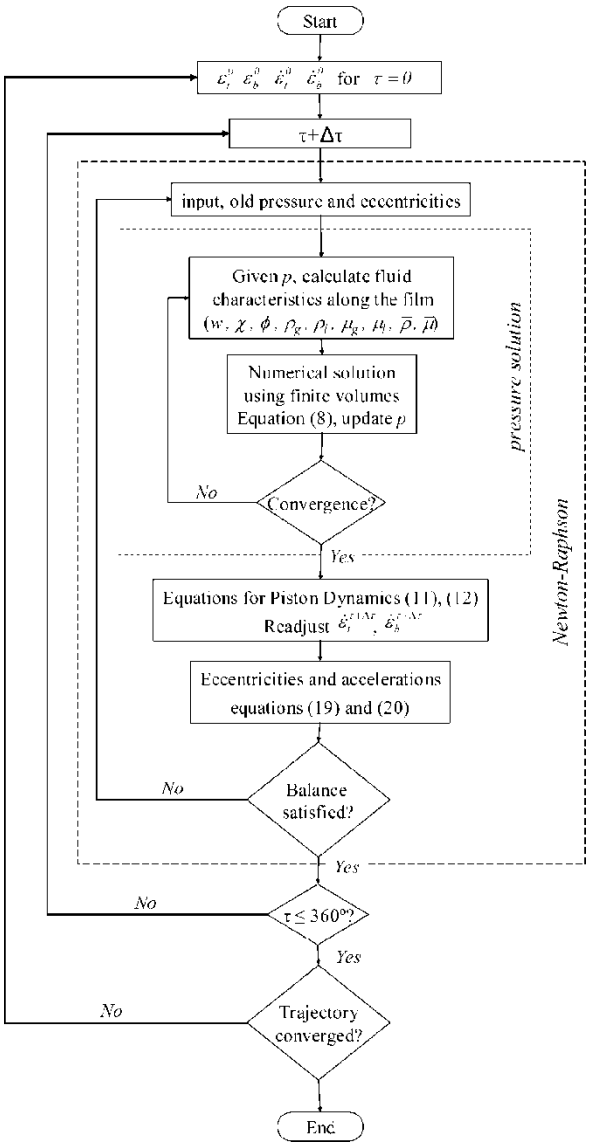

Fig. 3 Algorithm employed for the numerical methodology

system. A combination of a synthetic oil and a hydrofluorocarbon (HFC) refrigerant commonly adopted in domestic refrigeration compressors was considered. The properties for a mixture of the refrigerant HFC-134a and polyol ester EMKARATE RL10H were provided by the oil manufacturer and adjusted by curve fitting. Correlations used are presented in Appendix 2. For simplicity, the fluid is assumed to be at constant temperature.

Relevant compressor data required for the simulation is presented in Table 1, as well as the parameters defined for the numerical simulation.

In addition, pressure in the cylinder as a function of the crankshaft angle is required. Figure 4 graphically sketches this variation, which can also be compared to the shell pressure, assumed constant. Pressure in the cylinder can either be obtained

Table 1 Geometry and numerical data used in the simulations

	Parameter	Value
Geometry	R (mm)	10.5
	L (mm)	21.0
	c (μm)	5.0
	z_P (mm)	12.08
	z_{CM} (mm)	9.53
	C_{BP} (mm)	25.54
	C_{MP} (mm)	36.47
	d (mm)	2.0
	ω (rad/s)	370
	m (g)	34.6
	m_b (g)	24.2
	I_P (kg m^2)	0.287×10^{-5}
	p_{suc} (kPa)	238.50
	T (°C)	60
Numerical	Mesh (θ, ξ)	18×30
	$\Delta\tau$ (°)	5
	Tolerance (p)	1×10^{-6}
	Tolerance (ε_i)	1×10^{-4}

from numerical simulation of the compression cycle or be measured experimentally [**26**].

Referring to equation (4), two different absorption conditions were tested: the first simulated a low absorption condition ($\kappa = 0.05$), whereas the second ($\kappa = 0.50$) indicates easy dissolution of the refrigerant in the oil even at fast transients. The latter dissolves twice as much refrigerant as the former, which indicates a lower viscosity of the lubricant in such conditions, as well as a higher potential to release gas under negative pressure gradients, related to a higher saturation pressure. However, at lower coefficient of absorption refrigerant dissolves for a longer time.

Results of the two-phase model are compared to those obtained using classical methodologies, for a single-phase fluid. Different cavitation criteria are also used. Table 2 summarises the cases analysed in addition to the two-phase flow model.

The methodology requires only minor changes to incorporate the additional single-phase cases. To consider constant properties, the algorithm will not readjust them during the iterative process. Therefore, referring to Fig. 3, in the pressure solution stage, only the numerical solution for pressure, equation (8), is required. In addition, when a cavitation condition is considered, a routine to verify pressures is included. This basically requires that, if during the solution of the linear system a value below the cavitation pressure was obtained, it is replaced by the cavitation pressure. This procedure, along with an iterative solution for the linear system (e.g. CTDMA [**25**]), is the commonly adopted cavitation algorithm [**27**]. The three different criteria compared in this work with the two-phase flow modelling are characterized as follows.

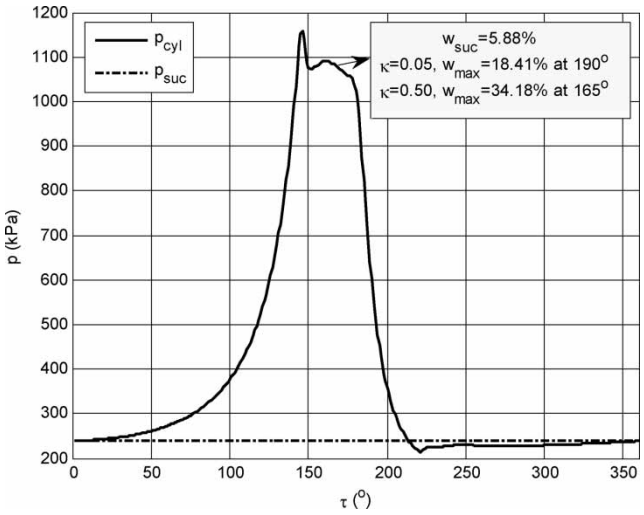

Fig. 4 Pressures in the cylinder and shell during operation and mixture characteristics

1. NCav: in this case, no cavitation pressure is assumed, i.e., the pressure is always that determined by the solution of the linear system. This criterion in nothing else than the Sommerfeld condition.
2. Cav: the cavitation pressure is assumed to vary linearly along the length of the piston, starting from the cylinder pressure at the top (p_{cyl}) and reaching the shell pressure at the bottom of the piston (p_{suc}). Whenever the pressure calculated from a given position is less than the cavitation pressure at that position, the former value is replaced by the latter.
3. Cav_{min}: the minimum value between cylinder and shell pressures is considered as a constant value for the cavitation pressure. When the value calculated is smaller than this minimum value, it is updated to the cavitation pressure.

Table 2 Different conditions explored

Fluid	Case	Cavitation criterion	μ (mPa s)
Oil	Oil NCav	None (Sommerfeld)	4.9481
	Oil Cav	Linear variation between p_{cyl} and p_{suc}	
	Oil Cav_{min}	Constant, minimum between p_{cyl} and p_{suc}	
Oil–refrigerant (saturated at p_{suc})	OR NCav	None (Sommerfeld)	4.2514
	OR Cav	Linear variation between p_{cyl} and p_{suc}	
	OR Cav_{min}	Constant, minimum between p_{cyl} and p_{suc}	
Oil–refrigerant	$2p_{05}$	Automatically determined from w_{sat}	Variable
Two-phase	$2p_{50}$		

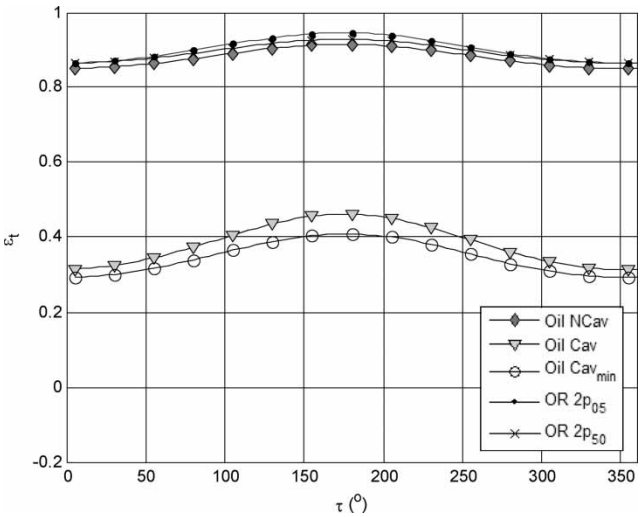

Fig. 5 Eccentricity at the top of the piston

Figure 5 presents the eccentricity for the top of the piston as a function of the crankshaft angle. Differences simply due to the lubricant viscosity, i.e. Oil NCav versus OR NCav, etc., were not shown to be significant. Thus, for clarity, results for oil–refrigerant single phase are omitted. However, the cavitation criteria adopted showed to be crucial in determining the trajectory. Higher eccentricities are observed when cavitation is not considered, whereas the top of the piston moves closer to the cylinder axis when cavitation criteria are adopted. The two-phase model results were similar to those neglecting cavitation. An increase in the eccentricity at the top is observed for the mixture absorbing a less amount of refrigerant (OR $2p_{05}$).

The behaviour of the piston is explained if Fig. 6 is analysed simultaneously with Fig. 5. Individually, the conclusions from the top of the piston can be drawn.

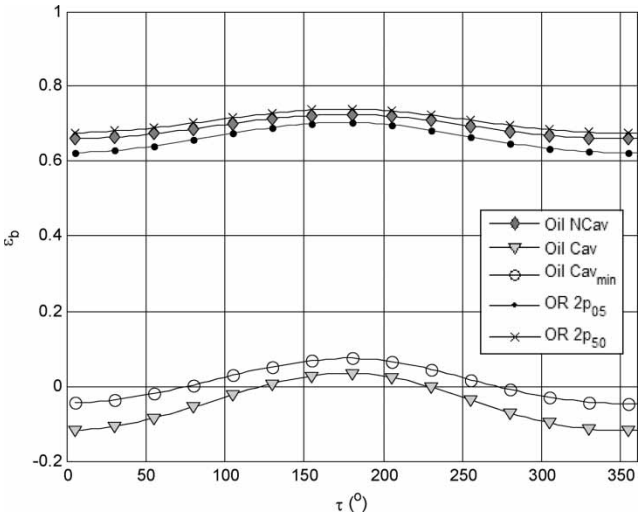

Fig. 6 Eccentricity at the bottom of the piston

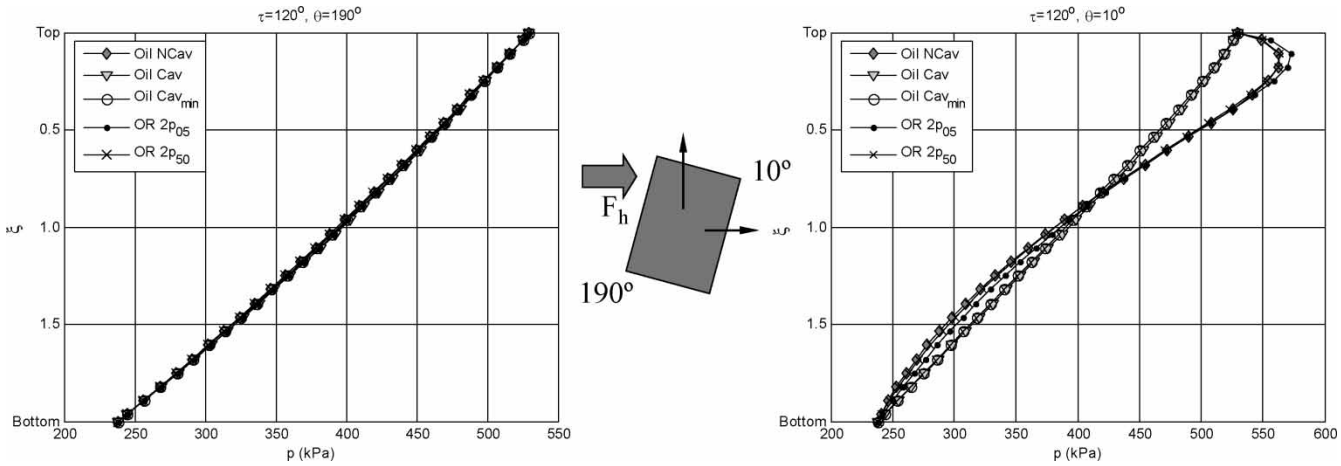

Fig. 7 Pressures for two opposite sides of the piston at $\tau = 120^{\circ}$

However, it can be noticed a greater amplitude of the movements for the results where cavitation criteria was adopted, indicating additional effort from the piston to balance the forces along the cycle. Along with the more inclined condition in which the piston moves, a hydrodynamic wedge effect is expected to balance the forces. On the other hand, the two-phase model has predicted a more stable motion, as also observed for the non-cavitated solution. For the piston lubricated with the less absorbent mixture, inclination slightly increases at the top dead centre region.

To evaluate deeper the differences in eccentricity, an analysis of pressure profiles along the piston trajectory was made. In Fig. 7, the profiles for circumferential positions $\theta = 10^{\circ}$ and $\theta = 190^{\circ}$ are presented for a crankshaft angle $\tau = 120^{\circ}$. Such circumferential positions are chosen among the discretized points for being the closest to thrust and anti-thrust surfaces of the piston, respectively. At this time, the piston is moving upwards. Owing to the high axial velocity, a significant wedge effect develops in the anti-thrust surface of piston, and hydrodynamic forces act pushing the piston against the wall at $\theta = 0^{\circ}$.

The two-phase flow model presents limited difference in this region, as the lubricant flows against a positive pressure gradient. Therefore, no release of gas takes place in the upward movement of the piston.

However, a different picture occurs for the piston returning to the bottom dead centre. Initially, a negative pressure gradient develops and a divergent gap exists for the flow along the minimum film thickness region ($\theta = 0^{\circ}$). Such a situation can be seen in Fig. 8, for a crankshaft angle of 240°. As the fluid reaches the divergent region, pressure tends to decrease and refrigerant is released from the oil, giving rise to a two-phase flow with further expansion of the gas to accommodate changes in geometry. As the shell pressure at the bottom of the piston is communicated, pressure recovery also takes place. The

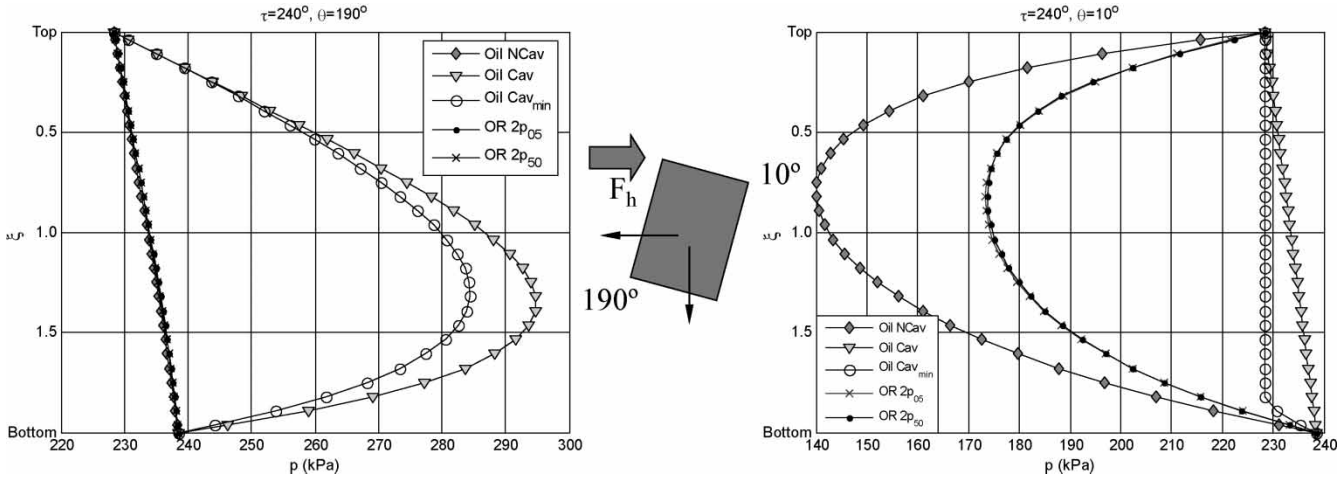

Fig. 8 Pressures for two opposite sides of the piston at $\tau = 240$

Table 3 Cycle averaged values for power consumption due to viscous friction

Case	P_{ot} (W)
Oil NCav	6.904
Oil Cav	4.249
Oil Cav_{min}	4.240
OR NCav	5.941
OR Cav	3.663
OR Cav_{min}	3.652
$2p_{05}$	5.960
$2p_{50}$	6.189

effect of gas expansion is clear when comparing the results with those for a non-cavitated condition. On the other hand, when a cavitation criterion is applied, the behaviour is exactly the opposite. The low pressures cause the rupture of the film, and a squeeze film effect provokes increase in pressure at $\theta = 190^{\circ}$, eventually resulting in the same effect on the piston.

As an important parameter for piston design, power consumption was also determined. After calculating the friction force using equation (15), power loss due to viscous friction can be averaged for the whole cycle as

$$P_{ot} = \frac{1}{2\pi}\int_0^{2\pi} F_f \cdot V_P \, d\tau \tag{21}$$

Values are presented in Table 3, where it can be seen that lower values are obtained when cavitation is artificially considered, as the cavitated points are removed from calculation (negligible shear stress). Here, viscosity plays a major role and when the oil–refrigerant is considered as the lubricant, lower values are obtained. Results for the two-phase flow model are closer to that for the oil–refrigerant lubricant disconsidering cavitation, although slightly higher. One of the reasons is that, when gas is released from the lubricant, the viscosity will actually increase as a result of a lower mass fraction of refrigerant and despite the presence of gas with lower viscosity. The correlation to calculate the viscosity of the oil–refrigerant liquid mixture is presented in Appendix 2 and is referred to this analysis. Minimal differences occur for the different mixture conditions, with higher friction for the mixture with more refrigerant dissolved, despite its lower viscosity.

Finally, the leakage of oil can also be estimated from the pressure profile determined. At the bottom of the piston, it is calculated as

$$q_{bottom} = \int_0^{2\pi} \left(-\frac{h^3}{12\bar{\mu}R}\frac{\partial p}{\partial \xi} + V_P \frac{h}{2} \right)\Bigg|_{z=L} R \, d\theta \tag{22}$$

Figure 9 presents results for flow rate. The main effect has been proved to be the axial movement of the piston (qVp), with only small differences between

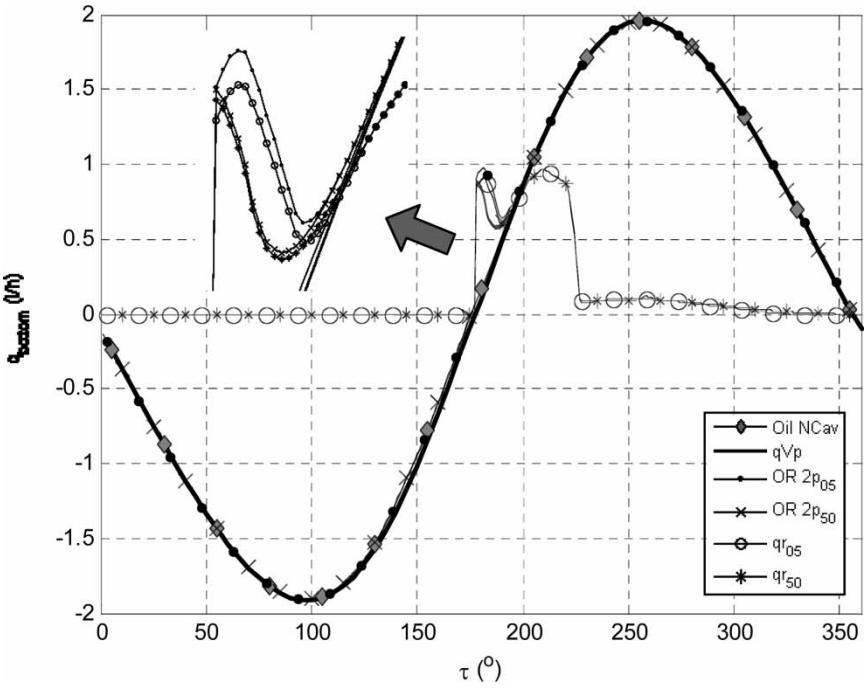

Fig. 9 Volumetric flow rate along the cycle and the participation of gas refrigerant for each two-phase case

the cases. This indicates the sealing capacity promoted by the small clearance. This value is significant for any of the single phase simulations, but an opportunity to estimate the leakage of refrigerant as gas can also be performed using the two-phase model, estimating such leakage from equation (5) with the void fraction of the liquid–gas lubricant leaving the piston skirt. This result is also presented. Refrigerant flow starts a little before 180°, when the piston changes direction; the presence of gas naturally increases the volumetric flow rate. The discontinuity results from the assumption that reverse flow starts with the change in direction of the piston. Therefore, a delay in the reverse flow is suggested, which is currently not predicted. Additional refinements will be required as pressure flow is conceivably important for that region. Nevertheless, it can be seen that maximum leakage occurs for the lowest piston velocities, as no resistence is imposed against the pressure gradient and the mixture presents has a high mass fraction. Thereafter, gas leakage gradually reduces as pressure in the cylinder starts to decrease, reducing the amount of refrigerant dissolved. A small difference can be observed as a result of the different absorption characteristics of the mixtures. Surprisingly, the mixture with a lower mass fraction presents a higher leakage than the one capable of absorbing more refrigerant, as can be seen in detail in Fig. 9. This is actually the reason to this behaviour: while the mixture with a higher coefficient of absorption has too much refrigerant dissolved from the start, as pressure decreases refrigerant is released as soon as cylinder pressure decreases. On the other hand, the mixture with lower coefficient of absorption can still absorb refrigerant; despite pressure decreases, levels are high and the refrigerant remains dissolving in the oil, therefore being carried out of the compression chamber. It should be stressed that the results intend to show the prediction capability of the model, although significant advances are required to the precise determination of the oil–refrigerant mixture inside the cylinder, thereby improving the understanding of the refrigerant release during suction.

4 CONCLUSIONS

A model considering the interaction of the oil and refrigerant during piston operation has been proposed. The model advances previous solutions available by including the variation of properties during the cycle. The change in properties is a result of the dissolution of the refrigerant in the oil and its release throughout the piston–cylinder clearance when negative pressure gradients are experienced.

1. Compared to the previous solutions considering pure oil with constant properties, small differences are observed in relation to non-cavitated conditions, and no agreement was found with cavitated solutions. This highlights the controversy regarding cavitation boundary conditions, as considerable discrepancy was observed.
2. The model predicts power consumption similarly to the single-phase model considering oil–refrigerant viscosity. Using cavitation criteria, a much lower value was predicted.
3. Differences in the oil leakage through the clearance during downstroke were not significant for most of the cycle, but close to the top dead centre the two-phase model predicts higher volumetric leakage. The model can estimate the amount of refrigerant released as gas with the oil, having calculated the volume ratio of the phases during pressure solution.
4. The influence of the coefficient of absorption in the mixture behaviour was not significant, although at lower rates of absorption a higher leakage was predicted. Nevertheless, additional studies to understand the transient behaviour of the oil–refrigerant mixture are crucial to the advances of the present model. Simultaneously, future work shall consider also a better estimate for the flow of oil close to the top dead centre, potentially the instant where maximum refrigerant leakage occurs.

Applying the model to more realistic geometries of the piston is also relevant. For instance, in recesses, where the clearance increases, the two-phase flow model is capable of predicting release of gas even during the upstroke, which may significantly affect piston trajectory.

ACKNOWLEDGEMENTS

This research was supported financially by the Programme Alβan, the European Union Programme of High Level Scholarships for Latin America, identification number E03D22219BR. Assistance from the Brazilian Compressor Company EMBRACO SA is also acknowledged.

REFERENCES

1 **Repàci, A.** Non linear modelling of the piston slap phenomenon in an alternative internal combustion engine. *Math. Model.*, 1987, **8**, 366–367.
2 **Zhu, D., Cheng, H. S., Takayuki, A.,** and **Hasmai, K.** A numerical analysis for piston skirt in mixed lubrication – Part I: basic modelling. *J. Tribol.*, 1992, **114**, 553–562.

3 **Zhu, D., Cheng, H. S., Takayuki, A.,** and **Hasmai, K.** A numerical analysis for piston skirt in mixed lubrication – Part II: deformations considerations. *J. Tribol.*, 1993, **115**, 125–133.

4 **Chittenden, R. J.** and **Priest, M.** Analysis of the piston assembly, bore distortion and future developments. *Tribol. Ser.*, 1993, **26**, 241–270.

5 **Gamble, R., Priest, M., Chittenden, R. J.,** and **Taylor, C. M.** Preliminary study of the influence of piston secondary motion on piston ring lubrication. *Tribol. Ser.*, 2000, **38**, 679–691.

6 **Mufti, R. A.** *Total and component friction in a motored and firing engine*. PhD Thesis, University of Leeds, Leeds, 2004.

7 **Prata, A. T., Fernandes, J. R. S.,** and **Fagotti, F.** Dynamic analysis of piston secondary motion for small reciprocating compressors. *J. Tribol.*, 2000, **122**, 752–760.

8 **Rigola, J., Perez-Segarra, C. D.,** and **Oliva, A.** Numerical simulation of the leakage through the radial clearance between piston and cylinder in hermetic reciprocating compressors. Proceedings of the International Conference of *Compressors and their systems*, London, UK, 2003, pp. 313–321.

9 **Cho, J. R.** and **Moon, S. J.** A numerical analysis of the interaction between the piston oil film and the component deformation in a reciprocating compressor. *Tribol. Int.*, 2005, **38**(5), 459–468.

10 **Akei, M., Mizuhara, K., Taki, T.,** and **Yamamoto, T.** Evaluation of film-forming capability of refrigeration lubricants in pressurized refrigerant atmosphere. *Wear*, 1996, **196**, 180–187.

11 **Na, B. C., Chun, K. J.,** and **Han, D. C.** A tribological study of refrigeration oils under HFC-134a environment. *Tribol. Int.*, 1997, **30**(9), 707–716.

12 **Safari, S.** and **Hadfield, M.** Wear behaviour of the piston/gudgeon pin in a hermetic compressor with replacement CFC refrigerants. *Wear*, 1998, **219**, 8–15.

13 **Ciantar, C., Hadfield, M., Smith, A. M.,** and **Swallow, A.** The influence of lubricant viscosity on the wear of hermetic compressor components in HFC-134a environments. *Wear*, 1999, **236**, 1–8.

14 **Lacerda, V. T., Prata, A. T.,** and **Fagotti, F.** Experimental characterisation of oil-refrigerant two-phase flow. Proceedings of the ASME – Advanced Energy Systems Division, 2000, vol. 40, pp. 101–109.

15 **Castro, H. O. S., Gasche, J. L.,** and **Conti, W. P.** Foam flow of oil-refrigerant R134a mixture in a small diameter tube. In Proceedings of the 10th International Refrigeration and Air Conditioning Conference at Purdue, Purdue, USA, 2004, paper R171.

16 **Grando, F. P.** and **Prata, A. T.** Computational modeling of oil-refrigerant two-phase flow with foam formation in straight horizontal pipes. In Proceedings of the 2nd International Conference on *Heat transfer, fluid mechanics and thermodynamics – HEFAT*, Zambia, 2003, paper GF2.

17 **Barbosa, Jr., J. R., Lacerda, V. T.,** and **Prata, A. T.** Prediction of pressure drop in refrigerant–lubricant oil flows with high contents of oil and refrigerant outgassing in small diameter tubes. *Int. J. Refrig.*, 2004, **27**, 129–139.

18 **Dowson, D.** and **Taylor, C. M.** Cavitation in bearings. *Annu. Rev. Fluid Mech.*, 1979, **11**, 35–66.

19 **Grando, F. P., Priest, M.,** and **Prata, A. T.** Lubrication in refrigeration systems: performance of journal bearings lubricated with oil and refrigerant mixtures. Life cycle tribology, Proceedings of the 31st Leeds-Lyon Symposium on *Tribology*, Leeds 2004, Tribology and Interface Engineering Series, 2005, pp. 481–491 (Elservier, Amsterdam).

20 **Grando, F. P., Priest, M.,** and **Prata, A. T.** A two-phase flow approach to cavitation modeling in journal bearings. *Tribol. Lett.*, 2006, in press, DOI: 10.1007/s11249-006-9027-6.

21 **Yokozeki, A.** Time-dependent behavior of gas absorption in lubricant oil. *Int. J. Refrig.*, 2002, **25**, 695–704.

22 **Silva, A.** *Kinetics and dynamics of gas absorption by lubricant oil*. DEng thesis, Federal University of Santa Catarina, Florianopolis, Brazil, 2004.

23 **Pinkus, O.** and **Sternlicht, B.** *Theory of hydrodynamic lubrication*, 1961 (McGraw-Hill, New York).

24 **Carey, V. P.** *Liquid–vapor phase-change phenomena*, 1992 (Hemisphere, New York).

25 **Patankar, S. V.** *Numerical heat transfer and fluid flow*, 1980 (McGraw-Hill, New York).

26 **Rigola, J., Perez-Segarra, C. D., Raush, G., Oliva, A., Escriba, M., Jover, J.,** and **Escanes, F.** Experimental studies of hermetic reciprocating compressors with special emphasis on pv diagrams. Proceedings of the 16th International Compressor Engineering Conference at Purdue, Purdue, USA, 2002, paper C4-1.

27 **Venner, C. H.** and **Lubrecht, A. A.** *Multilevels methods in lubrication*. Tribology Series 37, 2000 (Elsevier, Amsterdam)

28 **McLinden, M. O., Klein, S. A., Lemmon, E. W.,** and **Peskin, A. W.** REFPROP: Thermodynamic and transport properties of refrigerants and refrigerant mixtures, version 6.0. Washington (DC): NIST, 1998.

APPENDIX 1

Notation

A_P	piston axial acceleration (m/s^2)
c	radial clearance between piston and cylinder (m)
C_{BP}	distance between connecting rod centre of mass and the piston gudgeon pin (m)
C_{MB}	connecting rod length (m)
d	distance between the crankshaft centre and the cylinder axis, 'offset' (m)
e	eccentricity (m)
F_f	friction force (N)
F_g	force due to the compression of the gas (N)
F_h	hydrodynamic force (N)
F_{rx}	connecting rod force, direction x(N)
F_{rz}	connecting rod force, direction z(N)
h	lubricant film thickness (m) $= c - [e_t + (e_b - e_t)\xi R/L]\cos\theta$
I_P	moment of inertia of the piston about the gudgeon pin (kg m^2)

L	piston length (m)
m	mass of the piston (kg)
m_b	connecting rod mass (kg)
m_l	total mass of liquid (oil + refrigerant) (kg)
m_{lr}	mass of liquid refrigerant (kg)
M_f	moment due to viscous friction, in relation to the pin (N m)
M_h	hydrodynamic moment about the pin (N m)
p	absolute pressure (Pa)
P_{ot}	power consumption by viscous friction (W)
q_{bottom}	volumetric flow rate at the bottom of the piston (m^3/s)
r	radial coordinate (m)
R	piston radius (m)
t	time (s)
T	temperature (°C)
V_P	piston axial velocity (m/s)
w	refrigerant mass fraction (kg_{ref}/kg_{mixt})
w_o	overall refrigerant mass fraction (kg_{ref}/kg_{mixt})
w_r	mass fraction immediately before the instant considered (kg_{ref}/kg_{mixt})
w_{sat}	refrigerant solubility in the oil (kg_{ref}/kg_{mixt})
x	coordinate of the Cartesian system (m)
y	coordinate of the Cartesian system (m)
z	axial coordinate of the Cartesian system (m)
z_P	pin location from the top of the piston (m)

γ	axial coordinate for the polar system (m)
$\Delta\tau$	step in the crankshaft angle (rad, °)
ε	eccentricity ratio ($= e/c$) (–)
$\dot{\varepsilon}$	velocity in the radial direction (1/s)
$\ddot{\varepsilon}$	acceleration in the radial direction ($1/s^2$)
θ	angular coordinate, polar system (rad, °)
κ	coefficient of absorption (–)
μ	dynamic viscosity (Pa s)
$\bar{\mu}$	homogeneous viscosity, equation (7) (Pa s)
ξ	dimensionless axial coordinate ($=\gamma/R$) (–)
ρ	density (kg/m^3)
$\bar{\rho}$	homogeneous density, equation (6) (kg/m^3)
τ	crankshaft angle ($= \omega t$)(rad, °)
ø	void fraction, equation (5) (–)
χ	gas quality, equation (3) (kg/m^3)
ω	crankshaft angular velocity (rad/s)

Superscripts and subscripts

b	bottom of the piston
cyl	cylinder
CM	centre of mass
g	gas phase
l	liquid phase
mixt	mixture
ref	refrigerant
suc	at the suction or shell
t	top of the piston
τ	previous crankshaft position
$\tau+\Delta\tau$	current crankshaft position

APPENDIX 2: CALCULATION OF PHYSICAL PROPERTIES

Empiricism is the most common procedure in determining physical properties for oil–refrigerant mixtures, very often adjusting curves from experimental data that have been made available. In this work, properties for the mixture of refrigerant R134a and oil ICI EMKARATE RL10H were calculated using data provided in graphical form by the oil manufacturer. For pure refrigerant, data were obtained from the software REFPROP [**28**]. This section presents the numerical correlations adopted to calculate the physical properties required. Further discussion on the properties of the fluids and the behaviour of this specific mixture can be found by Silva [**22**].

A.1 Solubility

The solubility of R134a in the polyol ester oil ICI EMKARATE RL10H was provided by the oil manufacturer in a diagram and adjusted by curve fitting for the interval $0 < p < 1000$ kPa and $0 < T < 60$ °C as

$$w_{sat} = \frac{a_1 + b_1 p + c_1 T + d_1 p^2 + e_1 T^2 + f_1 Tp}{a_2 + b_2 p + c_2 T + d_2 p^2 + e_2 T^2 + f_2 Tp} \tag{23}$$

where $a_1 = 0.6825$, $b_1 = 0.0701$, $c_1 = 0.0699$, $d_1 = -1.2087 \times 10^{-4}$, $e_1 = -1.7157 \times 10^{-3}$, $f_1 = 2.4124 \times 10^{-3}$, $a_2 = 1.0$, $b_2 = -3.1315 \times 10^{-3}$, $c_2 = 0.0503$, $d_2 = 1.0541 \times 10^{-6}$, $e_2 = 1.3645 \times 10^{-3}$, $f_2 = -6.4074 \times 10^{-5}$.

A.2 Density

The density for the mixture R134a–EMKARATE RL10H is calculated using the additive law of mixtures. Considering an ideal mixture, the result is presented in the following equation

$$\rho_l = \frac{\rho_{oil}}{1 + w_r((\rho_{oil}/\rho_{lr}) - 1)} \tag{24}$$

where ρ_l is the density of the liquid mixture, ρ_{oil} the density of the pure oil, ρ_{lr} the density of the liquid refrigerant, and w_r is the refrigerant mass fraction.

The oil density provided by the manufacturer and adjusted in the range $20 < T < 120\,^{\circ}\text{C}$ is given by

$$\rho_{oil} = a_3 + b_3 T + c_3 T^2 \tag{25}$$

where $a_3 = 966.4364$, $b_3 = -0.5739$, $c_3 = -2.4476 \times 10^{-4}$, and ρ_{oil} the density in kg/m^3.

The density of the liquid refrigerant is obtained from the software REFPROP [**28**] and validated for the interval $-5 < T < 60\,^{\circ}\text{C}$ as follows

$$\rho_{lr} = a_4 + b_4 T + c_4 T^2 \tag{26}$$

where $a_4 = 1294.6790$, $b_4 = -3.2213$, $c_4 = -0.0123$, and ρ_{lr} the density in kg/m^3.

A.3 Dynamic viscosity

The viscosity of the liquid mixture R134a and the polyol ester oil was provided by the oil manufacturer and the following fit is proposed for the interval $0 < T < 60\,^{\circ}\text{C}$ and $0 < w_r < 1$

$$\mu_l = \frac{a_5 + b_5 T + c_5 w_r + d_5 T^2 + e_5 w_r^2 + f_5 T w_r}{a_6 + b_6 T + c_6 w_r + d_6 T^2 + e_6 w_r^2 + f_6 T w_r} \tag{27}$$

where $a_5 = 0.0371$, $b_5 = 9.1603 \times 10^{-5}$, $c_5 = -0.0800$, $d_5 = -2.7390 \times 10^{-7}$, $e_5 = -0.0435$, $f_5 = -6.0485 \times 10^{-5}$, $a_6 = 1.0$, $b_6 = 0.0531$, $c_6 = 2.2309$, $d_6 = 1.1656 \times 10^{-3}$, $e_6 = -0.3053$, $f_6 = 0.0334$, and μ_l the viscosity (Pa s).

A.4 Properties for the refrigerant in gas phase

The properties of the gas were obtained using the software REFPROP [**28**], and for the interval $0 < p < 1600$ kPa and $0 < T < 60\,^{\circ}\text{C}$ the following fits are proposed for density ρ_g (kg/m^3) and viscosity μ_g (Pa s), respectively

$$\rho_g = \frac{a_7 + b_7 p + c_7 T + d_7 p^2 + e_7 T^2 + f_7 T p}{a_8 + b_8 p + c_8 T + d_8 p^2 + e_8 T^2 + f_8 T p} \tag{28}$$

where $a_7 = 4.2473 \times 10^{-3}$, $b_7 = -1.9077 \times 10^{-4}$, $c_7 = 0.0448$, $d_7 = 3.4605 \times 10^{-5}$, $e_7 = -2.4624 \times 10^{-5}$, $f_7 = 5.3830 \times 10^{-4}$, $a_8 = 1.0$, $b_8 = 0.0155$, $c_8 = -8.2500 \times 10^{-4}$, $d_8 = 4.5680 \times 10^{-5}$, $e_8 = 6.9326 \times 10^{-8}$, $f_8 = -2.1388 \times 10^{-6}$

$$\mu_g = \frac{a_9 + b_9 p + c_9 T + d_9 T^2 + e_9 p^3}{a_{10} + b_{10} p + c_{10} p^2 + d_{10} T} \times 10^{-6} \tag{29}$$

where $a_9 = 10.8186$, $b_9 = -2.6052 \times 10^{-3}$, $c_9 = 0.1451$, $d_9 = 3.7658 \times 10^{-4}$, $e_9 = -2.0170 \times 10^{-7}$, $a_9 = 1.0$, $b_{10} = -2.1278 \times 10^{-4}$, $c_{10} = -7.752 \times 10^{-9}$, $d_{10} = 9.6695 \times 10^{-3}$.